The University Of Sheffield.

Modelling the Effects of Moisture Absorption on the Thermo-Mechanical Properties of Thermoset Resins

By:

Ben Christen Holmes

A thesis submitted in partial fulfilment of the requirements for the degree of Doctor of Philosophy

The University of Sheffield
Faculty of Engineering
Department of Materials Science and Engineering

May 2018

Summary

A revised approach for investigating the hydrolysis of DGEBA-DDA epoxy resin has been proposed and this has allowed the initial properties of the material, before ageing occurs, to be deduced. A model was developed, incorporating aspects of Group Interaction Modelling (GIM), and this has allowed the change in material mass, as a result of hydrolysis, to be linked to the change in the glass transition temperature of the resin. The second focus of this work has been to apply GIM to modelling the thermo-mechanical properties of phenolic resins as a function of cure and formaldehyde/phenol ratio. This modelling has highlighted the effect of ether bridges upon the engineering properties of these materials and their potential for increasing the residual stresses within phenolic based composites. The impact of polymer free volume on the hygrothermal behaviour of phenolic resins has also been investigated. This was achieved through modification of the GIM molar volume equation and has suggested a possible beneficial effect of absorbed water, upon the engineering moduli of the resin, before free volume has been filled. Finally, the hygrothermal behaviour of low-fired carbon-fibre composites have been investigated. This analysis suggests that the presence of low-fired carbon-fibre within composites reduces the water concentration gradients throughout the material. This has led to the proposal that the presence of this hygroscopic fibre may reduce the impact of cyclic conditioning upon the polymer matrix by reducing the differential swelling stresses within the material.

Acknowledgement

This work was funded by the UK Defence Science and Technology Laboratory (DSTL) under contract number DSTLX-1000086095.

I would like to thank Dr Foreman for supervising my PhD, Dr Swan, Dr Stone, Dr Denham, and Dr Berridge, at DSTL, and Prof. Arnold and Dr Alston at Swansea University, for the informative conversations that we had and for providing experimental data that was essential for parts of the modelling undertaken in this work. I would also like to thank Dr Lafferty for the training in laboratory instruments that he kindly provided. And finally, a thank you to Roderick Ramsdale-Capper for the discussions that we had and the help you provided when I needed it.

Dedication

I dedicate this work to my Mum, my Dad, and Annette, for all your loving support.

Table of Contents

Introduction

Epoxy and Phenolic resins are a group of thermosetting polymers that have found widespread use in engineering applications; particularly in the role as the matrix component of fibre reinforced composites. These materials are well suited to this application as they possess good mechanical properties, are resistant to corrosion, and bind strongly to the fibre reinforcement. However, they are susceptible to absorbing moisture from their ambient environment and this has an effect upon their engineering properties [1-4]. As a consequence, it is necessary to understand the hygrothermal behaviour of these polymers in a variety of different environmental conditions to ensure that they will perform as required in their service environment. In this work the hydrothermal behaviour of epoxy and phenolic resins will be investigated through both experimental, and modelling, approaches.

In chapter two, the hydrolysis of an epoxy resin, synthesised from the reaction of the diglycidyl ether of bisphenol A (DGEBA) with the amine hardener dicyandiamide (DDA), will be investigated. This material is known to absorb moisture when exposed to atmospheric water vapour, or when immersed in liquid water. This water chemically reacts with the polymer network, breaking the cross-links between polymer chains, and thus reducing the glass transition temperature of the material. Although this phenomenon has received substantial treatment in the literature [5-7], the coupling of the diffusion and hydrolysis processes has complicated the analysis of these experimental studies. In this work samples of much smaller dimensions will be employed, and it will be shown that this enables them to attain equilibrium with their environment on a much shorter time scale than that associated with the hydrolysis reaction. Thus, the two processes are decoupled. This allows the diffusive properties of unaged DGEBA-DDA, solubility and diffusion coefficient, to be determined. A diffusion model is then developed, based on the formalism of Yagoubi et al [8] to describe the combined diffusion and hydrolysis processes and by fitting to the experimental data, the rate constants for the hydrolysis process are obtained. Finally, it will be shown that these rate constants can be employed within Group Interaction Modelling (GIM) to predict the glass transition temperature of DGEBA-DDA as a function of conditioning time.

In chapter three, Group Interaction Modelling will be employed to predict the thermo-mechanical properties of phenolic resins with respect to their chemical group constituents, cure time, and formaldehyde/phenol (F/P) ratio. During the cure of phenolic resins, two distinct intermediate chemical structures can be formed, methylol groups and ether bridges, and these are dependent upon the initial F/P ratio that was employed in their synthesis. GIM is used to deduce the effect of each of these chemical groups upon the thermo-mechanical properties of the resin, and it will be shown that although methylol groups provide a small improvement to the material's properties, the impact of ether bridges is significant. In the second part of this work, the effect of initial F/P ratio on the thermo-mechanical properties, of fully cured phenolic resins, is investigated. A methodology for identifying the initial chemical constituents of phenolic resins in their gelled state, before cross-linking between adjacent polymer chains has occurred, is introduced, and then their evolution with cure time predicted via rate equations. This analysis will show that the Young's modulus, and glass transition temperature, increase with increasing F/P ratio. However, the effect of F/P ratio on polymer properties is reduced in the mid F/P ratio range 1.4-1.8. Furthermore, above an F/P ratio of 2.5, no further change in Young's modulus or glass transition temperature can occur and this is attributed to the point at which no further cross-links can be incorporated into the chemical structure of the resin (cross-link saturation). Finally, the residual stress within a phenolic resin matrix, of a long fibre composite, is calculated and this analysis indicates that although no improvement in material properties occurs above an F/P ratio of 2.5, residual stresses continue to increase. It is shown that this results from the loss of ether bridges, through the formation of formaldehyde, and the subsequent shrinkage of the resin matrix that occurs as formaldehyde diffuses through the matrix and evaporates.

In chapter four, Group Interaction Modelling will be employed to model the effect of absorbed water on the thermo-mechanical properties of phenolic resins. These predictions will allow the behaviour of these materials, over the entire relative humidity spectrum, to be investigated. It will be shown that the swelling behaviour of phenolic resins, predicted by the model, shows considerable discrepancy from that behaviour expected experimentally. A modification to GIM is proposed, in which the actual volume of liquid water is included directly in the molar volume equation, and it will be shown that the predictions of this new model are in better agreement with the experimental behaviour. Finally, the GIM molar volume equation is adjusted to account for the presence of polymer free volume, allowing the effect of free volume, upon the thermo-mechanical properties of the resin under a range of humidity environments, to be predicted. These predictions indicate that, before polymer free volume is completely filled, the effect of absorbed water molecules is to increase the Young's modulus of the material. This result is unexpected as such behaviour is not commonly reported for epoxy and phenolic resins in the

literature. Several proposals, for the scarcity of experimental evidence of this phenomenon, are presented and discussed.

In chapter five, the hygrothermal behaviour of low-fired carbon-fibre is investigated. A simple model will be developed to describe the absorption/desorption process, associated with the fibre, and this will then be applied to characterise a low-fired carbon-fibre using data from dynamical vapour sorption (DVS). Having obtained the rate constants, describing the uptake of water by the fibre, a model for modelling the hygrothermal behaviour of low-fired carbon-fibre phenolic composites is developed. This is then used to understand the effect of low-fired carbon-fibre on the moisture uptake behaviour of the resin matrix. This analysis indicates that at high relative humidity, the fibre causes the uptake behaviour of the matrix to be perturbed significantly. This is attributed to the absorption of water, from the matrix, into fibre pore volume. Finally, the effect of low-fired carbon-fibre on the concentration, and glass transition temperature, profiles of the matrix, throughout the composite's geometry, is predicted. These results show that low-fired carbon-fibre reduces the water concentration gradients, and thus by extension property gradients, within the matrix compared to those it would usually encounter when no fibre is present. Thus, it suggests that low-fired carbon-fibre may reduce the material's susceptibility to water induced ageing phenomena, such as cracking induced through variation in the material's swelling response.

1. Literature Review

1.1. Epoxy Resin Synthesis

Epoxy resins are synthesised through the reaction of two separate chemical species commonly referred to as epoxy and hardener [9]. The epoxy contains the epoxide functional group which undergoes reaction with functional groups within the hardener to form covalent bonds between the two species. A common group of hardeners employed in this reaction are amine based and in this case the formation of covalent bonds arises as a consequence of the reaction of epoxide groups with primary or secondary amines. The reaction between an epoxide group and a primary amine is described by:

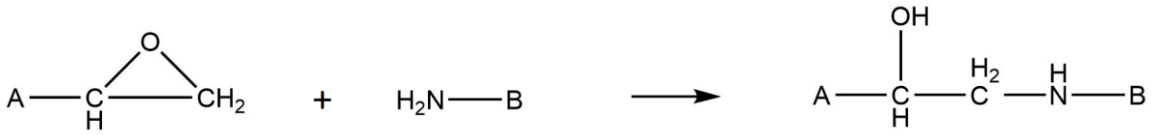

Figure 1: Reaction of an Epoxide group with a primary amine.

Where A and B represent the chemical structures of the epoxy and hardener molecules respectively to which the epoxide and amine functional groups belong. Secondary amines can undergo further reaction with epoxide groups to form:

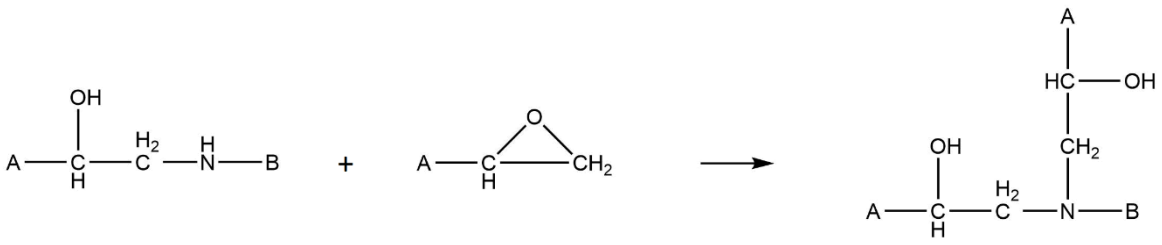

Figure 2: Reaction of an Epoxide group with a secondary amine.

Both of these processes involve the reaction of an epoxide group with an amine group resulting in the formation of a covalent bond between epoxy and hardener molecules with the introduction

of an OH functional group into the chemical structure. A third process is possible, after the formation of secondary or tertiary amines, whereby an epoxide group reacts with the OH functional group:

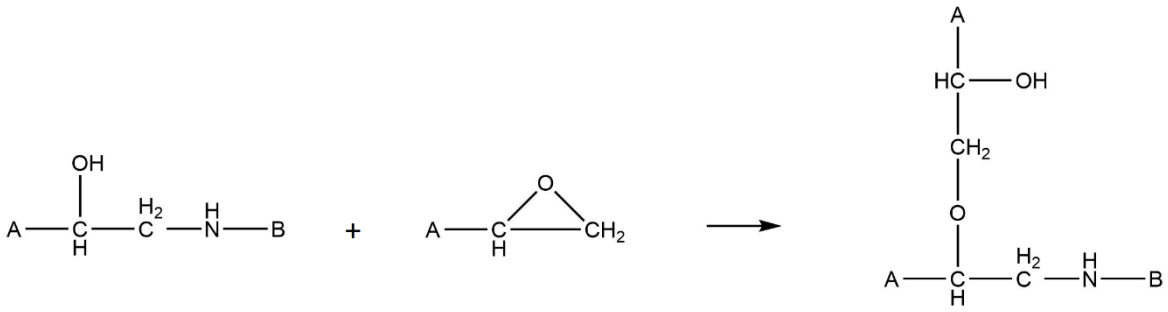

Figure 3: Reaction of an Epoxide group with the OH group to form an ether functional group.

This reaction results in the formation of a covalent bond with the introduction of an ether functional group into the polymer structure.

Each of these three chemical processes results in the creation of a covalent bond between the two reacting species that are involved. These reactions initially lead to the formation of linear polymer chains, followed by the formation of covalent bonds between adjacent chains; termed cross-linking. Thus, the cross-link density of the material increases with the eventual formation of a thermoset polymer; this process is referred to as cure.

The final cross-link density of the resin is dependent upon the number of covalent bonds that each epoxy and hardener molecule can form. This quantity is termed the functionality. Each epoxide group can form one covalent bond whereas each primary amine group can form two, thus they are referred to as mono-functional and di-functional groups respectively. A wide variety of epoxies and hardeners have been synthesised with a range of different functionalities. As the glass transition temperature (T_g) is a function of cross-link density, which in turn is dependent upon the functionalities of the underlying reactants, the T_g of the resin is affected by the choice of epoxy and hardener with higher functionality reactants generally resulting in cured resins that possess higher glass transition temperatures [10].

1.2. Phenolic Resins

Phenolic resins were some of the first polymers to be developed synthetically in the early part of the 20th century and were successful commercially under the Bakelite brand. They are synthesised from the reaction of phenol with formaldehyde, in the presence of an acidic or basic catalyst, and are characterised by two distinct chemical structures dependent upon the initial ratio of reactants and the catalyst employed [11]. When formaldehyde is in excess and the catalyst is basic the resulting polymer network exhibits a high degree of cross-linking and as a result possesses a high T_g; this form of phenolic resin is termed resole. When phenol is in excess and the catalyst is acidic the cross-link density of the polymer network is low and thus the T_g follows a similar trend; these phenolic resins are termed novolac. Phenolic resins exhibit excellent fire resistance and thus they are often employed in environments where fire resistance is essential [12, 13] . They also possess unique high temperature stability through the formation of a char boundary layer at the material/atmosphere interface. This char layer reduces the rate of material ablation and as a result phenolic resins are often employed as the matrix component in composites developed for high temperature applications [14] .

1.2.1. Mechanism of Cure

Phenolic resins are synthesised through the reaction of phenol with formaldehyde in the presence of an acidic, or basic, catalyst [11]. The transformation from individual molecules of phenol and formaldehyde to a cured polymer network occurs through several reaction steps. In the first step, phenol gains methylol groups through the addition of formaldehyde to the ortho and para sites of the phenyl ring (Figure 4).

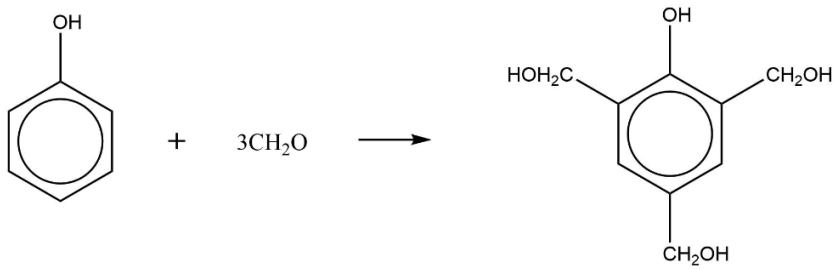

Figure 4: Reaction between phenol and formaldehyde.

The exact number of methylol groups on any given phenol molecule will vary between zero and three. The distribution of phenol molecules with respect to the number of methylol groups on their phenyl ring is a function of the initial formaldehyde/phenol ratio employed in the synthesis.

Increasing the quantity of formaldehyde, relative to phenol, will promote greater addition of methylol groups to the phenol molecule. In the second step of the reaction, the methylol groups on phenol molecules react with either the unreacted sites (ortho/para) on neighbouring phenol molecules (Figure 5), or with other methylol groups (Figure 6). In each case the process takes the form of a condensation reaction with the evolution of one molecule of water and the formation of a methylene, or ether, bridge between the two phenol molecules.

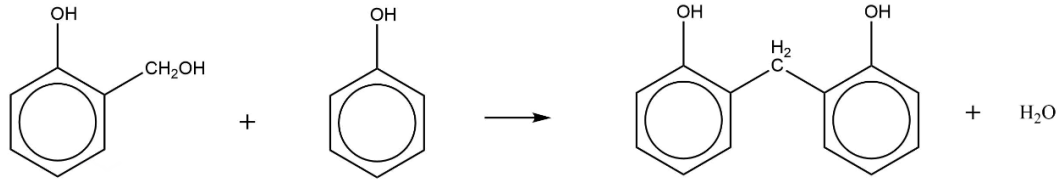

Figure 5: Methylene bridge formation.

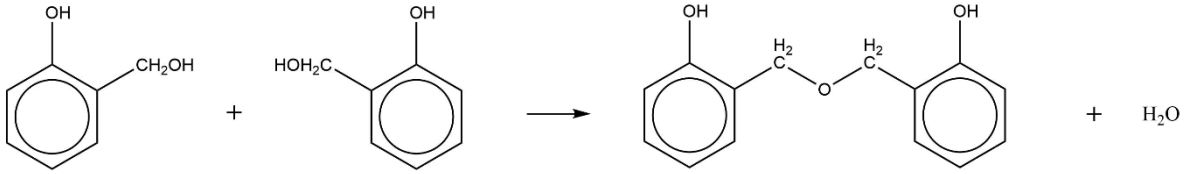

Figure 6: Ether bridge formation.

As the second step of the reaction proceeds, the average molecular weight of the mixture's constituents increases until sufficient polymerisation has occurred to cause resin gelation. Further reaction occurs in the material's rubber phase and thus proliferation of the second reaction leads to an increase in the cross-link density. A third reaction step can occur at elevated temperatures (in excess of 160℃) [15] in which an ether bridge undergoes molecular rearrangement to form an energetically more stable methylene bridge with the evolution of one molecule of formaldehyde (Figure 7). It should be noted that the third reaction step has no impact upon the polymer's cross-link density.

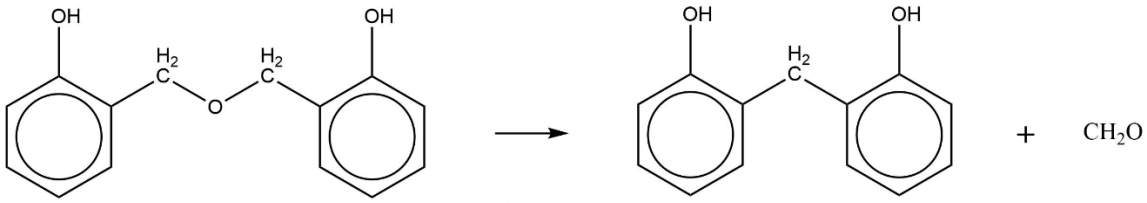

Figure 7: Molecular rearrangement of an ether bridge to form an energetically more stable methylene bridge with the evolution of one molecule of formaldehyde.

1.2.2. Pressure Considerations in the Cure of Phenolic Resins

As discussed previously, cross-link formation during the cure of phenolic resins is brought about by a series of condensation reactions with the formation of water and formaldehyde. Thus, a proportion of the initial reactant mass will be transformed into water molecules. At cure temperatures in excess of 100℃, and under normal atmospheric conditions (pressure of one atmosphere), these molecules vaporise to form pockets of water vapour within the reactant mixture. The consequence of this vaporisation is foaming of the reactant mixture which, if gelation occurs before all vapour pockets have evaporated, results in a final cured material that possesses a high proportion of voids and thus poor mechanical properties [16]. To prevent foaming of the reactant mixture it is necessary to either slow the rate of reaction or to apply external pressure. The rate of reaction can be reduced by modifying the cure cycle to include longer isotherms at lower temperatures. This has the effect of allowing evolved water molecules to evaporate before they can accumulate to form pockets of water vapour. Alternatively, external pressure can be applied to the reactant mixture by curing the material in a hot-press or autoclave. The pressure required to prevent vaporisation of condensation water, at a temperature T, is equal to the partial saturated vapour pressure of water, at that temperature [17]. When the applied pressure is equal to, or greater than, the partial saturated vapour pressure of water at the cure temperature T the condensation water will remain in the liquid phase; thus, foaming of the reaction mixture will be prevented.

1.2.3. Evolution of Chemical Species within Phenolic Resins during Cure

Freeman et al [18] studied the evolution of molecular species during the cure of phenolic resins using paper chromatography. Analysis of these results allowed the rate constants associated with each reaction process to be deduced. They observed that the reactivity of methylol phenols is affected by the position of the methylol group on the phenyl ring. The results also showed that when an alkaline catalyst is employed, as is the case in the synthesis of resole phenolic resins, the formation of methylene bridges is predominantly through the molecular rearrangement of ether bridges and not from the reaction of methylol groups with free sites on a nearby phenyl rings. Astarloa et al [19] studied the effect of temperature on the formation of chemical species during cure using NMR and liquid chromatography. These results showed that increasing temperature increased the rate at which each individual reaction occurred. However, the end chemical species after complete reaction had occurred were not affected by the temperature employed during cure. This work corroborated the findings of Freeman et al [18] that the para position, on the phenyl ring of the phenol molecule, is more reactive than the ortho position.

Monni et al [20] investigated the relationship between the underlying chemical species, and material properties, of phenolic resins throughout the cure process. Similar techniques as those applied by Astarloa et al were used to determine species concentration as a function of cure time. These were then combined with material property measurements, performed at various stages during cure, allowing the structure-property relations to be deduced. Manfredi et al [21] studied the thermo-mechanical properties of fully cured phenolic resins. They synthesised resins from a range of different F/P ratios, before measuring their material properties, allowing the relationship between thermo-mechanical properties and F/P ratio to be observed.

Manfredi et al [22], and Riccardi et al [23], modelled the initial cure reactions of the phenol/formaldehyde reactant mixture before gelation had occurred. This was achieved by identifying the various chemical structures that form during cure and associating a rate constant with each underlying reaction process. This was then fit to experimental data, for the evolution of chemical species with cure time, allowing the values of the rate constants to be obtained.

1.3. Environmental Stability - Hygrothermal Ageing

The chemical structures of epoxy and phenolic resins possess high densities of polar functional groups in the form of the OH group. With regards to epoxies, these are introduced during the reaction of epoxide groups with primary or secondary amines. In the case of phenolics they are an intrinsic component of the reactants in the form of the OH group of the phenol molecule. The OH group is a polar functional group and as a result, water molecules that diffuse into the polymer structure from the outside environment, can hydrogen bond to it. Lee et al [24] performed molecular modelling on the behaviour of water molecules within an epoxy resin and this work indicated a high density of water molecules clustered around the OH functional groups of the polymer. Similar clustering was also observed around the tertiary amine group. Hydrogen bound water is less likely to diffuse out of the material and thus the net effect of the presence of polar groups within a polymer's chemical structure is to cause the material to absorb, and retain, moisture from the surrounding atmosphere.

1.3.1. Dependence of Moisture Content upon Polar Group Density

Soles et al [25] investigated the effect of polar group density and nanovoid volume upon the magnitude of the equilibrium moisture content of epoxy resins. This was achieved by conditioning a variety of epoxies, of differing polar group densities and nanovoid volumes, in liquid water and determining their equilibrium moisture content gravimetrically. Polar group density was altered by changing the functionality of the epoxy molecule and nanovoid volume by

varying the molecular length of the hardener molecule. The equilibrium moisture content was observed to be a strong function of polar group density. It also exhibited a dependence, although smaller, on nanovoid volume with increasing nanovoid volume resulting in larger equilibrium moisture contents. This was explained by the suggestion that water molecules have a greater volume in which they can reside, unhindered by the morphology of the polymer network, when the nanovoid volume is larger.

A similar dependence on polar group density was observed by Nishitani et al [26]. They identified the functional groups in a variety of epoxies and used this information to calculate the Hoy's solubility parameters representative of each chemical structure. The Hoy's solubility parameters describe the individual contributions of three separate interactions to the total cohesive energy of the polymer. These three interactions are: dispersive forces, polar forces, and hydrogen bonding. The polarity parameter describes the contribution of polar forces to the total cohesive energy of the polymer. It is dependent on the density of polar functional groups within the material, and thus it allows the effect of polar group density on equilibrium moisture content to be characterised. For the set of epoxies investigated, equilibrium moisture content was observed to be a positive function of the polarity parameter, and hence a positive function of polar group density.

Carfagna et al [27] synthesised a range of resins from different epoxy/hardener ratios. They observed that the equilibrium moisture content of the material increased with increasing hardener content. This was attributed to the polar nature of the amine hardener increasing the ability of the polymer network to interact with, and retain, water molecules that had diffused into the material. Similar behaviour has also been reported by Grave et al [28] for another epoxy resin system.

1.3.2. Dependence of Moisture Content upon Relative Humidity and Temperature

For a given epoxy/phenolic structure, of fixed polar group density, the equilibrium moisture content is observed to be a function of both relative humidity and temperature. However, the effect of relative humidity upon moisture content is the dominant effect with changes induced by temperature being relatively small [3]. As the conditioning relative humidity, at a fixed temperature, increases there is a corresponding increase in the observed equilibrium moisture content of the material. A general relationship describing this behaviour is of the form [29]:

$$M = a\,RH^{b} \qquad (1)$$

Where M is the magnitude of the equilibrium moisture content, RH is the percentage relative humidity of the environment, and a and b are material specific constants with b taking values in the range:

$$b \geq 1 \tag{2}$$

In the scenario where $b = 1$, the relationship between equilibrium moisture content and relative humidity is linear and equation (1) is equivalent to Henry's law. When the relationship between the equilibrium moisture content and relative humidity, at a given temperature, is linear the behaviour can be described by Henry's law [8, 30]:

$$C_{(T)} = S_{(T)}\, p_{sat\,(T)}\, RH_f \tag{3}$$

Where $C_{(T)}$ is the concentration of water molecules absorbed within the polymer at equilibrium, in units of $mol.mm^{-3}$, $S_{(T)}$ and $p_{sat\,(T)}$ are the solubility of water within the material and the partial saturation vapour pressure of water vapour in the conditioning atmosphere, at a temperature T, in units of $mol.mm^{-3}.Pa^{-1}$ and Pa, respectively, and RH_f is the fractional relative humidity. Henry's law is obeyed in systems where the interaction between water molecules is negligible. Thus, at high water concentrations the interaction between diffusing water molecules becomes important and the behaviour of material equilibrium moisture content deviates from that described by Henry's law.

1.3.3. Mechanism of Absorption/Desorption - Diffusion

Moisture absorption in epoxy and phenolic resins is precipitated by the diffusion of water molecules through the free volume of the polymer network followed by subsequent hydrogen bonding of these water molecules to polar functional groups within the material. The diffusion process is often observed to be Fickian in nature and thus can be described by Fick's second law [31]:

$$\frac{\partial C}{\partial t} = D\,\frac{\partial^2 C}{\partial x^2} \tag{4}$$

Where C is the concentration of water molecules in units of $mol.mm^{-3}$, t is time in units of minutes, D is the diffusion coefficient in units of $mm^2.min^{-1}$, and x is a position within the material in units of mm. Diffusion is defined as Fickian if the moisture content of the material, with respect to the square root of conditioning time, can be described by a solution to Fick's second law.

The diffusion coefficient governs the rate at which moisture is absorbed/desorbed and is specific to both the type, and temperature, of the material involved [32-34]. As temperature increases there is a corresponding increase in the kinetic energy of the water molecules within the material which is manifested as an increase in their average velocity. Diffusion occurs through the random motion of molecules, thus an increase in molecule velocity will have the effect of increasing the rate at which the diffusion process occurs. The relationship between the diffusion coefficient and temperature can be described by an Arrhenius law of the form [35]:

$$D_{(T)} = D_0 \, e^{\frac{-E_d}{RT}} \tag{5}$$

Where $D_{(T)}$ and D_0 are the diffusion coefficient at a temperature T, and the diffusion coefficient as T tends to infinity respectively, both in units of $mm^2.min^{-1}$, E_d is the activation energy for diffusion in $J.mol^{-1}$, and T is the temperature in K.

The diffusion coefficient has been found to be closely related to the solubility of water in polymer materials [8, 36, 37]. As the solubility of water in the polymer increases, there is a corresponding decrease in the diffusion coefficient and this relationship is approximately linear such that a doubling of solubility leads to the diffusion coefficient being reduced by a factor of two; thus, the material will take twice as long to attain equilibrium with its conditioning environment. This observation was explained by Merdas et al [36] who proposed that absorption in epoxy resins is governed by two processes: diffusion of water molecules between polar groups, and the bonding/de-bonding of water molecules to these polar groups. They suggested that the time required for water molecules to diffuse between polar groups is negligible compared to that required for water molecules to bond/de-bond to polar groups. Thus, the rate of absorption/desorption, and hence the diffusion coefficient, will be limited by the density of polar groups within the material. In other words, the diffusion coefficient will be inversely proportional to the solubility of water within the polymer.

1.3.4. Deviations from Fickian Behaviour

When the observed diffusive behaviour deviates from the definition of Fickian diffusion it is termed non-Fickian. There are extensive accounts in the literature of non-Fickian behaviour being observed in epoxy resins. These are often attributed to complex underlying phenomena which perturb the observed absorption/desorption behaviour. Examples include: binding/unbinding of water molecules to the polymer network [38] (Langmuir model), leeching of hydrolysed polymer chain segments [39], and two-stage diffusion [40] (polymer relaxation), to name a few.

1.3.4.1. Langmuir Model

Carter et al [38] investigated the hygrothermal ageing of a commercial epoxy resin over an extended conditioning period of 3.5 years. The initial absorption behaviour was observed to be Fickian with the material initially displaying a clear plateau in moisture content after conditioning for ~1.5 months. However, over a longer conditioning period of 3.5 years a gradual increase in moisture content occurred with approach to a second equilibrium plateau. They suggested that water molecules could exist in two separate states within the resin: bound and un-bound. A free water molecule absorbed within the resin, termed un-bound, has a probability p_b, in units of min^{-1}, to become strongly bound to the polymer network. Bound water molecules can also become free with a probability p_f in units of min^{-1}. Bound water does not participate in diffusion and thus if $p_f \ll p_b$ the net result is an increase in the moisture content of the material above its initial equilibrium plateau. They modified Fick's second law to include this phenomenon as follows:

$$\frac{\partial C}{\partial t} = D\,\frac{\partial^2 C}{\partial x^2} + p_f C_b - p_b C \tag{6}$$

Where C and C_b are the concentrations of unbound and bound water respectively both in units of $mol.mm^{-3}$. The ratio of the concentration of unbound water to bound water is equal to the ratio of the probability of a bound water molecule becoming free to the probability of a free molecule becoming bound:

$$\frac{C}{C_b} = \frac{p_f}{p_b} \tag{7}$$

The time taken for the material to attain the second equilibrium plateau is dependent on the magnitude of the underlying probabilities.

The observation of a double plateau in epoxy resins, under hygrothermal conditions, has been reported extensively in the literature and the model of Carter et al [38] has been shown to be successful in encompassing this behaviour [41].

1.3.5. Hydrolysis of Epoxy Resins under Hygrothermal Conditions

1.3.5.1. Hydrolysis in DGEBA-DDA Epoxy Resin

The epoxy resin DGEBA-DDA is synthesised from the reaction of the diglycidyl ether of bisphenol A (DGEBA) with the amine hardener dicyandiamide (DDA). The occurrence of hydrolysis in DGEBA-DDA resin has been proposed by several authors [5, 6, 39] and is supported by observations from gravimetric, DMTA and FTIR experiments. When DGEBA-DDA is aged hygrothermally, either through immersion in liquid water or through exposure to water vapour, a permanent reduction in the dry T_g of the resin is observed and this reduction is not reversed upon the complete removal of moisture from the material [6, 7]. As T_g is a function of cross-link density [10] this suggests that water molecules interact with the polymer network causing hydrolysis of polymer chains and thus an overall reduction in resin T_g. This proposal is supported by the work of De'Neve et al [5, 42] who measured the modulus of DGEBA-DDA resin in the rubber phase for samples aged hygrothermally over a range of conditioning times. Applying the theory of rubber elasticity these modulus measurements were used to estimate the average molecular mass between cross-links in the underlying polymer structure. They observed that the effect of hygrothermal conditioning was to increase the average molecular mass between cross-links, consistent with the idea that the action of water in DGEBA-DDA is to hydrolyse the polymer network.

Samples dried post-conditioning also exhibit a permanent increase in their dry mass and this mass increase is a function of conditioning time [6, 7, 43]. This suggests that the hydrolysis reaction results in the chemical addition of water molecules to the polymer network. Xiao et al [44] summarised the hydrolysis mechanism as taking the form shown below in Figure 8.

Figure 8: Mechanism for hydrolysis proposed by Xiao et al [44].

Fata et al [6] suggested that not all cross-links would be susceptible to hydrolysis and proposed a more specific reaction pathway, shown below in Figure 9:

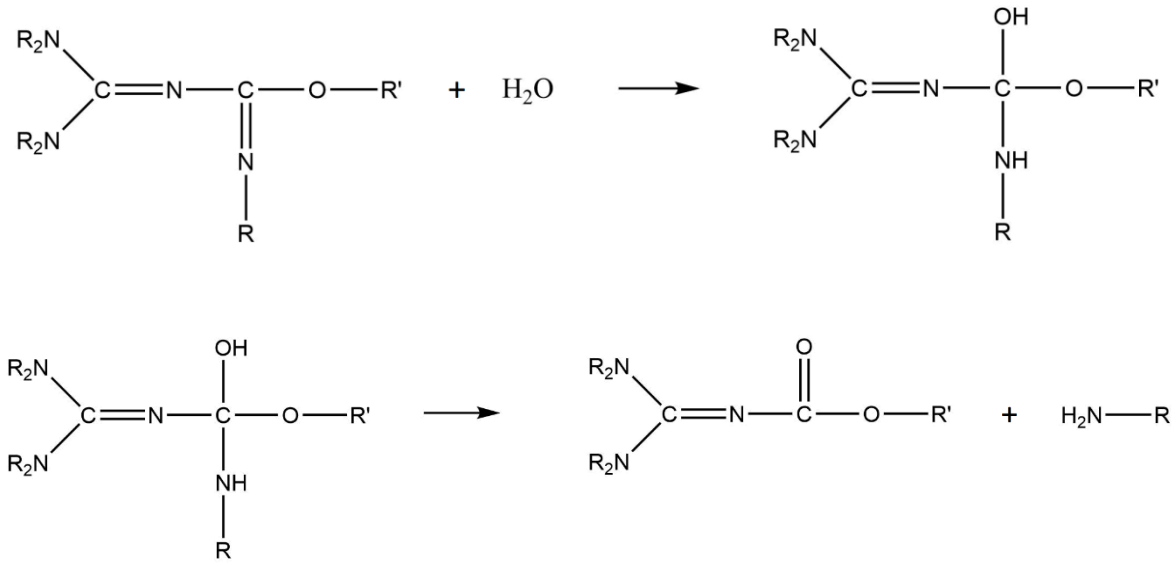

Figure 9: Reaction pathway for hydrolysis proposed by Fata et al [6].

Xiao et al [7] investigated the effect of hygrothermal conditioning on DGEBA-DDA samples immersed in liquid water at a temperature of 90℃, which is in excess of the wet T_g of the resin. An initial mass increase followed by a permanent loss in resin mass over extended conditioning times was observed. They suggested that the polymer chains within the resin could be hydrolysed in more than one location, creating chain segments free from the covalent bonds of the polymer network. These can then leech out of the resin into the conditioning medium. At conditioning temperatures below the wet resin T_g no permanent mass loss occurs suggesting that free chain segments are constrained when the resin is in its glassy phase which prevents them from leeching out of the polymer structure. After ageing at temperatures sufficient for leeching to occur, samples were removed from conditioning and the liquid water evaporated. After removal of the conditioning water a residue was obtained from the bottom of the conditioning chamber. This was analysed with FTIR and found to comprise of chemical species that are present in unaged DGEBA-DDA resin, confirming the suggestion of leeching of hydrolysed chain segments [7, 39].

Xiao et al [44] developed a model for the diffusion-hydrolysis process by modifying Fick's second law to allow for the loss of water molecules through their addition to the polymer. A solution to this modified form of Fick's law second was obtained and combined with a term describing the loss of hydrolysed chain segments from the material through their leeching into the conditioning medium. This solution was able to reproduce the behaviour observed experimentally

and allowed them to quantify several parameters governing the hydrolysis process in DGEBA-DDA epoxy resin.

1.3.5.2. Hydrolysis in a DGEBA, PGE, DDM Epoxy Resin

Damian et al [45] investigated the effect of hygrothermal conditioning, through liquid immersion at a range of temperatures, upon an epoxy resin synthesised from DGEBA, PGE, and DDM. At low temperatures of 30℃ the material showed a typical response, absorbing water until an equilibrium plateau was obtained after conditioning for ~11 months. However, at higher temperatures (>50℃), although the material initially gained mass, at longer conditioning times it was observed to lose mass. A residue from the conditioning water was obtained and analysed with ^{1}H NMR. This indicated the presence of plasticiser, but also of chemical segments that had originated from the polymer network, suggesting that hydrolysis had occurred. The dry glass transition temperature of the resin was measured and found to be 60℃. This led them to suggest that as the resin is in its glassy state at 35℃, hydrolysed polymer chain segments are unable to leech out of the material. In contrast, at conditioning temperatures at, and in excess of, 50℃, the resin is in the rubber phase and thus hydrolysed segments have enough mobility to diffuse out of the polymer network and into the conditioning medium. The overall result is a loss of material mass when the resin is conditioned at temperatures sufficient for its transformation from glass to rubber during conditioning.

1.4. Effect of Absorbed Moisture upon the Thermo-mechanical Properties of Polymers

The presence of absorbed moisture within epoxy and phenolic resins has been observed to have an effect upon the thermo-mechanical properties of these materials including: reduction in engineering moduli [2, 46, 47], depression of glass transition temperature [3, 5, 48, 49], and moisture induced swelling [4, 50]. These effects can be separated into two distinct categories: reversible and irreversible.

If the thermo-mechanical property changes, resulting from absorbed moisture, are reversed on complete drying of the material then the effects are termed reversible. When the process is reversible the observed effect of moisture upon thermo-mechanical properties can be attributed entirely to the physical presence of water molecules within the polymer network. If full recovery of engineering properties is not observed, after complete removal of absorbed moisture, then the effects are termed irreversible. Irreversible processes can be attributed to chemical

changes occurring within the polymer network during the conditioning process; such as hydrolysis.

1.4.1. Dynamic Mechanical Thermal Analysis (DMTA)

Dynamic mechanical thermal analysis (DMTA) is a characterisation technique for investigating the viscoelastic properties of materials. This is achieved by measuring the response of the material to a sinusoidally oscillating stress [51]. Typically, rectangular samples are employed which are then clamped at both ends within the DMTA instrument. One clamp is fixed, whereas the other is connected to the driveshaft which can move freely. A sinusoidally oscillating force is then applied to the driveshaft causing the driveshaft to oscillate about its equilibrium position. As the sample is attached to a fixed clamp at one end this results in it being subjected to a sinusoidal stress. The response of the material, in terms of its strain, is then measured allowing the dynamic modulus of the material to be obtained. The strain response is also compared against the applied stress. When a material is in its elastic region, the strain is directly proportional to the applied stress and thus the stress and strain waveforms are in phase. However, when the material begins to exhibit inelastic behaviour the stress and strain are no longer directly proportional and as a result the stress and strain waveforms move out of phase. The phase difference is termed the phase angle and is used by the DMTA to calculate the damping behaviour of the material. Polymers exhibit a local maximum in their damping behaviour when undergoing transitions that involve a reduction in modulus, thus DMTA can be employed to obtain the temperatures at which a wide range of transitions occur; examples include the glass transition in polymer materials, and the beta transition in epoxy resins.

The DMTA instrument is capable of measuring the strain response of materials over a wide range of temperatures (-180℃ to 450℃) and thus can be used to characterise the material's modulus behaviour as a function of temperature. The stress cycle can also be applied at a range of frequencies allowing the modulus and damping behaviour of the polymer to be investigated as a function of strain rate. DMTA has found extensive application in polymer research and has been employed in the study of polymer blends, cure monitoring, and investigating the effect of absorbed water on the glass transition temperature.

Bikiaris et al [52], and others [53, 54], employed DMTA to investigate the miscibility of various polymer blends. If the blended materials are immiscible then they will exist in their own distinct domains. This results in the observation of two distinct glass transition temperatures,

provided the glass transition temperatures of the pure materials are sufficiently different. If the two components are miscible then only a single glass transition temperature is observed.

Xie et al [55] utilised DMTA to monitor the cure of an epoxy composite. Uncured composite samples were prepared from epoxy prepreg. These were then loaded into the DMTA and a scan was performed at a fixed temperature. The evolution of the storage modulus as a function of time, for a range of different curing temperatures, was recorded. This allowed the change in the mechanical properties of the epoxy composite, and thus the extent of mechanical cure, to be characterised as a function of both cure time and temperature.

Another field of study that DMTA has been applied to is the investigation of absorbed water inside polymer materials. This is discussed in detail in the section that follows.

1.4.2. Glass Transition Temperature Depression

The effect of absorbed moisture on the glass transition temperature of epoxy and phenolic resins has been investigated extensively within the literature [3, 5, 48, 49, 56]. The general observation is that absorbed moisture reduces the glass transition temperature of the material, with the magnitude of the T_g depression being proportional to the moisture content. Water molecules bond to polar groups within the polymer network and their presence disrupts the van der Waals forces and hydrogen bond interactions between adjacent polymer chains; this is termed plasticisation [3]. The reduced attraction between polymer chains means that less energy is required to separate them to a distance where further chain motions become possible (additional degrees of freedom), the so-called glass transition. If the energy applied to the system is in the form of thermal energy, then the effect of plasticisation is manifested as a reduction in the temperature at which the glass transition occurs.

There is debate within the literature with regards to the nature of absorbed water in epoxy resins as to whether it exists in one, or two, states. The loss tangent/temperature spectra obtained from DMTA of resin's containing absorbed moisture often exhibit two observable peaks that are associated with the glass transition event [57-59]. The presence of multiple T_g peaks can be attributed to materials that possess a variety of states, with each state possessing its own unique T_g. When moisture isn't present, these distinct states can arise as a result of the differing properties of separate phases within the material; for example, in polymer blends where the two components

are immiscible [52-54]. Differences in cross-link density throughout the geometry of the material can also lead to the observation of multiple states in DMTA spectra.

Thus, the observation of two loss tangent peaks in material's containing absorbed moisture has led researchers to suggest that absorbed water exists in two distinct states [60]; one in which the disruption of the van der Waals and hydrogen bond interactions is negligible leading to a small decrease in material T_g, and a second in which the disruption of the van der Waals and hydrogen bond interactions is more severe leading to increased plasticisation of the network and thus effecting a much greater reduction in material T_g. However, it has also been speculated that the observation of a double loss tangent peak is an artefact arising from drying of the polymer material during the course of the DMTA scan [61].

Chateauminois et al [61] investigated the effect of drying of the material during the DMTA experiment on the spectra that they obtained. Two separate samples composed of identical material were analysed. Prior to the DMTA experiment both were conditioned in the same environment until they had attained equilibrium, indicated by a plateau in their moisture content with respect to time. One sample was then sealed in aluminium foil with epoxy adhesive to prevent its absorbed moisture from escaping while the other was left untreated. Analysis of the DMTA spectra of both coupons revealed a double loss tangent peak in the open material, however only a single peak was observed in the coupon enclosed in aluminium foil. This lead them to suggest that the presence of multiple peaks in the DMTA spectra of conditioned materials, results from the evaporation of moisture from the material during the experiment. Thus, the initial loss tangent peak represents the glass transition temperature of the wet material. As the temperature of the DMTA increases further, the material enters the rubber phase in which the diffusion process can occur at a much higher rate. Rapid drying ensues and the glass transition temperature of the polymer recovers sufficiently for it to exceed the temperature of the DMTA during the scan. This results in the recording of a second loss tangent peak. This hypothesis was supported by accompanying TGA performed at the same heating rate as the DMTA experiment. This confirmed that non-negligible moisture loss occurs during the DMTA scan and that when the material enters the rubber phase rapid moisture loss occurs.

1.4.3. Moisture Induced Swelling

Adamson et al [4] investigated the swelling response of a commercial epoxy resin as a function of moisture content. The material was conditioned hygrothermally by immersion in liquid water for a range of temperatures. At various points in the conditioning process samples

were removed and their weight and dimensions recorded. This allowed the volume of the samples for a range of moisture contents to be determined. Once the material had attained its equilibrium moisture content its percentage change in volume was compared to that expected by a simple rule of mixtures. The expected percentage change in sample volume was calculated by referring to the mass of water in the sample at equilibrium and using the density of water at each specific conditioning temperature to calculate the volume of water absorbed within the material. This was then combined with the sample dry volume allowing the expected percentage change in sample volume to be obtained.

They observed that the percentage change in sample volume was less than that expected from simply adding the volume of absorbed water to the dry volume of the sample. They attributed this difference to the existence of free volume within the polymer and suggested that initially, water molecules diffuse into the free volume between polymer chains and only once this free volume is filled does subsequent moisture absorption induce swelling of the polymer material. This hypothesis was supported by the experimental relationship they obtained between percentage volume change and moisture content. Early in the conditioning process, when the moisture content of the epoxy was small, the effect of increasing moisture content on the percentage change in material volume was negligible. However, above a certain threshold, increasing moisture content further had a large impact on the percentage change in volume of the sample. In this region the change in sample volume was approximately equal to the volume of water absorbed indicating that the free volume had become saturated. The percentage of the sample's volume that can be identified as free was obtained from the difference between the expected percentage volume change and that observed experimentally in the material once it has attained its equilibrium moisture content.

They also calculated the free volume for a range of different temperatures and observed that free volume decreased with increasing temperature. They suggested that the greater thermal energy of polymer chains at higher temperatures will increase the magnitude of their thermal vibrations. This would reduce the volume within which water molecules could reside without interacting with the polymer network and thus free volume would be reduced. Similar swelling behaviour, initially negligible followed by a rapid increase after a threshold water content is exceeded, has been reported extensively throughout the literature for a wide range of epoxy resins [50].

1.5. Hygrothermal Behaviour of Fibre Reinforcements

1.5.1. Moisture Absorption in Low-fired Carbon-fibres

Low-fired carbon-fibre is a form of carbon with a chemical structure similar to that of standard carbon-fibre. It is formed through the same manufacturing process as standard carbon-fibre [62], however the final graphitisation step, at high temperature, is omitted [29]. The low firing temperature prevents complete graphitisation of the carbon-fibres and thus the resulting material is characterised by a structure that possesses some degree of porosity. This porosity allows the material to absorb large quantities of water (~15% w/w) [63], when it is exposed to hygrothermal conditions [29]. The equilibrium water content of the fibre is observed to be related to the degree of graphitisation of the material, with increasing levels of graphitisation leading to a reduction in the ability of the fibre to absorb water [29]. The hygrothermal behaviour of a variety of different low-fired carbon-fibres, as a function of relative humidity, have been investigated by Stokes [29]. The relationship between equilibrium moisture content and relative humidity, in all of these materials, was found to be characterised by the so-called S-shaped absorption behaviour. This S-shaped behaviour varies between different fibres, but its general form can be summarised as follows. At low conditioning relative humidity (<40%) the equilibrium moisture content of the fibre is linear with respect to relative humidity. Above a threshold relative humidity (~40%), the equilibrium moisture content increases rapidly with increasing relative humidity. At higher relative humidity (>60%) the equilibrium moisture content/relative humidity gradient decreases and equilibrium moisture content appears to approach a plateau.

1.5.2. Moisture Absorption in Activated Carbon

The equilibrium moisture content/relative humidity behaviour of activated carbons has been observed to be characterised by an S-shaped absorption behaviour [64, 65]. Dubinin [66] proposed a mathematical relation to describe the uptake behaviour of different chemical species by carbonaceous materials:

$$V = V_0 \, e^{-\left(\frac{RT}{\beta E_0} ln\left(\frac{1}{a}\right)\right)^2} \tag{8}$$

Where V is the volume of the species adsorbed/absorbed by the material, V_0 is the maximum volume of the species that the material can adsorb/absorb, β is a constant specific to the type of chemical species and carbonaceous material, E_0 is the energy of adsorption, and a is the activity of the chemical species in the atmosphere surrounding the carbonaceous material. Although this

equation can describe the hygrothermal behaviour of activated carbons it does not account for the different carrying capacities of the material surface, and that of the pore volume, instead treating them as the same entity in V_0.

Because of these, and other limitations, Do et al [65] proposed a new model for moisture uptake in activated carbons. They suggested that initially, the moisture uptake process is governed by surface adsorption. This is followed by absorption of water clusters into pore volume when surface water concentrations are high enough to allow the formation of water clusters. In the first stage of the process, water molecules in the surrounding atmosphere adsorb to functional groups at the activated carbon surface through intermolecular interactions. These adsorbed water molecules can act as secondary adsorption sites and thus clusters of water molecules can form around surface functional groups. At this early stage no absorption of water clusters into pore volume is possible. If atmospheric moisture concentrations are high enough to promote the formation of large water clusters, containing at least five water molecules, then it becomes energetically favourable for these clusters to move from the carbon surface into the pore volume. This absorption of water clusters into pore volume accounts for the large increase in the equilibrium moisture content of activated carbons that is observed above a certain relative humidity threshold. At high relative humidity the pore volume becomes saturated with water clusters and thus no further significant increases in equilibrium moisture content, with relative humidity, occur. They developed a mathematical model to describe the uptake of moisture by activated carbons by deriving the rate equations governing each of the steps in the adsorption/absorption process. This model was shown to be capable of describing the experimental uptake/relative humidity behaviour of a range of different activated carbons.

1.6. Effect of Hygrothermal Conditioning upon Epoxy and Phenolic Based Composite Materials

Epoxy and Phenolic resins are employed as the matrix component in fibre-reinforced composite materials. Thus, the effect of absorbed moisture upon the thermo-mechanical properties of the polymer will also impact upon the engineering performance of their composites.

Ellyin et al [67] investigated the effect of liquid immersion upon the engineering properties of glass-fibre/epoxy composites. Two conditioning environments were employed, one at ambient temperature, and a second at 90℃. Composite samples conditioned at ambient temperature initially gained mass, through water absorption, before eventually appearing to approach a plateau in their moisture content after conditioning for ~4 months. The samples aged

at 90℃ rapidly absorbed moisture and, at the time at which the experiment was concluded (~1.2 months), no observable plateau in moisture content was apparent. The transverse cracking behaviour of the wet samples was then investigated by applying a tensile stress to the materials. The strain was recorded as stress was increased and the number of transverse cracks in the matrix were also counted. This analysis indicated that the strain threshold, required to induce cracking in the composite aged at 90℃, is less than for unaged materials. This was attributed to damage to the composite material during hygrothermal conditioning. However, the strain threshold for cracking in the samples aged at ambient temperature was increased. They attributed this effect to the plasticising nature of water molecules absorbed within the matrix of the composite.

Zhou et al [68] investigated the behaviour of graphite/epoxy composites, immersed in liquid water, at four different temperatures: 45℃, 60℃, 75℃, and 90℃. The samples aged at the two lower temperatures, 45℃ and 60℃, were observed to initially gain mass before approaching an approximate plateau in moisture content after conditioning for ~9 months and ~6 months respectively. The samples conditioned at 75℃ also appeared to approach an approximate plateau after conditioning for ~3.6 months, however the moisture content of these materials was greater than that observed in the samples aged at 45℃ and 60℃. Microscopy of the surface of these samples indicated the formation of micro-cracks during the conditioning process. They suggested that water molecules could fill these cracks, increasing the equilibrium moisture content of the material. The composite samples aged at 90℃ initially gained mass, reaching an equilibrium plateau in moisture content after ~1 month of conditioning. However, after conditioning for ~2.5 months they begun to lose mass. Microscopy of these samples indicated the presence of two different phenomena: micro-cracking and peeling of the matrix. Although micro-cracking increases the equilibrium moisture content of the material, peeling of the matrix from the sample surface leads to mass loss and this effect is dominant resulting in a net loss in sample mass at temperatures of 90℃. They suggested that micro-cracking and peeling occur as a result of a mismatch between the swelling behaviour of the matrix and fibre in the presence of absorbed water molecules.

Newman et al [69] investigated the effect of cyclic hygrothermal conditioning on flax-fibre/epoxy composites. Samples were subjected to a varying conditioning environment in which they were cyclically saturated with water, followed by drying. They observed that, as the number of cycles increased, both the equilibrium moisture content, and diffusion coefficient, of the material also increased. Surface microscopy indicated that micro-cracking of the matrix was occurring. Density measurements indicated a reduction in material density, as the number of conditioning cycles increased, and this was used to estimate the percentage of voids introduced

into the material, through the formation of micro-cracks, as a function of conditioning time. This analysis showed that both the equilibrium moisture content, and diffusion coefficient, increase with increasing void volume. Water molecules can be absorbed into these voids, thus increasing the equilibrium moisture content of the material. As water can exist as liquid within these voids its ingress into the composite is much more rapid than when diffusing through the polymer matrix. This accounts for the observed increase in the diffusion coefficient.

Lundgren et al [70] investigated the effect of hygrothermal conditioning on the absorption behaviour of pre-cracked glass-fibre/epoxy composites. Materials possessing a range of micro-crack densities were obtained through the application of differing tensile loads. These were then immersed in liquid water, at a fixed temperature, and their moisture content as a function of time observed gravimetrically. This analysis indicated that crack density had no impact on the moisture content/time relationship of the samples. As other researchers [68, 69] have observed an increase in material equilibrium moisture content, as the quantity of micro-cracks increases, this led them to suggest that, early in the conditioning experiment, absorbed water is capable of inducing crack closure through swelling of the matrix. This prevents filling of cracks deeper within the composite and thus leads to the observed independence of equilibrium moisture content on micro-crack density. However, they highlighted that the ability of absorbed water to induce crack closure will be material specific, depending on the type of matrix and fibre, and thus may not always occur.

1.7. Group Interaction Modelling (GIM)

Group Interaction Modelling (GIM) is a modelling formalism, developed by Porter [71], in which knowledge of the chemical constituents of a polymer's mer unit can be employed to predict the bulk thermo-mechanical properties of the material: Young's Modulus, glass transition temperature etc. Both amorphous and crystalline polymers can be encompassed within this framework, however the model does not account for anisotropy and thus it is only applicable to isotropic materials. In its original formulation GIM was applied to simple polymer systems, however, it has been subsequently extended to successfully predict the thermo-mechanical properties of more complicated systems such as epoxy resins where two different chemical species, epoxy and hardener, combine to form the polymer network [72-75]. Later advancements focused on the application of GIM to natural polymers [76, 77], more specifically silks, in which the mixed structural characteristic of these materials, being both crystalline and amorphous, can be captured and modelled within GIM. The effect of hygrothermal ageing, through the absorption of atmospheric moisture, on the thermo-mechanical properties of spider silks has also been investigated by including the water molecule within GIM as a diluent and these model predictions have shown close agreement with experimental observations [78].

Group Interaction Modelling was developed by David Porter and a full treatment of the theory, and its application, is presented in his book 'Group Interaction Modelling of Polymer Properties' [71]. As GIM will be employed extensively throughout this work, its basic principles and governing equations have been summarised in the section that follows.

1.7.1. Group Interaction Modelling: A Summary

Within GIM a polymer's structure is simplified to one consisting of infinitely long polymer chains stacked together in a hexagonal packing pattern (Figure 10).

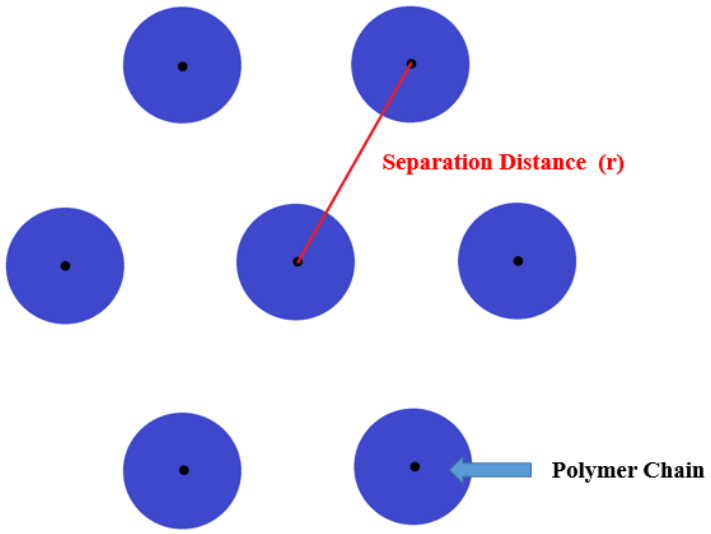

Figure 10: Polymer geometry within GIM.

Covalent bonds can exist between adjacent polymer chains depending on the degree of cross-linking within the polymer network. In this simplified structure the basic repeat unit of the polymer, referred to as the mer unit, is surrounded by, and thus can interact with, six other repeat units. The interactions between these mer units can be mediated by both van der Waals forces and hydrogen bonding. To increase the separation distance between adjacent mer units energy must be supplied to the polymer system; for example, by increasing the temperature of the material. This increases the thermal energy of the mer units allowing them to partially overcome the intermolecular forces and thus increasing their average separation distance.

The average mer unit separation distance, and thus the average distance between adjacent polymer chains, as a function of energy, can be linked to the thermo-mechanical properties of the material. For example, the change in mer unit separation for a given change in thermal energy can be used to calculate the thermal expansion coefficient: the fractional change in polymer volume with respect to a temperature change ΔT. An important concept of the model is that changes in the energy of the polymer system have a negligible impact upon the separation distance of mer units in the polymer main chain axis. This is because the mer units within the polymer chain axis are bound together by covalent bonds which are much stronger than the van der Waals and hydrogen bond forces acting between the mer units in adjacent polymer chains.

The average separation distance of two adjacent mer units can be described by the GIM potential function. The potential function is given below in equation (9) and in Figure 11 its behaviour, as a function of the mer unit separation distance r, is shown:

$$\phi = -\phi_{0_{(E_{coh})}} + H_c + H_{T_{(N,\Theta,T)}} + H_m = \phi_{0_{(E_{coh})}}\left[\left(\frac{r_{0_{(V_w)}}}{r}\right)^{12} - 2\left(\frac{r_{0_{(V_w)}}}{r}\right)^{6}\right] \qquad (9)$$

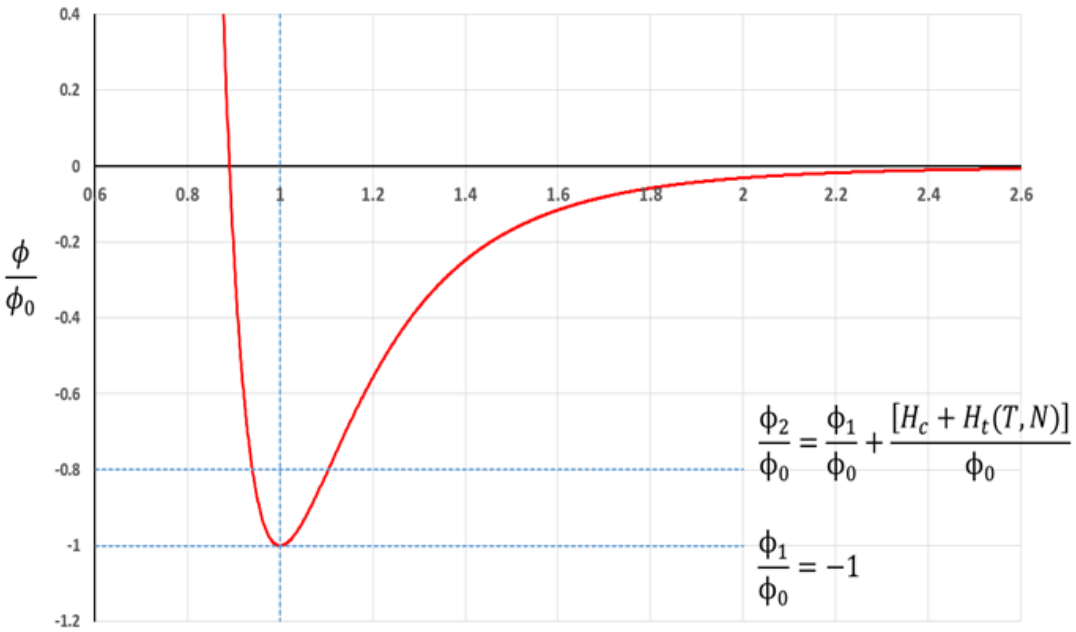

Figure 11: GIM Potential Function.

The term ϕ_0 describes the depth of the potential well and thus represents the energy required to completely overcome the van der Waals and hydrogen bond attractive forces between two adjacent mer units. It is a positive function of the strength of the intermolecular forces between the two mer units.

The term H_c is the configurational energy and describes the energy that is 'frozen' into a polymer in the form of polymer chains that are unable to attain their lowest energy configurations as a result of the morphological constraints of the polymer network. The configurational energy takes a fixed value dependent upon whether the polymer is amorphous or crystalline. For polymers in the amorphous state, H_c takes a value of $0.107\phi_0$, and a value of $0.04\phi_0$ for the crystalline state. The configurational energy of crystalline polymers is less than that of amorphous materials and this is because the slow cooling rate, required for crystal formation, provides sufficient time for polymer chains to relax to their minimum energy configurations.

The term H_T is the thermal energy and describes the combined thermal energy of two adjacent mer units at a temperature T. It is important to note that this thermal energy is not the total thermal energy of the two mer units but the thermal energy capable of increasing mer unit separation. As described previously, negligible separation of mer units occurs in the polymer main chain axis due to the presence of strong covalent bonding. Thus, mer unit separation only occurs in the two dimensions perpendicular to the polymer main chain axis. The thermal energy of polymer chain vibrations is contained within three vibrational modes, however only two are perpendicular to the main chain axis. Thus, only the thermal energy contained within the two vibrational modes perpendicular to the polymer main chain axis contribute to mer unit separation and hence the term H_T is not representative of the total thermal energy of the two mer units.

The term H_m is the mechanical energy and represents the energy applied to two adjacent mer units through the application of an external force. Finally, ϕ is the potential energy of two mer units at a separation distance r and r_0 is the equilibrium separation distance; the separation distance between two adjacent mer units when no external energy is applied to the system, in other words the configurational, thermal, and mechanical energy are zero.

To summarise, when energy is supplied to the two mer units their potential energy increases (left-hand side of equation (9)) which implies that their average separation distance r must also increase (right-hand side of equation (9)). It is possible to derive equations for the

prediction of polymer thermo-mechanical properties from the GIM potential function. These relationships are known as the GIM constitutive equations and are usually expressed in terms of the mer unit parameters of the polymer; described in the following section.

1.7.2. Obtaining the Thermal Energy H_T, Potential Well Energy ϕ_0, and Equilibrium Separation Distance r_0, from the Polymer's Mer Unit Parameters

To employ the GIM constitutive equations to predict polymer thermo-mechanical properties it is first necessary to obtain values for H_T, ϕ_0, and r_0. These can be calculated from the mer unit parameters of the polymer to be modelled. The five fundamental mer unit parameters are: E_{coh}, N, Θ, V_w, and M. The term E_{coh} is the cohesive energy and describes the energy required to separate one mole of mer units from their equilibrium separation distance, r_0, to an infinite distance. The term N represents the degrees of freedom that contribute to chain separation i.e. those vibrations perpendicular to the polymer main chain axis. The term Θ is the characteristic temperature and is related to the frequency of polymer chain vibrations parallel to the polymer chain axis. The term V_w is the van der Waals volume, and M is the molar mass. The values of these parameters, for the mer unit, are obtained either from group addition tables or through a molecular modelling approach.

Molecular modelling can be employed to obtain the cohesive energy and van der Waals volume of the mer unit. This has an advantage over the group addition approach, as although group addition tables give cohesive energy values for a wide range of functional groups, they are averages obtained from a multitude of polymer materials. As a result, interactions dependent on the morphology of the polymer structure, such as hydrogen bonding, are not specifically accounted for.

The van der Waals volume of the mer unit, obtained from group addition, assumes that the total van der Waals volume is equal to the sum of the van der Waals volumes of each of the constituent functional groups. In practice, covalent bonding in the polymer structure allows overlapping of the van der Waals surfaces of adjacent atoms and thus this approach will tend to overestimate the van der Waals volume of the mer unit. In molecular modelling, the bond distance of the covalent interaction is modelled and thus the overlapping of van der Waals surfaces is accounted for. This provides a more accurate prediction of the van der Waals volume of the mer unit.

The group addition approach has the advantage of allowing the parameter values for complicated structures to be obtained rapidly. It is also relatively simple, not requiring the need for specialist software. Using group addition, each of the functional group constituents of the mer unit is identified and assigned its representative parameter values; these being obtained from group additivity tables such as those compiled by van Krevelen et al [79] or Porter [71]. The parameter values representative of the mer unit as a whole are then obtained by summing the parameter values associated with each of the mer unit's underlying functional groups. The values of H_T, ϕ_0, and r_0, can then be obtained from the following three equations:

$$H_T \approx \frac{N}{3} k \left(T - \frac{\Theta}{6.7} tan^{-1} \left(\frac{6.7T}{\Theta} \right) \right) \tag{10}$$

$$\phi_0 = \frac{4}{3N_A} E_{coh} \tag{11}$$

$$r_0 = \frac{r_w}{0.89} \tag{12}$$

Where k is Boltzmann's constant, N_A is Avogadro's number, and r_w is the van der Waals radius of the mer unit. Thus, having obtained these three parameters they can now be inserted into the GIM constitutive equations allowing the prediction of polymer thermo-mechanical properties. However, it is common within GIM to express the constitutive equations in terms of the parameters of the mer unit. Below, the GIM expressions for five key thermo-mechanical properties are introduced in terms of mer unit parameters.

1.7.3. Glass Transition Temperature (T_g)

The glass transition temperature is expressed within GIM by:

$$T_g = 0.224\theta + 0.0513 \frac{E_{coh}}{N} \tag{13}$$

Where E_{coh} is the cohesive energy, in units of $J.mol^{-1}$, N is the degrees of freedom in units of mer^{-1}, θ is the characteristic temperature of polymer chain vibrations parallel to the polymer chain axis, in units of K, and T_g is the glass transition temperature of the polymer, in units of K.

The glass transition is defined within GIM as the point at which the intermolecular attractive force between two mer units, reaches a maximum:

$$\frac{dF}{dr} = 0 \tag{14}$$

As the mer units are separated further, the strength of the intermolecular forces falls, and thus this describes the point at which polymer chains have separated sufficiently to allow new molecular motions to become possible. Equation (13) indicates that T_g is a function of the ratio of the cohesive energy to the degrees of freedom ($\frac{E_{coh}}{N}$). The cohesive energy describes the depth of the potential well and thus the strength of the van der Waals and hydrogen bond forces between mer units. The degrees of freedom describe the number of modes, within which thermal energy can be stored, at a given temperature. Thus, a polymer with a greater number of degrees of freedom will attain the thermal energy required for polymer chains to separate, to the point associated with the glass transition, at a lower temperature and thus will possess a lower T_g.

1.7.4. Thermal Expansion Coefficient (α)

The thermal expansion coefficient is expressed within GIM by:

$$\alpha_{(T)} = \frac{1.38}{8.31} \frac{C_{(N,\theta,T)}}{E_{coh}} \tag{15}$$

Where T is the temperature in K, $\alpha_{(T)}$ is the thermal expansion coefficient in units of K^{-1}, and $C_{(N,\theta,T)}$ is the heat capacity of one mole of mer units in units of $J.mol^{-1}.K^{-1}$. It is important to note that, within GIM, the molar heat capacity $C_{(N,\theta,T)}$ is not representative of the polymer's molar heat capacity that would be measured experimentally.

There are two components to the heat capacity: atomic vibrations and polymer chain vibrations. Only polymer chain vibrations influence the average separation distance of adjacent polymer chains. Thus, the molar heat capacity $C_{(N,\theta,T)}$, employed in equation (15) in the calculation of $\alpha_{(T)}$, is the molar heat capacity of the material when only polymer chain vibrations are considered. Furthermore, only polymer chain vibrations in the two dimensions perpendicular to the polymer main chain axis are accounted for as only these chain vibrations contribute to

increasing polymer chain separation. Thus, the actual molar heat capacity of the polymer, as measured by experiment, will be greater than the value of $C_{(N,\theta,T)}$ used in GIM.

1.7.5. Molar Volume (V)

The molar volume is expressed within GIM by:

$$V_{(T)} = 1.4364\, V_w \left[1 + \int_0^T \alpha_{(T)}\, dT\right] \tag{16}$$

Where $V_{(T)}$ is the volume of one mole of mer units in units of $cc.mol^{-1}$, and V_w is the van der Waals volume of one mole of mer units in units of $cc.mol^{-1}$.

1.7.6. Density (ρ)

Density is calculated within GIM from:

$$\rho_{(T)} = \frac{M}{V_{(T)}} \tag{17}$$

Where $\rho_{(T)}$ is the density in units of $g.cc^{-1}$.

1.7.7. Young's Modulus (E)

Young's Modulus is calculated within GIM from:

$$E_{(T)} = 18\, \frac{\left(0.89E_{coh} - H_{(N,\theta,T)}\right)}{V_{(T)}} \tag{18}$$

Where $E_{(T)}$ is the Young's modulus in units of MPa.The term $H_{(N,\theta,T)}$ is the thermal energy that acts to increase the polymer chain separation distance of one mole of mer units, at a temperature T. This is different than the actual thermal energy of the polymer as atomic vibrations, and polymer chain vibrations in the polymer main chain axis, do not contribute to polymer chain

separation, as discussed previously, and are therefore omitted from the calculation of $H_{(N,\theta,T)}$. Equation (18) indicates that an increase in molar volume reduces the magnitude of the Young's modulus, whereas increasing the cohesive energy increases its magnitude. On the top line of the fraction in equation (18) it is also apparent that the cohesive energy is reduced by an amount equal to the molar thermal energy. Thus, increasing the thermal energy of the polymer also leads to a decrease in the Young's modulus which agrees with the general observation that the engineering moduli of materials reduce with increasing temperature.

1.8. Modelling the Hygrothermal Conditioning Process in Polymers

Modelling allows the parameters that characterise the hygrothermal behaviour of materials, such as solubility and the diffusion coefficient, to be obtained through the fitting of model predictions to experimental data. Once these material parameters have been obtained, the expected hygrothemal behaviour of the material under a wide range of different conditions, such as for different material dimensions and conditioning temperatures, can be predicted. Thus, modelling allows the results from a small number of experiments to be used to predict the behaviour of materials in a wide range of environments, without the need for experimentally investigating every possible condition.

There are two different approaches to modelling hygrothermal conditioning in polymer systems. The first involves solving the equation that describes the diffusion process, occurring within the material, subject to a series of boundary conditions. This approach is most appropriate for systems in which the diffusion process is not complicated by the presence of other phenomena, and in which the material parameters: diffusion coefficient, solubility, remain constant with respect to position and time.

In more complicated systems, such as where the solubility and diffusion coefficient are functions of both time and position, solving the diffusion equation can be mathematically complex. In these circumstances numerical methods are often applied, namely the finite difference [80] and finite element methods [81]. In the finite difference method, the differentials within the diffusion equation are approximated such that these infinitesimal differences become finite differences. Thus, a drawback compared to the exact solution approach is that care must be taken to ensure these differences are sufficiently small, at the expense of computation time, or the predicted material behaviour can vary significantly from that observed experimentally.

1.8.1. Exact Solution Approach to Modelling Moisture Diffusion

If the diffusion behaviour within a material is observed to be Fickian then the absorption/desorption process can be described by Fick's second law [31]. A general solution for Fickian diffusion, in one dimension, is given by [82]:

$$M_t = M_\infty \left(1 - e^{-7.3\left(\frac{Dt}{h^2}\right)^{0.75}}\right) \quad (19)$$

Where M_t and M_∞ are the moisture content of the material at a time t and at equilibrium respectively, D is the diffusion coefficient, and h is the material thickness in the dimension in which diffusion is occurring. Equation (19) can be fit against experimental measurements of material moisture content as a function of conditioning time allowing the diffusion coefficient, and equilibrium moisture content, at a given temperature and relative humidity to be determined.

A second approach is to plot the change in material moisture content as a function of the square root of conditioning time [82]. Equation (20) below can then be employed to obtain the diffusion coefficient:

$$D = \frac{\pi h^2}{16{M_\infty}^2}\, g^2 \quad (20)$$

Where g is the gradient of the initial linear portion of the material's $M_t/t^{\frac{1}{2}}$ relationship. Both of these approaches have been employed extensively in modelling the hygrothermal conditioning process in polymers where the overall behaviour is either Fickian, or approximately Fickian [83-85].

As equations (19) and (20) assume that diffusion occurs only in one dimension, diffusion of water in the other two dimensions is neglected and thus the diffusion coefficient obtained from fitting these equations to experimental data is an overestimate of the actual diffusion coefficient. To obtain an approximation to the actual diffusion coefficient, the so called 'edge-correction' formula, proposed by Shen et al [86], can be employed:

$$D_{obs} = D_{act}\left(1 + \frac{h}{w} + \frac{h}{l}\right)^2 \quad (21)$$

Where D_{obs} and D_{act} are the diffusion coefficients obtained from fitting either equation (19) or (20) to experimental data, and the actual diffusion coefficient respectively, both in units of $mm^2.min^{-1}$, h is the material dimension employed in equation (19), and w and l are the material dimensions in the other two dimensions all in units of mm. The 'edge-correction' formula assumes that the material is isotropic with regards to diffusing water molecules and thus that the diffusion coefficient is identical in all three dimensions. Thus, it is unsuitable for materials which have direction dependent diffusion coefficients. Examples include long-fibre reinforced composite materials where the diffusion coefficient along the fibre direction can be significantly different than the diffusion coefficient in the direction normal to the fibre layers [87, 88].

More complicated phenomena, such as processes where water can become bound/unbound to the polymer network, or where the diffusion coefficient is concentration dependent, can be accounted for by modification of Fick's second law. This can then be solved, subject to boundary conditions, allowing the full hygrothermal conditioning process to be modelled.

1.8.2. Numerical Methods

For polymer systems whose hygrothermal behaviour deviates significantly from that described by Fick's second law, or in which obtaining an exact solution to the diffusion equation is not practical, numerical methods can be applied. The two most common forms employed are the finite difference [80] and finite element methods [81].

1.8.2.1. Finite Difference and Finite Element Methods

In the finite difference method derivative terms are approximated with reference to Taylor's expansion [80]. For example, to a first order approximation, the first derivative of the function $f_{(x)}$ with respect to the variable x can be expressed as:

$$\frac{d}{dx}f_{(x)} \approx \frac{f_{(x+\Delta x)} - f_{(x)}}{\Delta x} \tag{22}$$

And, rearranging:

$$f_{(x+\Delta x)} \approx f_{(x)} + \Delta x \frac{d}{dx}f_{(x)} \tag{23}$$

Thus, the value of the function $f_{(x)}$ at the position $x + \Delta x$ can be approximated from the value, and the gradient of the function $f_{(x)}$ at the position x; provided that the step Δx is sufficiently small.

Another approach is the finite element method [81]. In this approach the system is first divided into a series of elements. These are typically triangular in shape for a two-dimensional system. The equation describing the evolution of a system parameter, such as concentration, temperature etc., is then solved for each element subject to the boundary conditions of that element. This simplifies the problem, as although the boundary conditions of the system as a whole might be complex, owing to the geometry of the material, they are relatively simple for the geometry of an individual element. The calculated parameters of every element, at a given point in time, can then be combined to predict the behaviour of the bulk material.

1.8.2.2. Numerical Modelling Approaches to Complex Hygrothermal Phenomena

Numerical methods have been applied to model complex hygrothermal conditioning processes in a wide range of polymers. Sullivan et al [89] investigated the effect of absorbed moisture on the ply-normal modulus of low-fired carbon-fibre phenolic composites. The ply-normal modulus is the elastic modulus in the direction normal to the composite plys, in other words normal to the fibre layers. Therefore, it is the modulus of the matrix, not that of the fibre-reinforcement. A series of tensometer experiments were performed to determine the ply-normal modulus in a range of composite samples, of varying moisture contents, at two different temperatures: 177℃ and 260℃. Above a moisture content threshold, the composite samples exhibited a significant decrease in their ply-normal modulus in the temperature range 177-260℃. This was attributed to absorbed moisture, plasticising the polymer matrix and thus reducing the glass transition temperature of the material. A function was then derived that described the behaviour of the ply-normal modulus as a function of both moisture content and temperature. The diffusion coefficient of the composite was determined from composite hygrothermal conditioning data obtained from a range of different conditioning environments. In this analysis, differences in the diffusion coefficient in the fibre direction, and in the direction normal to the fibre plys, were accounted for within a finite element model. The finite element method was then applied to calculate the moisture content of a composite sample, as a function of temperature, under an increasing temperature regime from 21℃ to 500℃ at a ramp rate of 5.55℃. s^{-1}. At each time-step, the value of the diffusion coefficient was recalculated to account for the change in temperature occurring within that time period. They then applied the function derived earlier from the ply-normal modulus data to predict the average ply-normal modulus of the composite throughout the course of the heating regime.

Yagoubi et al [8] investigated the hygrothermal behaviour of a commercially available epoxy resin. This material initially exhibited a brief plateau in its moisture content before increasing further at extended conditioning times. They attributed this phenomenon to a diffusion-reaction process whereby water molecules diffusing into the polymer can interact with chemical groups within the polymer network to form water/functional group complexes. As water molecules bound within these complexes are unable to diffuse, they remain trapped within the polymer. Thus, the net effect is an increase in the moisture content of the material over extended conditioning times as more water/functional group complexes are formed. This process was modelled by allowing the local solubility of water within the polymer to vary as a function of the local water complex concentration. The local diffusion coefficient was also assumed to be dependent upon the local water complex concentration as the diffusion coefficient in polymers has been observed to be a function of material solubility [36]. This diffusion equation was then subjected to numerical methods, in the form of the finite element method, allowing the moisture content of the polymer to be predicted as a function of conditioning time. To determine the values of the unknown parameters, such as the initial and final diffusion coefficients, model predictions were compared against experiment and the input parameter values varied through an iterative process. This was repeated until those parameter values that produced the best fit between model and experiment were obtained.

Numerical methods are also adopted in situations where the diffusion process is relatively simple but the complex structure of the material renders obtaining an exact solution to the diffusion equation difficult [90]. This is essential for understanding the evolution of the water concentration profile in composite materials where the presence of reinforcing fibres can significantly complicate the structure of the material. Another application of numerical methods is in modelling diffusion in materials in which the boundary conditions change with time [91]. This applies to conditioning environments whose temperature and relative humidity change with time and thus encompasses both real world environments and cyclic conditioning experiments.

1.8.3. Diffusion in Materials with Variable Solubility

Fick's second law describes diffusion in materials that possess a uniform solubility profile throughout their geometry. However, in some materials the solubility, and hence equilibrium moisture concentration, varies throughout the materials geometry. This is common in the electronic packaging industry where two component materials are often utilised in which two materials, of differing solubility, are bound together [30]. Non-uniform solubility profiles can also be created through modification of the polymer structure, such as through the formation of water/functional group complexes as described by Yagoubi et al [8].

One approach to this problem has been to normalise the water concentrations within the two materials [30, 92, 93]:

$$\phi = \frac{C_1}{C_{sat_1}} \tag{24}$$

$$\phi = \frac{C_2}{C_{sat_2}} \tag{25}$$

Where C_1 and C_2 are the concentrations of water within the first, and second, material respectively, C_{sat_1} and C_{sat_2} are the concentrations within the two materials at equilibrium, and ϕ is the normalised water concentration. Thus, the concentration term in Fick's second law can then be replaced with the quantity ϕC_{sat}, where C_{sat} is a function of position within the material.

Yagoubi et al [8] employed a different approach by deriving Fick's second law in terms of a chemical potential dependent flux:

$$J_{(x)} = -\frac{1}{RT} D_{(x)} C_{(x)} \frac{d\mu_{(x)}}{dx} \tag{26}$$

Where $J_{(x)}$ is the diffusive flux of water molecules, in units of $mol.mm^{-2}.min^{-1}$, $D_{(x)}$ is the diffusion coefficient for water molecules, in units of $mm^2.min^{-1}$, $C_{(x)}$ is the concentration of the water molecules, in units of $mol.mm^{-3}$, and $\mu_{(x)}$ is the chemical potential of the water molecules, in units of $J.mol^{-1}$. The chemical potential is given by:

$$\mu = \mu_0 + RTln(a) \tag{27}$$

Where μ is the chemical potential at a position x within the material, with activity a and temperature T, and μ_0 is the chemical potential of the standard state; that being the state in which the activity is equal to unity at the temperature T. They showed that the activity of water molecules in the gas phase can be written as:

$$a = \frac{C}{C_{sat}} \tag{28}$$

Where C is the concentration of water molecules at a position x within the material and C_{sat} is the equilibrium water concentration at that position. The equilibrium concentration C_{sat} can be allowed to vary as a function of time and position to account for changes in the solubility profile of the material. Thus, this modelling approach is analogous to the normalised approach.

2. Gravimetric and DMTA Investigation into the Hydrolysis of DGEBA-DDA Resin under Hygrothermal Conditions

2.1. Introduction

It is well documented in the literature that when conditioned hygrothermally, DGEBA-DDA resin is susceptible to hydrolysis by absorbed water molecules [5, 6, 39]. The result is a reduction in the cross-link density of the polymer network with an accompanying reduction in the glass transition temperature of the resin [6, 7] (see section 1.3.5.1, page 14).

In previous work on the hygrothermal ageing of DGEBA-DDA resin, square samples have been utilised with thickness dimensions in the range 1.2-2.0 mm [6, 7]. However, with these sample dimensions the time required for the materials to attain equilibrium, with their conditioning environments, is similar to that over which hydrolysis of the resin occurs. For example, the approximate dimensions of the samples conditioned at 50℃ by Xiao et al [7] were 1.2 x 30 x 30 mm. Using the diffusion coefficient representative of the unaged resin (obtained later in this work, see section 2.3.2.5.5.2, page 123), the time required for these samples to attain 90% of their equilibrium moisture content can be calculated and is found to be ~80 hrs. In contrast, the time required for the effect of hydrolysis to become detectable by DMTA, in other words through the observation of a reduction in the glass transition temperature of the resin, is ~ 4.33 hours (calculated from the rate constants for hydrolysis obtained later in this work, see section 2.3.2.5.5.3, page 125). Thus, the diffusion and hydrolysis processes are strongly coupled. As a result, it is not possible to obtain the diffusive properties of the material prior to ageing. Furthermore, the extent of hydrolysis after a given conditioning time has been determined with reference to the change in the dry T_g of the resin. However, as the diffusion and hydrolysis phenomena are coupled the extent of hydrolysis, at a time t, will vary throughout the geometry of the sample. Thus, the T_g profile within the sample will be non-uniform leading to distortion of the loss tangent peak, obtained from DMTA spectra, rendering determination of a precise T_g difficult.

The aims of this chapter are two-fold: first to measure the rate of the hydrolysis reaction with high precision, and second to determine the change in DGEBA-DDA resin's diffusive properties (diffusion coefficient, solubility) as a function of temperature and conditioning time.

2.2. Methods

2.2.1. Experimental Methods

2.2.1.1. Rate of the hydrolysis reaction

2.2.1.1.1. Coupon Size

The extent of hydrolysis in conditioned DGEBA-DDA can be determined by thoroughly drying the material and then comparing its aged T_g to the T_g of the resin prior to conditioning. This allows the extent of reaction to be observed as both a function of time and temperature and thus the rate of hydrolysis can be deduced. However, this methodology assumes that the rate of hydrolysis is uniform throughout the material and constant with respect to time. If the rate of hydrolysis varies, as a function of position, within the material then this will lead to the formation of a non-uniform T_g profile. A variable T_g profile results in a broadening of the loss tangent peak, obtained from DMTA, making precise determination of resin T_g as a function of conditioning time impossible. Before a material attains its equilibrium moisture, content a water concentration gradient exists throughout the material resulting in a hydrolysis rate that is both time and position dependent. Thus, the T_g profile is non-uniform. To decouple the diffusion and hydrolysis phenomena it is necessary to reduce the material thickness such that the time required for the material to attain its equilibrium moisture content is much smaller than the timescale required for significant hydrolysis to occur.

To meet this criterion, thin films of resin (d < 0.075 mm) were employed for samples that were to be subsequently analysed with DMTA, post-conditioning, to establish the extent of hydrolysis. The experimental results in section 2.3 (page 78) indicate that this thickness dimension is more than sufficient to decouple the diffusion and hydrolysis processes.

2.2.1.1.2. Conditioning Temperature

A minimum of three different conditioning temperatures are required to determine the rate of hydrolysis as a function of temperature. In selecting appropriate temperatures, it is important to take into account the wet T_g of the resin. Xiao et al [7] conditioned DGEBA-DDA samples at 50℃, 70℃, and 90℃. The initial dry T_g of these samples, before conditioning commenced, was determined by DMTA and found to be 159℃. Subsequent analysis of these samples, after complete ageing had occurred, gave wet resin T_g's of 98℃, 84℃, and 82℃, respectively. The larger T_g depression, observed at higher temperatures, likely arises as a consequence of these samples undergoing a phase transition (glass to rubber) as the conditioning temperature exceeds the wet T_g of the material [7]. Gravimetric analysis of the samples conditioned at 90℃ showed that these materials had an initial equilibrium moisture content of ~9.5% w/w, compared to ~6.75% w/w at 50℃. The samples conditioned at 70℃ displayed an initial equilibrium plateau at ~8% w/w, which slowly increased over extended conditioning times. When the proximity of the 70℃ samples to their wet T_g (84℃) is accounted for, the gravimetric analysis suggests that these materials were slowly undergoing a transition from a glass to a rubber. These observations are in agreement with the suggestion of Leger et al [94] that an increase in free volume accompanies a material's transition from the glass to the rubber phase. Thus, the solubility of water in the resin will be expected to increase as it undergoes its phase transition. An increase in solubility during conditioning leads to an increase in water concentration within the material and thus an increase in the rate of hydrolysis. Thus, these three conditioning temperatures are unsuitable for accurate determination of the rate of hydrolysis. A more suitable range of temperatures is: 35℃, 50℃, and 60℃, and these will be employed in the experiments that follow.

The wet T_g of fully aged DGEBA-DDA resin at equilibrium, at 70℃ and 100% relative humidity, is ~84℃ [7]. Thus, if a similar degree of T_g depression occurs in samples aged at 60℃, then the wet T_g of these samples will be ~24℃ above the conditioning temperature. As a result, DGEBA-DDA samples conditioned at or below 60℃ will not undergo a glass-rubber transition during the conditioning experiment. Furthermore, the experimental results obtained later in this work have shown that the equilibrium moisture content of fully aged DGEBA-DDA resin, at 35℃/100% RH and 60℃/100% RH, is 4.79% w/w and 4.84% w/w respectively (see Figure 34 and Figure 32 in section 2.3.2.3, page 102). The similarity in equilibrium moisture content at the two temperatures suggests that the solubility of water within the resin at 60℃ is not increasing as a result of a glass-rubber phase transition. These two experimental observations indicate that a maximum conditioning temperature of 60℃ is not sufficient to induce a phase change within the material and thus this temperature is suitable for investigating the rate of hydrolysis, as a function of temperature, in DGEBA-DDA resin in the glassy state.

2.2.1.1.3. Atmospheric Conditioning over Liquid Immersion

Previous work on the hygrothermal ageing of DGEBA-DDA has focused almost predominantly on liquid immersion [6, 7, 43] with only a single paper investigating the behaviour of DGEBA-DDA in humid atmospheres [42]. However, as discussed previously, loss of material dry mass has been observed at conditioning temperatures of 70℃, and above, and this has been attributed to hydrolysed polymer chain segments leeching out of the material and into the conditioning medium. This loss of mass during conditioning makes determination of equilibrium moisture content difficult and may affect the solubility of water within the resin, either through the loss of polar groups attached to the free chain segments, or through the creation of free volume. With regards to hydrolysis rate determination, a change in solubility during conditioning will affect the concentration of water within the material and this will directly influence the rate of the hydrolysis reaction. It can also be conjectured that the loss of hydrolysed chain segments may have an impact upon the dry T_g of the material as even fully hydrolysed chains will interact with the surrounding polymer network through van der Waals forces and/or hydrogen bonding.

Previous work on DGEBA-DDA suggests that the leeching phenomenon occurs as a consequence of the material transforming from a glassy, to a rubbery, state during conditioning [6, 7, 44]. This is because a net loss in the mass of the resin is not observed at temperatures at, or below, 60℃ and only occurs at higher temperatures when the resin is in its rubber state. However, the samples employed in these experiments were ~1.2-2.0 mm in thickness, ~16-27 times thicker than the thin film samples to be employed in this work. Thus, although no measurable mass loss was observed within these materials this insight should not be applied to thin film samples where the reduction in dimension will amplify the percentage mass loss occurring within a given time period. To avoid any unanticipated effect of leeching upon the conditioning experiments performed within this work an atmospheric conditioning environment of 100% relative humidity will be employed.

2.2.1.2. Material Diffusive Properties as a Function of Conditioning Time

Earlier, the coupling of the diffusion and hydrolysis processes was discussed (see section 2.2.1.1.1, page 40) with the necessity of decoupling them to prevent concentration gradients within the material from affecting the determination of T_g as a function of conditioning time. A similar approach is required for thicker samples, employed in gravimetric analysis, if the initial diffusive properties (diffusion coefficient, solubility) of the material, before ageing occurs, are to be determined. Thin film samples are not appropriate for this purpose as significant desorption of moisture will occur during removal from their conditioning environments for weighing. A method where gravimetric analysis is possible inside the conditioning chamber, such as Dynamical

Vapour Sorption (DVS), would remove this unwanted effect. However, this piece of equipment was unavailable for the experiments that were performed in this work. Preliminary experiments on samples of ~0.25 mm thickness suggested that they would be suitable for the determination of the initial equilibrium moisture content of DGEBA-DDA resin. However, due to their small dimension, absorption occurred so rapidly that few data points could be obtained in the initial linear portion of their uptake/√time relationships. To improve the accuracy in determining the initial diffusion coefficients of the resin, a second set of coupons, of thickness ~0.72 mm, were employed to allow a larger quantity of data points in the initial linear region to be gathered.

2.2.1.3. Resin Synthesis

The resin investigated in this work was synthesised from DGEBA cured with the amine hardener DDA. A mixing ratio of epoxy to hardener of 100:7 by mass, suggested by Fata et al [6], was employed as this mixing ratio has been shown to result in a high final T_g of ~171℃ [6]. Prior to mixing, DGEBA was pre-heated at 80℃ to lower its viscosity. After the initial heating step, DDA was added to the epoxy and stirred mechanically for ~10 minutes to ensure adequate dispersion of the DDA powder within the mixture. The DDA powder used in this experiment had first been pulverised down to a grain size of ~0.05 mm. This increases the surface area of the hardener, in contact with the epoxy, and thus increases the rate of reaction between the two components. This step is essential as DDA is insoluble in DGEBA and thus if the grain size is too large then the mixture will attain gelation with these large grains of DDA still intact. This prevents complete reaction of DGEBA with DDA during cure as the cure kinetics in the gelled phase are diffusion controlled. DDA molecules trapped within the large grains of hardener have insufficient time to diffuse out into the polymer network and thus are unable to undergo reaction with epoxide groups.

After stirring for ~10 minutes the mixture is transferred to a vacuum oven at 80℃ and degassed for ~15 minutes. After degassing, the mixture is then cured according to the cure cycle suggested by Fata et al [6]. This initially involves stirring mechanically for ~1 hour at 150℃ until no visible DDA grains remain. The solution is then cast directly onto glass plates primed with release agent, which are then transferred to a fan assisted oven preheated at 150℃. The oven employed in this work was a Heratherm OMH60. The oven is ramped to 180℃ at 3℃.min^{-1}, followed by a 1-hour dwell. After the cure cycle is complete, the DGEBA-DDA castings are immediately placed under vacuum for storage to prevent any reaction between the resin and atmospheric moisture.

2.2.1.4. Sample Preparation

Three types of sample were machined from the cured resin casting, each of differing dimensions. These are shown below in Table 1.

Sample Type	d_i (mm) (Thickness)	w_i (mm) (Width)	l_i (mm) (Length)
Film	~0.075	~10	~20
Thin	~0.25	~29	~29
Thick	~0.72	~12	~28

Table 1: Average dimensions of the three different sample types.

Rough initial dimensions were achieved by machining with a diamond saw. This was followed by grinding with various grades of silicon carbide abrasive paper, using an ATM Saphir 320, to obtain the final dimensions. All samples were taken from the core of the resin casting by abrading away an equal quantity of material from both the top and bottom surfaces to achieve the desired thickness. This ensures that differences in the thermo-mechanical properties of the resin occurring at the resin/air and resin/glass interface, as a result of possible thermal gradients during cure, are removed from the samples. The total machining time for any individual sample, during which the resin was exposed to the laboratory atmosphere and the water of the grinder, was ~45 minutes. The DMTA experiments performed later in this work indicate that, at 35℃, the change in the T_g of DGEBA-DDA films after 45 minutes conditioning, as a result of hydrolysis, is negligible. Thus, the change in T_g occurring in the materials during the machining process, at room temperature, will be undetectable by DMTA. Therefore, any hydrolysis occurring within this time frame will have no impact upon the results of the experiment.

2.2.1.5. Conditioning Environment Preparation

An atmospheric relative humidity of 100% was achieved by partially filling glass jars with distilled water which were then sealed and placed in a fan assisted oven at the desired temperature. After preparation, the filled jars were left for 48 hours before any experiments were initiated to ensure uniform temperature and relative humidity throughout the containers. The jars were 150 mm in height and 150 mm diameter. They were filled with distilled water to a depth of 100 mm leaving a 50 mm air gap where the coupons could be suspended on a wire mesh, hung from the lid of the jar. Where no fan is present in the conditioning container, and thus mixing of

air only occurs through convection, ISO 483:2005 [95] recommends that the height of the air gap above the fluid (h) should not be greater than the diameter of the fluid surface (d):

$$h \leq d \tag{29}$$

Using the diameter of the conditioning containers employed in this work, this gives a maximum value of h of no greater than 150 mm. As the height of the air gap above the fluid (h) is 50 mm, the requirements of ISO 483:2005 [95] are satisfied.

2.2.1.6. Conditioning Experiments - DMTA (~0.075 mm films)

Film samples were suspended inside conditioning containers at temperatures of 35℃, 50℃, and 60℃. Periodically, at time intervals appropriate for the rate at which hydrolysis is occurring at each of the three conditioning temperatures, one to three samples were removed, dried superficially, and placed inside a vacuum oven at 50℃ for 24 hours, in preparation for DMTA. Using the diffusion coefficient representative of unaged DGEBA-DDA resin, calculated later in this work (see Table 25 in section 2.3.2.5.5.2, page 123), the drying time required for complete removal of absorbed moisture, from films of 0.075 mm thickness at 50℃, is less than 1 hour. Thus, the drying time employed is more than adequate to ensure complete removal of moisture prior to the DMTA experiment commencing.

For DMTA, films were tested in tension at a frequency of 1 Hz using a PerkinElmer DMTA 8000. To minimise moisture absorption during the scan, the DMTA was ramped at 20℃. min^{-1} to 100℃, followed by a 10-minute dwell, before ramping to 200℃ at 2℃. min^{-1}. The DMTA measurement data below 100℃ is not required, as only the dry T_g of the resin needs to be determined, and it is known that this falls in the range $140℃ < T_g < 185℃$, dependent upon the extent of hydrolysis (see section 2.3.1.2.1, page 89). Thus, the low temperature data can be discarded as at high ramp rates (20℃. min^{-1}) there is the potential for temperature discrepancy between thermocouple and sample. The dwell for 10 minutes at 100℃ ensures evaporation of any moisture absorbed by the films during the time period required to setup the DMTA experiment. As well as the conditioned samples, DMTA was performed on four unaged films to determine the initial dry T_g of unaged DGEBA-DDA resin.

2.2.1.7. Conditioning Experiments - Gravimetric Analysis - Unaged Resin (~0.25 mm and ~0.72 mm samples)

At each of the three conditioning temperatures: 35℃, 50℃, and 60℃, no less than three samples were conditioned. Samples were removed periodically, their removal time recorded, dried superficially and then weighed on a balance (A&D GR-200) with a precision of ±50μg. They were then returned to their conditioning environment and their return time also recorded. This allowed the time the samples spent outside of their conditioning environment, during the weighing process, to be determined and thus by accounting for this factor exact conditioning times could be obtained. The average time a sample spent outside of its conditioning environment during weighing was 5 minutes.

2.2.1.8. Conditioning Experiments - Gravimetric Analysis - Aged Resin (~0.25 mm and ~0.72 mm samples)

After conditioning for a time period, sufficient for complete hydrolysis to occur, the six samples conditioned at 60℃ were removed, dried superficially, and placed under vacuum at 50℃ to allow complete removal of absorbed moisture. The time required for complete hydrolysis to occur, at 60℃, was determined by referring to the DMTA data for thin films (see Figure 23 later in this work) and was taken to be the point at which an approximate plateau in T_g was observed after a conditioning time of 60 $\sqrt{hrs}$. The vacuum dried samples were removed periodically for weighing and drying continued until a final dry mass could be obtained; this being indicated by a plateau in the moisture content/√time relationship of the material. After complete drying, these six samples were reconditioned at each of the three conditioning temperatures (35℃, 50℃, 60℃) and investigated gravimetrically using the same methodology that was applied to the unaged samples. After attaining equilibrium at each temperature, the samples were thoroughly dried under vacuum before proceeding to the next conditioning temperature.

2.2.2. Modelling Methods: Formulation of Diffusion-Hydrolysis Model for Understanding the Hygrothermal Ageing Process in DGEBA-DDA Resin

2.2.2.1. Modelling the Hydrolysis Process

2.2.2.1.1. Describing the Hydrolysis Reaction in Terms of Fundamental Units

After conditioning for an extended time period, sufficient for complete hydrolysis to occur, a permanent increase in resin dry mass is observed that cannot be reversed through drying. This has been attributed to the chemical addition of water molecules to the polymer structure as

a result of hydrolysis [7]. In this description each water molecule that reacts with the polymer network hydrolyses one polymer chain. As the reaction proceeds it becomes possible for polymer chains to be cut in two or more locations, freeing them from the covalent bonds of the polymer network. If the resin is immersed in water when it is in the rubbery state, then it becomes possible for these free chain segments to leech out of the material and into the conditioning medium.

To simplify the modelling of this process it is assumed that the polymer consists of long chains of repeat units stacked parallel to one another in a hexagonal packing pattern. Two adjacent chains are then considered as shown below in Figure 12.

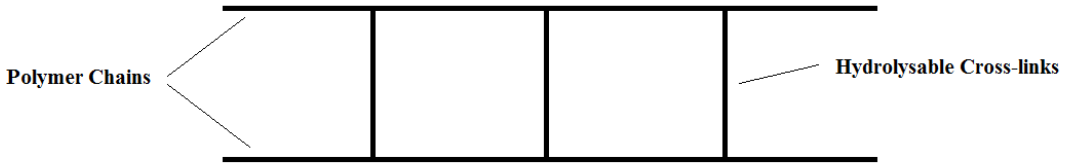

Figure 12: Simplified polymer structure of DGEBA-DDA resin.

The cross-links shown in this figure represent those that are susceptible to hydrolysis. Fata et al [6] suggest that a variety of different cross-links are formed during the cure of DGEBA-DDA but that only a certain type can be hydrolysed by water molecules. As the focus of this work is on the change in cross-link density that results from hydrolysis, these stable cross-links are not shown. Each section of polymer containing a hydrolysable cross-link is referred to as a fundamental unit; of which there are three different types, shown below in Figure 13.

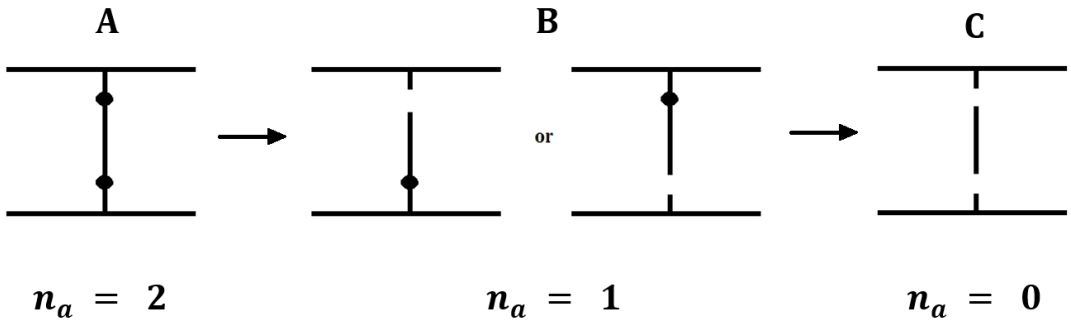

Figure 13: Structures of the three types of fundamental unit in DGEBA-DDA resin.

In this scheme, A and C are representative of the initial and fully hydrolysed systems respectively. During hygrothermal conditioning, the polymer system will consist of fractional proportions of each type of fundamental unit dependent upon the extent to which hydrolysis has occurred. For simplicity, it is assumed that the fully hydrolysed material is composed of hydrolysable cross-links cut in no more than two places. This assumption is reasonable as any hydrolysis process occurring in polymer chains already free from the polymer network (cut in two places) would be negligible until the later stages of conditioning when the proportion of fundamental units of type C becomes dominant. One would also expect this tertiary hydrolysis process to lead to an increase in the solubility of water within the material, as it involves the further addition of polar OH groups to the polymer structure.

However, after conditioning for 60 $\sqrt{hrs}$ at 60℃ (the approximate time required for complete hydrolysis to occur) the change in the sample moisture content, with time, is negligible with an apparent plateau having been attained (see Figure 30 later in this work). This implies either that tertiary hydrolysis does not occur, or that it occurs at such a low rate that its influence is negligible during the time-scale of these conditioning experiments (~6.5 months).

Within each fundamental unit the points of the polymer network that are susceptible to hydrolysis are termed reactive sites and denoted by n_a. Assuming that the hydrolysis reaction is governed by first order kinetics, the rate equations for the transformation of $A \rightarrow B$ can be written as:

$$\frac{d}{dt}[B] = 2K_{AB}S_f[W][A] \tag{30}$$

$$\frac{d}{dt}[A] = -\frac{d}{dt}[B] = -2K_{AB}S_f[W][A] \tag{31}$$

And $B \rightarrow C$ as:

$$\frac{d}{dt}[C] = K_{BC}S_f[W][B] \tag{32}$$

$$\frac{d}{dt}[B] = -\frac{d}{dt}[C] = -K_{BC}S_f[W][B] \tag{33}$$

The rate equations for the entire hydrolysis process ($A \rightarrow B \rightarrow C$) are obtained by combining those from each individual step outlined above:

$$\frac{d}{dt}[A] = -2K_{AB}S_f[W][A] \tag{34}$$

$$\frac{d}{dt}[B] = 2K_{AB}S_f[W][A] - K_{BC}S_f[W][B] \tag{35}$$

$$\frac{d}{dt}[C] = K_{BC}S_f[W][B] \tag{36}$$

Where $[A]$, $[B]$, and $[C]$ are the molar concentrations of fundamental units A, B, and C, respectively in units of $mol.mm^{-3}$, K_{AB} and K_{BC} are the rate constants associated with processes $A \rightarrow B$ and $B \rightarrow C$ respectively in units of $mm^3.mol^{-1}.min^{-1}$, [W] is the concentration of water molecules in $mol.mm^{-3}$ and S_f is the so-called solubility fraction.

In this chapter the concept of solubility fraction will be introduced to prevent the concentration of water molecules, that are available for hydrolysis $[W]$, from increasing as hydrolysis proceeds and the solubility of water within the material increases. It is defined by:

$$S_f = \frac{S_A}{S} \tag{37}$$

Where S_A is the solubility of water in fundamental unit A i.e. the solubility of water in the initial unaged system, and S is the solubility of water within the resin at conditioning time t, both measured in units of $mol.mm^{-3}.Pa^{-1}$. The solubility fraction is important as the solubility of water within the resin increases as hydrolysis proceeds through the incorporation of polar OH groups into the polymer network each time a cross-link is cut. This increase in solubility increases the equilibrium moisture content of the material and thus there is a corresponding increase in water concentration. However, this increased water capacity is associated with water molecules clustering around the new OH groups that have been introduced into the polymer network at the location were polymer chains have been hydrolysed. Thus, water molecules located in the vicinity of these groups are in regions of the network where hydrolysis has already occurred and so are

less likely to contribute to further hydrolysis reactions. Furthermore, the ability of these water molecules to diffuse to un-hydrolysed sites is restricted from their hydrogen bonding to the OH functional group. These arguments suggest that an increase in the rate of hydrolysis, resulting from an increase in the solubility of water within the resin, is unlikely. The solubility fraction accounts for changes in material solubility to ensure that the concentration of water available for hydrolysis, in a sample having attained its equilibrium moisture content, remains constant throughout the conditioning process.

In the unaged resin, all fundamental units are of type A and thus the initial values of $[B]$ and $[C]$ are zero. An initial value for $[A]$ can be determined as two moles of water molecules are required to fully hydrolyse one mole of units of type A to type C. Therefore, with reference to n_{abs}, the moles of water chemically combined with the polymer network in the fully aged resin, we can write:

$$n_A = n_{FU} = \frac{n_{abs}}{2} \tag{38}$$

Where n_A, n_{FU}, and n_{abs}, are the moles of fundamental units of type A, the moles of fundamental units of all types, and the moles of chemically reacted water, respectively. The moles of chemically reacted water n_{abs} can be re-expressed in terms of the percentage mass of water retained ($\%_{abs}$) in the dried, fully aged resin, as follows. The water chemically combined with the fully aged resin can be written as:

$$am_i = m_i + m_{abs} \tag{39}$$

Where m_i and m_{abs} are the initial mass of the unaged resin, and the mass of water chemically combined with the polymer network in the fully aged resin, respectively. The term a is the fractional increase in mass. This can be rearranged to express the fractional increase in mass in terms of a percentage:

$$\%_{abs} = 100\ \frac{m_{abs}}{m_i} \tag{40}$$

Where $\%_{abs}$ is the percentage, by mass, of water that is retained in the dry, fully aged resin. Rewriting the initial mass of the resin in terms of its volume and density:

$$\%_{abs} = 100\ \frac{m_{abs}}{\rho_{R_i}\, V_i} \tag{41}$$

Where ρ_{R_i} and V_i are the initial density and volume of the resin, before ageing, in units of $g.mm^{-3}$ and mm^3, respectively. Rearranging equation (41) in terms of m_{abs}, the mass of retained water in the dry fully aged resin, the following expression is obtained:

$$m_{abs} = \frac{\%_{abs}\, \rho_{R_i}\, V_i}{100} \tag{42}$$

The moles of water chemically combined with the polymer network, in the dry fully aged resin, can therefore be obtained from:

$$n_{abs} = \frac{m_{abs}}{18} \tag{43}$$

Substituting equation (42) into equation (43):

$$n_{abs} = \frac{\%_{abs}\, \rho_{R_i}\, V_i}{1800} \tag{44}$$

Substituting equation (44) into equation (38), the moles of fundamental units of type A is given by:

$$n_A = \frac{\%_{abs}\, \rho_{R_i}\, V_i}{3600} \tag{45}$$

The initial concentration of fundamental units of type A, within the resin before conditioning, is given by:

$$[A] = \frac{n_A}{V_i} \tag{46}$$

Where $[A]$ is in units of $mol.mm^{-3}$. Substituting equation (45) into equation (46):

$$[A] = \frac{\%_{abs}\,\rho_{R_i}}{3600} \tag{47}$$

Finally, before ageing the resin is composed entirely of fundamental units of type A. Thus, the total concentration of fundamental units, of all types, is given by:

$$[FU] = [A] \tag{48}$$

Where $[FU]$ is the total concentration of fundamental units of all types in units of $mol.mm^{-3}$.

2.2.2.1.2. Using GIM to Predict the Glass Transition Temperature of DGEBA-DDA resin from Fundamental Unit Concentrations

In the previous section the rate equations governing the hydrolysis reaction in DGEBA-DDA resin were derived allowing the concentrations of fundamental units to be predicted as a function of conditioning time. A method is now required to link these fundamental unit concentrations to the glass transition temperature of DGEBA-DDA resin. To achieve this objective, the formalism of GIM will be employed.

Within GIM a mer unit can be associated with each type of fundamental unit. As the structures of these three fundamental units are different, they will each possess their own unique mer unit parameter values. Table 2 below shows the cohesive energy (E_{coh}) and degrees of freedom (N) associated with the mer unit of each type of fundamental unit.

Fundamental Unit	E_{coh} $(J.mol^{-1})$ Cohesive Energy	N (mer^{-1}) Degrees of Freedom
A	E_{coh_A}	N_A
B	$E_{coh_A} + \frac{E_H}{2}$	$N_A + \frac{N_H}{2}$
C	$E_{coh_A} + E_H$	$N_A + N_H$

Table 2: Cohesive energy and degrees of freedom for the mer units associated with each type of fundamental unit.

Where E_{coh_A} and N_A are the cohesive energy and degrees of freedom associated with the mer unit of fundamental unit A. The terms E_H and N_H are the increase in cohesive energy and degrees of freedom that result from a single hydrolysis event ($A \rightarrow B$ or $B \rightarrow C$). The mer unit parameters for fundamental units B and C have been expressed in terms of the cohesive energy, and degrees of freedom, of fundamental unit A, and the terms E_H and N_H. A single hydrolysis event transforms fundamental unit A into fundamental unit B. However, the chemical structure of fundamental unit A is composed of two mer units linked together by a hydrolysable cross-link. Thus, although the hydrolysis event introduces a cohesive energy E_H and degrees of freedom N_H to fundamental unit A, this is shared between two mer units and hence the cohesive energy and degrees of freedom, associated with the mer unit of fundamental unit B, are $E_{coh_A} + \frac{E_H}{2}$, and $N_A + \frac{N_H}{2}$, respectively. In fundamental unit C, two hydrolysis events have occurred and these are shared between two mer units. Thus, the cohesive energy and degrees of freedom for the mer unit of fundamental unit C are $E_{coh_A} + E_H$, and $N_A + N_H$, respectively.

The cohesive energy and degrees of freedom that are introduced to the fundamental unit by a single hydrolysis event can be determined with reference to the underlying chemical process. Assuming the reaction pathway for hydrolysis proposed by Xiao et al [44], a single hydrolysis event involves the breaking of a covalent bond, creating two free chain ends, and the introduction of an OH functional group into the polymer network. In the context of GIM, each free chain end introduces three degrees of freedom to the mer unit. The OH functional group increases the cohesive energy by 13000 $J.mol^{-1}$, and as a side group to the main polymer chain, contributes two degrees of freedom. Thus, each hydrolysis event increases the cohesive energy of the fundamental unit by 13000 $J.mol^{-1}$ and the degrees of freedom by eight. These values for E_H and N_H are shown below in Table 3.

E_H $(J.mol^{-1})$ **Cohesive Energy**	N_H (mer^{-1}) **Degrees of Freedom**
13000	8

Table 3: Cohesive energy and degrees of freedom introduced to the fundamental unit by a single hydrolysis event.

To obtain the values of E_{coh_A} and N_A by group addition, the chemical structure of fundamental unit A must be known. However, this is complicated by the fact that there is still debate within the literature as to the exact chemical structures that are formed during the cure of DGEBA-DDA resin [96]. In recognition of these difficulties, no attempt will be made to speculate on the possible chemical structure of fundamental unit A and instead the values of E_{coh_A} and N_A will be inferred from experimental measurements of the glass transition temperature.

The glass transition temperature of fundamental unit A can be expressed in terms of the GIM equation for T_g (equation (13)) as:

$$T_{g_A} = 0.224\Theta + 0.0513 \frac{E_{coh_A}}{N_A} \tag{49}$$

And fundamental unit C as:

$$T_{g_C} = 0.224\Theta + 0.0513 \left[\frac{E_{coh_A} + E_H}{N_A + N_H}\right] \tag{50}$$

The term Θ is the characteristic temperature of polymer chain vibrations parallel to the polymer chain axis and takes an approximate value of 550K for polymers that possess phenyl rings in their polymer chains [71], such as DGEBA-DDA. As the hydrolysis reaction does not affect the phenyl structure of DGEBA-DDA, the value of Θ is approximately identical in all three fundamental unit types.

This allows equations (49) and (50) to be solved simultaneously to obtain expressions for E_{coh_A} and N_A:

$$E_{coh_A} = \frac{\left(T_{g_A} - 0.224\Theta\right)}{\left(T_{g_C} - T_{g_A}\right)}\left[E_H - N_H \frac{\left(T_{g_C} - 0.224\Theta\right)}{0.0513}\right] \quad (51)$$

$$N_A = \frac{0.0513\, E_H - N_H\left(T_{g_C} - 0.224\Theta\right)}{\left(T_{g_C} - T_{g_A}\right)} \quad (52)$$

The glass transition temperatures of fundamental units A (T_{g_A}) and C (T_{g_C}), in other words of the unaged and fully hydrolysed resin, can be obtained experimentally. In this work these measurements were performed by DMTA (see section 2.2.1.6, page 45). Employing the values of T_{g_A} and T_{g_C} that were obtained from these experiments (Table 8, page 92) in equations (51) and (52), the cohesive energy and degrees of freedom, associated with the mer unit of fundamental unit A, were calculated and are shown below in Table 4.

E_{coh_A} $(J.mol^{-1})$ **Cohesive Energy**	N_A (mer^{-1}) **Degrees of Freedom**
294956	45.53

Table 4: Cohesive energy and degrees of freedom associated with the mer unit of fundamental unit A.

It is now possible to calculate the cohesive energy and degrees of freedom of the mer units associated with fundamental units B and C. Substituting the previously obtained values of E_{coh_A}, N_A, E_H, and N_H, for the parameters in Table 2., the parameter values for the mer units of each type of fundamental unit are obtained.

Fundamental Unit	E_{coh} $(J.mol^{-1})$ **Cohesive Energy**	N (mer^{-1}) **Degrees of Freedom**
A	294956	45.53
B	301456	49.53
C	307956	53.53

Table 5: Cohesive energy and degrees of freedom for the mer units associated with each type of fundamental unit.

The cohesive energy and degrees of freedom associated with the mer units of each type of fundamental unit are now known. However, during hygrothermal conditioning each type of fundamental unit will be present, in proportions dependent on the extent to which hydrolysis has occurred. The mer unit parameters of a mixed state can be obtained by combining those parameters for each distinct state (A,B,C) on a mole fraction basis [71]. Thus, the average cohesive energy at a given point in the conditioning process is obtained from:

$$E_{avg} = f_A E_{coh_A} + f_B E_{coh_B} + f_C E_{coh_C} \quad (53)$$

And the average degrees of freedom:

$$N_{avg} = f_A N_A + f_B N_B + f_C N_C \quad (54)$$

Where f_A, f_B, and f_C, are the mole fractions of fundamental units A, B, and C, at a given point in the conditioning process. They are obtained from:

$$f_A = \frac{[A]}{[FU]} \quad (55)$$

$$f_B = \frac{[B]}{[FU]} \quad (56)$$

$$f_C = \frac{[C]}{[FU]} \quad (57)$$

Where $[A]$, $[B]$, and $[C]$, are the concentrations of units A, B, and C, in units of $mol.mm^{-3}$, and $[FU]$ is the total concentration of all types of fundamental unit, in units of $mol.mm^{-3}$. Thus, for a given proportion of each type of fundamental unit, the glass transition temperature can be calculated using the GIM equation for T_g (equation (13)):

$$T_g = 0.224\Theta + 0.0513 \frac{E_{avg}}{N_{avg}} \quad (58)$$

Where E_{avg} is the average cohesive energy, in units of $J.mol^{-1}$, and N_{avg} is the average degrees of freedom, in units of mer^{-1}.

2.2.2.2. Modelling the Diffusion Process

2.2.2.2.1. Diffusion Model Formulation

For simplicity, it is assumed that the samples under conditioning are sheets of infinite area and finite thickness, thus implying that diffusion of water occurs in only one dimension. The effect of water diffusing through the sample edges, the so-called edge effect, is small as $d \ll w, l$. Thus, this effect can be accounted for by the edge-correction formula proposed by Shen et al [86], given below in equation (59):

$$D_{obs} = D_{act}\left(1 + \frac{d}{w} + \frac{d}{l}\right)^2 \tag{59}$$

Where D_{obs} and D_{act} are the observed, and actual, diffusion coefficients respectively in units of $mm^2.min^{-1}$, and d, w, and l, are the sample thickness, width, and length dimensions in units of mm. Thus, edge effects are accounted for by increasing the diffusion coefficient by a factor that is dependent upon the dimensions of the sample to be modelled. When modelling a system where the actual diffusion coefficient and coupon dimensions are already known, the edge correction formula is used to calculate D_{obs} and it is this diffusion coefficient that is then employed within the model. This ensures that the time predicted by the model, for the material to attain a given moisture content, is in agreement with that which is observed experimentally. However, the predicted concentration gradients within the material before equilibrium is achieved will contain some degree of error compared to the gradients within the actual material. As the edge correction factors, for the sample dimensions employed in this work, are small (1.02 to 1.21), these errors are negligible.

In the work that follows the diffusion model developed by Yagoubi et al [8] is adopted as this will allow the effect of solubility gradients on the observed diffusion behaviour of the resin to be predicted. This model also involves a reaction scheme where water molecules can bind with functional groups within the polymer network to form water complexes. These complexes can subsequently break down allowing water molecules to become free, thus it is a reversible reaction. However, the hydrolysis reaction follows a different process (permanent binding of water

molecules to the polymer network) and so this part of the model has been adjusted to account for the specific nature of the hydrolysis phenomenon occurring in DGEBA-DDA resin.

2.2.2.2.2. Description of the Yagoubi [8] Derivation of the Diffusive Flux Equation in terms of Material Solubility

In this section, the diffusive flux equation in terms of material solubility, that was derived by Yagoubi et al [8], is described. Although this derivation has already been outlined in Yagoubi's paper [8], a number of intermediate steps were not shown and thus the purpose of this work is to describe the derivation step by step, with the inclusion of appropriate background material where necessary.

Assuming that diffusion occurs only in the x-coordinate, the diffusive flux of water molecules can be written as [8]:

$$J_{(x)} = -\frac{1}{RT} D_{(x)} C_{(x)} \frac{d\mu_{(x)}}{dx} \quad (60)$$

Where $J_{(x)}$ is the diffusive flux of water molecules in the x-coordinate in units of $mol.mm^{-2}.min^{-1}$, $D_{(x)}$ is the diffusion coefficient in units of $mm^2.min^{-1}$, $C_{(x)}$ is the concentration of water molecules in units of $mol.mm^{-3}$, and $\mu_{(x)}$ is the chemical potential of water molecules in units of $J.mol^{-1}$; with all parameters being measured at a position x. The chemical potential of a state is defined as:

$$\mu = \mu_0 + RT \ln a \quad (61)$$

Where μ is the chemical potential of the state, with activity a, in units of $J.mol^{-1}$, μ_0 is the chemical potential of the standard state in $J.mol^{-1}$, R is the universal gas constant in $J.mol^{-1}.K^{-1}$, and T is the temperature of the system in K. When interactions between a species and itself are negligible it can be approximated as an ideal gas and the activity is then expressed by [8]:

$$a = \frac{P}{P_0} \quad (62)$$

Where p and p_0 are the partial pressures of the species in the state of interest, and in the standard state, respectively. This can be rewritten in terms of concentrations with reference to the ideal gas equation:

$$PV = nRT \tag{63}$$

$$P = n\frac{RT}{V} \tag{64}$$

Where P is the partial pressure of the species in $J.mm^{-3}$, V is the volume occupied by the diffusing species in mm^3, n is the number of moles of the diffusing species, and T is the temperature of the system in K. Thus, the partial pressures of the species within the two states are given by:

$$P = n\frac{RT}{V} \tag{65}$$

$$P_0 = n_0\frac{RT}{V} \tag{66}$$

Substituting (65) and (66) into (62), and noting that the volume and temperature of both states are identical:

$$\Rightarrow \quad a = \frac{n}{n_0} \tag{67}$$

The concentration of species within the state of interest, and in the standard state, are given by:

$$C = \frac{n}{V} \tag{68}$$

$$C_0 = \frac{n_0}{V} \tag{69}$$

Where C and C_0 are the concentration of the diffusing species in the state of interest, and in the standard state, respectively both in units of $mol.mm^{-3}$. Thus, rearranging (68) and (69), and substituting into (67):

$$\Rightarrow \ a = \frac{C}{C_0} \tag{70}$$

The derivation outlined above is only valid if the temperature and volume of the state of interest are the same as those of the standard state. Thus, to evaluate the validity of this derivation, the standard state must first be identified in the material of interest. Within the context of the model, the standard state is defined as that in which the material is in equilibrium with its conditioning atmosphere, at a given temperature and relative humidity. In other words, the net diffusive flux of water molecules into, or out of, the material is zero. For a material comprised of an infinite sheet, of thickness Δx, the time taken for it to attain its equilibrium moisture content within a given conditioning environment (t_{sat}) is observed to $t_{sat} \to 0$ as $\Delta x \to 0$. Thus, in a slice of material of thickness dx, at the material/atmosphere interface, equilibrium is attained in an infinitesimal time period dt. This implies that the surface of the material is representative of the standard state. Thus, if another state of thickness dx, at position x, is considered the above criteria are met if the temperature at the material surface, and at the position x, are identical.

In this work it is assumed that the time scale associated with a given DGEBA-DDA resin sample reaching thermal equilibrium, with its conditioning environment, is much smaller than that required for the material to attain its equilibrium moisture content. Thus, the heat and moisture diffusion processes are sufficiently decoupled to allow the thermal gradients within the material to be regarded as negligible. This implies that the temperature of the standard state (material surface) and any state of interest will be approximately equal. Hence the temperature requirement of the activity as a function of concentration derivation, is satisfied.

The equilibrium concentration of a species, absorbed within a material, can be related to the partial vapour pressure of the same species in the surrounding atmosphere by Henry's Law, provided that the interactions between the species and itself are negligible. Henry's Law is given by the following expression [8, 30]:

$$C_{(T)} = \ S_{(T)}\, p_{sat_{(T)}}\, RH_f \tag{71}$$

Where $C_{(T)}$ is the equilibrium concentration of the species within the material in $mol.mm^{-3}$, $S_{(T)}$ is the solubility of the species within the material in $mol.mm^{-3}.Pa^{-1}$, $p_{sat_{(T)}}$ is the partial vapour pressure of the species in the surrounding atmosphere, when the atmosphere is saturated with that species, in Pa, and RH_f is the ratio of the actual partial vapour pressure of the species in the surrounding atmosphere to its saturated partial vapour pressure. In the case of water vapour, RH_f is related to relative humidity by the following expression:

$$RH_f = \frac{RH}{100} \tag{72}$$

The solubility and saturated partial vapour pressure are both temperature dependent. The relationship between solubility and temperature takes the form of an Arrhenius relation [97]:

$$S_{(T)} = S_0 \, e^{\frac{-E_s}{RT}} \tag{73}$$

Where $S_{(T)}$ is the solubility in $mol.mm^{-3}.Pa^{-1}$, S_0 is the solubility as $T \to \infty$ in $mol.mm^{-3}.Pa^{-1}$, E_s is the activation energy in $J.mol^{-1}$, and T is the temperature in K. The terms S_0 and E_s are dependent upon both the material and absorbent species under consideration and must be determined experimentally.

The relationship between the saturated partial vapour pressure of water, and temperature, is well understood experimentally with various functions being proposed to describe the observed behaviour [98-100]. In this work the function suggested by Wagner et al [100] will be employed:

$$Ln\left(\frac{p}{p_c}\right) = \frac{T_c}{T}(a_1 v + a_2 v^{1.5} + a_3 v^3 + a_4 v^{3.5} + a_5 v^4 + a_6 v^{7.5}) \tag{74}$$

Where p is the saturated partial vapour pressure of water, in units of MPa, and T is the temperature in K. The term v is calculated from:

$$v = 1 - \frac{T}{T_c} \tag{75}$$

Values for the constants in equation (74) have been proposed by Wagner et al [100] and are shown below in Table 6.

Parameter	Value
p_c (MPa)	22.064
T_c (K)	647.096
a_1	-7.85951783
a_2	1.84408259
a_3	-11.7866497
a_4	22.6807411
a_5	-15.9618719
a_6	1.80122502

Table 6: Values for the constants in equation (74) proposed by Wagner et al [100].

The concentration of water in the standard state can be written, with reference to Henry's law (equation (3)), as:

$$C_{0_{(T)}} = S_{(T)}\, p_{sat_{(T)}}\, RH_f \tag{76}$$

Thus, the expression for activity becomes:

$$a = \frac{C}{C_0} = \frac{C}{S_{(T)}\, p_{sat_{(T)}}\, RH_f} \tag{77}$$

Substituting into the expression for chemical potential:

$$\mu = \mu_0 + RT\, ln\left[\frac{C}{S_{(T)}\, p_{sat_{(T)}}\, RH_f}\right] \tag{78}$$

Differentiating with respect to the x coordinate:

$$\frac{d\mu}{dx} = RT \frac{d}{dx}\left[\ln\left(\frac{C}{S_{(T)}\, p_{sat_{(T)}}\, RH_f}\right)\right] \tag{79}$$

$$\frac{d\mu}{dx} = \frac{S_{(T)}\, RT}{p_{sat_{(T)}}\, RH_f\, {S_{(T)}}^2\, C}\left[\left(S_{(T)}\, p_{sat_{(T)}} RH_f \frac{dC}{dx}\right) - \left(C\, p_{sat_{(T)}}\, RH_f \frac{dS}{dx}\right)\right] \tag{80}$$

After cancelling and collecting terms, equation (80) can be written as:

$$\frac{d\mu}{dx} = RT\left[\frac{1}{C}\frac{dC}{dx} - \frac{1}{S_{(T)}}\frac{dS}{dx}\right] \tag{81}$$

Thus, the chemical potential gradient has been expressed in terms of the solubility and concentration gradients. Substituting this expression into equation (60) for the diffusive flux:

$$J_{(x)} = -D_{(x)}\left[\frac{dC}{dx} - \frac{C}{S}\frac{dS}{dx}\right] \tag{82}$$

Equation (82) above is the expression derived by Yagoubi et al [8]. They then employed this equation in a finite element model to predict the evolution of water concentration with time. However, in this work a finite difference model will be employed. To model diffusion using the finite difference method, an expression relating the change in species concentration with time, at a position x, is required.

2.2.2.2.3. Extending the Yagoubi [8] Equation for use in the Finite Difference Method

The expression below describes the change in water concentration occurring in a time ∂t:

$$\frac{\partial C_{(x)}}{\partial t} = D_{(x)}\frac{\partial^2 C_{(x)}}{\partial x^2} \tag{83}$$

This is known as Fick's second law, where ∂C and ∂t are the infinitesimal change in concentration and time, in units of $mol.mm^{-3}$ and min respectively, and $D_{(x)}$ is the diffusion coefficient at a position x in units of $mm^2.min^{-1}$. It is possible to derive Fick's second law in terms of the expression for the diffusive flux in equation (82). Consider a volume element of area A and thickness Δx. If it is assumed that diffusion occurs only in the x-coordinate then the mass balance for this element can be written as:

$$\Delta N = (J_1 - J_2)\, A\, \Delta t \tag{84}$$

Where ΔN is the change in moles of the diffusive species within the volume element, Δt is the time period in min, and J_1 and J_2 are the fluxes through the left-hand and right-hand sides of the element respectively in units of $mol.mm^{-2}.min^{-1}$. Equation (84) can be rewritten in terms of concentration as:

$$\frac{\Delta C}{\Delta t} = (J_1 - J_2)\, \frac{A}{V} \tag{85}$$

As the volume of the element is given by $A\Delta x$, equation (85) becomes:

$$\frac{\Delta C}{\Delta t} = \frac{(J_1 - J_2)}{\Delta x} \tag{86}$$

The change in flux over the distance Δx can be written as:

$$\Delta J = J_2 - J_1 \tag{87}$$

Substituting (87) into (86):

$$\frac{\Delta C}{\Delta t} = -\frac{\Delta J}{\Delta x} \tag{88}$$

Which, in the limit when $\Delta t \rightarrow 0$ and $\Delta x \rightarrow 0$, becomes:

$$\frac{\partial C}{\partial t} = -\frac{\partial J}{\partial x} \tag{89}$$

With reference to (80), the flux gradient can be written as:

$$\frac{\partial J}{\partial x} = -\frac{\partial}{\partial x}\left[D_{(x)}\frac{\partial C}{\partial x} - \frac{D_{(x)}C_{(x)}}{S_{(x)}}\frac{\partial S}{\partial x}\right] \tag{90}$$

To aid the clarity of the derivations that follow, equation (90) can be written as:

$$\frac{\partial J}{\partial x} = -(A - B) \tag{91}$$

Where:

$$A = \frac{\partial}{\partial x}\left(D_{(x)}\frac{\partial C}{\partial x}\right) \tag{92}$$

And:

$$B = \frac{\partial}{\partial x}\left(\frac{D_{(x)}C_{(x)}}{S_{(x)}}\frac{\partial S}{\partial x}\right) \tag{93}$$

Applying the product rule for differentiation to equation (92), A can be expressed as:

$$A = \left(\frac{\partial C}{\partial x}\frac{\partial D}{\partial x}\right) + \left(D_{(x)}\frac{\partial^2 C}{\partial x^2}\right) \tag{94}$$

Applying the product rule for differentiation to equation (93), B becomes:

$$B = \left(\frac{\partial S}{\partial x}\frac{\partial}{\partial x}\left(\frac{D_{(x)}C_{(x)}}{S_{(x)}}\right)\right) + \left(\frac{D_{(x)}C_{(x)}}{S_{(x)}}\frac{\partial^2 S}{\partial x^2}\right) \tag{95}$$

Differentiating the first term in equation (95) using the quotient rule:

$$B = \left(\left(\frac{1}{S_{(x)}}\frac{\partial}{\partial x}\left(D_{(x)}\,C_{(x)}\right)\right) - \left(\frac{D_{(x)}\,C_{(x)}}{{S_{(x)}}^2}\frac{\partial S}{\partial x}\right)\right)\frac{\partial S}{\partial x} + \left(\frac{D_{(x)}\,C_{(x)}}{S_{(x)}}\frac{\partial^2 S}{\partial x^2}\right) \tag{96}$$

And finally, differentiating the term $\left(D_{(x)}\,C_{(x)}\right)$ with respect to x and multiplying out the bracket, B can be expressed as:

$$B = \left(\frac{C_{(x)}}{S_{(x)}}\frac{\partial D}{\partial x}\frac{\partial S}{\partial x}\right) + \left(\frac{D_{(x)}}{S_{(x)}}\frac{\partial C}{\partial x}\frac{\partial S}{\partial x}\right) - \left(\frac{D_{(x)}\,C_{(x)}}{{S_{(x)}}^2}\left(\frac{\partial S}{\partial x}\right)^2\right) + \left(\frac{D_{(x)}\,C_{(x)}}{S_{(x)}}\frac{\partial^2 S}{\partial x^2}\right) \tag{97}$$

Substituting the expressions for A and B, equations (94) and (97), into equation (91), the diffusive flux gradient can be written as:

$$\frac{\partial J}{\partial x} = \left(\frac{C_{(x)}}{S_{(x)}}\frac{\partial D}{\partial x}\frac{\partial S}{\partial x}\right) + \left(\frac{D_{(x)}}{S_{(x)}}\frac{\partial C}{\partial x}\frac{\partial S}{\partial x}\right) - \left(\frac{D_{(x)}\,C_{(x)}}{{S_{(x)}}^2}\left(\frac{\partial S}{\partial x}\right)^2\right) + \left(\frac{D_{(x)}\,C_{(x)}}{S_{(x)}}\frac{\partial^2 S}{\partial x^2}\right) - \frac{\partial C}{\partial x}\frac{\partial D}{\partial x} - D_{(x)}\frac{\partial^2 C}{\partial x^2} \tag{98}$$

Substituting equation (98) into equation (89), the following expression is obtained:

$$\frac{\partial C}{\partial t} = -\left(\frac{C_{(x)}}{S_{(x)}}\frac{\partial D}{\partial x}\frac{\partial S}{\partial x}\right) - \left(\frac{D_{(x)}}{S_{(x)}}\frac{\partial C}{\partial x}\frac{\partial S}{\partial x}\right) + \left(\frac{D_{(x)}\,C_{(x)}}{{S_{(x)}}^2}\left(\frac{\partial S}{\partial x}\right)^2\right) - \left(\frac{D_{(x)}\,C_{(x)}}{S_{(x)}}\frac{\partial^2 S}{\partial x^2}\right) + \frac{\partial C}{\partial x}\frac{\partial D}{\partial x} + D_{(x)}\frac{\partial^2 C}{\partial x^2} \quad (99)$$

When the diffusion coefficient and solubility are uniform throughout the material this reduces to:

$$\frac{\partial C_{(x)}}{\partial t} = D_{(x)}\frac{\partial^2 C_{(x)}}{\partial x^2} \quad (100)$$

Which is Fick's Second Law as introduced earlier in equation (83). Equation (89) describes the local change in water concentration resulting from diffusion of water molecules in the x-coordinate. It does not account for the local loss of water molecules, and hence concentration, that occurs as a consequence of the addition of water molecules to the polymer network as the hydrolysis reaction proceeds. To model this phenomenon, the term C_{abs} must be introduced to the diffusion equation.

2.2.2.2.4. Accounting for the Change in Water Concentration Resulting from the Addition of Water Molecules to the Polymer Network through the Hydrolysis Reaction

The expression below is the modified form of the diffusion equation (89) to account for the loss of water molecules as a result of hydrolysis.

$$\frac{\partial C}{\partial t} = -\frac{\partial J}{\partial x} - C_{abs} \quad (101)$$

Where C_{abs} is the concentration of water molecules binding to the polymer network per minute, as a result of the hydrolysis reaction, in units of $mol.mm^{-3}.min^{-1}$.

Earlier in this work it was suggested that the hydrolysis reaction could be modelled as a transformation from a state A to a state C in the form:

$$A \rightarrow B \rightarrow C$$

One mole of water molecules is required to hydrolyse one mole of fundamental units of type A to type B, or of type B to type C. Thus, the combined molar change in units A and B per minute is equal to the moles of water molecules binding with the polymer network per minute. With reference to the rate equations C_{abs} can be written as:

$$C_{abs} = -\frac{d}{dt}[A] + \frac{d}{dt}[C] \quad (102)$$

$$C_{abs} = K_{BC}S_f[W][A] + 2K_{AB}S_f[W][A] \quad (103)$$

$$C_{abs} = (K_{BC}[B] + 2K_{AB}[A])\, S_f[W] \quad (104)$$

Substituting this expression for C_{abs} into the diffusion equation (101):

$$\frac{\partial C}{\partial t} = -\frac{\partial J}{\partial x} - (K_{BC}[B] + 2K_{AB}[A])\, S_f[W] \quad (105)$$

Which accounts for the change in water concentration that arises from both the diffusion and hydrolysis processes.

2.2.2.2.5. Determination of the Local Diffusion Coefficient and Solubility within a Volume Element Located at a Position x within the Material

The diffusion coefficient and solubility of water within a material are properties determined by that material's chemical and physical structure. As hydrolysis proceeds there is an increase in OH group density with a corresponding reduction in cross-link density. These chemical and physical changes cause the material's diffusion coefficient and solubility to evolve as a function of the extent of hydrolysis. Thus, in a partially aged material it is possible for a range

of diffusion coefficients and solubilities to exist throughout the material's geometry. The extent of these property gradients is dependent upon the coupling between the diffusion and hydrolysis processes, becoming more pronounced as sample dimensions are increased and the processes become increasingly coupled. To model the diffusion coefficient and solubility as a function of the extent of hydrolysis, these two properties need to be related to the three fundamental unit types: A, B, and C. In the unaged state, the material is composed only of fundamental units of type A, and in the fully hydrolysed state only of type C. If the terms D_i and S_i are defined as the initial material diffusion coefficient and solubility respectively, and D_f and S_f as the values of the same parameters in the fully hydrolysed material, then:

$$D_A = D_i \tag{106}$$

$$D_C = D_f \tag{107}$$

$$S_A = S_i \tag{108}$$

$$S_C = S_f \tag{109}$$

Where D_A and D_C are the diffusion coefficients associated with fundamental units A and C respectively, in units of $mm^2.min^{-1}$, and S_A and S_C are the solubilities associated with units A and C in units of $mol.mm^{-3}.Pa^{-1}$. It is not possible to determine D_B and S_B experimentally, the diffusion coefficient and solubility associated with unit B, as no intermediate state comprised purely of unit B occurs during hydrolysis as the rate constants associated with the two hydrolysis processes (K_{AB}, K_{BC}) do not satisfy the requirement that $K_{BC} \ll K_{AB}$ necessary to decouple the two hydrolysis steps. However, as both reaction steps: $A \rightarrow B$ and $B \rightarrow C$, are chemically identical, involving hydrolysis of one cross-link and the addition of one OH group to the polymer network, it is reasonable to assume that the changes in diffusion coefficient and solubility brought about by each hydrolysis step are identical. That is to say, each hydrolysis reaction contributes a fixed quantity to the fundamental unit's diffusion coefficient and solubility. Thus, D_B and S_B can be expressed as:

$$D_B = \frac{1}{2}(D_A + D_C) \tag{110}$$

$$S_B = \frac{1}{2}(S_A + S_C) \quad (111)$$

The average value of the solubility and diffusion coefficient, within a volume element of DGEBA-DDA resin at a given point in the hydrolysis process, can be obtained by fractionally combining the contributions from each type of fundamental unit:

$$D_{ve} = D_A \frac{[A]}{[FU]} + D_B \frac{[B]}{[FU]} + D_C \frac{[C]}{[FU]} \quad (112)$$

$$S_{ve} = S_A \frac{[A]}{[FU]} + S_B \frac{[B]}{[FU]} + S_C \frac{[C]}{[FU]} \quad (113)$$

Where D_{ve} and S_{ve} are the average diffusion coefficient and average solubility for the volume element, in units of $mm^2.min^{-1}$ and $mol.mm^{-3}.Pa^{-1}$ respectively.

2.2.2.2.6. Numerical Analysis of the Diffusion-Hydrolysis Equation

To predict the evolution of the water molecule concentration profile within a material, as a function of conditioning time, the governing diffusion equation must be solved subject to a set of boundary conditions. However, the complexity of the combined diffusion-hydrolysis phenomena renders the task of obtaining an exact analytical solution difficult. In this work numerical methods have been employed, more specifically the finite difference method, to approximate the derivatives within the governing equation allowing the complex behaviour occurring within the material to be modelled.

2.2.2.2.7. Finite Difference Method

The mathematical formalism that underpins the finite difference method is that of the Taylor series expansion [80]. The value of a function $f_{(a)}$ at a position $a + h$ can be expressed in the form of a Taylor Expansion as:

$$f_{(a+h)} = f_{(a)} + f'_{(a)}\, h + \frac{1}{2} f''_{(a)}\, h^2 + \ldots + \frac{1}{n!} f^n{}_{(a)}\, h^n + O_{(h^{n+1})} \quad (114)$$

The value of the derivative of $f'_{(a)}$ can be approximated by considering just the first two terms of the Taylor expansion:

$$f_{(a+h)} \approx f_{(a)} + f'_{(a)}h \tag{115}$$

$$f'_{(a)} \approx \frac{f_{(a+h)} - f_{(a)}}{h} \tag{116}$$

Where the approximation tends to the true value of $f'_{(a)}$ in the limit where the step size h tends to zero. The error in the approximation is related to the truncation of terms in the Taylor expansion. With reference to equation (114) the exact solution of $f'_{(a)}$ can be written as:

$$f'_{(a)} = \frac{f_{(a+h)} - f_{(a)}}{h} + O_{(h)} \tag{117}$$

Thus, the difference between the approximation and the actual value of $f'_{(a)}$ can be written as:

$$\frac{f_{(a+h)} - f_{(a)}}{h} - f'_{(a)} = O_{(h)} \tag{118}$$

Thus, it is apparent that the difference between the approximation and the actual value of $f'_{(a)}$, in other words the error, is proportional to h. This is termed a first order approximation. Higher order approximations can be obtained by considering further terms in the Taylor expansion with a corresponding reduction in the approximation error. A second order approximation to $f'_{(a)}$ can be deduced by considering the values of the function $f_{(x)}$ at two equidistant points either side of $f_{(a)}$: $f_{(a+h)}$ and $f_{(a-h)}$. These can be expanded into Taylor series to give:

$$f_{(a+h)} = f_{(a)} + f'_{(a)}\,h + \frac{1}{2} f''_{(a)}\,h^2 + O_{(h^3)} \tag{119}$$

$$f_{(a-h)} = f_{(a)} - f'_{(a)}\,h + \frac{1}{2} f''_{(a)}\,h^2 + O_{(h^3)} \tag{120}$$

Subtracting equation (120) from equation (119), the following expression is arrived at:

$$\frac{f_{(a+h)} - f_{(a-h)}}{2h} = f'_{(a)} + O_{(h^2)} \quad (121)$$

Thus, the value of $f'_{(a)}$ can be approximated as:

$$f'_{(a)} \approx \frac{f_{(a+h)} - f_{(a-h)}}{2h} \quad (122)$$

Which is a second order approximation with an error proportional to h^2.

The second derivative of the function $f_{(x)}$, at a point a, namely $f''_{(a)}$, can be approximated through a similar treatment as that employed for the second order approximation of $f'_{(a)}$. Considering two equidistant points either side of $f_{(a)}$; $f_{(a+h)}$ and $f_{(a-h)}$, then their Taylor expansions can be written as:

$$f_{(a+h)} = f_{(a)} + f'_{(a)} h + \frac{1}{2} f''_{(a)} h^2 + \frac{1}{6} f'''_{(a)} h^3 + O_{(h^4)} \quad (123)$$

$$f_{(a-h)} = f_{(a)} - f'_{(a)} h + \frac{1}{2} f''_{(a)} h^2 - \frac{1}{6} f'''_{(a)} h^3 + O_{(h^4)} \quad (124)$$

Combining these two expressions through addition:

$$\frac{f_{(a+h)} + f_{(a-h)} - 2f_{(a)}}{h^2} = f''_{(a)} + O_{(h^2)} \quad (125)$$

Thus, the second order approximation to the second derivative $f''_{(a)}$ is given by:

$$f''_{(a)} \approx \frac{f_{(a+h)} + f_{(a-h)} - 2f_{(a)}}{h^2} \quad (126)$$

2.2.2.2.8. Mesh Construction

As discussed previously, the finite difference method works by discretising a continuous function $f_{(x)}$ over a variable x. Thus, the function is represented by an array of discrete points separated by a step h in the x coordinate. The derivatives of $f_{(x)}$ can then be evaluated at each discrete point with reference to the appropriate finite difference approximation. The governing equation for the diffusion-hydrolysis process describes the change in water concentration, with respect to time, at a position x (see equation (105)). The boundary conditions for x are:

$$0 \leq x \leq d \quad (127)$$

Where d is the material thickness in mm. The material/atmosphere interface is located at $x = 0$ and $x = d$; $x = \frac{d}{2}$ represents the centre of the material. Under certain conditions, the resulting concentration profile within the material will be symmetrical about the plane $x = \frac{d}{2}$ for all conditioning times t. The criteria for symmetry are given in the list below:

1. Diffusion occurs through both sides of the material.

2. The conditioning environments on either side of the material are identical; more specifically that the concentration boundary conditions at $x = 0$ and $x = d$ are identical for all conditioning times ($C_{(0,t)} = C_{(d,t)}$ for $t: 0 \rightarrow \infty$).

3. The diffusion coefficient, solubility, and fundamental unit concentration profiles are symmetrical about the plane $x = \frac{d}{2}$ at $t = 0$.

4. The temperature profile throughout the material is symmetrical, about the plane $x = \frac{d}{2}$, for all conditioning times t.

For the materials modelled in this work the conditions for symmetry are satisfied; thus, the governing equation only needs to be solved in the range:

$$0 \leq x \leq \frac{d}{2} \tag{128}$$

This simplification has the effect of improving the efficiency of the finite difference model by reducing the computation time required to predict the concentration profile, throughout the material, at a conditioning time t. The computation time that is saved can be invested in increasing the resolution of the calculated concentration profiles (reducing h and thus increasing the density of discrete position points within the material) or improving the model accuracy by reducing the time step employed in the finite difference approximations.

In Figure 14 below the mesh representation is depicted for one half of a material, satisfying the symmetry criteria, exposed to a conditioning atmosphere at the material/atmosphere interface located at $x = 0$.

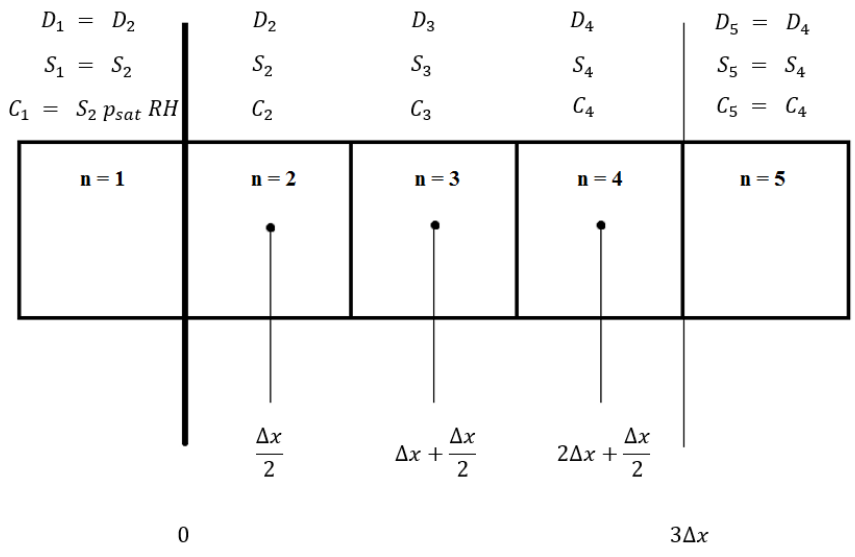

Figure 14: Mesh representation of a material exposed to a conditioning environment.

The material/atmosphere interface is located at $x = 0$, and the material centre at $x = 4\Delta x$, thus the thickness of the material is $8\Delta x$. An element is associated with each discrete point in the x-coordinate, with a volume given by:

$$V_E = wl\Delta x \tag{129}$$

Where V_E is the volume of the element in mm^3, Δx is the thickness of the element in mm, and w and l are the material width and length in the y and z coordinates respectively in units of mm. The total number of elements within the mesh is given by:

$$n_E = \frac{d}{2\Delta x} + 1 \tag{130}$$

The first and last elements, $n = 1$ and $n = n_E$ respectively, are boundary elements representing the material/atmosphere interface and material centre respectively. These boundary elements are comprised of infinitesimally thin slices of material of thickness dx and volume dV located at $x = 0$ and $x = \frac{d}{2}$. The volumes of these elements depicted in Figure 14 are only figurative to aid visualisation of the material mesh and are not representative of their actual size in relation to the other elements. C_n, S_n, and D_n are the concentration, solubility, and diffusion coefficient associated with element n, where n takes values in the range:

$$1 \leq n \leq n_E \tag{131}$$

The boundary element at the material/atmosphere interface, designated element one ($n = 1$), takes the diffusion coefficient and solubility values of its neighbour: element two ($n = 2$).

$$D_1 = D_2 \tag{132}$$

$$S_1 = S_2 \tag{133}$$

The boundary element has an infinitesimal thickness dx and thus attains equilibrium with the conditioning atmosphere in the infinitesimal time period dt. Furthermore, the conditioning

atmosphere is assumed to be an infinite source, in other words the partial vapour pressure of water in the atmosphere is unaffected by the loss of water molecules that arises from absorption of water vapour by the material. Under these two conditions, the boundary element is always at equilibrium with the conditioning atmosphere and thus, with reference to Henry's law (equation (3)), the concentration of the boundary element can be expressed as:

$$C_{(0,t)} = S_{(T)}\, p_{sat\,(T)}\, RH_f \tag{134}$$

Which is true for all conditioning times t.

The boundary element at the material centre, designated as element n_E ($n = n_E$), takes the diffusion coefficient, solubility, and concentration value of its neighbouring element: $n = n_E - 1$. This is an approximation, as before equilibrium is achieved a concentration gradient will exist over the distance $\frac{\Delta x}{2}$; between element $n_E - 1$ and the element at the material centre n_E. This will also be true of the material diffusion coefficient and solubility if these parameters are time dependent. Therefore, care should be taken when interpreting model predictions at the centre of the material ($x = \frac{d}{2}$). As the property profiles of the material are symmetrical about the plane $x = \frac{d}{2}$ the net diffusive flux at $x = \frac{d}{2}$ is zero. When modelling only one half of a material, in a symmetrical system, this condition is satisfied by setting the diffusive parameters of the boundary element (n_E), at $x = \frac{d}{2}$, equal to those of its neighbouring element at $x = \frac{d}{2} - \frac{\Delta x}{2}$. Thus:

$$D_{n_E} = D_{(n_E - 1)} \tag{135}$$

$$S_{n_E} = S_{(n_E - 1)} \tag{136}$$

$$C_{n_E} = C_{(n_E - 1)} \tag{137}$$

2.2.2.2.9. Finite Difference Approximation of the Governing Equation

Having discretised the dimension of the material in the x-coordinate into a number of discrete points, or elements, finite difference approximations are then applied to the diffusion equation. The governing equation for diffusion, in DGEBA-DDA resin, is given by:

$$\frac{\partial C}{\partial t} = -\frac{\partial J}{\partial x} - C_{abs} \tag{138}$$

Replacing the derivative $\frac{\partial J}{\partial x}$ with the second order, and $\frac{\partial C}{\partial t}$ with the first order, finite difference approximations:

$$\frac{\partial}{\partial t} C_{(t,x)} \approx \frac{C_{(t+\Delta t,x)} - C_{(t,x)}}{\Delta t} \tag{139}$$

$$\frac{\partial}{\partial x} J_{(t,x)} \approx \frac{J_{(t,x+\Delta x)} - J_{(t,x-\Delta x)}}{2\Delta x} \tag{140}$$

Where x is the coordinate of the element within the mesh, t is the time elapsed since conditioning was initiated, Δx is the step between mesh points or element thickness in the x coordinate, and Δt is the time-step. Substituting equations (139) and (140) into equation (138), one obtains:

$$\frac{C_{(t+\Delta t)} - C_{(t,x)}}{\Delta t} = -\left[\frac{J_{(t,x+\Delta x)} - J_{(t,x-\Delta x)}}{2\Delta x}\right] - C_{abs} \tag{141}$$

Which can be rearranged to obtain:

$$C_{(t+\Delta t,x)} = -\left[\frac{J_{(t,x+\Delta x)} - J_{(t,x-\Delta x)}}{2\Delta x}\right]\Delta t + C_{abs}\Delta t + C_{(t,x)} \tag{142}$$

This can be simplified by introducing the variable G:

$$G = -\left[\frac{J_{(t,x+\Delta x)} - J_{(t,x-\Delta x)}}{2\Delta x}\right] + C_{abs} \tag{143}$$

Where G is the concentration gradient with respect to time, at time t and position x, in units of $mol.mm^{-3}.min^{-1}$. Substituting equation (143) into equation (142):

$$C_{(t+\Delta t,x)} = G\Delta t + C_{(t,x)} \quad (144)$$

Thus, the concentration at a time $t + \Delta t$, at a position x, can be obtained by taking the concentration at an earlier time $C_{(t,x)}$ and adding to it the change in concentration that occurs over the time-step Δt, namely $G\Delta t$.

2.3. Results and Discussion

2.3.1. DMTA Investigation

2.3.1.1. Analysis of DMTA Data

The DMTA spectra for film samples aged at a range of temperatures, and for a variety of conditioning times, have been obtained. It is now necessary to extract the relevant parameters (glass transition temperature, full width at half maximum (FWHM), loss tangent peak height, background loss tangent) so that the behaviour of these properties as a function of time, and temperature, can be understood. Observation of the DMTA spectra would suggest that a Lorentzian function is a good approximation to the shape of the loss tangent curve. Therefore, the four desired parameters can be obtained by fitting a Lorentzian function to the loss tangent/temperature relationship of each DMTA spectrum. However, the accuracy of the fitting process is affected by how closely the loss tangent curve resembles a Lorentzian function.

The presence of artefacts, or noise, in the DMTA spectrum can result in deviations from this functional form leading to the introduction of errors into the parameters obtained through the fitting process. For this reason, it is first necessary to inspect each DMTA spectrum to ensure that it is free of noise and/or artefacts. If either are present, then steps will be taken to remove these anomalies without affecting the validity of the parameters to be obtained through the fitting process. In the section that follows two important anomalies are discussed: an artefact that is associated with the tensile geometry employed in the DMTA of thin films, and noise that is inherent to all DMTA experiments. A methodology is then outlined for removing these effects from the DMTA data prior to the function fitting process.

2.3.1.1.1. Noise in the Loss Tangent Above T_g

Figure 15 and Figure 16 below show the loss tangent/temperature and storage modulus/temperature profiles for two epoxy resin films.

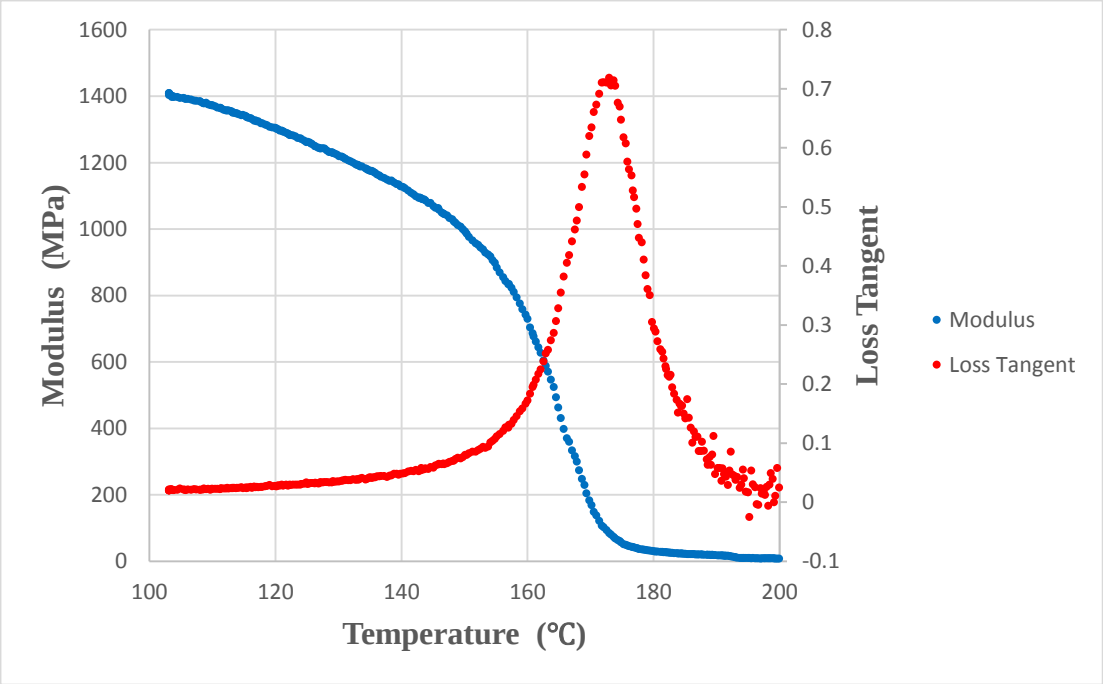

Figure 15: DMTA spectrum for an epoxy film in which the force precision of the instrument is not exceeded.

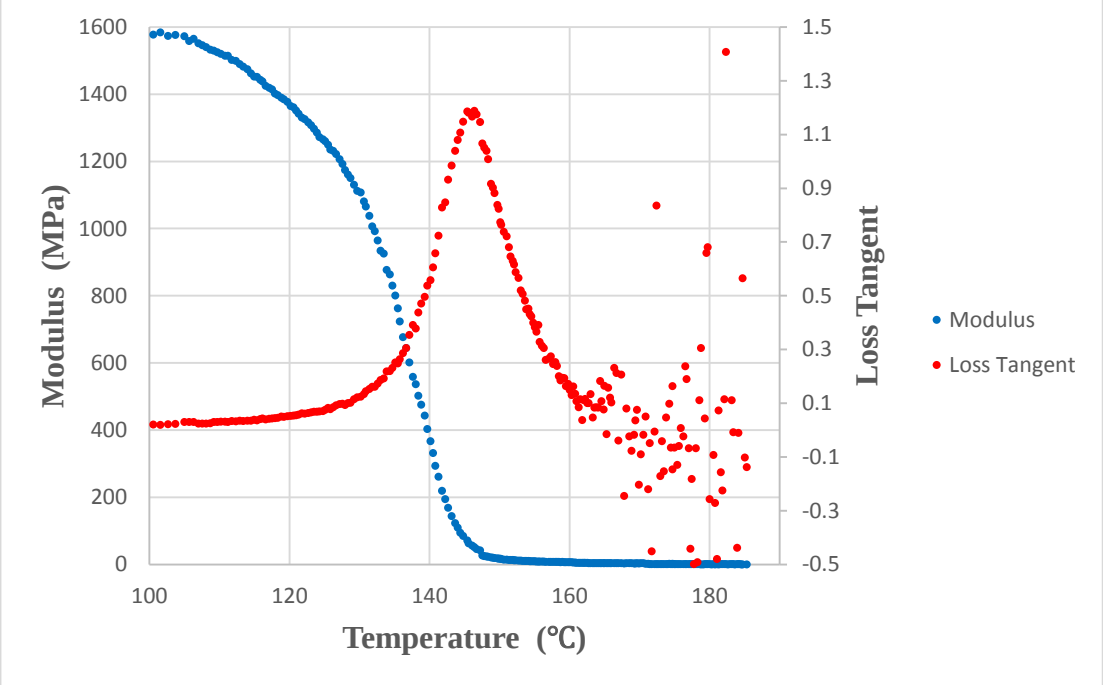

Figure 16: DMTA spectrum for an epoxy film in which the force precision of the instrument is exceeded above 160°C.

Referring to the loss tangent curve in Figure 15 it is apparent that the loss tangent data becomes noisier when the film is above its glass transition temperature ($T_g \approx 174$℃) as the measurements of the loss tangent exhibit a greater degree of dispersion when temperatures are in excess of the T_g of the material. This arises as a consequence of the magnitude of the dynamic force, this being the force employed to achieve the selected strain in the DMTA experiment, approaching the limits of the precision to which this quantity can be determined by the instrument. If the dynamic force drops below the force precision of the DMTA then the resulting data becomes meaningless as the DMTA is unable to precisely measure the value of the dynamic force and this variable is required for the calculation of material properties (loss tangent, storage modulus). In the DMTA spectrum shown in Figure 16, the dynamic force falls below the force precision of the instrument at a temperature of ~165℃ resulting in a large amount of dispersion in the measured loss tangent data points.

When initiating a DMTA scan, the user specifies a strain to be employed during the course of the experiment. A dynamic force is then applied to the sample to achieve the desired strain. As the temperature of the material increases, during a scan with an increasing temperature profile, its Young's modulus falls and thus the dynamic force required to achieve the given strain will also decrease. When the material passes through its glass transition, transforming from a glassy to a rubbery state, there is large reduction in material modulus and hence a corresponding large reduction in the dynamic force. This accounts for the tendency of the dynamic force to fall below the precision of the instrument when the DMTA exceeds the T_g of the material being tested. The impact of this effect can be mitigated by selecting a higher strain at the start of the DMTA experiment. This increases the magnitude of the dynamic force ensuring that its value will remain above the force precision of the instrument at temperatures in excess of T_g. However, a caveat of increasing the strain is that there is an accompanying increase in the stress within the epoxy film which increases the potential for the film to break during the experiment.

Breakage of a sample during a DMTA experiment results in the loss of any data that would have been obtained at temperatures above the failure temperature. In most circumstances this renders the DMTA spectrum unusable and thus the data must be discarded. As the samples employed within this work have been conditioned over extended time periods, ~6.5 months for films conditioned at 60℃, it is important to reduce the risk of sample breakage from occurring. As a result, lower strain values have been employed in these DMTA experiments even though this produced greater noise in the loss tangent data at temperatures in excess of T_g. However, this was preferable than to risk sample failure during the DMTA experiment.

This decision appears reasonable as noise in the loss tangent data above T_g only impacts the determination of the FWHM, associated with the loss tangent curve, and the value of the background loss tangent in the region above the T_g. As the loss tangent curve is approximately symmetrical, and the value of the background loss tangent is similar on either side of the peak, the effect of noise affecting the fitting process can be negated by only considering loss tangent measurements for the material when it is the glassy, or glassy/rubbery, phase and neglecting all measurements of the loss tangent in the rubber phase. This was achieved through the following methodology. First, the height of the loss tangent peak was determined by eye and then this value was divided by two. Two temperatures are associated with this value of the loss tangent and their difference is equal to the FWHM. The higher of these two temperatures was taken as the cut off point for the loss tangent/temperature data with no measurements above this temperature being employed in the Lorentzian fitting process. In Figure 17 below the effect of this cutting process on the DMTA spectrum is shown before the application of the function fitting process. Although a large number of samples exhibited negligible amounts of noise in the region above their T_g, the cutting process was performed on the spectra of all samples to ensure uniformity in the processing of the experimental data.

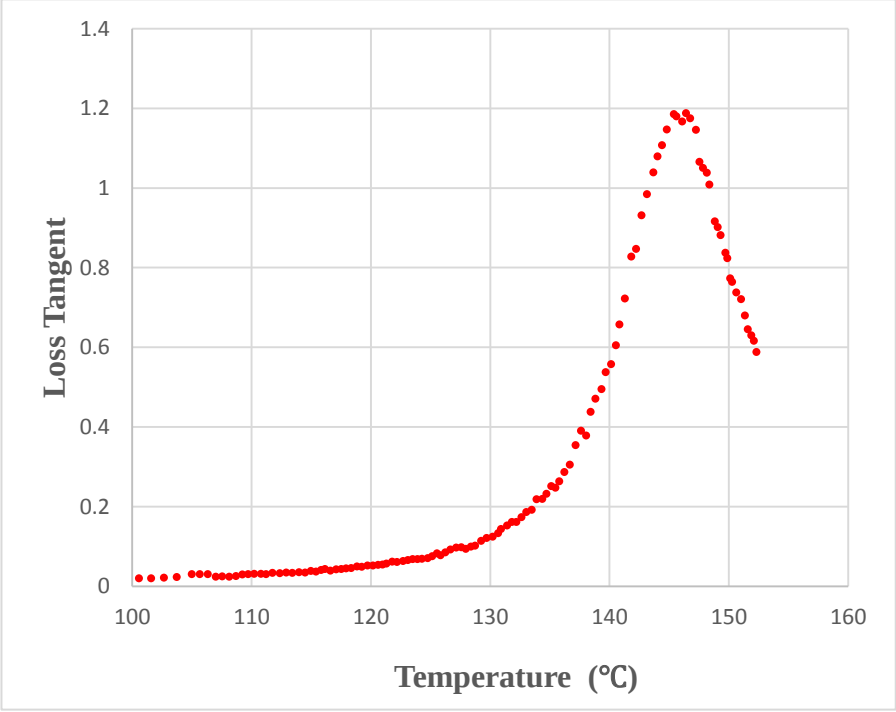

Figure 17: DMTA spectrum for an epoxy film showing the removal of noisy data points above material T_g prior to the fitting process.

2.3.1.1.2. Tensile Geometry Artefacts

The DMTA spectrum presented below in Figure 18 exhibits artefacts in both the loss tangent and storage modulus in the temperature range ~131℃ to ~142℃, just below the material T_g of 146℃. These artefacts arise as a consequence of inadequate static force being applied to the film in the initial setup of the DMTA experiment.

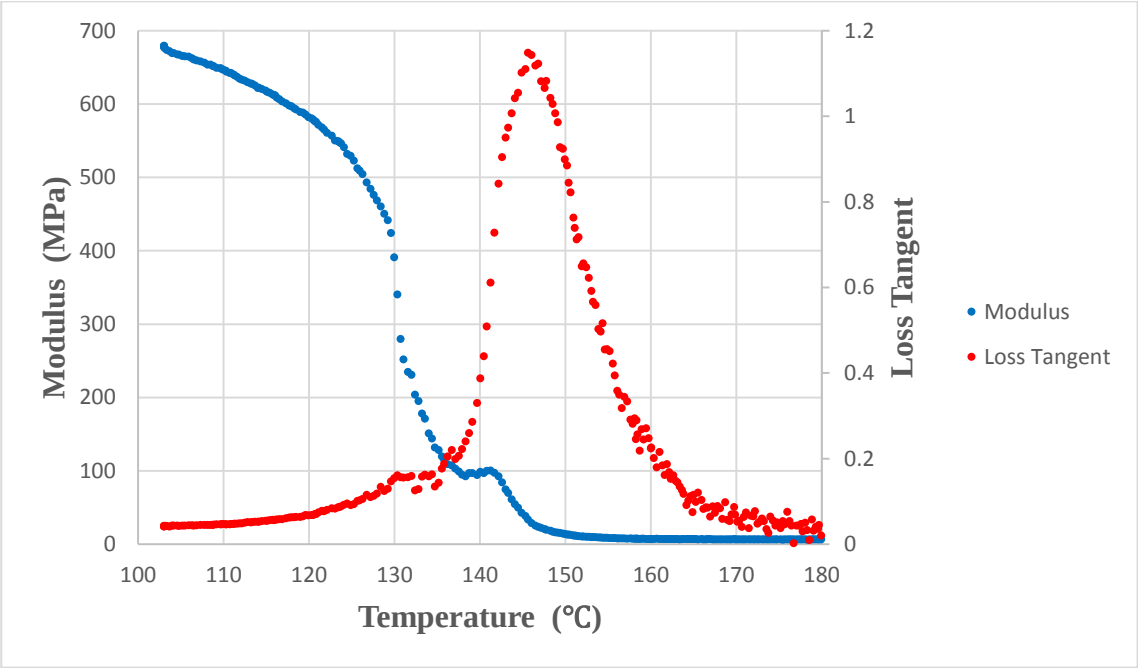

Figure 18: DMTA spectrum for an epoxy film showing tensile artefacts in the 131℃-142℃ temperature range.

In order to explain this artefact, it is first necessary to understand the mechanism that underlies a tensile geometry DMTA experiment. When a sample is tested in tensile geometry [51], one end is clamped to the driveshaft of the DMTA and the other end to the tensile geometry frame; this being located directly above the driveshaft. The sample is then subjected to a stress cycle whereby a dynamic force is first applied in a downwards direction, putting the sample under tension, until the desired strain is attained. After this maximum strain is attained the dynamic force relaxes before being applied in an upwards direction, putting the sample under compression, until the desired strain is attained once again. Finally, the dynamic force is relaxed to zero and the sample returns to its original length. The above process represents one complete stress cycle. The value of the dynamic force in both halves of the stress cycle (tensile and compressive) is used to determine the DMTA measured parameters: loss tangent and storage modulus, as the force required to achieve a given strain is identical, regardless of whether it be a tensile or compressive stress. However, when the samples are in the form of thin films (d < 0.075 mm), such as the DGEBA-DDA films employed in this work, it is possible for the sample to buckle when a

compressive stress is applied. This phenomenon significantly reduces the dynamic force required to attain the desired strain in the upwards dimension and thus the two dynamic forces, tensile and compressive, are no longer identical which leads to incorrect measurement of the loss tangent and storage modulus.

To prevent the sample from buckling during tensile DMTA experiments a pre-load is applied to the sample when the DMTA experiment is being setup. This involves clamping the sample to the driveshaft as before, however, before the sample is clamped to the tensile frame a pre-load is applied to the driveshaft in the form of a static force. This displaces the driveshaft in the upwards direction. The sample is then clamped to the tensile frame and the pre-load removed. This application of a static force puts the sample under tension. It is recommended that the value of the static force be twice the value of the dynamic force being employed within the DMTA experiment to achieve the desired strain [101]. With the sample under tension, it is not possible for buckling to occur in the second half of the stress cycle when the upwards directional force is applied.

Although the static force is initially selected to be at least twice the value of the dynamic force, it is possible for it to fall below the value of the dynamic force during the course of the DMTA experiment. This can occur because as the sample is heated during the experiment it expands and this expansion has the effect of reducing the tensile pre-load acting upon the material, thus causing the static force to decrease. This effect becomes more pronounced as the material approaches its glass transition temperature and begins to yield under the applied static force. This yielding increases the length of the sample, decreasing the tensile pre-load and thus further decreasing the static force. Inspecting the force data that accompanies the DMTA spectrum in Figure 18, it is evident that at 100℃ the static force is already less than the dynamic force (Figure 19).

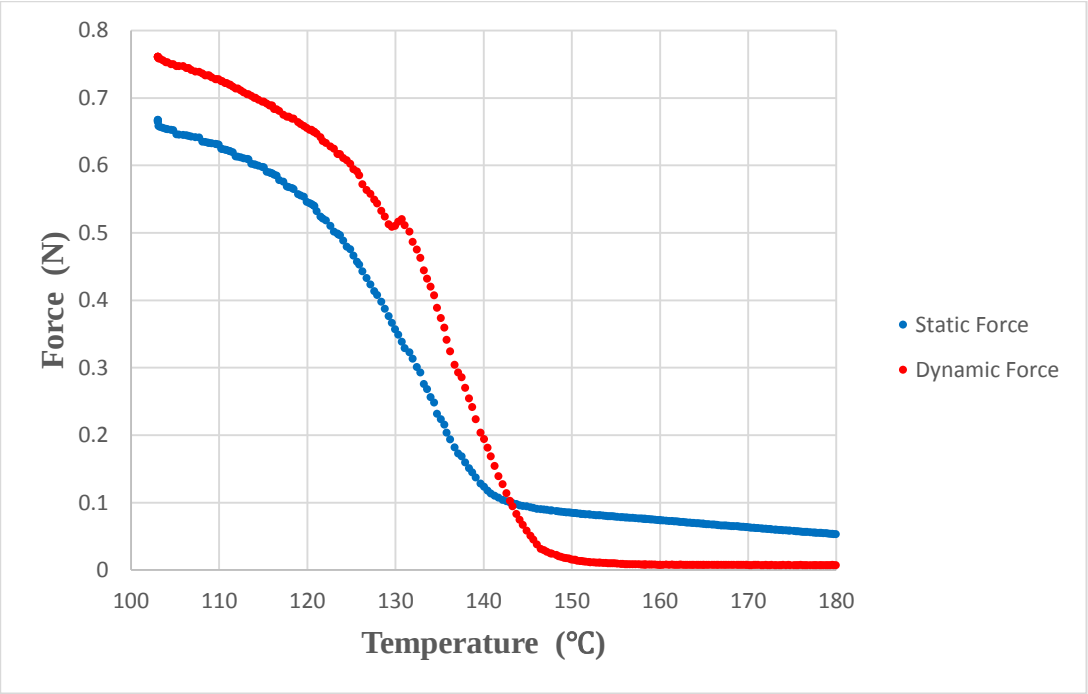

Figure 19: Accompanying dynamic and static force data for the DMTA spectrum in Figure 18.

However, the loss tangent and storage modulus show no unusual behaviour until a temperature of ~131℃ is reached. As the material T_g is 146℃ this would suggest that the effect of sample buckling only becomes substantial in the region where the material begins to undergo its glass/rubber transition. A possible explanation for this observed effect is that the large reduction in material modulus, associated with the onset of the glass transition, makes the sample more susceptible to buckling when placed under compression. As the glass transition is approached, the dynamic force falls below the static force at a temperature of ~142℃ and an accompanying recovery in modulus can be observed in Figure 18, indicating that buckling is no longer occurring. For the remainder of the DMTA experiment the static force remains greater than the dynamic force and no further artefacts are observed. In Figure 20 the DMTA spectrum for a different epoxy film is shown along with its accompanying force data in Figure 21.

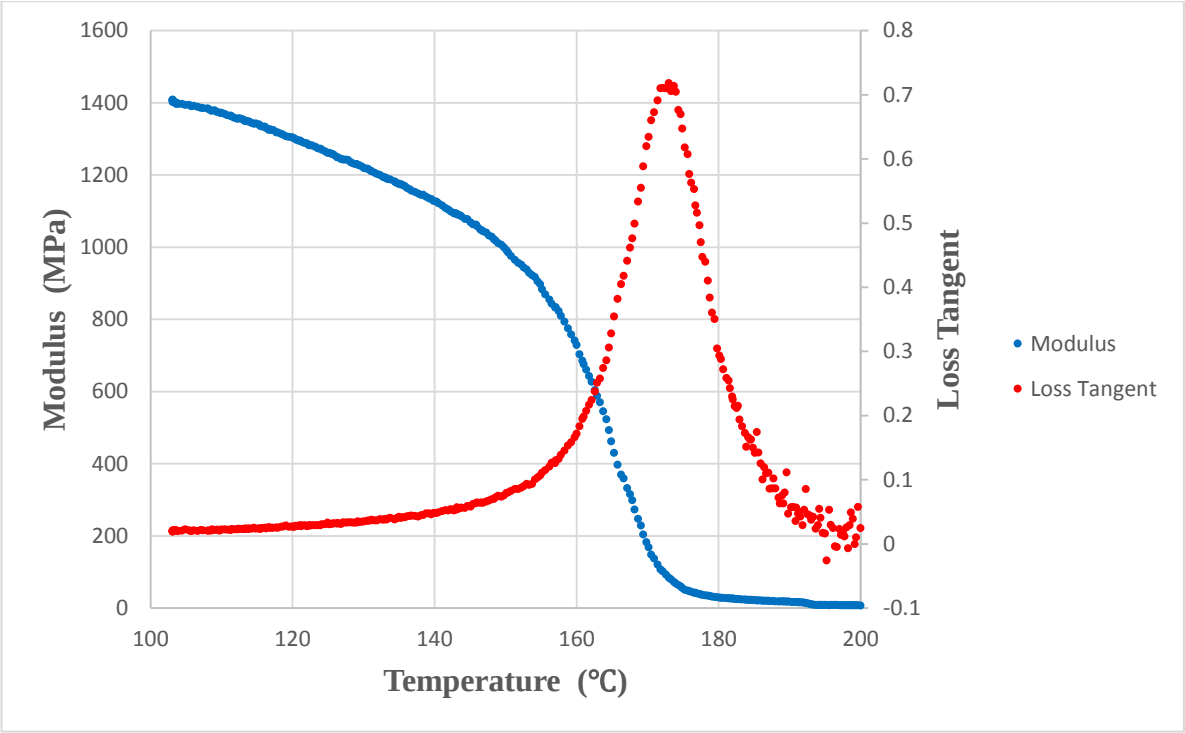

Figure 20: DMTA spectrum for an epoxy resin film.

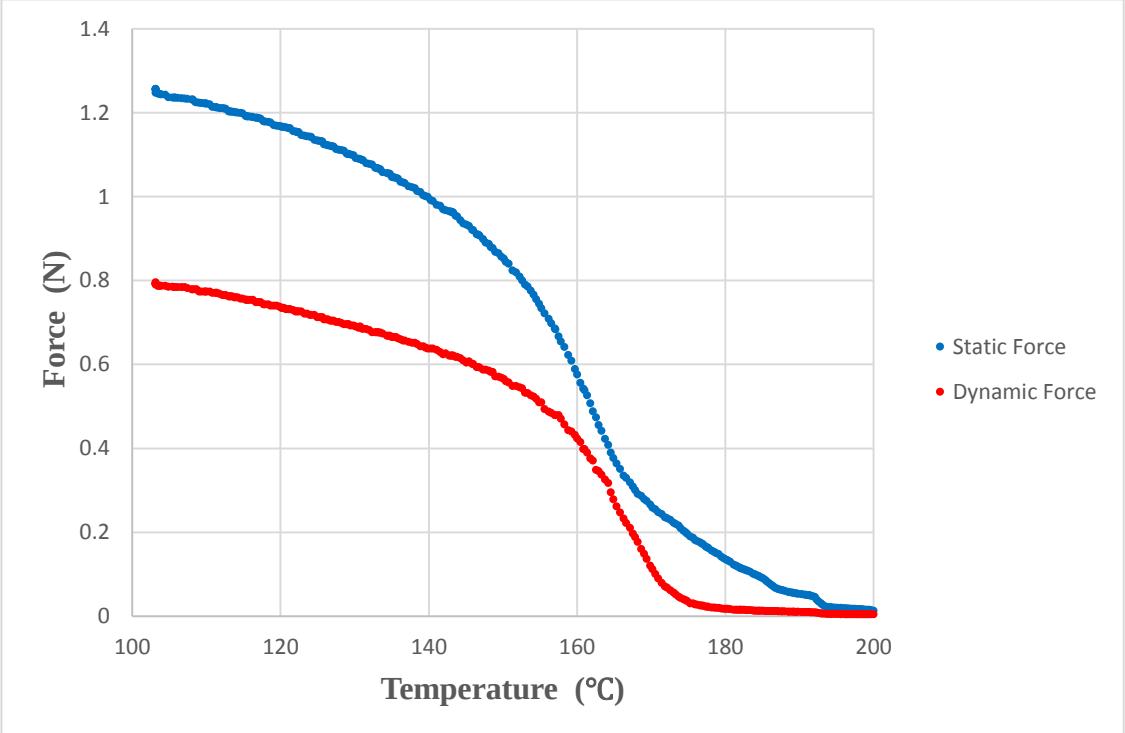

Figure 21: Accompanying dynamic and static force data for the DMTA spectrum in Figure 20.

No buckling artefacts are present in the DMTA spectrum shown in Figure 20, and Figure 21 confirms that the static force is always greater than the dynamic force, even in the region of the glass transition temperature.

One method for ensuring that the static force always remains greater than the dynamic force is to apply a large pre-load to the sample during the initial setup of the DMTA experiment. However, as with the case for the magnitude of the dynamic force discussed in the previous section, utilisation of high static forces increases the risk of coupon failure during the DMTA experiment. For this reason, only the recommended pre-load was applied at the beginning of each DMTA experiment, that being twice the value of the initial dynamic force that is required to achieve the desired strain [101].

As the region of the DMTA experiment affected by this artefact coincides with the onset of the loss modulus curve, it has a significant effect upon the Lorentzian fitting process. However, in all the DMTA spectra where this artefact was present, the value of the static force always rose above the value of the dynamic force before the peak of the loss tangent curve was observed. Thus, the value of the glass transition temperature, loss tangent peak height, and background loss tangent, are unaffected by this artefact. The FWHM cannot be accurately deduced in these spectra however as the artefact distorts one side of the loss tangent curve and thus the value of this parameter is affected.

The methodology for removing the buckling artefact from the DMTA spectra was as follows. The affected region of the DMTA spectrum was determined by identifying discontinuities in the loss tangent/temperature and storage modulus/temperature profiles. The loss tangent data points in this region where then removed. As this can involve removing a substantial number of data points from one side of the loss tangent curve, the FWHM values obtained from these spectra were discarded. In Figure 22 below, the effect of this cutting process on the DMTA spectrum shown in Figure 18, is depicted.

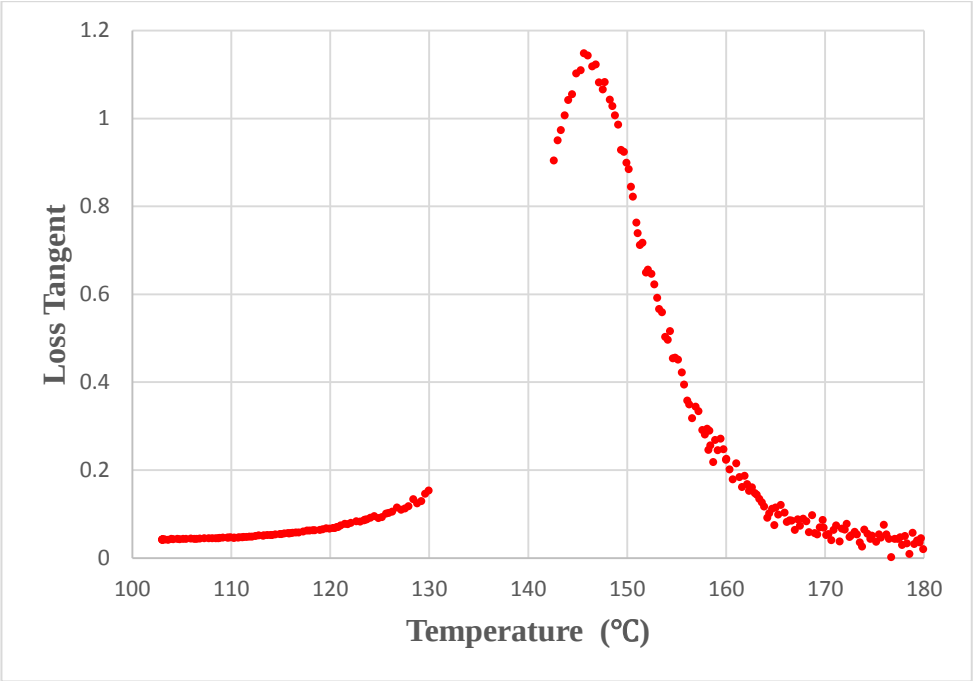

Figure 22: DMTA spectrum for an epoxy resin film showing removal of the buckling artefact prior to the fitting process.

2.3.1.1.3. Extent of the Presence of DMTA Artefacts

All of the DMTA spectra exhibited some degree of noise at temperatures in excess of the glass transition temperature of the material and for this reason the first cutting process was applied to all of the spectra. Four samples were affected by the buckling artefact, and of these four, three could be cleaned with the second cutting process. These samples have been designated with an (A) after their sample identifier. However, one of these samples was affected extensively by the buckling artefact such that the second cutting process was not appropriate. For this sample, no function fitting was undertaken and the glass transition temperature was determined by visual observation. No other parameters were taken from this spectrum as the presence of the buckling artefact made their determination difficult. This sample is designated with an (E) following its sample identifier.

2.3.1.1.4. Determination of Loss Tangent Peak Height

Fitting a Lorentzian function to the loss tangent curve allows the determination of the four parameters that characterise the shape of the distribution: the height of the loss tangent peak above the background loss tangent (H), the background loss tangent ($tan\delta_b$), the FWHM (w), and the glass transition temperature (T_g). With regards to the loss tangent peak height, it is the

actual height of the peak observed in the DMTA spectrum that is required. This can be obtained from:

$$H_a = H + tan\delta_b \quad (145)$$

Where H_a is the actual height of the loss tangent peak.

2.3.1.1.5. Estimation of Errors

Errors associated with each of the five parameters were estimated by referring to the parameter values obtained from unconditioned samples. Four unconditioned samples were tested and thus each parameter was measured four times. The standard deviations of the measurements associated with each parameter were then calculated. These were taken to be representative of the error associated with each parameter at any point during the conditioning process.

Parameter	$\boldsymbol{\Delta H}$	$\boldsymbol{\Delta w}$ (℃)	$\boldsymbol{\Delta T_g}$ (℃)	$\boldsymbol{\Delta tan\delta_b}$	$\boldsymbol{\Delta H_a}$
Error	0.0084	0.28	0.33	0.003	0.0089

Table 7: Errors associated with each of the Lorentzian parameters. These were taken to be equal to the standard deviations of the parameters obtained from the unconditioned samples.

Where H is the height of the loss tangent peak above the background loss tangent, w is the full width at half maximum (FWHM), $tan\delta_b$ is the background loss tangent, and H_a is the actual height of the loss tangent peak as observed in the DMTA spectrum.

2.3.1.1.6. Loss Tangent Curve Parameters Obtained for Each Sample as a Function of Conditioning Time and Temperature

The parameter values obtained for each sample, from the Lorentzian fitting process, are given in the appendices in Table 62, Table 63, Table 64, and Table 65 (see Appendix A, page 319).

2.3.1.2. Interpretation of Parameter Values Obtained from DMTA

2.3.1.2.1. Glass Transition Temperature as a Function of Conditioning Time and Temperature

In Figure 23 the evolution of the glass transition temperature (T_g), of dry DGEBA-DDA resin films, is shown as a function of conditioning time and temperature.

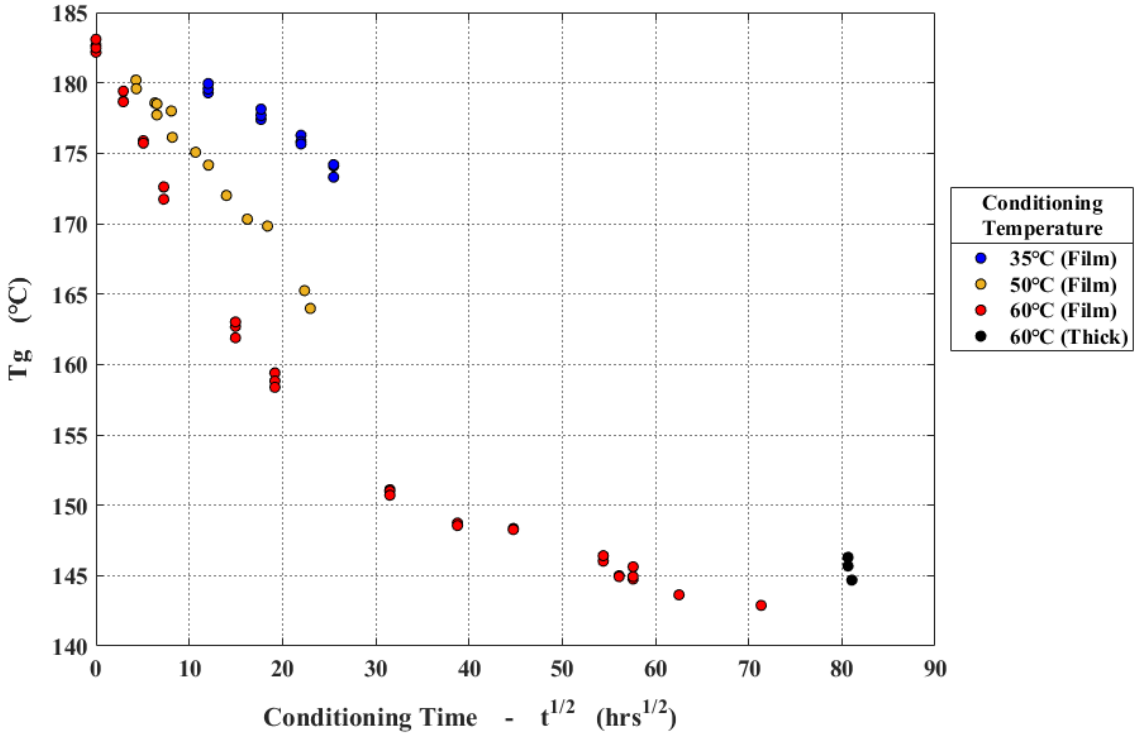

Figure 23: Glass transition temperature of DGEBA-DDA films as a function of time and temperature.

All data points have been obtained from the DMTA spectra of thin film samples (~0.075 mm) aged for specific time periods, at fixed conditioning temperatures. In the case of conditioning at 60℃, three further samples were obtained from two ~0.25 mm and ~0.72 mm samples: HC2 and HC6, after the gravimetric experiments they were required for had been completed. These samples had been initially conditioned at 60℃ for ~71 $hrs^{\frac{1}{2}}$, before being employed sequentially in reconditioning experiments at 60℃, 50℃, and 35℃. Thus, they have not been conditioned exclusively at 60℃. However, as an approximation it has been assumed that their total conditioning time, the time they spent conditioning at all three temperatures, is representative of their conditioning time at 60℃. These extra films were obtained by grinding away an equal proportion of material from both sides of samples HC2 and HC6, to obtain core specimens. This precaution was taken as condensation often formed upon the samples during the conditioning

process and this could potentially allow hydrolysed chain segments, located near the sample surface, to leech out of the material. The effect of hydrolysed chain segments upon the glass transition temperature of DGEBA-DDA is unknown and thus it is important to prevent any possible leeching from occurring. Machining films from the core of the sample minimises the likelihood of obtaining material within which significant leeching has occurred. After machining, the films were placed in a vacuum oven at 50℃ and dried for ~48 hrs to ensure that no residual moisture remained. In Figure 23, Figure 24, Figure 25, and Figure 26, the three new films that were obtained from the thicker samples are denoted as 'thick'.

The initial dry T_g of DGEBA-DDA, before ageing, was ~182.5℃ and this was observed to decrease with conditioning time at each of the three conditioning temperatures. The rate of T_g reduction is observed to increase with increasing temperature. These observations are in agreement with those reported in the literature and have been attributed to a reduction in cross-link density, as a result of hydrolysis, leading to a reduction in the T_g of the material [6, 7]. At 60℃, material T_g appears to be approaching a plateau at ~143℃ after conditioning for ~71 $hrs^{\frac{1}{2}}$. However, the films obtained from the 'thick' samples exhibited higher glass transition temperatures at ~145℃ even though these films were conditioned for a longer time period. This recovery of T_g with extended conditioning time is unusual and inconsistent with the concept of cross-link density reducing as hydrolysis occurs. In the literature there have been no observations of a recovery in the T_g of DGEBA-DDA resin over extended conditioning periods, however the final T_g of the resin after complete hydrolysis has occurred has been observed to take two different values; with these being dependent on the conditioning temperature [7]. At a conditioning temperature of 50℃, the final dry T_g of DGEBA-DDA resin has been observed to be ~144℃ , however at conditioning temperatures of 70℃, and higher, the final T_g is ~140-141℃. It should be noted that Fata et al [6] also measured the dry T_g of DGEBA-DDA after conditioning at 60℃ for a time sufficient for complete hydrolysis to occur. They determined the dry T_g of the resin to be ~132.5℃, however, this value cannot be compared with those obtained by Xiao et al [7], with DMTA, as they employed a different technique; namely differential scanning calorimetry (DSC). The T_g of polymers is a function of strain rate [102], and thus T_g values determined in a DMTA experiment, where a cyclic strain is applied, are not directly comparable with those obtained by DSC where no strain is applied. Only at very low frequencies will T_g values measured by DMTA begin to approximate those obtained by DSC.

Xiao et al [7] measured the wet T_g of DGEBA-DDA resin immersed in liquid water at 50℃, after complete hydrolysis had occurred, and found it to be ~98℃. Thus, it can be hypothesised that the observed relationship between conditioning temperature and final T_g may

be associated with the material approaching, and exceeding, its wet glass transition temperature during the conditioning experiment.

2.3.1.2.2. Post Ageing T_g Recovery through the Relaxation of Hydrolysed Polymer Chains

In the context of GIM, two polymers with identical chemical compositions but existing in two different states, one amorphous, the other crystalline, will possess different glass transition temperatures [71]. This is because, in an amorphous polymer not all of the polymer chains have attained their lowest energy configurations (see section 1.7.1, page 25). Thus, the overall energy of the system is greater than that of its crystalline counterpart, and as a result, less energy is required for the material to undergo its glass transition. As a consequence, the glass transition temperature of the amorphous material is lower than that of its crystalline counterpart. As the hydrolysis reaction alters the morphology of the polymer network, it can be hypothesised that a post ageing relaxation process can occur resulting in a subsequent recovery in T_g.

At temperatures of 60℃ and above, the resin is partially in its rubber phase and as a result the free chain segments are unconstrained. When the resin samples are removed from the 60℃ conditioning environment, and dried, they return to their glassy state. In this phase the free polymer chains, introduced through the hydrolysis process, are constrained and thus an extended time period is necessary in order for them to relax to their lowest energy states. In the DMTA experiments performed in this work the DGEBA-DDA films, aged at 60℃, were only dried for a time period sufficient for the removal of absorbed moisture (~48 hrs). Thus, it can be concluded that the drying process provides insufficient time for free polymer chains to relax and hence no T_g recovery is observed in samples conditioned at temperatures of 60℃ and above.

When DGEBA-DDA resin is conditioned at 50℃ the material remains in its glassy state throughout the ageing process and thus free polymer chain relaxation can occur simultaneously with the hydrolysis reaction. Thus, the observed final T_g of ~145℃, in samples conditioned at 50℃, is that representative of fully hydrolysed DGEBA-DDA resin in which all free polymer chains have relaxed to their lowest energy configurations. The final T_g of ~140℃, observed in samples conditioned at temperatures of 60℃ and above, is that representative of fully hydrolysed DGEBA-DDA resin in which no free polymer chains have been able to relax to their lowest energy configurations. This explanation for the temperature dependence of the dry T_g of fully hydrolysed DGEBA-DDA resin is consistent with the conditioning data in Figure 23.

At extended conditioning times, the T_g of films aged at 60℃ dropped below ~145℃. However, when fully hydrolysed materials were reconditioned at 50℃ and 35℃, as occurred with the films that were obtained from samples HC2 and HC6 (labelled as 'Thick' samples in Figure 23), a final T_g of ~145℃ was observed. Thus, subjecting these samples to the two lower temperatures, where the material is in its glassy state, provided sufficient time for the relaxation of free polymer chains to occur.

If the above hypothesis is correct then chain relaxation, and thus T_g recovery, will occur throughout the conditioning process as it is only when the resin is almost fully hydrolysed (dry T_g of ~ 145℃) that the wet T_g of the material approaches the conditioning temperature, which interferes with the relaxation process. It is not possible to accurately determine the time period associated with T_g recovery from the conditioning data and thus it will be assumed that the measured dry T_g of each film is that associated with DGEBA-DDA resin in which all free polymer chains have relaxed to their lowest energy states. From this assumption it follows that the final dry T_g of fully hydrolysed DGEBA-DDA resin is ~145℃. In the analysis that follows the two films with glass transition temperatures below 145℃, namely H25 and H26, were neglected as these do not meet the criterion for their free polymer chains having attained complete relaxation.

In Table 8 below the values of T_{g_A} and T_{g_C} are shown; these being the glass transition temperature of unaged and fully hydrolysed DGEBA-DDA resin respectively. The subscripts A and C refer to the fundamental unit types that are representative of each of these two material states (unaged and fully aged).

Parameter	Temperature (℃)
T_{g_A}	182.5
T_{g_C}	145.3

Table 8: Glass transition temperature of unconditioned and fully hydrolysed DGEBA-DDA resin.

2.3.1.2.3. Loss Tangent Curve Parameters as a Function of the dry T_g of DGEBA-DDA Resin

As discussed previously, the T_g of DGEBA-DDA resin is directly related to the extent to which the material has been hydrolysed. Thus, it is more appropriate to understand the loss tangent curve parameters in terms of T_g than in terms of two different variables: time and temperature. In the figures that follow (Figure 24, Figure 25, Figure 26) the parameters H_a, w, and $tan\delta_b$, have been expressed as functions of the dry T_g of DGEBA-DDA resin.

2.3.1.2.3.1. Loss Tangent Peak Height (H_a) as a Function of T_g

Figure 24 displays the relationship between the height of the loss tangent peak and the glass transition temperature of the resin.

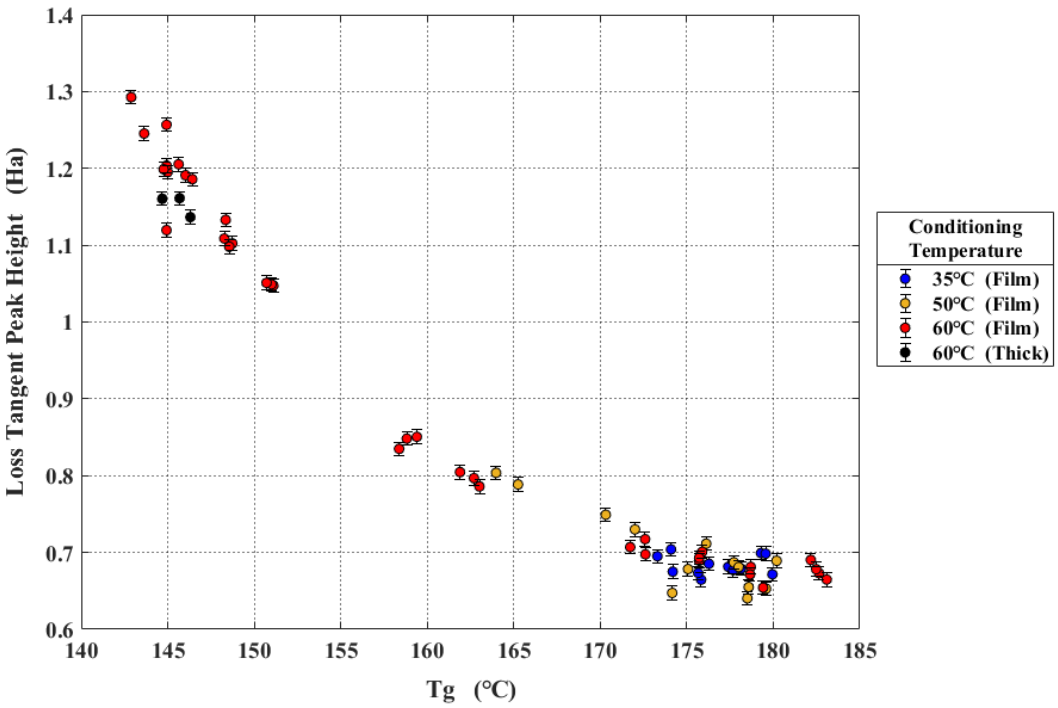

Figure 24: Loss tangent peak height as a function of glass transition temperature. Each data point represents one measurement and the error bars associated with each point are an estimate of the error, showing one standard deviation either side of the measured value. These standard deviations were obtained by DMTA measurements on unaged samples, as detailed in section 2.3.1.1.5, page 88.

During the initial stages of hydrolysis, when resin T_g is in the range 175℃-182.5℃, the loss tangent peak height (H_a) takes an approximately constant value of ~0.66. However, once T_g falls below 175℃ H_a increases rapidly, attaining a final value of ~1.3 when the T_g of the resin is

~142.5℃. As it was earlier assumed that 145℃ represents the T_g of fully hydrolysed material then the value of H_a that is representative of fully aged DGEBA-DDA resin is ~1.2. Thus, the loss tangent peak height approximately doubles in magnitude after complete hydrolysis of the resin has occurred. In the literature, the height of the loss tangent peak, in thermosetting polymers, has been observed to decrease with increasing degree of cure, and hence with increasing T_g [103, 104]. Thus, the observed increase in H_a, as T_g is reduced, is consistent with that behaviour that has been observed in other thermosets.

The area under the loss tangent curve is proportional to the damping of the material. As cross-link density increases, the damping ability of the material decreases. Thus, if the full width half maximum (FWHM) of the loss tangent curve remains constant as a function of T_g, as is observed in these experiments (Figure 25), then it is the loss tangent peak height that must decrease with increasing T_g to account for the reduction in the damping ability of the resin with increasing cross-link density. This is consistent with the trend observed in Figure 24.

2.3.1.2.3.2. Full Width at Half Maximum (w) as a Function of T_g

The behaviour of the FWHM as a function of T_g is important as it describes how well the diffusion and hydrolysis processes have been decoupled. If the time required for a sample to attain moisture equilibrium with its environment (uniform concentration gradient throughout the sample geometry) is comparable to, or greater than, the time scale over which detectable hydrolysis occurs, then the two processes will become coupled (see section 2.2.1.1.1, page 40). This results in the extent to which hydrolysis occurs varying throughout the sample geometry forming a non-uniform T_g profile within the material. When DMTA is performed on such a material, each T_g state within the material will contribute to the measured properties. As a consequence, the loss tangent curve becomes broader making precise determination of resin T_g, and loss tangent peak height, impossible. To decouple the diffusion and hydrolysis processes thin films (~0.075 mm) have been employed in the DMTA experiments of this work. To determine whether these sample dimensions are sufficient to decouple the two processes, the behaviour of the FWHM as a function of T_g, and hence hydrolysis, must be studied (Figure 25).

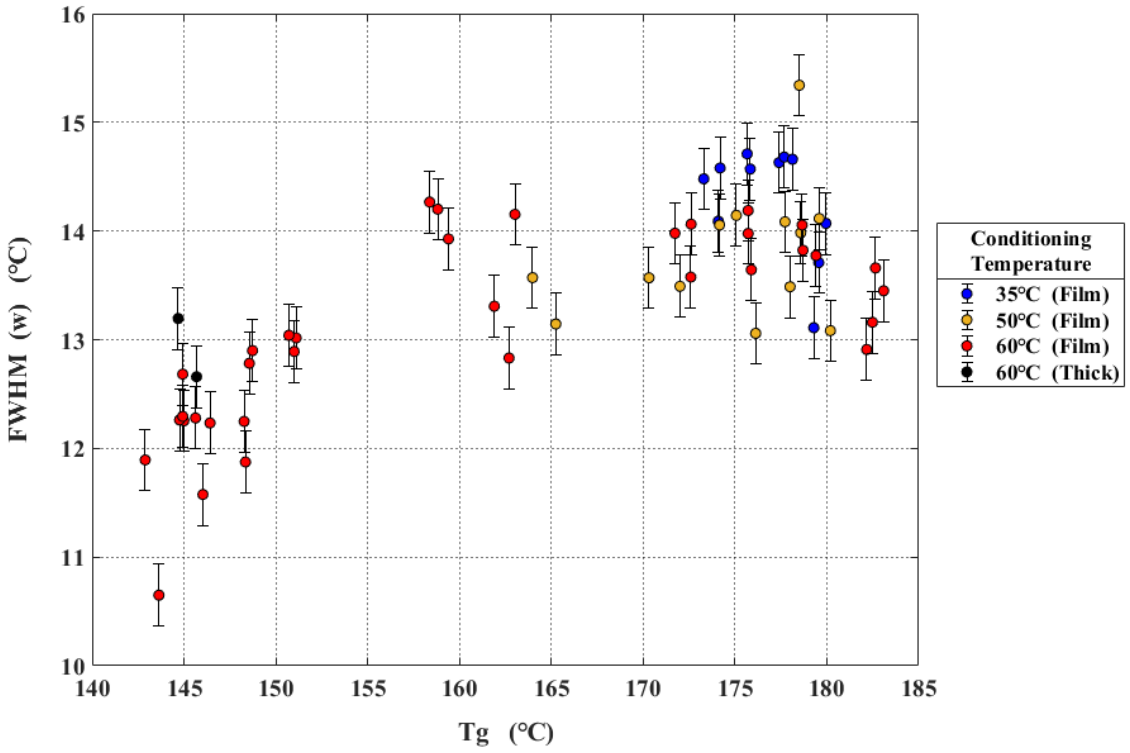

Figure 25: Full width half maximum (FWHM) as a function of glass transition temperature. Each data point represents one measurement and the error bars associated with each point are an estimate of the error, showing one standard deviation either side of the measured value. These standard deviations were obtained by DMTA measurements on unaged samples, as detailed in section 2.3.1.1.5, page 88.

The FWHM of the unaged material is ~13.5℃. This appears to increase slightly to ~14℃ in the initial stages of hydrolysis when resin T_g falls to ~175℃. When resin T_g has fallen to ~155℃ the FWHM regains its initial value of ~13.5℃. The FWHM of fully hydrolysed DGEBA-DDA resin, having a T_g of 145℃, is ~12.5℃. Distortion effects arising from the coupling of the diffusion and hydrolysis processes will act to broaden the loss tangent curve, increasing the FWHM. Thus, the behaviour in Figure 25 shows that the greatest effect of coupling in these films is to increase the FWHM by ~0.5℃. As the error on the FWHM (Table 7) is 0.28℃, the observed distortion effect is negligible which confirms that the film dimensions are sufficient to decouple the hydrolysis and diffusion processes. The FWHM of the fully hydrolysed resin is observed to fall by ~1℃ when compared to its initial value in the unaged material. The mechanism behind this decrease cannot be explained at present, however it is small and as its effect is only to sharpen the loss tangent curve it does not have a negative impact upon the precision of the T_g measurements.

2.3.1.2.3.3. Background Loss Tangent ($tan\delta_b$) as a Function of T_g

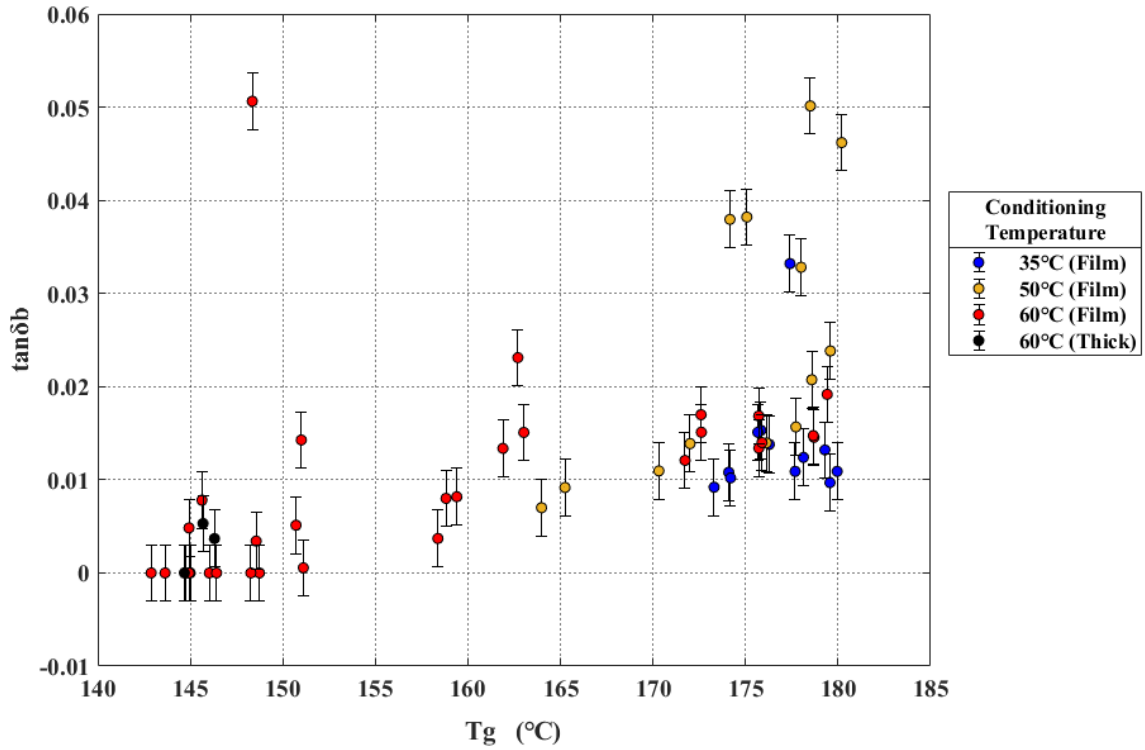

Figure 26: Background loss tangent as a function of the glass transition temperature. Each data point represents one measurement and the error bars associated with each point are an estimate of the error, showing one standard deviation either side of the measured value. These standard deviations were obtained by DMTA measurements on unaged samples, as detailed in section 2.3.1.1.5, page 88.

The value of the background loss tangent remains constant during the early stages of hydrolysis, when resin T_g is in the range 170℃-182.5℃, taking a value of ~0.015. However, there is significant scatter in the data points with several falling in the range ~0.03 to ~0.05. When the resin T_g falls below 152℃ the background loss tangent appears to become zero, however this is an artefact of the Lorentzian function fitting process. As discussed previously (section 2.2.1.6, page 45), when performing DMTA upon films the initial temperature ramp was 20℃. min^{-1}, from room temperature to 100℃, with no data being recorded in this range. This action was taken to prevent significant hydrolysis of the resin from occurring during the DMTA scan through the absorption of atmospheric moisture. As the glass transition temperature of all samples is in excess of 100℃, the lowest glass transition temperatures being greater than 140℃, this methodology was justified. However, as a consequence, when fitting the Lorentzian function to loss tangent curves with low glass transition temperatures (T_g < 152℃) there were not enough data points to the left of the loss tangent curve for the background loss tangent to be clearly observed. As a result, the fitting software assumed that the background loss tangent was zero in these DMTA spectra. This difficulty did not arise when the Lorentzian function was fit to films with higher glass transition

temperatures. This is because there were sufficient data points to the left of their loss tangent curves to allow the background loss tangent to be clearly discerned.

2.3.2. Gravimetric Analysis

2.3.2.1. Gravimetric Analysis (Unaged DGEBA-DDA Resin)

2.3.2.1.1. Unaged DGEBA-DDA Resin Conditioned at 35℃

Figure 27 shows the percentage change in mass of 'thin' samples (~0.25 mm thickness) conditioned at a temperature of 35℃ and relative humidity (RH) of 100%.

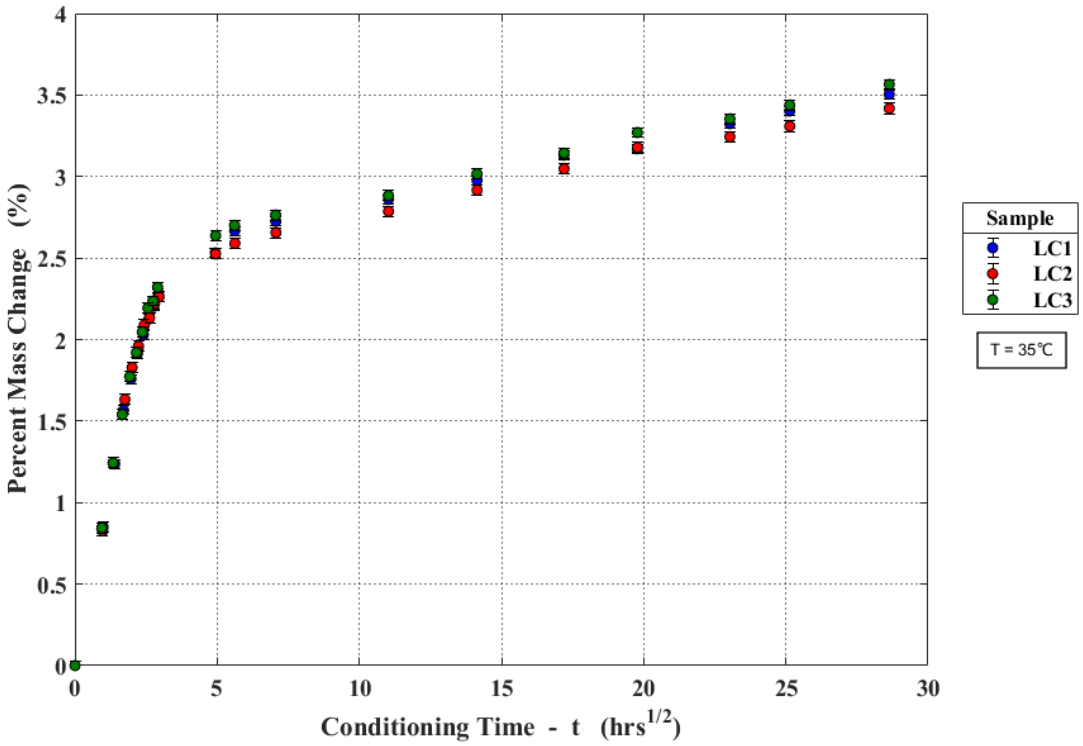

Figure 27: Percentage change in mass of DGEBA-DDA samples conditioned at a temperature of 35℃ and 100% relative humidity. The errors bars on each data point are proportional to the precision of the balance and were calculated by propagation of errors.

All three samples appear to approach an initial equilibrium moisture content of ~2.6% w/w, however with increasing conditioning time the samples continue to gain mass and no definite plateau is observed. This gradual increase above ~2.6% w/w can be explained by the increasing solubility of water in DGEBA-DDA resin, arising from the addition of OH groups to the polymer network as hydrolysis proceeds. The role of hydrolysis in increasing the equilibrium moisture content of the material is confirmed with reference to the T_g/conditioning time profile in Figure 23.

Figure 23 shows that at 35℃ a negligible decrease in T_g, of ~1.5℃, occurs in the first 25 hours of conditioning. The drop in T_g occurring in this time period is for thin films that attain their equilibrium moisture content quickly; the time taken for films to attain equilibrium at 35℃, calculated later in this work, is ~1 hour. Figure 27 indicates that the ~0.25 mm samples take considerably longer to reach equilibrium, ~25 hours. As a result, after 25 hours conditioning, the extent of hydrolysis that has occurred throughout the material geometry of the thin films will be much greater than that which has occurred in the thicker ~0.25 mm samples. Thus, the partial plateau that is observed at ~2.6% w/w is approximately representative of the equilibrium moisture content of the unaged material before hydrolysis has occurred.

With increasing conditioning time, the moisture content increases, and this is matched by a corresponding reduction in resin T_g, thus confirming the link between the observed moisture content and the extent to which hydrolysis has occurred.

2.3.2.1.2. Unaged DGEBA-DDA Resin Conditioned at 50℃

At 50℃ similar behaviour is observed. An initial rapid increase in mass of ~2.6% w/w, followed by a slow gradual increase over extended conditioning times.

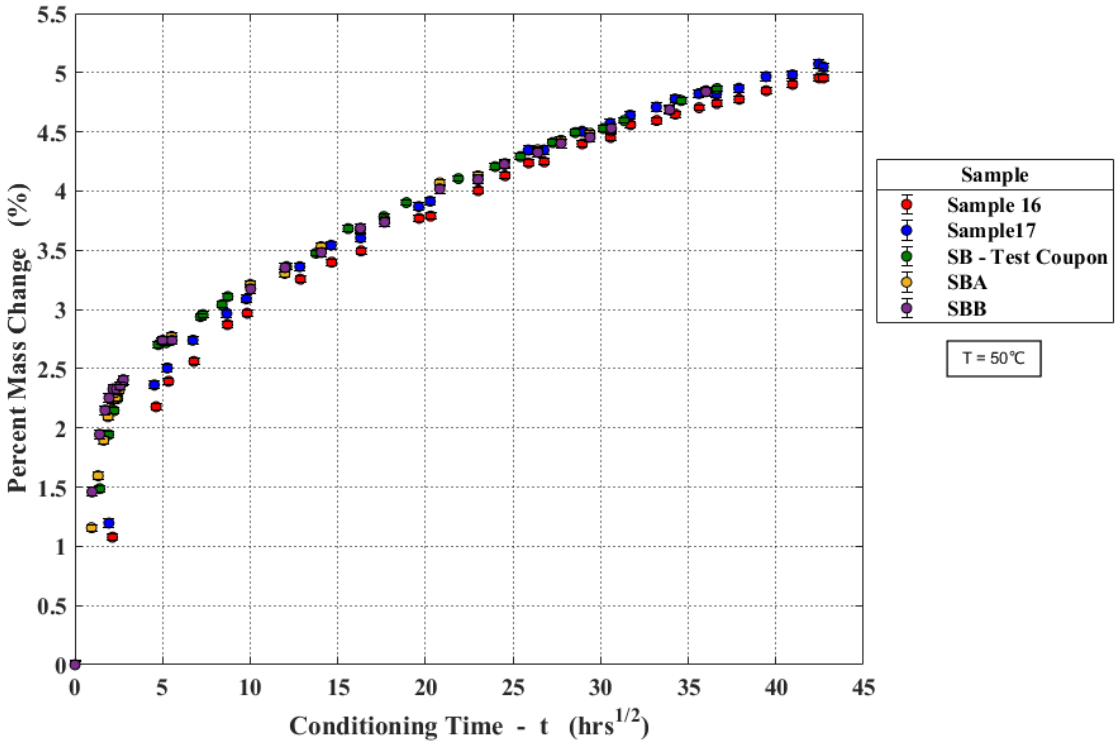

Figure 28: Percentage change in mass of DGEBA-DDA samples conditioned at a temperature of 50℃ and 100% relative humidity. The errors bars on each data point are proportional to the precision of the balance and were calculated by propagation of errors.

No final plateau in moisture content is discerned, however the secondary mass increase behaviour occurring as a result of hydrolysis shows some indication of moving towards a plateau after conditioning times of ~42 $hrs^{\frac{1}{2}}$. Figure 29 shows the uptake behaviour of all five samples at 50℃ at early conditioning times (t < 8 $hrs^{\frac{1}{2}}$).

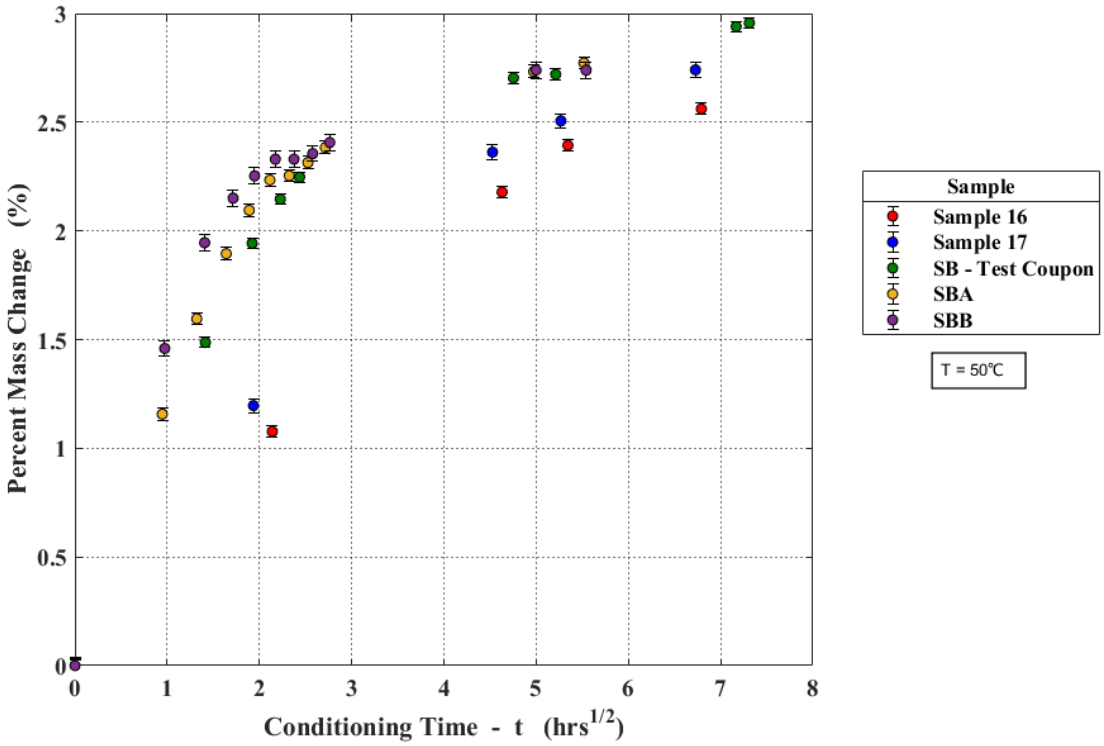

Figure 29: Percentage change in mass of DGEBA-DDA samples conditioned at a temperature of 50℃ and 100% relative humidity (Early conditioning times). The errors bars on each data point are proportional to the precision of the balance and were calculated by propagation of errors.

A clear initial plateau in moisture content is not observable in the 'thick' (~0.72 mm thickness) samples (Sample 16 and Sample 17) as the diffusion and hydrolysis processes are too strongly coupled. The three 'thin' (~0.25 mm thickness) samples (SB-Test Coupon, SBA, SBB) show two separate plateaus, one at ~2.4% w/w and a second at ~2.75% w/w. This might suggest the occurrence of a bound/unbound water phenomenon such as that suggested by Carter et al [38]. If this hypothesis is correct, then the initial equilibrium moisture content of unaged DGEBA-DDA resin at 50℃ is ~2.4% w/w, which increases to ~2.75% w/w as water molecules become strongly bound to the polymer network. As no gravimetric measurements exist between these two plateaus a second explanation would be that the samples experienced water loss during the weighing process. This loss accumulated each time the samples were removed from their conditioning environments and thus, after ~8 hours of conditioning, the moisture content of the samples was less than their actual equilibrium moisture content. After this initial conditioning period the samples were not weighed for ~17 hours which would provide adequate time for the

samples to attain equilibrium. This would result in the two equilibria plateau observed in Figure 29.

2.3.2.1.3. Unaged DGEBA-DDA Resin Conditioned at 60℃

In Figure 30 the percentage change in mass of the samples conditioned at 60℃ is shown. At this conditioning temperature, a final plateau in the percentage change in mass is observed at extended conditioning times of ~72 $hrs^{\frac{1}{2}}$.

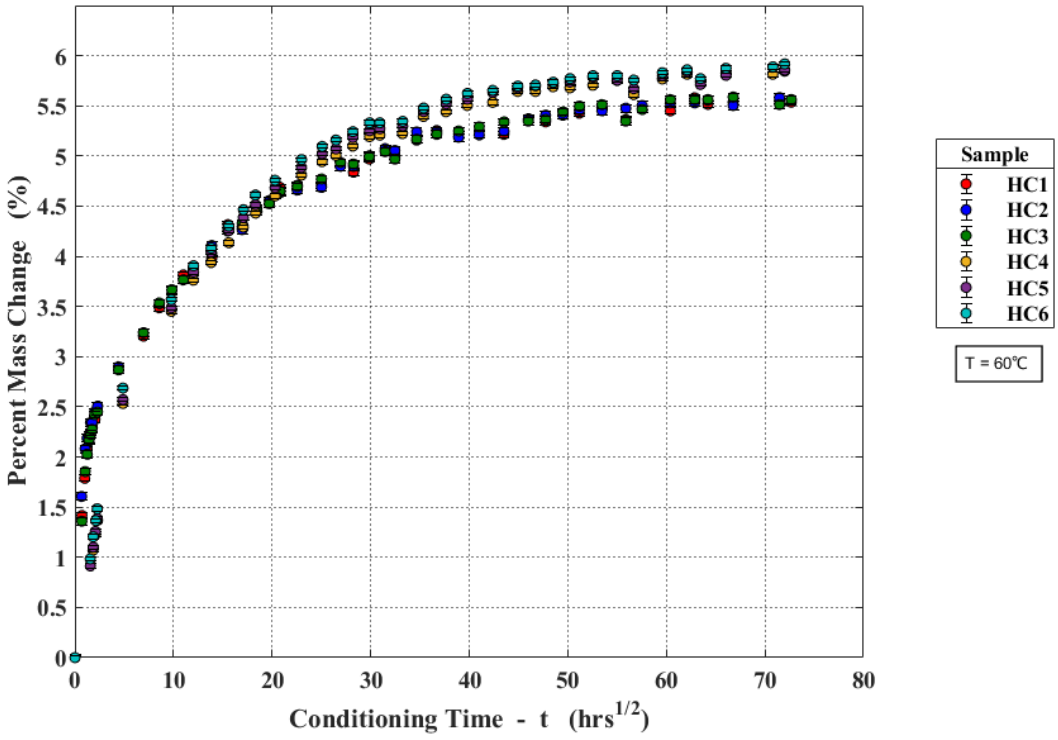

Figure 30: Percentage change in mass of DGEBA-DDA samples conditioned at a temperature of 60℃ and 100% relative humidity. The errors bars on each data point are proportional to the precision of the balance and were calculated by propagation of errors.

Referring to Figure 23 it is apparent that this coincides with the approximate plateau in T_g occurring at ~145℃ that is associated with fully hydrolysed DGEBA-DDA resin. This is expected as once the material is fully hydrolysed there will be no further increases in solubility or reductions in cross-link density. Thus, conditioning at 60℃ for ~72 $hrs^{\frac{1}{2}}$ is sufficient to completely hydrolyse all hydrolysable cross-links that are initially present in the unaged resin. As a result, after conditioning, samples HC1, HC2, HC3, HC4, HC5, and HC6, are representative of fully hydrolysed DGEBA-DDA resin. The 'thick' samples (~0.72 mm thickness) exhibited a final plateau of ~5.8% w/w whereas the 'thin' samples (~0.25 mm thickness) plateaued at ~5.5% w/w. This difference in percentage mass change can be attributed to the evaporation of absorbed

moisture that occurs when the 'thin' samples are removed from their conditioning environments for weighing.

The mass change behaviour at early conditioning times (Figure 31) is similar to that observed at 50℃ with a partial plateau at ~2.4% w/w being present. However, no secondary plateau is observed as the high rate of hydrolysis occurring at this conditioning temperature results in a rapid increase in the solubility of water within the resin as conditioning proceeds.

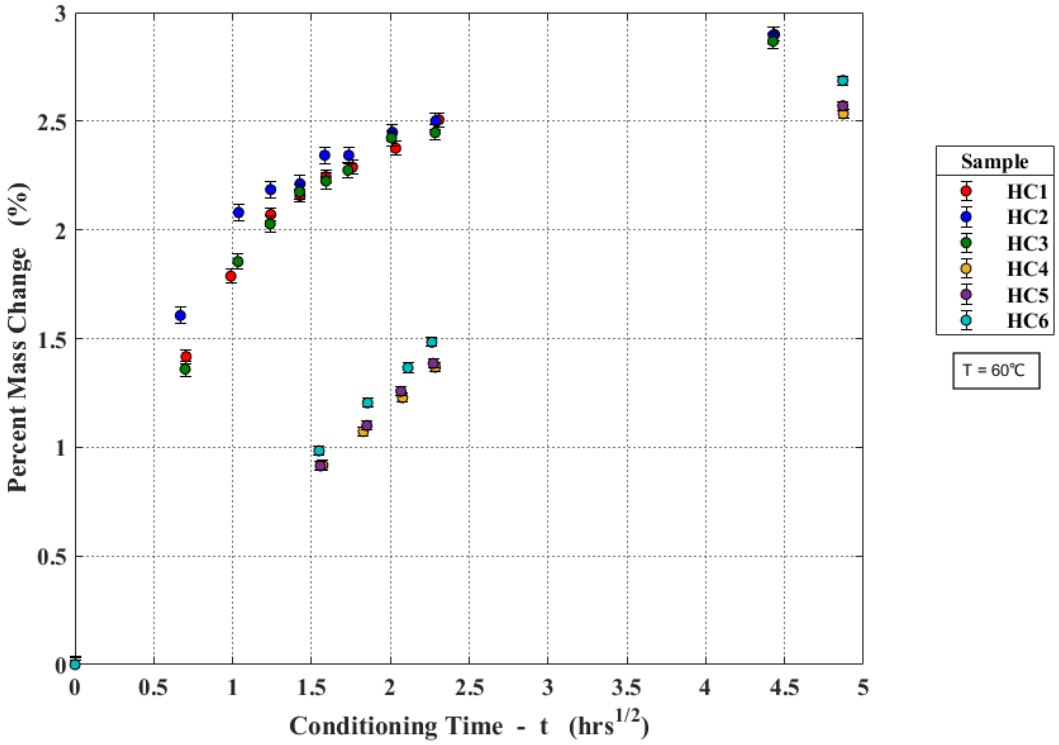

Figure 31: Percentage change in mass of DGEBA-DDA samples conditioned at a temperature of 60℃ and 100% relative humidity (Early conditioning times). The errors bars on each data point are proportional to the precision of the balance and were calculated by propagation of errors.

2.3.2.2. Increase in the Dry Mass of DGEBA-DDA Resin Through the Chemical Addition of Water to the Polymer Network

After conditioning at 60℃ for ~72 $hrs^{\frac{1}{2}}$ no further changes in material mass were observed, indicative of complete hydrolysis of the resin. The fully hydrolysed samples were then removed from their conditioning environments and dried under vacuum, at 60℃, until a final dry mass was obtained. In the literature, the dry mass of DGEBA-DDA has been observed to increase with conditioning time, with the magnitude of this increase being dependent upon both time and temperature. This behaviour has been attributed to the chemical addition of the water molecule to

the polymer network each time a cross-link is hydrolysed. The increase in dry mass has been observed to be ~1% w/w in DGEBA-DDA resin that has been fully hydrolysed [6, 7, 43].

Table 9 below shows the average percentage increase in the dry mass of fully hydrolysed DGEBA-DDA resin obtained from samples HC1, HC2, HC3, HC4, HC5, HC6.

$\%_a$ (%)	$\Delta\%_a$ (%)
0.994	0.024

Table 9: Percentage increase in dry mass of fully hydrolysed DGEBA-DDA resin.

Where $\%_a$ is the average increase in dry mass and $\Delta\%_a$ is the associated error, taken to be equal to the standard deviation. The percentage increase in dry mass that occurs in these fully hydrolysed samples is therefore consistent with that previously observed in the literature [6, 7, 43].

2.3.2.3. Gravimetric Analysis (Fully Hydrolysed DGEBA-DDA Resin)

The fully hydrolysed samples (HC1,HC2,HC3,HC4,HC5,HC6) were reconditioned at each of the three conditioning temperatures to determine the effect of the hydrolysis reaction on the diffusion coefficient and solubility of DGEBA-DDA resin. Figure 32 below shows the absorption behaviour of fully aged samples reconditioned at 60℃.

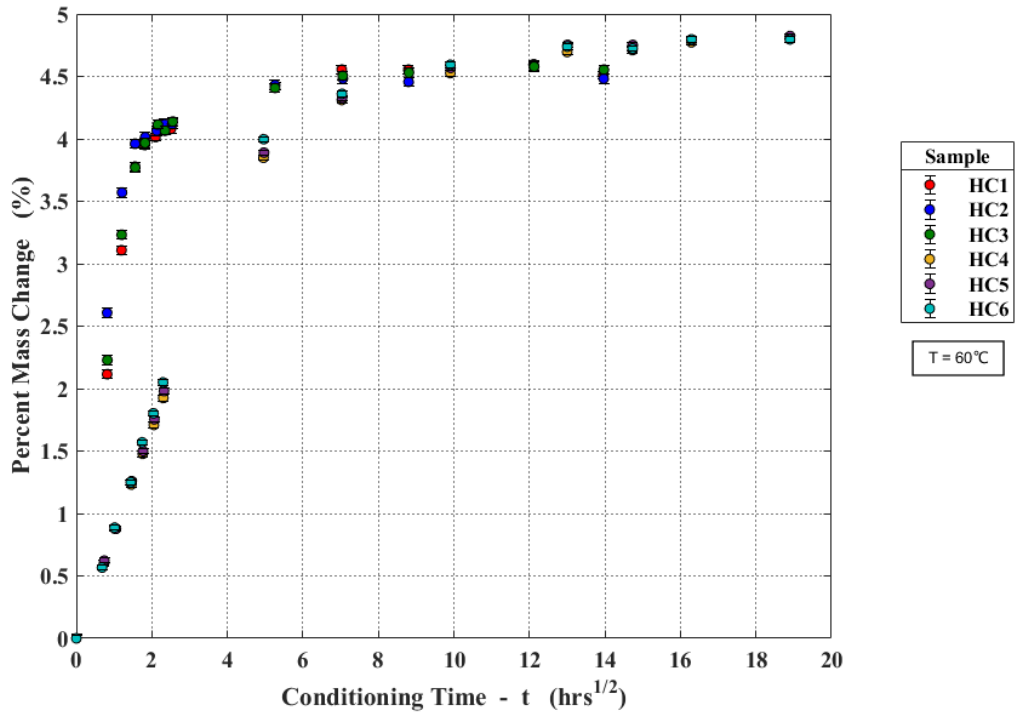

Figure 32: Percentage change in mass of fully hydrolysed DGEBA-DDA resin as a function of conditioning time at a temperature of 60℃ and 100% relative humidity. The errors bars on each data point are proportional to the precision of the balance and were calculated by propagation of errors.

The ‘thick’ (~0.72 mm thickness) samples (HC4,HC5,HC6) exhibited a plateau in their mass change behaviour corresponding to ~4.75% w/w of absorbed moisture. ‘Thin’ (~0.25 mm thickness) samples (HC1,HC2,HC3) plateaued slightly lower at ~4.5% w/w. This difference in equilibrium moisture content between the thick and thin samples was only observed when reconditioning at 60℃. When reconditioned at the two lower temperatures, 35℃ and 50℃, almost identical equilibrium levels were observed in both types of samples. Thus, this difference can be attributed to the evaporation of moisture from the thinner samples during the weighing process. This also explains the difference in percentage uptake that was observed between the ‘thick’ and ‘thin’ samples conditioned at 60℃ (see Figure 30).

Similar absorption behaviour was observed at 50℃ and 35℃ (Figure 33 and Figure 34) with all samples attaining a final equilibrium uptake of ~4.75% w/w at each temperature.

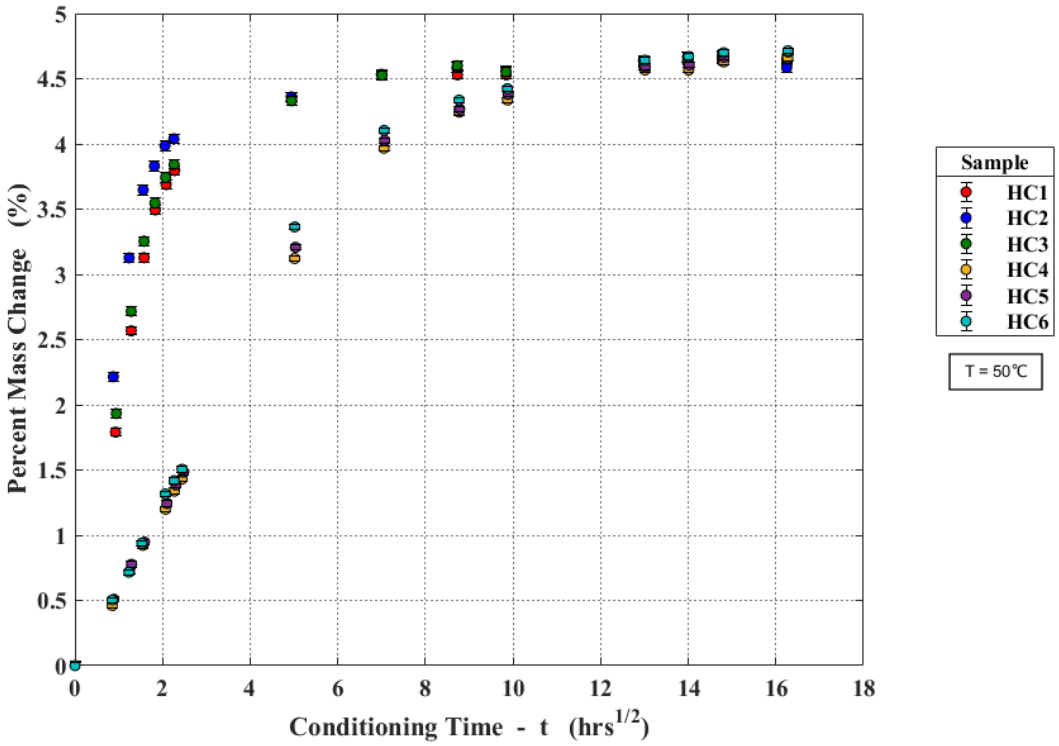

Figure 33: Percentage change in mass of fully hydrolysed DGEBA-DDA resin as a function of conditioning time at a temperature of 50℃ and 100% relative humidity. The errors bars on each data point are proportional to the precision of the balance and were calculated by propagation of errors.

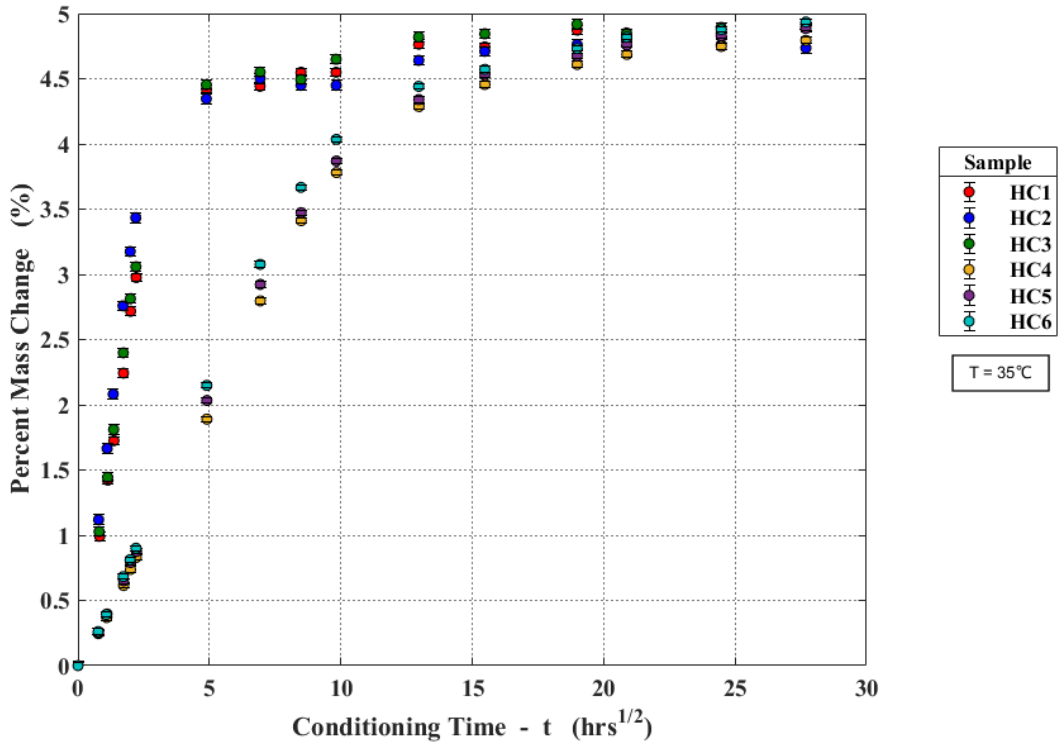

Figure 34: Percentage change in mass of fully hydrolysed DGEBA-DDA resin as a function of conditioning time at a temperature of 35℃ and 100% relative humidity. The errors bars on each data point are proportional to the precision of the balance and were calculated by propagation of errors.

The rate of moisture absorption was observed to be dependent upon the conditioning temperature as expected for diffusion controlled processes.

As discussed previously (section 2.3.2.2, page 101), hydrolysis leads to an increase in resin dry mass through the chemical addition of water molecules to the polymer structure. As a result, these new dry mass values must be taken as the initial mass of the resin in the reconditioning experiments. However, a consequence of this is that it is not possible to directly compare the percentage change in mass of the reconditioned samples with that observed in the samples before reconditioning. This is because their initial dry masses are different and thus even if both types of sample (unconditioned and fully hydrolysed) contain an identical quantity of moisture their percentage changes in mass will be different.

In this work, the change in the equilibrium moisture content of DGEBA-DDA resin during conditioning has been attributed to the process of hydrolysis. Water molecules chemically react with the resin, becoming part of the polymer network and increasing the solubility of water

within the material. The net effect is an increase in DGEBA-DDA's equilibrium moisture content, from ~2.6% w/w in the unaged material, to ~5.8% w/w after complete hydrolysis has occurred.

However, another explanation is that no change in solubility occurs and that the slow gradual increase in mass, above the initial plateau, arises as a result of the bound/unbound water phenomenon proposed by Carter et al [38] (see section 1.3.4.1, page 13). If this explanation is correct then one would expect the time taken to achieve the final plateau in percentage mass change (~6% w/w) to be identical when comparing reconditioned samples (fully hydrolysed) to samples conditioned for the first time (unaged). To make this comparison the percentage mass change at equilibrium in the reconditioned sample must be recalculated in terms of their initial dry masses before ageing, in other words neglecting the increase in dry mass that resulted from the chemical addition of water to the polymer structure. Table 10 shows the adjusted equilibrium percentage mass change for the three reconditioned 'thick' (~0.72 mm thickness) samples.

Sample	Adjusted Equilibrium Percentage Mass Change (%) (w/w)
HC4	*5.85*
HC5	*5.86*
HC6	*5.87*

Table 10: Adjusted equilibrium percentage mass change for 'thick' samples reconditioned at 60℃.

Taking an average, the percentage mass change at equilibrium in 'thick' samples, reconditioned at 60℃, is ~5.86% w/w after a conditioning time of ~12.5 $hrs^{\frac{1}{2}}$. In the initial conditioning experiment, 'thick' samples took ~72 $hrs^{\frac{1}{2}}$ to reach the same percentage change in mass. Thus, the gradual increase in percentage mass change with conditioning time can be attributed to an increase in material solubility, and the chemical addition of water, resulting from the hydrolysis reaction and not to a bound/unbound water phenomenon.

2.3.2.4. Calculating the Initial Density of Unaged DGEBA-DDA Resin

The initial density of each sample, before ageing, was determined by calculating their mass to volume ratio. Sample masses were obtained by weighing with a gravimetric balance with a precision of ±50 μg. Dimensions were obtained using a micrometer, with a precision of ±0.5

μm, for thickness measurements and calipers, with a precision of ±5 μm, for length and width measurements. Table 11 shows the calculated density, and corresponding error, for each sample employed in the gravimetric experiments.

Sample	$\boldsymbol{\rho_i}$ $\left(\boldsymbol{g.mm^{-3}}\right)$	$\boldsymbol{\Delta\rho_i}$ $\left(\boldsymbol{g.mm^{-3}}\right)$
HC1	*1.032E-03*	*4.890E-05*
HC2	*1.093E-03*	*9.466E-05*
HC3	*1.044E-03*	*7.045E-05*
HC4	*1.171E-03*	*4.539E-05*
HC5	*1.171E-03*	*3.397E-05*
HC6	*1.173E-03*	*1.759E-05*
Sample 16	*1.305E-03*	*1.643E-05*
Sample 17	*1.310E-03*	*2.486E-05*
SB-Test Coupon	*1.070E-03*	*5.226E-05*
SBA	*1.099E-03*	*3.010E-05*
SBB	*1.104E-03*	*1.934E-05*
LC1	*1.169E-03*	*2.131E-05*
LC2	*1.080E-03*	*4.760E-05*
LC3	*1.114E-03*	*1.664E-05*

Table 11: Initial sample densities before ageing.

A large distribution in density values is observed with any given measurement falling in the range $1.032 \times 10^{-3}\ g.mm^{-3}$ to $1.31 \times 10^{-3}\ g.mm^{-3}$. However, as all samples where machined from the same resin casting this degree of variation is not expected. On average, the 'thick' samples (~0.72 mm thickness) have higher densities than the 'thin' samples (~0.25 mm thickness) which suggests that sample dimensions are responsible for the observed variation. This may result from the difficulties inherent in accurate volume determination of samples with small dimensions.

The percentage change in mass at equilibrium, observed in both the 'thin' and 'thick' samples reconditioned at 35℃ (Figure 34) and 50℃ (Figure 33), is almost identical irrespective of the supposedly different initial densities of these two types of sample. This would suggest that the actual sample densities are approximately the same and that the observed variations in density most likely arise as a result of the errors introduced during sample volume determination.

In the work that follows it is assumed that the initial densities of all samples are identical. An average density was obtained from the five thick samples (HC4, HC5, HC6, Sample 16, Sample 17) and this was taken to be representative of the density of each sample in all the calculations that follow (Table 12).

$\boldsymbol{\rho_{avg}}$ $\boldsymbol{(g.mm^{-3})}$	$\boldsymbol{\Delta\rho_{avg}}$ $\boldsymbol{(g.mm^{-3})}$
1.226E-03	*6.653E-05*

Table 12: Average initial density of DGEBA-DDA resin before ageing (Obtained from densities of 'thick' samples).

2.3.2.5. Obtaining the Diffusion Coefficients and Solubility Representative of Fully Hydrolysed and Unaged DGEBA-DDA Resin

In this section, a methodology is outlined for obtaining the diffusion coefficients, and solubility, representative of unaged and fully hydrolysed DGEBA-DDA resin. Conventional methods for obtaining these two parameters cannot be employed, at least not at the two higher conditioning temperatures, as the diffusion and hydrolysis processes become coupled. The consequence of this coupling is that significant hydrolysis can occur before the sample can attain equilibrium with its conditioning environment. The conditioning experiments conducted previously (see section 2.3.2.1, page 97) have indicated that the solubility of water within DGEBA-DDA resin is strongly dependent upon the extent of hydrolysis. Thus, the consequence of this hydrolysis is to increase the solubility of the material before the initial equilibrium plateau in moisture content can be observed. This renders precise determination of the initial equilibrium moisture content, and hence solubility, impossible.

Standard methods for obtaining the diffusion coefficient of polymer materials involve either fitting the one-dimensional solution to Fick's second law to experimental data, or determining the gradient of the initial linear portion of the material's uptake/$\sqrt{t}$ relationship and then applying equation (20) [82] (see section 1.8.1, page 33). Both methods assume that the equilibrium moisture content of the material remains constant during the absorption process. This criterion is only approximately met by the samples conditioned at 35℃ where the T_g, of resin located at the sample surface, is observed to fall by ~1.5℃ in the time frame required for initial equilibrium to be attained. At 50℃, the reduction in T_g of resin at the sample surface is ~4.5℃ when initial equilibrium is attained, and at 60℃ no discernible plateau, indicative of initial equilibrium, is observed as a result of the rapid progression of the hydrolysis reaction at this

temperature. To obtain the solubility and diffusion coefficients at these higher conditioning temperatures it is necessary to model the diffusion-hydrolysis process. This allows model predictions to be fit to the experimental data and then, by systematically adjusting the input parameters, those values that best fit the empirical data can be obtained.

The initial parameters required for the model/fitting process are $S_{C_{(T)}}$ and $D_{C_{(T)}}$, the solubility and diffusion coefficient associated with fundamental unit type C, in other words the solubility and diffusion coefficients representative of the fully hydrolysed resin, at a temperature T. As only one process occurs in the fully hydrolysed resin, namely diffusion, the constant solubility criterion discussed above is satisfied and a standard method for obtaining solubility and diffusion coefficients can be employed. This has the advantage of allowing the errors associated with these two parameters to be calculated using propagation of errors.

Once these two parameters have been determined, at each of the three conditioning temperatures, they can then be employed as inputs in the model fitting process. There are four unknown parameters that describe the uptake behaviour of the unaged resin: $S_{A_{(T)}}$, $D_{A_{(T)}}$, K_{AB}, and K_{BC}. Appropriate values are estimated for each parameter by referring to the gravimetric and DMTA data (see section 2.3.1.2.1 and 2.3.2.1 on pages 89 and 97) and these values are then employed as initial inputs to the model. The diffusion-hydrolysis process is simulated within the model and the predicted percentage change in mass as a function of time generated as an output. This output is then compared to the experimental data and the goodness of fit characterised through the calculation of R^2:

$$R^2 = 1 - \frac{A}{B} \tag{146}$$

Where A and B are given by:

$$A = \frac{1}{N}\sum_{i=1}^{N}(E_i - M_i)^2 \tag{147}$$

$$B = \frac{1}{N}\sum_{i=1}^{N}\left(E_i - \hat{E}\right)^2 \tag{148}$$

Where N is the total number of experimental measurements, E_i is the value of the i^{th} experimental measurement, M_i is the corresponding value predicted by the model, and $\hat{E}$ is the average value of all experimental measurements. The initial input parameters are then adjusted, systematically, and the process repeated until the parameter values that maximise the value of R^2 are obtained.

2.3.2.5.1. Determining Solubility ($S_{C_{(T)}}$) as a Function of Temperature in Fully Hydrolysed DGEBA-DDA Resin

The concentration of water absorbed within the resin at equilibrium, when it is conditioned at 100% relative humidity and assuming that it obeys Henry's law, is related to the solubility of water within the resin by:

$$C_{m_{(T)}} = S_{(T)}\, p_{sat_{(T)}} \tag{149}$$

Where $C_{m_{(T)}}$ is the concentration of water at equilibrium, at 100% relative humidity, in units of $mol.mm^{-3}$, $S_{(T)}$ is the material solubility in units of $mol.mm^{-3}.Pa^{-1}$, and $p_{sat_{(T)}}$ is the partial saturation vapour pressure of water in the conditioning atmosphere. Thus, material solubility can be expressed as:

$$S_{(T)} = \frac{C_{m_{(T)}}}{p_{sat_{(T)}}} \tag{150}$$

In the earlier gravimetric analysis (presented in section 2.3.2.3, page 102) the moisture content of samples was expressed in terms of their percentage change in mass as a function of the square root of conditioning time. To employ equation (150) in calculating the solubility of water within the resin, the gravimetric data must first be re-expressed in terms of water concentration. Water concentration can be expressed in terms of the percentage change in mass, as follows. The percentage change in mass of the resin $\%_u$, brought about by the absorption of water, can be expressed in terms of the mass of absorbed water m_w and the initial dry mass of the resin prior to conditioning m_R:

$$\%_u = 100\,\frac{m_w}{m_R} \tag{151}$$

The mass of absorbed water m_w can be written in terms of its concentration C_w and the volume it occupies V as:

$$m_w = C_w V \tag{152}$$

Similarly, re-expressing the mass of the dry resin in terms of its dry density ρ_R and volume V:

$$m_R = \rho_R V \tag{153}$$

Substituting equations (152) and (153) into equation (151) leads to:

$$\Rightarrow \%_u = 100 \frac{C_w}{\rho_R} \tag{154}$$

Rearranging equation (154) and expressing C_w as a molar concentration, one obtains:

$$C_w = \frac{\%_u \rho_R}{1800} \tag{155}$$

Where $\%_u$, m_w, m_R, C_w, ρ_R, and V, are in units of %, g, g, $mol.mm^{-3}$, $g.mm^{-3}$, and mm^{-3} respectively. Having re-expressed the gravimetric data in terms of water concentration the plateau in the concentration/$\sqrt{t}$ relationship, representative of the equilibrium water concentration of the material, is then identified. The average value of the water concentration at equilibrium for each sample is taken from at least two data points, dependent upon the stability of the concentration measurements within the plateau region. Equation (150) is then applied, using the values of $C_{m_{(T)}}$ obtained for each sample. Below in Table 13 the calculated solubility, and its corresponding error, is shown for fully hydrolysed samples as a function of conditioning temperature. The final column of the table expresses the error in solubility as a percentage of the calculated solubility.

T (℃)	Sample	$S_{C_{(T)}}$ $(mol.mm^{-3}.Pa^{-1})$	$\Delta S_{C_{(T)}}$ $(mol.mm^{-3}.Pa^{-1})$	Percentage Error on $S_{C_{(T)}}$ (%)
35	HC1	5.99E-10	1.89E-11	3.16
35	HC2	5.88E-10	1.86E-11	3.17
35	HC3	6.01E-10	1.65E-11	2.74
35	HC4	5.88E-10	2.27E-11	3.85
35	HC5	5.99E-10	2.31E-11	3.85
35	HC6	6.05E-10	2.33E-11	3.85
50	HC1	2.61E-10	7.14E-12	2.73
50	HC2	2.60E-10	7.15E-12	2.74
50	HC3	2.60E-10	7.13E-12	2.74
50	HC4	2.61E-10	1.00E-11	3.85
50	HC5	2.63E-10	1.01E-11	3.85
50	HC6	2.64E-10	8.29E-12	3.14
60	HC1	1.58E-10	4.33E-12	2.74
60	HC2	1.56E-10	3.83E-12	2.46
60	HC3	1.59E-10	6.15E-12	3.88
60	HC4	1.67E-10	6.41E-12	3.85
60	HC5	1.66E-10	4.52E-12	2.72
60	HC6	1.67E-10	6.41E-12	3.85

Table 13: Solubility as a function of temperature for fully hydrolysed samples.

In Table 14 the average solubility of fully hydrolysed DGEBA-DDA resin has been calculated, at each of the three conditioning temperatures. Also shown is the average equilibrium moisture content, at 100% relative humidity, of fully hydrolysed DGEBA-DDA resin. These values are given in terms of the percentage change in mass and were obtained from the gravimetric analysis presented earlier in section 2.3.2.3.

T (℃)	Average $S_{C_{(T)}}$ $(mol.mm^{-3}.Pa^{-1})$	Average Percentage Change in Mass (Fully Hydrolysed) (%)
35	5.97E-10	4.84
50	2.62E-10	4.67
60	1.66E-10	4.79

Table 14: Average solubility and percentage mass change for fully hydrolysed DGEBA-DDA resin as a function of temperature.

As discussed earlier, when conditioning at 60℃ non-negligible amounts of water are lost through evaporation during the weighing of the 'thin' samples (~0.25 mm thickness).

Consequently, the equilibrium plateau observed in 'thin' samples conditioned at 60℃ is not representative of the actual equilibrium moisture content of the material. For this reason, the solubility values of samples HC1, HC2, and HC3, were not included when calculating the average solubility in Table 14. Although negligible evaporation occurred within the 'thin' samples at the two lower temperatures, only the solubility of thick samples was employed in the averaging process at each temperature.

The results in Table 14 show that solubility falls with increasing temperature but that the equilibrium moisture content of the resin remains approximately constant. As the equilibrium water concentration of the resin can be expressed by Henry's law (equation (3)), this suggests that the product $S_{(T)}\, p_{sat_{(T)}}$ is approximately constant over the temperature range 35-60℃. This implies that the equilibrium moisture content is independent of temperature and takes an average value of ~4.77% (w/w). The observation that the equilibrium moisture content, of fully hydrolysed DGEBA-DDA resin, is independent of temperature is consistent with that behaviour observed in other epoxy resins [3].

2.3.2.5.2. Determining Diffusion Coefficients ($D_{C_{(T)}}$) as a Function of Temperature in Fully Hydrolysed DGEBA-DDA Resin

A standard method for calculating diffusion coefficients in polymers involves plotting moisture content against the square root of conditioning time and then determining the gradient of the initial linear portion of this relationship [82]. Equation (156) below can then applied to calculate the observed diffusion coefficient:

$$D_{obs_{(T)}} = \frac{\pi\, d^2}{16\, {C_{eq}}_{(T)}^{\,2}}\, {g_{(T)}}^2 \qquad (156)$$

Where $D_{obs_{(T)}}$ is the observed diffusion coefficient in units of $mm^2.min^{-1}$, d is the sample thickness in units of mm, ${C_{eq}}_{(T)}$ is the concentration of water within the resin at equilibrium in units of $mol.mm^{-3}$, and $g_{(T)}$ is the gradient of the initial linear portion of the uptake curve in units of $mol.mm^{-3}.min^{-\frac{1}{2}}$. Equation (156) assumes that diffusion only occurs in one dimension, in a direction perpendicular to the sample surface. This assumption implies that the sample consists of an infinite sheet, of finite thickness, such that diffusion of water only occurs through two sides of the material. As equation (156) does not account for the diffusion of water through

the other four sides of the sample, the value of the diffusion coefficient obtained through this expression will over-estimate the actual value. To obtain the actual diffusion coefficient, diffusion through the sides of the sample must be accounted for by applying the 'edge-effect' correction factor [86]:

$$c_f = \left(1 + \frac{d}{w} + \frac{d}{h}\right)^2 \tag{157}$$

Where w and l are the sample width and length respectively both in units of mm. The actual diffusion coefficient is then obtained from:

$$D_{obs(T)} = D_{C(T)}\, c_f \tag{158}$$

$$D_{C(T)} = \frac{D_{obs(T)}}{c_f} \tag{159}$$

Where $D_{C(T)}$ is the actual diffusion coefficient in units of $mm^2.min^{-1}$. Table 15 shows the observed and actual diffusion coefficients for each sample along with their associated dimension correction factors.

T (℃)	Sample	$D_{obs(T)}$ $(mm^2.min^{-1})$	$\Delta D_{obs(T)}$ $(mm^2.min^{-1})$	c_f	$D_{C(T)}$ $(mm^2.min^{-1})$	$\Delta D_{C(T)}$ $(mm^2.min^{-1})$	Percentage Error on $D_{C(T)}$ (%)
35	*HC1*	*1.38E-05*	*1.64E-06*	*1.03*	*1.34E-05*	*1.59E-06*	*11.84*
35	*HC2*	*1.24E-05*	*2.34E-06*	*1.02*	*1.21E-05*	*2.29E-06*	*18.83*
35	*HC3*	*1.38E-05*	*2.07E-06*	*1.03*	*1.34E-05*	*2.01E-06*	*15.01*
35	*HC4*	*1.50E-05*	*1.78E-06*	*1.21*	*1.24E-05*	*1.48E-06*	*11.89*
35	*HC5*	*1.51E-05*	*1.64E-06*	*1.19*	*1.27E-05*	*1.39E-06*	*10.91*
35	*HC6*	*1.41E-05*	*1.39E-06*	*1.17*	*1.21E-05*	*1.19E-06*	*9.84*
50	*HC1*	*3.40E-05*	*3.76E-06*	*1.03*	*3.29E-05*	*3.64E-06*	*11.05*
50	*HC2*	*3.40E-05*	*6.18E-06*	*1.02*	*3.32E-05*	*6.03E-06*	*18.16*
50	*HC3*	*3.53E-05*	*5.17E-06*	*1.03*	*3.42E-05*	*5.01E-06*	*14.64*
50	*HC4*	*3.79E-05*	*4.25E-06*	*1.21*	*3.13E-05*	*3.52E-06*	*11.23*
50	*HC5*	*3.64E-05*	*3.61E-06*	*1.19*	*3.07E-05*	*3.05E-06*	*9.94*
50	*HC6*	*3.42E-05*	*2.56E-06*	*1.17*	*2.92E-05*	*2.19E-06*	*7.49*
60	*HC1*	*6.13E-05*	*6.71E-06*	*1.03*	*5.95E-05*	*6.50E-06*	*10.93*
60	*HC2*	*5.79E-05*	-	*1.02*	*5.65E-05*	-	-
60	*HC3*	*6.15E-05*	*9.57E-06*	*1.03*	*5.96E-05*	*9.28E-06*	*15.57*
60	*HC4*	*6.80E-05*	*7.45E-06*	*1.21*	*5.62E-05*	*6.17E-06*	*10.97*
60	*HC5*	*6.55E-05*	*5.21E-06*	*1.19*	*5.52E-05*	*4.40E-06*	*7.97*
60	*HC6*	*5.99E-05*	*4.99E-06*	*1.17*	*5.12E-05*	*4.27E-06*	*8.34*

Table 15: Observed and actual diffusion coefficients for fully hydrolysed DGEBA-DDA samples as a function of temperature.

To enable comparison, the average diffusion coefficient at each of the three conditioning temperatures has been calculated. 'Thin' samples attained equilibrium much more rapidly than the 'thick' samples and thus it was difficult to obtain several data points in the initial linear portion of their uptake/$\sqrt{t}$ relationships. This had an impact upon the precision to which the gradient could be determined in these samples. As a consequence, only the diffusion coefficients of 'thick' samples (HC4, HC5, HC6) were employed in calculating the average diffusion coefficients shown below in Table 16.

T (℃)	Average $D_{C(T)}$ $(mm^2.min^{-1})$
35	*1.24E-05*
50	*3.04E-05*
60	*5.42E-05*

Table 16: Average diffusion coefficient of fully hydrolysed DGEBA-DDA as a function of temperature.

The diffusion coefficient is observed to increase with increasing temperature which is expected behaviour as at higher temperatures water molecules have greater kinetic energy. As diffusion arises from the random motion of particles, increasing particle kinetic energy increases the rate at which diffusion occurs.

2.3.2.5.3. Determining Diffusion Coefficients, Solubility, and Rate Constants in Unaged DGEBA-DDA Resin

Having obtained the average solubility and diffusion coefficients, representative of fully hydrolysed DGEBA-DDA resin, these can now be used as inputs in the model fitting process. This allows the values of the diffusion coefficient and solubility in the unaged resin to be determined as a function of temperature, along with the rate constants that govern the hydrolysis reaction. In the work that follows, the diffusion-hydrolysis model (developed in section 2.2.2, page 46) is employed to predict the percentage change in mass of each sample as a function of conditioning time. These predictions have then been compared to the gravimetric data for the initially unaged samples conditioned at three different temperatures (Figure 27, Figure 28, Figure 30) and the four unknown input parameters: $S_{A(T)}$, $D_{A(T)}$, $K_{AB(T)}$, and $K_{BC(T)}$, adjusted systematically until the parameter values that maximised the value of R^2 were deduced.

The results of the model/data fitting process for three unaged samples, at each of the three conditioning temperatures, are shown below in Figure 35, Figure 36, and Figure 37 . The model/data fits for the complete set of samples can be found in the appendices (see Appendix B, page 322). The maximum value of R^2 and the values of the four deduced parameters are shown alongside each figure. The red line represents the model predicted percentage mass change of the sample. This is composed of two components: water that has reacted chemically with the polymer network as a consequence of the hydrolysis reaction, and free water molecules absorbed within

the resin. These two components are shown separately alongside the net mass change to aid interpretation of the observed behaviour.

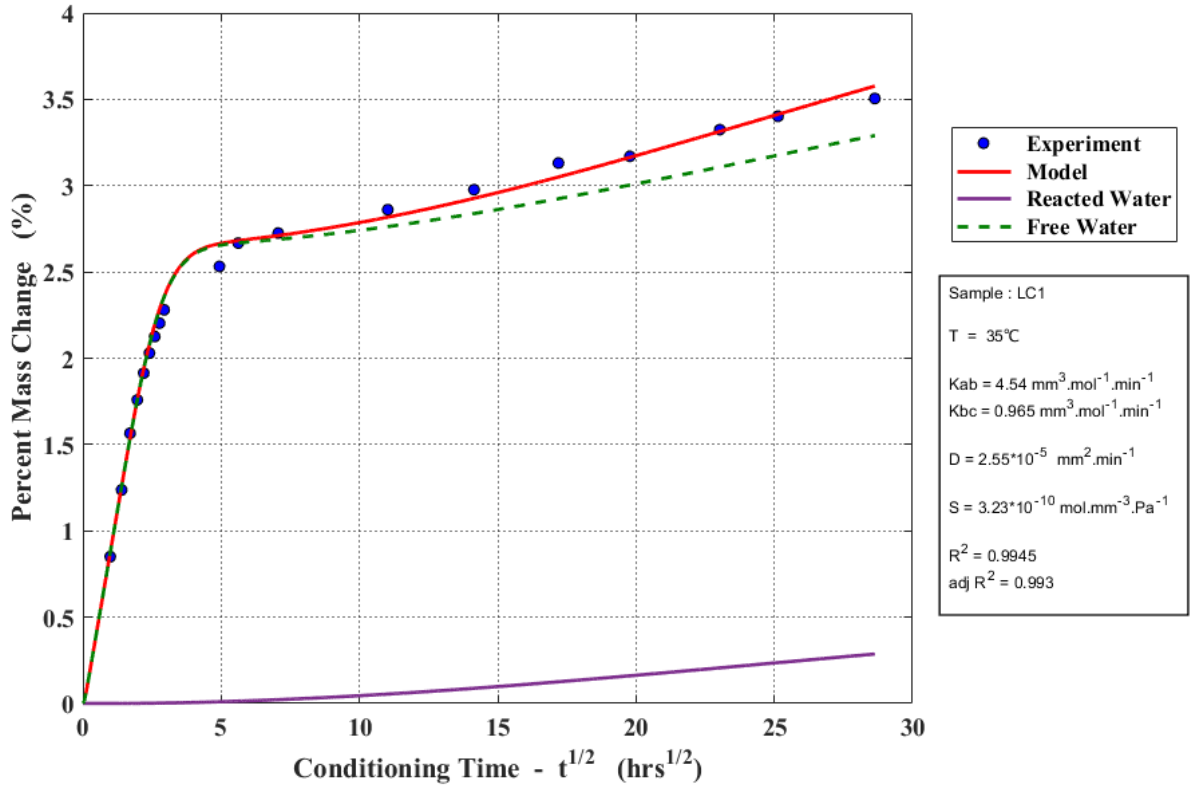

Figure 35: Result of model/data fitting process for sample LC1 conditioned at 35℃ and 100% relative humidity.

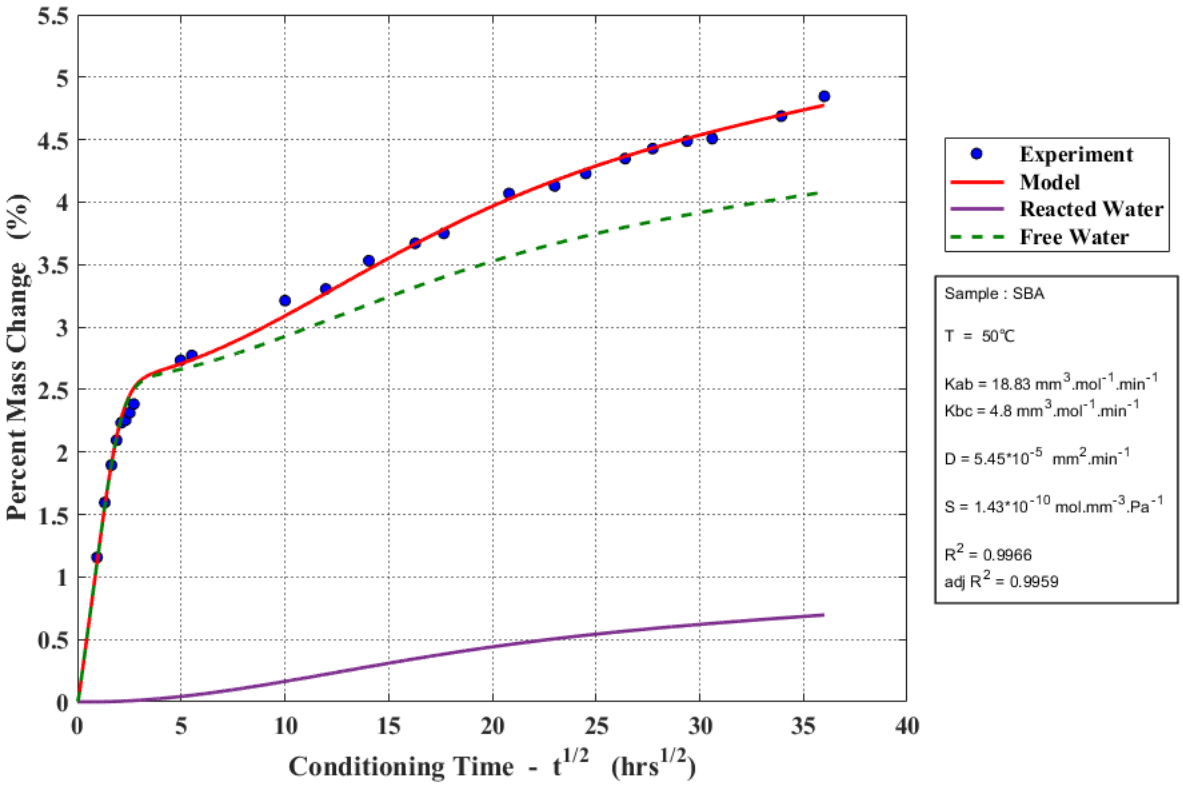

Figure 36: Result of model/data fitting process for sample SBA conditioned at 50℃ and 100% relative humidity.

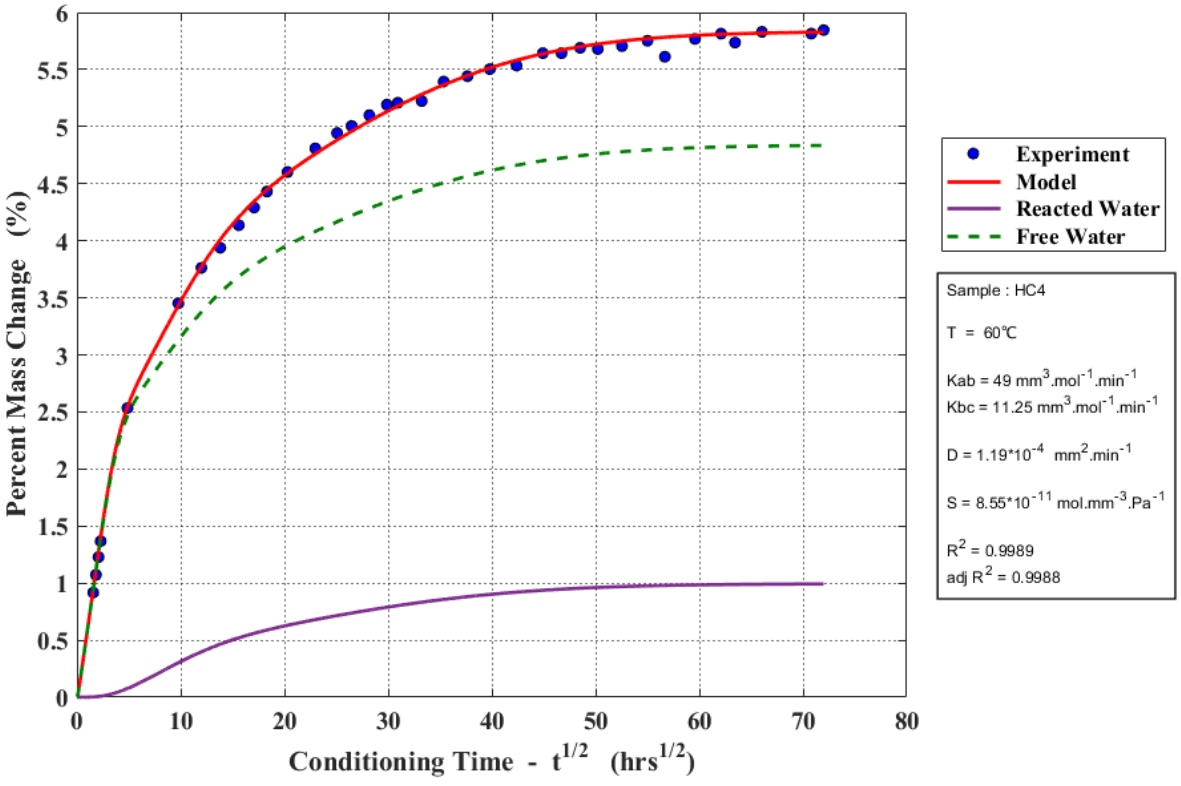

Figure 37: Result of model/data fitting process for sample HC4 conditioned at 60℃ and 100% relative humidity.

These results show that the diffusion-hydrolysis model, developed in this chapter, is capable of describing the anomalous hygrothermal behaviour of DGEBA-DDA resin at each of the three conditioning temperatures. This supports the hypothesis that hydrolysis causes an increase in the solubility of water, within the material, which has the effect of increasing the equilibrium moisture content of the resin as conditioning proceeds.

2.3.2.5.4. Estimation of Errors Associated with Model Derived Parameters

When determining the diffusion coefficient, and solubility, associated with the fully hydrolysed material it was possible to calculate the corresponding errors on these parameters by propagation of errors. In the model/data fitting process that has been employed above, this is not possible. This difficulty arises as an exact analytical solution to the governing equation, describing the diffusion-hydrolysis process, is not known. The solution of the governing equation (equation (138)), as a function of time, is approximated in the model using the finite difference method. This allows the expected mass change as a function of time to be predicted, however without an analytical solution the method of propagation of errors cannot be employed in determining the errors associated with each of the derived parameters.

In an attempt to resolve this issue, the error on the model obtained parameters is estimated by referring to the errors calculated previously, for the diffusion coefficient and solubility (Table 15 and Table 13), for fully hydrolysed samples. This approximation appears justified as the main sources of error associated with these two parameters are related to sample mass, in the case of solubility, and sample mass and dimensions in the case of the diffusion coefficient. Both these sources of error are related to the type of sample: 'thin' (~0.25 mm thickness) or 'thick' (~0.72 mm thickness), as these two sample types have different average masses and dimensions. Thus, for a given sample type, one would expect that the magnitude of the errors associated with the solubility and diffusion coefficients of the unaged material to be roughly proportional to the errors calculated for the fully hydrolysed materials. Below, in Table 17 and Table 18, the average percentage error on the value of the solubility and diffusion coefficient are shown as both a function of conditioning temperature and sample type.

T (℃)	Sample Type	Average Percentage Error on $S_{C(T)}$ (%)
35	Thin	3.02
35	Thick	3.85
50	Thin	2.74
50	Thick	3.62
60	Thin	3.02
60	Thick	3.47

Table 17: Average percentage error on the value of the solubility as a function of both temperature and sample type.

T (℃)	Sample Type	Average Percentage Error on $D_{C(T)}$ (%)
35	Thin	15.23
35	Thick	10.88
50	Thin	14.62
50	Thick	9.56
60	Thin	13.25
60	Thick	9.09

Table 18: Average percentage error on the value of the diffusion coefficient as a function of both temperature and sample type.

The following methodology has been employed in estimating the errors on the model derived values of parameters $S_{A(T)}$ and $D_{A(T)}$. First, each sample is designated as either 'thick' or 'thin' dependent upon the following criteria:

Thin: $d < 0.35\ mm,\ w, l > 28\ mm$

Thick: $d > 0.55\ mm,\ w < 13.5\ mm,\ l > 26.5\ mm$

In Table 19, the type associated with each sample is shown, determined with reference to the above selection criteria.

Sample	Type
LC1	Thin
LC2	Thin
LC3	Thin
Sample 16	Thick
Sample 17	Thick
SB - Test Coupon	Thin
SBA	Thin
SBB	Thin
HC4	Thick
HC5	Thick
HC6	Thick

Table 19: Sample type designation.

The error associated with each of the model derived parameters, $S_{A(T)}$ and $D_{A(T)}$, was then estimated by referring to Table 17 and Table 18 and applying the appropriate average percentage error to the model obtained values.

2.3.2.5.5. Results of the Model Fitting Process

2.3.2.5.5.1. Results of the Model Fitting Process - Solubility ($S_{A_{(T)}}$)

Table 20 below shows the values of the initial solubility obtained for each sample from the model/data fitting process.

T (℃)	Sample	$S_{A(T)}$ $(mol.mm^{-3}.Pa^{-1})$	Average Percentage Error on $S_{C_{(T)}}$ (%)	$\Delta S_{A(T)}$ $(mol.mm^{-3}.Pa^{-1})$
35	*LC1*	*3.23E-10*	*3.02*	*9.74E-12*
35	*LC2*	*3.17E-10*	*3.02*	*9.56E-12*
35	*LC3*	*3.26E-10*	*3.02*	*9.83E-12*
50	*Sample 16*	*1.40E-10*	*3.62*	*5.07E-12*
50	*Sample 17*	*1.46E-10*	*3.62*	*5.28E-12*
50	*SB-Test Coupon*	*1.49E-10*	*2.74*	*4.07E-12*
50	*SBA*	*1.43E-10*	*2.74*	*3.93E-12*
50	*SBB*	*1.39E-10*	*2.74*	*3.80E-12*
60	*HC4*	*8.55E-11*	*3.47*	*2.97E-12*
60	*HC5*	*8.69E-11*	*3.47*	*3.02E-12*
60	*HC6*	*8.88E-11*	*3.47*	*3.09E-12*

Table 20: Solubility of unaged DGEBA-DDA resin as a function of temperature.

In Table 21 below, the average value of the solubility and equilibrium moisture content as a function of temperature, have been calculated for unaged DGEBA-DDA resin.

T (℃)	Average $S_{A(T)}$ $(mol.mm^{-3}.Pa^{-1})$	Average Percentage Change in Mass (Unaged DGEBA-DDA Resin) (%)
35	*3.22E-10*	*2.64*
50	*1.43E-10*	*2.58*
60	*8.71E-11*	*2.53*

Table 21: Average solubility and equilibrium moisture content of unaged DGEBA-DDA resin as a function of temperature.

In Table 21, the average value of the initial equilibrium moisture content appears to show a slight decrease with increasing temperature, taking an average value of ~2.58% w/w across all three temperatures. It is of interest to note that this initial equilibrium water content is similar to that observed in the epoxy resin composed of DGEBA, cross-linked with the amine hardener DDM. The equilibrium moisture content of epoxy resins is strongly dependent on the functionality of the epoxy component [25] (number of epoxide groups) as it is the reaction of these groups, with the hardener, that result in the formation of polar OH groups. Although these two resins are formed from different hardeners, they are both based on the difunctional DGEBA molecule. Thus, they might be expected to possess similar absorption properties.

When immersed in liquid water, and conditioned to equilibrium, DGEBA-DDM is observed to absorb ~2.75%, by mass, of water [25]. However, the densities of the DGEBA-DDA resin employed in this work, and that of DGEBA-DDM, are different, $1.226 \times 10^{-3}\ g.mm^{-3}$ and $1.193 \times 10^{-3}\ g.mm^{-3}$ respectively, and thus this must be accounted for before a direct comparison between their moisture contents can be made. The water content within a given volume of DGEBA-DDM resin is first calculated. This mass of water is then added to the mass of an identical volume of dry DGEBA-DDA resin. This indicated that if DGEBA-DDA resin was to absorb this quantity of water then its mass would increase by 2.675%. This is very close to the value of ~2.58%, obtained in this work, and thus, when at equilibrium at 100% relative humidity, DGEBA-DDA and DGEBA-DDM both contain similar quantities of water molecules within a given volume.

Thus, it can be concluded that the initial equilibrium moisture content of DGEBA-DDA resin is similar to that of other DGEBA based resins and it is the occurrence of hydrolysis which leads to an increase in material solubility. The end result of this reaction is that the equilibrium moisture content of fully aged DGEBA-DDA resin at 100% relative humidity, is greater than that which is observed in other DGEBA systems where hydrolysis does not occur. Table 22 below shows the comparison between the solubility of DGEBA-DDA resin before, and after, complete hydrolysis has occurred.

T (℃)	$S_{A(T)}$ $(mol.mm^{-3}.Pa^{-1})$	$S_{C(T)}$ $(mol.mm^{-3}.Pa^{-1})$	Equilibrium Moisture Content (Unaged) (%) (w/w)	Equilibrium Moisture Content (Fully Aged) (%) (w/w)	$\frac{S_{C(T)}}{S_{A(T)}}$
35	*3.22E-10*	*5.97E-10*	*2.64*	*4.84*	*1.86*
50	*1.43E-10*	*2.62E-10*	*2.58*	*4.67*	*1.83*
60	*8.71E-11*	*1.66E-10*	*2.53*	*4.79*	*1.91*

Table 22: Comparison of the solubility of unaged, and fully hydrolysed, DGEBA-DDA resin as a function of temperature.

This comparison indicates that, as a consequence of the hydrolysis reaction, material solubility increases and that the solubility of fully hydrolysed DGEBA-DDA resin is approximately twice that of the unaged material.

2.3.2.5.5.2. Results of the Model Fitting Process - Diffusion Coefficient ($D_{A_{(T)}}$)

Table 23 below shows the values of the initial diffusion coefficient obtained for each sample from the model/data fitting process.

T (°C)	Sample	$D_{A_{(T)}}$ $(mm^2.min^{-1})$	Average Percentage Error on $D_{C_{(T)}}$ (%)	$\Delta D_{A_{(T)}}$ $(mm^2.min^{-1})$
35	*LC1*	*2.55E-05*	*15.23*	*3.89E-06*
35	*LC2*	*2.60E-05*	*15.23*	*3.96E-06*
35	*LC3*	*2.50E-05*	*15.23*	*3.81E-06*
50	*Sample 16*	*6.07E-05*	*9.56*	*5.80E-06*
50	*Sample 17*	*5.16E-05*	*9.56*	*4.93E-06*
50	*SB-Test Coupon*	*5.63E-05*	*14.62*	*8.23E-06*
50	*SBA*	*5.45E-05*	*14.62*	*7.97E-06*
50	*SBB*	*5.25E-05*	*14.62*	*7.67E-06*
60	*HC4*	*1.19E-04*	*9.09*	*1.08E-05*
60	*HC5*	*1.17E-04*	*9.09*	*1.06E-05*
60	*HC6*	*1.13E-04*	*9.09*	*1.02E-05*

Table 23: Diffusion coefficient of unaged DGEBA-DDA resin as a function of temperature.

Table 24 shows the average value of the diffusion coefficient as a function of temperature.

T (°C)	Average $D_{A_{(T)}}$ $(mm^2.min^{-1})$
35	*2.55E-05*
50	*5.51E-05*
60	*1.16E-04*

Table 24: Average value of the diffusion coefficient as a function of temperature for unaged DGEBA-DDA resin.

A similar trend to that which occurs in the fully hydrolysed resin is observed with the diffusion coefficient increasing with increasing temperature. In Table 25 below, the average diffusion coefficients of unaged, and fully hydrolysed, DGEBA-DDA resin are compared at each of the three conditioning temperatures.

T (°C)	$D_{A(T)}$ $(mm^2.min^{-1})$	$D_{C(T)}$ $(mm^2.min^{-1})$	$\frac{D_{C(T)}}{D_{A(T)}}$
35	*2.55E-05*	*1.24E-05*	*0.49*
50	*5.51E-05*	*3.04E-05*	*0.55*
60	*1.16E-04*	*5.42E-05*	*0.47*

Table 25: Comparison of the diffusion coefficients of unaged, and fully hydrolysed, DGEBA-DDA resin as a function of temperature.

This comparison indicates that the net effect of hydrolysis is to reduce the diffusion coefficient of water in DGEBA-DDA resin. More specifically, the diffusion coefficient of fully hydrolysed DGEBA-DDA resin is reduced approximately by a factor of two.

Thus, the net effect of the complete hydrolysis of DGEBA-DDA resin, at a given temperature, is to approximately double the solubility of water within the resin and reduce the diffusion coefficient by a factor of two. If the factor associated with the increase in solubility is expressed by α, then the conditioning experiments performed in this work show that the factor associated with the decrease in the diffusion coefficient is inversely proportional to the value of α. This relationship, between solubility and diffusion coefficient, has been observed for other epoxy resins in the literature in which some chemical change occurs within the material in the presence of absorbed moisture [8, 36, 37].

2.3.2.5.5.3. Results of the Model Fitting Process - Rate Constants ($K_{AB_{(T)}}$ and $K_{BC_{(T)}}$)

Table 26 below shows the values of the two rate constants obtained from each sample through the model fitting process, and in Table 27 their average values are shown.

T (℃)	Sample	K_{AB} $(mm^3.mol^{-1}.min^{-1})$	K_{BC} $(mm^3.mol^{-1}.min^{-1})$
35	*LC1*	*4.54*	*0.96*
35	*LC2*	*4.30*	*0.87*
35	*LC3*	*4.82*	*0.82*
50	*Sample 16*	*17.40*	*4.76*
50	*Sample 17*	*17.39*	*5.22*
50	*SB - Test Coupon*	*17.43*	*4.64*
50	*SBA*	*18.83*	*4.80*
50	*SBB*	*21.37*	*4.81*
60	*HC4*	*49.00*	*11.25*
60	*HC5*	*49.45*	*12.60*
60	*HC6*	*49.62*	*13.66*

Table 26: Hydrolysis rate constants obtained from samples conditioned at each of the three temperatures.

T (℃)	Average K_{AB} $(mm^3.mol^{-1}.min^{-1})$	Average K_{BC} $(mm^3.mol^{-1}.min^{-1})$	$\frac{K_{AB}}{K_{BC}}$
35	*4.56*	*0.88*	*5.16*
50	*18.48*	*4.85*	*3.81*
60	*49.36*	*12.51*	*3.95*

Table 27: Average hydrolysis rate constants as a function of temperature.

The results of the model fitting process indicate that both rate constants increase with increasing temperature. This behaviour is expected as at higher temperatures the average kinetic energy of water molecules is greater. Thus, it becomes statistically more probable that a water molecule, in the vicinity of a hydrolysable site, will have energy equal to, or greater than, the activation energy associated with the hydrolysis reaction; allowing the energy barrier to be overcome and the

hydrolysis reaction to occur. However, at a given temperature the magnitudes of the two rate constants are different which is unexpected as it had been assumed that the two hydrolysis reactions occurring in the fundamental unit, to produce one free polymer chain, involved identical chemical processes. Thus, one would expect the values of $K_{AB\,(T)}$ and $K_{BC\,(T)}$ to be equal at all temperatures. The hypothesis, that the two hydrolysis reactions involved in forming a free polymer chain are identical, is supported by the work of Fata et al [6] who have suggested that only one specific type of chemical reaction is responsible for hydrolysis in DGEBA-DDA resin.

In the work that follows, the activation energies associated with the two rate constants have been calculated and shown to be identical (see section 2.3.2.6.3, page 139). This suggests that the same chemical reaction is occurring in both hydrolysis steps. If the two hydrolysis reactions occurring in the fundamental unit are identical, then the possibility that the first hydrolysis reaction effects the rate of the second reaction, must be considered. The first hydrolysis reaction results in two polymer chains that are both bound at one end to the polymer network, and unbound and free to move at the other end. With this freedom of movement, the polymer chains can undergo reorientation to achieve a lower energy configuration which has the effect of altering the morphology of the polymer network. It is possible that in this new morphology, access to the second hydrolysable site in the fundamental unit, becomes constrained. This will result in a lower value of the rate constant for the second hydrolysis process, even though the underlying chemical reactions are identical.

In Table 27 the ratio of the magnitudes of two rate constants, K_{AB} and K_{BC}, was calculated at each of the three conditioning temperatures to allow the differences in their values to be quantified. At 60℃ and 50℃ the rate constant associated with the first hydrolysis reaction is observed to be approximately four times greater than that associated with the second reaction. This difference increases to approximately five times at 35℃. However, this deviation at 35℃ from the trend observed at the two higher temperatures most likely arises as a result of the slow rate of the hydrolysis reaction at 35℃. To accurately determine the values of the two rate constants, through the model fitting process, it is necessary that DGEBA-DDA samples are conditioned for a time period sufficient for both reaction processes to occur ($A \rightarrow B$ and $B \rightarrow C$). In Figure 38, Figure 39, and Figure 40, the predicted fractional proportions of each type of fundamental unit: A, B, and C, in DGEBA-DDA resin are shown as a function of both conditioning time and temperature, at 100% relative humidity. The values of the rate constants, K_{AB} and K_{BC}, employed in this analysis were those obtained earlier from the model fitting process (Table 27). It has also been assumed that the time required for the resin to attain equilibrium with

its conditioning environment is negligible. In other words, no water concentration gradients exist and the hydrolysis reaction proceeds uniformly throughout the geometry of the material.

Figure 38 indicates that at 60℃, complete hydrolysis of the resin occurs after a conditioning time of ~65 $hrs^{\frac{1}{2}}$ and thus the final state of the resin is one composed entirely of fundamental unit of type C.

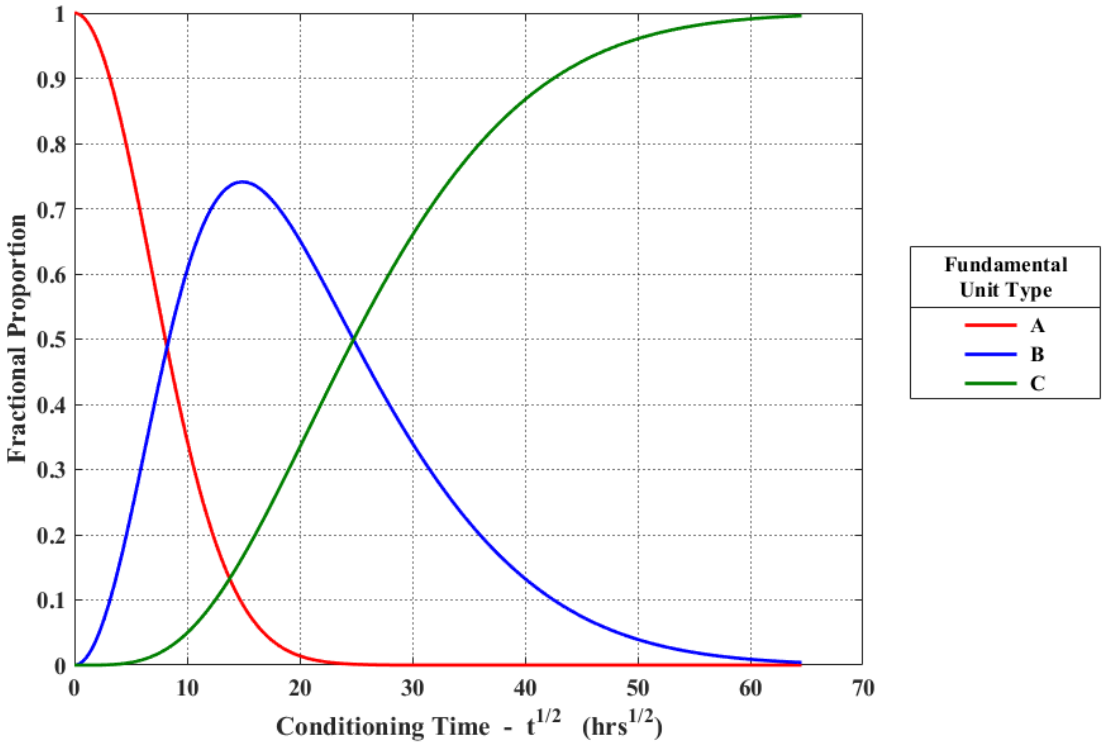

Figure 38: Evolution of the fractional proportions of each type of fundamental unit as a function of conditioning time at 60℃.

In Figure 39 below it is apparent that, after 65 $hrs^{\frac{1}{2}}$ conditioning at 50℃, hydrolysis is still occurring. All fundamental units have undergone at least one hydrolysis reaction and thus the fractional proportion of fundamental unit A, is zero. A small quantity of fundamental units (type B) have yet to undergo the second hydrolysis reaction, however the bulk of the resin is composed of fully hydrolysed units (type C).

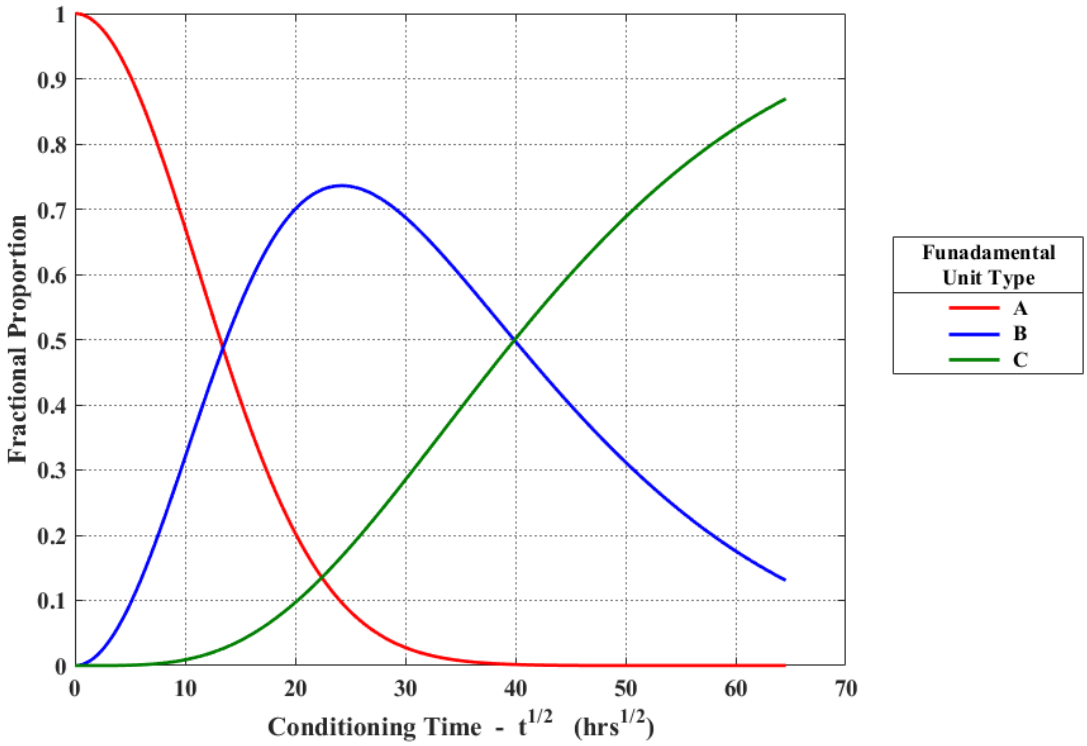

Figure 39: Evolution of the fractional proportions of each type of fundamental unit as a function of conditioning time at 50℃.

The evolution of fundamental units at 35℃ is shown below in Figure 40. These predictions indicate that, even after conditioning for 65 $hrs^{\frac{1}{2}}$, hydrolysis is far from completion. The bulk of the resin, ~75%, is composed of fundamental units in which only one hydrolysis reaction has occurred (type B). The remaining 25% of the resin is composed predominantly of fully hydrolysed units (type C), with only a very small quantity of unreacted units still remaining (type A).

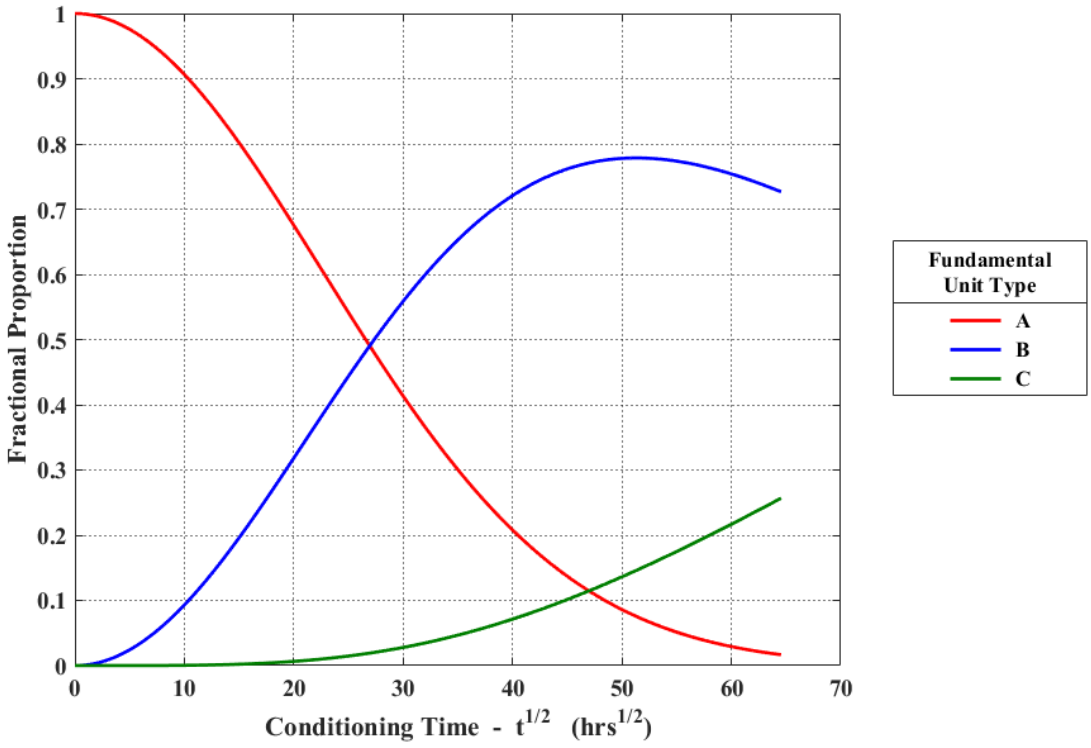

Figure 40: Evolution of the fractional proportions of each type of fundamental unit as a function of conditioning time at 35℃.

In Table 28 the approximate fractional proportions of each type of fundamental unit, within each group of resin samples at the time that their conditioning experiments were concluded, are shown for each of the three temperatures.

Temperature (℃)	**Mole Fraction of *A***	**Mole Fraction of *B***	**Mole Fraction of *C***
35	0.45	0.53	0.02
50	0	0.43	0.57
60	0	0	1

Table 28: Approximate fractional proportions of fundamental units within each group of samples at the point in time at which their conditioning was concluded.

At 60℃ and 50℃ the fraction of unit C is greater than 0.5, however at 35℃ this fraction is very small at 0.02. As unit C is a product of the second hydrolysis reaction, its very low proportion in

the samples conditioned at 35℃ would suggest that this conditioning time was insufficient for the second hydrolysis reaction to noticeably contribute to the change in material solubility. As a result, the error on the value of K_{BC} obtained at 35℃ will be large and thus this is the most likely cause of the difference in the rate constant ratio obtained at 35℃ (Table 27). This hypothesis could be tested by repeating the gravimetric conditioning experiment at 35℃ for an extended conditioning period to ensure that both hydrolysis processes contribute to the increase in material solubility. The model fitting process could then be applied to this new conditioning data and the ratio between the two rate constants re-calculated. If the hypothesis is correct, then the ratio obtained from the new 35℃ data should be similar to that observed at the two higher conditioning temperatures. However, using the adjusted values of the rate constants in Table 29, the conditioning time required to obtain a fractional proportion of unit C equal to, or greater than, 0.57, at 35℃, is predicted to be ~10 months. Thus, repeating the 35℃ conditioning experiment for a time period sufficient for the significant formation of fundamental unit C, was impractical.

In the work that follows, the hypothesis that was explored above is taken to account for the difference in the rate constant ratio at 35℃. To estimate the actual value of K_{BC}, the ratio at 35℃ is first approximated to being equal to the average of the ratios at the two higher temperatures. The expected value of K_{BC} can then be calculated from the adjusted ratio and the value of K_{AB}:

$$K_{BC} = \frac{K_{AB}}{(Adjusted\ Ratio)} \tag{160}$$

Table 29 shows the corrected average value of K_{BC}, at 35℃, obtained from equation (160) and in Table 30 the value of K_{BC} has been corrected for samples LC1, LC2, and LC3.

T (℃)	Average K_{AB} $(mm^3.mol^{-1}.min^{-1})$	Average K_{BC} $(mm^3.mol^{-1}.min^{-1})$	Adjusted $\left(\frac{K_{AB}}{K_{BC}}\right)$
35	*4.56*	*1.17*	*3.88*
50	*18.48*	*4.85*	*3.81*
60	*49.36*	*12.51*	*3.95*

Table 29: Adjusted average hydrolysis rate constants as a function of conditioning temperature.

T (℃)	Sample	K_{AB} $(mm^3.mol^{-1}.min^{-1})$	K_{BC} $(mm^3.mol^{-1}.min^{-1})$
35	*LC1*	*4.54*	*1.17*
35	*LC2*	*4.30*	*1.11*
35	*LC3*	*4.82*	*1.24*
50	*Sample 16*	*17.40*	*4.76*
50	*Sample 17*	*17.39*	*5.22*
50	*SB - Test Coupon*	*17.43*	*4.64*
50	*SBA*	*18.83*	*4.80*
50	*SBB*	*21.37*	*4.81*
60	*HC4*	*49.00*	*11.25*
60	*HC5*	*49.45*	*12.60*
60	*HC6*	*49.62*	*13.66*

Table 30: Rate constants obtained for each sample where the values of K_{BC} for samples LC1, LC2, and LC3, have been corrected to account for the adjusted ratio.

In the section that follows the activation energy and limiting value, associated with the rate constant K_{BC}, will be determined. In this analysis the adjusted values of K_{BC}, in Table 30, will be employed.

2.3.2.6. Calculating the Arrhenius Relationships for the Solubility, Diffusion Coefficient, and Rate Constants

In the previous work, (section 2.3.2.5, page 107) the values for the solubility, diffusion coefficient, and rate constants, at three different temperatures, were calculated for both unaged, and fully hydrolysed, DGEBA-DDA resin. However, in order to predict the long-term behaviour of DGEBA-DDA resin within its engineering environment, the values of these parameters over a wide temperature range are required. A standard method for obtaining the value of a temperature dependent parameter, at an unmeasured temperature, is to assume that it follows an Arrhenius relation. The Arrhenius relation [105] is defined by equation (161):

$$r_{(T)} = r_0 \, e^{-\frac{E_r}{RT}} \tag{161}$$

Where $r_{(T)}$ is the value of the parameter at a temperature T, r_0 is the limiting value the parameter tends towards as temperature tends towards infinity, E_r is the activation energy for the process in

units of $J.mol^{-1}$, R is the universal gas constant in units of $J.mol^{-1}.K^{-1}$, and T is the temperature in K. A temperature dependent parameter obeys an Arrhenius law if the relationship obtained from plotting the natural logarithm of the parameter, as a function of the inverse of the observation temperature, is represented by a straight line. Although each of the four parameters has only been measured at three different temperatures, it will be shown below that their general trends are linear. The solubility and diffusion coefficients, reported in the literature for a wide range of epoxy resins, have been observed to obey an Arrhenius law [35, 97]. Thus, it is reasonable to assume that the behaviour of the diffusion coefficient and solubility, in the unaged and fully hydrolysed resin, obeys an Arrhenius relationship in the temperature range: 35℃ to 60℃. The rates associated with chemical reactions are widely observed to obey the Arrhenius relation [105] and thus its application to the rate constants, governing the hydrolysis reaction, is justified.

The value of the activation energy (E_r) and limiting parameter (r_0) can be calculated by obtaining the gradient, and intercept, of the line of best fit to the $ln(r_{(T)})/T^{-1}$ plot.

$$E_r = -mR \tag{162}$$

$$r_0 = e^c \tag{163}$$

Where m and c are the gradient, and intercept, respectively of the line of best fit.

2.3.2.6.1. Determining the Activation Energy (E_s) and Limiting Value (S_0) Associated with the Solubility of Unaged and Fully Hydrolysed DGEBA-DDA Resin

Below, the natural logarithm of the solubility of each sample, for unaged (Table 31) and fully hydrolysed (Table 32) DEGBA-DDA resin, has been calculated along with their corresponding values of inverse temperature. The Arrhenius plots for the solubility of the unaged (S_A), and fully hydrolysed (S_C), resin are displayed in Figure 41, and Figure 42, and Table 33shows the values of the activation energy (E_s) and limiting value (S_0) of each state.

T (℃)	Sample	$S_{A(T)}$ $(mol.mm^{-3}.Pa^{-1})$	$\Delta S_{A(T)}$ $(mol.mm^{-3}.Pa^{-1})$	T^{-1} (K^{-1})	$Ln\left(S_{A(T)}\right)$	$\Delta Ln\left(S_{A(T)}\right)$
35	LC1	3.23E-10	9.74E-12	3.247E-03	-21.85	0.0302
35	LC2	3.17E-10	9.56E-12	3.247E-03	-21.87	0.0302
35	LC3	3.26E-10	9.83E-12	3.247E-03	-21.85	0.0302
50	Sample 16	1.40E-10	5.07E-12	3.096E-03	-22.69	0.0362
50	Sample 17	1.46E-10	5.28E-12	3.096E-03	-22.65	0.0362
50	SB - Test Coupon	1.49E-10	4.07E-12	3.096E-03	-22.63	0.0274
50	SBA	1.43E-10	3.93E-12	3.096E-03	-22.67	0.0274
50	SBB	1.39E-10	3.80E-12	3.096E-03	-22.70	0.0274
60	HC4	8.55E-11	2.97E-12	3.003E-03	-23.18	0.0347
60	HC5	8.69E-11	3.02E-12	3.003E-03	-23.17	0.0347
60	HC6	8.88E-11	3.09E-12	3.003E-03	-23.14	0.0347

Table 31: Natural logarithm of sample solubility as a function of temperature for unaged DGEBA-DDA resin.

T (℃)	Sample	$S_{C(T)}$ $(mol.mm^{-3}.Pa^{-1})$	$\Delta S_{C(T)}$ $(mol.mm^{-3}.Pa^{-1})$	T^{-1} (K^{-1})	$Ln\left(S_{C(T)}\right)$	$\Delta Ln\left(S_{C(T)}\right)$
35	HC1	5.99E-10	1.89E-11	3.247E-03	-21.24	0.0316
35	HC2	5.88E-10	1.86E-11	3.247E-03	-21.25	0.0317
35	HC3	6.01E-10	1.65E-11	3.247E-03	-21.23	0.0274
35	HC4	5.88E-10	2.27E-11	3.247E-03	-21.25	0.0385
35	HC5	5.99E-10	2.31E-11	3.247E-03	-21.24	0.0385
35	HC6	6.05E-10	2.33E-11	3.247E-03	-21.23	0.0385
50	HC1	2.61E-10	7.14E-12	3.096E-03	-22.07	0.0273
50	HC2	2.60E-10	7.15E-12	3.096E-03	-22.07	0.0274
50	HC3	2.60E-10	7.13E-12	3.096E-03	-22.07	0.0274
50	HC4	2.61E-10	1.00E-11	3.096E-03	-22.07	0.0385
50	HC5	2.63E-10	1.01E-11	3.096E-03	-22.06	0.0385
50	HC6	2.64E-10	8.29E-12	3.096E-03	-22.06	0.0314
60	HC1	1.58E-10	4.33E-12	3.003E-03	-22.57	0.0274
60	HC2	1.56E-10	3.83E-12	3.003E-03	-22.58	0.0246
60	HC3	1.59E-10	6.15E-12	3.003E-03	-22.56	0.0388
60	HC4	1.67E-10	6.41E-12	3.003E-03	-22.52	0.0385
60	HC5	1.66E-10	4.52E-12	3.003E-03	-22.52	0.0272
60	HC6	1.67E-10	6.41E-12	3.003E-03	-22.52	0.0385

Table 32: Natural logarithm of sample solubility as a function of temperature for fully hydrolysed DGEBA-DDA resin.

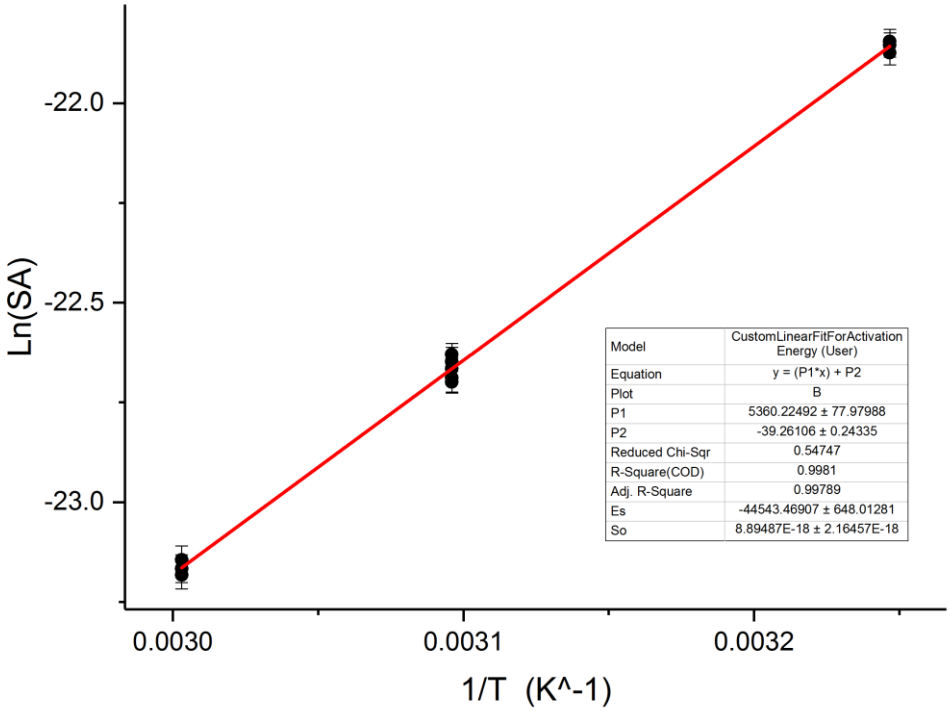

Figure 41: Arrhenius plot for the solubility of unaged DGEBA-DDA resin.

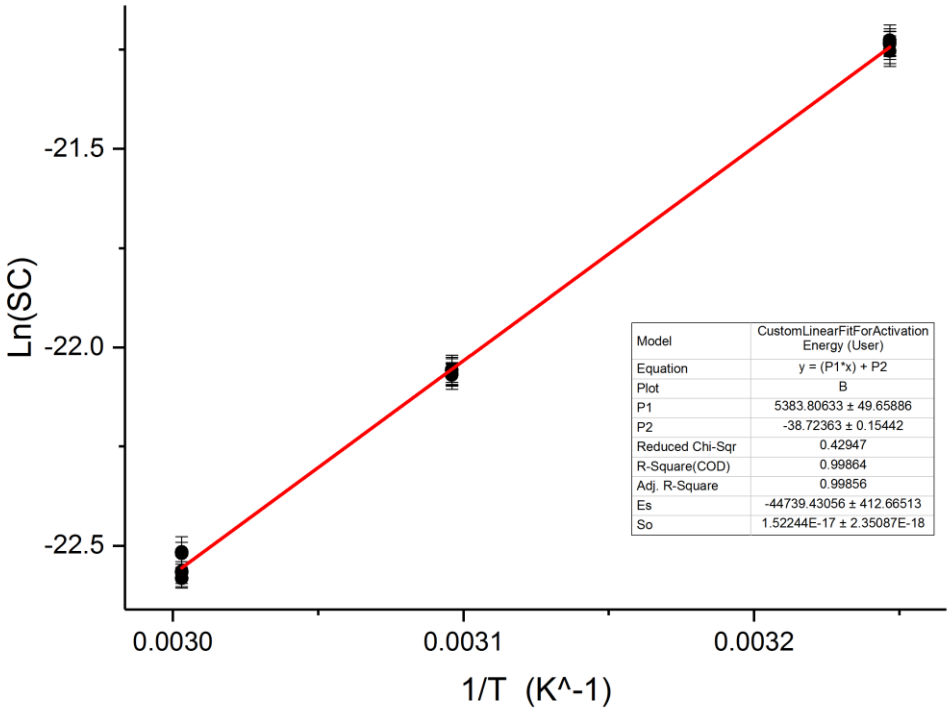

Figure 42: Arrhenius plot for the solubility of fully hydrolysed DGEBA-DDA resin.

Parameter	E_s $(kJ.mol^{-1})$	S_0 $(mol.mm^{-3}.Pa^{-1})$	ΔE_s $(kJ.mol^{-1})$	ΔS_0 $(mol.mm^{-3}.Pa^{-1})$	Percentage Error on E_s (%)	Percentage Error on S_0 (%)
S_A	*-44.54*	*8.89E-18*	*0.65*	*2.16E-18*	*1.46*	*24.30*
S_C	*-44.74*	*1.52E-17*	*0.41*	*2.35E-18*	*0.92*	*15.46*

Table 33: Activation energy and limiting value for the solubility of unaged and fully Hydrolysed DGEBA-DDA resin.

The results in Table 33 show that the activation energies associated with the two different states (unaged and fully hydrolysed) are identical. The activation energy E_s, also referred to as the heat of dissolution, is dependent on the intermolecular interactions between water molecules and functional groups within the polymer structure [97]. In DGEBA-DDA these interactions are dominated by the interaction of water with polar OH groups. The observation that the activation energy of both the unaged, and fully hydrolysed, states is identical suggests that the chemical groups responsible for the increase in solubility in the hydrolysed state are identical to those present in the unaged state. This is consistent with the hypothesis that hydrolysis results in the introduction of polar OH groups to the polymer network leading to an increase in the equilibrium moisture content of the material. This is because the functional groups responsible for water absorption in the unaged state are also polar OH groups; formed through the reaction of epoxide groups with amines during cure. Referring to Table 33, the limiting value of the solubility (S_0) in the fully hydrolysed state is greater than that of the unaged state. This is expected as the hydrolysed material contains a greater quantity of OH groups than the unaged material and thus the concentration of water that the material can absorb, and hence its solubility, will be greater than that of the unaged material as $T \to \infty$.

2.3.2.6.2. Determining the Activation Energy (E_d) and Limiting Value (D_0) Associated with the Diffusion Coefficient of Unaged and Fully Hydrolysed DGEBA-DDA Resin

In Table 34 and Table 35 below, the natural logarithm of the diffusion coefficient is shown as a function of the inverse of temperature, for both the unaged and aged material. Figure 43 and Figure 44 show the Arrhenius plots obtained for the diffusion coefficient, in the two different material states, and Table 36 shows the values of the activation energy, and limiting value, obtained from these two Arrhenius plots.

T (℃)	Sample	$D_{A(T)}$ $(mm^2.min^{-1})$	$\Delta D_{A(T)}$ $(mm^2.min^{-1})$	T^{-1} (K^{-1})	$Ln\left(D_{A(T)}\right)$	$\Delta Ln\left(D_{A(T)}\right)$
35	LC1	2.55E-05	3.89E-06	3.2468E-03	-10.58	0.152
35	LC2	2.60E-05	3.96E-06	3.2468E-03	-10.56	0.152
35	LC3	2.50E-05	3.81E-06	3.2468E-03	-10.60	0.152
50	Sample 16	6.07E-05	5.80E-06	3.0960E-03	-9.71	0.096
50	Sample 17	5.16E-05	4.93E-06	3.0960E-03	-9.87	0.096
50	SB - Test Coupon	5.63E-05	8.23E-06	3.0960E-03	-9.79	0.146
50	SBA	5.45E-05	7.97E-06	3.0960E-03	-9.82	0.146
50	SBB	5.25E-05	7.67E-06	3.0960E-03	-9.86	0.146
60	HC4	1.19E-04	1.08E-05	3.0030E-03	-9.04	0.091
60	HC5	1.17E-04	1.06E-05	3.0030E-03	-9.06	0.091
60	HC6	1.13E-04	1.02E-05	3.0030E-03	-9.09	0.091

Table 34: Natural logarithm of sample diffusion coefficient as a function of temperature for unaged DGEBA-DDA resin.

T (℃)	Sample	$D_{C(T)}$ $(mm^2.min^{-1})$	$\Delta D_{C(T)}$ $(mm^2.min^{-1})$	T^{-1} (K^{-1})	$Ln\left(D_{C(T)}\right)$	$\Delta Ln\left(D_{C(T)}\right)$
35	HC4	1.24E-05	1.48E-06	3.2468E-03	-11.30	0.119
35	HC5	1.27E-05	1.39E-06	3.2468E-03	-11.27	0.109
35	HC6	1.21E-05	1.19E-06	3.2468E-03	-11.32	0.098
50	HC4	3.13E-05	3.52E-06	3.0960E-03	-10.37	0.112
50	HC5	3.07E-05	3.05E-06	3.0960E-03	-10.39	0.099
50	HC6	2.92E-05	2.19E-06	3.0960E-03	-10.44	0.075
60	HC4	5.62E-05	6.17E-06	3.0030E-03	-9.79	0.110
60	HC5	5.52E-05	4.40E-06	3.0030E-03	-9.80	0.080
60	HC6	5.12E-05	4.27E-06	3.0030E-03	-9.88	0.083

Table 35: Natural logarithm of sample diffusion coefficient as a function of temperature for fully hydrolysed DGEBA-DDA resin.

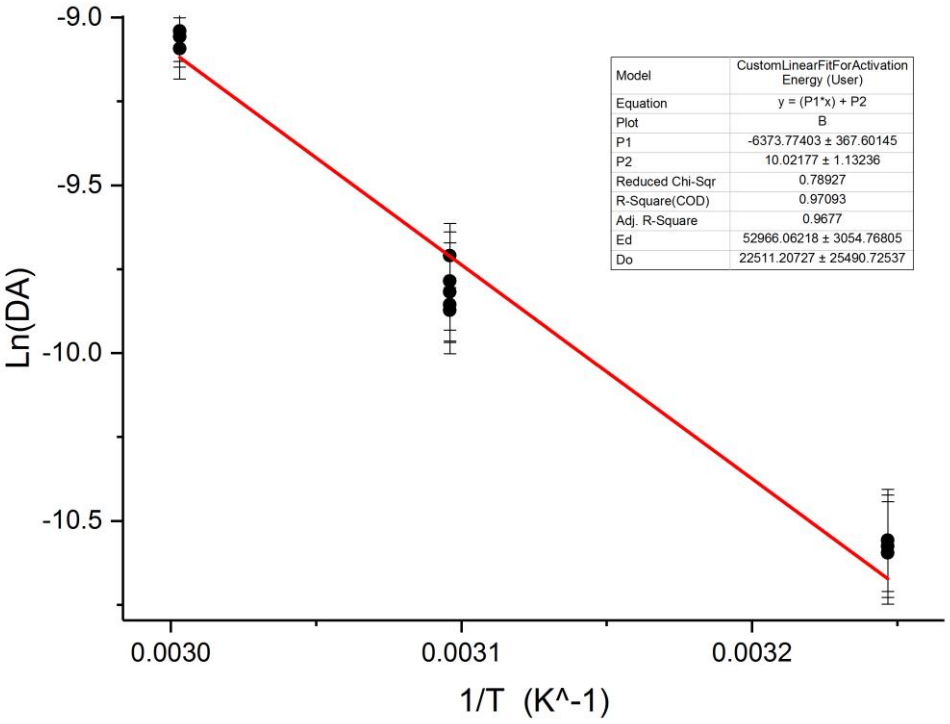

Figure 43: Arrhenius plot for the diffusion coefficient of unaged DGEBA-DDA resin.

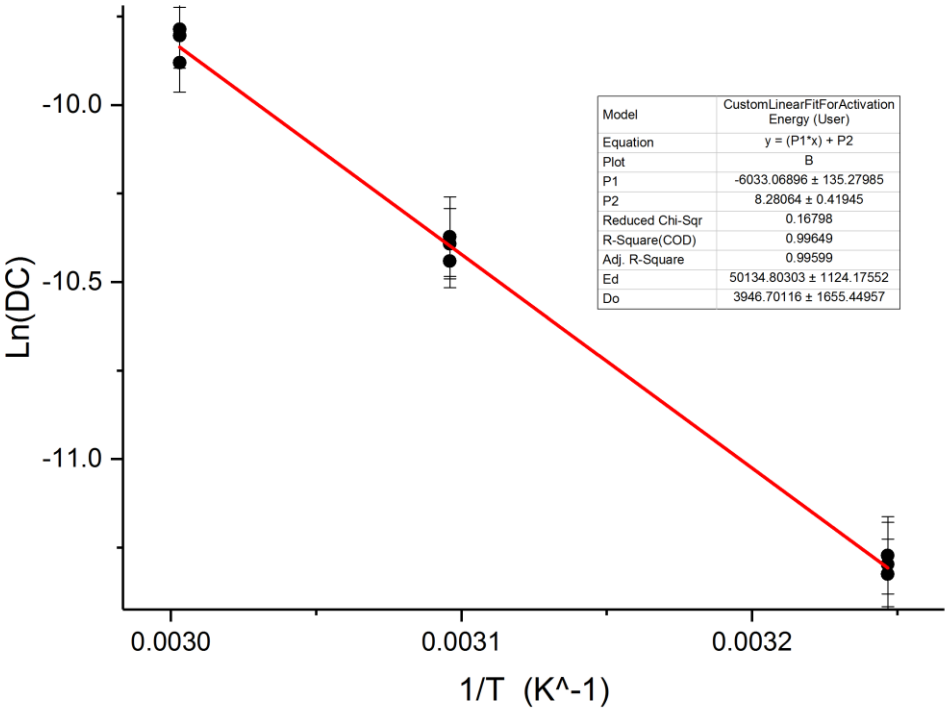

Figure 44: Arrhenius plot for the diffusion coefficient of fully hydrolysed DGEBA-DDA resin.

Parameter	E_d ($kJ.mol^{-1}$)	D_0 ($mm^2.min^{-1}$)	ΔE_d ($kJ.mol^{-1}$)	ΔD_0 ($mm^2.min^{-1}$)	Percentage Error on E_d (%)	Percentage Error on D_0 (%)
D_A	*52.97*	*22511*	*3.05*	*25491*	*5.76*	*113.24*
D_C	*50.13*	*3847*	*1.12*	*1655*	*2.23*	*43.02*

Table 36: Activation energy and limiting value for the diffusion coefficient of unaged and fully hydrolysed DGEBA-DDA resin.

Referring to Table 36, the activation energy (E_d) associated with diffusion in both the unaged, and fully hydrolysed, states is approximately the same when the errors on the parameters are accounted for. This observation is consistent with the description of the diffusion of water molecules in polymers proposed by Merdas et al [36]. In this model, the time required for one water molecule to diffuse from one polar group to another, is negligible when compared to the time frame required for a water molecule to de-bond from a given polar group, thus allowing it to diffuse to another. Thus, the rate at which water molecules move between adjacent polar groups, and hence the rate at which bulk diffusion occurs, is dependent upon the strength of the intermolecular interaction between water molecules and the constituent chemical groups of the polymer. This implies that the activation energy of diffusion is representative of the energy required for a bound water molecule to become de-bonded, allowing it to diffuse to an adjacent polar functional group.

The dominant polar group affecting diffusion in the unaged resin is the OH group. As the net effect of hydrolysis is to increase the quantity of OH groups within the resin then one would expect the activation energy for diffusion to remain unchanged as there is no change in the chemical composition of the polar species responsible for inhibiting the diffusion of water molecules. The identical activation energies observed in both states confirms this expectation. The limiting value (D_0) associated with the fully hydrolysed state is lower than the value of the unaged state. This reduction in limiting value arises as a result of the increased quantity of polar groups within the hydrolysed state This inhibits diffusion by increasing the number of bonding/de-bonding events a water molecule experiences when traversing a given distance. This increases the time-frame required for a water molecule to travel a given distance and thus decreases the rate at which bulk diffusion occurs.

It should be noted that the error associated with the limiting value (D_0) of both states is large (in the range ~43% to ~113%). This is expected because the limiting value represents the value of the diffusion coefficient as the conditioning temperature tends to infinity. The diffusion coefficient has only been measured at three temperatures, in the range 35℃ to 60℃, and thus small inaccuracies in the determination of the line of best fit in this region, when performing the Arrhenius analysis, will lead to large errors in the predicted value of the diffusion coefficient at temperatures which are far outside of the range of tested temperatures. As the purpose of this work is to predict the ageing behaviour of DGEBA-DDA in its engineering environment (-20℃ to 60℃), inaccuracies in the diffusion coefficient outside of this temperature range have no bearing upon the predictive capability of the diffusion-hydrolysis model.

2.3.2.6.3. Determining the Activation Energies (E_k) and Limiting Values (K_0) Associated with the Two Rate Constants

In Table 37 below, the natural logarithms of the two rate constants, obtained from each sample, have been calculated along with their associated inverse temperatures. These results have been presented in the form of Arrhenius plots in Figure 45 and Figure 46, and the activation energies and limiting values of the two states are shown in Table 38.

T (℃)	Sample	$K_{AB(T)}$ $(mm^3.mol^{-1}.min^{-1})$	$K_{BC(T)}$ $(mm^3.mol^{-1}.min^{-1})$	T^{-1} (K^{-1})	$Ln\left(K_{AB(T)}\right)$	$Ln\left(K_{BC(T)}\right)$
35	LC1	4.54	1.17	3.247E-03	1.51	0.16
35	LC2	4.30	1.11	3.247E-03	1.46	0.10
35	LC3	4.82	1.24	3.247E-03	1.57	0.22
50	Sample 16	17.40	4.76	3.096E-03	2.86	1.56
50	Sample 17	17.39	5.22	3.096E-03	2.86	1.65
50	SB - Test Coupon	17.43	4.64	3.096E-03	2.86	1.54
50	SBA	18.83	4.80	3.096E-03	2.94	1.57
50	SBB	21.37	4.81	3.096E-03	3.06	1.57
60	HC4	49.00	11.25	3.003E-03	3.89	2.42
60	HC5	49.45	12.60	3.003E-03	3.90	2.53
60	HC6	49.62	13.66	3.003E-03	3.90	2.61

Table 37: Natural logarithms of the two rate constants obtained from each sample as a function of temperature.

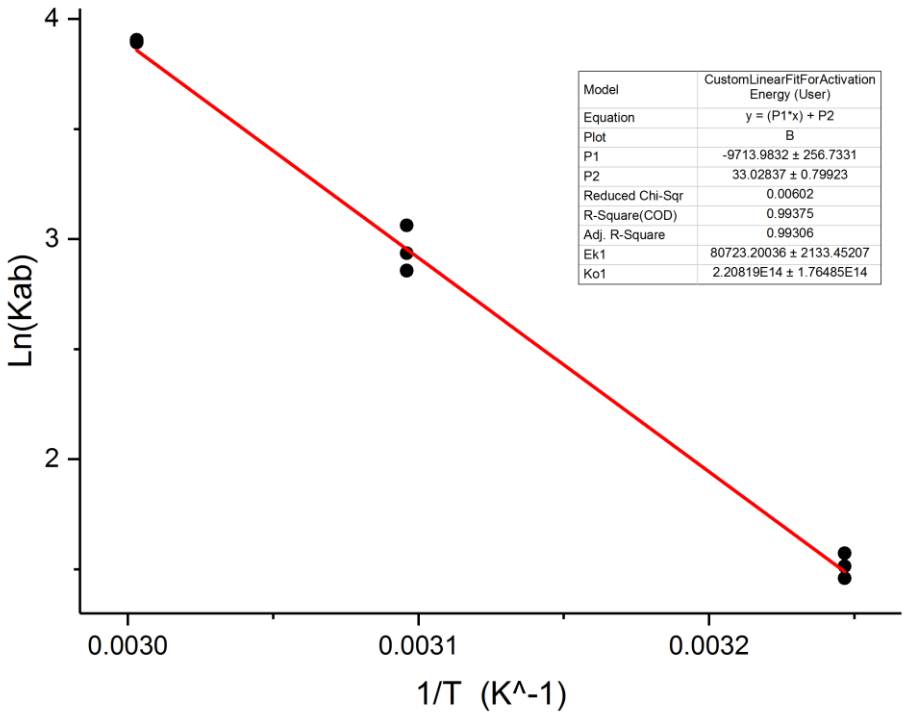

Figure 45: Arrhenius plot for the rate constant K_{AB}.

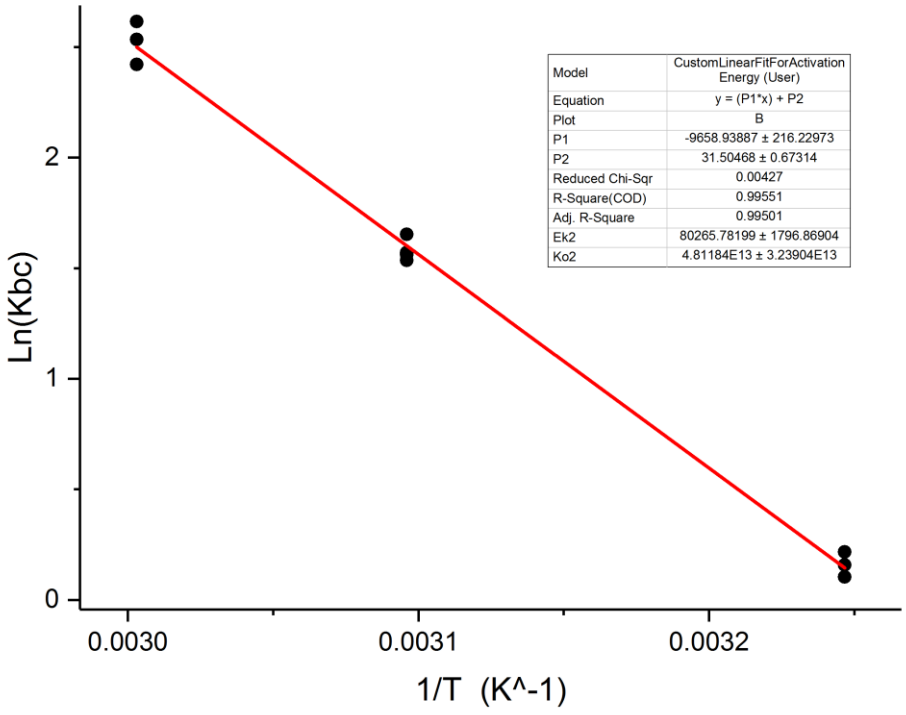

Figure 46: Arrhenius plot for the rate constant K_{BC}.

Parameter	E_k ($kJ.mol^{-1}$)	K_0 ($mm^3.mol^{-1}.min^{-1}$)	ΔE_k ($kJ.mol^{-1}$)	ΔK_0 ($mm^3.mol^{-1}.min^{-1}$)	Percentage Error on E_k (%)	Percentage Error on K_0 (%)
K_{AB}	*80.72*	*2.21E+14*	*2.13*	*1.76E+14*	*2.64*	*79.64*
K_{BC}	*80.27*	*4.81E+13*	*1.8*	*3.24E+13*	*2.24*	*67.36*

Table 38: Activation energy and limiting value for the rate constants K_{AB} and K_{BC}.

Referring to Table 38, the activation energies associated with the two rate constants are observed to be identical. This suggests that the same chemical reaction is responsible for both hydrolysis processes ($A \rightarrow B$ and $B \rightarrow C$). This is consistent with the proposal of Fata et al [6] that a single reaction pathway is responsible for hydrolysis in DGEBA-DDA resin. The limiting values associated with the two rate constants are different, with the limiting value of K_{AB} being greater than that of K_{BC}. This accounts for the greater magnitude of the rate constant governing the first hydrolysis step K_{AB}, over that governing the second K_{BC}, and this was hypothesised to result from a change in polymer morphology as discussed earlier (see section 2.3.2.5.5.3, page 125).

It is of interest to note that the calculated activation energy for hydrolysis of 80.5 $kJ.mol^{-1}$, is similar to that presented by Xiao et al [43] for the activation energy of diffusion, in DGEBA-DDA resin, of 70.4 $kJ.mol^{-1}$. In their work, square samples of ~1.5 mm thickness were employed in conditioning experiments whereby samples were immersed in liquid water, over a range of temperatures, and their absorption behaviour tracked gravimetrically as a function of time. The relatively large sample thickness (~1.5 mm) coupled the diffusion and hydrolysis processes and as a result the initial equilibrium moisture content of ~2.6% w/w (Figure 27) observed in this work, was not discernible in their experiments. As a result, it wasn't possible for them to detect the change in material solubility that results from hydrolysis and thus they assumed that the final equilibrium moisture content was representative of the resin before, and after, complete hydrolysis had occurred.

In this work it has been shown that the percentage change in mass of the resin, observed in the range: ~2.6% w/w to ~5.8% w/w, occurs as a result of both the chemical addition of water molecules to the polymer structure and the change in material solubility brought about by hydrolysis. In the work by Xiao et al [43] they assumed that the change in mass observed in this region was governed by diffusion and employed these observations in the calculation of the

diffusion coefficient. However, as the behaviour in this region results from hydrolysis, and not diffusion, the relationship between diffusion coefficient and temperature that they obtained was actually the relationship between the rate of hydrolysis and temperature. This accounts for the similarity between the activation energy for hydrolysis, obtained in this work, and that proposed for diffusion in the work of Xiao et al [43].

2.3.3. Comparison of Model Predicted T_g, as a Function of Temperature and Conditioning Time, with Experimental Observation

Earlier, the experimental observations of the glass transition temperature of DGEBA-DDA films, as a function of conditioning time and temperature, were discussed (section 2.3.1.2.1, page 89), and in the previous section the values of the two rate constants, K_{AB} and K_{BC}, were deduced at the three conditioning temperatures (section 2.3.2.5.5.3, page 125). The rate constants govern the rate of hydrolysis and thus their values can be used to determine the fractional proportions of fundamental units A, B, and C, within the resin at any point in the conditioning process. This is achieved by employing their values in the rate equations (equations (34), (35), and (36), page 49) whose solutions are then approximated, as a function of conditioning time and temperature, by a finite difference method. The fractional proportions of each unit type, at a given point in the conditioning process, can then be used within GIM to predict the glass transition temperature of the resin (see section 2.2.2.1.2, page 52). Thus, the values of the rate constants obtained from the gravimetric analysis can be used to predict the evolution of the quantities of fundamental units, and thus T_g, in the thin film samples as a function of time and temperature. These predictions can then be compared to the T_g behaviour that is observed experimentally to establish whether the model, linking solubility and glass transition temperature, is consistent with the experimental data.

The modelling is simplified by assuming that the concentration of water, corrected to account for the solubility fraction S_f (equation (37)), within each film takes a fixed value throughout the conditioning experiment. This assumption is reasonable as the small thickness dimension of the films ensures that the time scale required for them to attain equilibrium with their conditioning environment is much smaller than the time-scale associated with hydrolysis. As a result, the diffusion and hydrolysis processes can be decoupled. In Figure 47, Figure 48, and Figure 49, the model predicted evolution of material T_g, as a function of time and temperature, is compared against the experimental observations obtained through DMTA.

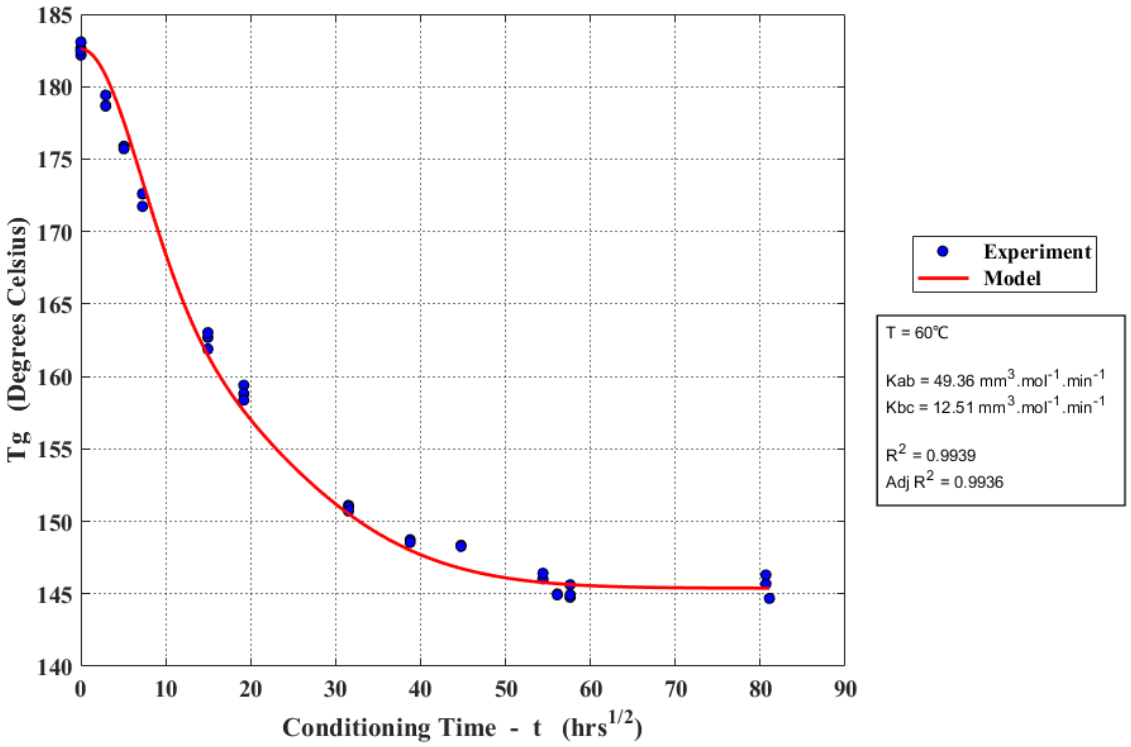

Figure 47: Model predicted T_g of DGEBA-DDA resin films, as a function of conditioning time at 60℃, compared to experimental measurements.

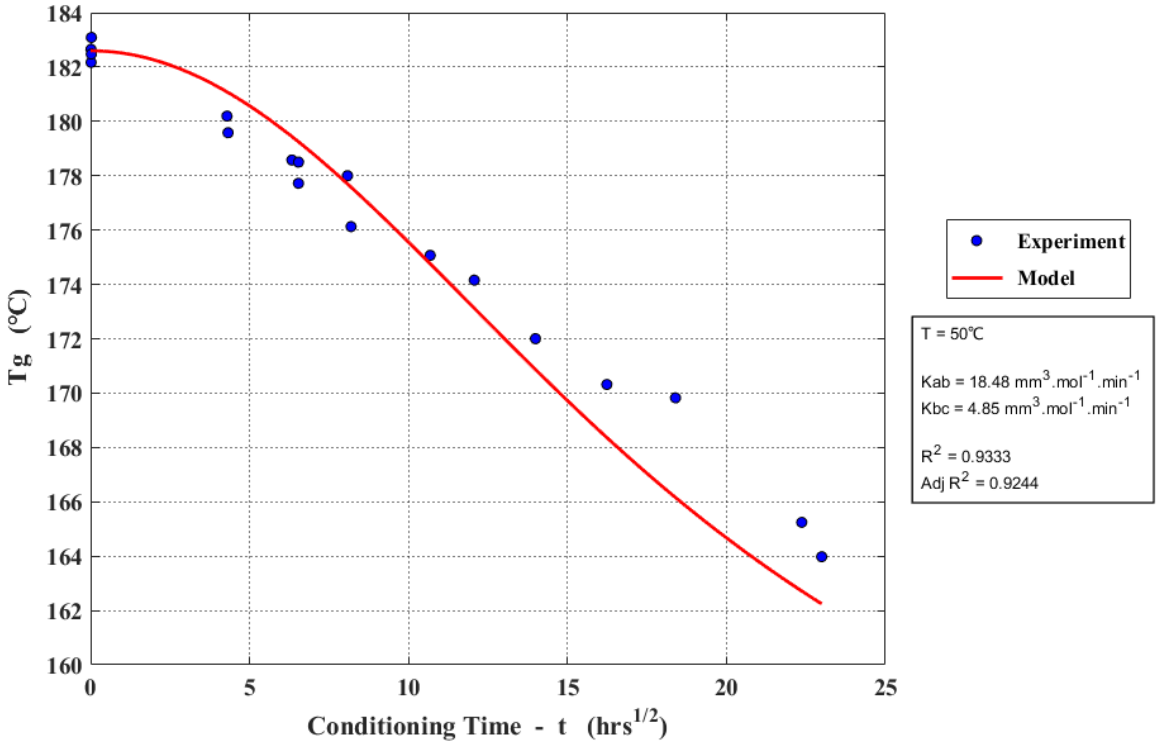

Figure 48: Model predicted T_g of DGEBA-DDA resin films, as a function of conditioning time at 50℃, compared to experimental measurements.

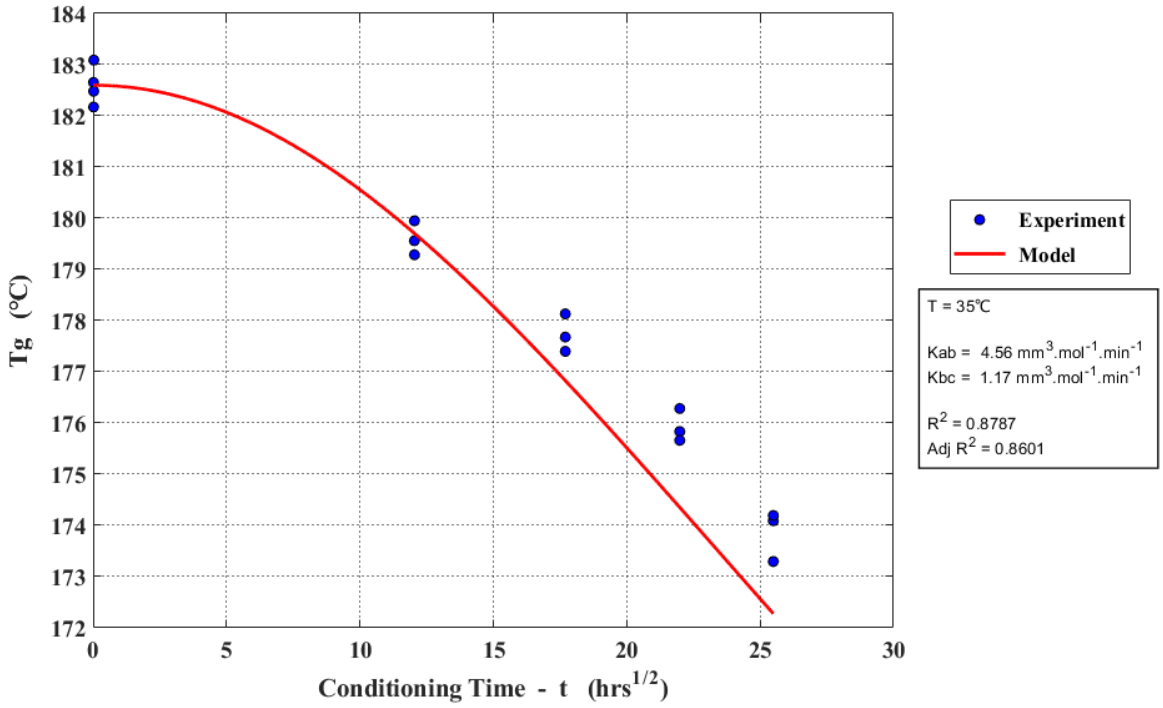

Figure 49: Model predicted T_g of DGEBA-DDA resin films, as a function of conditioning time at 35°C, compared to experimental measurements.

As discussed previously, only the 'thick' and 'thin' samples and films aged at 60°C were conditioned for a time period sufficient to allow complete hydrolysis to occur. Thus, the values of the two rate constants obtained from the model fitting process at this temperature will display the highest degree of accuracy as they were obtained from fitting model predictions to data that encompassed the entire hydrolysis process (unaged to fully hydrolysed resin). The results in Figure 47 show that the model predicted values of T_g and those obtained from the DMTA experiments are in good agreement ($adj\ R^2 = 0.9936$). However, this agreement falls at the two lower temperatures (Figure 48 and Figure 49) with the value of adjusted R^2 being 0.9244 at 50°C and 0.8601 at 35°C.

The most likely explanation for the deviation of the model from experiment at the two lower conditioning temperatures, is the absence of complete conditioning data (unaged to fully hydrolysed resin) at these temperatures. At 60°C (Figure 47), the disagreement between model and experiment at early conditioning times (~2 $hrs^{\frac{1}{2}}$) is ~2°C, which is similar to the largest deviation of ~1.8°C observed at 35°C. However, the agreement between model and experiment at extended conditioning times ($t_{con} > 10\ hrs^{\frac{1}{2}}$) at 60°C is much closer (~1°C) resulting in a high value of adjusted R^2, when all the conditioning data is accounted for. Thus, there is insufficient

conditioning data at 35℃ to determine the goodness of fit between model and experiment. However, the behaviour observed at 60℃ would suggest that the values of the rate constants obtained at 35℃ are likely to be reasonable approximations. This would need to be confirmed by conditioning at 35℃ for a time period sufficient for complete hydrolysis to occur. However, using the experimentally determined values of the rate constants in Table 29, the predicted time frame required for complete hydrolysis to occur, at 35℃, is ~2.8 years making such an experiment impractical.

2.4. Chapter Conclusions

In this work, the hydrolysis of DGEBA-DDA resin has been investigated through a combined experimental and modelling approach. The susceptibility of DGEBA-DDA resin to hydrolysis, through its reaction with absorbed water, has been investigated by several researchers [5-7]. The principal techniques that have been employed are gravimetric analysis, to observe the uptake of water by the resin, and DMTA, to observe the reduction in T_g that occurs as a result of hydrolysis. However, in these studies, the interpretation of the results is problematic as the time-frame associated with detectable hydrolysis, using DMTA, is similar to that over which the material attains equilibrium with its conditioning environment. In other words, the diffusion and hydrolysis processes are coupled. In this chapter, the diffusion and hydrolysis processes were sufficiently decoupled by reducing the thickness of the samples that were employed in both DMTA, and gravimetric, experiments.

The gravimetric analysis of DGEBA-DDA samples, conditioned at 100% relative humidity and for a range of temperatures, indicated that the moisture content of the resin initially plateaus at ~2.58% w/w, before slowly increasing, over extended conditioning times, to ~5.86% w/w. The results of the DMTA experiments show that, when the samples attain their second equilibrium moisture content at ~5.86% w/w, no further reduction in T_g is observed, indicating that complete hydrolysis has occurred. Furthermore, when dried and reconditioned, all samples rapidly reached equilibrium at ~5.86% w/w and the initial plateau, followed by a gradual increase in moisture content with conditioning time, was no longer present. Thus, the change in equilibrium moisture content with conditioning time can be attributed to a change in material solubility, occurring as a result of the addition of polar OH groups to the polymer network each time a polymer chain is hydrolysed. This was accompanied by a reduction in the diffusion coefficient which is consistent with behaviour observed in other epoxy resins, where the diffusion coefficient has been shown to be inversely proportional to the solubility of water within the material [8, 36, 37]. The initial solubility and diffusion coefficient of DGEBA-DDA resin, before significant hydrolysis occurs, have not been observed previously by other researchers [5-7] as in prior experiments both the

diffusion and hydrolysis processes were too strongly coupled to allow the initial state of the material to be characterised.

A finite difference diffusion model was developed using the diffusive flux equation, as a function of concentration and solubility, derived by Yagoubi et al [8]. This was modified to allow for the loss of water molecules that occurs, through their addition to the polymer network, during the hydrolysis reaction. A simple model was developed to describe the hydrolysis process in terms of a transformation of chemical species ($A \rightarrow B \rightarrow C$), depending on how many times a given cross-link had been hydrolysed. Rate equations were derived to describe the evolution of each of these species as a function of time. Each species was assumed to possess its own unique solubility and diffusion coefficient. The average solubility and diffusion coefficient, within a volume element of DGEBA-DDA resin, was obtained by combining the contributions of each species on a mole fraction basis. The moisture content/time profile for DGEBA-DDA resin, predicted by the model, was fit to the experimental gravimetric data. The rate constants, and diffusion parameters, were then varied until those values that best fit the data were obtained. This allowed the activation energy for the diffusion coefficient, solubility, and the hydrolysis process, to be obtained.

The activation energies for diffusion, and hydrolysis, were obtained from the fitting process and found to be 51.55 $kJ.mol^{-1}$, and 80.5 $kJ.mol^{-1}$, respectively. The activation energy for diffusion calculated by Xiao et al [43] was 70.4 $kJ.mol^{-1}$, which is similar to that obtained for hydrolysis in this work. This was attributed to the fact that in Xiao's work thicker sample dimensions were employed which coupled the diffusion and hydrolysis processes. As a result, no initial equilibrium plateau, representing the moisture content of unaged DEGBA-DDA resin, was observed. Thus, they assumed that the gradual increase in moisture content that occurs above ~2.58% w/w, was representative of diffusion when in fact this work has shown that it occurs as a result of hydrolysis increasing the solubility of water within the resin. Thus, they unknowingly measured the rate of the hydrolysis process, and not diffusion, and this accounts for the similarity between their activation energy and the one obtained for hydrolysis in this work.

Finally, Group Interaction Modelling was employed to model the T_g of DGEBA-DDA resin during the conditioning process. Mer unit parameters for each type of chemical species: A, B , and C, were obtained with reference to the T_g of unaged, and fully hydrolysed, DGEBA-DDA resin as measured by DMTA. This allowed the T_g of the material to be predicted as a function of the fractional proportions of each type of chemical species. The rate constants governing the hydrolysis process, obtained by fitting the predictions of the diffusion model to the gravimetric

data, were then employed to calculate the fractional proportion of each species, in DGEBA-DDA films, as a function of conditioning time. GIM was then used to convert these proportions, at a given time in the conditioning process, into a resin T_g and these predictions were compared against the T_g/conditioning time data. The predictions of GIM were shown to be in good agreement with the experimentally determined glass transition temperatures of DGEBA-DDA resin, when the material was conditioned hygrothermally at 60℃.

3. Group Interaction Modelling on the Thermo-mechanical Properties of Phenolic Resins

3.1. Introduction

Phenolic resins are employed within the composites industry as the matrix component of fibre-reinforced materials. Unfortunately, the chemical structures of phenolic resins possess a high density of polar functional groups and thus they are susceptible to absorbing atmospheric moisture from their working environment. As discussed previously in this work (section 1.4, page 16), absorption of atmospheric moisture has an effect upon the thermo-mechanical properties of these materials. However, it is not possible to adjust the density of polar groups within phenolic resins, and thus the extent to which they absorb moisture, as the polarity arises from the OH functional group of the phenol molecule.

Phenolic resins are synthesised from the reaction of phenol with formaldehyde whereby formaldehyde reacts to form covalent bonds between phenol molecules. Increasing the formaldehyde/phenol ratio (F/P) of the reactants results in the formation of a greater quantity of covalent bonds between phenol molecules. Thus, it leads to an increase in the cross-link density of the polymer. However, the F/P ratio has no impact upon the density of OH groups within the structure of the fully cured polymer as they are not a product of the curing reaction. They are incorporated into the polymer network, irrespective of the F/P ratio, as they are a constituent functional group of the phenol molecule. As the high density of polar OH groups is inherent to the fundamental structure of phenolic resins, it is not possible to alter their susceptibility to absorbing moisture. Thus, it becomes of importance to develop modelling capabilities to understand the hygrothermal ageing process within these polymers and the resulting impact that this may have upon their engineering performance.

In the first part of this chapter the mer unit parameter values associated with each chemical species are determined and GIM is then employed to predict their thermo-mechanical properties. This analysis is then used to determine the effect of specific chemical functional groups on the overall thermo-mechanical properties of the resin.

In the second part of this chapter the F/P ratio associated with each chemical species is identified. These species can exist either temporarily as intermediate cure products or as the constituents of fully cured phenolic resins. By referring to the ratios representative of each species, it is possible to estimate the initial proportions of species present in a phenolic resin before cross-linking between adjacent polymer chains has occurred. The evolution of each chemical species, and therefore the thermo-mechanical properties of the resin, are then predicted as a function of both cure time and F/P ratio.

In the third part of this chapter the thermo-mechanical properties of fully cured phenolic resins are predicted as a function of F/P ratio. Various property trends associated with different regions of F/P ratio are identified and their underlying influences discussed.

Finally, the residual stress remaining in a phenolic composite after cure, arising as a result of shrinkage of the polymer material, is estimated. It is shown that this stress is a function of F/P ratio and its relation to other thermo-mechanical properties is discussed.

3.2. Methods

3.2.1. Group Interaction Modelling of Phenolic Resins

To predict the thermo-mechanical properties of a given phenolic resin the parameter values (E_{coh}, N, V_w, M) of its characteristic repeat unit, the so-called mer unit, must first be determined. As discussed previously in this work (section 1.2.1, page 6), the cure of phenolic resins is complicated by the existence of several reaction pathways leading to the formation of a variety of different chemical structures. Thus, any given phenolic resin will be composed of a variety of different mer unit structures each possessing its own unique parameter values. The average mer unit parameter values for the resin are obtained by combining the contributions from each underlying mer unit on a mole fraction basis. The framework of GIM requires that the network structure of the polymer to be modelled, to have undergone sufficient reaction for gelation to have occurred. The gelled state of the resin can be represented as consisting of infinitely long polymer chains stacked in a hexagonal packing pattern. Cross-links can form between a polymer chain and any of its six surrounding neighbours. However, as each phenyl ring can undergo only one cross-link reaction, the system can be simplified to one consisting of just two adjacent polymer chains (Figure 50).

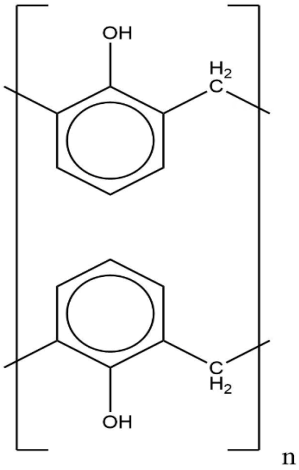

Figure 50: Simplified structure of a phenolic resin.

The structure presented above can be generalised to represent any phenolic resin by expressing it in the form shown below in Figure 51.

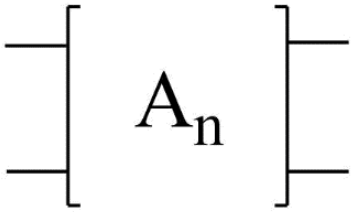

Figure 51: Generalisation of the structure of a phenolic resin.

Where A_n represents the chemical structure of the two polymer chains at a position n. A_n can take the form of a variety of different chemical structures, dependent upon the cure state of the resin and the initial formaldehyde/phenol ratio of reactants employed in its synthesis. The various chemical structures that A_n can represent are depicted below in Figure 52.

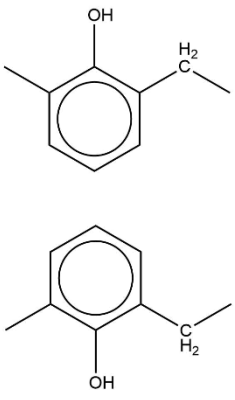

A

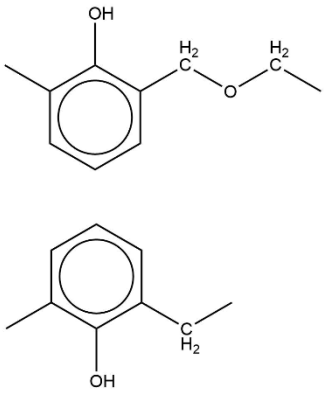

B

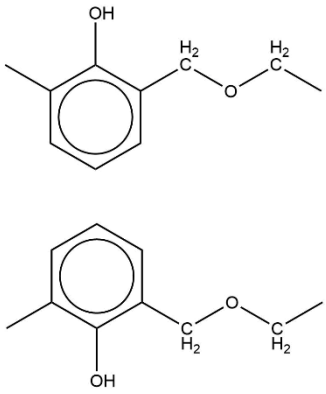

C

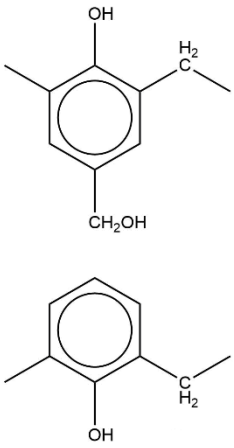

D

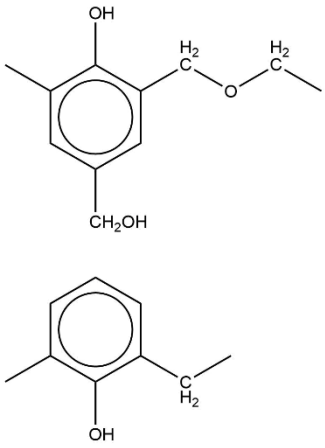

E

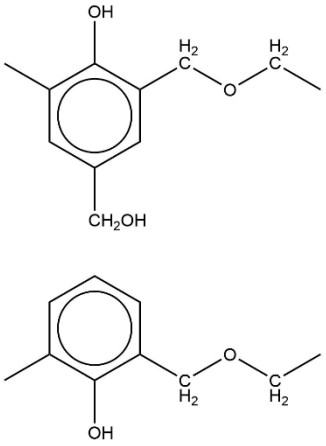

F

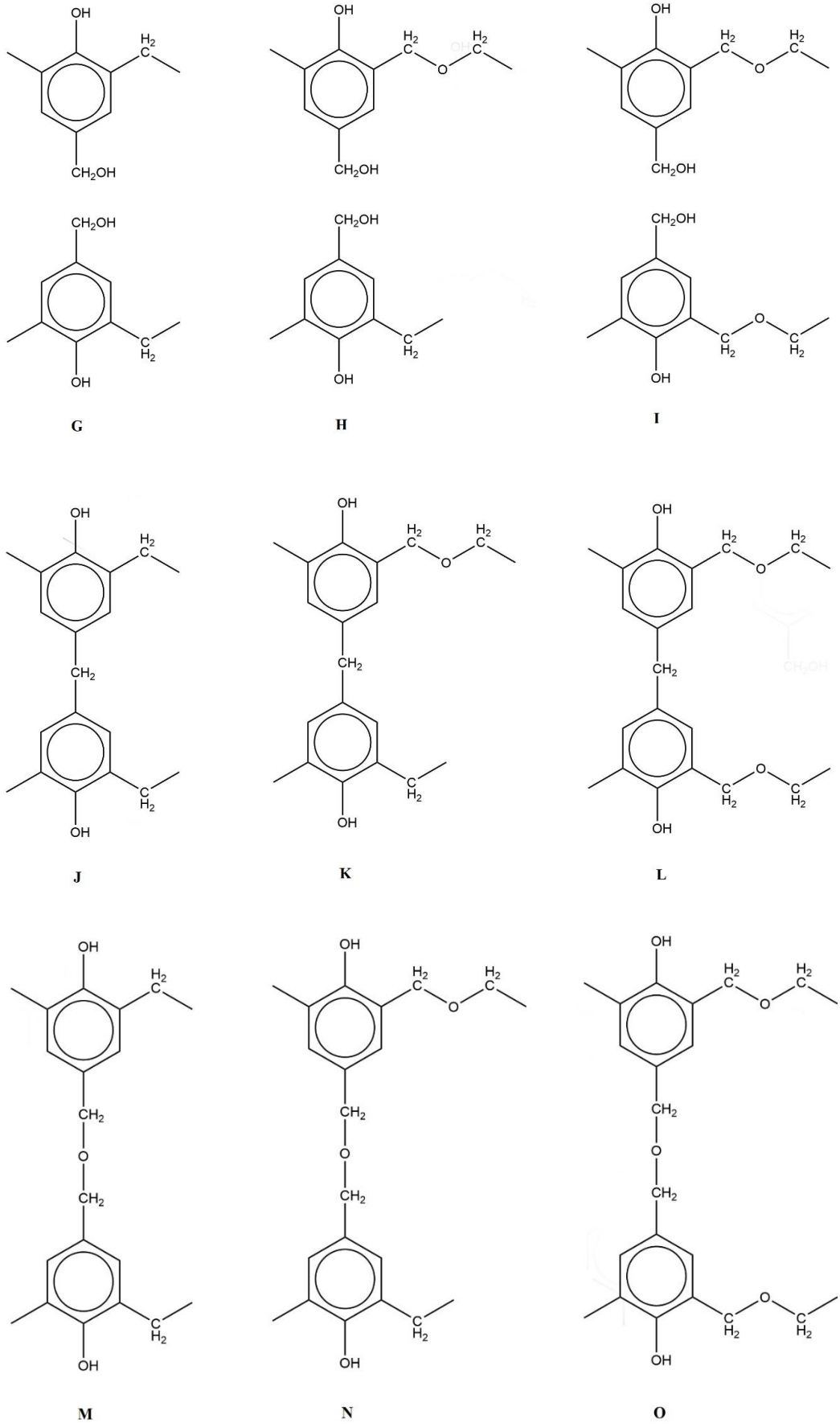

Figure 52: Possible chemical structures of A_n.

In total, there are fifteen different chemical structures that can be associated with A_n. As cure proceeds, the fractional proportions of each of these underlying chemical structures will change; thus, in order to model the evolution of the polymer's thermo-mechanical properties as a function of cure, the transformation of one chemical structure to another must be considered. In this work a methodology similar to that applied by Manfredi et al [22], and Riccardi et al [23],will be employed but for the later stages of reaction after gelation has occurred. The initial structure of the gelled resin, before the onset of cross-linking between adjacent polymer chains, is estimated by referring to the formaldehyde/phenol ratio employed in the resin's synthesis. Assuming first order kinetics [105], the rate equations governing the concentration behaviour of each of the fifteen different types of chemical species are given by:

$$\frac{d}{dt}[A] = K_3[B] \tag{164}$$

$$\frac{d}{dt}[B] = 2K_3[C] - K_3[B] \tag{165}$$

$$\frac{d}{dt}[C] = -2K_3[C] \tag{166}$$

$$\frac{d}{dt}[D] = K_3[E] - K_1[D] \tag{167}$$

$$\frac{d}{dt}[E] = 2K_3[F] - K_3[E] - K_1[E] \tag{168}$$

$$\frac{d}{dt}[F] = -2K_3[F] - K_1[F] \tag{169}$$

$$\frac{d}{dt}[G] = K_3[H] - K_2[G] \tag{170}$$

$$\frac{d}{dt}[H] = 2K_3[I] - K_3[H] - K_2[H] \tag{171}$$

$$\frac{d}{dt}[I] = -2K_3[I] - K_2[I] \tag{172}$$

$$\frac{d}{dt}[J] = K_1[D] + K_3[K] + K_3[M] \quad (173)$$

$$\frac{d}{dt}[K] = K_1[E] + 2K_3[L] + K_3[N] - K_3[K] \quad (174)$$

$$\frac{d}{dt}[L] = K_1[F] + K_3[O] - 2K_3[L] \quad (175)$$

$$\frac{d}{dt}[M] = K_2[G] + K_3[N] - K_3[M] \quad (176)$$

$$\frac{d}{dt}[N] = K_2[H] + 2K_3[O] - 2K_3[N] \quad (177)$$

$$\frac{d}{dt}[O] = K_2[I] - 3K_3[O] \quad (178)$$

Where the rate constants K_1, K_2, and K_3, are all in units of min^{-1}. The rate constant K_1 represents the reaction of methylol with an unreacted site on the phenyl ring, K_2 the reaction of two methylol groups to form an ether bridge, and K_3 the molecular rearrangement of an ether bridge to form a methylene bridge. The terms in square brackets represent the concentration of each type of chemical species, in units of $mol.mm^{-3}$. To calculate the evolution of species concentration as a function of time, the first derivative of each rate equation is replaced with its first order finite difference approximation. Thus, each rate equation can be written in the form:

$$\frac{d}{dt}[Species]_t \approx \frac{[Species]_{t+\Delta t} - [Species]_t}{\Delta t} \quad (179)$$

$$[Species]_{t+\Delta t} \approx \Delta t \frac{d}{dt}[Species]_t + [Species]_t \quad (180)$$

The species concentration at a time $t + \Delta t$ is calculated by combining the species concentration at time t with the change in concentration that occurs in the time step Δt. Species concentration

at each time step can then be calculated through an iterative process allowing the relationship between species concentration and time to be deduced.

The mer unit parameters (E_{coh}, N, V_w, M) associated with each type of chemical species are obtained by summing the functional group contributions of their underlying chemical constituents. Where a cross-link exists between two adjacent polymer chains, two free chain ends are lost reducing the degrees of freedom of the structure by six. This is because each free polymer chain end can vibrate in three dimensions, thus having three degrees of freedom. Finally, it should be noted that each chemical structure consists of two mer units and thus, to obtain the parameter values for a single mer unit, the parameter values associated with each structure are divided by two. The parameter values of a phenolic resin's characteristic mer unit are obtained by combining those from each of its underlying chemical species on a mole fraction basis:

$$f_{Species} = \frac{[Species]}{[Total\ Species]} \tag{181}$$

Where $f_{Species}$ is the mole fraction of a specific species, $[Species]$ is the species' concentration, and $[Total\ Species]$ is the total concentration of all types of species, structures A through O (Figure 52), within the resin and whose value is independent of time. Thus, by way of example, the cohesive energy of the phenolic resin's characteristic mer unit is expressed as:

$$E_{coh} = \sum_{n=1}^{n} f_n E_{coh_n} \tag{182}$$

Where f_n is the mole fraction of the nth species and E_{coh_n} is its associated cohesive energy.

3.2.2. Determining the Initial Mole Fraction of Each Species

The initial state of the resin is assumed to be composed of infinitely long polymer chains, with no cross-linking between adjacent polymer chains having yet occurred. Further reaction is possible leading to the development of cross-linking between polymer chains and it is this stage of the cure process that is modelled within GIM. However, before the cure can be modelled, the initial mole fraction of each underlying species (Figure 52) must be determined. As the early stages of cure are not modelled by GIM, a methodology must be developed for the estimation of

the initial species composition of the resin. This is achieved by referring to the chemical structure of each species and determining the number of phenol and formaldehyde molecules required to create each structure. There are nine possible initial chemical structures (*A* through to *I*), as earlier it was assumed that no cross-linking between adjacent polymer chains exists in the initial state of the resin. It is further assumed that the methylene bridges within these initial structures arise as a result of the reaction of methylol groups with unreacted sites on phenyl rings, in other words they are not products of the molecular rearrangement of ether bridges. Following from these assumptions, the molecules of phenol and formaldehyde required to create each species are calculated and given below in Table 39.

Species	Formaldehyde Molecules	Phenol Molecules	F/P Ratio
A	*2*	*2*	*1*
B	*3*	*2*	*1.5*
C	*4*	*2*	*2*
D	*3*	*2*	*1.5*
E	*4*	*2*	*2*
F	*5*	*2*	*2.5*
G	*4*	*2*	*2*
H	*5*	*2*	*2.5*
I	*6*	*2*	*3*
J	*3*	*2*	*1.5*
K	*4*	*2*	*2*
L	*5*	*2*	*2.5*
M	*4*	*2*	*2*
N	*5*	*2*	*2.5*
O	*6*	*2*	*3*

Table 39: Molecules of phenol and formaldehyde required to form each type of chemical species.

An observation of this analysis is that none of these structures possess an F/P ratio that is less than one. This implies that the assumption of an initial resin state consisting of infinitely long polymer chains, stacked in a hexagonal packing pattern, is unsuitable for modelling novolacs because the F/P ratio employed in synthesising these resins is always less than one. A novolac structure can

be modelled within GIM if it is assumed that the polymer chains are of finite length. This implies that the chains terminate in a phenol group in which addition of formaldehyde, to form a methylol group, has occurred at only one location on the phenyl ring. This limits the number of covalent bonds the phenol molecule can form with other phenol molecules, to one, thus terminating the polymer chain. The modelling work that follows focuses exclusively on resole phenolic resins in which the initial F/P ratio is always greater than one. Thus, the earlier assumption of infinitely long polymer chains is appropriate. From the F/P ratio analysis in Table 39, five distinct groups of chemical structures, each associated with a specific F/P ratio, can be identified. These groups are shown below in Table 40.

F/P Ratio	Associated Species
1	*A*
1.5	*B,D*
2	*C,E,G*
2.5	*F,H*
3	*I*

Table 40: Chemical species associated with five different F/P ratios.

In the initial resin structure, it will be assumed that, for a given F/P ratio, the proportions of each species associated with that ratio are equal. Thus, if the F/P ratio employed in the resin synthesis is 2.5 then the initial resin structure, in GIM, will have a mole fraction of species F of $\frac{1}{2}$ and a corresponding mole fraction of species H of $\frac{1}{2}$.

To determine the mole fraction of each species, for an arbitrary F/P ratio, the following methodology is adopted. By way of example, assume that the F/P ratio for a given phenolic resin is 1.75. With reference to Table 40, the upper and lower F/P ratio bounds, R_u and R_l, are given by:

$$R_u = 2 \tag{183}$$

$$R_l = 1.5 \tag{184}$$

Then the fraction of the F/P ratio associated with the upper and lower bounds, f_u and f_l respectively, can be expressed as:

$$f_u = \frac{R - R_l}{R_u - R_l} \tag{185}$$

$$f_l = 1 - f_u \tag{186}$$

Where R is the F/P ratio of the initial reactants; in this example taking a value of 1.75. Thus, the values of f_u and f_l are:

$$f_u = \frac{1}{2} \tag{187}$$

$$f_l = \frac{1}{2} \tag{188}$$

The fractional contribution of each species in the upper and lower bounds is given by:

$$F_u = \frac{f_u}{n_u} \tag{189}$$

$$F_l = \frac{f_l}{n_l} \tag{190}$$

Where F_u and F_l are the fractional contributions of each species in the upper and lower bounds, and n_u and n_l are the number of species in each bound respectively. In this example:

$$n_u = 3 \tag{191}$$

$$n_l = 2 \tag{192}$$

Thus, the values of F_u and F_l are:

$$F_u = \frac{1}{6} \tag{193}$$

$$F_l = \frac{1}{4} \tag{194}$$

Thus, the initial structure of a phenolic resin with a F/P ratio of 1.75, before cross-linking between adjacent polymer chains occurs, is represented by five different chemical species: B, D, C, E, and G. The fractional contributions of each species to the structure as a whole are $\frac{1}{4}$, for species B and D, and $\frac{1}{6}$, for species C, E, and G. The parameter values of the characteristic mer unit are obtained by combining the mer unit parameters of each of these five species, in the fractional proportions determined above.

3.3. Results and Discussion

3.3.1. Effect of Specific Chemical Group Constituents upon the Thermo-mechanical Properties of Phenolic Resins

Before modelling more complex phenolic resins it is beneficial to study the thermo-mechanical properties of pure systems; those consisting of only one type of chemical species ($A \rightarrow O$ in Figure 52). This allows the influence of individual chemical groups, such as methylol and ether bridges, on the bulk engineering properties of the polymer to be understood, thus enabling the relationship between underlying chemistry and engineering properties to be identified. It also assists in the interpretation of the thermo-mechanical property/cure time profiles of phenolic resins, as in these systems a variety of different chemical species are present.

The thermo-mechanical properties of each specific species ($A \rightarrow O$) can be predicted by considering pure systems. For example, the thermo-mechanical properties of species H can be identified by setting $f_H = 1$ and the mole fractions of all other species equal to zero. Thus, only the mer unit parameter values associated with species H will be employed in the GIM constitutive equations for thermo-mechanical property prediction. In the modelling that follows, all property predictions are for materials at room temperature (25℃).

Table 41 below shows the mer unit parameter values associated with each species. These were obtained by applying a group additivity methodology using the functional group parameters suggested by Porter [71]. In Table 42, their GIM predicted thermo-mechanical properties are also presented.

Species	E_{coh} $(J.mol^{-1})$ Cohesive Energy	N (mer^{-1}) Degrees of Freedom	V_W $(cc.mol^{-1})$ van der Waals Volume	M $(g.mol^{-1})$ Molar Mass
A	42500	8	61.53	106
B	47900	10	69.145	121
C	53300	12	76.76	136
D	51250	9.5	70.645	121
E	56650	11.5	78.26	136
F	62050	13.5	85.875	151
G	60000	11	79.76	136
H	65400	13	87.375	151
I	70800	15	94.99	166
J	44750	6	66.645	112
K	50150	8	74.26	127
L	55550	10	81.875	142
M	50150	8	74.26	127
N	55550	10	81.875	142
O	60950	12	89.49	157

Table 41: Calculated mer unit parameters for each chemical species, using the functional group parameters suggested by Porter [71].

Species	T_g (℃)	M $(g.mol^{-1})$ Molar Mass	α (K^{-1}) Thermal Expansion Coefficient	V $(cc.mol^{-1})$ Molar Volume	ρ $(g.cc^{-1})$. Density	Young's Modulus (MPa)
A	122.03	106	0.00024751	93.13	1.1382	3125
B	95.27	121	0.00027778	105.4	1.148	2446
C	77.44	136	0.00030401	117.74	1.155	1884
D	126.24	121	0.00024343	106.83	1.1327	3380
E	102.24	136	0.00026906	119.05	1.1424	2761
F	85.36	151	0.00029155	131.33	1.1498	2235
G	129.3	136	0.00024055	120.53	1.1283	3577
H	107.6	151	0.00026279	132.72	1.1378	3008
I	91.69	166	0.00028256	144.96	1.1452	2517
J	231.89	112	0.00017355	99.24	1.1286	4634
K	170.99	127	0.00020764	111.4	1.1401	3938
L	134.44	142	0.00023589	123.6	1.1489	3330
M	170.99	127	0.00020764	111.4	1.1401	3938
N	134.44	142	0.00023589	123.6	1.1489	3330
O	110.08	157	0.00026001	135.84	1.1558	2800

Table 42: GIM predicted thermo-mechanical properties for each chemical species.

3.3.1.1. Effect of Methylol Groups and Ether Bridges on the Thermo-mechanical Properties of Species Possessing no Cross-linking

First, the effect of methylol groups and main chain ether bridges upon the thermo-mechanical properties of those species that possess no cross-linking: A, B, C, D, E, F, G, H, and I, will be investigated. These species can be characterised in terms of the number of methylol groups they contain allowing them to be separated into three distinct categories:

$n_{methylol} = 0$: Where there are no methylol groups present on either of the phenyl rings

$n_{methylol} = 1$: Where one of the phenyl rings contains a methylol group

$n_{methylol} = 2$: Where both phenyl rings contain methylol groups

Similarly, they can be characterised in terms of the number of ether bridges, in the main chain of their polymer backbones, as follows:

$n_{ether} = 0$: Where there are no ether bridges in either polymer chains

$n_{ether} = 1$: Where one polymer chain possesses an ether bridge

$n_{ether} = 2$: Where both polymer chains possess an ether bridge

Thus, before cross-linking occurs, there are a total of nine distinct chemical structures each possessing their own unique number of methylol groups and main chain ether bridges.

In the results that follow, for a given quantity of main chain ether bridges, the three thermo-mechanical property predictions for 0, 1, and 2, methylol groups have been connected by straight lines to aid visualisation of the data. It is important to note that these lines do not describe the thermo-mechanical properties of the resin between data points. This is because only whole number quantities of methylol groups exist, in other words the distribution of methylol groups is discrete, not continuous. The same approach is applied in section 3.3.1.2 where the predicted thermo-mechanical properties of the species before, and after cross-linking, have been connected by a straight line even though the distribution of the number of cross-links is discrete.

3.3.1.1.1. Glass Transition Temperature

Figure 53 below shows the GIM predicted effect of methylol groups and main chain ether bridges upon the T_g of phenolic resins in which no cross-linking has occurred.

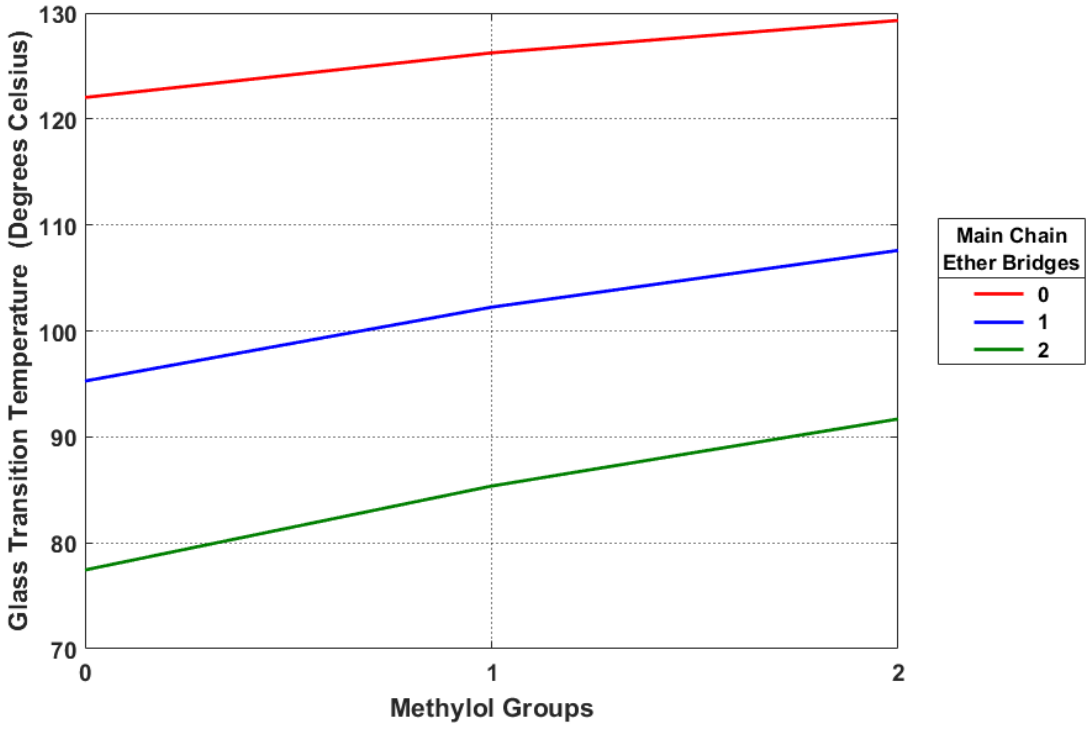

Figure 53: T_g as a function of the number of methylol groups and backbone ether bridges in phenolic resins in which no cross-linking has occurred.

The glass transition temperature is ~122℃ for a system that contains neither methylol side groups or ether bridges in the main chain of the polymer. Increasing the number of methylol groups is observed to increase T_g slightly, reaching a final temperature of ~129℃ for a species containing two methylol groups. Thus, the net effect of the addition of a methylol group to the phenyl ring is a slight increase in resin T_g. The inclusion of ether bridges in the polymer backbone is observed to have a large impact on T_g. For a resin in which no methylol groups are present, the addition of ether bridges reduces T_g to a final value of ~77℃ when there are two ether bridges present in the polymer backbone; a reduction of ~45℃.

The overall behaviour can be summarised as follows. For a species in which no methylol groups or backbone ether bridges are initially present (species A), the addition of two methylol groups to the two phenyl rings increases T_g by ~7℃, whereas the addition of two backbone ether bridges reduces T_g by ~45℃.

Thus, GIM predicts that the inclusion of methylol groups in the mer unit has a slight positive impact on T_g, however the contribution from ether bridges is negative resulting in a large depression in T_g. This result can be understood in terms of the functional group parameters associated with each of these two types of chemical species. The GIM equation for T_g (equation (13)) indicates that T_g is a function of two parameters: the characteristic temperature of polymer chain vibrations parallel to the polymer chain axis (θ), and the ratio of the mer unit's cohesive energy to its degrees of freedom $\left(\frac{E_{coh}}{N}\right)$. The presence of phenyl rings in the polymer backbone dominates the value of θ and as a consequence neither of the functional groups (methylol/ether bridge) have a significant impact upon the value of this parameter. Thus, the observed changes in T_g must be attributed to the ratio $\left(\frac{E_{coh}}{N}\right)$ associated with each functional group. Table 43 below shows the calculated cohesive energy and degrees of freedom for each chemical entity, obtained by group additivity using the functional group parameters suggested by Porter [71]. The ratio $\left(\frac{E_{coh}}{N}\right)$ for each chemical entity has also been calculated.

Structure	$\mathbf{E_{coh}}$ $\mathbf{(J.mol^{-1})}$ **Cohesive Energy**	$\mathbf{N}$ $\mathbf{(mer^{-1})}$ **Degrees of Freedom**	**Ratio** $\left(\frac{\mathbf{E_{coh}}}{\mathbf{N}}\right)$ $\boldsymbol{(J.mer.mol^{-1})}$	$\mathbf{Ratio^{-1}}$ $\boldsymbol{\left(\frac{E_{coh}}{N}\right)^{-1}}$ $\boldsymbol{(mol.J^{-1}.mer^{-1})}$
Methylol	17500	3	5833	0.000171
Ether bridge	10800	4	2700	0.00037
Species A	42500	8	5313	0.000188

Table 43: Cohesive energy, degrees of freedom, and ratio $\left(\frac{E_{coh}}{N}\right)$ associated with the three different chemical entities. Parameters were obtained by group additivity using the functional group parameters suggested by Porter [71].

It is important to note that for the purposes of comparing these two functional groups with species A, it is has been assumed that the ether bridge is represented by the following chemical structure: $-O-CH_2-$, as one of the CH_2 groups of the ether bridge is already included in species A, and thus it is only the $-O-CH_2-$ section that changes the mer unit parameters of species A when an ether bridge is added to its chemical structure.

The ratio $\left(\frac{E_{coh}}{N}\right)$ of species A is 5313 $J.mer.mol^{-1}$. Referring to Table 42 it can be seen that this corresponds to a T_g of 122.03℃. Thus, addition of functional groups to species A with ratios higher than 5313 will increase the T_g of the resin, whereas the addition of groups with ratios

below 5313 will cause a net reduction in T_g. Table 43 shows that the methylol functional group has a ratio $\left(\frac{E_{coh}}{N}\right)$ slightly higher than that of species A, accounting for the small predicted increase in T_g. By comparison, the ratio associated with the ether bridge is less than half that of species A. Thus, addition of ether bridges to species A results in a large decrease in the T_g of the resin.

3.3.1.1.2. Thermal Expansion Coefficient

Figure 54 below shows the GIM predicted effect of methylol groups and main chain ether bridges upon the thermal expansion coefficient of phenolic resins in which no cross-linking has occurred.

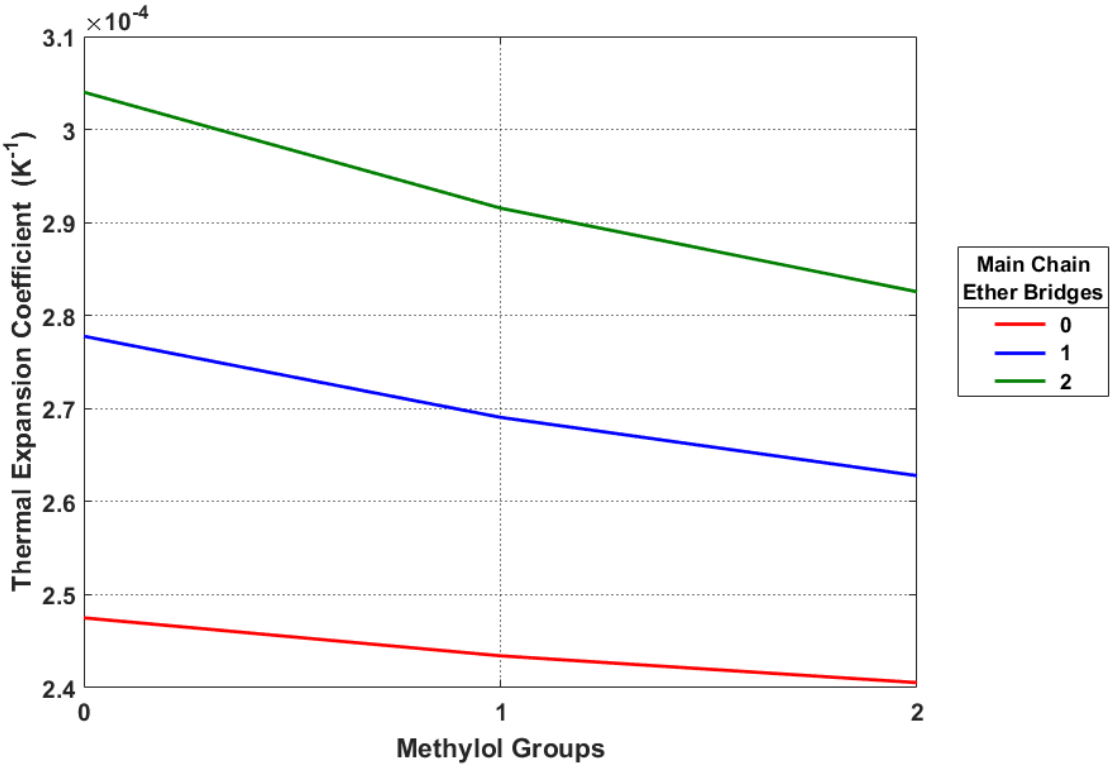

Figure 54: Thermal expansion coefficient as a function of the number of methylol groups and backbone ether bridges in phenolic resins in which no cross-linking has occurred.

The inclusion of methylol groups within the chemical structure of species A is observed to decrease the value of the thermal expansion coefficient by ~3% when two methylol groups are present. The addition of ether bridges to the chemical structure of species A is observed to markedly increase the thermal expansion coefficient by ~37% when two backbone ether bridges are present. These trends in thermal expansion coefficient can be related to the earlier discussion of glass transition temperature behaviour. The thermal expansion coefficient is a function of cohesive energy and degrees of freedom, see equation (15), more specifically it is proportional to

the inverse of the ratio $\left(\frac{E_{coh}}{N}\right)$. Thus, with reference to Table 43 it is apparent that the addition of methylol groups will cause a slight reduction in the value of the thermal expansion coefficient whereas the addition of backbone ether bridges will result in its value increasing by a large amount.

3.3.1.1.3. Molar Volume

Figure 55 below shows the GIM predicted effect of methylol groups and main chain ether bridges upon the molar volume of phenolic resins in which no cross-linking has occurred.

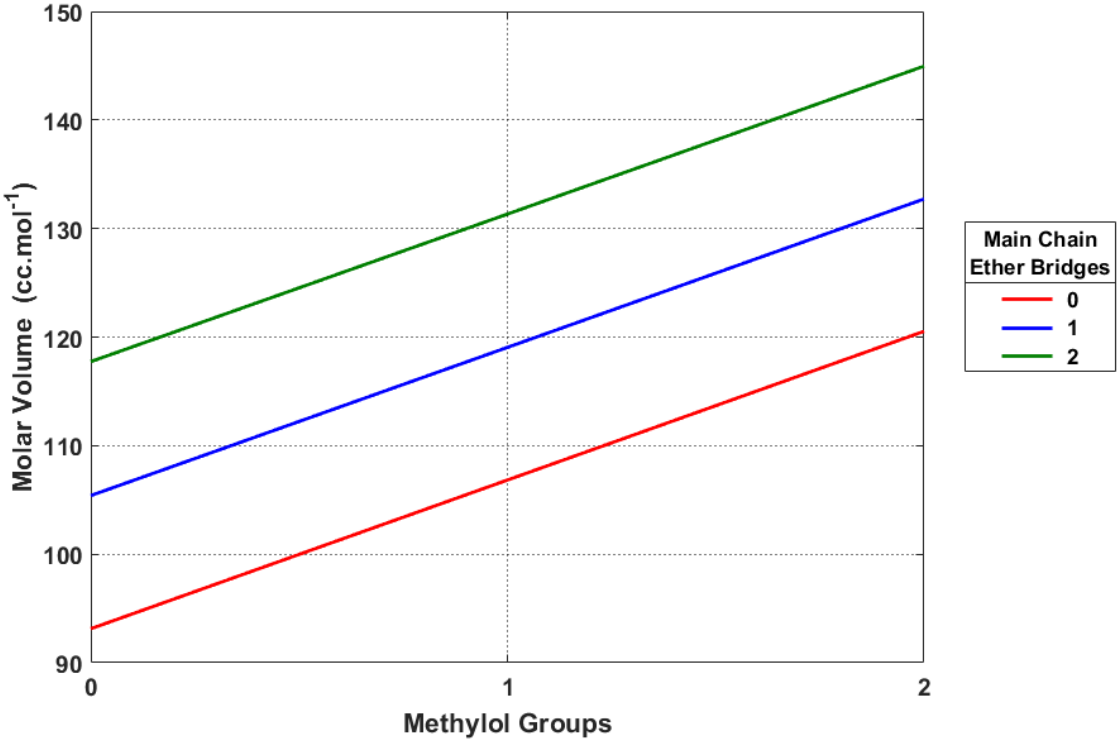

Figure 55: Molar volume as a function of the number of methylol groups and backbone ether bridges in phenolic resins in which no cross-linking has occurred.

The addition of methylol groups to species *A* is observed to increase the molar volume of the mer unit with molar volume increasing by ~30% when two methylol groups are present. The addition of two ether bridges has a similar but slightly reduced effect, increasing molar volume by ~27%. Thus, both types of functional groups affect an increase in the molar volume of species *A*. This is because the molar volume of the resin is a function of both the van der Waals volume of the functional group constituents of the mer unit, and the thermal expansion coefficient. Although the methylol group decreases the thermal expansion coefficient slightly, as was discussed previously (section 3.3.1.1.2, page 164), the dominant effect is the extra van der Waals volume that it brings

to the mer unit and thus its net effect is to increase the molar volume of species A. Table 44 below shows the calculated van der Waals volumes for both the methylol and ether bridge functional groups. These were obtained by group additivity using the functional group parameters suggested by Porter [71].

Functional Group	$\mathbf{V_W}$ $(\mathbf{cc.\,mol^{-1}})$
Methylol	18.23
Ether bridge	15.23

Table 44: Calculated van der Waals volumes for the methylol and ether bridge functional groups. These values were obtained by group additivity using the functional group parameters suggested by Porter [71].

The van der Waals volume of the methylol group is ~20% larger than that of the ether bridge and thus, although the methylol group acts to reduce the thermal expansion coefficient, its net effect is to increase the molar volume of species A slightly more than that which is brought about by the addition of the ether bridge.

3.3.1.1.4. Density

Figure 56 below shows the GIM predicted effect of methylol groups and main chain ether bridges on the density of phenolic resins in which no cross-linking has occurred.

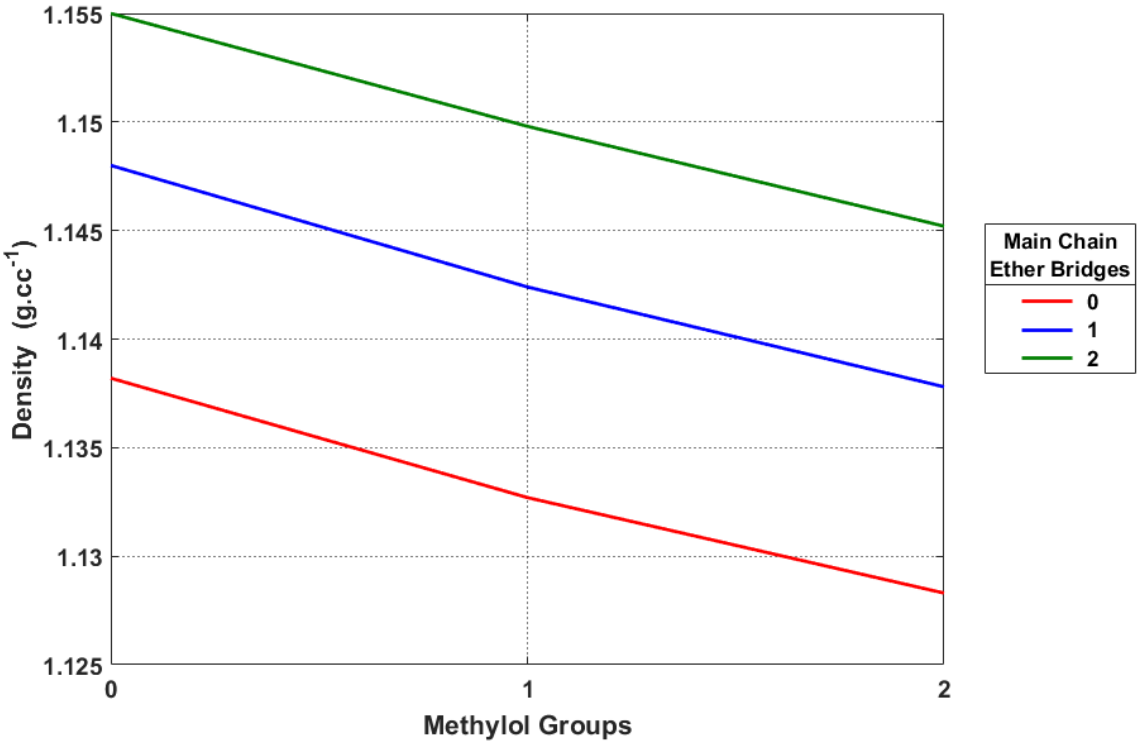

Figure 56: Density as a function of the number of methylol groups and backbone ether bridges in phenolic resins in which no cross-linking has occurred.

The incorporation of methylol groups into the structure of species *A* leads to a decrease in resin density of ~0.9% when two methylol groups are present. In comparison, the addition of two ether bridges to the polymer backbone causes resin density to increase by ~1.44%.

3.3.1.1.5. Young's Modulus

Figure 57 below shows the GIM predicted effect of methylol groups and ether bridges upon the Young's modulus of phenolic resins in which no cross-linking has occurred.

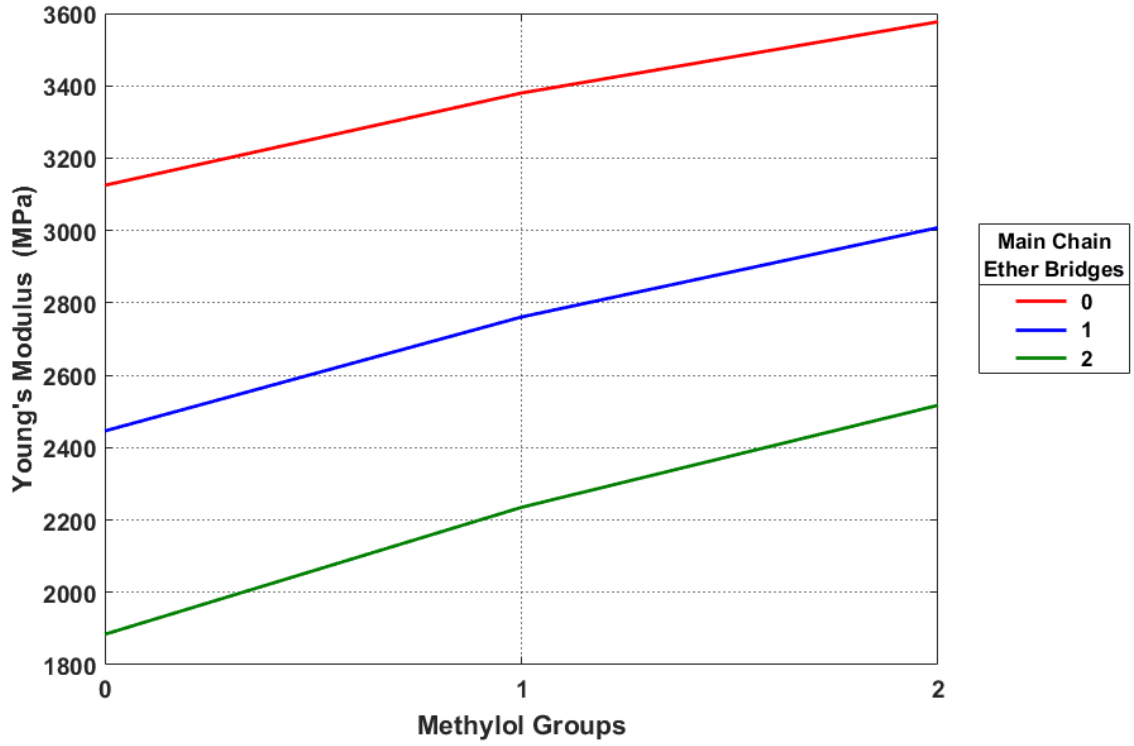

Figure 57: Young's modulus as a function of the number of methylol groups and backbone ether bridges in phenolic resins in which no cross-linking has occurred.

Young's modulus is observed to increase from the addition of methylol groups by ~14.7% when two methylol groups are included in the chemical structure of species A. The opposite trend is observed as the quantity of backbone ether bridges is increased, with the Young's modulus being reduced by ~39.4% when two ether bridges are present in the backbone of both polymer chains. This trend in modulus with respect to each functional group is similar to that observed for the glass transition temperature.

3.3.1.2. Effect of Cross-linking and Cross-link Type upon the Thermo-mechanical Properties of Phenolic Resins

In this section the effect of cross-linking and cross-link type, methylene or ether bridge, upon the predicted thermo-mechanical properties of phenolic resins is investigated. The species of interest are: D, E, F, G, H, I, J, K, L, M, N, and O (Figure 52). Species D, E, and F, each contain one methylol group and thus can undergo a cross-linking reaction to form a methylene bridge between the two adjacent phenyl rings, forming species J, K, and L, respectively. Species G, H, and I, each contain two methylol groups and can undergo reaction to form species with an ether bridge between the two adjacent phenyl rings: M, N, and O, respectively. These ether bridges can then undergo molecular rearrangement to form species cross-linked by a methylene bridge: J, K, and L, with the evolution of one molecule of formaldehyde.

3.3.1.2.1. Glass Transition Temperature

Figure 58 below shows the GIM predicted effect of cross-linking and cross-link type upon the glass transition temperature of phenolic resins.

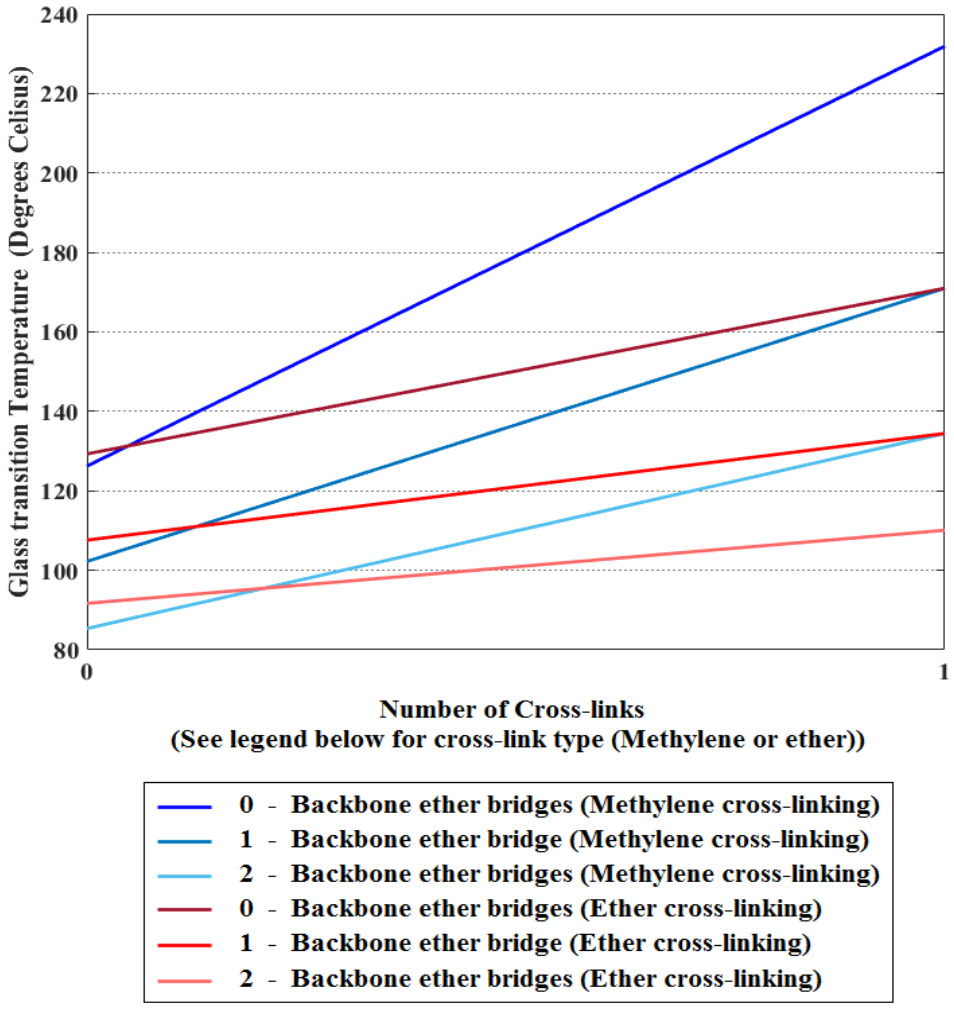

Figure 58: Phenolic resin T_g as a function of cross-linking and cross-link type.

The glass transition temperature is observed to increase with cross-link formation irrespective of the type of cross-link that is formed (methylene or ether bridge). This is because a large number of degrees of freedom (six) are lost when a cross-link is formed between the two phenyl rings and, for both methylene and ether bridges, the net effect is to increase the ratio $\left(\frac{E_{coh}}{N}\right)$ of the underlying structure. Thus, the formation of any type of cross-link leads to an increase in T_g. The increase in T_g is greatest when the cross-link takes the form of a methylene bridge with T_g increasing by a value in the range ~50-105℃, with the largest increase in T_g observed when no backbone ether bridges are present. When the cross-link takes the form of an ether bridge the corresponding increase in T_g is in the range ~19-40℃.

The explanation for the reduced effect of ether bridge cross-linking, on resin T_g, can be understood with reference to the earlier discussion on the relationship between T_g and the number of ether groups in the polymer chain backbone (see section 3.3.1.1.1, page 162). The addition of ether bridges to the polymer backbone lowers the T_g of the resin because the ratio $\left(\frac{E_{coh}}{N}\right)$ associated with these groups is much less than the ratio associated with the structure of species A (Table 43). However, as the formation of a cross-link reduces the degrees of freedom of the mer unit, the net effect is an increase in T_g, although much smaller in magnitude than that observed from the formation of methylene bridges. Finally, the T_g of a fully cross-linked system is seen to be dependent only on the number of ether groups within the mer unit and not on their location, whether they were identified as being in the backbone or as a cross-link between the two adjacent polymer chains. This is consistent with the formulation of GIM as the selection of polymer backbone is arbitrary.

3.3.1.2.2. Thermal Expansion Coefficient

Figure 59 below shows the effect of cross-linking and cross-link type upon the thermal expansion coefficient of phenolic resins.

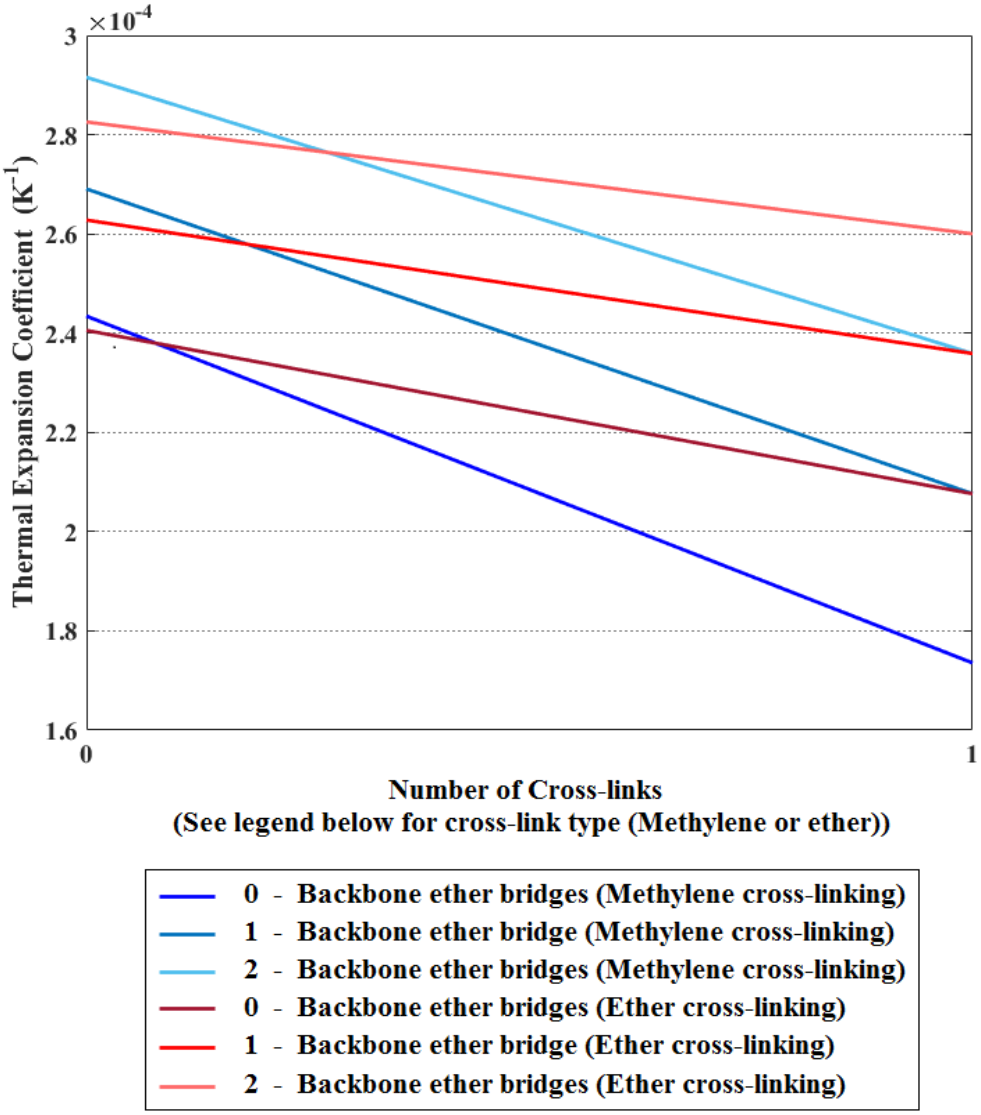

Figure 59: Phenolic resin thermal expansion coefficient as a function of cross-linking and cross-link type.

Formation of either type of cross-link is observed to decrease the value of the thermal expansion coefficient. If a methylene bridge is formed then the reduction is in the range ~19-28%, with a reduction of ~8-13% observed through the formation of an ether bridge. The large reduction in degrees of freedom upon cross-link formation (six) ensures that both cross-link types lead to a reduction in the thermal expansion coefficient. The effect is less pronounced for the ether link as, ordinarily, the addition of an ether group to the mer unit leads to an increase in the thermal expansion coefficient (see section 3.3.1.1.2, page 164). It is only as a result of the degrees of freedom lost through cross-linking that the net effect is an overall reduction in the value of the thermal expansion coefficient.

3.3.1.2.3. Molar Volume

Figure 60 below shows the effect of cross-linking and cross-link type upon the molar volume of phenolic resins.

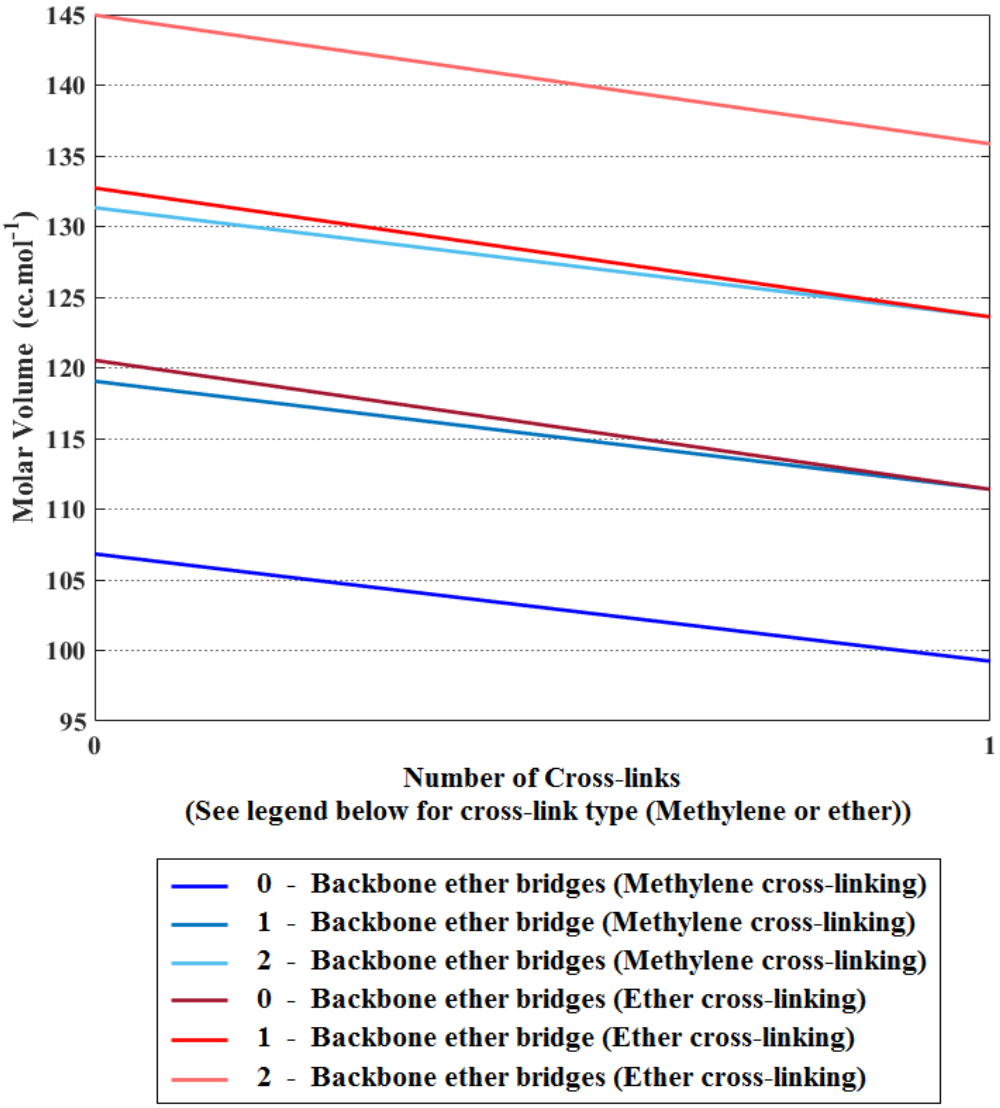

Figure 60: Phenolic resin molar volume as a function of cross-linking and cross-link type.

Both types of cross-links effect an almost identical reduction in the molar volume of the resin, of ~5.7-7.5%, with the presence of ether backbone groups appearing to have a negligible effect upon this value.

3.3.1.2.4. Density

Figure 61 below shows the effect of cross-linking and cross-link type upon the density of phenolic resins.

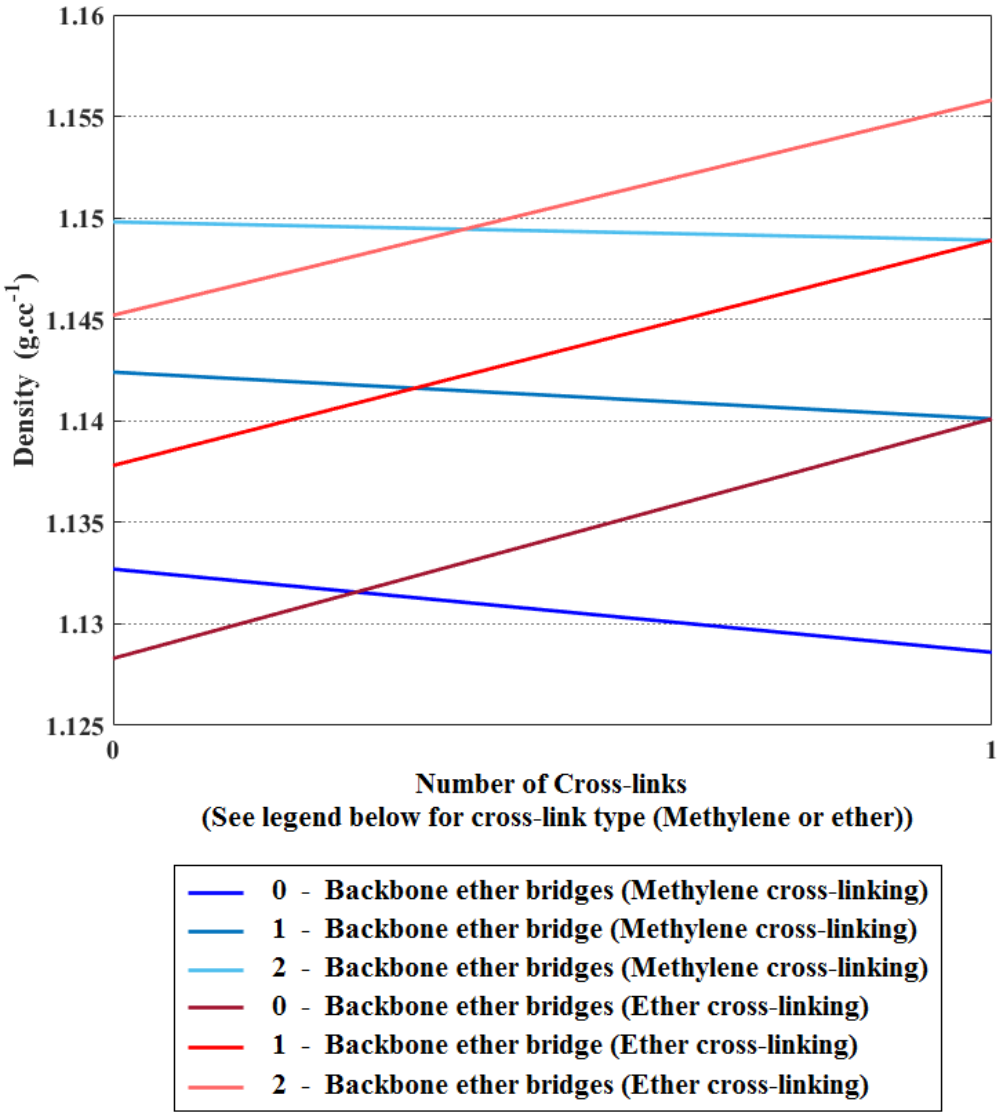

Figure 61: Phenolic resin density as a function of cross-linking and cross-link type.

The formation of a methylene bridge cross-link causes the density of the resin to reduce by ~0.1-0.33% whereas the formation of an ether bridge cross-link increases resin density by a value in the range ~0.96-1.02%.

3.3.1.2.5. Young's Modulus

Figure 62 below shows the GIM predicted effect of cross-linking and cross-link type upon the Young's modulus of phenolic resins.

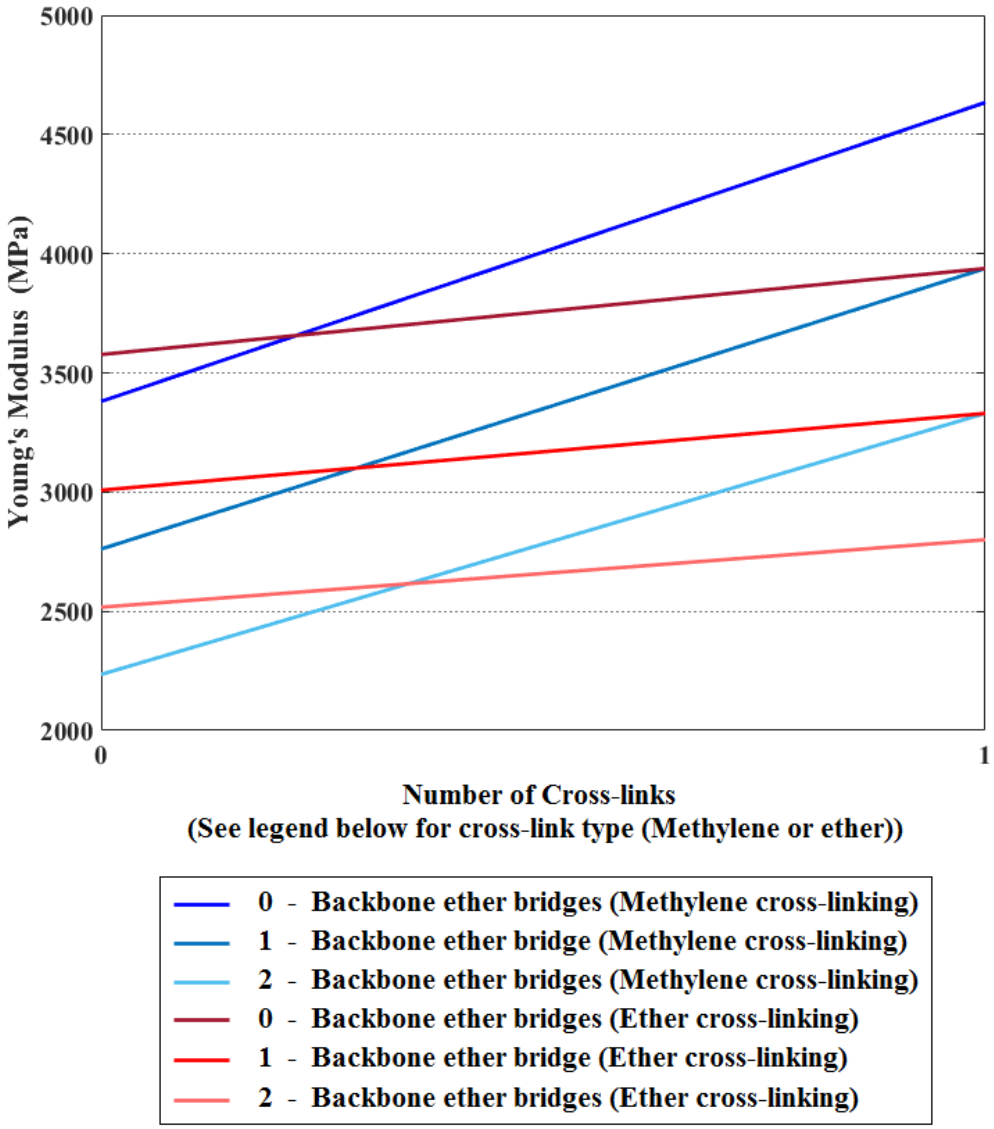

Figure 62: Phenolic resin Young's modulus as a function of cross-linking and cross-link type.

As expected, both types of cross-link effect an increase in the resin's Young's modulus. The magnitude of this effect is proportional to the increase in T_g that accompanies the formation of each type of cross-link. Thus, the increase in Young's modulus is greatest for methylene bridges ~37-47%, where the T_g increase is in the range ~50-105℃, and only marginal for ether bridges, ~8.3-12%, where the increase in T_g is much smaller, being in the range ~19-40℃.

3.3.2. Modelling the Thermo-mechanical Properties of Phenolic Resins as a Function of Cure Time and F/P Ratio

In this section the modelling methodology outlined in section 3.2, page 149, has been employed to predict the thermo-mechanical properties of phenolic resins as a function of both cure time and F/P ratio. This involves calculating the fractional proportions of each chemical species present at a given time during the cure process. This information can be then used as an input for GIM allowing the evolution of the thermo-mechanical properties of the phenolic resin to be predicted, as cure progresses.

3.3.2.1. Predicting the Fractional Proportion of each Chemical Species as a Function of Cure Time and F/P Ratio

The initial chemical species present within the phenolic resin before cross-linking occurs, are estimated from the initial F/P ratio of reactants employed in the synthesis of the resin. The species associated with a range of F/P ratios are shown below in Table 45 and in Table 46 the fractional proportions of each species are presented. The data for both tables was obtained by applying the methodology outlined in section 3.2.2, page 155.

F/P Ratio	Associated Chemical Species
1	*A*
1.125	*A,B,D*
1.25	*A,B,D*
1.375	*A,B,D*
1.5	*B,D*
1.625	*B,D,C,E,G*
1.75	*B,D,C,E,G*
1.875	*B,D,C,E,G*
2	*C,E,G*
2.125	*C,E,F,G,H*
2.25	*C,E,F,G,H*
2.375	*C,E,F,G,H*
2.5	*F,H*
2.625	*F,H,I*
2.75	*F,H,I*
2.875	*F,H,I*
3	*I*

Table 45: Initial chemical species present within a phenolic resin before cross-linking occurs, as a function of F/P ratio.

F/P Ratio	f_A	f_B	f_C	f_D	f_E	f_F	f_G	f_H	f_I	f_J	f_K	f_L	f_M	f_N	f_O
1	*1*														
1.125	*3/4*	*1/8*		*1/8*											
1.25	*1/2*	*1/4*		*1/4*											
1.375	*1/4*	*3/8*		*3/8*											
1.5		*1/2*		*1/2*											
1.625		*3/8*	*1/12*	*3/8*	*1/12*		*1/12*								
1.75		*1/4*	*1/6*	*1/4*	*1/6*		*1/6*								
1.875		*1/8*	*3/12*	*1/8*	*3/12*		*3/12*								
2			*1/3*		*1/3*		*1/3*								
2.125			*3/12*		*3/12*	*1/8*	*3/12*	*1/8*							
2.25			*1/6*		*1/6*	*1/4*	*1/6*	*1/4*							
2.375			*1/12*		*1/12*	*3/8*	*1/12*	*3/8*							
2.5						*1/2*		*1/2*							
2.625						*3/8*		*3/8*	*1/4*						
2.75						*1/4*		*1/4*	*1/2*						
2.875						*1/8*		*1/8*	*3/4*						
3									*1*						

Table 46: Initial mole fraction of each chemical species within a phenolic resin before cross-linking occurs, as a function of F/P ratio.

Having obtained the initial proportions of each chemical species, their evolution as a function of time is predicted by applying the methodology outlined in section 3.2.1, page 149. The rate constants (K_1, K_2, K_3), governing the chemical processes responsible for cure, were assumed to be identical and each assigned an arbitrary value of 0.01 min^{-1}. In practice, the rate constants will not be identical. They can be determined experimentally by measuring the concentration of each type of species as a function of cure time. However, these experiments were not performed in this work and thus the rate constants were assigned identical arbitrary values to allow a basic understanding of the cure kinetics to be obtained from the model. Figure 63 and Figure 64 below contrast the predicted change in the proportion of each chemical species, as a function of cure time, for resins synthesised from both low, and high, F/P ratios. Predictions for a wider range of F/P ratios are given in the appendices (see Appendix C, page 326). To aid the interpretation of the model results, the chemical structures for each species, given previously in Figure 52, are shown again below.

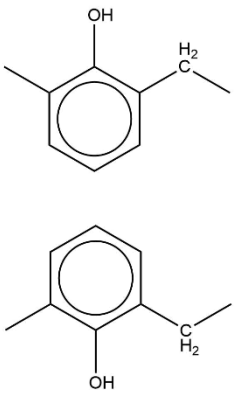

A

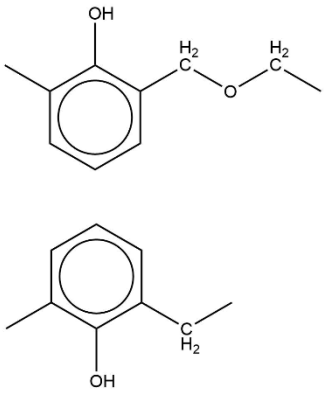

B

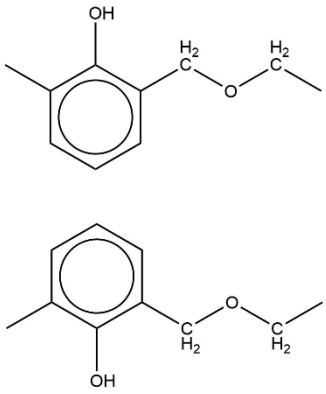

C

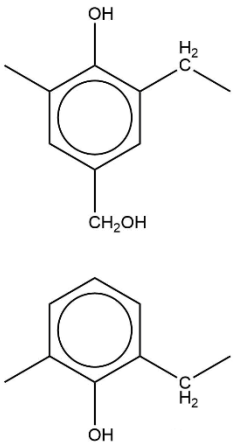

D

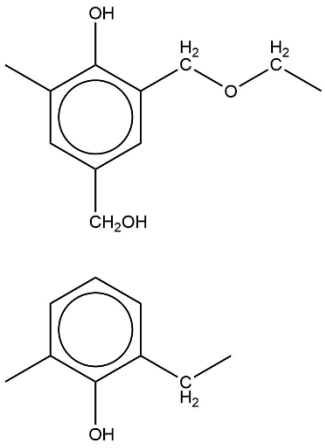

E

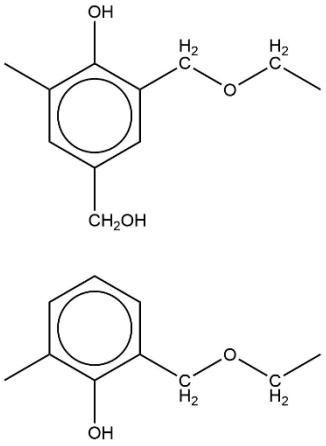

F

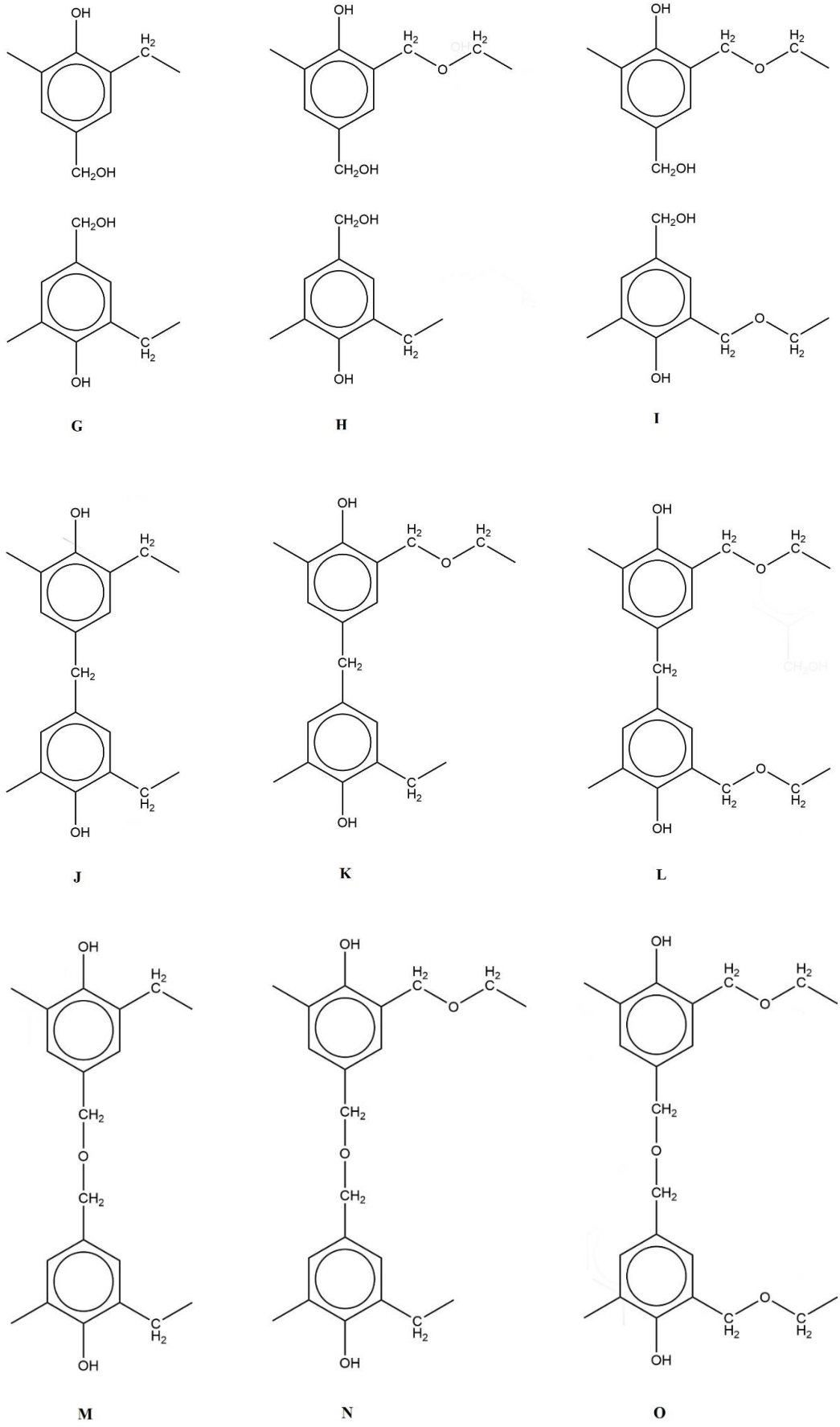

Figure 52: Representative chemical structures of each species.

3.3.2.1.1. Species Evolution in Phenolic Resins Synthesised from an F/P Ratio of 1.25

Figure 63 below shows the evolution of chemical species, as a function of cure time, in a phenolic resin synthesised from an initial F/P ratio of reactants of 1.25.

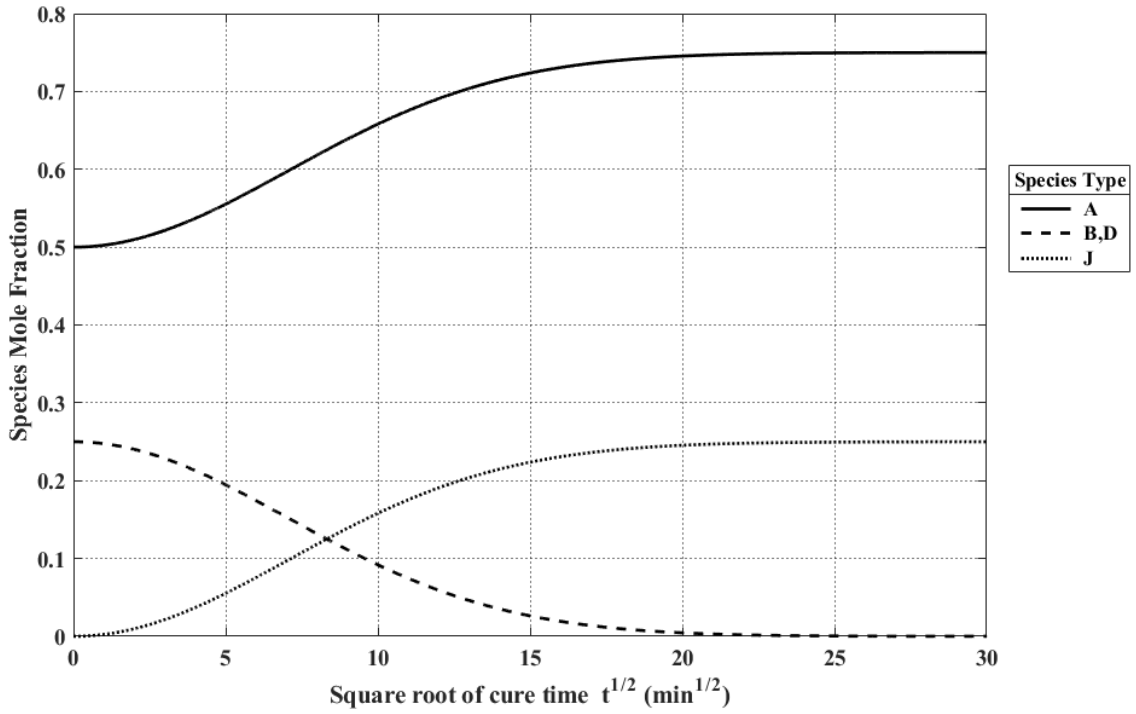

Figure 63: Species evolution as a function of cure time (F/P = 1.25).

The initial structure of a phenolic resin synthesised from an F/P ratio of 1.25 contains three different chemical species, namely A, B, and D. Species A is represented by two adjacent phenyl rings that contain no methylol groups or backbone ether bridges. Thus, species A is stable and does not undergo reaction during the cure process. The other two species can each react once to form stable chemical structures. In the case of species B, this involves the molecular rearrangement of a backbone ether bridge to form a methylene bridge, and thus results in the formation of species A. This accounts for the gradual increase in the mole fraction of species A with cure time. In species D, one phenyl ring contains a methylol group and thus a cross-linking reaction can occur between the two adjacent polymer chains resulting in the formation of a methylene bridge. This cross-linked species is represented by J, and thus the molar quantity of J is observed to increase as species D is consumed through cross-linking reactions. The final structure of the fully cured phenolic resin is composed of two species, one in which no cross-linking has occurred (species A), and another in which a methylene bridge cross-link exists between the two polymer chains (species J).

3.3.2.1.2. Species Evolution in Phenolic Resins Synthesised from an F/P ratio of 2.5

Figure 64 and Figure 65 below show the evolution of chemical species, as a function of cure time, in a phenolic resin synthesised from an initial F/P ratio of reactants of 2.5.

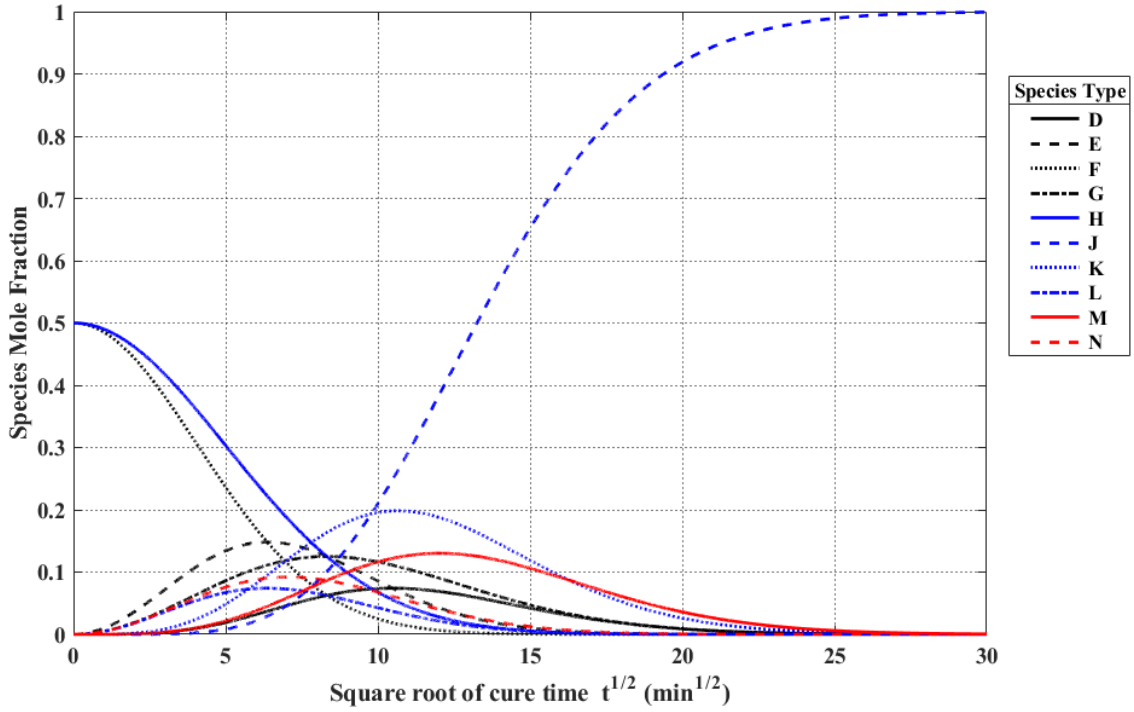

Figure 64: Species evolution as a function of cure time (F/P = 2.5).

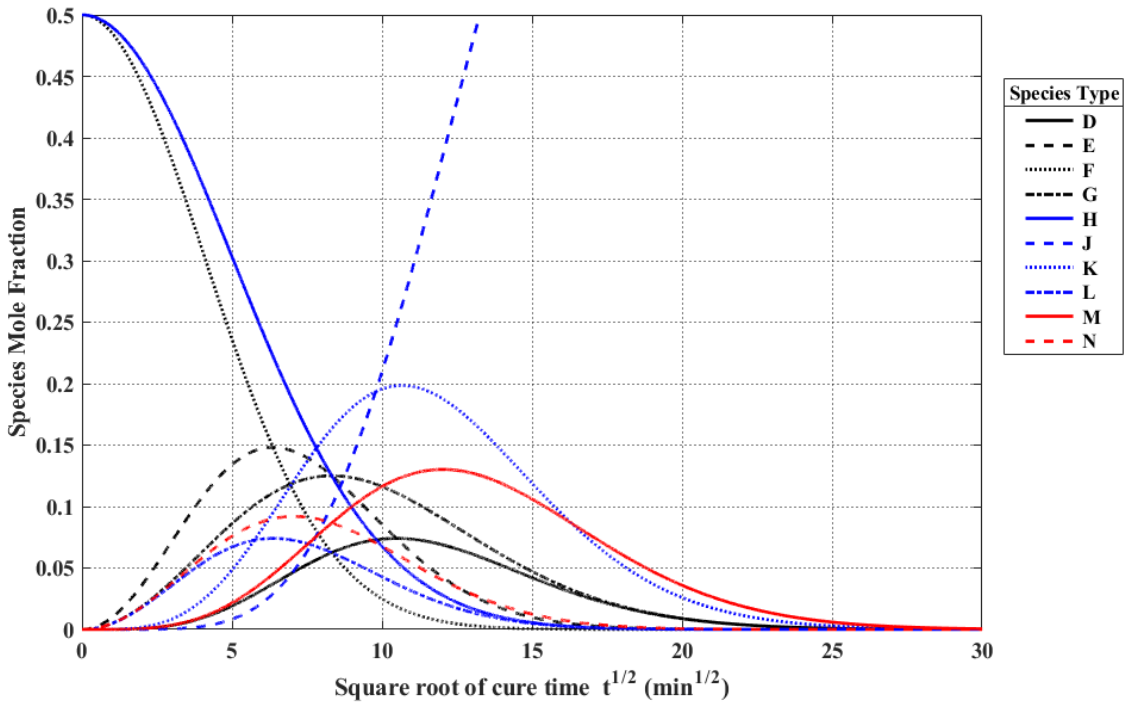

Figure 65: Species evolution as a function of cure time (F/P = 2.5). Figure has been scaled to allow the behaviour of species with low fractional proportions to be observed.

The high F/P ratio results in the inclusion of a large number of ether containing species in the initial structure of the resin. This allows for the formation of a variety of intermediate structures resulting in a complex evolution of chemical species.

The initial structure of the phenolic resin is composed of species F and H. These species can both undergo reaction to form intermediate structures. Species F can either lose one of its two backbone ether bridges to form species E, or undergo a cross-linking reaction to form a methylene bridge with the creation of species L. Thus, as cure proceeds the proportion of F is reduced as it reacts to form species E and L. Two separate reactions can lead to the formation of species E, a molecular rearrangement of either of the two backbone ether bridges present in species F. In contrast, species L can only be formed through one reaction pathway, namely a cross-linking reaction to form a methylene bridge. As a result, a greater proportion of species E is formed through the reaction of species F, than of species L.

The other chemical structure initially present in the resin, before cure begins, is species H. This can either lose a backbone ether bridge, to form species G, or undergo a cross-linking reaction to form an ether bridge between the two adjacent polymer chains, leading to the creation of species N. Each of these reactions can occur only through one reaction pathway and thus, equal proportions of both are formed as species H undergoes reaction. The rate at which the proportion of species H is lost is less than that observed for species F. This is because the total number of reaction pathways available for the breakdown of species H is two, which is less than the three available fir species F.

The mole fraction proportions of intermediate species peak at various times in the cure process. The general trend observed is that the quantity of species possessing two ether bridges peaks at early cure times (species N and L at ~6.5 $hrs^{\frac{1}{2}}$). As cure progresses, more ether bridges have had time to react and thus the peak in species containing single ether bridges occurs at later cure times (species K and M at ~11 $hrs^{\frac{1}{2}}$).

3.3.2.1.3. Discussion

The results in Figure 63, Figure 64, and Figure 65, above and those in Appendix C indicate that the final chemical composition, of a fully cured phenolic resin (cure time $\rightarrow \infty$), is always represented by a mixture of two species, namely A and J. Species A is represented by two phenyl rings which have not undergone cross-linking, whereas species J represents the same two phenyl rings but in which a cross-link, in the form of a methylene bridge, exists linking the two

adjacent polymer chains. As ether bridges are unstable at elevated temperatures [15], any ether containing species will undergo molecular rearrangement, provided the cure temperature is high enough, and thus as a consequence, these species will not be present in the fully cured phenolic resin. This implies that the final chemical structure of a fully cured phenolic resin is composed of only two distinct chemical species.

The exact proportions of these two species, in a fully cured phenolic resin, is dependent upon the initial F/P ratio of reactants employed in the synthesis of the resin. The proportion of species J increases with increasing F/P ratio until, at an F/P ratio of 2.5, it becomes the only species present. This is because, with increasing F/P ratio, a larger proportion of phenyl rings will possess methylol groups at their para sites. This allows a greater degree of cross-linking, between adjacent polymer chains, to occur. When the F/P ratio is equal to 2.5, all of the initial species contain at least one methylol group. This group can undergo reaction to form a methylene bridge and this structure is represented by species J. Increasing the F/P ratio further introduces species that contain two methylol groups. These undergo reaction to form ether bridges (M, N, O) which can then undergo molecular rearrangement to form methylene bridges, becoming species J. It is this molecular rearrangement of ether bridges that is responsible for the chemical structures, of fully cured phenolic resins, being composed entirely of species J when the F/P ratio is equal to, or greater than, 2.5.

3.3.2.2. Predicting Phenolic Resin Thermo-Mechanical Properties as a Function of Cure time and F/P Ratio with GIM

The species mole fraction profiles, obtained in the previous section, are now used as inputs for GIM allowing the evolution of a phenolic resin's engineering properties, as a function of cure time and F/P ratio, to be predicted. It was assumed previously that the values of the rate constants (K_1,K_2,K_3) were identical. However, in practice, the rate constants will not be equal and thus the GIM predicted properties of partially cured phenolic resins will differ from those observed experimentally. Thus, the thermo-mechanical property predictions that follow, for partially cured phenolic resins, should only be taken as approximations indicative of the broad overall trends in material properties.

3.3.2.2.1. Glass Transition Temperature and Young's Modulus

Figure 66 and Figure 67 below show the evolution of the glass transition temperature, and Young's modulus, of phenolic resins as a function of both cure time and the initial F/P ratio of reactants.

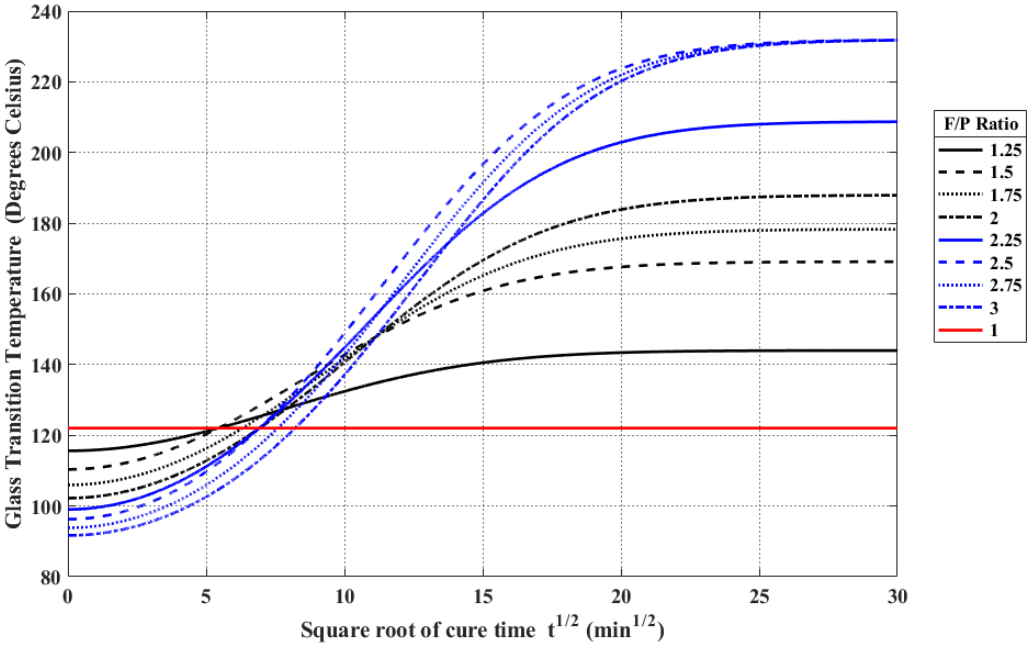

Figure 66: Glass transition temperature as a function of cure time and F/P ratio.

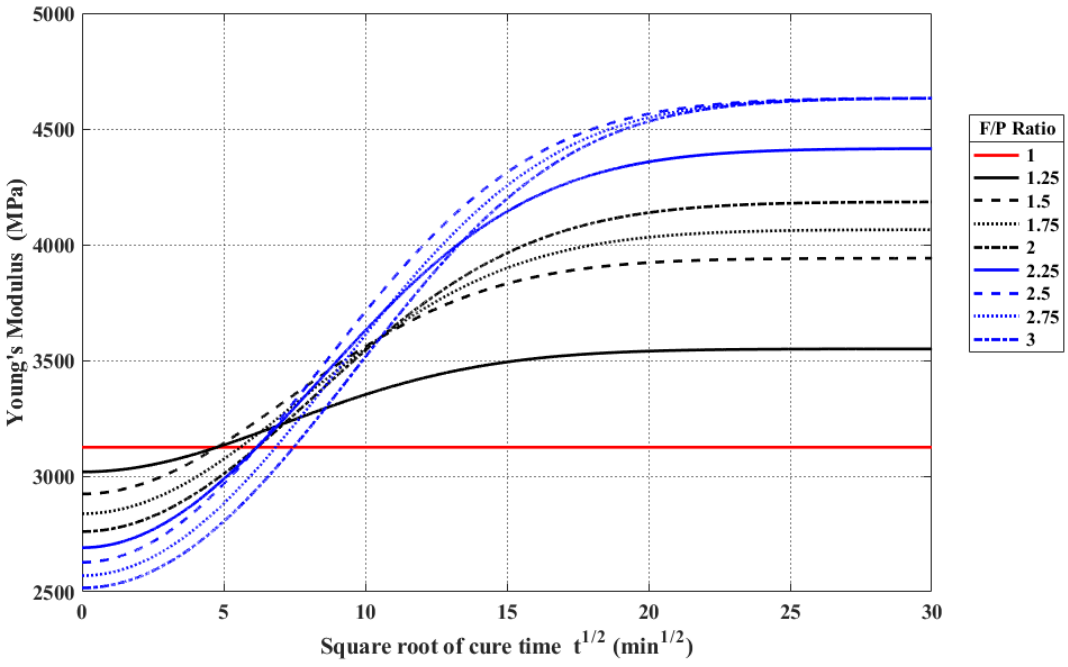

Figure 67: Young's modulus as a function of cure time and F/P ratio.

When the F/P ratio is equal to 1 the initial state of the resin, that being the state in which no cross-linking between adjacent polymer chains has occurred, is composed entirely of species A. Neither of the phenyl rings in species A possess methylol groups and thus no cross-linking reactions can occur. As a consequence, there is no development of cross-linking as a function of cure time and thus the glass transition temperature is observed to remain constant at a value of ~122℃. Increasing the F/P ratio to 1.25, the initial state of the resin becomes represented by three different species: A, B, and D. Species D represents two phenyl rings, with one possessing a methylol group, allowing this species to undergo a cross-linking reaction to form a methylene bridge. Thus, the fully cured system exhibits an overall increase in T_g when compared to its initial state before cross-linking had occurred.

At early cure times $\left(t^{\frac{1}{2}} < 5\right)$, the predicted T_g of the phenolic resin is less than that of species A; a species in which no cross-linking occurs. This can be explained by the initial presence of ether bridges in the polymer backbone of the resin, in the form of species B. This has the effect of reducing T_g, as predicted previously in section 3.3.1.1.1, page 162. As cure proceeds these ether bridges are lost through molecular rearrangement and therefore they do not impact upon the final T_g of the fully cured phenolic resin. The general trend that is observed, with increasing F/P ratio, is a decrease in the initial T_g of the phenolic resin, before cross-linking has occurred, and an increase in the final T_g of the fully cured material.

When the F/P ratio is greater than 2.5, no further increase in the T_g of the fully cured phenolic resin is observed. This is because when the F/P ratio is equal to 2.5 the structure of the fully cured phenolic resin is composed entirely of species J. As species J represents two phenyl rings cross-linked by a methylene bridge, no further cross-linking reactions are possible. In other words, the system has attained cross-link saturation. Increasing the F/P ratio above 2.5 leads to the formation of a greater proportion of initial species that contain bridges. However, as these undergo molecular rearrangement to form methylene bridges, they do not affect the final T_g of the fully cured phenolic resin. There is still, however, an effect upon both the initial T_g, and the T_g of the partially cured materials, arising from the introduction of ether bridges into the phenolic resin structure.

Thus, in conclusion, it would appear that employing F/P ratios in excess of 2.5, in the synthesis of phenolic resins, provides no benefit to the T_g of the fully cured system. When the F/P ratio is in excess of 3, every phenol molecule can undergo reaction with formaldehyde and thus

there is an excess of formaldehyde that is unable to react. Thus, no further changes in the thermo-mechanical properties of either partially cured, or fully cured, phenolic resins occurs.

Similar trends are observed in the Young's modulus and this is expected as the elastic moduli, and T_g (extent of cross-linking), are closely related [10].

3.3.2.2.2. Thermal Expansion Coefficient

Figure 68 below shows the evolution of the thermal expansion coefficient of phenolic resins as a function of both cure time and the initial F/P ratio of reactants.

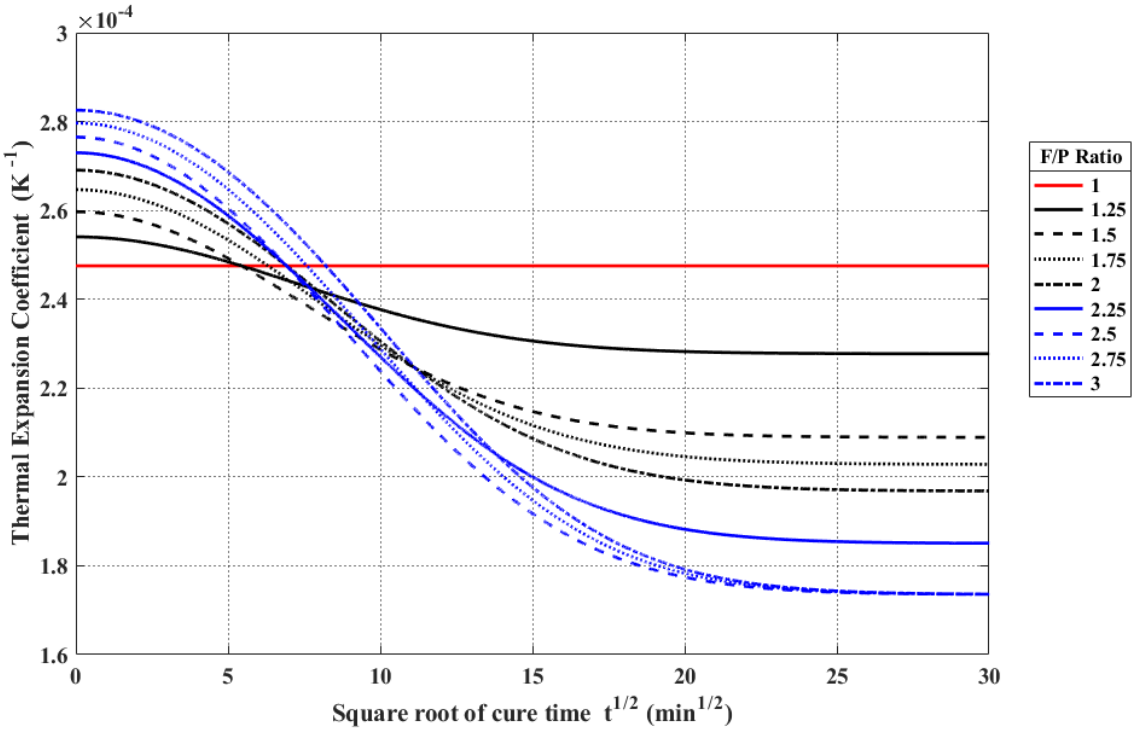

Figure 68: Thermal expansion coefficient as a function of cure time and F/P ratio.

The initial value of the thermal expansion coefficient, in phenolic resins before cross-linking occurs, is observed to increase with increasing F/P ratio and this can be attributed to the increasing quantity of ether bridges in the backbone of the polymer. Previously it was shown (section 3.3.1.1.2, page 164) that the presence of ether bridges, within a species, has the effect of increasing that species thermal expansion coefficient. As cure proceeds, the thermal expansion coefficient decreases, for all F/P ratios, as a result of the development of cross-linking within the polymer structure and from the loss of ether bridges. At F/P ratios in excess of 2.5 there is no further

change in the thermal expansion coefficient, of fully cured phenolic resins, because cross-link saturation has been reached.

3.3.2.2.3. Density

Figure 69 below shows the evolution of the density of phenolic resins as a function of both cure time and the initial F/P ratio of reactants.

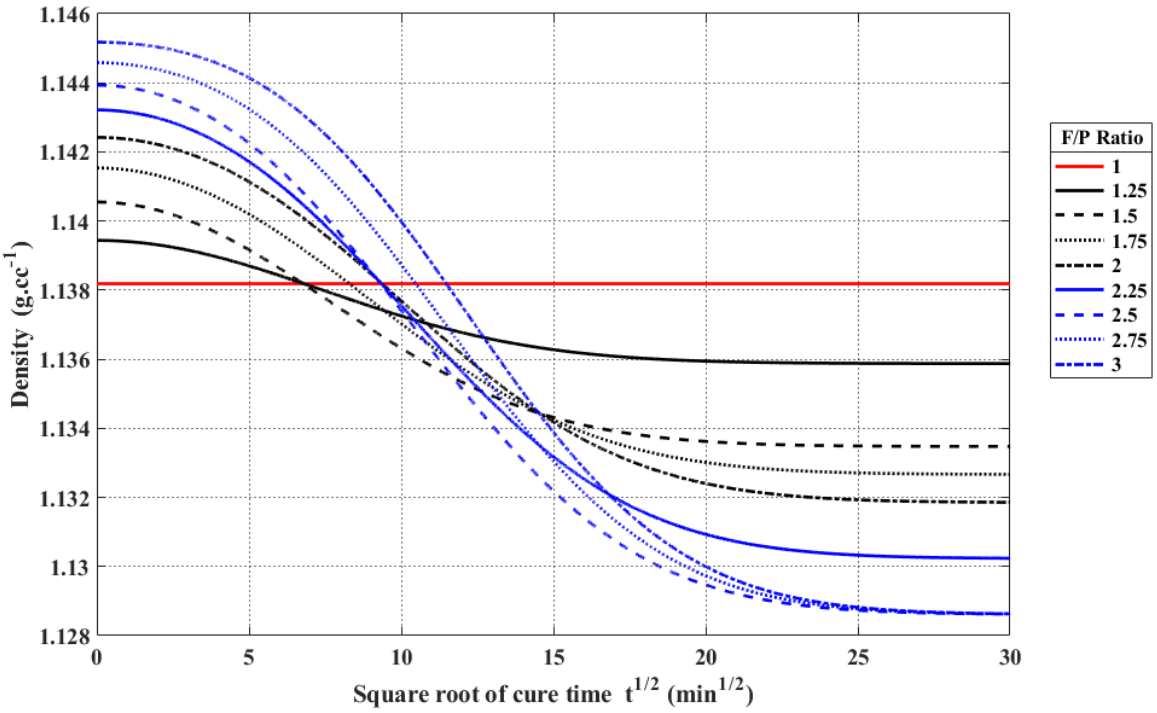

Figure 69: Density as a function of cure time and F/P ratio.

The initial density of the phenolic resin increases, with increasing F/P ratio, and this is expected as it was earlier deduced (section 3.3.1.1.4, page 167) that the addition of ether bridges, to the chemical structure of a species, has the effect of increasing its density. The overall trend is a reduction in the density of fully cured phenolic resins with increasing F/P ratio, with no further effect observed when the F/P ratio is greater than 2.5 as a consequence of cross-link saturation.

3.3.2.2.4. Mass Loss and Volume Reduction

Figure 70 and Figure 71 below show the percentage mass loss, and volume reduction, of phenolic resins as a function of both cure time and the initial F/P ratio of reactants.

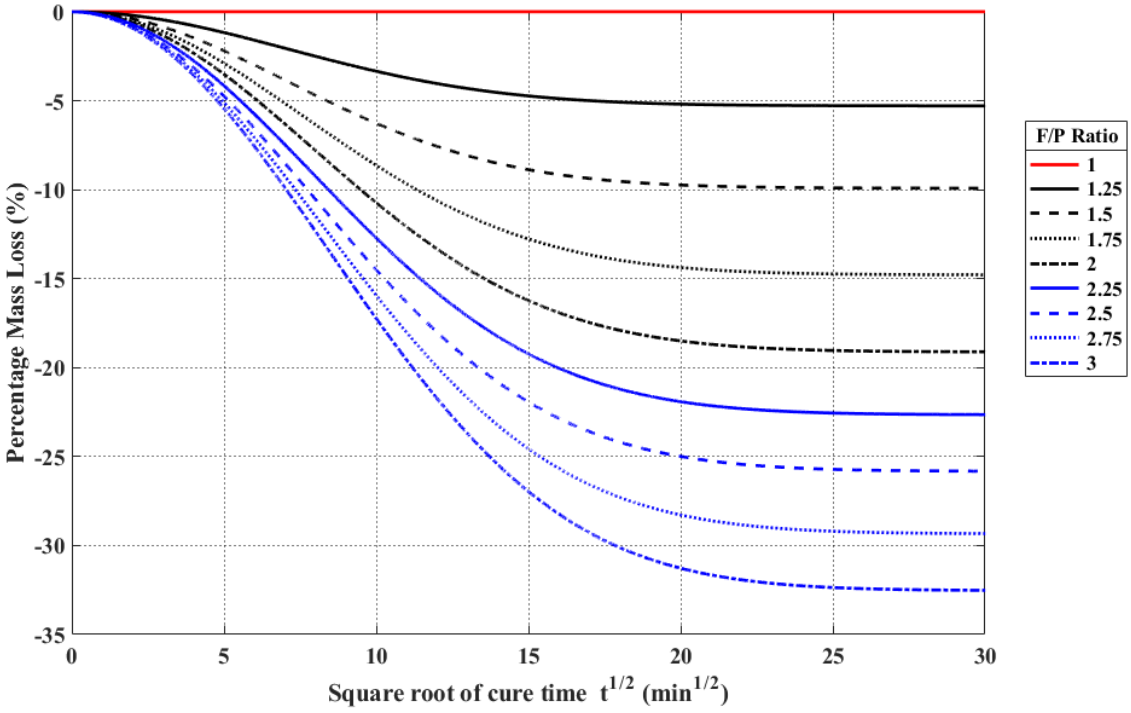

Figure 70: Percentage mass loss as a function of cure time and F/P ratio.

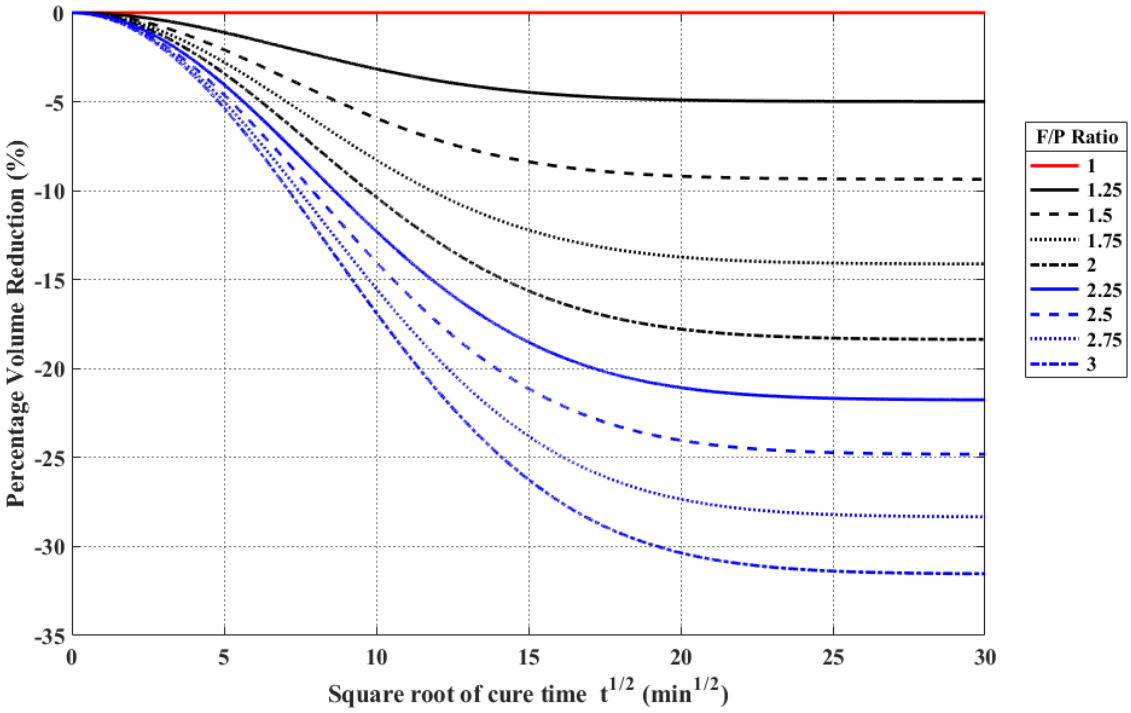

Figure 71: Percentage volume reduction as a function of cure time and F/P ratio.

The mass of the phenolic resin is observed to decrease as a function of cure time, with the magnitude of the mass loss being related to the F/P ratio. Larger F/P ratios result in greater mass loss. The cure of phenolic resins occurs through a series of condensation reactions. These are of two general forms:

Type I Reaction of methylol with a free site on a phenyl ring to form a methylene bridge, with the evolution of one water molecule (I) (Figure 5).

Type II Reaction of two methylol groups to form an ether bridge (Figure 6), and one molecule of water, with subsequent molecular rearrangement to form a methylene bridge and one molecule of formaldehyde (II) (Figure 7).

The net loss in molar mass that occurs, through each of these reaction pathways, is shown in Table 47.

Cross-link Type	**Mass Loss** $(g.mol^{-1})$
I	*18*
II	*48*

Table 47: Mass loss resulting from the formation of each type of cross-link.

Both types of cross-linking reaction are positive functions of the F/P ratio, with type I being dominant initially, before being superseded by type II, as the F/P ratio is further increased. Thus, mass loss is an increasing function of F/P ratio and this agrees with the predicted behaviour shown in Figure 70.

A similar trend is observed in the reduction of resin volume during cure and this arises from the combined effect of the loss of degrees of freedom, following cross-link formation, coupled with the loss in van der Waals volume arising from the evaporation of the reaction products (water and formaldehyde).

3.3.3. Thermo-mechanical Properties of Fully Cured Phenolic Resins as a Function of F/P Ratio

In the previous section, the effect of both cure time and the initial F/P ratio of reactants, on phenolic resin thermo-mechanical properties, was discussed. In this section, the relationship between F/P ratio, and the engineering properties of fully cured materials, will be investigated. The figures below show the thermo-mechanical properties of fully cured phenolic resin as a function of the initial F/P ratio of reactants.

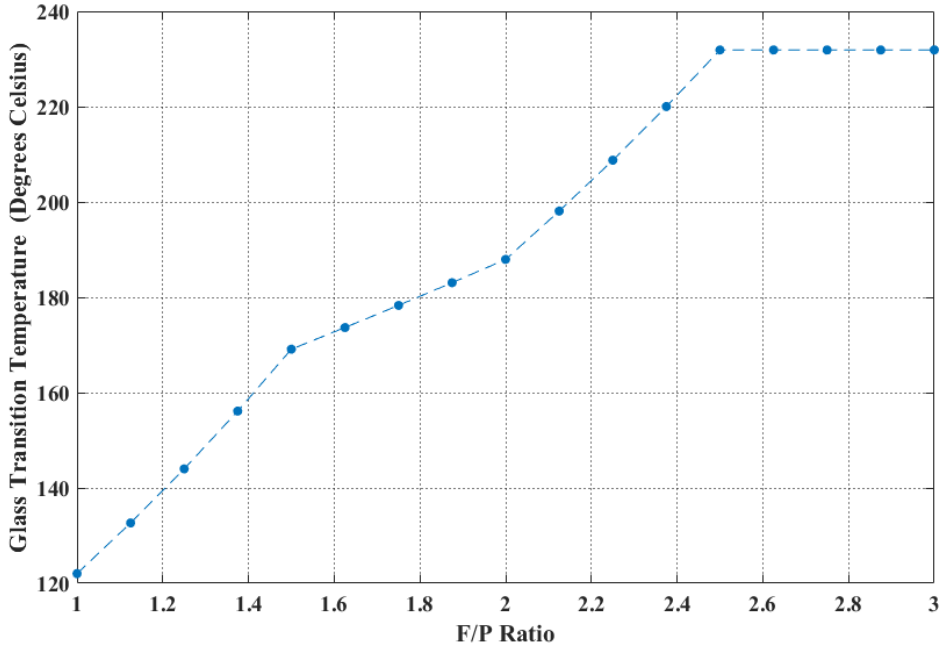

Figure 72: Glass Transition Temperature of fully cured phenolic resin as a function of F/P ratio.

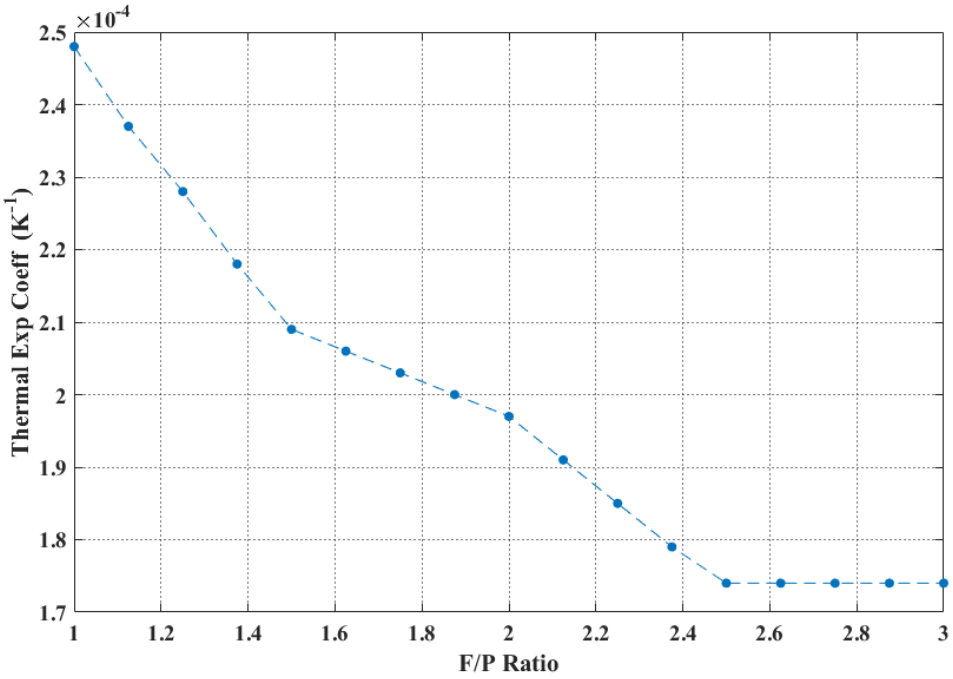

Figure 73: Thermal Expansion Coefficient of fully cured phenolic resin as a function of F/P ratio.

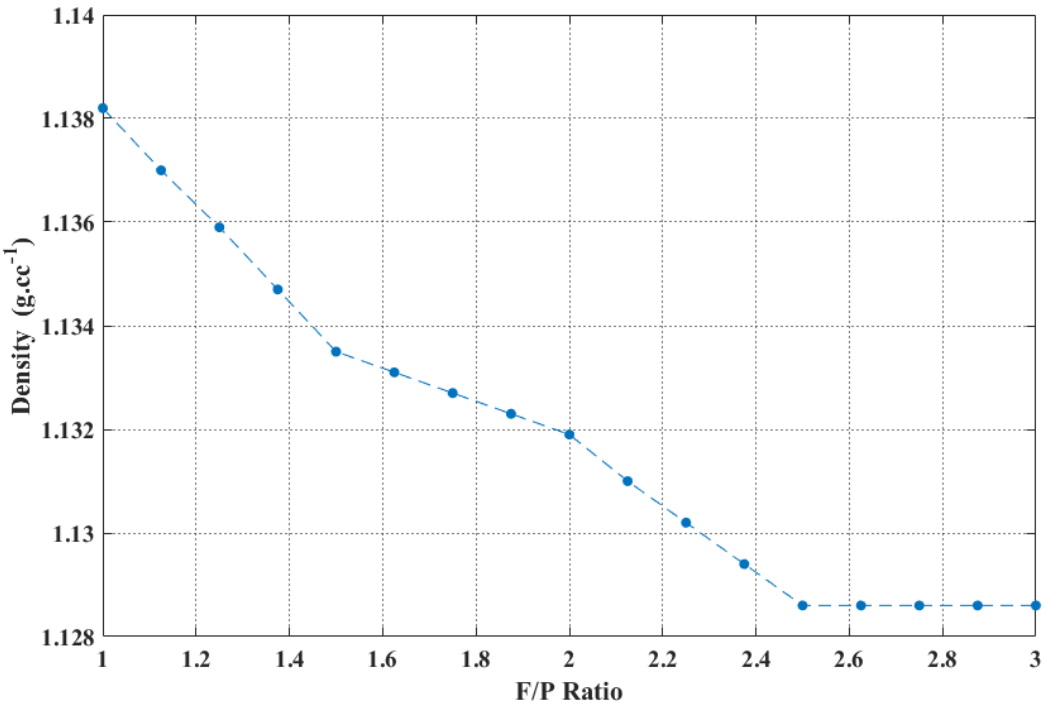

Figure 74: Density of fully cured phenolic resin as a function of F/P ratio.

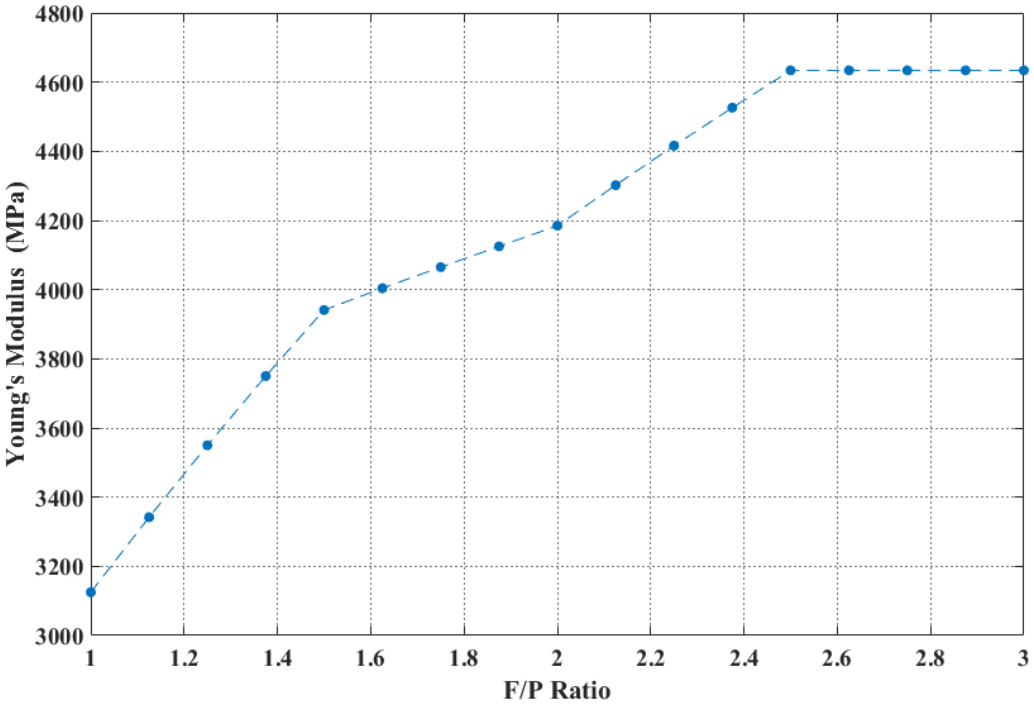

Figure 75: Young's modulus of fully cured phenolic resin as a function of F/P ratio.

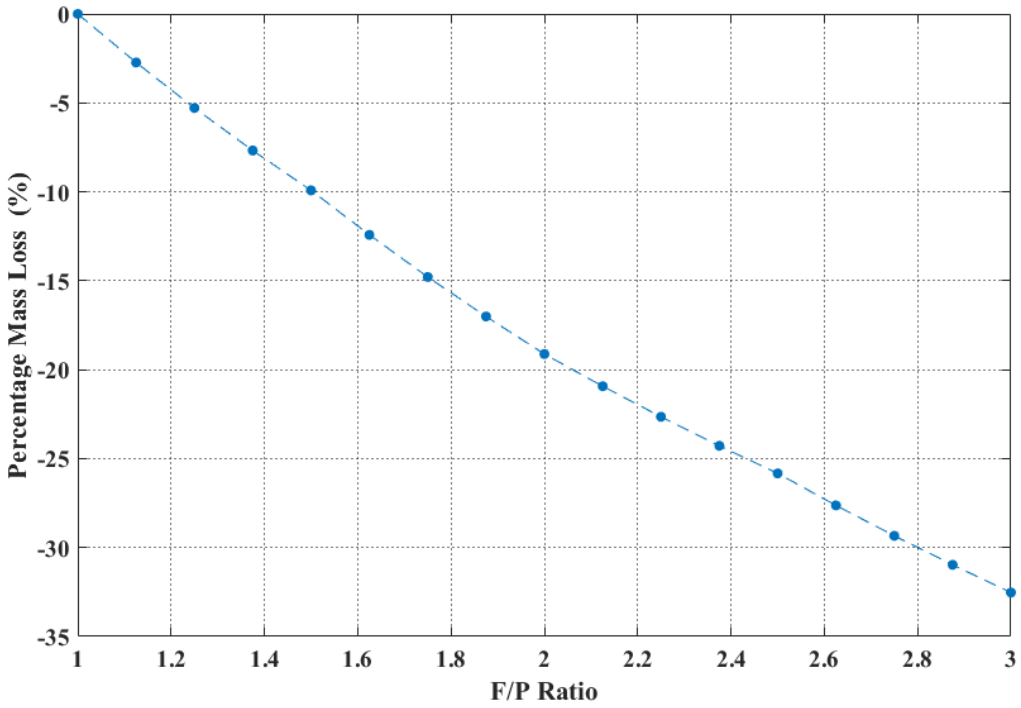

Figure 76: Percentage mass loss of fully cured phenolic resin as a function of F/P ratio.

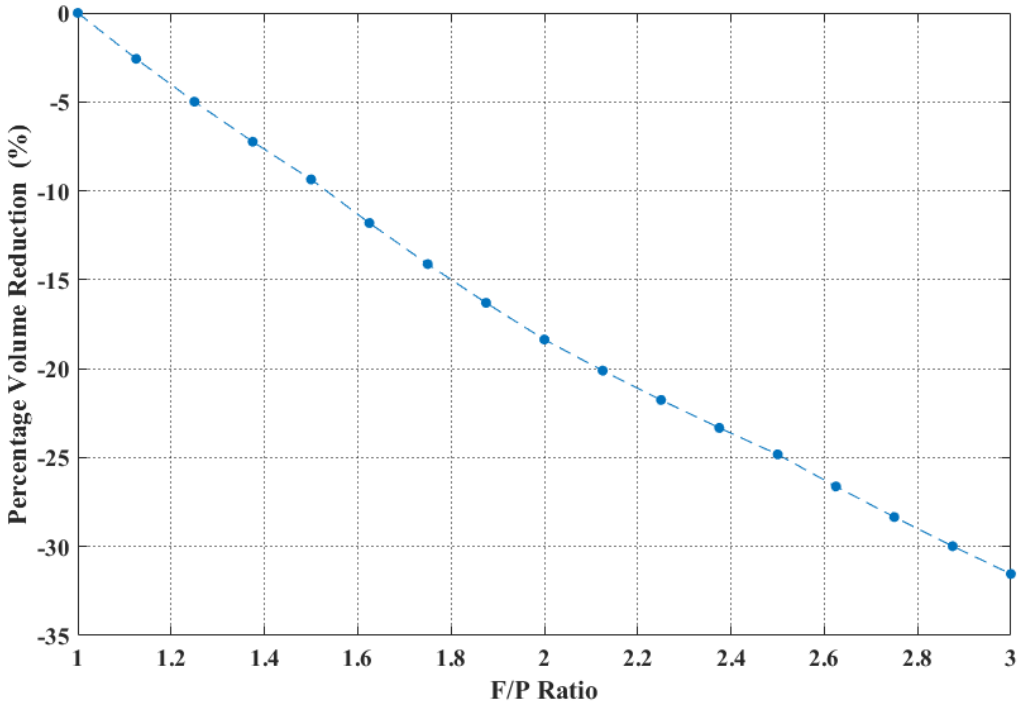

Figure 77: Percentage volume reduction of fully cured phenolic resin as a function of F/P ratio.

Two distinct property trends are observed with respect to the F/P ratio: an approximately linear decrease in both the percentage mass loss and percentage volume reduction, and a more complex relationship for the other four engineering properties: T_g, thermal expansion coefficient, density, and Young's modulus. These exhibit four distinct regions of behaviour that can be categorised, with respect to the initial F/P ratio of reactants, as follows.

$\mathbf{1 < F/P < 1.5}$

Glass transition temperature and Young's modulus increase, whereas the thermal expansion coefficient and density decrease, with increasing F/P ratio.

$\mathbf{1.5 < F/P < 2}$

The trends in all four engineering properties remain unchanged, however the magnitude of the property change with respect to increasing F/P ratio is greatly decreased. Thus, changes in the F/P ratio effect much smaller changes in the resin's underlying thermo-mechanical properties than in the first region.

$2 < F/P < 2.5$

The trends remain unchanged, however the magnitude of the property change with increasing F/P ratio becomes similar to that observed in the first region.

$F/P > 2.5$

All properties are constant with respect to the F/P ratio and this is attributed to cross-link saturation, as was discussed previously (see section 3.3.2.2.1, page 183).

3.3.4. Investigation into Residual Stress Arising from Material Contraction During Cure

In the previous section, it was predicted that the effect of increasing the initial F/P ratio of reactants, employed in the synthesis of phenolic resins, is to increase the degree of cross-linking within the polymer network and that this is accompanied by a reduction in the volume of the material. When phenolic resins are employed as the matrix component within composite materials, this contraction may be restricted by the presence of the fibre reinforcement. Resins are utilised as matrices within composite materials to enable effective load transfer between individual fibres. Thus, the forces involved in reducing the volume of the resin will be transferred to the reinforcement, which will inhibit the ability of the matrix to achieve a stress-free state. As a consequence, there will be residual stress frozen into the resin after cure which could result in, or facilitate, cracking of the matrix and subsequent delamination leading to catastrophic failure of the composite. In this section the residual stress inside the phenolic matrix, of a fibre-based composite, will be estimated, related to the F/P ratio, and finally related to the phenolic resin T_g and Young's Modulus.

Assume a simple unidirectional fibre-reinforced composite with a matrix composed of phenolic resin. The resin is assumed to be able to expand and contract freely in the axes perpendicular to the fibre direction, but is constrained in the direction parallel to the fibre axis. The Young's modulus of the fibre is assumed to be infinite, that is to say that there is no strain induced in the fibre as a consequence of resin contraction. This assumption is reasonable as, taking approximate values for the Young's modulus of carbon fibre [106] and phenolic resin [107] from the literature, the Young's modulus of carbon fibre is ~66 times greater than that of a typical phenolic resin. The initial state of the resin, for a given F/P ratio, is assumed to be fully bonded to the fibre such that any volume reduction, occurring during cure, will be experienced as a longitudinal stress within the resin. For simplicity, the Young's Modulus of the resin is assumed

to independent of strain, in other words constant. This approximation should give reasonable estimates at small strain values but will become increasingly inaccurate as the longitudinal strain increases and the resin stress/strain behaviour leaves the elastic region. Internal stresses, resulting from thermal contraction of the resin or expansion of the fibre, upon cooling after cure, are omitted. All predictions are made for a composite at room temperature (T = 25℃).

The final volume of the resin can be expressed in terms of the initial volume as:

$$aV_i = V_f \tag{195}$$

Where V_i is the initial volume of the resin, that is to say the volume of the resin before cross-linking between adjacent polymer chains has occurred, and V_f is the final volume of the fully cured resin, both in units of mm^3. The term a is the final volume expressed as a fraction of the initial volume. Equation (195) can be rewritten in terms of length as:

$$(bL_i)^3 = V_f \tag{196}$$

Where L_i is the initial length of the side of a cube of resin, of volume V_i, in units of mm, and b is the final length of the resin expressed as a fraction of the initial length. Substituting equation (196) into equation (195):

$$aV_i = b^3{L_i}^3 \tag{197}$$

$$a{L_i}^3 = b^3{L_i}^3 \tag{198}$$

$$a = b^3 \tag{199}$$

$$b = a^{\frac{1}{3}} \tag{200}$$

For the purposes of calculating the strain, the length of the resin (L) is taken to be the dimension that the fully cured material would have if no fibre reinforcement were present.

$$L = L_f = bL_i \tag{201}$$

Where L, L_f, and L_i, are the length of the resin for the strain calculation, and the final and initial lengths respectively in units of mm. The change in resin length that arises, as a result of its bonding to the fibre, is therefore:

$$\Delta L = L_i - L \tag{202}$$

$$\Delta L = L_i - L_f \tag{203}$$

$$\Delta L = L_i - bL_i \tag{204}$$

$$\Delta L = (1 - b)L_i \tag{205}$$

Thus, the longitudinal strain within the resin, in the fibre axis direction, is given by:

$$\varepsilon = \frac{\Delta L}{L} = \frac{(1 - b)L_i}{bL_i} \tag{206}$$

$$\varepsilon = \frac{1}{b} - 1 \tag{207}$$

Where ε is the longitudinal strain. The stress within the resin in the fibre axis direction is:

$$\sigma = E\varepsilon = E\left(\frac{1}{b} - 1\right) \tag{208}$$

Where σ is the stress in units of MPa and E is the Young's Modulus of the resin, at 25℃, in units of MPa.

3.3.4.1. Longitudinal Stress as a Function of F/P Ratio and Thermo-mechanical Properties

The longitudinal stress within a fully cured phenolic resin is shown below, in Figure 78 to be an approximately linear function of the initial F/P ratio of reactants.

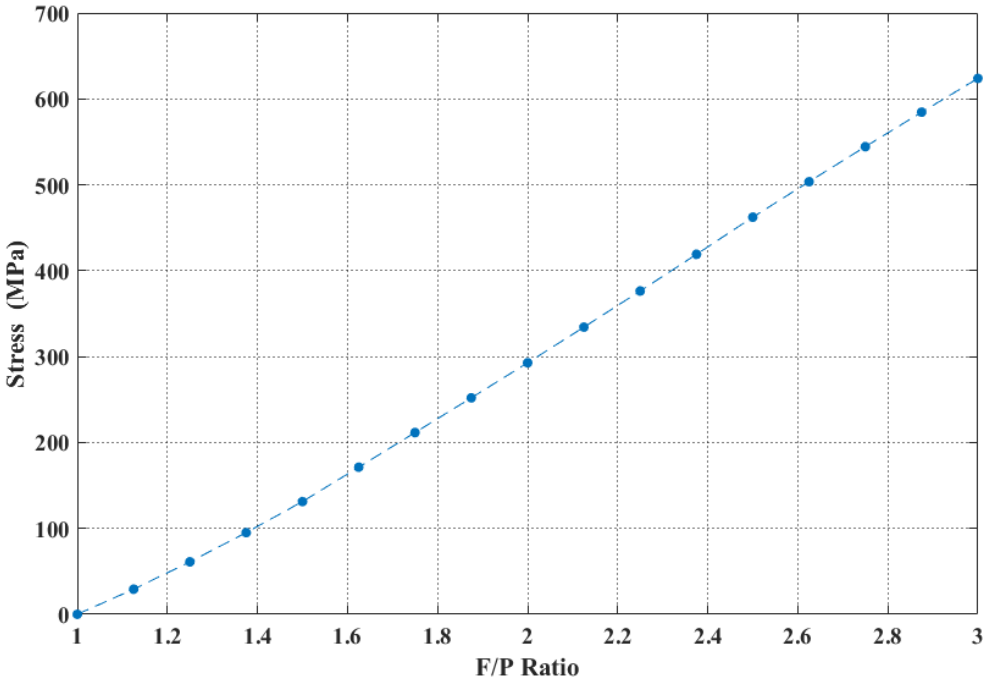

Figure 78: Longitudinal stress within a fully cured phenolic resin matrix as a function of F/P ratio.

By plotting the longitudinal stress against both the glass transition temperature, and Young's modulus, it is possible to identify the 'cost' that is incurred, in the form of internal stress within the matrix of the composite, in obtaining the desired engineering properties. This is shown below in Figure 79 and Figure 80.

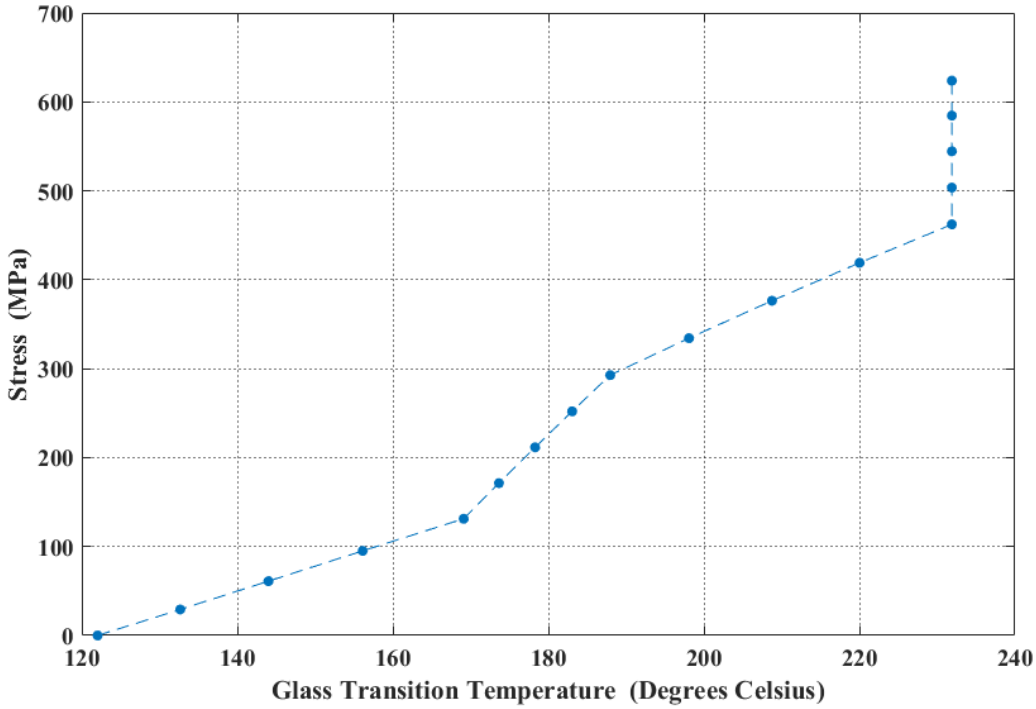

Figure 79: Longitudinal stress within a fully cured phenolic resin matrix as a function of the glass transition temperature.

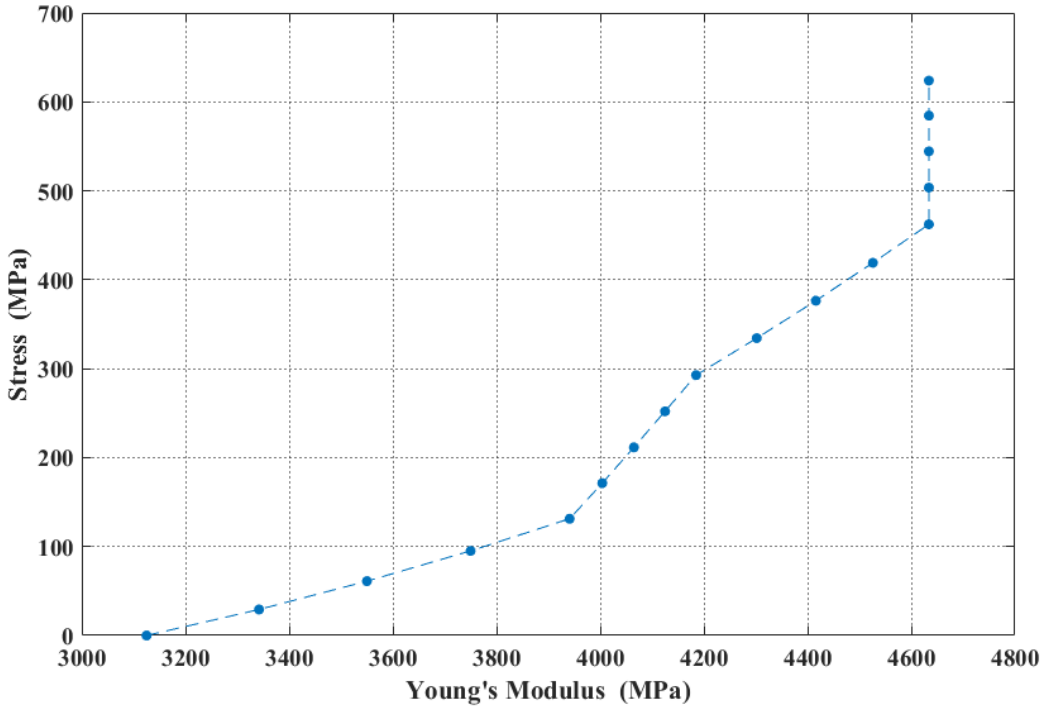

Figure 80: Longitudinal stress within a fully cured phenolic resin matrix as a function of the Young's modulus.

The longitudinal stress initially increases linearly with glass transition temperature. Moving from an initial T_g of ~122℃, to ~169℃, the longitudinal stress increases by ~132 MPa, approximately 2.8 $MPa.℃^{-1}$. However, on moving from a T_g of ~169℃, to ~188℃, the longitudinal stress increases by ~163 MPa, approximately 8.6 $MPa.℃^{-1}$. Thus, improvements in T_g above 169℃ incur large penalties, in the form of internal stresses within the matrix, for only small gains in the glass transition temperature. Above ~188℃, the behaviour reverts back to that observed at lower temperatures and when a T_g of ~232℃ has been attained, the stress has increased by a further ~169 MPa, approximately 3.9 $MPa.℃^{-1}$. Once a glass transition temperature of ~232℃ is reached, no further improvement in T_g is obtained from increasing the F/P ratio further as the material has attained cross-link saturation. However, although increasing the F/P ratio further has no effect upon the glass transition temperature, it does increase the residual stress within the resin. This is because increasing the F/P ratio increases the number of ether bridges in the initial resin structure. These are subsequently lost, through molecular rearrangement, resulting in a larger volume reduction than that which is observed in resins where fewer ether bridges are present initially. Thus, the net effect of this increase in ether bridges, at F/P ratios in excess of 2.5, is to increase the residual stress within the cured matrix with no benefit to the glass transition temperature. A similar trend is observed in the Young's modulus as expected, as the glass transition temperature and Young's modulus are closely related [10].

3.3.5. Comparison of Model Predicted Thermo-Mechanical Property Behaviour with data in the Available Literature

The model results obtained previously (section 3.3.1, page 159) indicate that the inclusion of ether bridges, within the chemical structure of phenolic resins, will have an effect on the overall thermo-mechanical properties of the material. The effect of ether bridges on the flexural modulus of phenolic resins was investigated by Parameswaran et al [108]. They synthesised resins from a range of different initial F/P ratios using the same cure cycle. They suggested that resins synthesised from higher F/P ratios would contain a greater proportion of ether bridges. This is supported by the proposal of Maciel et al [15] that temperatures in excess of 160℃ are required to induce the loss of ether species, through their molecular rearrangement to methylene bridges. The highest temperature employed by Parameswaran et al [108] was 120℃ and thus the resins synthesised from higher F/P ratios would be expected to contain a higher proportion of ether bridges. Measurements of the flexural modulus indicated that it reached a maximum when the F/P ratio was 1.7, and thereafter decreased with increasing F/P ratio. They attributed this decrease to the greater proportion of ether bridges present in those phenolic resins synthesised from higher F/P ratios, disrupting the hydrogen bonding between polymer chains.

The decrease in flexural modulus with increasing ether bridge concentration is supported by the model predictions of GIM where it was shown that the inclusion of ether bridges, in the structure of phenolic resins, reduces the Young's modulus of the material (Figure 57). However, in these model predictions the effect of hydrogen bonding, from the polar OH groups in phenolic resins, have not been included. Thus, GIM suggests that it is not the disruption of hydrogen bonding that accounts for the reduction in modulus with ether bridge content, but instead the reduction in the ratio $\left(\frac{E_{coh}}{N}\right)$ of the mer unit.

Gabilondo et al [109] also investigated the effect of F/P ratio on the flexural modulus of phenolic resins. Although no DSC was performed, the final cure temperature was 190℃, sufficient for the molecular rearrangement of ether bridges to methylene bridges. Thus, the modulus reducing effect of ether bridges can be discounted and the trends in these results can be compared against those predicted by GIM for fully cured resins in Figure 75. Their measurements indicate that the flexural modulus increases with increasing F/P ratio which is in agreement with the behaviour predicted by the model. Importantly, they observed this trend for F/P ratios up to 2.2, this being the highest ratio employed in their study. This agrees with the model prediction in Figure 75 that Young's modulus will continue to increase with increasing F/P ratio, for F/P ratios less than 2.5, as cross-link saturation has not yet been reached.

Manfredi et al [21] investigated the T_g of fully cured phenolic resins for a range of different F/P ratios. Care must be taken in the interpretation of their results as no DSC was performed to verify that the resins were fully cured. The loss tangent/temperature spectrum obtained for one of these materials, through DMTA, showed a significant 'shoulder' on the left-hand side of the loss tangent curve. This can be indicative of post-curing of the material during the DMTA scan. However, assuming that the materials were fully cured, the following trends were observed. When the F/P ratio was equal to 1, the T_g of the fully cured material was 172℃. This increased, with increasing F/P ratio, to 255℃ when the F/P ratio was 1.3, and to 263℃ when the F/P ratio was 2. Thereafter, no appreciable change in T_g was observed with increasing F/P ratio. This appears to contradict the findings of Gabilondo et al [109] as they observed an increase in modulus, at F/P ratios in excess of 2, which would be expected to be accompanied by an increase in T_g. However, in the data of Manfredi et al [21] there is only one measurement of T_g for a resin with an F/P ratio greater than 2. Thus, the observation that the glass transition temperature is constant, above an F/P ratio of 2, is most likely as a result of an erroneous data point. Comparing the observations of Manfredi et al [21] with the predictions of the model in Figure 72, considerable disagreement is apparent. In the following section it is proposed that this

deviation can be accounted for by including the effect of hydrogen bonding in the mer unit parameter values of each phenolic resin chemical species (A through O).

3.3.6. Hydrogen Bonding in Phenolic Resins

The GIM cohesive energy parameter, calculated for each type of phenolic resin species in Table 41, was calculated by group additivity using the functional group parameters suggested by Porter [71]. The cohesive energy describes the energy required to completely overcome the intermolecular forces of attraction between mer units. Thus, it describes both the van der Waals and hydrogen bond interactions. However, the cohesive energy values of each functional group, provided in the additivity tables of Porter [71], are average values obtained from systems containing many different chemical species. These systems can possess complex morphologies and as a result it is not always possible for specific functional groups to participate in hydrogen bonding, even if ordinarily they are capable of doing so. To model polymers in which every functional group capable of undergoing hydrogen bonding participates in this interaction, the cohesive energy parameter must be increased to account for the increased intermolecular attraction. Porter et al [110] have suggested that each hydrogen bond contributes 10,000 $J.mol^{-1}$ to the cohesive energy parameter of the mer unit. This has been employed within GIM, by Foreman et al [75], to predict the thermo-mechanical properties of epoxy resin blends in which strong hydrogen bonding interactions are possible. These results showed that, when hydrogen bonding was accounted for, model predictions were in good agreement with that material behaviour which was observed experimentally.

In phenolic resins, OH groups are located on both the phenyl ring and, before complete cross-linking has occurred, on methylol groups. These are highly polar groups possessing lone pairs of electrons and thus are capable of forming hydrogen bonds. Thus, this would suggest that hydrogen bonding plays an important role in the properties of phenolic resins. As discussed previously, the cohesive energies of each species in Table 41 were calculated using the group additivity tables of Porter [71]. These values do not account for situations in which every instance of a specific functional group can participate in hydrogen bonding. In the work that follows, the cohesive energies of each species in Table 41 have been recalculated for the scenario where hydrogen bonding occurs in every functional group that is capable of participating in hydrogen bonding. Thus, each OH group within the mer unit forms one hydrogen bond contributing 10,000 $J.mol^{-1}$ to the cohesive energy. Figure 81 below shows the GIM predicted relationship between T_g and F/P ratio, for when only average hydrogen bonding is considered, and for the situation where every OH group participates in hydrogen bonding. These results have been compared to the data of Manfredi et al [21].

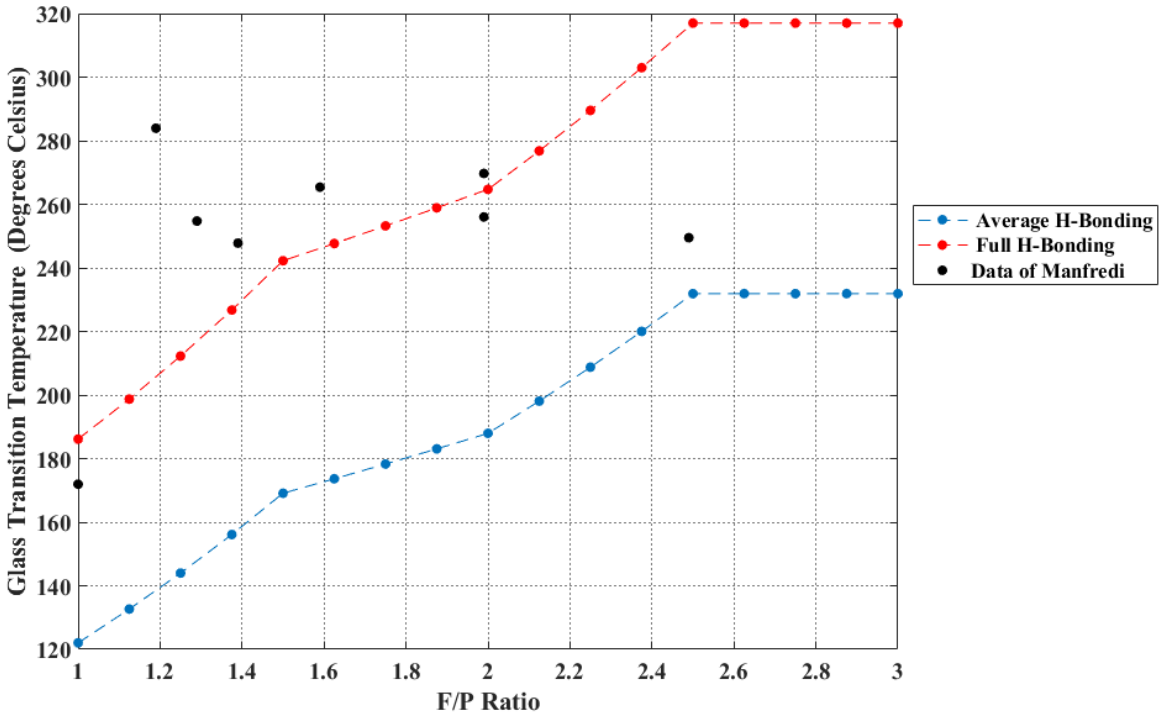

Figure 81: GIM predicted T_g for fully cured phenolic resins, as a function of F/P ratio, for both the average and full hydrogen bonding scenarios. The experimental data of Manfredi et al [21] is also shown to allow comparison.

These results show that the model predictions agree more closely with experiment when it is assumed that all OH groups participate in hydrogen bonding (full H-bonding). The T_g of phenolic resins synthesised from an initial F/P ratio of reactants of 1, predicted by the full hydrogen bonding model, is within 15℃ of that which was observed experimentally by Manfredi et al [21]. The increase in T_g in the range 1 < F/P < 1.5, followed by the temporary reduction in the increase of T_g, with increasing F/P ratio, in the range 1.5 < F/P < 2 also appears to broadly agree with their experimental measurements. If the model predictions are correct, then this implies that the reduced dependence of T_g, on F/P ratio in the range 1.5 < F/P < 2 may have led Manfredi et al [21] to assume that this was indicative of a plateau in T_g, leading them to conclude that, above an F/P ratio of 1.6, no further changes in T_g occur.

3.4. Chapter Conclusions

In the first part of this chapter, GIM was employed to predict the thermo-mechanical properties of the fundamental chemical structures that can exist within phenolic resins. These results were then employed to characterise the effect of methylol groups, and ether bridges, upon the properties of phenolic materials. This modelling showed that the addition of methylol groups to the phenyl rings had a slight positive effect on thermo-mechanical properties; e.g. an increase in T_g and Young's modulus. However, the presence of ether bridges was shown to reduce both the glass transition temperature and Young's modulus. These observations were supported by the findings of Parameswaran et al [108]. The effect of cross-link type: ether or methylene bridge, was also investigated. This indicated that T_g, and Young's modulus, increase slightly when an ether bridge is formed, however a much larger increase is affected through the formation of a methylene bridge.

In the second part of this chapter, the thermo-mechanical properties of phenolic resins were predicted as a function of both cure time and F/P ratio. This analysis showed that the T_g, thermal expansion coefficient, density, and Young's modulus, of fully cured phenolic resins, initially increased with increasing F/P ratio. However, above an F/P ratio of 2.5, no further changes occurred. The model suggested that this was because when the F/P ratio is 2.5, all phenyl rings in the material can form their maximum number of cross links, and hence cross-link saturation is attained. Thus, increasing the F/P ratio further has no impact on the T_g, thermal expansion coefficient, density, or Young's modulus. It does however have an effect on the percentage mass, and volume reduction, of the fully cured resin. This is because, as the F/P ratio is increased above 2.5 more ether groups are introduced into the initial structure of the phenolic resin. These are subsequently lost, through molecular rearrangement, to form methylene bridges with the evolution of formaldehyde which results in the loss of material mass and volume. However, as the final structure of these resins is identical to that obtained from a F/P ratio of 2.5, no improvements in T_g, Young's modulus, thermal expansion coefficient, or density, are observed. Thus, an implication of the model is that F/P ratios in excess of 2.5 should be avoided as they provide no benefit to the thermo-mechanical properties of the fully cured material. They do however increase the proportion of ether groups in partially cured resins, which has an effect on their engineering properties.

In the third part of this chapter, the residual stress within the phenolic resin matrix of a composite, was investigated. The stress was found to be related to the initial F/P ratio employed in the synthesis of the resin. Stress was then plotted against the thermo-mechanical properties of the fully cured resin allowing the 'cost' incurred, in the form of internal stress within the matrix, in obtaining the desired resin properties, to be deduced. This analysis showed that although the T_g, Young's modulus, thermal expansion coefficient, and density, of fully cured phenolic resins

synthesised from F/P ratios in excess of 2.5, are identical to those obtained from an F/P ratio of 2.5, their residual stress is increased. This is because these materials initially contain greater proportions of ether bridges which are subsequently lost through molecular rearrangement with the evolution of formaldehyde. This loss of volume, through the evolution and loss of formaldehyde molecules, increases the shrinkage of the material and thus leads to an increase in the internal stress within the matrix.

Finally, the model predicted T_g of fully cured phenolic resins, as a function of F/P ratio, was compared with the experimental results of Manfredi et al [21]. This analysis showed a large discrepancy between the predictions of the model and experiment which was attributed to the manner in which the hydrogen bonding of the OH groups had been handled within the model. When the mer unit parameters for each species were adjusted to account for full hydrogen bonding, that is to say every OH group was assumed to form one hydrogen bond, then closer agreement between the model and the data of Manfredi et al [21] was obtained. This suggests that in future work, the mer unit parameter values for each phenolic resin species should be adjusted to account for the participation of all OH groups in the hydrogen bonding interaction.

4. Group Interaction Modelling on the Effect of Hygrothermal Conditioning upon the Thermo-mechanical Properties of Phenolic Resins

4.1. Introduction

To model the effect of hygrothermal ageing upon the thermo-mechanical properties of a polymer, the polymer must first be characterised in terms of its chemical structure and diffusive properties. Determination of a polymer's underlying chemical structure allows the GIM parameter values associated with its representative mer unit to be deduced. These parameter values can then be combined with those of the water molecule, on a molar basis, to predict the effect of absorbed moisture upon the engineering properties of the material. The moles of water molecules per mer unit, required for this calculation, are determined from the polymer's diffusive properties.

In the first section of this chapter, DMTA and gravimetric data that have been provided by Alston et al [111, 112], for a hygrothermally conditioned phenolic resin, are presented and analysed. These experimental results are then employed in characterising the phenolic resin in terms of its representative mer unit and diffusion properties (solubility and diffusion coefficient).

In the second section, GIM is extended to allow the volume of the absorbed molecules to be correctly accounted for. The parameters derived in the first section are then employed within this model to predict the thermo-mechanical properties of a phenolic resin as a function of both relative humidity and polymer free volume.

4.2. Methods

4.2.1. Modelling the Thermo-mechanical Properties of Phenolic Resins as a Function of Relative Humidity and Temperature

To predict the effect of absorbed moisture upon the engineering properties of a polymer, the GIM parameter values for the water molecule are combined with those of the material's representative mer unit, on a mole fraction basis [78,110]. Thus, the moles of water molecules per mole of mer units, must first be calculated. The concentration of water molecules at equilibrium, absorbed within a material at a given relative humidity, can be calculated from:

$$C = C_{Max}\, RH_f \tag{209}$$

Where RH_f is the conditioning relative humidity expressed as a fraction of 100% relative humidity, and C and C_{Max} are the concentrations of water molecules at a relative humidity of RH_f, and 100%, respectively both in units of $mol.mm^{-3}$. The moles of mer units per unit volume can be calculated from the GIM predicted polymer density, at the conditioning temperature of interest, and mer unit molar mass:

$$C_{Mer_{(T)}} = \frac{\rho_{R(T)}}{M_{Mer}} \tag{210}$$

Where $C_{Mer_{(T)}}$ is the concentration of mer units at a temperature T, in units of $mol.mm^{-3}$, $\rho_{R(T)}$ is the GIM predicted density of the polymer at a temperature T, in units of $g.cc^{-1}$, and M_{Mer} is the GIM predicted molar mass of the mer unit, in units of $g.mol^{-1}$. The molar ratio of water molecules to mer units can now be calculated from equations (209) and (210):

$$R_{(T)} = \frac{C}{C_{Mer_{(T)}}} = \frac{C_{Max}\, RH_f\, M_{Mer}}{\rho_{R(T)}} \tag{211}$$

Having obtained the molar ratio of water molecules to mer units, the parameter values that are representative of the wet mer unit can now be calculated. By way of example, the degrees of freedom associated with the wet mer unit is calculated as follows:

$$N_{Wet} = N_{Mer} + R_{(T)} N_{Water} \quad (212)$$

Where N_{Wet} and N_{Mer} are the degrees of freedom of the wet and dry mer units respectively and N_{Water} is the degrees of freedom associated with a single water molecule. The other four mer unit parameters are calculated by employing the same methodology.

The cohesive energy, and degrees of freedom, associated with the water molecule have been suggested by Porter et al [110] and have been successfully applied within GIM to predict the effect of absorbed moisture upon the glass transition temperature of spider silks [78]. The GIM equation for the glass transition temperature is given by:

$$T_g = 0.224\theta + 0.0513\frac{E_{coh}}{N} \quad (213)$$

Where T_g is the glass transition temperature in K, E_{coh} and N are the mer unit cohesive energy and degrees of freedom respectively, and θ is the characteristic temperature of polymer chain vibrations parallel to the polymer chain axis, in units of K. Of these three variables, only two are affected by the presence of water, namely E_{coh} and N, because water, existing as free molecules that interact via van der Waals forces and hydrogen bonding, do not possess long chains of covalently bound atoms in which chain vibrations can exist. As a result, the value of θ for the water molecule is 0 K. Thus, knowing only two of the four parameter values associated with the water molecule is sufficient to predict its effect on the glass transition temperature of the polymer. This is also true of the thermal expansion coefficient. However, for the other three thermo-mechanical properties investigated in this work: molar volume, density, and Young's modulus, a further two parameters are required: the molar mass and van der Waals volume of the water molecule.

Although at first glance the inclusion of the van der Waals volume of the water molecule within GIM appears trivial, this work will show that such an approach leads to erroneous predictions that do not agree with experimental observation (see section 4.3.2, page 231).

4.2.2. Calculating the Expected Percentage Change in Material Volume for a Given Quantity of Absorbed Moisture

To assess the validity of the polymer swelling behaviour predicted by GIM, it is first necessary to calculate the expected change in polymer volume as a function of moisture content. The effect of absorbed moisture upon the volume of epoxy resins was described earlier in section 1.4.3, page 19. This behaviour can be summarised as follows. Initially, absorbed water molecules fill the free volume of the polymer and thus there is no associated change in material volume. When the volume of absorbed water is greater than the polymer's free volume, swelling behaviour is observed; more specifically, the increase in material volume is equal to the volume of water absorbed, discounting that which is contained within the free volume of the polymer. It is also observed that the density of water, absorbed within epoxy and phenolic resins, is that of liquid water [4].

If the free volume of a given polymer is zero, then the expected percentage change in the molar volume of the material, at a given temperature and relative humidity, can be calculated as follows. The density of liquid water, at a temperature T, can be expressed as:

$$\rho_{Water_{(T)}} = \frac{m_{Water}}{V_{Water_{(T)}}} \tag{214}$$

Where T is temperature in units of K, $\rho_{Water_{(T)}}$ is the density of liquid water in units of $g.cc^{-1}$, m_{Water} is the mass of absorbed water molecules in units of g, and $V_{Water_{(T)}}$ is the volume of absorbed water molecules in units of cc. The mass of absorbed water molecules can be expressed as a molar quantity by:

$$m_{Water} = 18\, moles_{Water} \tag{215}$$

Where $moles_{Water}$ represents the moles of absorbed water molecules. Substituting equation (215) into equation (214) gives:

$$\rho_{Water_{(T)}} = 18\, \frac{moles_{Water}}{V_{Water_{(T)}}} \tag{216}$$

Rearranging equation (216) in terms of the volume of absorbed water molecules:

$$V_{Water_{(T)}} = 18 \frac{moles_{Water}}{\rho_{Water_{(T)}}} \quad (217)$$

Thus, the volume occupied by one mole of absorbed water molecules can be written as:

$$V_{M_{(T)}} = \frac{18}{\rho_{Water_{(T)}}} \quad (218)$$

Where $V_{M_{(T)}}$ is the molar volume of absorbed water molecules in units of $cc.mol^{-1}$.

The density of liquid water, at a given temperature, can be calculated from empirical property relations. In this chapter the function proposed by Kell [113] will be used. Thus, the expected percentage change in a material's molar volume resulting from the absorption of water, assuming that the material possesses zero free volume, at a given temperature and relative humidity, can be expressed as:

$$aV_{(T)} = V_{(T)} + R_{(T)} V_{M_{(T)}} \quad (219)$$

$$\%_{MV_{(T)}} = 100 \frac{R_{(T)} V_{M_{(T)}}}{V_{(T)}} \quad (220)$$

Where $\%_{MV_{(T)}}$ is the percentage change in the material's molar volume in units of %, and $R_{(T)}$ is the ratio of the moles of water molecules to moles of mer units.

4.2.3. Re-formulation of GIM to Account for the Volume of Absorbed Water Molecules in Terms of the Liquid Volume of Water

Later in this work (see section 4.3.2, page 231) it will be shown that incorporating the van der Waals volume of water molecules directly into GIM leads to thermo-mechanical property predictions that are inconsistent with experimental observations. More specifically, the predicted

change in molar volume, resulting from the absorption of water molecules, is less than expected. To identify the source of these inconsistencies it is necessary to study the underlying model construction of GIM.

In GIM, the van der Waals surface associated with a single mer unit (repeat unit) is simplified to that of a sphere. This sphere has a van der Waals volume equal to the sum of the van der Waals volumes of each of the functional group constituents of the mer unit. However, as absorbed water molecules do not covalently bond to the mer unit, instead interacting via van der Waals forces and hydrogen bonding, it is incorrect to add the van der Waals volume of the water molecule to that of the mer unit.

In Figure 82 below, the average distance between two chemical species, for both the covalent and van der Waals and hydrogen bond interactions, is shown. The term r_0 describes the van der Waals radius of each species.

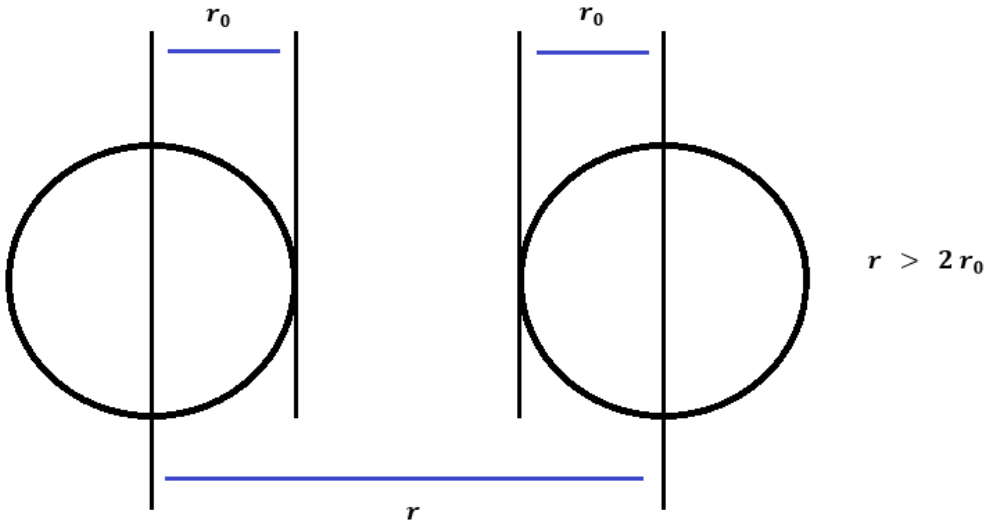

Figure 82: Average separation distance (r) associated with both the covalent, and van der Waals and hydrogen bonding, interactions.

As can been seen, when the two chemical species are covalently bonded it is possible for their van der Waals surfaces to overlap. However, when only van der Waals forces and hydrogen bonds are present, no overlapping of their surfaces is possible. This is because at close separation distances the repulsive forces, between electrons in the outer shells of both species, dominate. Thus, it is not possible for the van der Waals surfaces of the two species to come into contact at

ordinary temperatures and pressures. As a consequence, the volume occupied by the two chemical species is greater than that which is expected when only the van der Waals volume of the two species is considered. The separation distance between the mer unit and the water molecule can be understood in the same terms, as this interaction is mediated by van der Waals and hydrogen bond forces. Thus, the apparent increase in volume that a water molecule brings to the van der Waals volume of the mer unit will be greater than the van der Waals volume of the water molecule. The conclusion of this analysis is that the model structure of GIM does not permit the van der Waals volume of water molecules to be simply combined with the van der Waals volume of the mer unit and thus another approach must be sought.

Having ascertained that the van der Waals volume of water cannot be simply combined with that of the mer unit, a new model is proposed in which the van der Waals volume of water is taken to be zero. In this new model, water molecules do not affect the van der Waals volume of the mer unit; instead, the volume of water molecules is added directly to the polymer's molar volume. This modified form of the molar volume equation (221) is expressed below alongside the standard GIM equation (222) to enable comparison:

$$V_{(T)} = 1.4364\, V_w \left[1 + \int_0^T \alpha_{(T)}\, dT\right] + R_{(T)}\, V_{M\,(T)} \tag{221}$$

$$V_{(T)} = 1.4364\, V_w \left[1 + \int_0^T \alpha_{(T)}\, dT\right] \tag{222}$$

Where T is temperature in units of K, $V_{(T)}$ is the mer unit molar volume in units of $cc.mol^{-1}$, V_w is the van der Waals volume of one mole of mer units in units of $cc.mol^{-1}$, $\alpha_{(T)}$ is the thermal expansion coefficient in units of K^{-1}, $R_{(T)}$ is the molar ratio of water molecules to mer units, and $V_{M\,(T)}$ is the molar volume of liquid water in units of $cc.mol^{-1}$.

The molar volume of liquid water is suitable for extending the molar volume equation because it accounts for the reduced packing efficiency of water molecules, as a result of repulsive forces, at small separation distances. Furthermore, adding the volume that the absorbed water molecules would occupy, in the liquid phase, directly to the volume of the polymer is in agreement with the swelling behaviour observed in hygrothermally conditioned polymers after their free

volume has been filled [4, 50]. In summary, in this modified molar volume equation, absorbed water molecules bring both cohesive energy and degrees of freedom to the mer unit, however they do not affect the mer unit's van der Waals volume. The volume of absorbed water molecules is accounted for by calculating the volume that they would occupy in the liquid phase and then adding this volume directly to the standard mer unit molar volume equation (equation (222)).

A complication arising from this new model formulism is in the amount of thermal energy that absorbed water molecules bring to the polymer network. As water molecules possess their own degrees of freedom, the net effect of water absorption is to increase the degrees of freedom of the polymer system, and hence the thermal energy at a given temperature. This increase in thermal energy effects an increase in the average separation distance of adjacent polymer chains, thus increasing the polymer's volume. However, the thermal energy of absorbed water molecules has already been incorporated into the model through the term that describes their volume: $V_{M(T)}$, the molar volume of liquid water. The thermal energy of water molecules in the liquid phase increases with increasing temperature. This increase in thermal energy allows water molecules to partially overcome the van der Waals and hydrogen bond interactions, and thus the average separation distance between water molecules increases. The net effect is to increase the volume of liquid water, with an associated reduction in its density. The function describing the density of liquid water as a function of temperature, proposed by Kell [113] and employed in calculating $V_{M(T)}$, accounts for this decrease in density with temperature and thus, the increase in water molecule thermal energy with temperature is already incorporated into the term $V_{M(T)}$. This presents a problem as the thermal energy of water molecules is now incorporated into the model through two separate terms: N, and $V_{M(T)}$. As a consequence, the impact of thermal energy on any thermo-mechanical properties that are functions of both of these parameters: N and $V_{M(T)}$, will be overestimated.

In the section that follows this new model formulism is employed to predict the thermo-mechanical properties of phenolic resin, as a function of relative humidity, at 25℃. These results are then compared with those obtained using the standard formalism of GIM (using the van der Waals volume of water) and the validity of the two approaches is discussed.

4.2.4. Accounting for Polymer Free Volume within the New Model Formulism

As stated previously (section 1.4.3, page 19), the swelling behaviour of epoxy resins during hygrothermal conditioning, can be divided into two distinct phases. The first phase is characterised by the diffusion of water molecules into polymer free volume, which has no observable effect on the polymer's total volume. Behaviour transitions to the second phase when the volume of absorbed water molecules is in excess of the free volume of the polymer. In this phase, the total volume of the polymer increases with increasing water content; more specifically the change in the total volume of the polymer is directly proportional to the volume of water absorbed [4, 50]. The impact of free volume upon the swelling behaviour of the polymer, and hence upon other volume dependent thermo-mechanical properties (density and Young's modulus), can be simply incorporated into the framework of the new model. The methodology applied in this model extension is outlined below.

First, the molar volume of the polymer, discounting the effect of absorbed water, is calculated from equation (223):

$$V_{(T)} = 1.4364\, V_w \left[1 + \int_0^T \alpha_{(T)}\, dT\right] \tag{223}$$

Where $V_{(T)}$ is the molar volume of the polymer in units of $cc.mol^{-1}$. The molar free volume can then be calculated from:

$$V_{Free_{(T)}} = v_{Free}\, V_{(T)} \tag{224}$$

Where $V_{Free_{(T)}}$ is the molar free volume in units of $cc.mol^{-1}$, and v_{Free} is the free volume fraction. The volume of water molecules, absorbed within one mole of mer units, is given by:

$$V_{Water_{(T)}} = R_{(T)}\, V_{M_{(T)}} \tag{225}$$

Where $V_{Water_{(T)}}$ is in units of $cc.mol^{-1}$. The concept of the apparent volume of absorbed water is introduced, this being defined as the volume of absorbed water molecules that are not contained within free volume. The methodology for calculating the apparent volume of absorbed water is

outlined below. First, the difference between the volume occupied by water molecules, absorbed within one mole of mer units, and the molar free volume, is calculated:

$$B_{(T)} = V_{Water_{(T)}} - V_{Free_{(T)}} \tag{226}$$

Where $B_{(T)}$ is the molar volume difference in units of $cc.mol^{-1}$. The molar volume difference is then evaluated with respect to the logic below allowing the value of the apparent volume to be deduced.

$$if \quad B_{(T)} \leq 0 \quad then \quad V_{App_{(T)}} = 0$$

$$if \quad B_{(T)} > 0 \quad then \quad V_{App_{(T)}} = B_{(T)}$$

Where $V_{App_{(T)}}$ is the apparent volume of water molecules, absorbed within one mole of mer units, in units of $cc.mol^{-1}$. When $B_{(T)}$ is less than or equal to zero, this implies that the volume of the absorbed water molecules can be accommodated within the free volume of the polymer. Thus, no swelling occurs and the apparent volume of the water molecules $V_{App_{(T)}}$, absorbed within the polymer, is zero. When $B_{(T)}$ is greater than zero this implies that there is an excess volume of water molecules that cannot be accommodated within the free volume of the polymer. As a result, swelling of the polymer volume occurs and this swelling is equal to $B_{(T)}$; the difference between the volume of absorbed water and that which can be accommodated within the free volume of the polymer. Thus, the apparent volume of the absorbed water molecules $V_{App_{(T)}}$ is equal to $B_{(T)}$.

As only water molecules that are not contained within free volume contribute to the swelling behaviour, and therefore impact upon the molar volume, the molar volume equation of the liquid volume model can be rewritten in terms of the apparent volume as:

$$V_{(T)} = 1.4364\, V_w \left[1 + \int_0^T \alpha_{(T)}\, dT\right] + V_{App_{(T)}} \tag{227}$$

Equation (227) is the modified form of the molar volume equation to account for polymer free volume.

4.3. Results and Discussion

4.3.1. Characterisation of a Phenolic Resin's Chemical Structure and Diffusive Properties from Experimental Data

4.3.1.1. Characterisation of a Phenolic Resin's Chemical Structure

In section 3.2.2 (page 155), the initial F/P ratio of reactants was related to the fractional proportion of chemical species initially present within a phenolic resin, before cross-linking between adjacent polymer chains occurs (see Table 46, page 176)). The mer unit parameter values for each structure were then combined on a mole fraction basis, allowing the parameter values of the resin's characteristic mer unit to be deduced and thus allowing the thermo-mechanical properties of the material to be predicted. However, the phenolic resin investigated by Alston et al [111, 112], and modelled in the work that follows, is a commercially available resin and thus the F/P ratio employed in its synthesis has not been made publicly available. As a consequence, it is not possible to establish the initial chemical structural composition of the resin by referring to its initial F/P ratio. Instead, the F/P ratio, and thus the chemical composition, must be inferred by comparing those resin properties that have been determined experimentally to those predicted by GIM, for a wide range of F/P ratios. This will allow the F/P ratio that results in the observed thermo-mechanical properties to be determined. The glass transition temperature is the most suitable property for this purpose as it can be determined with high precision using DMTA and it is also the most well defined property within GIM [71].

Figure 66, presented earlier in this work in section 3.3.2.2.1 (page 183), shows the relationship between resin glass transition temperature, cure time, and the initial F/P ratio of reactants. These predictions indicate that, for a partially cured system, glass transition temperature cannot be related to one unique F/P ratio. Depending on the extent of cure, resins of different ratios can share the same glass transition temperature. It is only in fully cured materials (when no further change in T_g with cure time occurs) that T_g can be related directly to the initial F/P ratio of the reactants. Thus, to apply this methodology to determine the initial chemical structural composition of a phenolic resin, the material must first be fully cured. Figure 83 below shows the DMTA spectrum, provided by Alston et al [111], for a fully cured commercial phenolic resin.

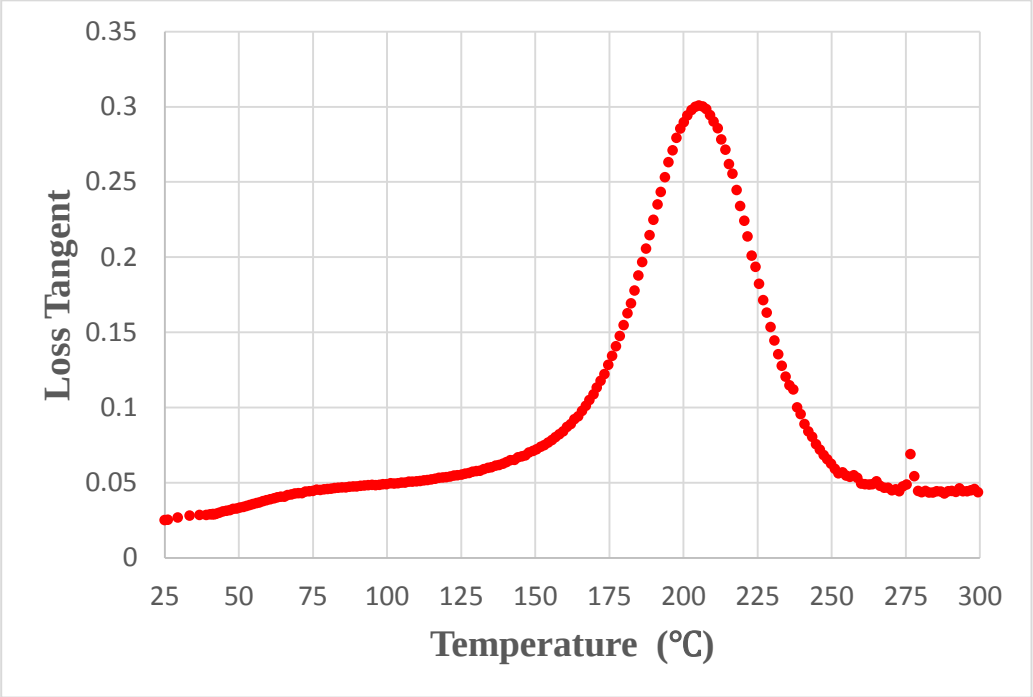

Figure 83: DMTA spectrum, provided by Alston et al [111], for a fully cured commercial phenolic resin.

The parameters describing the form of the loss tangent peak can be obtained by fitting an appropriate function to the experimental data. In chapter two, DMTA was performed on thin films of epoxy resin (thickness ~ 0.075 mm) and the form of the loss tangent curve was found to be best approximated by a Lorentzian function (see Figure 15 on page 79, section 2.3.1). However, the loss tangent curve for the phenolic resin in Figure 83, deviates from this Lorentzian form and appears to be better approximated by a Gaussian function. The probable explanation for this deviation is that non-negligible thermal gradients formed within the sample during the DMTA scan. This is possible as the phenolic resin tested in these DMTA experiments was not in the form of a thin film, instead being a much larger sample with a thickness of ~1.77 mm. As a consequence, various portions of the material undergo their glass transition at different times in the experiment, dependent on their local temperature. Thus, the material will be observed to possess a range of different glass transition temperatures and this has the effect of broadening the loss tangent curve, such that it deviates from the Lorentzian form. Therefore, in the analysis that follows, a Gaussian function will be employed in obtaining the parameters that describe the form of the loss tangent curve. Four parameters are obtained by fitting a Gaussian function to the DMTA spectrum in Figure 83. These are: the glass transition temperature (T_g), the height of the loss tangent peak above the background loss tangent (H) at $T = T_g$, the full width at half maximum (w), and the background loss tangent ($tan\delta_b$). The glass transition temperature is used to determine the initial F/P ratio of the resin whereas the peak height and full width half maximum

describe the shape of the Gaussian curve and are required by GIM when predicting resin thermo-mechanical properties at temperatures near, and above, the glass transition temperature.

Before function fitting is performed, the DMTA spectrum must first be 'cleaned' to remove any artefacts from the data. This ensures that a good fit to the data is obtained, thus providing accurate parameters. The Gaussian function employed in the fitting process has been modified by the inclusion of an offset term to represent the background loss tangent. This offset term is assumed to be independent of temperature. The DMTA spectrum in Figure 83 shows that the background loss tangent is approximately constant, taking a value of ~0.05 in the temperature range 75-300℃. However, below 75℃ the background loss tangent decreases reaching a value of ~0.025 at 25℃.

As the offset term in the modified Gaussian is assumed to be constant, this reduction in background loss tangent at lower temperatures will impact the accuracy of the fit. This can be avoided by considering only the loss tangent data above 75℃. This decision is reasonable as the value of the background loss tangent above, and below, the glass transition temperature, at temperatures in excess of 75℃, is approximately constant. The constancy of this parameter over a large temperature range (~225℃), compared to the small temperature range over which it is observed to decrease (~50℃), suggests that the anomalous behaviour observed below 75℃ is unlikely to be indicative of the actual background loss tangent. As this anomalous behaviour is observed at low temperatures, and thus early in the DMTA experiment, a possible explanation for its cause would be sample movement within the DMTA clamps. After this initial sample movement, no further movement occurred resulting in the background loss tangent assuming a constant value.

A second observable artefact in the DMTA spectrum in Figure 83 is the asymmetrical shape of the loss tangent curve. When the loss tangent is greater than 0.175 the peak is approximately symmetrical, however at lower values a difference between the left and right-hand sides of the peak becomes apparent. The left-hand side of the loss tangent peak appears to exhibit a small 'shoulder' in the temperature range 125℃ to 180℃. Several explanations have been proposed for these types of artefacts including: post-curing, plasticisation by absorbed moisture [57-59], and the existence of multiple phases within the material with each phase possessing its own distinct glass transition temperature [52-54].

In the experiments performed by Alston et al [111] the resin was fully cured by subjecting it to a temperature of 230℃ for 2 hours. It was then cooled, followed by DMTA, to obtain the spectrum shown above in Figure 83. As the material was fully cured prior to starting the DMTA experiment, post-curing processes do not account for the 'shoulder'. However, it is possible that the material absorbed a small quantity of moisture from the atmosphere after cure, during the cool down period before the DMTA experiment was performed. This would reduce the T_g of the resin material located close to the surface of the sample, resulting in a range of glass transition temperatures being measured in the DMTA experiment. These would distort the form of the loss tangent peak, associated with the dry resin, through the introduction of a 'shoulder' in the temperature range where the wet T_g of the resin was approached/exceeded during the DMTA experiment.

The final possible explanation for this artefact is the existence of multiple phases within the resin, each possessing its own unique glass transition temperature. As the cure mechanism of phenolic resins is complicated, involving many different chemical species (see section 1.2.1, page 6, and section 3.2.1, page 149), it is possible that the rate constants governing each type of chemical reaction may vary throughout the reaction mixture during cure, dependent upon the local concentrations of each type of chemical species. This might result in the final state of the fully cured resin possessing regions of different cross-link density, and thus it would be represented by a range of glass transition temperatures leading to distortion of the loss tangent peak observed in the DMTA spectrum.

Although it is not possible to determine the exact cause of the 'shoulder', its overall impact on the form of the loss tangent curve is small which suggests that the Gaussian curve, centred on ~205℃, is representative of the bulk of the resin material. To prevent the presence of the 'shoulder' from affecting the fitting process, loss tangent measurements below 0.175, on the left-hand side of the curve, are omitted from the fitting process (Figure 84).

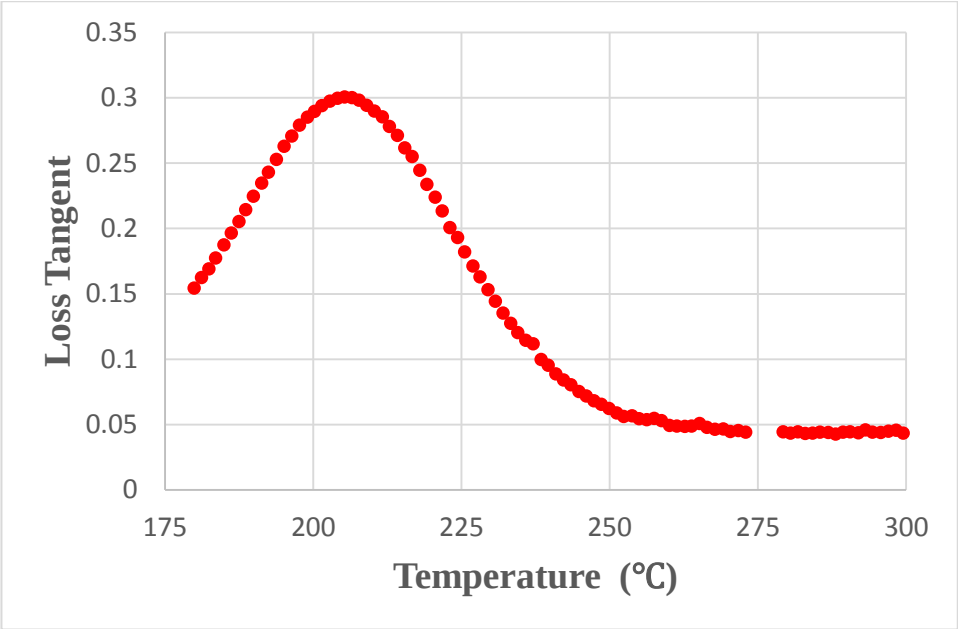

Figure 84: DMTA spectrum, provided by Alston et al [111], showing the omitted loss tangent measurements in the 'shoulder' region.

Figure 85 below shows the result of fitting a Gaussian function, with offset, to the 'cleaned' DMTA spectrum in Figure 84. The four parameters obtained from the fitting process are shown in Table 48.

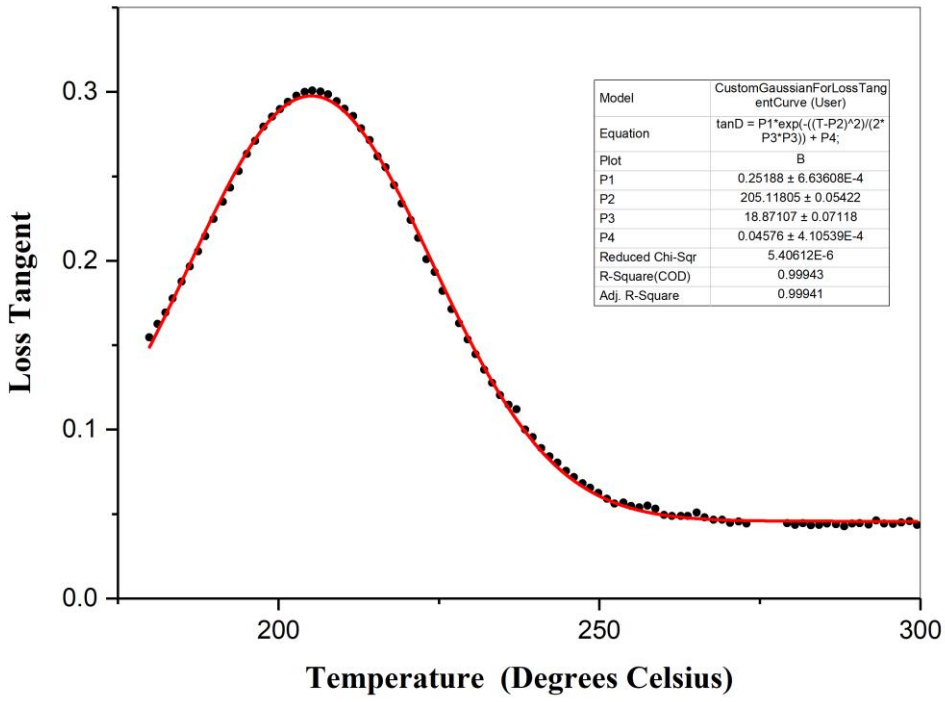

Figure 85: DMTA spectrum, provided by Alston et al [111], with fitted Gaussian function.

T_g (℃)	w (℃)	H	$\tan\delta_b$
205.12	18.87	0.252	0.046

Table 48: Parameters obtained from fitting a Gaussian function to the DMTA spectrum in Figure 84.

The glass transition temperature of the fully cured phenolic resin is obtained from the fitting process and found to be 205.12℃. This T_g can now be compared with those predicted by GIM for fully cured phenolic resins as a function of F/P ratio (Figure 66). The model predictions indicate that an initial F/P ratio of reactants of 2.25 results in a fully cured phenolic resin with a T_g of 210℃. As this prediction is within 5℃ of the experimentally observed value of 205.12℃, it is a good approximation of the initial F/P ratio of the phenolic resin investigated by Alston et al [111, 112], and thus this F/P ratio is employed in the modelling that follows.

As discussed earlier, to determine the characteristic mer unit associated with a phenolic resin, the fractional proportions of its constituent chemical structures must first be deduced. With reference to Table 40, the initial chemical species present within a phenolic resin synthesised from an F/P ratio of 2.25, before cross-linking has occurred, are: C, E, F, G,and H. The mole fraction contribution of each of these species can be obtained by referring to Table 47. Figure 86 below shows the chemical structures associated with each of these five different species.

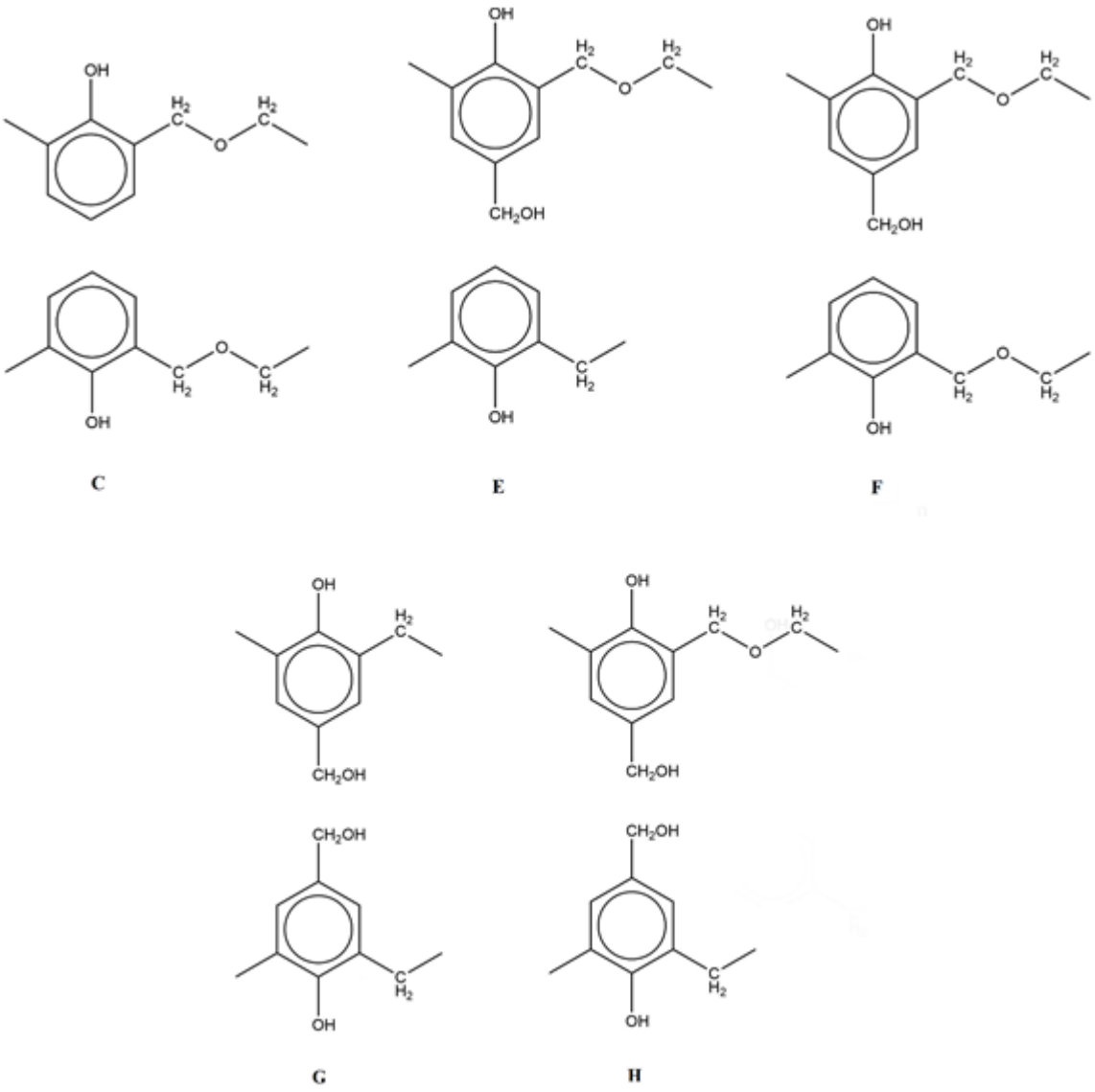

Figure 86: Chemical structures associated with species C, E, F, G, and H.

However, as stated previously, these species are those associated with the resin before cross-linking between adjacent polymer chains has occurred. To determine the fractional proportions of species present in the fully cured material, the fate of each of the initial species, throughout the cure process, must be deduced. Species C is composed of two adjacent polymer chains that are unable to undergo cross-linking due to the absence of methylol groups on either phenyl ring. Both polymer chains possess an ether bridge in their main chain backbone that will undergo molecular rearrangement to form a methylene bridge in the fully cured system. Thus, species C is transformed entirely into species A. All of the other species: E, F, G, and H, undergo cross-linking reactions as they possess methylol groups on their phenyl rings. Some of these species contain, or form through cross-linking reactions, ether bridges which will undergo molecular rearrangement to form methylene bridges, as occurs in species C. When all possible cure reactions

have occurred, these five species are all transformed entirely into species J; two adjacent polymer chains cross-linked via a methylene bridge. Thus, the chemical structure of the fully cured phenolic resin studied in this work is represented by two chemical species: A and J, in the mole fraction proportions shown below in Table 49.

f_A	f_J
$1/6$	$5/6$

Table 49: Mole fraction proportions of species A and J.

Combining the mer unit parameter values associated with each of these two chemical species, on a mole fraction basis, the parameter values for the characteristic mer unit of the fully cured phenolic resin are obtained. Table 50 below shows the mer unit parameter values pertaining to each individual chemical species, and those for the fully cured phenolic resin.

Type	E_{coh} $(J.mol^{-1})$	N (mer^{-1})	V_w $(cc.mol^{-1})$	M $(g.mol^{-1})$	N_c (mer^{-1})	**Atoms** (mer^{-1})
A	42500	8	61.53	106	12	14
J	44750	6	66.645	112	12	14.5
Combined	44375	6.333	65.793	111	12	14.417

Table 50: Mer unit parameter values for species A, J, and for the fully cured phenolic resin.

4.3.1.2. Characterisation of a Phenolic Resin's Diffusive Properties

The moisture absorption/desorption behaviour of phenolic resins, or more generally most polymers, is dependent upon two parameters: the diffusion coefficient and the solubility of water within the material. The rate at which moisture is absorbed/desorbed into/out of the polymer is governed by the diffusion coefficient, whereas the equilibrium moisture content is dependent upon the solubility of water within the material. Both parameters are material specific and are functions of the conditioning temperature. They are determined from fitting an appropriate function to the uptake/$\sqrt{t}$ relationship obtained from conditioning the material, at a fixed temperature and relative humidity, until it attains its equilibrium moisture content. In the work

that follows, the gravimetric data provided by Alston et al [112] has been employed to characterise the diffusive properties of the phenolic resin introduced in the previous section.

4.3.1.2.1. Absorption/Desorption of a Phenolic Resin Exposed to a Cyclic Hygrothermal Conditioning Environment

Figure 87 below shows the gravimetric data provided by Alston et al [112]. This shows the percentage change in mass of six phenolic resin samples subjected to a cyclic conditioning regime at 70℃, whereby they were alternately switched between environments at low (~0%) and high (~85%) relative humidity.

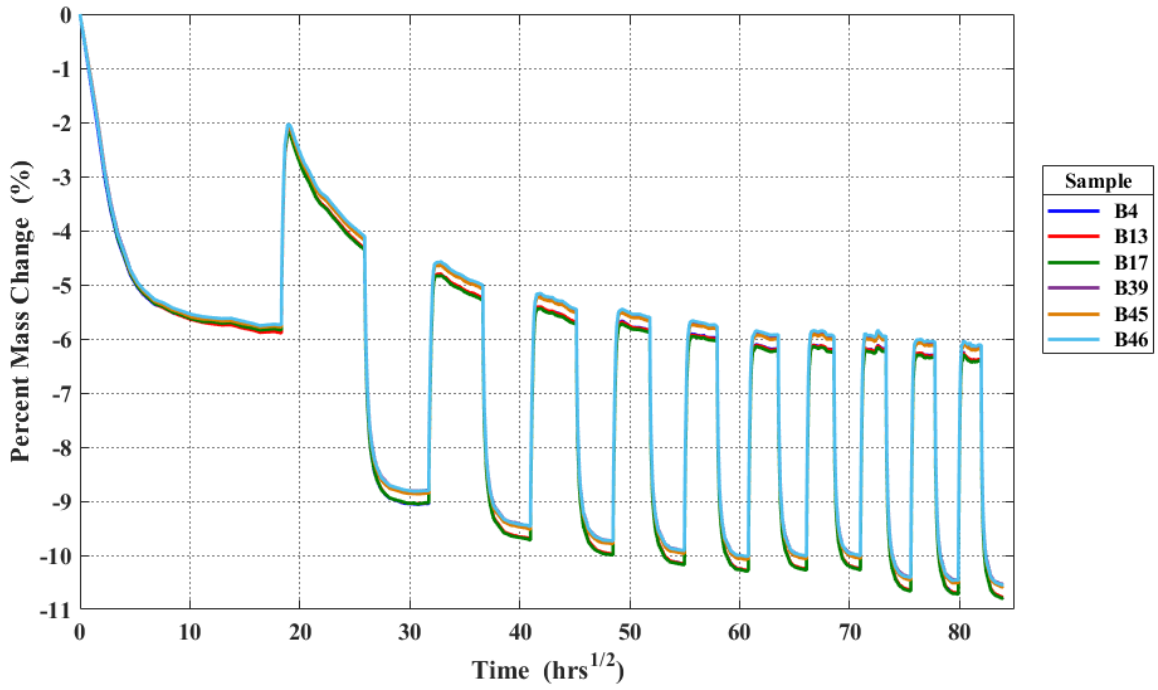

Figure 87: Gravimetric measurements provided by Alston et al [112] showing the percentage change in mass, as a function of time, for six phenolic resin samples exposed to a cyclic conditioning environment.

The experiment was begun by conditioning initially at 0% relative humidity, for a fixed time period, followed by conditioning at 85% relative humidity for an identical period of time. Thereafter, the samples were cycled between the two environments. The phenolic resin samples were not vacuum dried prior to conditioning, thus they are representative of the state of the material just after cure. As discussed in section 1.2.1 (page 6), the cure of phenolic resins occurs through a series of condensation reactions. Thus, a large quantity of water and formaldehyde is evolved during cure. Ordinarily, at the high temperatures experienced during cure, these molecules evaporate and as a result are not present in the cured resin. However, the intention of the work performed by Alston et al [114] was to understand the effect of these reaction products

on the thermo-mechanical properties of phenolic resins under conditions in which they are unable to evaporate during cure, thus becoming trapped in the cured material.

To retain the bulk of these cure products, they cured the phenolic resin in long glass tubes. Only the surface of the resin at the top of the tube is exposed to the atmosphere and thus this is the only surface through which cure products, water and formaldehyde, can be lost. If the surface of the resin exposed to the atmosphere is small, with respect to the total volume of resin within the tube, then the cured phenolic resin will retain a large proportion of its cure products. As a consequence, when these samples are exposed to an environment at 70℃ and 0% relative humidity, at the start of the cyclic conditioning experiment, these cure products will begin to diffuse to the resin surface and evaporate, leading to a net loss in resin mass. Figure 87 indicates that, after a time period of ~18 $hrs^{\frac{1}{2}}$, this mass loss is approaching a plateau indicating that these cure products account for ~5.8% w/w of the initial mass of the phenolic resin.

4.3.1.2.2. Evaporation of Residual IPA Solvent in Plasticising Conditioning Environments

An unusual phenomenon is observed in the cyclic conditioning experiment when samples are transferred from the dry (0%) to the wet (85%) relative humidity environments. Initially these samples gain mass, which is expected, as phenolic materials are susceptible to absorbing moisture from their surrounding atmosphere (see section 1.3, page 9). However, after this initial increase in mass, the samples begin to lose mass. This mass loss is unexpected and occurs only when the samples are exposed to the wet conditioning environment. This behaviour continues throughout the cyclic conditioning experiment but becomes less pronounced, appearing to approach a plateau after a conditioning time of ~80 $hrs^{\frac{1}{2}}$. After this plateau is observed, the mass of the samples in the 0% relative humidity environment, in other words the mass of the dry samples, is ~10.8% w/w less than that prior to the start of the conditioning experiment. It was determined previously that cure products account for ~5.8% w/w of the initial mass of the phenolic resin samples. This implies that there is a further ~5% w/w mass loss that cannot be accounted for by the loss of cure products. Investigations by Alston et al [114] have determined that this extra mass loss of ~5% w/w results from the evaporation of solvent, namely isopropyl alcohol (IPA), that remains trapped within the resin after cure.

The phenolic resin under investigation in this work is a commercial resin that is supplied in a beta staged state, in other words it is partially cured during the manufacturing process. As a consequence, the resin possesses a high viscosity. High viscosity resins have poor handling properties and are unsuitable for composite applications as their fibre wetting capability is

impaired [115]. To resolve these complications solvent, in the form of IPA, is added to the beta staged phenolic resin. This has the effect of lowering the resin's viscosity sufficiently such that its handling properties are no longer impaired. Ordinarily, this solvent evaporates during cure, however as the phenolic resin in this work was cured in long glass tubes this process is inhibited and thus the resulting cured resin contains a non-negligible quantity of solvent.

When these phenolic samples are exposed to a dry atmosphere, at 70℃ and 0% relative humidity, no resulting mass loss from solvent evaporation is observed. This suggests that when the resin is in its glassy state the IPA molecules are constrained by the morphology of the polymer network and thus the diffusion of these molecules is inhibited. When the same samples are exposed to a wet environment, at 70℃ and 85% relative humidity, they initially gain mass as expected. However, upon attaining equilibrium with their conditioning environment, characterised by a plateau in their mass change with respect to time, a gradual loss in mass is observed which suggests that the residual IPA solvent is evaporating.

Moisture induced loss of solvent can be explained by the plasticisation of the polymer network by water molecules. It is well documented throughout the literature that generally, the impact of absorbed moisture upon the engineering properties of epoxy, and phenolic, resins is a reduction in a range of thermal and mechanical properties; for example, both the engineering moduli [2, 46, 116] and glass transition temperature are reduced [3, 5, 48, 49]. It is hypothesised that these effects result from the disruption of the van der Waals and hydrogen bond interactions between polymer chains. The ability of water to disrupt these interactions is termed plasticisation [3]. As plasticisation increases the average separation distance between adjacent polymer chains, the morphological constraints on absorbed IPA molecules are relaxed and thus they become able to diffuse. Thus, by absorbing moisture from their environment the phenolic materials become plasticised allowing the evaporation of IPA solvent, and the associated mass loss, to occur. This explanation for the anomalous mass loss behaviour observed in wet environments is supported by FTIR measurements, performed by Alston et al [114], on the volatile products that are evolved from the phenolic material upon heating. This analysis indicates that the samples retain a substantial quantity of IPA solvent after cure and thus this supports the hypothesis that evaporation of residual solvent accounts for the ~5 % w/w mass loss observed during the course of the cyclic conditioning experiment.

4.3.1.2.3. Absorption Behaviour of Cure Product and Solvent Free Phenolic Resin

The two effects discussed previously; evaporation of cure products and residual solvent, affect the form of the phenolic resins mass change/$\sqrt{t}$ behaviour. To obtain the diffusion coefficient and equilibrium moisture content, characteristic of the resin, these two evaporation processes must be removed from the experimental data so that only the effect of the absorption/desorption of atmospheric moisture, on sample mass, remains. This can be achieved by exposing the resin samples to a wet environment for a time period sufficient for the complete evaporation of cure products and residual IPA solvent. As discussed previously in section 4.3.1.2.2 (page 224), this criterion is achieved in the cyclic conditioning experiment after a time period of ~80 $hrs^{\frac{1}{2}}$ where the mass loss occurring in samples in the wet environment, after equilibrium is achieved, is negligible. The mass of these samples in the dry state, after ~80 $hrs^{\frac{1}{2}}$ conditioning, is thus taken to be representative of the initial dry mass of the material. At $t =$ 80 $hrs^{\frac{1}{2}}$ the samples are transferred from the dry to the wet environment. The percentage change in mass, resulting from the absorption of atmospheric moisture, is now recalculated using the new initial mass values (free of water and formaldehyde, formed during the cure of the phenolic resin, and residual IPA solvent). These results are displayed below in Figure 88.

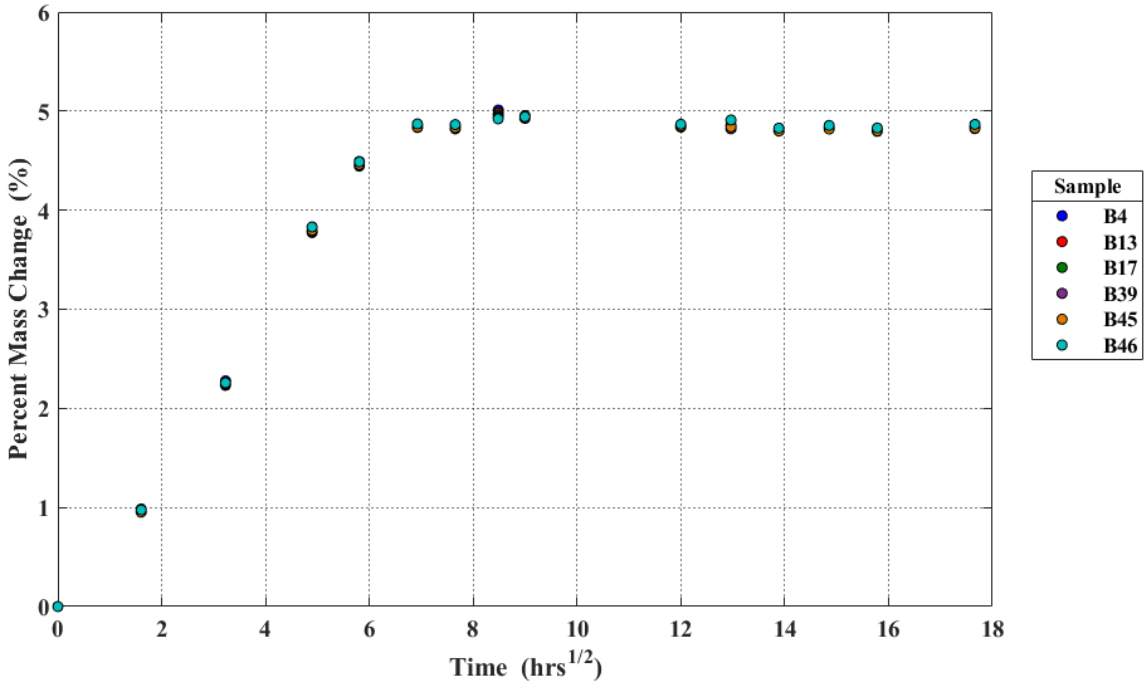

Figure 88: Percentage change in sample mass, as a function of time, for initially dry phenolic resin samples exposed to a conditioning environment at 70°C and 85% relative humidity. Gravimetric data provided by Alston et al [112].

All six samples attain an initial equilibrium moisture content of ~5% w/w. Over extended conditioning times a small amount of mass loss is observable, most likely as a result of the evaporation of residual IPA. However, this quantity is negligible (~0.1% w/w) and thus all data

points are assumed to be representative of the moisture absorption process. The diffusion coefficient and equilibrium moisture content of each sample can now be obtained by fitting an appropriate function to their mass change/$\sqrt{t}$ relationships. As the behaviour of each sample is Fickian, and assuming that diffusion only occurs in one dimension (through the sample thickness, diffusion through sample edges being neglected), a function of the form shown below in equation (228) is suitable for this purpose.

$$M_t = M_{eq}\left(1 - e^{-7.3\left(\frac{Dt}{h^2}\right)^{\frac{3}{4}}}\right) \quad (228)$$

Where M_t and M_{eq} are the percentage, by mass, of absorbed water at conditioning time t and at equilibrium respectively, D is the diffusion coefficient in units of $mm^2.min^{-1}$, and h is the sample thickness in units of mm. The sample thickness is known, the diffusion coefficient and equilibrium moisture content are unknown parameters to be obtained from the fitting process. However, before the fitting process can be performed the effect of the evaporation of cure products and residual IPA solvent, on the dimensions of each sample, must be considered.

4.3.1.2.4. Correcting Sample Dimensions to Account for Shrinkage Resulting from the Loss of Cure Products and Solvent

The samples employed in the cyclic conditioning experiments are disks of approximate diameter (d) and thickness (h) of ~20 mm and ~1 mm respectively. However, these initial sample dimensions were determined just after cure when the material contains ~10.8% w/w, by mass, of cure products and residual solvent. The evaporation of these components has the potential to affect sample volume, and thus sample dimensions, as it is well documented in the literature that the presence of absorbed moisture in polymers can result in swelling of the material [4, 50]. The size of formaldehyde and IPA molecules, in terms of their van der Waals volume, is comparable to that of the water molecule and thus it can be hypothesised that the presence of these chemicals will induce a similar swelling effect. As the gravimetric data employed in the fitting process (Figure 88) is for samples that have lost all of their cure products and residual solvent, it is necessary to re-measure their dimensions. However, at the time this analysis was performed, this data was unavailable.

In this chapter, the volume of the resin after complete removal of cure products (water and formaldehyde) and residual IPA solvent, will be referred to as the actual volume. This will be estimated from the measured initial sample masses and the GIM predicted density, at 25℃,

using the mer unit parameter values determined in the previous section for the dry fully cured phenolic resin. (see Table 50 on page 222section 4.3.1.1).

The GIM predicted density of the dry phenolic resin, using the mer unit parameters from Table 50, is 0.0011 $g.mm^{-3}$ at 25℃. Using this value in equation (229) below, the actual volume can be expressed as:

$$\rho_{R25} = \frac{m_R}{V_{act}} \tag{229}$$

$$V_{act} = \frac{m_R}{\rho_{R25}} \tag{230}$$

Where ρ_{R25} is the GIM predicted density of the dry phenolic resin, at 25℃, in $g.mm^{-3}$, m_R is the dry phenolic resin mass in g, and V_{act} is the actual volume of the sample in mm^3. Thus, the percentage change in sample volume arising from the presence of cure products and solvent is given by:

$$a = \frac{V_{cs}}{V_{act}} \tag{231}$$

Where a is the percentage change in volume caused by the presence of absorbed cure products and residual IPA solvent, expressed as a top-heavy fraction, and V_{cs} is the initial sample volume when both cure product and solvent are present, in units of mm^3. The percentage change in length in a single dimension is therefore:

$$b = \sqrt[3]{a} \tag{232}$$

Where b is the percentage change in length expressed as a top-heavy fraction.

Having obtained the percentage change in length, it is now possible to calculate the actual thickness and diameter of each sample when no residual cure products, or solvent, are present.

The initial thickness and diameter of each sample can be expressed in terms of their actual values as:

$$bh_{act} = h_{cs} \tag{233}$$

$$bd_{act} = d_{cs} \tag{234}$$

Where h_{act} and d_{act} are the actual thickness and diameter, and h_{cs} and d_{cs} are the initial thickness and diameter when cure products and solvent are still present. Rearranging:

$$h_{act} = \frac{h_{cs}}{b} \tag{235}$$

$$d_{act} = \frac{d_{cs}}{b} \tag{236}$$

Table 51 shows the percentage change in volume (from equation (231)) and actual dimensions (from equations (235) and (236)) of each sample.

Sample	B4	B13	B17	B39	B45	B46
d_{cs} (mm)	22.98	22.97	23.03	23.01	22.98	22.95
h_{cs} (mm)	1.32	1.31	1.30	1.30	1.31	1.30
m_R (g)	0.5833	0.5888	0.5906	0.5915	0.5835	0.5825
ρ_{R25} $(g.mm^{-3})$	1.13E-03	1.13E-03	1.13E-03	1.13E-03	1.13E-03	1.13E-03
V_{cs} (mm^3)	546.11	543.68	543.18	539.88	544.16	539.03
V_{act} (mm^3)	514.95	519.77	521.35	522.19	515.06	514.19
a	0.981	0.985	0.986	0.989	0.982	0.984
d_{act} (mm)	22.54	22.63	22.71	22.75	22.56	22.60
h_{act} (mm)	1.29	1.29	1.29	1.28	1.29	1.28
$l_{act} = w_{act}$ (mm)	15.94	16.00	16.06	16.09	15.95	15.98

Table 51: Percentage change in volume, and actual dimensions of each sample.

4.3.1.2.5. Function Fitting to the Phenolic Resin Conditioning Data to Obtain the Observed Diffusion Coefficient and Equilibrium Moisture Content

The actual sample thickness can now be used in equation (228) allowing the fitting process to be performed. The diffusion coefficient and equilibrium moisture content of each sample, obtained from the fitting process, are shown below in Table 52.

Sample	B4	B13	B17	B39	B45	B46
M_{eq} (%)	4.97	4.96	4.94	4.94	4.94	4.97
D_{obs} $(mm^2.min^{-1})$	1.37E-04	1.34E-04	1.33E-04	1.34E-04	1.35E-04	1.34E-04

Table 52: Equilibrium moisture content, in terms of the percentage change in mass, and observed diffusion coefficient for each sample obtained from the function fitting process.

Finally, the equation used in the fitting process (equation (228)) assumes that diffusion occurs in only one dimension. As diffusion also occurs through the sides of each sample, the observed diffusion coefficient (D_{obs}), obtained from fitting equation (228) to the gravimetric data in Figure 88, will overestimate the value of the actual diffusion coefficient (D_{act}). The actual diffusion coefficient can be obtained by applying the edge correction formula, introduced previously in the form of equation (21) (page 33 in section 1.8.1), and these corrected values are shown below in Table 53.

Sample	B4	B13	B17	B39	B45	B46
D_{act} $(mm^2.min^{-1})$	1.02E-04	9.95E-05	9.90E-05	9.93E-05	9.99E-05	9.91E-05

Table 53: Actual sample diffusion coefficients obtained by correcting for 'edge effects'.

The average value of the percentage mass change at equilibrium, and actual diffusion coefficient, are shown below in Table 54 and these values are employed in the modelling work that follows.

Average M_{eq} (%)	Average D_{act} $(mm^2.min^{-1})$
4.95	9.97E-05

Table 54: Average value of the percentage mass change, at equilibrium, and actual diffusion coefficient.

4.3.2. GIM Predicted Effect of Hygrothermal Conditioning upon the Thermo-mechanical Properties of Phenolic Resin (Model 1 - Using the van der Waals Volume of Water)

Earlier in this work (section 4.3.1, page 215) a phenolic resin was characterised in terms of both its representative mer unit and its diffusive properties: diffusion coefficient, and equilibrium moisture content as a function of relative humidity. This information can be now employed within Group Interaction Modelling to allow the prediction of the phenolic resin's thermo-mechanical properties as a function of its conditioning environment.

The predictions in the work that follows are for materials that have attained equilibrium with their conditioning environment, that is to say the concentration of absorbed water molecules throughout the material's geometry is uniform; no concentration gradients being present. The parameter values of the dry phenolic resin mer unit are those that were determined earlier in this work (see Table 50 on page 222, section 4.3.1). The GIM parameter values for the cohesive energy and degrees of freedom of the water molecule, have been suggested by Porter [110] and are given below in Table 55. The van der Waals volume of the water molecule given by Franks [117], is also shown in the same table. All model predictions have been made for a conditioning temperature of 25℃.

E_{coh} $(J.mol^{-1})$ **Cohesive Energy**	N $(molecule^{-1})$ **Degrees of Freedom**	V_w $(cc.mol^{-1})$ **Van der Waals Volume**	M $(g.mol^{-1})$ **Molar Mass**
16300	6	6.92	18

Table 55: GIM parameter values for the water molecule. The cohesive energy and degrees of freedom were suggested by Porter [110]. The van der Waals volume is that given by Franks [117].

4.3.2.1. Effect of Relative Humidity upon the Glass Transition Temperature of Phenolic Resin at 25℃

The GIM predicted effect of relative humidity upon the glass transition temperature of phenolic resin, at 25℃, is shown below in Figure 89.

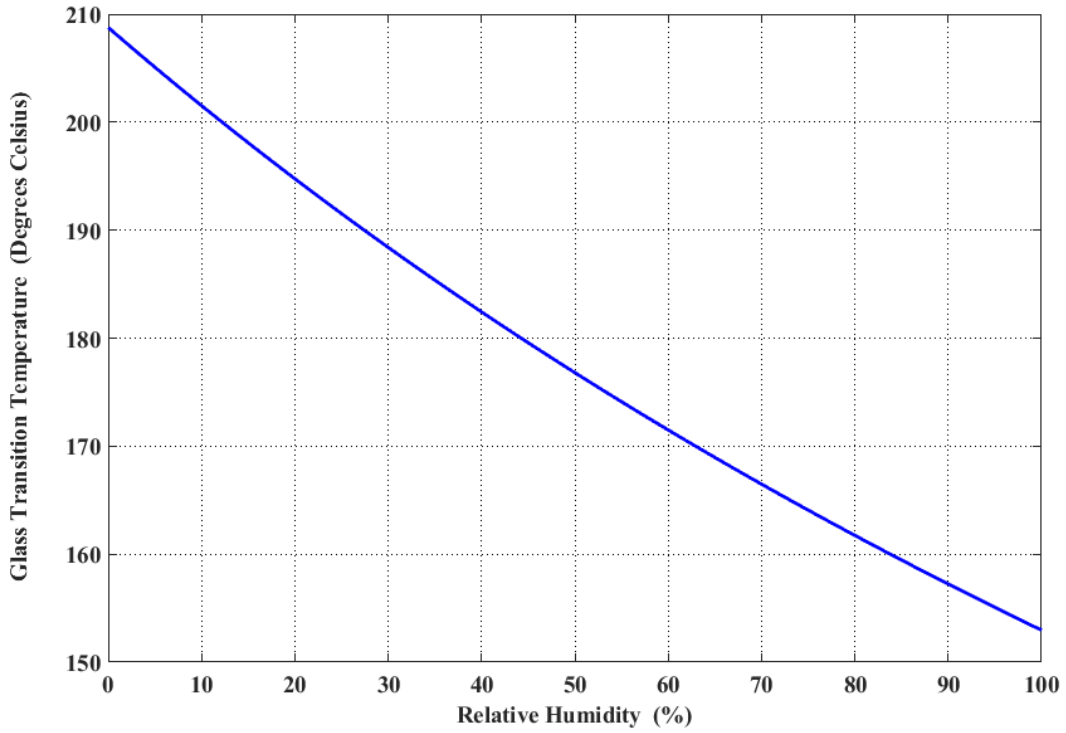

Figure 89: Glass transition temperature of phenolic resin, as a function of relative humidity, at 25℃.

The predictions of the model indicate that the glass transition temperature of the resin is inversely proportional to the conditioning relative humidity. This is in agreement with the glass transition behaviour reported in the literature for epoxy and phenolic resins exposed to hygrothermal environments [3, 5, 48, 49]. The glass transition temperature falls by ~55℃ from an initial dry value of ~208℃, at 0% relative humidity, to a final wet value of ~153℃ at 100% relative humidity. The fall in glass transition temperature, with increasing water molecule concentration, can be explained within the context of GIM as follows.

The glass transition of a polymer can be described as the point at which the separation distance, of adjacent polymer chains, becomes sufficient to allow new polymer chain vibrational modes to become active [71]. The energy required to reach this separation distance is dependent upon the strength of the van der Waals, and hydrogen bond, forces between adjacent polymer chains, that is to say, it is a function of the cohesive energy parameter E_{coh}. As water molecules

possess cohesive energy and degrees of freedom their addition to the phenolic resin increases both the cohesive energy, and degrees of freedom, of the characteristic mer unit. The cohesive energy of the mer unit increases, thus increasing the energy required to reach the chain separation distance at which the glass transition occurs. However, the degrees of freedom also increase, and thus, at a given temperature, the system will possess greater thermal energy. This allows polymer chains to reach the separation distance, associated with the glass transition, at lower temperatures and thus will act to reduce the glass transition temperature.

The overall effect on the glass transition temperature depends upon the ratio of the cohesive energy to the degrees of freedom. In the phenolic resin under investigation, the net effect of absorbed water molecules is to reduce the temperature at which the thermal energy of the system becomes sufficient to allow polymer chains to achieve the separation distance at which the glass transition occurs. Thus, moisture absorption causes a reduction in the glass transition temperature.

4.3.2.2. Effect of Relative Humidity upon the Thermal Expansion Coefficient of Phenolic Resin at 25℃

The GIM predicted effect of relative humidity upon the thermal expansion coefficient of phenolic resin, at 25℃, is shown below in Figure 90.

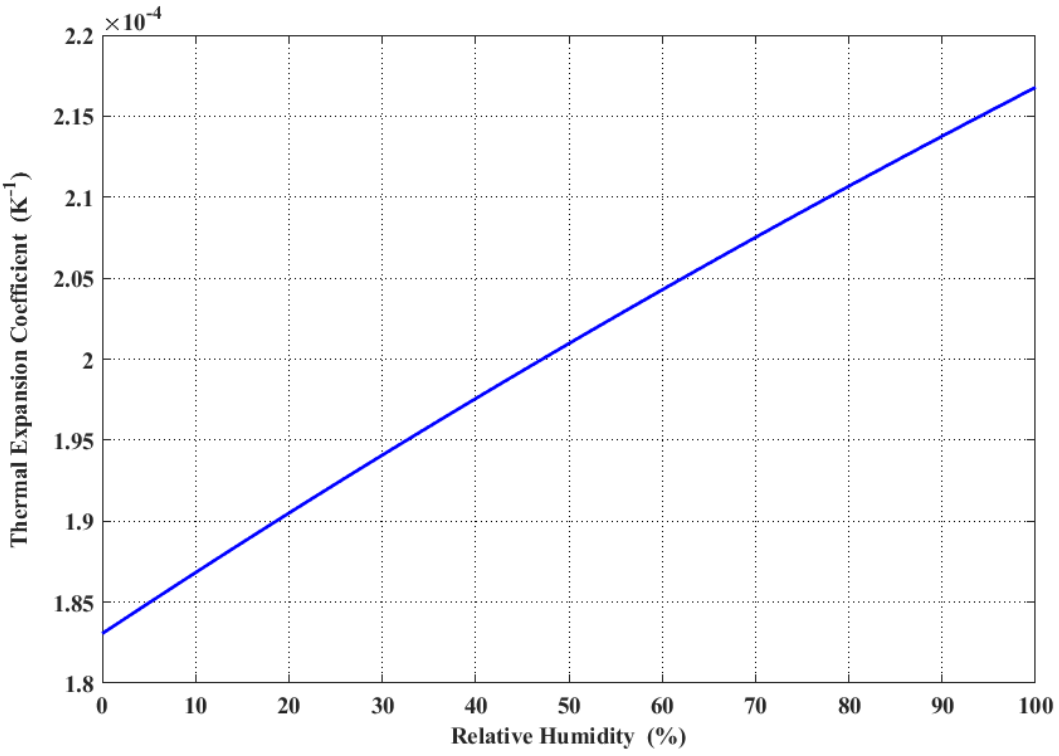

Figure 90: Thermal expansion coefficient of phenolic resin, as a function of relative humidity, at 25℃.

Model predictions suggest that the thermal expansion coefficient is a positive function of relative humidity. This is in agreement with the work of Adamson [4] who observed that the thermal expansion coefficient of an epoxy resin, increased by a factor of two after it was conditioned in liquid water for a time period sufficient for the material to attain equilibrium with its conditioning environment. The model predicts that the thermal expansion coefficient will increase by ~18%, from an initial value of ~$1.83 \times 10^{-4}\ K^{-1}$ at 0% relative humidity, to a final value of ~$2.16 \times 10^{-4}\ K^{-1}$ at 100% relative humidity.

The GIM equation for the thermal expansion coefficient, equation (15) (page 30, section 1.7.4), shows that this property is proportional to the ratio of the molar heat capacity to the cohesive energy. As discussed previously in section 4.3.2.1 (page 232), the addition of water molecules to the phenolic resin increases both the cohesive energy and degrees of freedom of the system. However, the increase in degrees of freedom is dominant and thus the net effect is to increase the molar heat capacity/cohesive energy ratio, leading to an increase in the thermal expansion coefficient. Within the context of GIM, an increase in molar heat capacity causes the thermal energy the system gains, in a temperature increment ΔT, to increase. Thus, the change in polymer chain separation distance, and hence polymer volume, occurring within this temperature increment also increases. This is reflected in an increase in the value of the thermal expansion coefficient.

The GIM equations for the glass transition temperature and thermal expansion coefficient are not functions of the van der Waals volume parameter (V_w). As a consequence, the difficulties that arise from the definition of the absorbed volume of water, in terms of its van der Waals volume, do not affect these property predictions. However, the van der Waals volume parameter does feature in the GIM equations for the molar volume, density, and Young's modulus. As a result, these property predictions will not necessarily agree with experimental observation; this is very apparent for the behaviour of the Young's modulus, as will be seen. As these results are erroneous, a detailed explanation of their predicted behaviour within the context of GIM is not appropriate.

4.3.2.3. Effect of Relative Humidity upon the Molar Volume of Phenolic Resin at 25℃

The GIM predicted effect of relative humidity on the molar volume of phenolic resin, at 25℃, is shown below in Figure 91.

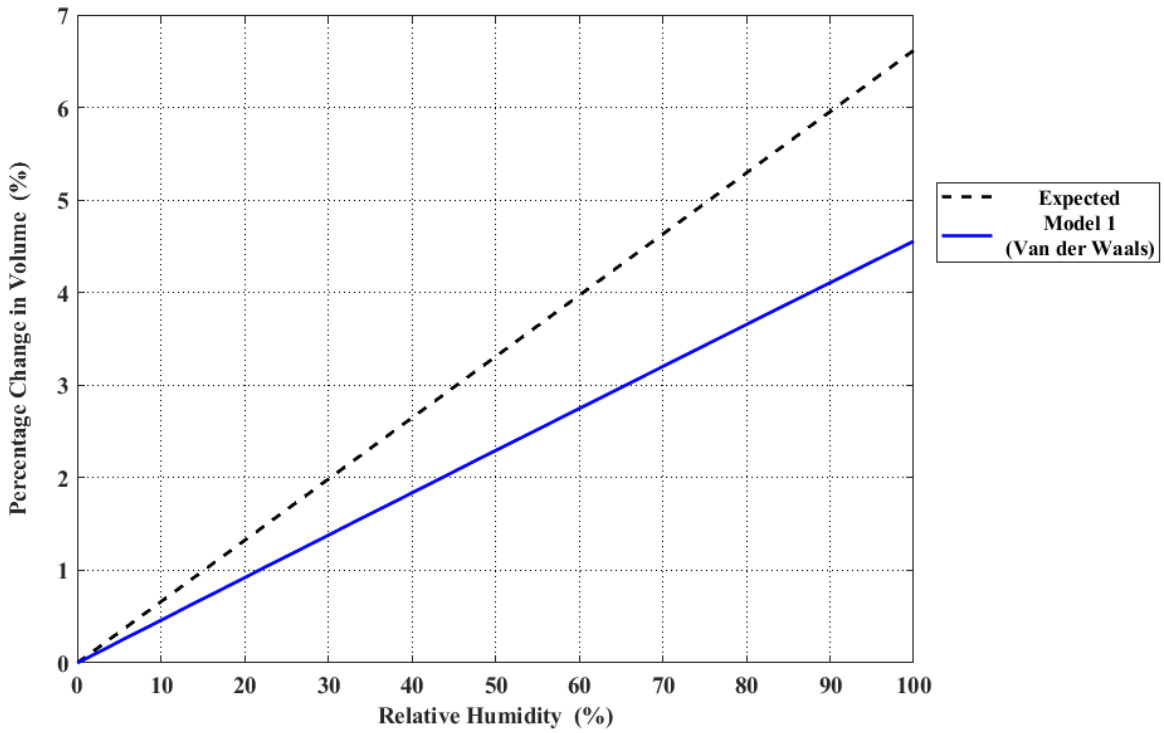

Figure 91: Molar volume of phenolic resin, as a function of relative humidity, at 25℃.

The expected percentage change in molar volume as a function of relative humidity, for a polymer with zero free volume, has been calculated and plotted on the same graph to allow model predictions to be compared against the expected behaviour. The expected percentage change in molar volume increases with increasing relative humidity, with the relationship being described by a straight line of constant gradient. The predicted percentage change in molar volume exhibits a similar behaviour, however, the gradient of the line describing this relationship is less than that which is expected. As a consequence, with increasing relative humidity, model predictions diverge from the expected behaviour. At 100% relative humidity, the expected percentage change in molar volume is ~6.5%, whereas only ~4.5% is predicted by the model.

The GIM equation that is employed in calculating a polymer's molar volume (equation (223)) is a function of both the van der Waals volume parameter and the thermal expansion coefficient. The thermal expansion coefficient is a function of the molar heat capacity (this being

a function of the degrees of freedom and the characteristic temperature of polymer chain vibrations parallel to the polymer chain axis) and cohesive energy. The values of the cohesive energy and degrees of freedom for the water molecule that have been employed in this work have been successfully applied to predicting the effect of absorbed moisture upon the glass transition temperature of spider silks [78]. Thus, it is unlikely that these parameters are responsible for the observed discrepancy between the expected and predicted behaviour. The characteristic temperature of polymer chain vibrations parallel to the polymer chain axis can also be discounted because water molecules do not covalently bond to the polymer network, interacting only via van der Waals forces and hydrogen bonding, and as a result do not contribute to this parameter. As work in the existing literature supports the value of the cohesive energy and degrees of freedom that have been employed in this model for the water molecule, and the impact of water molecules upon the characteristic temperature (θ) is zero, only the van der Waals volume parameter can account for the observed discrepancies between the predicted and expected behaviour. Referring to the equation for polymer molar volume (equation (223)) suggests that the van der Waals volume of the water molecule, taken from Table 55, is too small. As the van der Waals volume of the water molecule is a fixed quantity, being independent of the molecule's surrounding environment, this indicates that the volume of water absorbed within a polymer cannot be simply accounted for by its van der Waals volume. This inconsistency can only be resolved by reformulating GIM in terms of the liquid volume of water, as was outlined previously in section 4.2.3 (page 208).

4.3.2.4. Effect of Relative Humidity upon the Density of Phenolic Resin at 25℃

The GIM predicted effect of relative humidity upon the density of phenolic resin, at 25℃, is shown below in Figure 92.

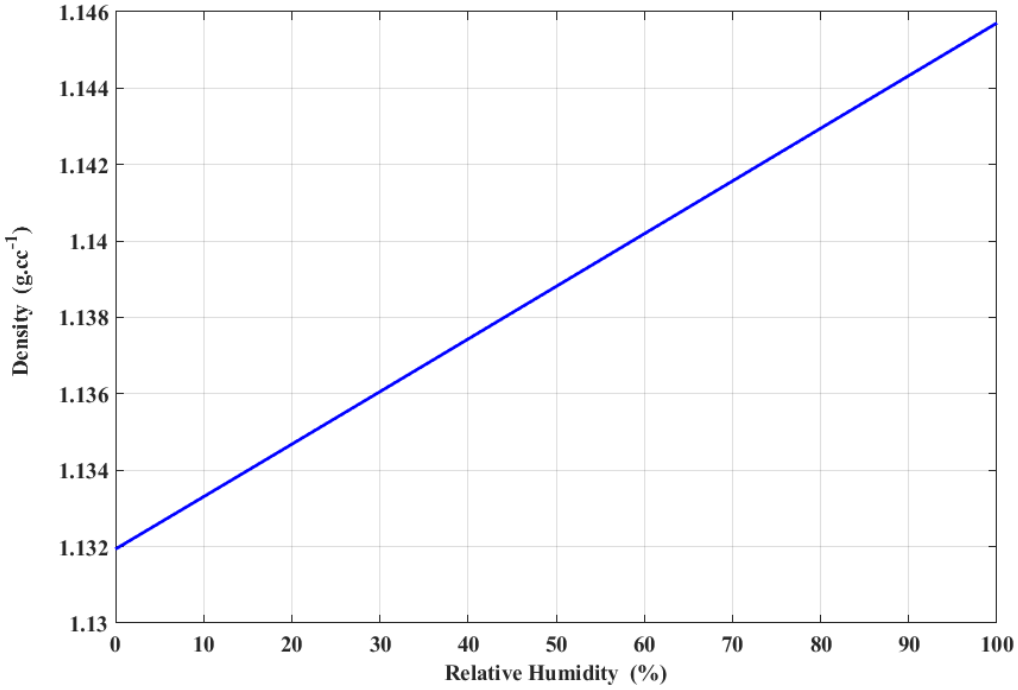

Figure 92: Density of phenolic resin, as a function of relative humidity, at 25℃.

Density increases by ~1.2%, from an initial value of ~1.132 $g.cc^{-1}$ at 0% relative humidity, to a final value of ~1.146 $g.cc^{-1}$ at 100% relative humidity. As the change in density is a function of both the mass of absorbed water molecules and the change in material volume that cause, this being dependent upon the free volume of the polymer, it is not possible to comment on the validity of these predictions as the expected behaviour will be material specific.

4.3.2.5. Effect of Relative Humidity upon the Young's Modulus of Phenolic Resin at 25℃

The GIM predicted effect of relative humidity upon the Young's modulus of phenolic resin, at 25℃, is shown below in Figure 93.

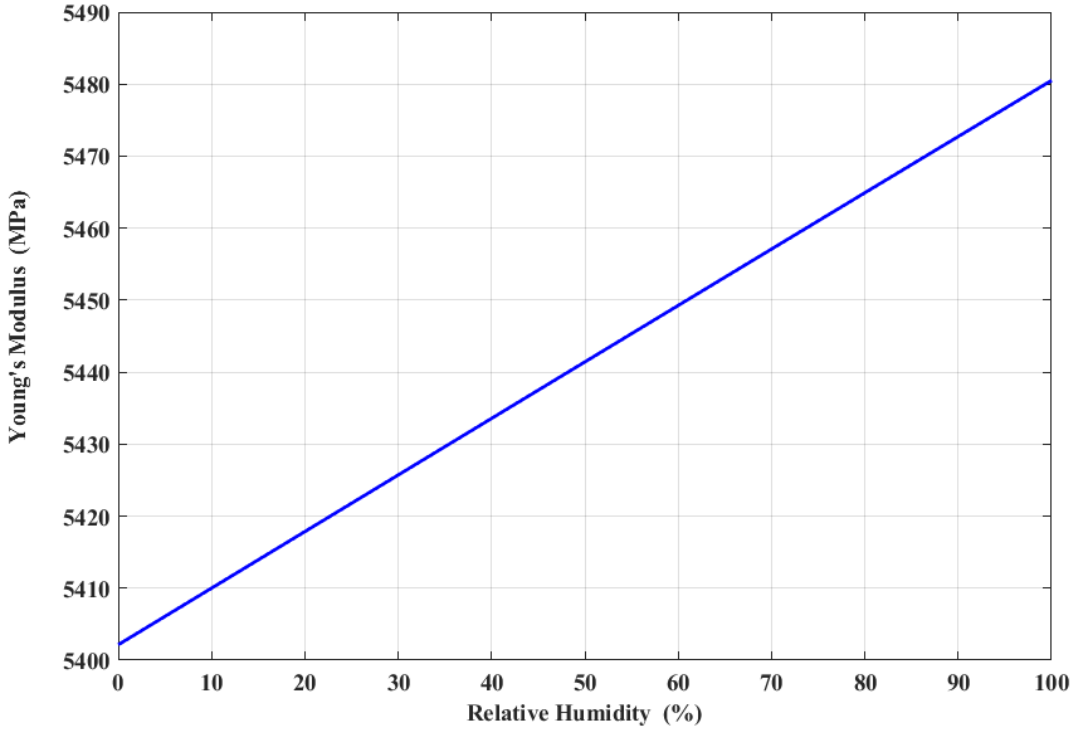

Figure 93: Young's modulus of phenolic resin, as a function of relative humidity, at 25℃.

These predictions indicate that the Young's modulus increases by ~1.4%, from an initial value of ~5402 MPa at 0% relative humidity, to a final value of ~5480 MPa at 100% relative humidity. This result is inconsistent with the behaviour of hygrothermally conditioned epoxy and phenolic resins reported in the literature [2, 46, 47] where the effect of absorbed moisture is observed to reduce the engineering moduli of the material.

The GIM equation for the Young's modulus (equation (18)) indicates that this property is proportional to the ratio of A to the polymer's molar volume $V_{(T)}$:

$$E_{(E_{coh},N,\theta,T)} = 18 \frac{A_{(E_{coh},N,\theta,T)}}{V_{(T)}} \quad (237)$$

Where A is proportional to a fraction of the cohesive energy, minus the thermal energy:

$$A_{(E_{coh},N,\theta,T)} = \left(0.89E_{coh} - H_{(N,\theta,T)}\right) \quad (238)$$

As A is a function of E_{coh}, N, and θ, its value is likely to be correct as these parameter values for the water molecule have been employed successfully within GIM by other researchers [78], as discussed previously (see section 4.3.2.3, page 235). Calculating the value of A as a function of relative humidity, indicates that the effect of absorbed water molecules is to increase the value of this function. Thus, for the predicted Young's modulus to fall, as is observed experimentally, the molar volume term $V_{(T)}$ must increase sufficiently such that the ratio, $\frac{A_{(E_{coh},N,\theta,T)}}{V_{(T)}}$, decreases. This implies that the erroneous prediction of increasing Young's modulus with increasing relative humidity, results from the under estimation of the effect of absorbed water molecules upon the molar volume of the polymer, as suggested previously (see section 4.3.2.3, page 235).

4.3.3. GIM Predicted Effect of Hygrothermal Conditioning upon the Thermo-mechanical Properties of Phenolic Resin (Model 2 - Using the Liquid Volume of Water)

4.3.3.1. Effect of Relative Humidity upon the Glass Transition Temperature and Thermal Expansion Coefficient of Phenolic Resin at 25℃

The behaviour of the glass transition temperature and thermal expansion coefficient of the phenolic resin, predicted by the new model, is identical to that obtained from the earlier model that employed the van der Waals volume of water. This is expected because the only GIM equation that was adjusted in the new model was that for the prediction of molar volume $V_{(T)}$. Thus, only molar volume and the thermo-mechanical properties that depend upon its value (density and Young's modulus) are affected by this change. As the predictions are identical, no further interpretation is required.

4.3.3.2. Effect of Relative Humidity upon the Molar Volume of Phenolic Resin at 25℃

Figure 94 below shows the percentage change in phenolic resin volume, as a function of relative humidity at 25℃, predicted by the two different models.

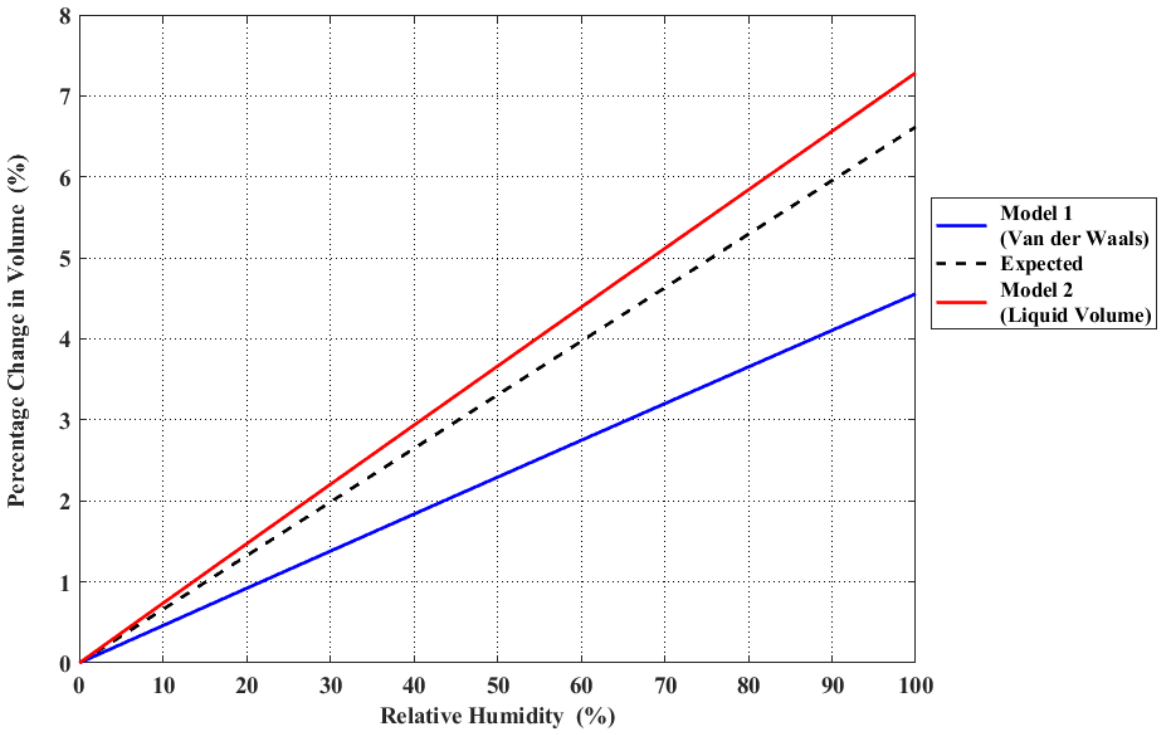

Figure 94: Percentage change in phenolic resin volume, as a function of relative humidity at 25℃, predicted by the two different models.

The expected behaviour has also been plotted to allow the validity, and accuracy, of both models to be compared. The results show that the predictions obtained from the model using the liquid volume of water are much closer to the expected behaviour. However, they diverge with increasing relative humidity, and at 100% relative humidity the predicted percentage change in volume is ~7.2%, compared to the ~6.5% that is expected. The cause of this overestimation can be identified by referring back to the modified GIM equation for molar volume (equation (221)). The volume of absorbed water is accounted for by the term $R_{(T)}\ V_{M\,(T)}$. However, water molecules bring cohesive energy and degrees of freedom to the system with the net effect being to increase the value of the thermal expansion coefficient. It is evident from equation (221),that an increase in the thermal expansion coefficient will affect an increase in the molar volume. Thus, the overestimation of molar volume in the liquid volume model can be attributed to the increase in thermal expansion coefficient that results from the presence of absorbed water molecules.

4.3.3.3. Effect of Relative Humidity upon the Density of Phenolic Resin at 25℃

Figure 95 shows the change in phenolic resin density, as a function of relative humidity at 25℃, predicted by the two different models.

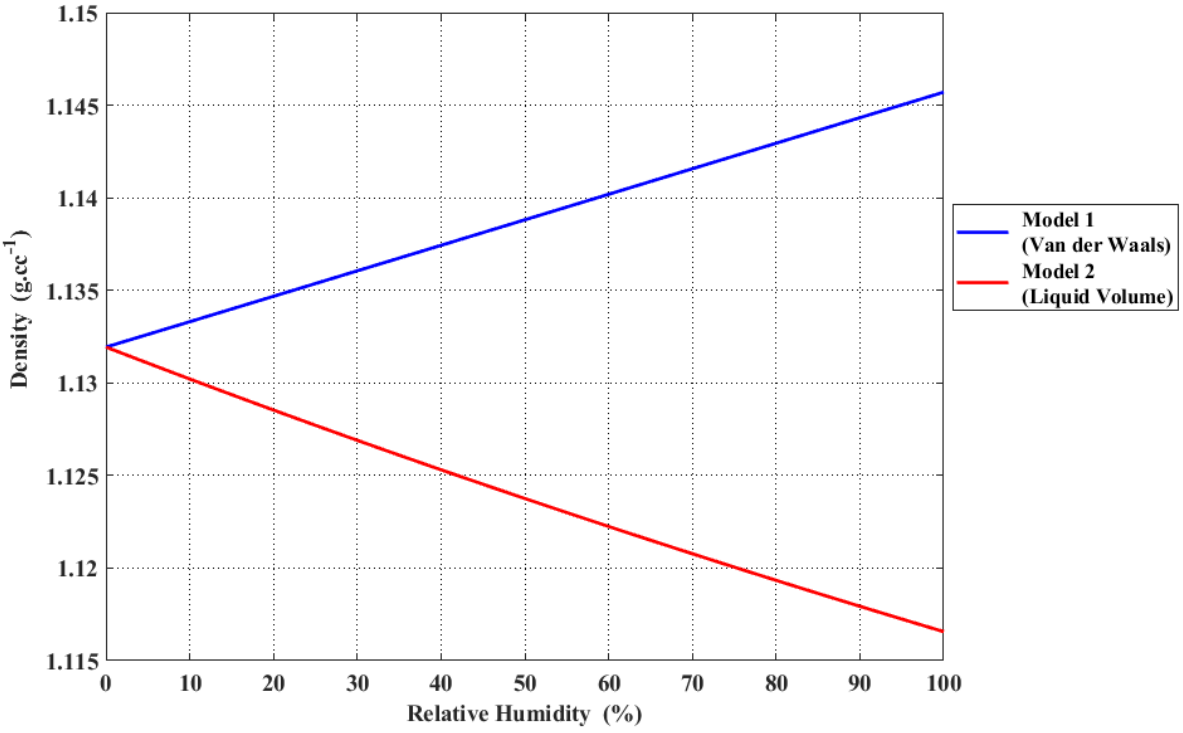

Figure 95: Change in phenolic resin density, as a function of relative humidity at 25℃, predicted by the two different models.

The predictions from the model using the van der Waals volume of water suggested that density could be expected to increase with increasing relative humidity. However, the predictions from liquid volume model indicate that density will fall by ~1.3%, from an initial value of ~1.132 $g.cc^{-1}$ at 0% relative humidity, to a final value of ~1.117 $g.cc^{-1}$ at 100% relative humidity. The density behaviour predicted by the liquid volume model is more likely to represent the actual density behaviour of the material. This is because density is a function of molar volume and the molar volume predictions of the liquid volume model are in greater agreement with expected behaviour than those of the van der Waals volume model (Figure 94).

4.3.3.4. Effect of Relative Humidity upon the Young's Modulus of Phenolic Resin at 25℃

Figure 96 shows the change in Young's modulus, as a function of relative humidity at 25℃, predicted by the two different models.

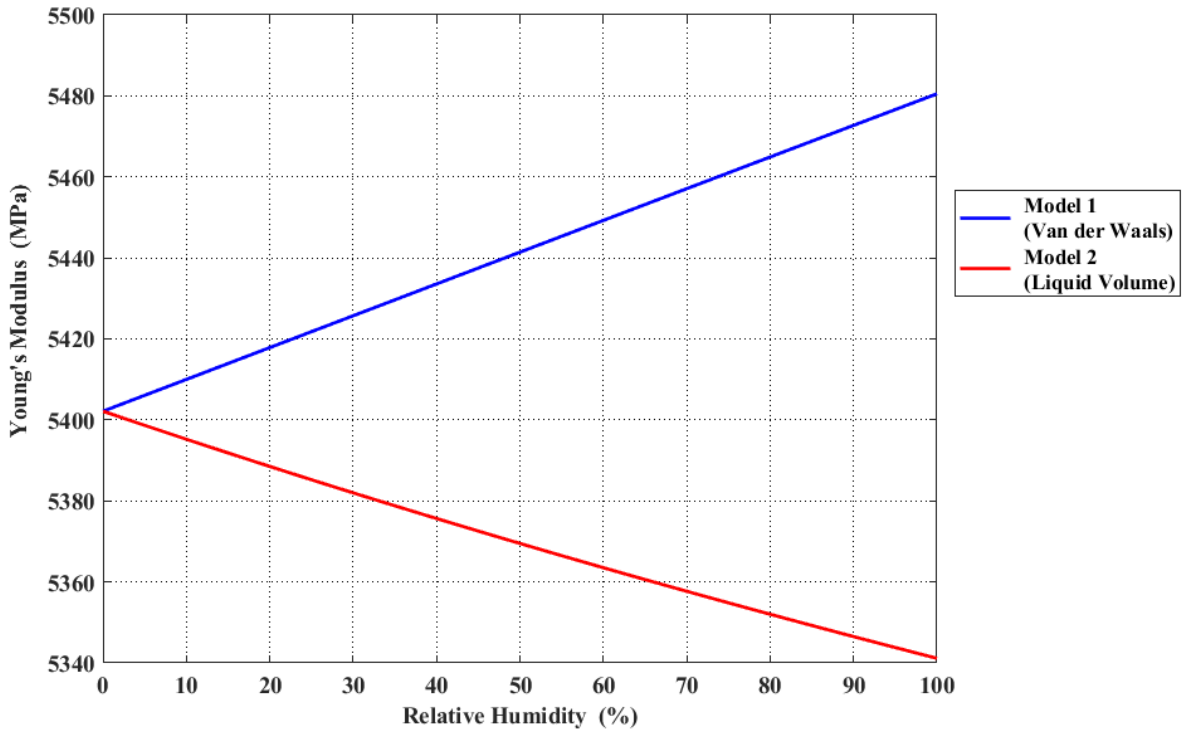

Figure 96: Change in the Young's modulus of phenolic resin, as a function of relative humidity at 25℃, predicted by the two different models.

These results show that the liquid volume model correctly predicts the reduction in modulus, with increasing relative humidity, that is observed experimentally in epoxy and phenolic resins [2, 46, 47]. The Young's modulus of the resin decreases by ~1.1%, from an initial value of ~5400 MPa at 0% relative humidity, to a final value of ~5340 MPa at 100% relative humidity. As discussed previously (see section 4.3.2.5, page 238), the value of the Young's modulus is proportional to the ratio $\frac{A_{(E_{coh},N,\theta,T)}}{V_{(T)}}$. In the reformulated model, the value of $A_{(E_{coh},N,\theta,T)}$ remains unchanged, however the predicted change in molar volume, resulting from water absorption, is greater than that predicted by the van der Waals volume model. The increase in molar volume that results from water absorption, is now sufficient to offset the increase in $A_{(E_{coh},N,\theta,T)}$ such that the net effect is a reduction in the ratio $\frac{A_{(E_{coh},N,\theta,T)}}{V_{(T)}}$. This corresponds to a decrease in the value of the Young's modulus.

4.3.4. Summary of the Validity of the Two Different Models

In the previous section the thermo-mechanical property predictions of the two different models have been compared. This has shown that the predictions of the liquid volume model are in greater agreement with the expected material behaviour, than those obtained by the van der Waals volume model. Of most importance, this new model formalism corrects the erroneous Young's modulus behaviour that is predicted by the standard GIM model when the van der Waals volume of water is included directly. However, as highlighted earlier, the effect of thermal energy is overestimated in the calculation of the molar volume, and thus the impact of absorbed water on any thermo-mechanical properties that are functions of both the degrees of freedom, and molar volume, will be overestimated. As a consequence, caution should be exercised when interpreting predictions obtained from this new model, with predictions being taken as representative of overall property trends rather than indicative of exact property values. The final benefit of this new model formalism is that the effect of polymer free volume can now be accounted for. The effects of free volume on the thermo-mechanical properties of phenolic resins, under hygrothermal conditions, is investigated in the next section.

4.3.5. Influence of Free Volume upon the Thermo-mechanical Property behaviour of Phenolic Resin under Hygrothermal Conditions at 25℃

In this section, the modified form of the molar volume equation of the liquid volume model (equation (227)), that accounts for polymer free volume, is employed in predicting the thermo-mechanical property behaviour of phenolic resins under hygrothermal conditions. In the work that follows, the thermo-mechanical properties of phenolic resin are predicted as a function of relative humidity, at 25℃, for two different free volume percentages: 0% and 3%. This will allow the influence of free volume upon the effects of hygrothermal ageing to be deduced. As the glass transition temperature and thermal expansion coefficient are not functions of molar volume, neither of these properties is affected by free volume and as a result these properties are not analysed in the work that follows.

4.3.5.1. Influence of Free Volume upon the Molar Volume Behaviour of Phenolic Resin under Hygrothermal Conditions at 25℃

Figure 97 shows the predicted percentage change in phenolic resin volume, as a function of relative humidity at 25℃, for materials with 0%, and 3%, free volume.

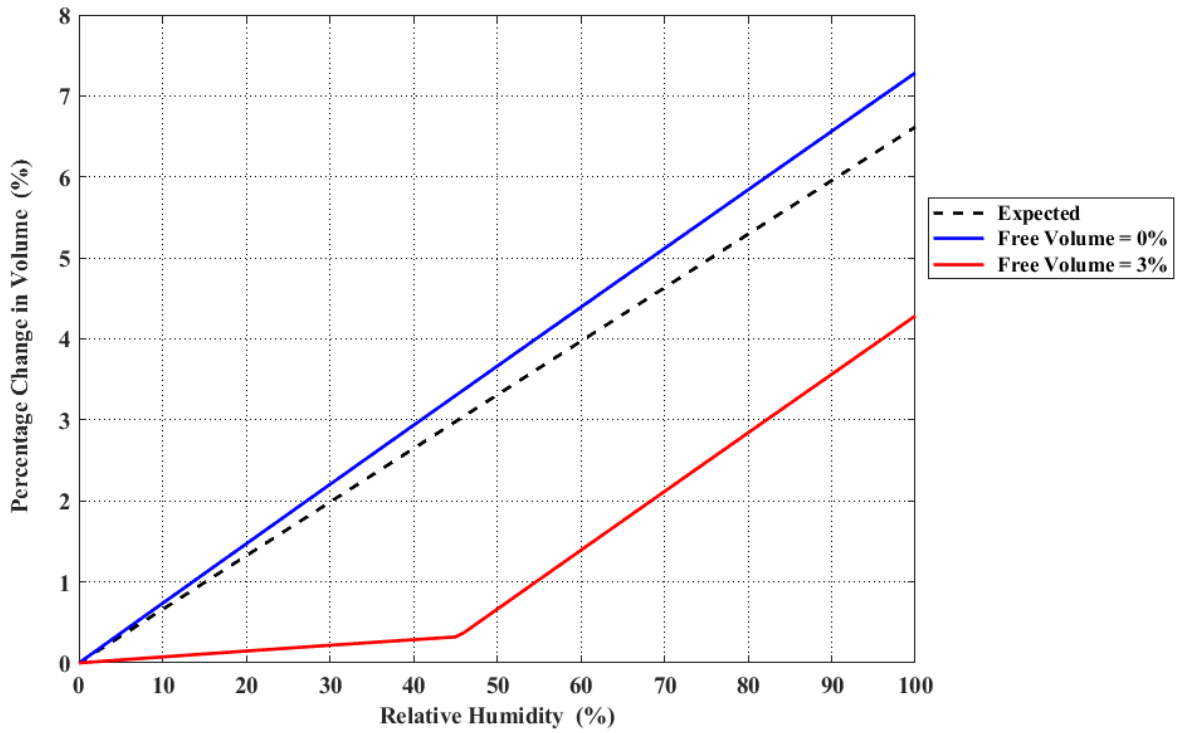

Figure 97: Percentage change in phenolic resin volume, as a function of relative humidity at 25℃, for materials with 0%, and 3%, free volume.

The predicted volume behaviour, for a material possessing 3% free volume, is similar to that observed in epoxy resins within the literature [4, 50]. The results indicate that for a polymer with 3% free volume, the effect of absorbed water molecules upon molar volume is negligible at conditioning relative humidities below 45%. At 45% relative humidity, an increase in molar volume of ~0.3% is exhibited by the material with 3% free volume, compared to ~3.3% in the material with no free volume. This is because the concentration of water molecules absorbed within the resin at relative humidities equal to, or less than 45%, is insufficient to completely fill the free volume of the polymer. In other words, the apparent volume of water ($V_{App_{(T)}}$) absorbed within the material with 3% free volume, is zero, and hence the molar volume of the polymer is unaffected.

The slight increase in molar volume of ~0.3% that is predicted, on moving from 0% to 45% relative humidity, can be attributed to the effect that absorbed water molecules have upon the thermal expansion coefficient of the polymer. As discussed previously, water molecules bring both cohesive energy and degrees of freedom to the polymer system with the net effect, in this phenolic resin, being to increase the value of the thermal expansion coefficient. Although water molecules absorbed within free volume have no impact upon the molar volume of the polymer, their cohesive energy and degrees of freedom must still be considered. This is because water molecules contained within free volume are still capable of interacting with surrounding polymer chains, through van der Waals forces and hydrogen bonding, and thus their cohesive energy, which describes the strength of this interaction, must be taken into account. Similarly, the thermal energy associated with absorbed water molecules can be transferred to the polymer network through their collision with polymer chains. Thus, free volume has no impact upon the cohesive energy and degrees of freedom that absorbed water molecules bring to the system.

At relative humidities greater than 45%, polymer free volume is completely filled and thus the effect of further water absorption defaults back to the behaviour expected for a polymer with zero free volume. At 100% relative humidity, the predicted percentage change in molar volume, for a material with 3% free volume, is ~4.25%, compared to ~7.25% for a material in which the free volume is zero. Thus, increasing free volume reduces the magnitude of the moisture induced swelling behaviour and increases the relative humidity threshold required for the effect of this phenomenon to become significant.

4.3.5.2. Influence of Free Volume upon the Density Behaviour of Phenolic Resin under Hygrothermal Conditions at 25℃

Figure 98 shows the predicted density behaviour of phenolic resin, as a function of relative humidity at 25℃, for materials with 0%, and 3%, free volume.

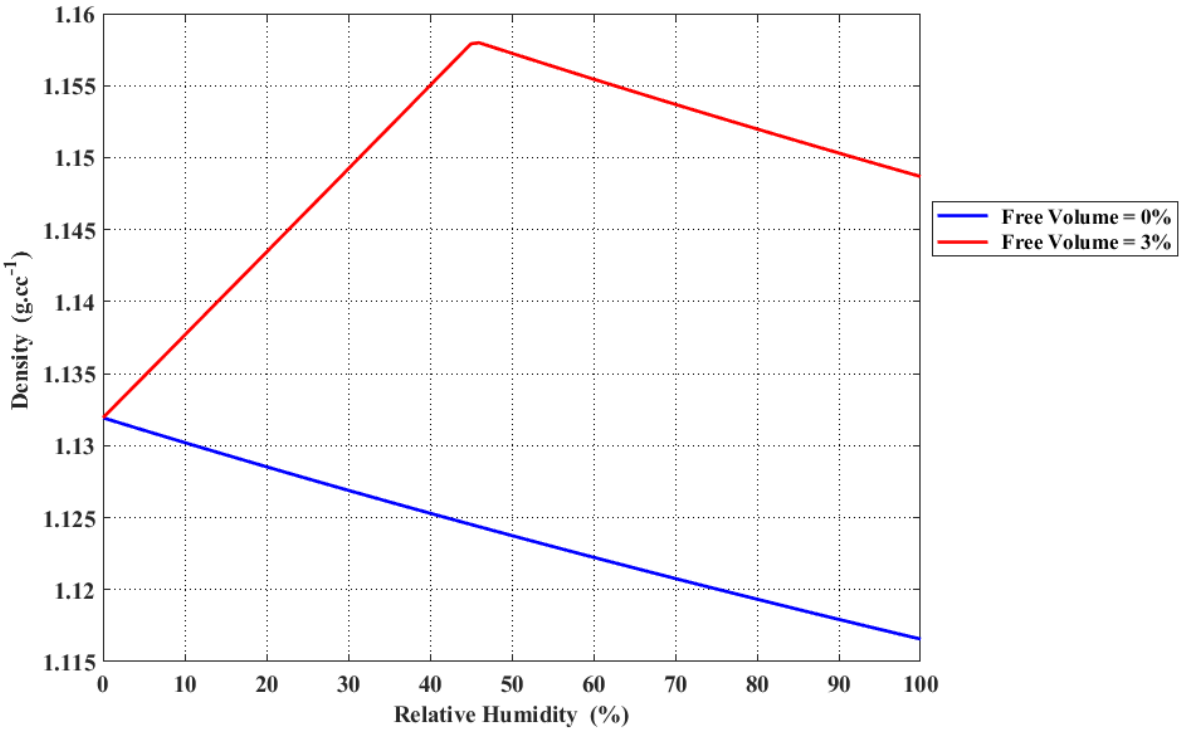

Figure 98: Density of phenolic resin, as a function of relative humidity at 25℃, for materials with 0%, and 3%, free volume.

The results indicate that, for a phenolic resin with 3% free volume, the initial effect of increasing relative humidity is to increase the density of the material. Density increases with relative humidity from an initial value of ~1.1325 $g.cc^{-1}$, at 0% relative humidity, to a value of ~1.1575 $g.cc^{-1}$ at 45% relative humidity. This increase in density can be attributed to the extra mass that absorbed water molecules bring to the polymer combined with the negligible change in volume that occurs when free volume has not been completely filled.

Above 45% relative humidity, the moisture content of the polymer becomes sufficient to completely fill the free volume and thus the change in molar volume with increasing relative humidity becomes considerable. Although the mass of the system is still increasing, the increase in volume becomes the dominant effect resulting in an overall reduction in density. In this region, density is reduced from an initial value of ~1.1575 $g.cc^{-1}$ at 45% relative humidity, to a final value of ~1.148 $g.cc^{-1}$ at 100% relative humidity.

For a phenolic resin in which the free volume is zero, the net effect of water absorption is to decrease the density of the polymer. By introducing free volume to the material this behaviour is initially reversed, with density increasing with relative humidity as long as unfilled free volume remains. When the conditioning relative humidity is sufficient to completely fill free volume, density behaviour defaults back to that expected for a polymer with zero free volume. Thus, if the free volume of the polymer is large enough, the effect of moisture absorption, at any relative humidity, will be to increase the density of the material.

4.3.5.3. Influence of Free Volume upon the Young's modulus behaviour of Phenolic Resin under Hygrothermal Conditions at 25℃

Figure 99 shows the predicted Young's modulus behaviour of phenolic resin, as a function of relative humidity at 25℃, for materials with 0%, and 3%, free volume.

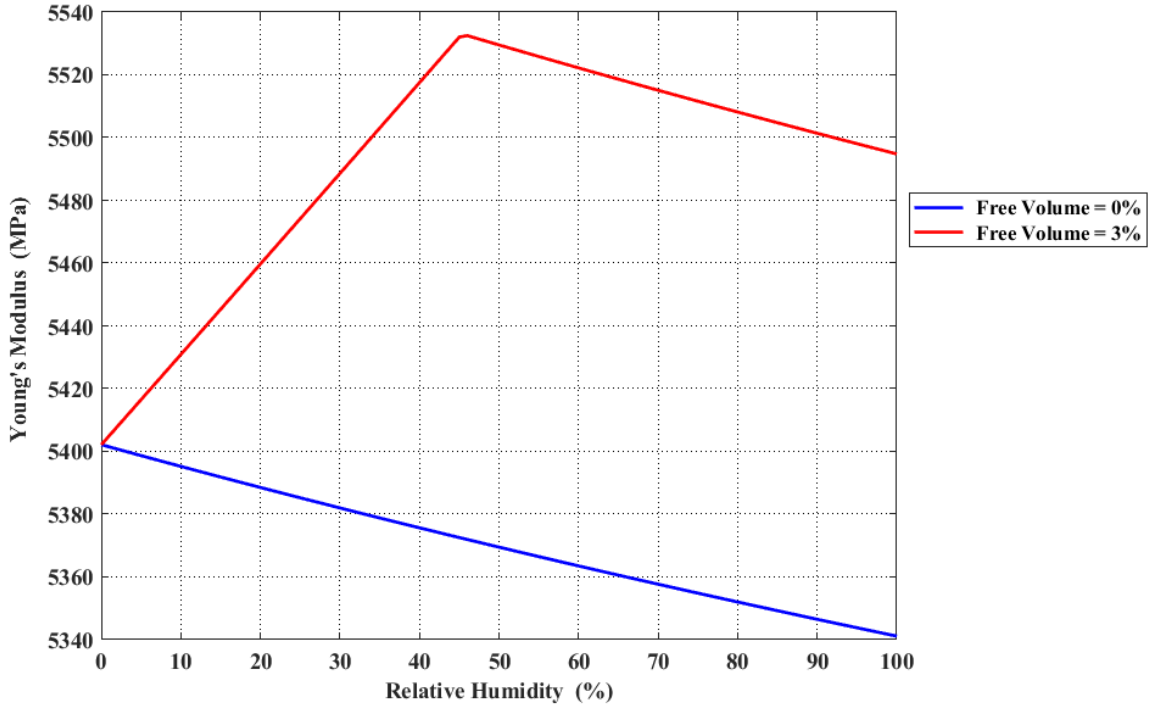

Figure 99: Young's modulus of phenolic resin, as a function of relative humidity at 25℃, for materials with 0%, and 3%, free volume.

The behaviour of the Young's modulus, with relative humidity, follows a trend similar to that predicted for density in Figure 98. Initially, Young's modulus increases with increasing relative humidity from a value of ~5400 MPa, at 0% relative humidity, to ~5530 MPa at 45%

relative humidity. However, above 45% relative humidity the behaviour is reversed with an overall reduction in Young's modulus observed from ~5530 MPa, at 45% relative humidity, to ~5495 MPa at 100% relative humidity. These trends can be understood by referring back to the GIM equation for the Young's modulus (equation (237)) that was discussed in section 4.3.2.5 (page 238).

Equation (237) indicates that the value of the Young's modulus is proportional to the ratio $\frac{A_{(E_{coh},N,\theta,T)}}{V_{(T)}}$. The term $A_{(E_{coh},N,\theta,T)}$ is a function of both the cohesive energy, and thermal energy, of the polymer system and was determined earlier to increase with increasing relative humidity (see section 4.3.2.5, page 238). As $A_{(E_{coh},N,\theta,T)}$ is independent of the molar volume of the polymer its behaviour is not affected by free volume. Thus, it is the change in the behaviour of the molar volume term $V_{(T)}$ at 45% relative humidity, when free volume becomes completely filled, that accounts for the change in the Young's modulus trend that is observed above this relative humidity. Below 45% relative humidity, absorbed water molecules occupy free volume and thus their effect upon molar volume is negligible. They do however contribute to the term $A_{(E_{coh},N,\theta,T)}$, which increases with increasing relative humidity, and thus the net effect is an increase in the ratio $\frac{A_{(E_{coh},N,\theta,T)}}{V_{(T)}}$ which corresponds to an increase in the Young's modulus. The term $A_{(E_{coh},N,\theta,T)}$ continues to increase as relative humidity is increased above 45%, however in this relative humidity range free volume is completely filled and the effect of absorbed water molecules upon molar volume is considerable. The increase in molar volume becomes dominant with the net effect being a reduction in the ratio $\frac{A_{(E_{coh},N,\theta,T)}}{V_{(T)}}$ corresponding to a decrease in the Young's modulus.

The results in Figure 99 suggest that for a phenolic resin, possessing a free volume of 3%, the overall effect of moisture absorption is to affect an increase in the value of the Young's modulus. As the actual free volume of the resin studied in this work is unknown, it is not possible to verify the validity of these model predictions through comparison with experimental measurements. However, in the literature there are no recorded observations of a net increase in the Young's modulus of epoxy or phenolic resins, when they are conditioned at high relative humidities (>50%) [2, 118-121].

In the work that follows the effect of relative humidity, upon the Young's modulus of phenolic resins, is predicted for resin materials possessing a range of different free volumes. These results indicate that it is possible to reconcile the predicted Young's modulus behaviour with that observed experimentally, provided that the free volume is small and the conditioning relative

humidity is low. These results, and the conclusions drawn from them, are discussed in the section that follows.

4.3.6. GIM Predicted Effect of Free Volume and Relative Humidity upon the Thermo-mechanical Properties of Phenolic Resin at 25℃

In the work that follows, the thermo-mechanical properties of phenolic resin, at 25℃, are predicted as a function of both the relative humidity of the environment, and of the free volume of the polymer. Only those properties that are affected by free volume are investigated; molar volume, density, and Young's modulus. The results for molar volume are expressed in terms of the percentage change in molar volume, compared to the initial molar volume of the dry material. The behaviour of the density and Young's modulus is presented in terms of their actual property values.

4.3.6.1. Effect of Relative Humidity and Free Volume upon the Molar Volume of Phenolic Resin at 25℃

Figure 100 below shows the predicted percentage change in the molar volume of phenolic resin, at 25℃, as a function of both relative humidity and polymer free volume.

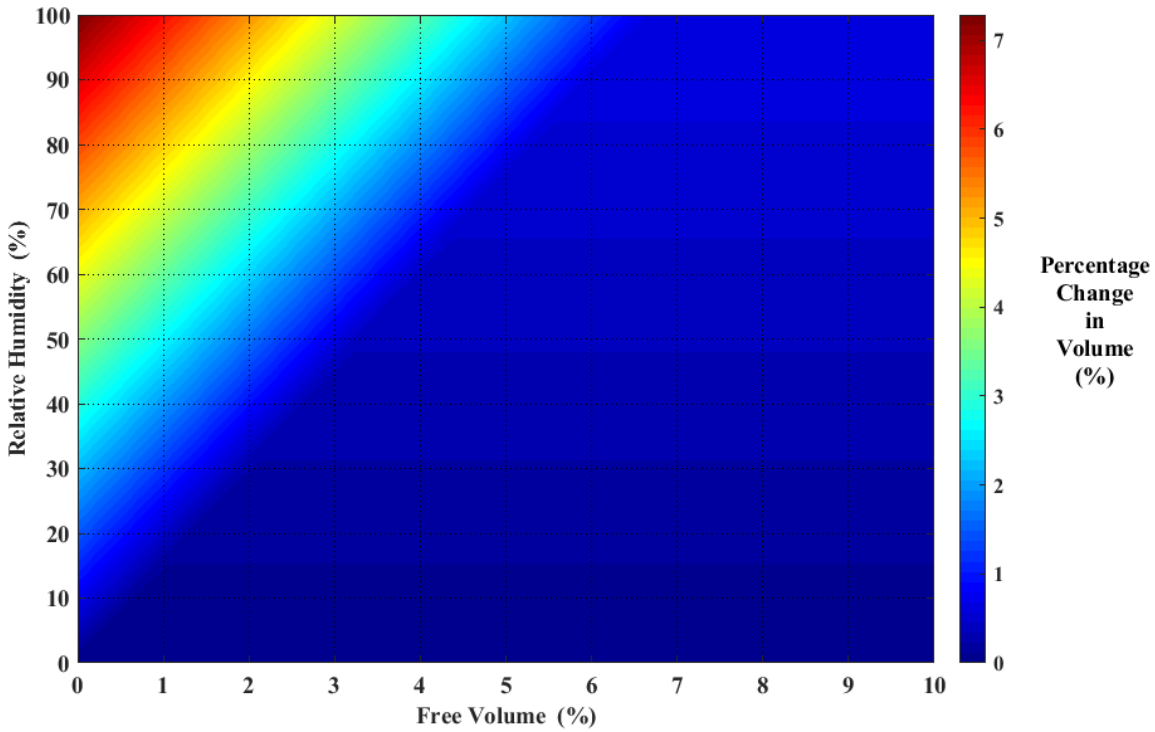

Figure 100: Percentage change in phenolic resin molar volume, at 25℃, as a function of both relative humidity and free volume.

The results indicate that the effect of increasing free volume is to increase the relative humidity threshold required for significant swelling of the polymer material to occur. This behaviour is expected because by increasing the free volume of the material the quantity of water molecules required to fill that free volume is also increased. As the quantity of absorbed water molecules is proportional to relative humidity, this implies that higher relative humidities are required to completely fill larger free volumes.

The relative humidity threshold, above which significant swelling occurs, increases with increasing free volume, from an initial value of 0% relative humidity for 0% free volume, to a final value of 100% relative humidity when the free volume is ~6.5%. Thus, if the free volume of the phenolic resin is equal to, or greater than, ~6.5% it becomes impossible to completely fill the free volume of the material. As a result, the impact of absorbed water molecules upon the molar volume of such a material will be negligible. A small increase in molar volume, with increasing relative humidity, is still predicted in phenolic resin materials with free volumes in excess of ~6.5%. This is because water molecules contained within free volume still contribute cohesive energy and degrees of freedom to the polymer. The net effect of these contributions were determined earlier in this work and found to have the effect of increasing the value of the thermal expansion coefficient (see section 4.3.2.2, page 233). As the molar volume is also a function of the thermal expansion coefficient, absorbed moisture contained within free volume still results in a slight increase in the molar volume of the polymer.

4.3.6.2. Effect of Relative Humidity and Free Volume upon the Density of Phenolic Resin at 25℃

Figure 101 below shows the predicted change in phenolic resin density, at 25℃, as a function of both relative humidity and polymer free volume.

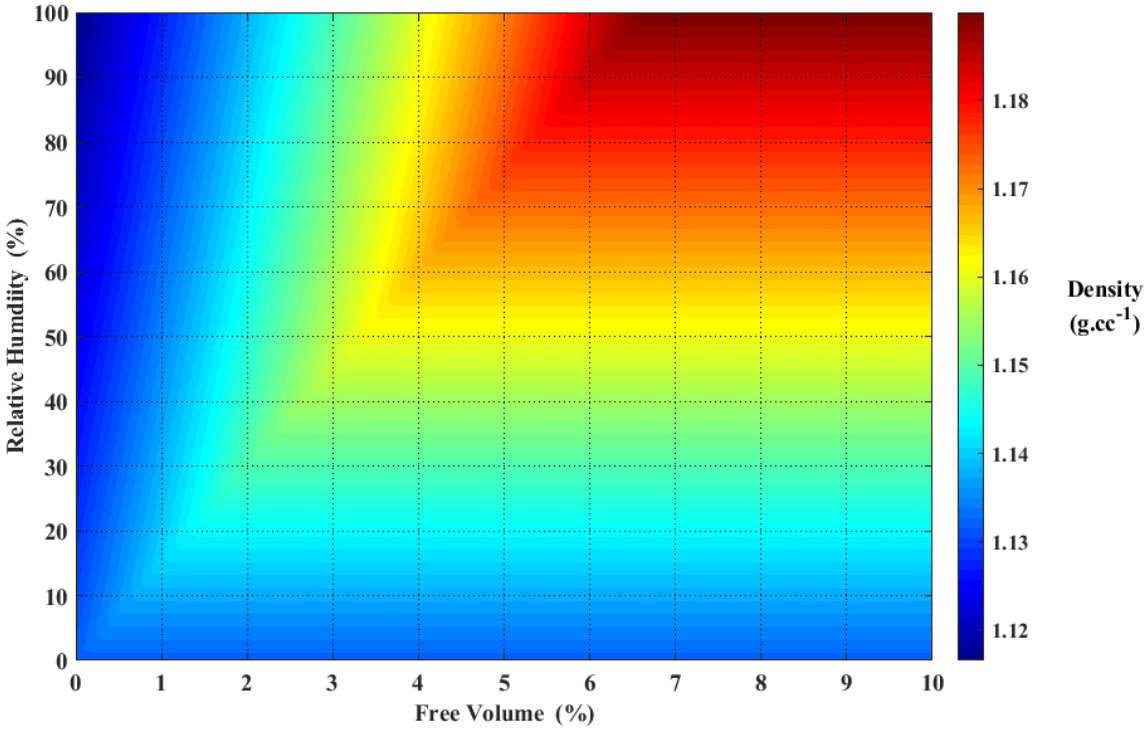

Figure 101: Phenolic resin density, at 25℃, as a function of both relative humidity and polymer free volume.

These results show that, for a given relative humidity, phenolic resin density initially increases with increasing free volume. This occurs because, as free volume is increased, a greater proportion of absorbed water molecules are able to occupy polymer free volume. This reduces the apparent volume of water ($V_{App_{(T)}}$) in the molar volume equation (equation (227)), and as free volume does not affect the mass of absorbed water molecules, the net effect is to increase the density of the polymer.

This behaviour continues until a threshold free volume is reached, above which no further changes in density are observed. The threshold free volume represents the minimum free volume required, at a given relative humidity, to ensure all absorbed water molecules occupy free volume. The threshold free volume increases with increasing relative humidity because at higher relative humidity a greater quantity of water molecules are absorbed within the polymer. Thus, a greater free volume is required to fully accommodate them. Increasing free volume above the threshold free volume, at a given relative humidity, yields no further increase in density. This is because at

the threshold free volume all absorbed water molecules are contained within free volume. Increasing free volume further has no impact upon the quantity of water molecules that occupy free volume and thus the molar volume, and hence the density, of the polymer remains unchanged.

The behaviour of material density with increasing relative humidity, for a given free volume, can be summarised as follows. Initially, density increases because absorbed water molecules occupy free volume and thus there is a negligible change in the molar volume of the polymer. After a threshold relative humidity is reached, at a given free volume, further increases in humidity result in a reduction in material density. This is because at the threshold relative humidity polymer free volume becomes completely filled. Further increases in relative humidity result in absorbed water molecules contributing to the apparent volume of water term $V_{App_{(T)}}$ in the molar volume equation. Thus, the molar volume of the polymer increases and this change in volume becomes the dominant term in the density equation, leading to a net decrease in density.

4.3.6.3. Effect of Relative Humidity and Free Volume upon the Young's Modulus of Phenolic Resin at 25℃

Figure 102 below shows the predicted change in the Young's modulus of phenolic resin, at 25℃, as a function of both relative humidity and polymer free volume.

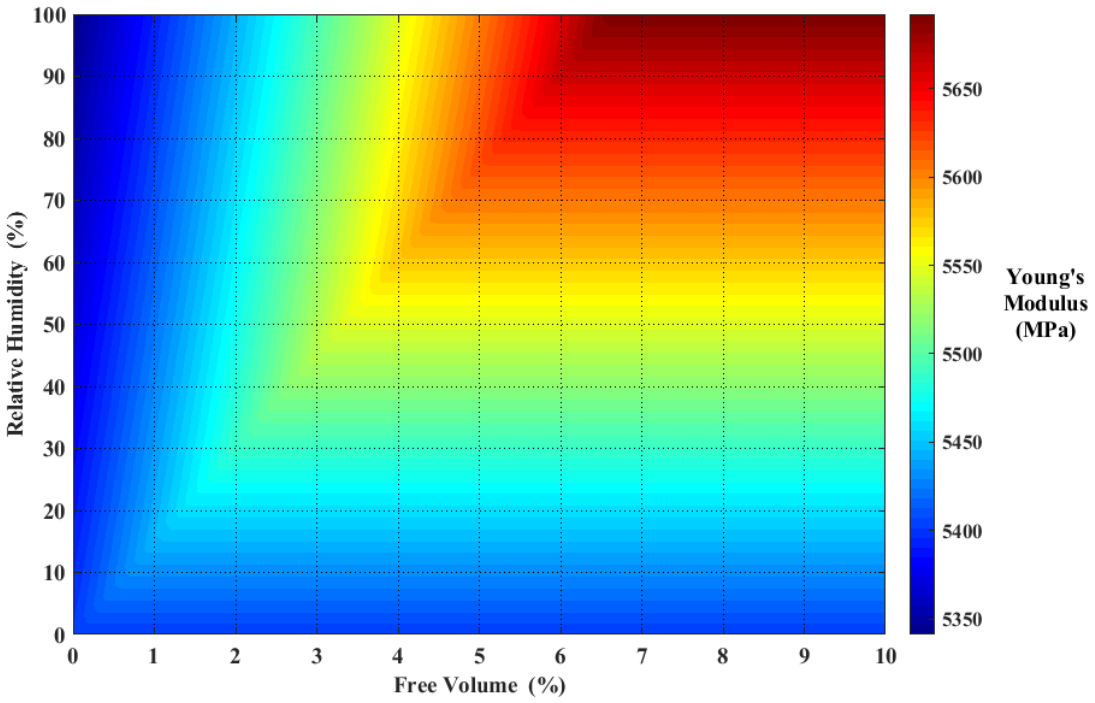

Figure 102: Young's modulus of phenolic resin, at 25℃, as a function of both relative humidity and polymer free volume.

The behaviour of the Young's modulus, with relative humidity and free volume, follows a trend similar to that observed for density (Figure 101). This is expected because the GIM equations for Young's modulus and density both involve a term that increases with increasing water content ($A_{(E_{coh},N,\theta,T)}$ in the case of Young's modulus and m_{water} in the case of density) divided by the molar volume of the polymer. Thus, the behaviour of the Young's modulus can be described by the same interpretation proposed for density in the previous section.

4.3.6.4. Discussion of the Predicted Effect of Free Volume on Phenolic Resin Thermo-Mechanical Properties under Hygrothermal Conditions

It is of interest to note that the results in Figure 102 indicate that if the free volume of the phenolic resin is ~0.5%, then the Young's modulus will increase slightly at relative humidities below ~40%. However, if the relative humidity is greater than 40% then a net decrease in Young's modulus is observed. In the literature, the majority of studies on the effect of hygrothermal ageing upon the engineering moduli of epoxy and phenolic resins, have focused on the mid, to high, relative humidity regimes [118-121]. Thus, the unusual model predictions, increasing Young's modulus with increasing moisture content, could be reconciled with experimental observations if the actual free volume of the phenolic resin is small (~0.5%). Then, the increase in Young's modulus would occur at low relative humidity (<40%), seldom probed by experiment, which would account for the lack of observations of this phenomenon in the literature.

The literature on the moduli of epoxy and phenolic resins, as a function of moisture content, has been examined in an attempt to validate the implication of the model that the Young's modulus of polymers, with small free volumes, can increase when they are conditioned at low relative humidities. However, the small amount of conditioning data at low relative humidities renders this process problematic. Furthermore, no work studying the relationship between free volume, Young's modulus, and relative humidity can be found. As a result, the modulus/RH data that has been analysed is for polymers in which the free volume is unknown. This makes comparison between the findings of separate studies problematic as the model indicates that free volume affects both the magnitude of the increase in Young's modulus, and the relative humidity range in which it occurs. Finally, studies investigating the effect of material moisture content upon all types of engineering moduli have been included, as pure Young's modulus data is scarce.

Botelho et al [120] investigated the effect of hygrothermal conditioning, at 90% relative humidity, on the engineering moduli of epoxy resins. Modulus measurements were performed on samples at various times during the conditioning process. Their results showed that the moduli of

samples that had attained equilibrium with their conditioning environment were less than those observed initially in the materials when dry. However, measurements of material modulus when the samples were only half way to equilibrium, thus possessing half their equilibrium moisture content, showed that there was no effect on the modulus at this point in the conditioning experiment. This observation is consistent with the predictions of the model developed in this work. This is because when these samples are half conditioned, the free volume of the material located closer to the sample surface will be filled, thus inducing swelling and lowering the modulus of the material. However, the material located closer to the sample centre will possess lower concentrations of water which may be insufficient to completely fill the material free volume within this region. Thus, in this region the effect of water molecules will be to increase the modulus. As the modulus measurements obtained by Botelho et al are an average for the entire material, this might result in a negligible change in modulus being observed at this point in the conditioning process.

Zanni et al [118] investigated the behaviour of the shear modulus of epoxy resins during conditioning at 100% relative humidity. Measurements were obtained for a range of conditioning times and in all cases showed that the shear modulus of the materials decreased with increasing moisture content. This behaviour is different than that observed by Botelho et al [120] as the moduli of the materials were reduced even at early conditioning times. However, in this work no gravimetric data was provided, thus it is not possible to determine the fractional water content of the material at each conditioning time. This information is required as the model suggests that an increase in modulus might only occur at low moisture contents. Yang et al [119] studied the effect of hygrothermal ageing, at 98% relative humidity in a cyclic conditioning environment 25-55℃, upon the flexural modulus of a phenolic resin composite. They showed that the flexural modulus decreased with moisture content. This effect was observed even when the moisture content of the material was low; possessing only half the moisture content it had at equilibrium.

Nkeuwa et al [122] observed the effect of hygrothermal ageing on the modulus of epoxy resins containing nano-clay fillers, conditioned to equilibrium at 20% relative humidity. Materials with a range of different fillers and weight fractions were investigated. All materials, except one, showed a reduction in modulus when conditioned to equilibrium at 20% relative humidity. The modulus of the outlier remained approximately constant, apparently unaffected by the moisture content. However, care must be taken in the interpretation of these results as their DMTA measurements indicated that a reduction in material modulus, associated with the onset of the glass transition, occurred at ~45℃ in the dry samples. As absorbed water reduces the T_g of epoxy resins [3, 5, 48, 49], the onset of modulus reduction when the materials are at equilibrium, at 20%

relative humidity, will be less than 45℃. Thus, it is possible that some modulus reduction, resulting from the onset of T_g, might occur at the temperature at which the modulus is measured, namely room temperature. Thus, any small increase in modulus at low relative humidity, resulting from absorbed water molecules occupying free volume, would be obscured by the reduction in modulus occurring at the onset of the glass transition. Klauser et al [2] investigated a phenol-resorcinol-formaldehyde resin, under hygrothermal conditions, and observed that the Young's modulus of these materials decreased with increasing water content. More specifically, at the low relative humidity of 30%, only a reduction in Young's modulus was observed.

The few studies available on the moduli of epoxy and phenolic resins [2, 122], at low relative humidity (≤30%), suggest that no improvement in modulus occurs; although moisture was observed to have no impact on modulus in one specific material. The results from conditioning experiments at higher relative humidities [118, 119, 121], but at early conditioning times before the free volume of the material has been completely filled, also do not generally support the model implication that modulus can increase at low material moisture contents. However, the work of Botelho et al [120] did show that no change in the modulus of an epoxy resin occurred when the moisture content of the material was half its equilibrium content. A difficulty in interpreting all these studies is that no free volume values are given for the materials and the model suggests that this is essential for understanding the behaviour of Young's modulus with water content. To summarise, those experimental data that are available do not generally support the model prediction of an increase in Young's modulus before free volume is filled. However, more data is required, specifically free volume and Young's modulus measurements as a function of relative humidity, to fully assess the validity of these model predictions.

4.4. Chapter Conclusions

In this work DMTA and gravimetric data for a commercial phenolic resin, supplied by Alston et al [111, 112], were analysed and used to characterise the material in terms of its chemical structure and diffusion properties. The diffusion coefficient and equilibrium moisture content, as a function of relative humidity, were obtained from the gravimetric data. The DMTA data allowed the T_g of the material to be determined. This was then compared against GIM predictions for T_g, as a function of F/P ratio, allowing the chemical species present in the fully cured resin, and thus the GIM mer unit parameters, to be deduced. The moles of water absorbed within the resin at a given relative humidity, were employed to determine the contribution of water to the mer unit parameter values of the dry phenolic resin. This allowed GIM to predict the influence of absorbed moisture on the thermo-mechanical properties of the material.

The predicted percentage change in polymer volume, obtained using the standard formalism of GIM, was shown to disagree with the expected swelling behaviour of the material. It was hypothesised that this resulted from the inclusion of the volume of water in terms of its van der Waals volume, as water molecules do not covalently bond to the polymer network. A new model was developed in which the apparent volume occupied by water molecules in the liquid state (termed the liquid volume) was combined directly with the mer unit molar volume. The percentage change in volume predicted by this model showed greater agreement with the expected swelling behaviour.

The liquid volume model was then modified to account for polymer free volume. The swelling response predicted by the free volume model, was in general agreement with the expected behaviour. However, the model also suggested that the Young's modulus could increase under certain free volume and relative humidity conditions. A search of the literature showed that no such effect has been observed to occur at mid, to high, relative humidities [118, 119, 121]. In general, no effect was observed at low relative humidity either [2, 122], although there were a few exceptions. Interpretation of data in the literature was complicated by the absence of free volume data for the materials being studied. The model suggests that this is essential for predicting the magnitude of the Young's modulus increase, and the relative humidity range in which it will occur. Thus, at present, there is not enough data available to validate the predictions of the free volume model.

5. Modelling the Hygrothermal Behaviour of Low-fired Carbon-fibre Phenolic Composites

5.1. Introduction

In this chapter, a model will be developed to describe the moisture absorption/desorption behaviour of low-fired carbon-fibre. This is then employed to investigate the effect of fibre volume fraction upon the hygrothermal ageing process occurring within phenolic based low-fired carbon-fibre composites. In the first section, dynamic vapour sorption (DVS) data provided by Stone [123], for a low-fired carbon-fibre, is reviewed and the overall behaviour discussed qualitatively. DVS is a characterisation technique which allows accurate measurement of a material's response to hygrothermal environments. The instrument allows a material to be subjected to range of atmospheric humidities whilst it is weighed in situ. The change in material mass with conditioning time, is constantly monitored, thus allowing the material's uptake/time response to be obtained. A benefit of this technique over gravimetric analysis by manual weighing is that the mass measurements are performed in situ. Thus, any errors in material mass introduced through the loss/gain of water during the weighing process, are avoided. In section 5.2 (page 257) a model is developed to describe the absorption/desorption behaviour of low-fired carbon-fibre enclosed within thermoset matrices. Finally, this model is employed to predict the effect of fibre volume fraction and relative humidity upon the thermo-mechanical property profiles of a phenolic resin matrix within a low-fired carbon-fibre composite.

5.2. Methods

In the literature, the hygrothermal behaviour of a low-fired carbon-fibre phenolic composite has been modelled by Sullivan et al [89] (see section 1.8.2.2, page 35). However, in this model no differentiation was made between the fraction of water that resided within the resin matrix, and that which was contained within the fibre. As a result, the model only described the water content of the composite as a whole, and thus the concentration profile of water throughout the resin matrix could not be obtained. Furthermore, no physical explanation was proposed for the underlying phenomena responsible for the S-shaped uptake behaviour of the low-fired carbon-fibre composite.

In the work that follows, insights from the literature on the hygrothermal behaviour of activated carbons have been applied to understand, and model, water absorption in low-fired carbon-fibres. The S-shaped absorption behaviour of low-fired carbon-fibre composites is not observed in fully fired carbon-fibre composites. It is however observed in activated carbons [64, 65]. As the structure of low-fired carbon-fibre possesses some degree of porosity, it appears reasonable to assume that the processes underlying moisture uptake in low-fired carbon-fibre will share some degree of similarity with those responsible for the same phenomenon in activated carbon. Thus, a simple model for the hygrothermal behaviour of low-fired carbon-fibre will be derived based on the assumption that water uptake in low-fired carbon-fibre occurs through a similar process to that responsible for water uptake in activated carbon.

5.2.1. Simplified Approach to Modelling the Hygrothermal Behaviour of Low-fired Carbon-fibre Exposed to Atmospheric Water Vapour

Although the model proposed by Do et al [65] provides a mechanism for, and accurately predicts, the moisture uptake behaviour of activated carbon, it is complicated mathematically by the presence of a large number of parameters that must be obtained through a fitting procedure. The aim of this work is to create a simple fibre model that allows the concentration profile of water molecules, absorbed within the polymer matrix of a low-fired carbon-fibre phenolic composite, to be predicted as a function of conditioning time. This will allow the fractional contribution of the water molecule to the mer unit parameter values of the polymer matrix, at a time t and position x within the material, to be determined.

GIM can then be applied to convert these characteristic mer unit parameters into polymer thermo-mechanical property predictions, thus enabling the engineering properties of the polymer matrix to be deduced as a function of conditioning time, throughout the composite's geometry. To achieve this aim, it is not necessary to model the underlying phenomena of the fibre absorption process, it is only necessary to determine the local effect of the fibre upon the concentration of water within the polymer matrix. Thus, the process is simplified by assuming that the fibre behaves as a simple source/sink for water molecules.

5.2.2. Fibre Model

5.2.2.1. Derivation

First, assume that the fibre is free, in other words not encapsulated within a matrix, and exposed to atmospheric water vapour. If all the water associated with the fibre, adsorbed at the surface and absorbed within the pore volume, is encompassed within a single quantity, then the concentration of water molecules within the fibre at equilibrium, at a given relative humidity and temperature, can be expressed as:

$$C_f = \frac{N_F}{V_F} \tag{239}$$

Where C_F is the concentration of water molecules associated with the fibre in units of $mol.mm^{-3}$, N_F is the moles of water molecules associated with the fibre, and V_F is the volume of the fibre in units of mm^3. The process by which water molecules become associated and dissociated, with the fibre, can be described by the reversible reaction:

$$w_m \leftrightarrow w_f$$

Where w_m and w_f represent water molecules within the surrounding medium, and those associated with the fibre, respectively. The rate equations describing the change in the concentration of water molecules within the medium, and associated with the fibre, are given by:

$$\frac{d}{dt} C_f = r_f C_m - r_b C_f \tag{240}$$

$$\frac{d}{dt} C_m = r_b C_f - r_f C_m \tag{241}$$

Where C_f and C_m are the concentrations of water associated with the fibre, and within the surrounding medium, respectively, in units of $mol.mm^{-3}$, and r_f and r_b are the rate constants describing the forward and reverse reactions, both in units of min^{-1}.

5.2.2.2. Determining the Equilibrium Constant *K*

At equilibrium, the concentration of water molecules associated with the fibre, and in the surrounding medium, is constant. Thus, equations (240) and (241) become:

$$\frac{d}{dt} C_f = 0 \tag{242}$$

$$\frac{d}{dt} C_m = 0 \tag{243}$$

Taking the equation for the change in fibre water concentration with respect to time (240), this condition can be expressed as:

$$\frac{d}{dt} C_f = r_f C_m - r_b C_f = 0 \tag{244}$$

Therefore:

$$r_f C_m = r_b C_f \tag{245}$$

And:

$$\frac{r_f}{r_b} = \frac{C_f}{C_m} \tag{246}$$

The ratio of the forward and reverse rate constants is known as the equilibrium constant and is given by:

$$K = \frac{r_f}{r_b} \tag{247}$$

And:

$$K = \frac{C_f}{C_m} \tag{248}$$

The magnitudes of the two rate constants depend upon the underlying processes involved. From the description of moisture uptake in activated carbon, proposed by Do et al [65], these are:

1. Adsorption/desorption of water molecules to fibre surface functional groups

2. Adsorption/desorption of water molecules to water molecules already adsorbed at the fibre surface

3. Absorption/desorption of water clusters, into/out of, fibre pores.

These processes depend, in turn, upon the concentration of water associated with the fibre. Thus, r_f and r_b can be expressed as functions of C_f.

5.2.2.3. Solution of the Rate Equation

The rate equation (equation (240)) can be solved to obtain C_f as a function of conditioning time, if the following assumptions are made. First, assume that the concentration of water within the conditioning atmosphere is constant, for all times t. This implies that the atmosphere behaves as an infinite source of water molecules. Second, assume that the processes governing the uptake of moisture by the fibre, in the range $C_{f_1} < C_{f_t} < C_{f_2}$, do not change; where C_{f_1} and C_{f_2} are the initial, and final, concentrations of water associated with the fibre, and C_{f_t} is the concentration of water associated with the fibre at conditioning time t. This implies that the values of the rate constants are constant within this fibre water concentration range. The fibre is initially at equilibrium, at a given relative humidity and temperature, having a fibre water concentration C_{f_1} at $t = 0$. The relative humidity is then incremented by an amount ΔRH, increasing the concentration of water in the surrounding atmosphere, and thus the concentration of water associated with the fibre, at equilibrium, increases to C_{f_2}.

The rate equation for C_f is:

$$\frac{d}{dt} C_f = r_f C_m - r_b C_f \tag{249}$$

Integrating (249) with respect to the concentration of water associated with the fibre, and time:

$$\int_{C_{f_1}}^{C_{f_t}} \frac{1}{(r_f C_m - r_b C_f)} \, dC_f = \int_0^t dt \tag{250}$$

Gives the solution to the rate equation:

$$-\frac{1}{r_b}\left[ln(r_f C_m - r_b C_f)\right]_{C_{f_1}}^{C_{f_t}} = t \tag{251}$$

This can then be rearranged:

$$-\frac{1}{r_b}\left[ln\left(r_f C_m - r_b C_{f_t}\right) - ln\left(r_f C_m - r_b C_{f_1}\right)\right] = t \tag{252}$$

$$\left[\frac{\left(r_f C_m - r_b C_{f_t}\right)}{\left(r_f C_m - r_b C_{f_1}\right)}\right] = e^{-r_b t} \tag{253}$$

$$r_f C_m - r_b C_{f_t} = \left(r_f C_m - r_b C_{f_1}\right) e^{-r_b t} \tag{254}$$

$$C_{f_t} = \frac{r_f}{r_b} C_m - \frac{1}{r_b}\left(r_f C_m - r_b C_{f_1}\right) e^{-r_b t} \tag{255}$$

Equation (255) describes the concentration of water associated with the fibre, at a conditioning time t.

5.2.2.4. Determining the Rate Constants r_f and r_b as a Function of C_f

5.2.2.4.1. Basic Principle

Having obtained a solution to the rate equation, the values of r_f and r_b, as a function of C_f, can be determined by fitting equation (255) to a series of appropriate data sets. To perform this analysis, the C_f/t relationships are required for a fibre, initially with an equilibrium concentration C_{f_1}, at a given relative humidity RH and temperature T, exposed to a new environment at relative humidity $RH + \Delta RH$ at an identical temperature T. The average value of C_f within each data set is:

$$\widehat{C_f} = \frac{C_{f_2} - C_{f_1}}{2} \tag{256}$$

If the change in fibre water concentration that occurs between these two steps is small, then the rate constants will be approximately constant during the conditioning process. This can be achieved by ensuring that the relative humidity step, ΔRH, is sufficiently small ($\Delta RH \sim 5\%$). By employing the above methodology to fibres exposed to a range of relative humidities, the values of r_f and r_b can be obtained for a range of C_f. Expressions for r_f and r_b, with respect to C_f, can then be obtained by plotting these two variables against C_f and fitting appropriate functions to the relationships that are obtained.

5.2.2.4.2. Complications

Equation (255) describes the concentration of water associated with the fibre as a function of conditioning time, when the concentration of water within the surrounding medium is increased by a small amount ΔC_m. This equation can be fit to the DVS fibre uptake data in Figure 107, Figure 108, Figure 109, and Figure 110, allowing the values of the rate constants at four distinct values of fibre water concentration (C_f) to be determined. The condition in equation (255), that the concentration of water within the surrounding medium remains constant during the conditioning process, is satisfied as the DVS chamber relative humidity, and hence atmospheric water concentration, was observed to be unaffected by the uptake of water by the fibre. Unfortunately, the change in the concentration of water within the medium that occurs in each of the relative humidity steps (Figure 107, Figure 108, Figure 109, Figure 110), is large. However, as a large amount of time was required for the fibre to attain equilibrium at each relative humidity (~65 hrs), employing smaller relative humidity steps was impractical. A more appropriate change

in relative humidity at each step would be ~5%, however this would have increased the number of steps from four to seventeen, increasing the overall time frame of the experiment from 12 to 48 days. As the change in concentration that occurs at each step is large, variation of the rate constants during the conditioning process must be considered. Thus, the rate constants obtained from fitting equation (255) to the fibre uptake data, for each relative humidity step, are approximations describing their average value within a given range of fibre water concentration.

The purpose of this work is to model the hygrothermal behaviour of low-fired carbon-fibre phenolic composites. More specifically, this involves modelling the influence of the fibre on the concentration of water molecules within the surrounding phenolic resin matrix. Thus, in equation (255) the concentration of water within the medium (C_m) represents the concentration of water within the resin matrix that surrounds the fibre. However, the DVS data in Figure 107, Figure 108, Figure 109, and Figure 110, is for low-fired carbon-fibre exposed to atmospheric water vapour. This presents a problem as the behaviour of the fibre within a resin medium is required. Below, a methodology is outlined for obtaining the rate constants, for fibre contained within a resin medium, from atmospheric fibre conditioning data. This analysis depends upon a number of assumptions.

Assumption One

It is assumed that the concentration of water associated with the fibre at equilibrium, at a given relative humidity and temperature, is dependent only upon the atmospheric water concentration of the conditioning environment and not upon the equilibrium water concentration of the surrounding medium. If the fibre water concentration at equilibrium depended upon the concentration of water within the surrounding medium, then much larger fibre water concentrations, and hence percentage change in fibre mass, would be expected when the medium is composed of resin. This is because the concentration of water that is absorbed within polymers at equilibrium, can be much greater than the concentration of water in their surrounding conditioning atmosphere. Tcharkhtchi et al [97] investigated the solubility of water in a range of epoxy resins derived from various epoxy/hardener ratios. In Table 56 below, the solubility they obtained for three different epoxy resins at 20℃ are given.

Resin	**1**	**2**	**3**
Solubility ($mol.m^{-3}.Pa^{-1}$)	2.47	1.88	1.95

Table 56: Solubility of water, in three different epoxy resins, measured by Tcharkhtchi et al [97].

To calculate the resin equilibrium water concentrations that these correspond to, Henry's law (equation (3)) is employed. In Table 57 below, the concentration of water absorbed within the three different epoxy resins has been calculated for when they are at equilibrium at 20℃ and 100% relative humidity.

Resin	1	2	3
$C_{Max}\ (mol.m^{-3})$	5724	4357	4519
$C_a\ (mol.m^{-3})$	0.953	0.953	0.953
C_{Max}/C_a	6006	4572	4742

Table 57: Comparison of the equilibrium concentration of water in the resins investigated by Tcharkhtchi et al [97], compared to the atmospheric water concentration.

Where C_{Max} is the maximum concentration of water absorbed within the resin at equilibrium, and C_a is the concentration of water in the surrounding atmosphere, calculated from the empirical relation given by Wagner et al [100]. This analysis indicates that, at 20℃, the equilibrium concentration of water within these epoxy resins is more than three orders of magnitude greater than the concentration of water in the surrounding atmosphere.

However, as will be shown later in this work (see section 5.3.8.1, page 294), the moisture content of low-fired carbon-fibre in a phenolic based composite is similar to that observed in the non-encapsulated fibre. This independence of fibre water concentration from the concentration of water in the surrounding medium, being dependent only on the concentration of water in the surrounding atmosphere, can be explained as follows.

Water molecules absorbed within phenolic resins can exist in two forms: free water molecules existing between polymer chains, and bound water molecules interacting with polar groups via van der Waals forces and hydrogen bonding. As free molecules are unbound, they are capable of diffusing between the resin and atmosphere and thus, at equilibrium, their concentration within the volume that they occupy will be the same as that of water in the conditioning atmosphere. As only free water molecules can diffuse between the resin and the fibre, and their concentration at equilibrium is equal to that of the atmosphere, then it follows that the concentration of water within the fibre at equilibrium will be independent of the concentration of water in the surrounding resin.

Assumption Two

It is assumed that at a given relative humidity, the presence of the surrounding resin medium does not affect the concentration of water associated with the fibre, at equilibrium, or the rate at which the uptake/loss of water, by the fibre, occurs. This assumption is problematic as the matrix may reduce the availability of functional groups at the fibre surface, through the morphological constraints imposed by the presence of the polymer network, thus reducing the quantity of water that can adsorb to the fibre surface. This would also impact the rate at which water molecules can adsorb to the fibre surface. In the present literature, no studies on the effect of an encapsulating matrix on the rate of water uptake/loss in low-fired carbon-fibre can be found. Thus, although in this work it will be assumed that the equilibrium moisture content and rate of the uptake process, in resin encapsulated fibre, is identical to that of free fibre, some caution should be taken when attempting to draw definitive conclusions from the results of this model.

As discussed earlier, at equilibrium the concentration of water within the atmosphere, at a given relative humidity, and within a polymer in contact with that atmosphere, are not necessarily the same. The concentration of water within some epoxy resins has been observed to be more than three orders of magnitude greater than the concentration of water within the conditioning atmosphere [97]. This difference in concentration, between the atmospheric and resin mediums, presents a problem as rate constants obtained from the atmospheric DVS data, using atmospheric concentrations, will not correctly describe the hygrothermal behaviour of the fibre when the medium is replaced with resin.

This is best illustrated by referring to the equation for the equilibrium constant. As discussed earlier, this is the ratio of the forward and reverse rate constants, or the ratio of the concentration of water associated with the fibre to the concentration of water in the surrounding medium, at equilibrium. At equilibrium at a given relative humidity, the concentration of water within the atmosphere, polymer, and associated with the fibre, are given by C_a, C_p, and C_f, respectively. The equilibrium constants for the fibre, in the presence of the two different mediums, are given by:

$$K_a = \frac{C_f}{C_a} \tag{257}$$

$$K_p = \frac{C_f}{C_p} \tag{258}$$

Where K_a and K_p are the equilibrium constants when the medium is composed of atmosphere, and polymer, respectively.

From the earlier assumption, that the concentration of water associated with the fibre at equilibrium is only a function of atmospheric water concentration, the concentration of water associated with the fibre at equilibrium, is identical in both mediums; thus, from equations (257) and (258):

$$K_a C_a = K_p C_p \tag{259}$$

And as, at a given relative humidity, the concentration of water absorbed within the phenolic resin polymer, at equilibrium, is much larger than the concentration of water within the atmosphere, this implies that:

$$K_a \gg K_p \tag{260}$$

The equilibrium constant K_a is that obtained from atmospheric DVS fibre conditioning data, where it has been assumed that the concentration of water within the surrounding medium (C_m) is equal to the concentration of water within the chamber atmosphere. If K_a is then used for the value of K when calculating the concentration of water associated with a fibre, at equilibrium, encased in a resin medium:

$$C_f = K C_m \tag{261}$$

Then it is apparent from expression (260) that the fibre water concentration will be greatly overestimated. Thus, the equilibrium constant K_a does not describe the equilibrium concentration of water, associated with the fibre, when the surrounding medium is composed of resin.

Earlier, it was assumed that the concentration of water associated with the fibre, at equilibrium at a given relative humidity, was dependent only upon the atmospheric water concentration and not upon the concentration of water within the surrounding polymer medium. Thus, it is apparent that the medium concentration (C_m), employed in the calculation of fibre concentration (C_f) in equation (261), should be the atmospheric water concentration, at the relative humidity of the conditioning environment, and not the equilibrium concentration of water

within the surrounding polymer medium. By switching the medium concentration in equation (261) with that of the concentration of water within the atmosphere, the correct fibre equilibrium water concentration is obtained. Thus, one possible method for applying rate constants obtained from atmospheric fibre conditioning data, to the behaviour of fibre within a resin medium, is to calculate the concentration of water molecules within the resin and then to take this value as being equal to the concentration of the medium (C_m). A second methodology, following from the assumption that fibre equilibrium water concentration is independent of the nature of the surrounding medium, is to take the atmospheric water concentration at each relative humidity step in the DVS data (Figure 107, Figure 108, Figure 109, Figure 110) and then to convert them to the corresponding equilibrium concentration of water, in the resin, at that relative humidity.

Thus, the value of C_m, in equation (261), becomes equal to the concentration of water within the phenolic resin at equilibrium, at the relative humidity of interest, and K takes the value K_p. The value of C_m, for a fibre surrounded by a phenolic resin matrix, is then obtained from:

$$C_m = C_{r_{Max}} RH_f \tag{262}$$

Where $C_{r_{Max}}$ is the maximum concentration of water that can be absorbed by the phenolic resin, in units of $mol.mm^{-3}$, and is equal to the concentration of water within the resin, at equilibrium, at 100% relative humidity.

Both methodologies outlined above allow the rate constants that describe the behaviour of fibre water concentration, for fibres surrounded by resin mediums, to be obtained from atmospheric fibre conditioning data. In the work that follows the second methodology, replacing atmospheric water concentrations with resin equilibrium water concentrations, will be adopted. This allows the concentration of water within the resin to be expressed in terms of its observed concentration, not the actual concentration seen by diffusing water molecules, which is beneficial as this is the concentration employed within GIM to calculate the effect of absorbed water upon the thermo-mechanical properties of the polymer.

The values of the rate constants, r_f and r_b, at four different fibre water concentrations (C_f), can now be obtained by fitting equation (255) to the fibre DVS data in section 5.3.4 (see page 279). The values of the rate constants at any fibre water concentration, can then be estimated

by fitting an appropriate function to the r_f/C_f, and r_b/C_f, relationships. However, this is made difficult by the fact that each relationship contains only four data points. Furthermore, the actual relationship between the rate constants and C_f is unknown, as the simplified model employed in this work is novel and thus no prior work within the literature has established the behaviour of these parameters with respect to C_f. As the relationship is unknown, there is uncertainty in the behaviour of the rate constants between data points which makes selection of an appropriate fitting function difficult. Inaccuracies in the predicted behaviour of the rate constants, as a function of C_f, will affect the accuracy of both the concentration of water associated with the fibre, at equilibrium, and the rate of the water uptake/loss process, predicted by the model. To prevent the introduction of inaccuracies into model predictions, a different methodology will be adopted in this work.

5.2.2.5. Methodology for Obtaining the Rate Constants as Functions of C_f and C_r in order to Minimise the Introduction of Errors into the Fitting Process

As discussed previously, the behaviour of the rate constants with respect to C_f is unknown and this complicates the fitting process as only limited data for the relationship between the rate constants, and C_f, is available. To minimise the introduction of errors into the predicted behaviour of the rate constants, resulting from inappropriate fitting function selection, the following approach will be taken.

The equation describing the behaviour of the forward rate constant with respect to C_f, $r_{f_{(C_f)}}$, is obtained by fitting an appropriate function to the r_f/C_f relationship. This is obtained from fitting the solution of the rate equation to the DVS data, as described previously. The equilibrium constant is then calculated as a function of the concentration of water within the resin at equilibrium:

$$K_{(C_r)} = \frac{C_f}{C_r} \tag{263}$$

Where C_f and C_r are the fibre and resin equilibrium water concentrations at a given relative humidity. Here it has been assumed that the relationship between resin water concentration, and relative humidity, obeys Henry's law (see section 1.3.2, page 10). Although the concentration of water associated with the fibre at equilibrium has only been measured at four distinct relative humidities, its expected behaviour can be inferred by referring to that which is observed in other low-fired carbon-fibres in the literature. As the behaviour of the equilibrium concentration of

water within the fibre and resin, as a function of relative humidity, is approximately known, the calculation of $K_{(C_r)}$ from these two parameters is considerably more accurate than employing equation (264) below, as the expected behaviour of the two rate constants, with respect to C_f, is unknown.

$$K_{(C_r)} = \frac{r_{f_{(C_f)}}}{r_{b(C_f)}} \tag{264}$$

Thus, for a given concentration of water within the resin and fibre, the forward rate constant is calculated from the function $r_{f_{(C_f)}}$, obtained from fitting to the r_f/C_f data, and the backward rate constant is calculated from equation (265) below.

$$r_{b(C_f,C_r)} = \frac{r_{f_{(C_f)}}}{K_{(C_r)}} \tag{265}$$

As the ratio of the two rate constants is determined by $K_{(C_r)}$, whose behaviour is well understood as discussed earlier, this parameter should exhibit a good degree of accuracy. This implies that the model predicted value of fibre equilibrium water concentration, at a given relative humidity, should be close to that observed experimentally. The magnitudes of the rate constants depend upon the function $r_{f_{(C_f)}}$, whose expected behaviour is unknown. Thus, the rate of fibre uptake/loss predicted by the model has the potential to deviate from that observed experimentally. The overall benefit of this alternative methodology for obtaining the rate constants, is an improvement in the accuracy of the predicted equilibrium water concentration of the fibre. There is no overall improvement in the accuracy of predictions relating to the rate at which the fibre gains/loses water.

5.2.3. Implementation of the Fibre Model Within the Framework of Previous Diffusion Modelling

Earlier in this work (section 2.2.2, page 46), a model was developed to describe the diffusion and hydrolysis phenomena that occur in DGEBA-DDA epoxy resin. This framework can be adapted to model the absorption/desorption behaviour of low-fired carbon-fibre phenolic composites. The structure of the composite is simplified to one in which the material consists of a homogenous blend of low-fired carbon-fibre with phenolic resin. In this simplification

anisotropy, resulting from fibre orientation, is omitted and thus the structure is approximated as being isotropic. Under this assumption, the composite structure reduces to that of a short-fibre composite in which fibres are randomly orientated and fibre length is negligible.

In the literature, no studies on the effect of adsorbed/absorbed water upon the engineering properties of low-fired carbon-fibre have been conducted. In contrast, water absorbed within epoxy and phenolic resins is known to have an effect upon their thermo-mechanical properties: reduction in glass transition temperature [3, 5], reduction in engineering moduli [118, 119] etc. If the effect of moisture upon the thermo-mechanical properties of the fibre is assumed to be negligible, then the fibre is essentially inert, and thus it is the effect of moisture upon the thermo-mechanical properties of the polymer matrix that impacts the mechanical performance of the composite.

This simplifies the composite modelling allowing the thermo-mechanical property profiles of the matrix to be easily obtained. These can then be inserted directly into a long-fibre composite model (non-diffusive) to determine the overall impact of absorbed moisture upon the engineering properties of the composite.

The rate equation derived earlier for non-encapsulated low-fired carbon-fibre, can be adapted for a volume element of composite as follows. The rate equation is given by:

$$\frac{d}{dt} C_f = r_f C_r - r_b C_f \tag{266}$$

Where C_r is the concentration of water molecules within the phenolic resin matrix, in units of $mol.mm^{-3}$. Thus, the governing equation for diffusion becomes:

$$\frac{\partial C_r}{\partial t} = -\frac{\partial J}{\partial x} - \frac{\partial C_f}{\partial t} \tag{267}$$

Substituting equation (266) into equation (267), one obtains:

$$\frac{\partial C_r}{\partial t} = -\frac{\partial J}{\partial x} + r_b C_f - r_f C_r \quad (268)$$

To determine the percentage change in mass, resulting from the absorption of water molecules, within a given volume element, it is necessary to account for the volume fraction of both the resin and fibre. Defining the fibre volume fraction as v_f, the volume of the resin, and of the fibre, within an element of volume V, can be expressed as $(1 - v_f)V$, and $v_f V$, respectively, both in units of mm^3. Thus, the percentage change in mass of a given volume element can be obtained from:

$$am_c = m_c + m_r + m_f \quad (269)$$

$$\%_c = 100\left(\frac{m_r + m_f}{m_c}\right) \quad (270)$$

$$\%_c = 100\left(\frac{(1 - v_f)C_r + v_f C_f}{(1 - v_f)\rho_r + v_f \rho_f}\right) \quad (271)$$

Where m_c is the dry mass of the composite, m_r and m_f are the mass of water molecules associated with the resin, and fibre, respectively, $\%_c$ is the percentage change in mass of the volume element, and ρ_r and ρ_f are the densities of the resin, and fibre, respectively both in units of $g.mm^{-3}$.

5.3. Results and Discussion

5.3.1. DVS Analysis of the Hygrothermal Behaviour of Low-Fired Carbon-Fibre

The DVS data discussed in this section, and shown below in Figure 103 is for a low-fired carbon-fibre and was provided courtesy of Stone [123]. All aspects of the DVS experiment, including sample preparation, were performed by Stone [123], with the purpose of the work that follows being to analyse their experimental results.

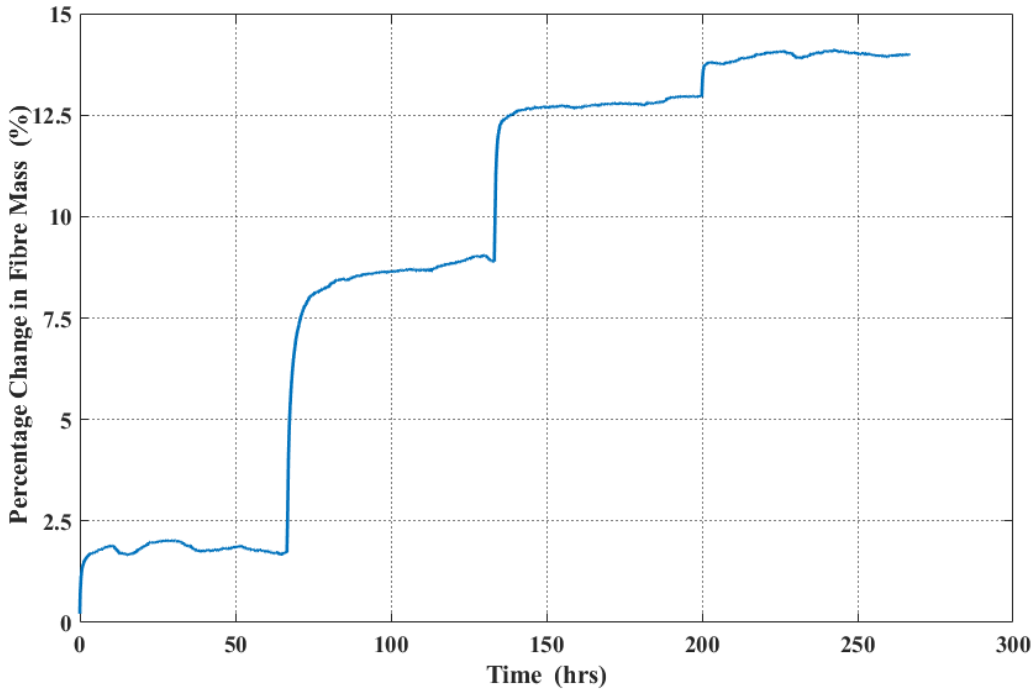

Figure 103: DVS data provided by Stone [123] showing the percentage change in mass of a low-fired carbon-fibre as a function of relative humidity and conditioning time.

The fibre material was free, in other words not encased within a thermoset matrix, and thus the observed behaviour is that representative of the movement of water between the fibre and atmosphere. Prior to the DVS experiment commencing, the fibre was heated to 150℃ and dried for 3 hours in free-flowing air to ensure complete evaporation of previously absorbed moisture. This step ensures that an accurate dry fibre mass is obtained and is essential as this parameter affects the calculation of the percentage change in mass, and thus the concentration of water associated with the fibre, at a given time in the DVS experiment. After the drying process was completed, the fibre was transferred to the conditioning chamber of the DVS instrument and an incremental relative humidity analysis was performed. This involves increasing the relative humidity of the chamber in distinct steps, with time provided at each step to allow the material moisture content to reach equilibrium with the surrounding atmosphere. Initially, the chamber relative humidity was 1.3%, this was then increased to 25% and held for ~65 hours. This was

followed by steps to 45%, 65%, and 85%. The fibre was exposed to each relative humidity for an identical period of time.

5.3.2. Converting Fibre Moisture Content from Mass Percentage to Water Concentration

Before interpreting the results of the DVS data provided by Stone [123], fibre moisture content will be re-expressed in terms of the concentration of water associated with the fibre, as these units are more suitable for the modelling that will be performed in this work. The percentage, by mass, of water associated with the fibre is given by:

$$\%_w = 100 \frac{m_w}{m_f} \tag{272}$$

Where m_w and m_f are the mass of the water, and fibre, respectively, both in units of g. The mass of the fibre can be expressed in terms of its density and volume as:

$$m_f = \rho_f V \tag{273}$$

Where ρ_f is the density of the fibre, in units of $g.mm^{-3}$, and V is the fibre volume in units of mm^3. The fibre density employed in this work was obtained from gas pycnometry and found to be 1.82 $g.mm^{-3}$. Similarly, the mass of water associated with the fibre can be expressed in terms of its concentration and the volume of the fibre, as:

$$m_w = C_f V \tag{274}$$

Where C_f is the concentration of water associated with the fibre, in units of $g.mm^{-3}$, and V is the fibre volume in units of mm^3. Substituting equation (273) and equation (274), into equation (272), gives:

$$\%_w = 100 \frac{C_f V}{\rho_f V} = 100 \frac{C_f}{\rho_f} \tag{275}$$

Rearranging equation (275) in terms of C_f:

$$C_f = \frac{\rho_f \, \%_w}{100} \tag{276}$$

And finally, the concentration of water associated with the fibre is expressed as a molar quantity:

$$C_f = \frac{\rho_f \, \%_w}{1800} \tag{277}$$

Where C_f is the concentration of water associated with the fibre in units of $mol.mm^{-3}$. It is important to note that 'water associated with the fibre' includes both that adsorbed at the fibre surface, and that absorbed within fibre pore volume. The assumption in deriving equation (275), that the volume occupied by adsorbed/absorbed water is equal to the volume of the fibre, is only approximately true. This is because, firstly, the volume occupied by water molecules adsorbed at the fibre surface is not part of the volume of the fibre itself. Secondly, the pores responsible for absorption in activated carbon are hypothesised by Do et al [65] to exist very close to the surface of the material. If the pores responsible for absorption in low-fired carbon-fibre are similar to those in activated carbon, then this would suggest that the bulk of the internal fibre volume is not susceptible to the absorption of water molecules. As a result, it is not possible to precisely determine the volume within which adsorbed/absorbed water is contained, and thus the value of C_f calculated by equation (277) is only an approximation. Figure 104 below shows the result of applying equation (277) to the DVS data of Stone [123] in Figure 103.

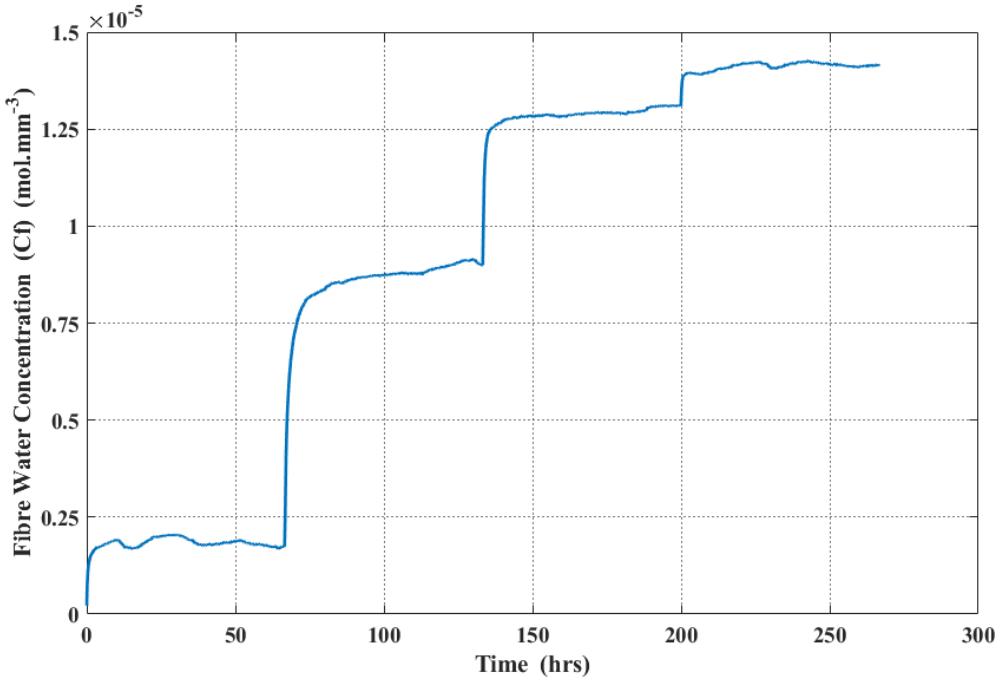

Figure 104: DVS data of Stone [123] adjusted to show the concentration of water associated with the fibre, C_f, as a function of conditioning time and relative humidity.

5.3.3. DVS Results Analysis - Concentration of Water Associated with the Fibre at Equilibrium as a Function of Relative Humidity

The DVS data in Figure 104 indicates that, on moving to a higher relative humidity, the concentration of water associated with the fibre initially increases, before subsequently reaching a plateau. The average value of C_f within this plateau region is equal to the concentration of water associated with the fibre, at equilibrium, at that specific relative humidity. In Figure 105 below, the concentration of water associated with the fibre, at equilibrium, has been plotted as a function of the fractional relative humidity; where the fractional relative humidity is given by:

$$RH_f = \frac{RH}{100} \tag{278}$$

Where RH is the relative humidity in units of %.

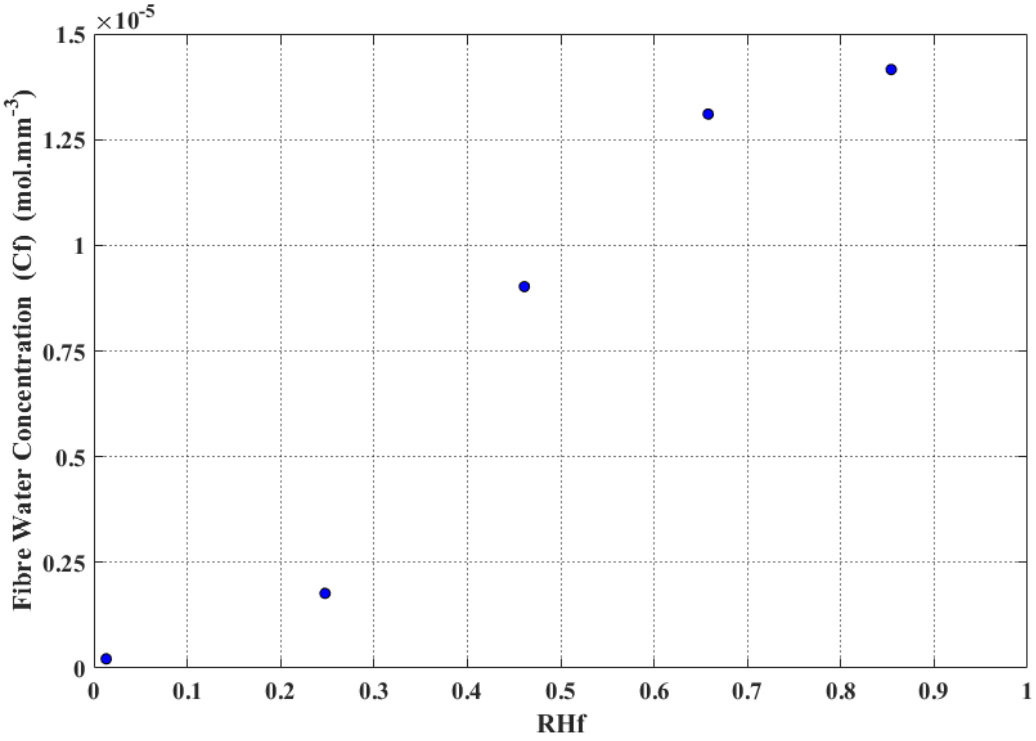

Figure 105: Concentration of water associated with the fibre, at equilibrium, as a function of the fractional relative humidity.

The experimental data indicates that initially, at low relative humidity (<25%), the concentration of water associated with the fibre, at equilibrium, increases slowly with increasing relative humidity. After a threshold relative humidity is reached (~25%), further increases in relative humidity result in a much larger increase in fibre equilibrium water concentration than was observed at lower relative humidities. Finally, above 65% relative humidity, the change in fibre equilibrium water concentration with increasing relative humidity becomes comparable to that observed at low relative humidity (<25%). This is the so-called S-Shaped absorption behaviour that is observed to be characteristic of the behaviour of low-fired carbon-fibres [29], and activated carbons [64, 65], under hygrothermal conditions.

In order to obtain the concentration of water associated with the fibre, at equilibrium, at any relative humidity, it is necessary to fit an appropriate function to the data in Figure 105. An inverse tangent function was deemed most suitable for this purpose as it is capable of describing the S-Shaped form of the C_f/RH_f relationship. The inverse tangent function employed was of the form:

$$C_{f_{(RH_f)}} = A_3 \, tan^{-1}\left(\left(A_1 RH_f\right) + A_2\right) + A_4 \qquad (279)$$

Where $C_{f_{(RH_f)}}$ is the concentration of water associated with the fibre at equilibrium, at a fractional relative humidity RH_f, in units of $mol.mm^{-3}$, and A_1, A_2, A_3, and A_4, are constants. The result of fitting equation (279) to the C_f/RH_f relationship in Figure 105 is shown below in Figure 106, along with the fit determined constants in Table 58.

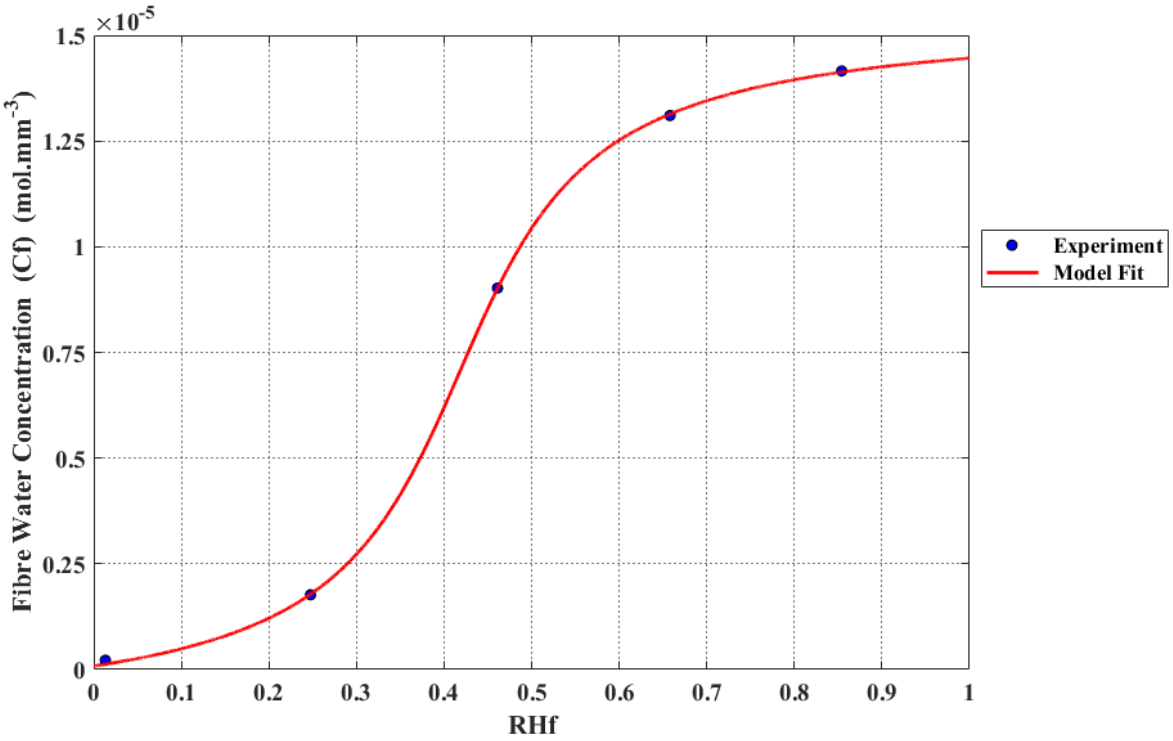

Figure 106: Result of fitting equation (279) to the C_f/RH_f data in Figure 105.

A_1	A_2	A_3	A_4
8.925	-3.737	5.346×10^{-6}	7.08×10^{-6}

Table 58: Constants obtained from fitting equation (279) to the C_f/RH_f data in Figure 105.

5.3.4. DVS Results Analysis - Fibre Uptake Behaviour within Distinct Relative Humidity Steps

The four steps in relative humidity in the DVS data of Stone [123], in Figure 104, are shown separately below in Figure 107, Figure 108, Figure 109, and Figure 110.

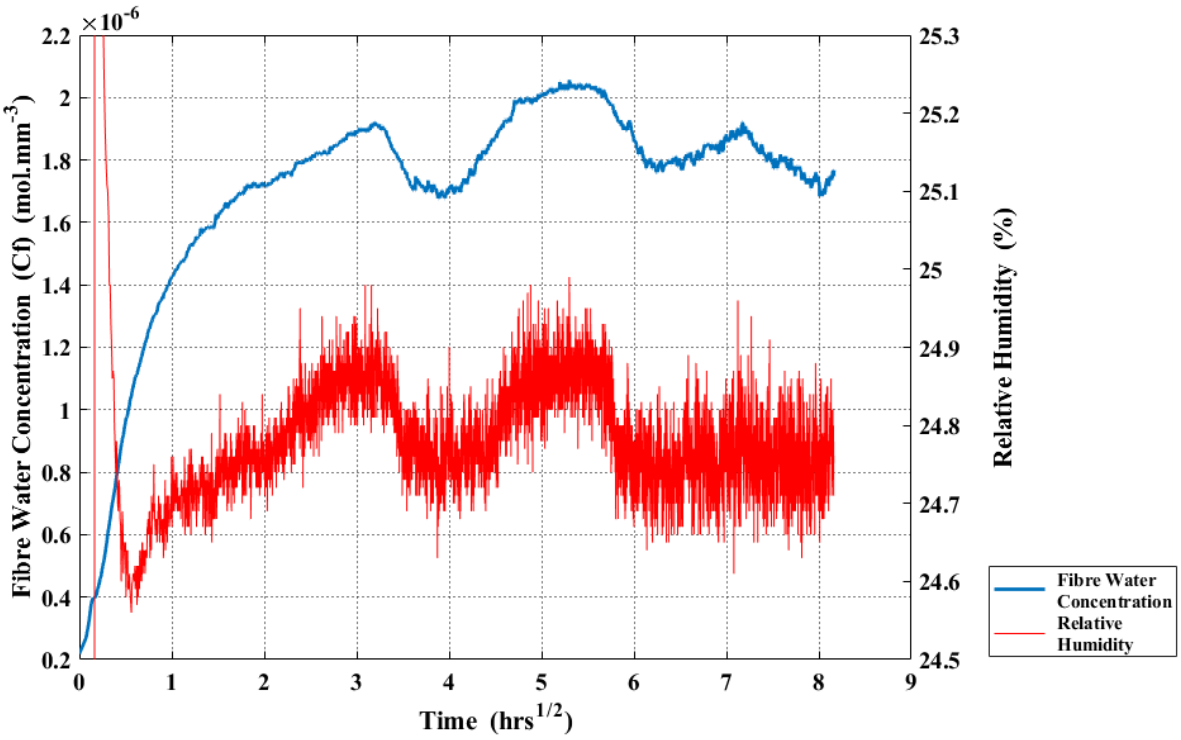

Figure 107: DVS data of Stone [123] showing the concentration of water associated with the fibre, C_f, as a function of conditioning time. The fibre is initially at equilibrium at a relative humidity of 1.32%, before being exposed to a relative humidity of 25%.

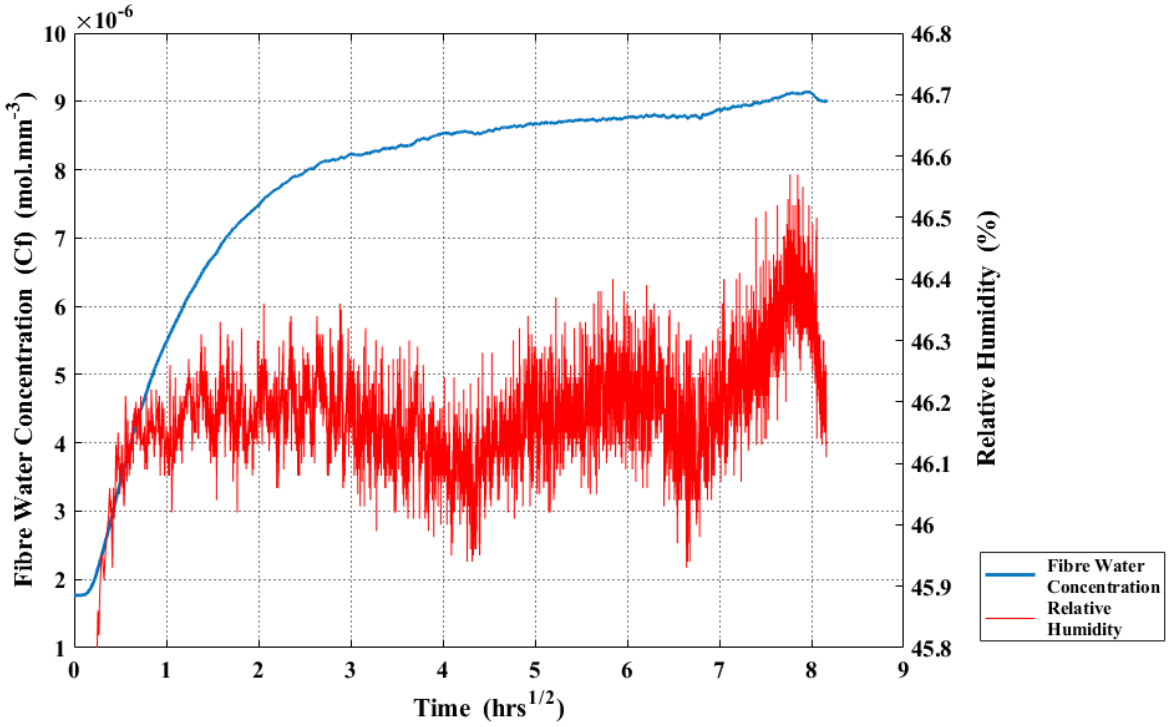

Figure 108: DVS data of Stone [123] showing the concentration of water associated with the fibre, C_f, as a function of conditioning time. The fibre is initially at equilibrium at a relative humidity of 25%, before being exposed to a relative humidity of 45%.

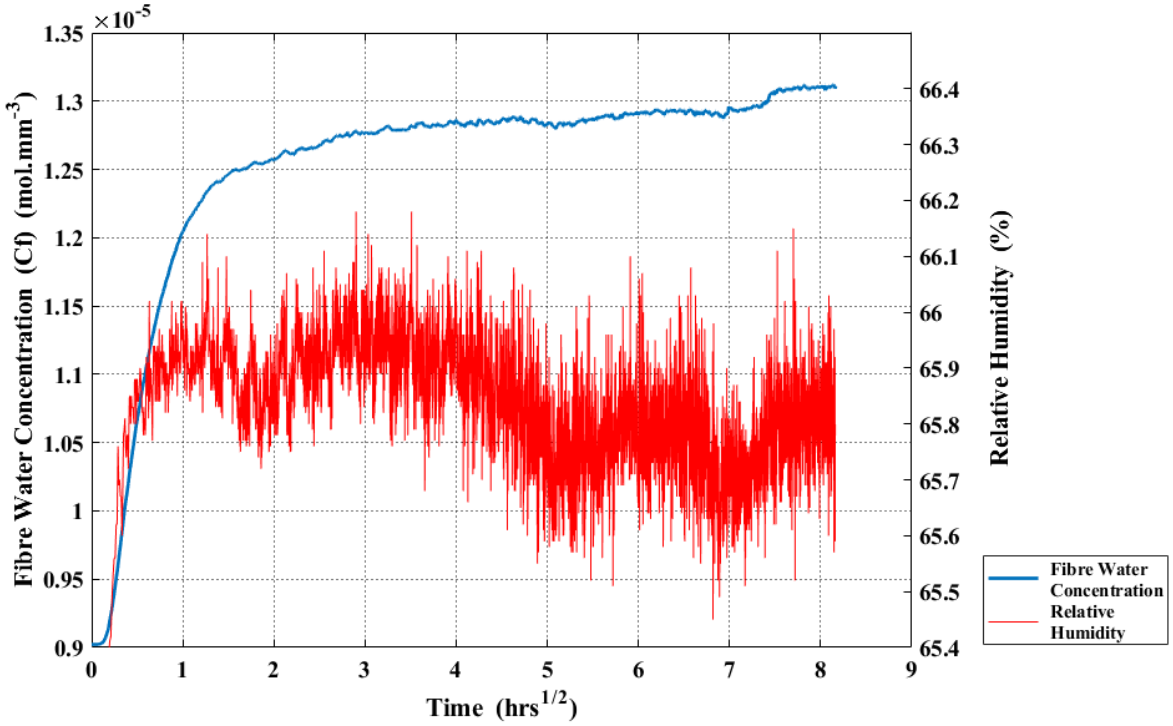

Figure 109: DVS data of Stone [123] showing the concentration of water associated with the fibre, C_f, as a function of conditioning time. The fibre is initially at equilibrium at a relative humidity of 45%, before being exposed to a relative humidity of 65%.

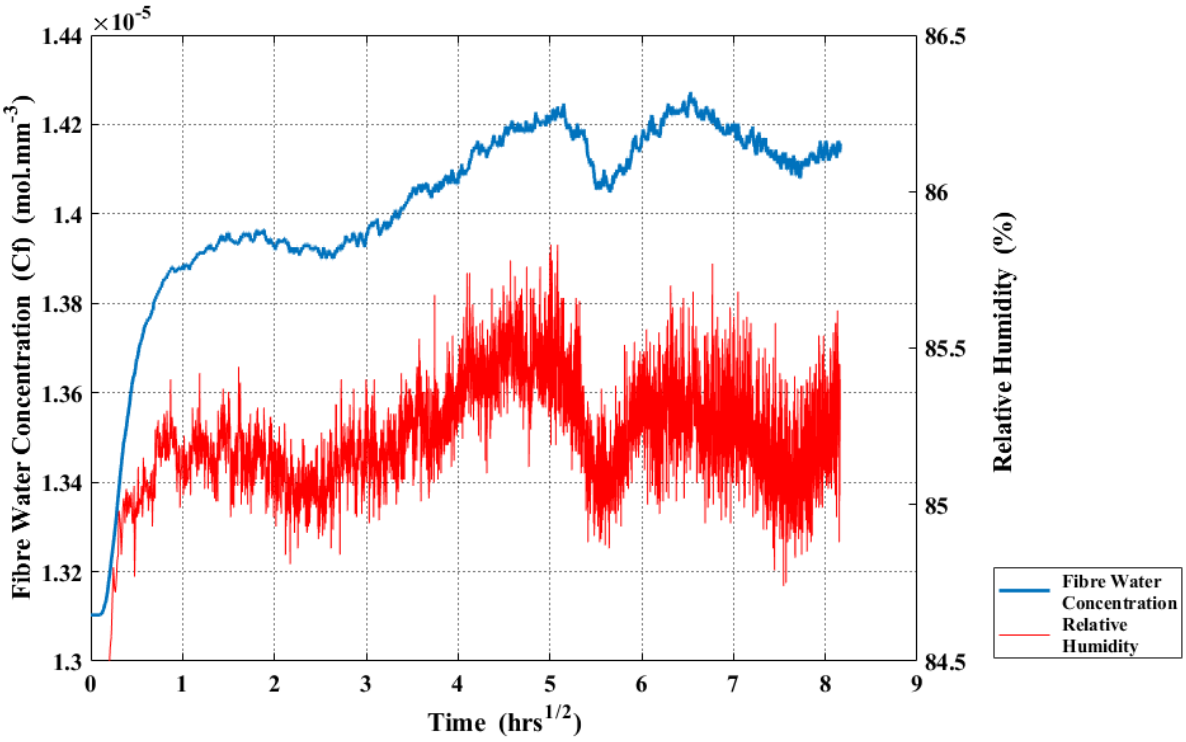

Figure 110: DVS data of Stone [123] showing the concentration of water associated with the fibre, C_f, as a function of conditioning time. The fibre is initially at equilibrium at a relative humidity of 65%, before being exposed to a relative humidity of 85%.

Here, both the concentration of water associated with the fibre (C_f), and the relative humidity of the DVS chamber, have been plotted as a function of the square root of conditioning time.

In Figure 107, depicting the fibre uptake behaviour in the 1.32% to 25% relative humidity step, fibre water concentration initially increases, before beginning to level off at extended conditioning times. However, the fibre then proceeds to sequentially lose, and gain, water in a broadly sinusoidal pattern. After a conditioning time of ~8 $hrs^{\frac{1}{2}}$, the magnitude of the oscillations in fibre water concentration have reduced, however more data would be required to determine whether a plateau in fibre water concentration has been achieved.

Anomalous behaviour is also apparent in Figure 110 which depicts the fibre uptake behaviour in the 65% to 85% relative humidity step. After a conditioning time of ~1 $hrs^{\frac{1}{2}}$, a plateau in fibre water concentration is observed. However, after ~2.5 $hrs^{\frac{1}{2}}$ a sharp increase in fibre water

concentration occurs, followed by broadly sinusoidal behaviour similar to that observed in the low relative humidity step data (Figure 107).

Small perturbations in fibre water concentration, in the plateau region, are also observed in the mid relative humidity range (Figure 108 and Figure 109). However, the overall increase in fibre water concentration that occurs in these steps, is much larger than that which occurs at the low and high relative humidities. As a result, the overall impact of these perturbations on the data, is reduced.

This anomalous behaviour can be explained by referring to the relative humidity/time relationship in each figure. It is apparent that at each step, the relative humidity of the DVS chamber oscillated about the desired relative humidity, throughout the course of the conditioning experiment. The periodic increase, and subsequent reduction, in fibre water concentration, occurring in the plateau region, tracks this increase, and decrease, in DVS chamber relative humidity. Thus, it is the limitation of the performance of the DVS instrument that is responsible for the observed oscillation in fibre water concentration in the plateau region.

5.3.5. Obtaining K as a Function of C_r

In the previous section the equilibrium constant K was introduced, which was defined as:

$$K = \frac{C_f}{C_r} \tag{280}$$

Where C_f and C_r are the concentration of water at equilibrium associated with the fibre, and in the surrounding resin medium, respectively. Thus, to obtain the value of the equilibrium constant at a given conditioning relative humidity, both the fibre and resin equilibrium water concentrations, at that relative humidity, must be known.

Figure 111 below shows the equilibrium water concentration of both the resin and fibre, as a function of relative humidity.

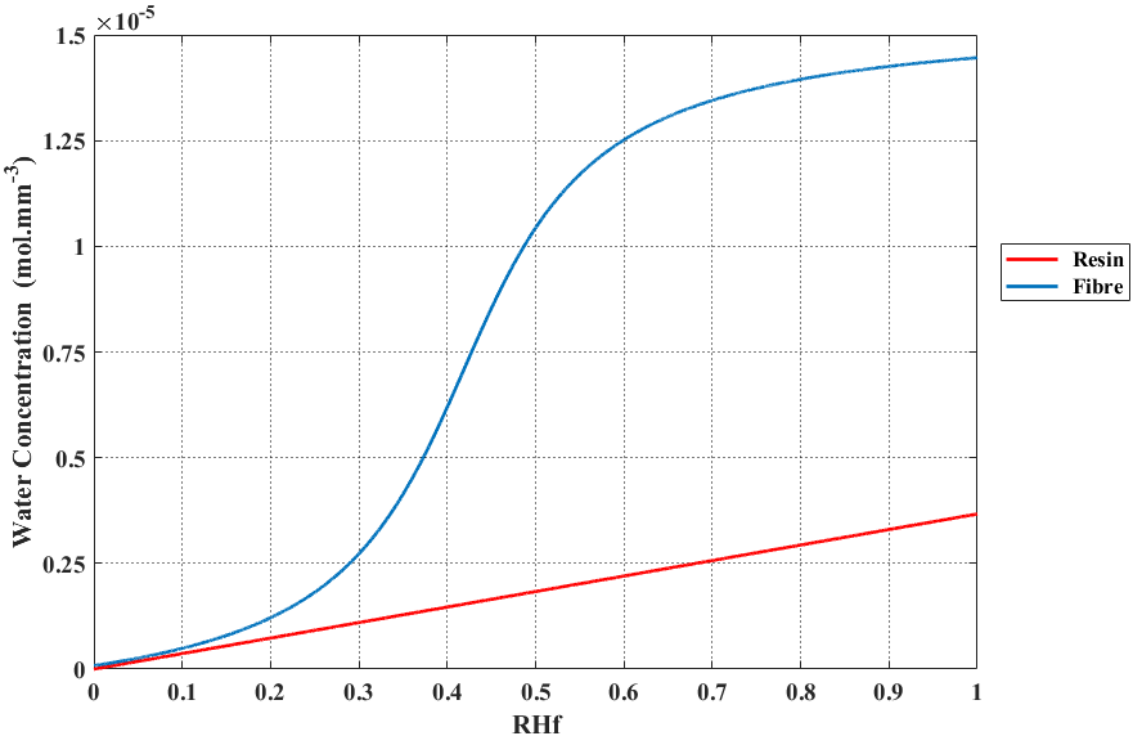

Figure 111: Resin and fibre equilibrium water concentration as a function of relative humidity.

The relationship between the equilibrium water concentration of the phenolic resin, and relative humidity, was estimated from equation (209) assuming that the material obeyed Henry's law. The value of C_{Max} in equation (209) was calculated from the diffusive properties of the phenolic resin that was investigated previously in section 4.3.1.2, page 222. The equilibrium water concentration of the fibre was predicted from the inverse tangent function (equation (279)), using the values of the constants in Table 58

The calculated fibre, and resin, equilibrium water concentrations, displayed in Figure 111, were then used to calculate the value of the equilibrium constant as a function of relative humidity, using equation (280). Below, in Figure 112, the calculated value of the equilibrium constant (K) has been plotted as a function of resin equilibrium water concentration.

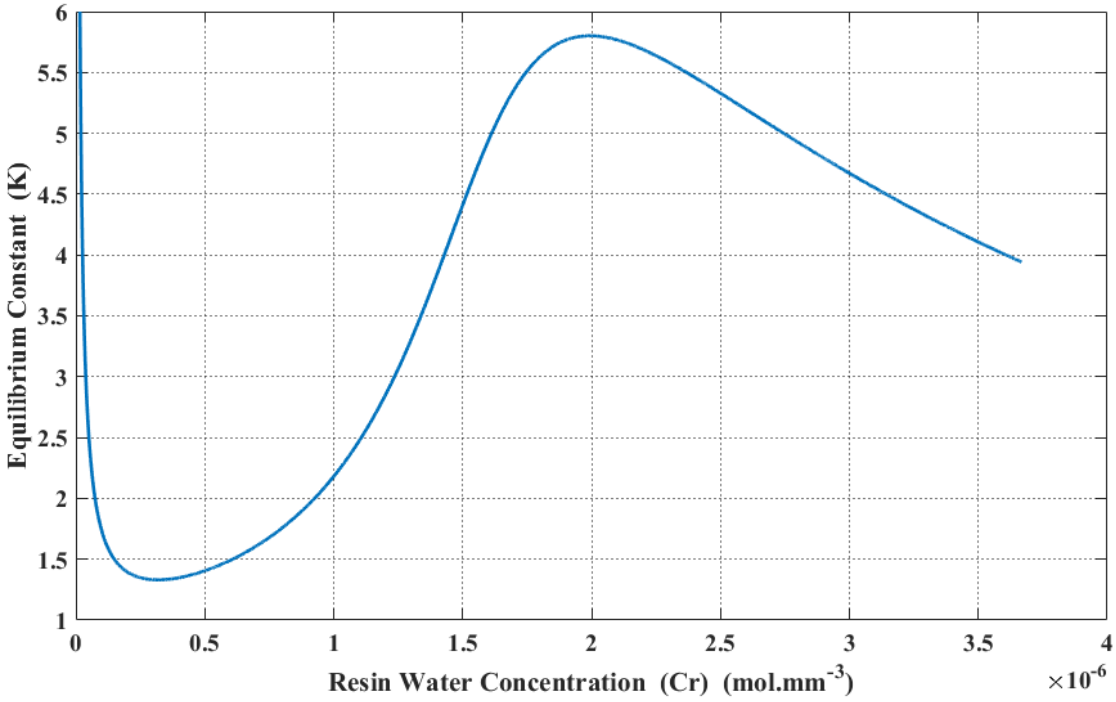

Figure 112: Equilibrium constant K as a function of resin equilibrium water concentration C_r.

Figure 112 shows that the value of the equilibrium constant varies considerably with the equilibrium water concentration of the surrounding resin medium. As C_r decreases below ~0.25 $mol.mm^{-3}$ the equilibrium constant increases rapidly, becoming infinite when C_r is equal to zero. As the equilibrium water concentration of both the fibre and resin, at 0% relative humidity, is zero, this behaviour is anomalous. However, the source of this inconsistency can be attributed to the inverse tangent function that was fit to the C_f/RH_f data in Figure 105. Inspecting the value of this function (equation (279)) at 0% relative humidity, using the values of the constants from Table 58, indicates that the predicted fibre water concentration, at equilibrium, is $8.033 \times 10^{-8}\ mol.mm^{-3}$, when in fact it should be zero. This discrepancy, between the value of C_f predicted by the fitted function and the expected value, is most likely as a result of the lack of experimental measurements of C_f in the low relative humidity range. There is only one measurement of C_f below 25% relative humidity, which effects the accuracy of the fit within this region. In the work that follows, the value of the equilibrium constant when C_r is less than ~0.25 $mol.mm^{-3}$ is assumed to take a constant value of 1.33. This ensures that fibre water concentration falls with resin water concentration, becoming zero when the relative humidity is zero.

As C_r is increased above ~0.25 $mol.mm^{-3}$ the equilibrium constant increases slowly. Assuming that the moisture uptake behaviour of the fibre can be described by the model proposed by Do et al [65] for activated carbon, fibre uptake in this region is dominated by surface adsorption. Thus, the change in both resin, and fibre, equilibrium water concentration will be expected to be approximately proportional to the change in water concentration of the conditioning atmosphere. The gradient of the equilibrium constant, as a function of C_r, continues to increase as C_r is increased further. This results in a rapid increase in the equilibrium constant in the range $\sim 0.75 \times 10^{-6}\ mol.mm^{-3} < C_r < \sim 1.75 \times 10^{-6}\ mol.mm^{-3}$. This can be attributed to the concentration of water at the fibre surface becoming sufficient to allow the formation of water clusters, with their subsequent absorption into fibre pore volume. Thus, a new fibre uptake process, namely absorption, becomes activated and the change in fibre water concentration with increasing relative humidity becomes amplified, resulting in a rapid increase in the value of the equilibrium constant. When C_r is increased beyond $\sim 1.75 \times 10^{-6}\ mol.mm^{-3}$ the equilibrium constant begins to decrease. This is because, at high relative humidity, the fibre pore volume becomes saturated and thus no further absorption can occur. This reduces the overall change in fibre water concentration that occurs within this region as relative humidity is increased.

Furthermore, if the results are interpreted in terms of the model proposed by Do et al [65] for water uptake in activated carbon, then the fibre uptake behaviour at low (<20%), and high (>70%) relative humidity, is dominated by adsorption. Figure 111 indicates that the change in the concentration of water adsorbed at the fibre surface, with increasing relative humidity, is less at high relative humidities than it is at low relative humidities. This could be attributed to the further growth of water clusters, at the fibre surface, becoming less energetically favourable as cluster size increases. Once fibre pore volume becomes saturated, this would manifest itself in an overall reduction in the change in the concentration of water, associated with the fibre, with increasing relative humidity. As overall, the change in resin water concentration, with relative humidity, is now greater than the change in fibre water concentration, the net effect is a reduction in the value of the equilibrium constant.

As the relationship between the equilibrium constant and C_r is complex, it is difficult to define a function that accurately encompasses the behaviour of K over the full range of values of C_r. Thus, the behaviour of the equilibrium constant is split into three separate regions. Within each region, a unique function describes the behaviour of K with respect to C_r. Table 59 below shows these three regions, designated A, B, and C, with their associated functions and applicable concentration ranges:

Region	Applicable range of C_r $(mol.mm^{-3})$	Function
A	$C_r \leq 3.9104 \times 10^{-7}$	$K_{(C_r)} = 1.33$
B	$3.9104 \times 10^{-7} < C_r \leq 1.75234 \times 10^{-6}$	$K_{(C_r)} = f_{A_{(C_r)}}$
C	$C_r > 1.75234 \times 10^{-6}$	$K_{(C_r)} = f_{B_{(C_r)}}$

Table 59: Functions describing K as a function of C_r for the three different concentration regions.

As discussed previously, the value of the equilibrium constant is assumed to be constant within region A. In regions B and C, the behaviour of the equilibrium constant, as a function of C_r, is obtained by fitting a sixth order polynomial to the K/C_r data. The sixth order polynomial functions, $f_{A_{(C_r)}}$ and $f_{B_{(C_r)}}$, are of the form:

$$f_{(C_r)} = A_1 {C_r}^6 + A_2 {C_r}^5 + A_3 {C_r}^4 + A_4 {C_r}^3 + A_5 {C_r}^2 + A_6 C_r + A_7 \quad (281)$$

Where the parameters $A_1 \rightarrow A_7$ are constants whose values are obtained by fitting each function to the data in Figure 112 within the appropriate concentration range (C_r), given above in Table 59. Table 60 below shows the values of these constants, for the functions $f_{A_{(C_r)}}$ and $f_{B_{(C_r)}}$, obtained from the fitting process:

Function	A_1	A_2	A_3	A_4	A_5	A_6	A_7
$f_{A_{(C_r)}}$	4.087×10^{36}	-2.936×10^{31}	8.054×10^{25}	-1.075×10^{20}	7.56×10^{13}	-25841900	4.679
$f_{B_{(C_r)}}$	-2.11×10^{35}	3.820×10^{30}	-2.882×10^{25}	1.16×10^{20}	-2.626×10^{14}	315777000	-150.772

Table 60: Values of the constants $A_1 \rightarrow A_7$ for the functions $f_{A_{(C_r)}}$ and $f_{B_{(C_r)}}$.

Figure 113 shows the behaviour of the equilibrium constant K, as a function of C_r, predicted by the three functions in Table 59 (dashed red line), compared to that calculated previously in Figure 112 (solid blue line). The results indicate that the two polynomial functions, $f_{A_{(C_r)}}$ and $f_{B_{(C_r)}}$, accurately predict the behaviour of K within their respective regions (B and C). The value of K, in region A, is approximated as taking a constant value. This is because, as was discussed earlier, the fibre equilibrium water concentration that is predicted by equation (279) at very low relative humidities, is erroneous, resulting in an equilibrium constant that becomes infinite at 0% relative

humidity. Thus, in the low relative humidity range, K isn't calculated from equation (280) and is instead approximated as taking a constant value.

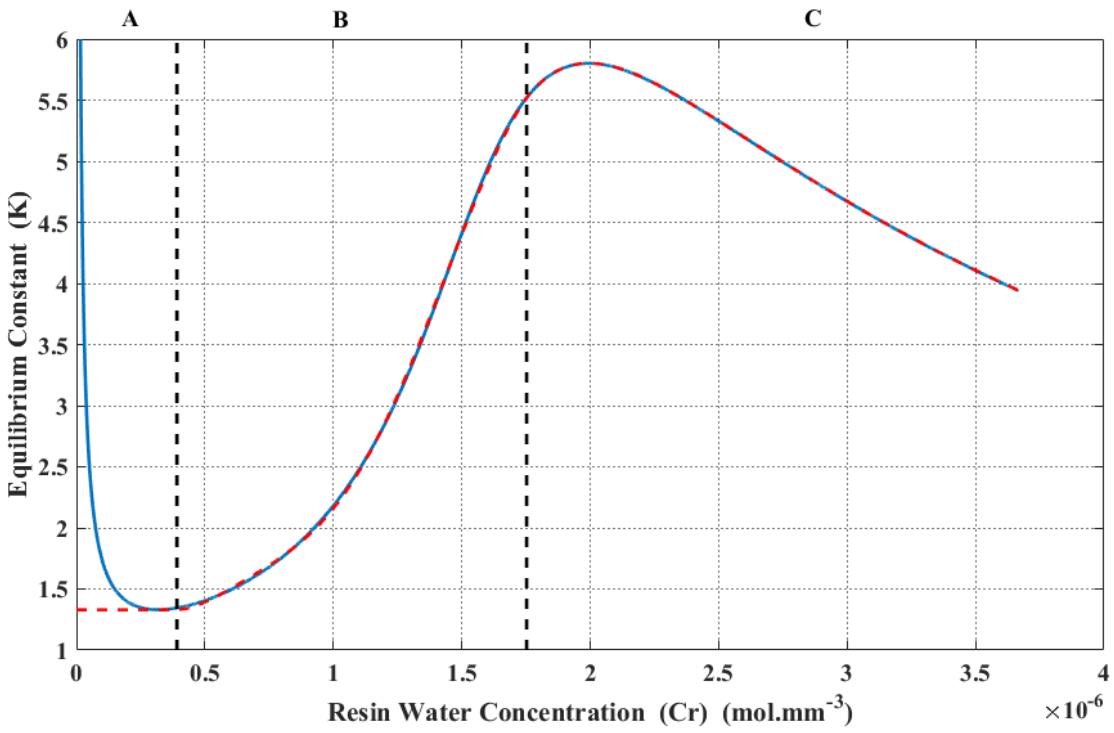

Figure 113: Result of fitting the three equilibrium constant functions to their respective regions A, B, and C.

5.3.6. Obtaining r_f as a function of C_f

The value of the rate constant (r_f) for a range of different fibre water concentrations (C_f), can be obtained by fitting equation (255) to the DVS fibre uptake data in Figure 107, Figure 108, Figure 109, and Figure 110. As discussed previously (see section 5.2.2.4.2, page 263), the change in relative humidity that occurs within these data sets, and hence atmospheric water concentration, is large and thus it is possible that the values of the rate constants will vary before the fibre attains its equilibrium moisture content. As a consequence, the rate constants obtained from the DVS data are approximate values, describing their average behaviour within each relative humidity range. The value of C_m in each step, the concentration of water in the medium, is the equilibrium concentration of water within the phenolic resin matrix at that relative humidity. This can be calculated from equation (209). Thus, by way of example, in Figure 107 where the relative humidity of the DVS chamber is increased from 1.32%, to 25%, the concentration of the medium is given by:

$$C_m = C_{r_{Max}} RH_f = 0.25\, C_{r_{Max}} \quad (282)$$

Where C_m is the concentration of water within the surrounding phenolic resin medium, at equilibrium, in units of $mol.mm^{-3}$, $C_{r_{Max}}$ is the maximum possible equilibrium concentration of water that the phenolic resin can absorb, in units of $mol.mm^{-3}$, and RH_f is the fractional relative humidity of the conditioning environment.

As highlighted previously, it is difficult to discern an equilibrium plateau in fibre water concentration in the DVS data for the low (1.32%-25%), and high (65%-85%), relative humidity steps, Figure 107 and Figure 110 respectively. Furthermore, although approximate plateaus in fibre water concentration can be observed in the mid-humidity steps (Figure 108 and Figure 109), a gradual increase in fibre water concentration occurs over extended conditioning times rendering the determination of a precise, equilibrium water concentration, impossible. Anomalous behaviour of fibre water concentration, within the region where equilibrium is expected, has an effect upon the quality of the fit obtained from fitting equation (255) to the fibre uptake DVS data.

Given these difficulties, it is more appropriate to obtain the rate constants that describe the bulk of the uptake process, at a given relative humidity, rather than attempting to account for small anomalous variations in fibre water concentration that occur over extended conditioning times. Thus, in the fitting process that follows, only data that describes the bulk of the fibre uptake process, in Figure 107, Figure 108, Figure 109, and Figure 110, has been employed. This was achieved by retaining the fibre mass change data at early conditioning times, with those anomalous measurements observed over extended conditioning times, being omitted. Below in Figure 114, Figure 115, Figure 116, and Figure 117, the results of fitting equation (255) to the truncated fibre DVS data of Stone [123], are shown.

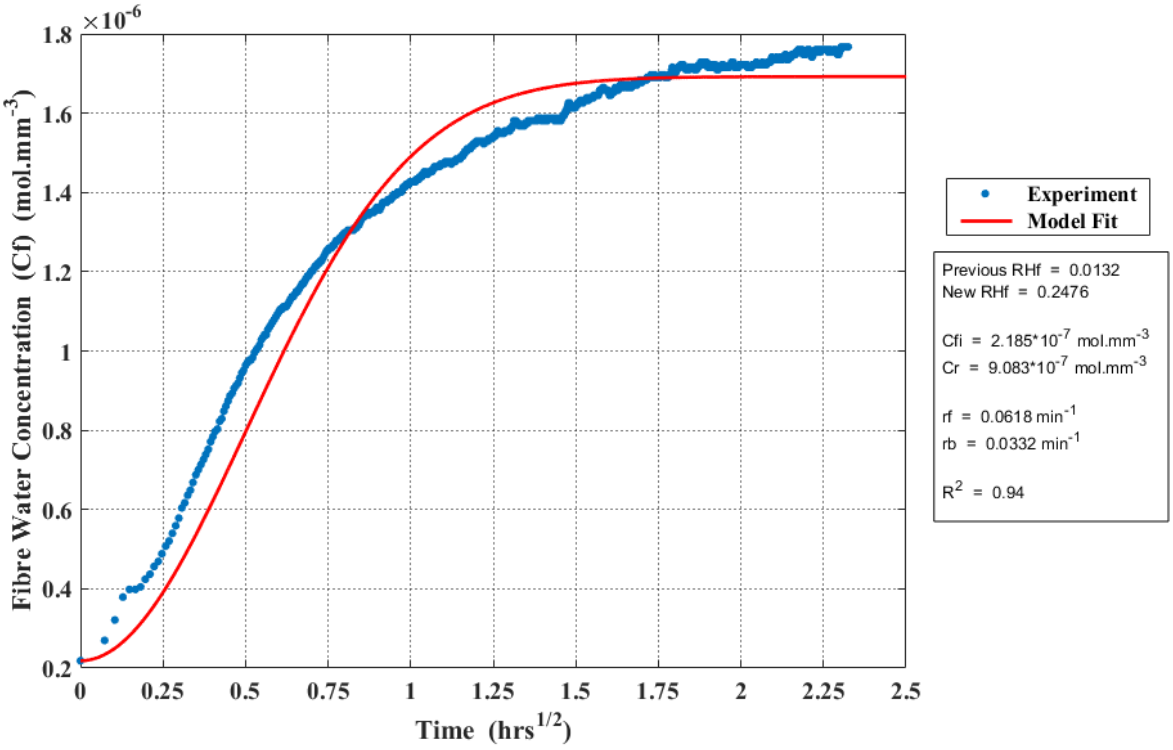

Figure 114: Result of fitting equation (255) to the truncated fibre DVS data of Stone [123], for fibre initially at a relative humidity of 1.32%, exposed to a relative humidity of 25%.

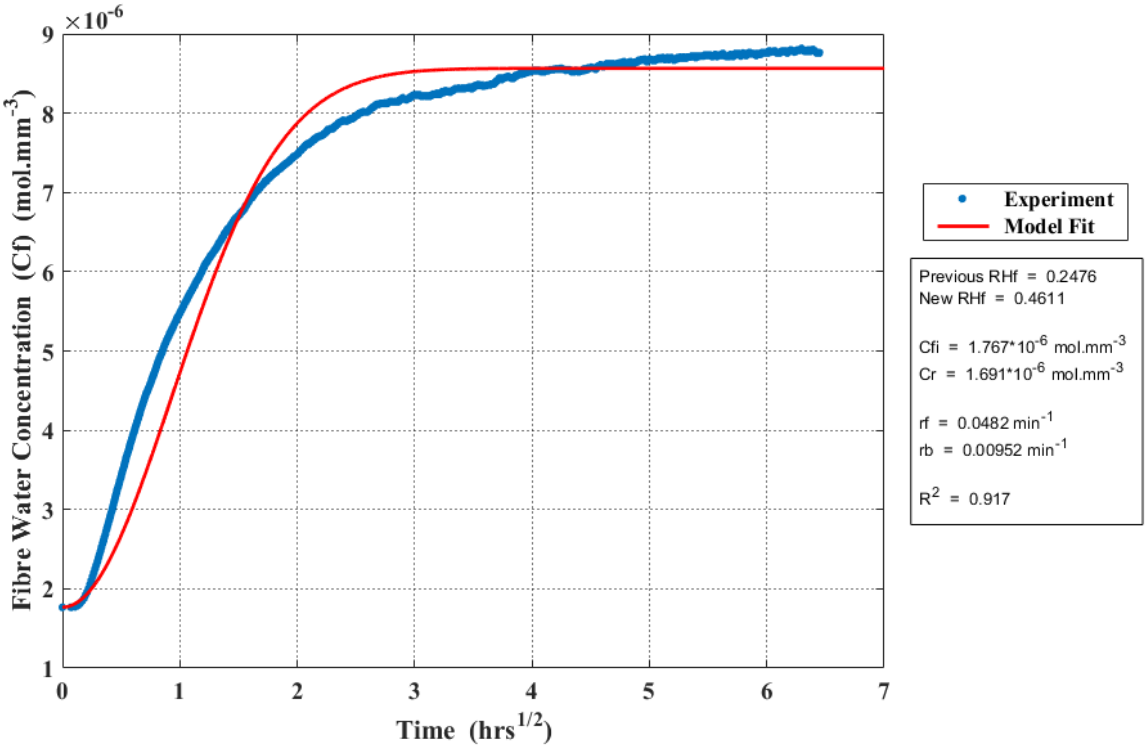

Figure 115: Result of fitting equation (255) to the truncated fibre DVS data of Stone [123], for fibre initially at a relative humidity of 25%, exposed to a relative humidity of 45%.

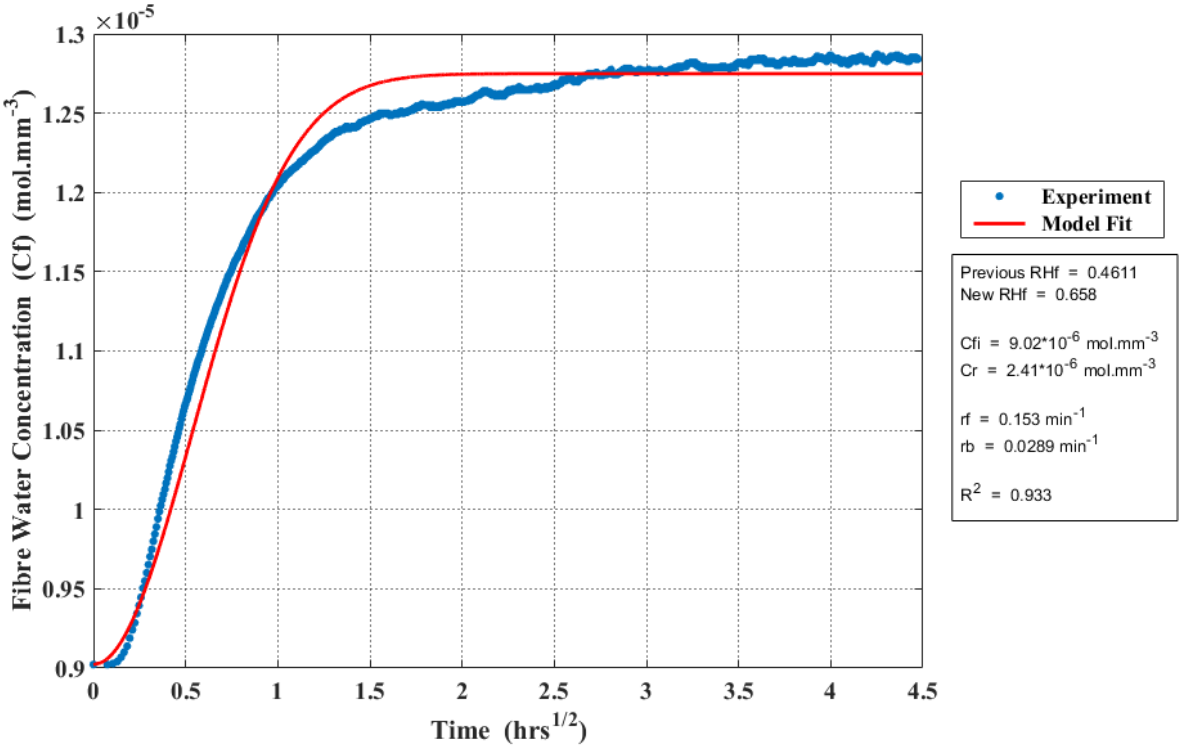

Figure 116: Result of fitting equation (255) to the truncated fibre DVS data of Stone [123], for fibre initially at a relative humidity of 45%, exposed to a relative humidity of 65%.

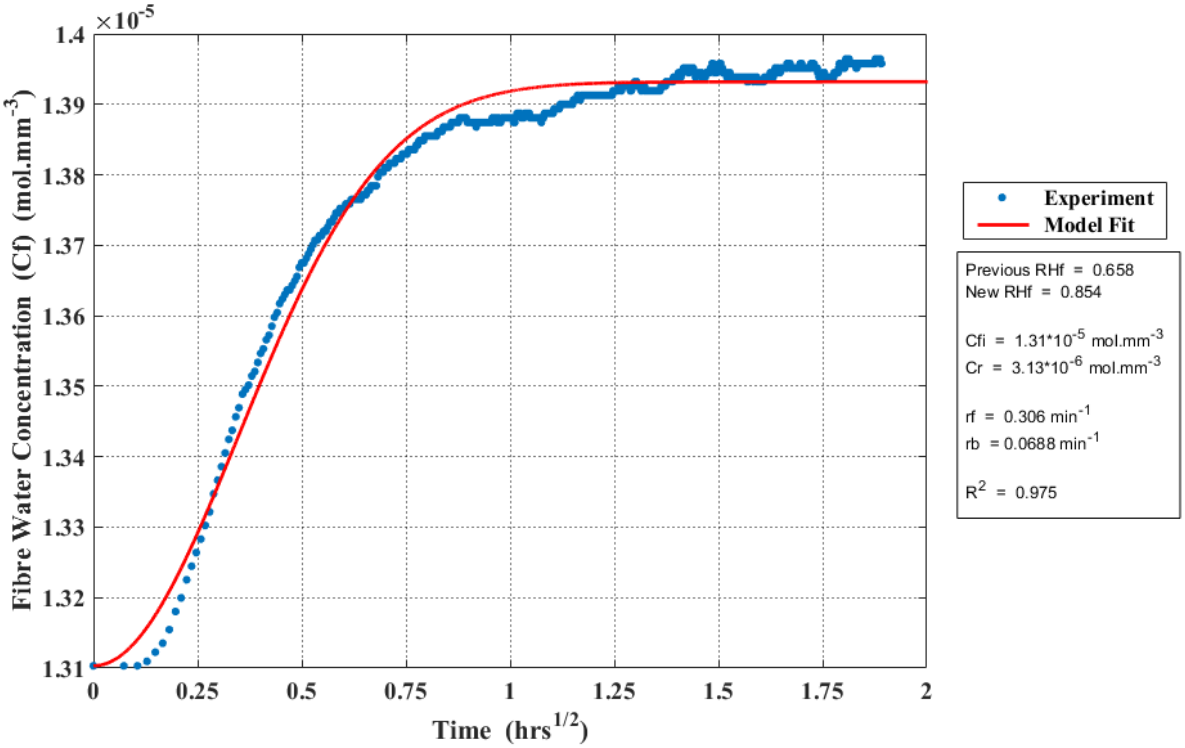

Figure 117: Result of fitting equation (255) to the truncated fibre DVS data of Stone [123], for fibre initially at a relative humidity of 65%, exposed to a relative humidity of 85%.

It is apparent from the results of the fitting process (Figure 114, Figure 115, Figure 116, Figure 117) that equation (255) is only partially successful in predicting the behaviour of fibre water concentration as a function of conditioning time. However, this is to be expected, as in formulating equation (255) the individual processes governing fibre uptake: adsorption of water to fibre surface functional groups, absorption of water clusters into fibre pore volume etc., were simplified into a single process described by a single equilibrium constant. In practice, each of the underlying mechanisms responsible for fibre uptake/loss will possess its own unique equilibrium constant and thus the overall uptake behaviour will be described by many more rate constants than the two employed in this simplified model.

This is supported by the experimental data in Figure 114, Figure 115, Figure 116, and Figure 117, which suggest that fibre uptake is governed by two distinct processes; one characterised by a rapid increase in C_f at early conditioning times, and a second characterised by a more gradual increase in C_f over an extended conditioning period. A minimum of four rate constants are required to describe this type of uptake behaviour. The general trend observed in each figure, between the model predicted fibre water concentration and that observed experimentally, is an underestimation of C_f at early conditioning times followed by its overestimation at extended conditioning times. This disagreement would be expected if the actual fibre behaviour was characterised by two processes, both occurring at different rates, as has been suggested.

As the values of the rate constants, r_f and r_b, obtained from each relative humidity step, are average values, the fibre water concentration that they are associated with is also taken as an average value. Thus, for a given relative humidity step:

$$\widehat{C_f} = \frac{C_{f_2} - C_{f_1}}{2} \tag{283}$$

Where $\widehat{C_f}$ is the average fibre water concentration, C_{f_2} is the equilibrium fibre water concentration at the final relative humidity of the DVS step, and C_{f_1} is the equilibrium fibre water concentration at the initial relative humidity of the DVS step.

In Figure 118 below, the value of the forward rate constant (r_f), obtained from fitting equation (255) to the fibre DVS data of Stone [123] (Figure 114, Figure 115, Figure 116, Figure 117), is expressed as a function of the average fibre water concentration $\widehat{C_f}$.

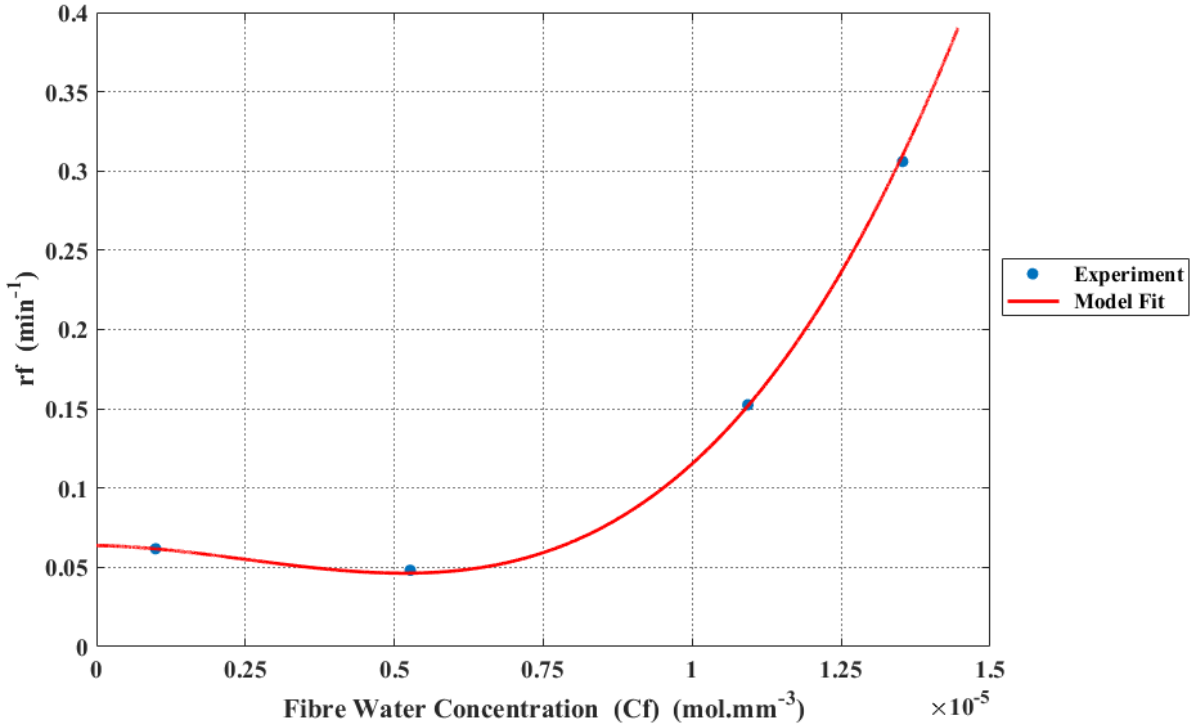

Figure 118: Forward rate constant r_f as a function of fibre water concentration C_f.

A third order polynomial appeared to fit the data well and thus the function, relating r_f to C_f, can be expressed as:

$$r_{f_{(C_f)}} = A_1 {C_f}^3 + A_2 {C_f}^2 + A_3 C_f + A_4 \qquad (284)$$

Where the parameters A_1, A_2, A_3, and A_4, are constants that are obtained from the fitting process. Their values are given below in Table 61.

A_1	A_2	A_3	A_4
2.3×10^{14}	-1.72×10^{9}	-633.92	0.0638

Table 61: Value of the constants A_1, A_2, A_3, A_4, obtained from fitting equation (284) to the experimental data in Figure 118.

5.3.7. Behaviour of r_f with respect to C_f

The results in Figure 118 indicate that when the fibre water concentration (C_f) is ~$0.1 \times 10^{-5}\ mol.mm^{-3}$, the value of the forward rate constant (r_f) is ~$0.6\ min^{-1}$. Increasing the fibre water concentration to ~$0.55 \times 10^{-5}\ mol.mm^{-3}$, has a negligible effect upon the value of the forward rate constant. Although the rate constant decreases slightly to ~$0.5\ min^{-1}$, the small magnitude of this change suggests that it is more likely attributed to error in the value of the rate constant, obtained from the fitting process, than as a result of an actual physical phenomenon. Referring back to Figure 111, it is apparent that when the equilibrium water concentration of the fibre is ~$0.55 \times 10^{-5}\ mol.mm^{-3}$ the concentration of water at the fibre surface is high enough to allow water cluster formation. This is followed by their subsequent absorption into fibre pore volume, as the fibre equilibrium water concentration increases rapidly in this region with increasing relative humidity. Sharp increases in the water concentration of activated carbons, with increasing relative humidity, have been associated by Do et al [65] with the absorption of water clusters into pore volume.

It is of interest to note that the forward rate constant in this region, where both adsorption and absorption occur, is identical to that at lower fibre water concentrations where only adsorption can occur. This suggests that the absorption of water clusters, into fibre pores, occurs more rapidly than the adsorption of water molecules to the fibre surface. Thus, the process that limits the rate at which the fibre uptakes water, is adsorption, and thus the forward rate constant is identical, regardless of whether adsorption, or adsorption with absorption, is occurring.

As C_f is increased beyond ~$0.75 \times 10^{-5}\ mol.mm^{-3}$ the forward rate constant begins to increase, with the rate of increase becoming larger with increasing C_f. Figure 111 shows that when the fibre equilibrium water concentration is ~$0.75 \times 10^{-5}\ mol.mm^{-3}$, the gradient of fibre water concentration with respect to relative humidity, has reached its maximum. Further increases in relative humidity result in smaller changes in fibre water concentration and this can be associated with the filling of fibre pores, reducing the overall free pore volume available for the further absorption of water clusters. As pore volume becomes saturated, water clusters will accumulate at the fibre surface. The increase in the rate constant within this region appears to suggest that this has the effect of increasing the rate at which atmospheric water molecules adsorb to the fibre surface. This agrees well with the activated carbon model of Do et al [65] in which the rate constant, associated with the adsorption of atmospheric moisture to water molecules already adsorbed at the fibre surface, is greater than that associated with the adsorption of atmospheric water to fibre surface functional groups.

5.3.8. Modelling the Hygrothermal Conditioning Process in Phenolic Based Low-fired Carbon-fibre Composites

In the work that follows, the methodology outlined in section 5.2.3 (page 270) is applied to model the hygrothermal conditioning of phenolic based low-fired carbon-fibre composites. The values of the rate constants, r_f and r_b, employed in the governing diffusion equation (equation (268)), are obtained from equations (284) and (265). The diffusion coefficient of the material is taken to be that of phenolic resin at 70℃, and was calculated earlier in this work (see section 4.3.1.2.5, Table 54 on page 230).

5.3.8.1. Comparison of Predicted Composite Moisture Content, as a Function of Relative Humidity, with the Experimental Data of Alston et al [124]

Figure 119 below shows the predicted water content of a phenolic based low-fired carbon-fibre composite, at equilibrium at 23℃, as a function of relative humidity. This has been compared against the experimental data of Alston et al [124]. The fibre volume fraction of the actual composite was measured by Denham [125] and found to be approximately 0.45. This value was employed in obtaining the model predictions in Figure 119.

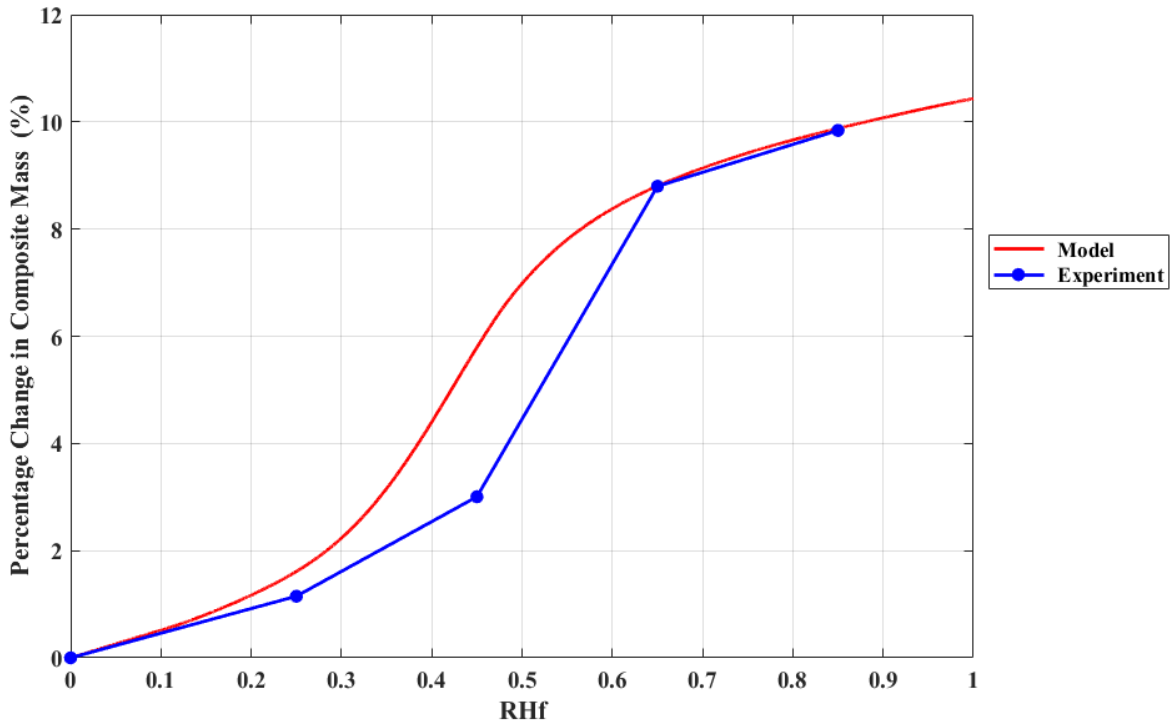

Figure 119: Model predicted moisture content of a phenolic based low-fired carbon-fibre composite, as a function of relative humidity at 23℃, compared against the experimental data of Alston et al [124].

In formulating the fibre model, it was assumed that the equilibrium moisture content of the fibre depended only upon the equilibrium concentration of water in the surrounding atmosphere, and not upon the equilibrium concentration of water within the surrounding resin medium. The results in Figure 119 support this assumption as, at relative humidities of 65% and above, no difference in the moisture content predicted by the model, and that measured experimentally by Alston et al [124], is observed. This also suggests that the presence of the resin matrix, surrounding the fibre surface, does not affect the quantity of water that can adsorb to the fibre surface, or absorb into fibre pore volume. However, the onset of the rapid increase in fibre moisture content that occurs at 25% relative humidity, associated with the absorption of water clusters into fibre pore volume, is delayed, and occurs at higher relative humidity in the composite. As both the moisture content predicted by the model and that obtained by Alston et al [124] experimentally, at and above 65% relative humidity, are identical, this suggests that the matrix is not affecting the quantity of fibre pores available for absorption.

Thus, the delayed onset for absorption can most likely be attributed to interaction of the matrix with water clusters at the fibre surface; for example, through hydrogen bonding. This initially prevents absorption from occurring at low fibre surface water concentrations. However, as the concentration of water at the fibre surface increases, with increasing relative humidity, a greater quantity of water clusters will become bound to matrix polar groups. Thus, the availability of matrix polar groups for further hydrogen bonding to occur, will be reduced. When no further water cluster/matrix polar group complexes can form, water clusters can then absorb into fibre pore volume. This explains the higher relative humidity required for absorption to occur when low-fired carbon-fibre is encapsulated within a phenolic resin matrix.

5.3.8.2. Relationship between Material Equilibrium Moisture Content and Relative Humidity as a Function of Fibre Volume Fraction

In order to understand the effect of fibre content on the overall hygrothermal behaviour of a composite, materials of varying fibre volume fraction have been modelled. The largest fibre volume fraction modelled was 0.7 as this is representative of the practical limit obtainable in actual composites. Modelling the behaviour of composites with fibre volume fractions in excess of the practical limit is avoided, as these predictions are not representative of real composites and thus cannot be verified by comparison with experiment.

Figure 120 below shows the model predicted relationship between material equilibrium moisture content and relative humidity, as a function of fibre volume fraction.

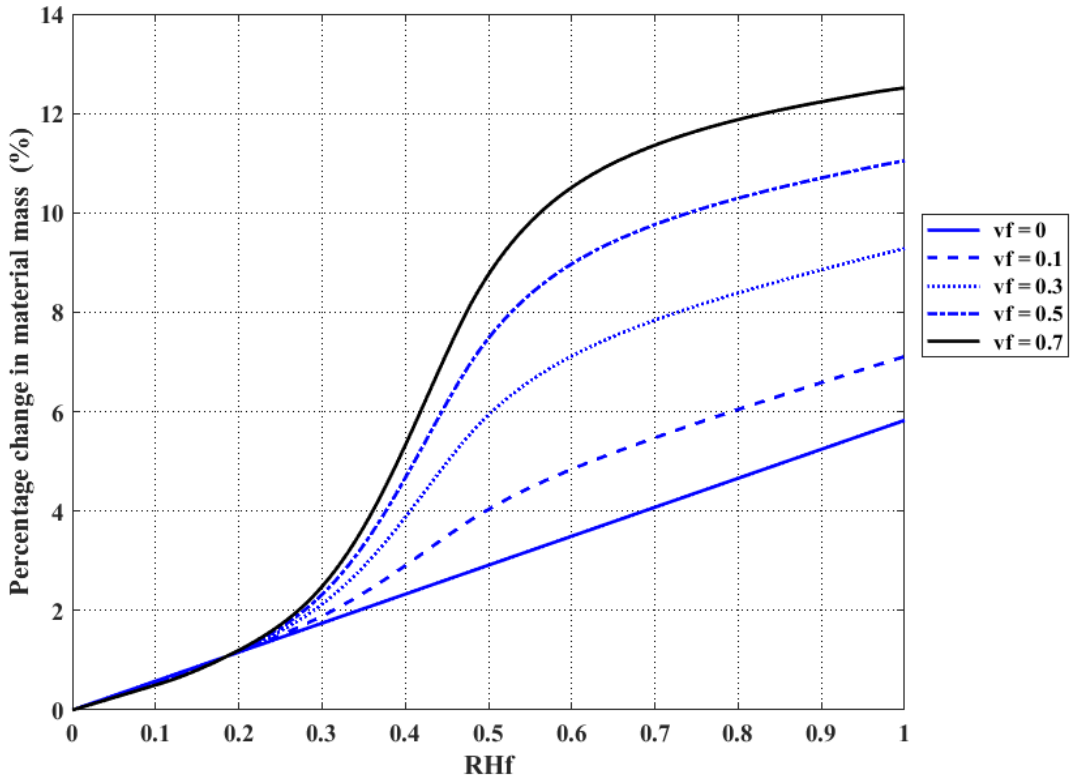

Figure 120: Relationship between material equilibrium moisture content and relative humidity, as a function of fibre volume fraction.

When v_f is equal to zero, the material is composed entirely of resin and thus its hygrothermal behaviour is identical to that of pure phenolic resin. Interestingly, fibre volume fraction has relatively little impact upon the moisture content of the material at low relative humidity (<20%). This suggests that the percentage change in mass, of both resin and fibre, that results from the uptake of moisture, is similar within this relative humidity range. When v_f is equal to 0.1, a small step in the percentage uptake of the material is observed between 20% and 50% relative humidity. Do et al [65] proposed that water clusters could form at the surface of activated carbons, followed by their subsequent absorption into the pore volume of the material. Thus, if the processes that govern moisture uptake in low-fired carbon-fibre are similar to those in activated carbon, then this step can be attributed to the absorption of water clusters into fibre pore volume. At relative humidities greater than 50%, the fibre pore volume becomes saturated with water clusters and the overall uptake behaviour, with increasing relative humidity, defaults back to that observed in the pure phenolic resin ($v_f = 0$). This is because after fibre pore volume becomes saturated, the increase in fibre water concentration with relative humidity, becomes less than that which occurs within the resin matrix, allowing the uptake behaviour of the resin matrix

to dominate within this region. The net effect is to increase the equilibrium moisture content of the material at 100% relative humidity, from 6% to 7%, in terms of the percentage change in mass.

Increasing the fibre volume fraction further, has the effect of increasing the size of the step in moisture content that is observed in the mid relative humidity range. Furthermore, the increased proportion of fibre within the composite causes the uptake behaviour at higher relative humidities (>60%) to more closely resemble that of the fibre, than that of the phenolic resin. The net effect at 100% relative humidity, of increasing the fibre volume fraction from zero to 0.7, is to effectively double the equilibrium moisture content of the material, from ~6% to ~12.5%, in terms of the percentage change in mass.

The results of this modelling suggest that at low relative humidity (<20%), the effect of fibre volume fraction, and hence of low-fired carbon-fibre, upon the moisture content of the composite, is negligible. Only in the mid relative humidity range, where the absorption of water clusters into fibre pore volume becomes possible, does the presence of low-fired carbon-fibre significantly influence the moisture content of the composite. However, the vast majority of composites will experience average relative humidities in excess of 20%, in their service environments.

5.3.8.3. Effect of Fibre Volume Fraction upon Material Moisture Content as a Function of Conditioning Time

The model predictions in Figure 120, in the previous section, indicated that at relative humidities greater than 20%, the effect of increasing fibre volume fraction is to increase the equilibrium moisture content of the material. In this section, the effect of low-fired carbon-fibre upon material moisture content, as a function of conditioning time, will be investigated at four different relative humidities: 25%, 45%, 65%, and 85%. This will be achieved by modelling the uptake behaviour of two different materials: one composed entirely of phenolic resin, with a fibre volume fraction equal to zero, and a second composed of both resin and fibre, with a fibre volume fraction equal to 0.7.

In each case, the material is assumed to be completely dry initially such that the concentration of water in both the resin (C_r), and fibre (C_f), is zero. The material is then exposed to one of the four relative humidities and the evolution of the material moisture content, with

conditioning time, is predicted until equilibrium is attained. The model results in the previous section show that, at relative humidities in excess of 20%, the general effect of increasing fibre volume fraction is to increase the equilibrium moisture content of the material. This makes comparison of the rate of the uptake process, at different relative humidities, problematic. To allow comparisons to be made, the predicted moisture content at each relative humidity was normalised using equation (285) below:

$$f_w = \frac{w_t}{w_{eq}} \tag{285}$$

Where f_w is the fractional water content, w_t is the total mass of water within the material at time t, and w_{eq} is the total mass of water within the material at equilibrium. The diffusion coefficient of both materials, that composed of pure resin ($v_f = 0$), and that composed of resin and fibre ($v_f = 0.7$), is that of pure phenolic resin at 70℃. As the diffusion coefficient of this phenolic resin is independent of relative humidity, being only dependent upon temperature, the time required for the pure resin to attain equilibrium, at each relative humidity, is identical, irrespective of the magnitude of the equilibrium moisture content. Thus, any difference between the rate of uptake in the pure resin material ($v_f = 0$), and that in the composite material, composed of both resin and fibre ($v_f = 0.7$), can be attributed directly to the time required to 'fill' the fibre at that relative humidity. Figure 121 below shows the model predicted fractional water content of the two materials (pure resin, and fibre/resin composite) as a function of conditioning time, at each relative humidity.

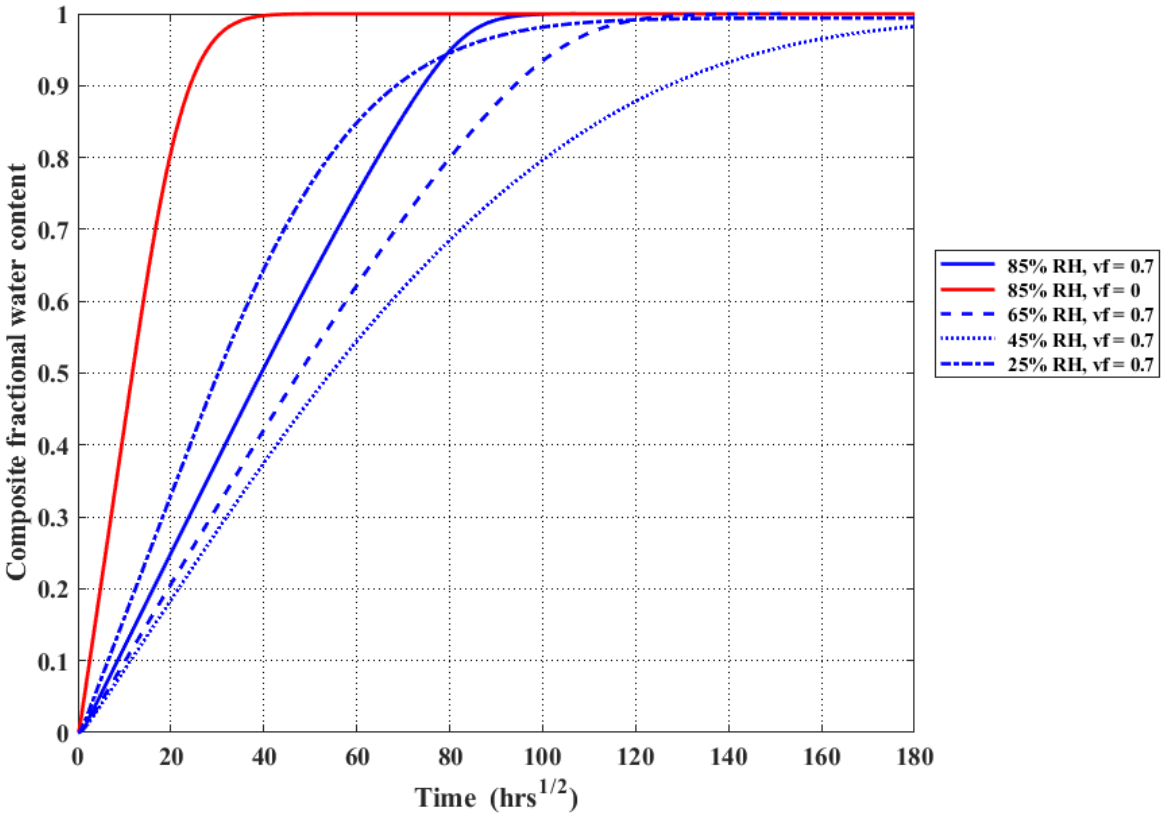

Figure 121: Relationship between fractional water content and conditioning time, as a function of relative humidity, for the two different materials.

As highlighted previously, the diffusion coefficient of the phenolic resin is independent of relative humidity and thus, as the uptake has been normalised, the uptake relationship shown above for the pure resin material ($v_f = 0$) (red line), at 85% relative humidity , is representative of the uptake behaviour of the pure resin material at all relative humidities. At 25% relative humidity, the rate at which uptake occurs in the composite material, that composed of both resin and fibre ($v_f = 0.7$), is significantly slower than that observed in the pure resin material. The relationship between its fractional water content and the square root of conditioning time, is initially linear. However, the rate of uptake begins to reduce after ~40 $hrs^{\frac{1}{2}}$ and extended time periods are required to observe the final approach to equilibrium. Thus, the overall uptake/$t^{\frac{1}{2}}$ relationship is non-Fickian.

The maximum possible fibre water concentration at 25% relative humidity is, from Figure 111, ~$0.2 \times 10^{-5}\ mol.mm^{-3}$. Referring back to Figure 118 for the relationship between the magnitude of the forward rate constant r_f, and fibre water concentration C_f, indicates that when

C_f is equal to, or less than ~$0.55 \times 10^{-5}\ mol.mm^{-3}$, the value of r_f is small at ~$0.055\ min^{-1}$. The slow uptake behaviour observed in the composite at 25% relative humidity, results from both the low value of the forward rate constant, and the low flux of water molecules diffusing into the material at this relative humidity.

At 45% relative humidity the rate of the uptake process is further reduced, however the overall trend in behaviour is similar to that observed at 25% relative humidity. The maximum fibre water concentration in this conditioning environment is ~$0.85 \times 10^{-5}\ mol.mm^{-3}$ which corresponds to a value of r_f of ~$0.075\ min^{-1}$, almost identical to that at 25% relative humidity. However, although the rate at which water becomes associated with the fibre (adsorbed/absorbed) is similar, the maximum fibre water concentration is increased as fibre surface water concentrations are now high enough to allow the formation, and absorption, of water clusters into fibre pore volume. Thus, to attain equilibrium, the fibre requires a greater quantity of water. Although at higher relative humidities the flux of water molecules diffusing into the material from the atmosphere, is increased, this is not sufficient to offset the increased quantity of water required for the fibre to attain equilibrium. Thus, the net effect is an increase in the time required for the material to attain equilibrium.

The uptake behaviour of the composite conditioned at 65% relative humidity, occurs at a faster rate than that observed at 45% relative humidity. Although initially, fibre water concentration throughout the composite will be low, and thus also the value of the forward rate constant, this will change as conditioning proceeds. At 65% relative humidity, the maximum fibre water concentration is ~$1.3 \times 10^{-5}\ mol.mm^{-3}$ which corresponds to a value of r_f of ~$0.26\ min^{-1}$, an approximate five-fold increase in its value compared to that at 45% relative humidity. Furthermore, the flux of water molecules diffusing into the material is increased. The uptake is however, still slower than that observed at 25% relative humidity, even though the forward rate constant and the flux of water molecules into the material have increased. This can be attributed to the much larger equilibrium moisture content of the fibre at 65% relative humidity, compared to that at 25% relative humidity. Thus, a much larger quantity of water is required to fill the fibre before equilibrium is achieved.

The rate of uptake observed in the composite conditioned at 85% relative humidity follows a similar trend, being greater than that observed at 65% relative humidity. The explanation for this behaviour is identical to that for conditioning at 65% relative humidity as both the forward rate constant, and flux of water molecules diffusing into the material, are increased.

The overall conclusion drawn from these model predictions is that the rate of uptake within a composite is limited by the value of the forward rate constant (r_f), the flux of water molecules diffusing into the material, and the equilibrium moisture content of the fibre at a given relative humidity. At low relative humidity (25%), fibre water concentrations are low resulting in the average value of r_f being small. Furthermore, the flux of water molecules into the material is also small. This results in the rate of uptake within the composite ($v_f = 0.7$) being slower than that observed in a pure resin material ($v_f = 0$). At high relative humidity (85%), the average value of r_f is increased as a result of increased fibre water concentrations. Furthermore, the flux of water molecules diffusing into the material is also increased. However, the equilibrium moisture content of the fibre is increased and thus a greater quantity of water is required for the fibre to attain equilibrium. The overall effect, at 85% relative humidity, is that the rate of uptake within the composite is still slower than that observed at low relative humidity (25%), however it is faster than that occurring in the mid relative humidity range (45%– 65%).

5.3.8.4. Effect of Fibre Volume Fraction on the Moisture Content of the Phenolic Resin Matrix as a Function of Conditioning Time

In the previous section, the fibre model was employed to predict the evolution of composite water content as a function of conditioning time, at four different conditioning relative humidities. In the work that follows, the impact of hygrothermal conditioning upon the thermo-mechanical properties of the phenolic resin matrix, of a low-fired carbon-fibre composite, will be investigated.

To understand the influence of the fibre on the moisture content of the surrounding phenolic resin matrix, the fractional water content of the phenolic resin matrix, as a function of conditioning time, has been predicted for two different materials. One material is composed of pure resin ($v_f = 0$), and the second is a composite of both resin and fibre ($v_f = 0.7$). Predictions were performed at the four different conditioning relative humidities that, employed in the previous section, and the results are shown below in Figure 122.

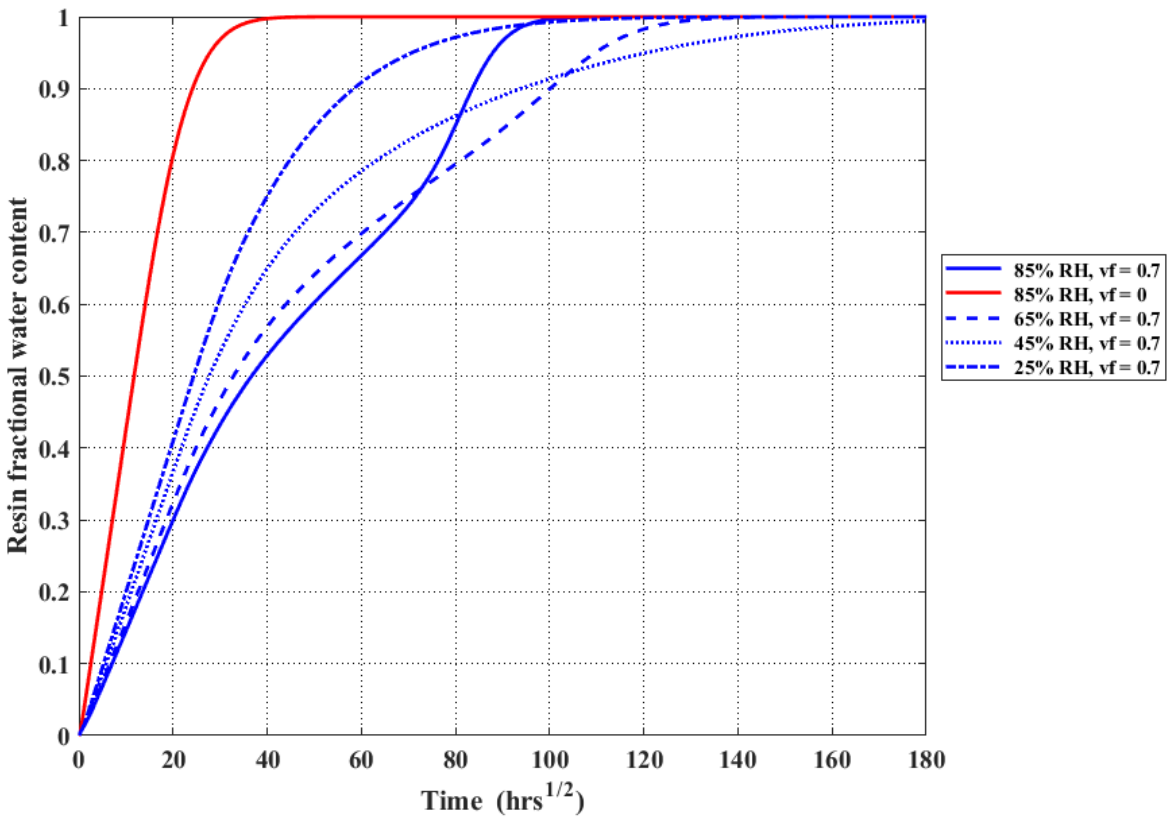

Figure 122: Relationship between the fractional water content of the phenolic resin matrix and conditioning time, as a function of relative humidity, for the two different materials.

The model results show that the presence of low-fired carbon-fibre, within a material, has the effect of reducing the rate at which the moisture content of the phenolic resin matrix increases with conditioning time, thus increasing the time period required for the phenolic resin matrix to attain equilibrium. This is expected, as for the material to reach equilibrium both the resin and fibre, throughout the entire geometry of the composite, must attain their equilibrium moisture content. However, as the fibre is encased within the resin and not exposed directly to the conditioning atmosphere, this 'extra' water content, required for overall material equilibrium, must be supplied by water molecules diffusing through the phenolic resin matrix. Thus, the time taken for the phenolic resin matrix to reach equilibrium is extended, as water molecules within the matrix are lost to the fibre, either through adsorption or absorption processes.

The rate of uptake continues to decrease with increasing relative humidity. However, at 65% relative humidity a new trend is observed. Initially, uptake within the phenolic resin matrix is slower than at 45% relative humidity. However, after a conditioning time of ~80 $hrs^{\frac{1}{2}}$, the rate of uptake increases and equilibrium within the phenolic resin matrix is attained faster than at 45%

relative humidity. Figure 111 showed the relationship between relative humidity and fibre equilibrium water concentration and indicated that, above 60% relative humidity, the change in fibre water concentration, with relative humidity, is reduced. This was attributed to the saturation of fibre pore volume. Thus, early in the 65% relative humidity conditioning experiment, the increase in the moisture content of the phenolic resin matrix is slow, as water is supplied to the fibre. However, after a sufficient time period, fibre pore volume becomes saturated and a greater proportion of water that diffuses into the phenolic resin matrix remains within the matrix, thus increasing the rate of uptake observed within the matrix. This, coupled with the larger value of the average forward rate constant and the increased flux of water molecules diffusing into the material, at higher relative humidity, allow the matrix to attain equilibrium more rapidly than at 45% relative humidity.

The same saturation of pore volume phenomenon is observed at 85% relative humidity, with a rapid increase in the rate of matrix uptake occurring after ~70 $hrs^{\frac{1}{2}}$. However, the increase in the rate of matrix uptake that this causes, is greater than at 65% relative humidity. This is because at 85% relative humidity, the flux of water molecules diffusing from the atmosphere into the phenolic resin matrix, is greater than at 65% relative humidity. Thus, the rate at which the fibre is filled with water is increased. The average value of the forward rate constant is also increased, allowing the fibre to attain equilibrium with its surrounding phenolic resin matrix, more rapidly.

5.3.8.5. Effect of Low-fired Carbon-fibre on the Water Concentration Profile of Phenolic Resin during Hygrothermal Conditioning

The results of the modelling in the previous section show that the presence of low-fired carbon-fibre within a material, effects the relationship between the fractional water content of the phenolic resin matrix and conditioning time. The uptake behaviour of the phenolic resin when the fibre volume fraction is zero, is observed to be Fickian. However, within a composite composed of both resin and fibre, with a fibre volume fraction of 0.7, this Fickian behaviour is lost. This implies that the water concentration profile within the phenolic resin matrix of the composite, does not evolve in the manner predicted by Fick's second law.

In the work that follows, this behaviour is investigated by using the fibre diffusion model to predict the water concentration profiles of two different materials at various points in their conditioning processes. One of these materials is composed purely of phenolic resin, with a fibre volume fraction of zero, the second is a composite composed of both resin and fibre, with a fibre

volume fraction of 0.7. Comparisons between these two materials were made when the moisture content of the phenolic resin matrix, in both materials, was identical. In the figures that follow, the resin moisture content of both materials is characterised by:

$$F = \frac{m_t}{m_{eq}} \tag{286}$$

Where F is the fractional water content of the phenolic resin matrix, m_t is the moisture content of the phenolic resin matrix at conditioning time t, and m_{eq} is the moisture content of the phenolic resin matrix at equilibrium.

Modelling was performed at three different relative humidities: 45%, 65%, and 85%, and in each case the initial water content of the material was zero. Figure 123, Figure 124, and Figure 125, show the concentration profiles predicted for the two different materials at each distinct relative humidity.

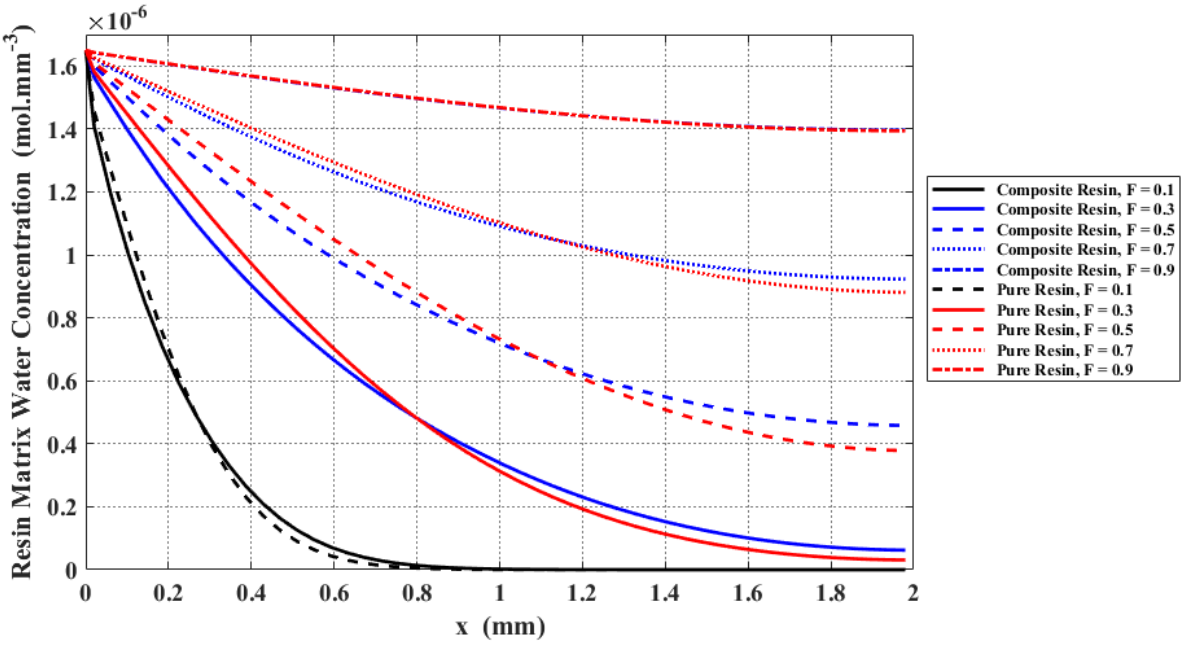

Figure 123: Water concentration profile of the phenolic resin matrix within the two different materials. One is composed entirely of phenolic resin ('Pure Resin'), the second is a composite of both resin and fibre ('Composite Resin') with a fibre volume fraction of 0.7. Concentration profiles are shown for a range of phenolic resin matrix fractional water contents (F): 0.1, 0.3, 0.5, 0.7, and 0.9. Both materials were initially dry before being exposed to a conditioning environment at 45% relative humidity.

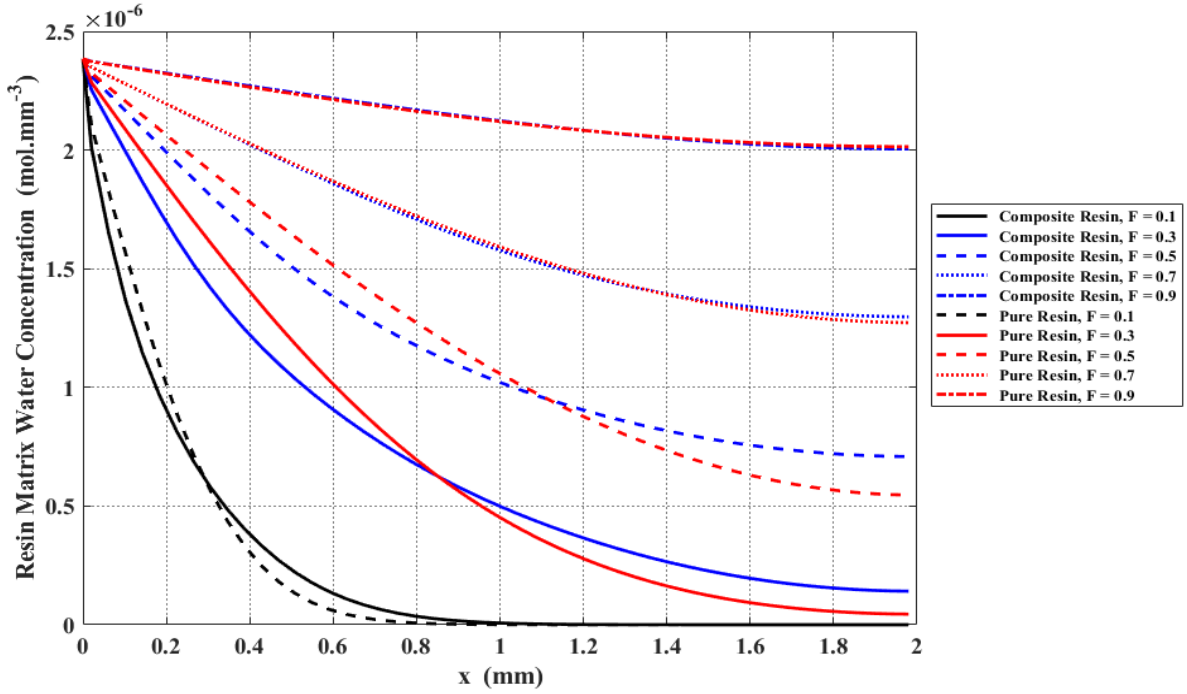

Figure 124: Water concentration profile of the phenolic resin matrix within the two different materials. One is composed entirely of phenolic resin ('Pure Resin'), the second is a composite of both resin and fibre ('Composite Resin') with a fibre volume fraction of 0.7. Concentration profiles are shown for a range of phenolic resin matrix fractional water contents (F): 0.1, 0.3, 0.5, 0.7, and 0.9. Both materials were initially dry before being exposed to a conditioning environment at 65% relative humidity.

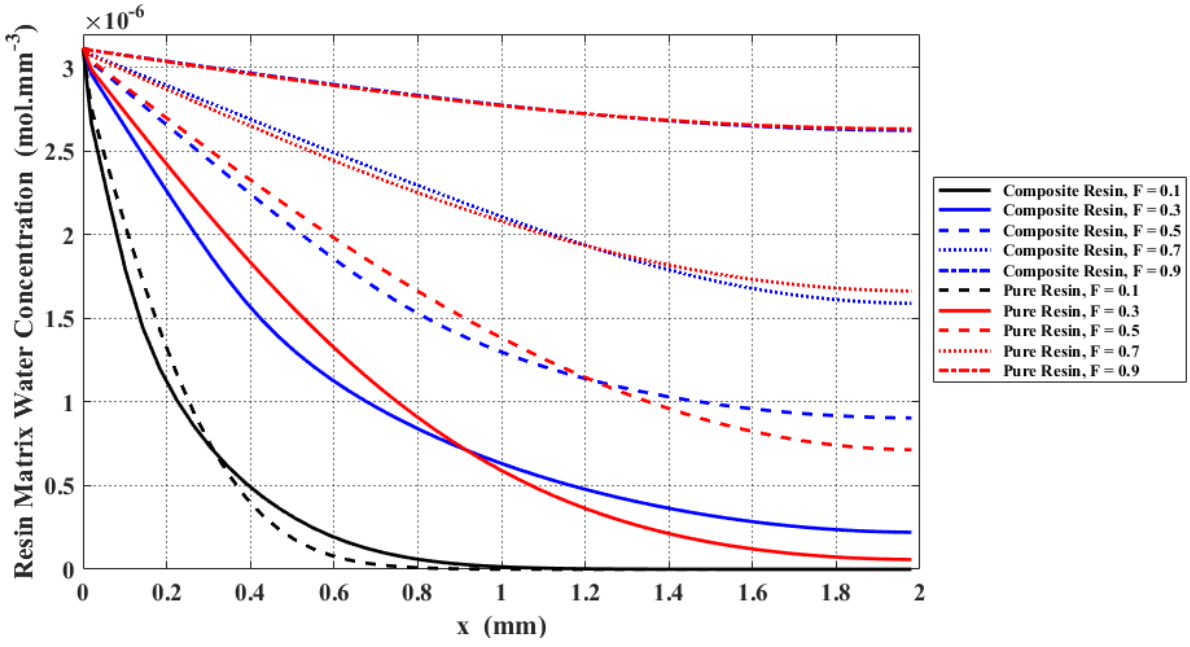

Figure 125: Water concentration profile of the phenolic resin matrix within the two different materials. One is composed entirely of phenolic resin ('Pure Resin'), the second is a composite of both resin and fibre ('Composite Resin') with a fibre volume fraction of 0.7. Concentration profiles are shown for a range of phenolic resin matrix fractional water contents (F): 0.1, 0.3, 0.5, 0.7, and 0.9. Both materials were initially dry before being exposed to a conditioning environment at 85% relative humidity.

Referring to the predicted concentration profiles above, the following observations can be made.

Conditioning Relative Humidity of 45% and 65%

In the region closer to the material surface, the concentration of water within the phenolic resin matrix of the pure material (that composed entirely of phenolic resin) is greater than that within the phenolic resin matrix of the composite material (that composed of both resin and fibre). At a certain depth below the material surface, the concentration of water within the phenolic resin matrix of both materials, becomes equal. At greater depths the behaviour is reversed, with the concentration of water within the phenolic resin matrix of the pure material, being less than that within the phenolic resin matrix of the composite. The difference between the water concentration profiles of the pure (phenolic resin only) and composite materials (resin and fibre), within the two regions described above, increases with increasing conditioning relative humidity. This is expected, as at higher relative humidity the equilibrium water concentration of the phenolic resin is increased, and thus the magnitude of any concentration differences between the two materials will also increase.

The difference between the concentration profiles of the two materials (pure phenolic resin, and the resin/fibre composite) is also observed to initially increase with the fractional water content of the phenolic resin matrix, reaching a maximum when $F = 0.3$. As the water content of the phenolic resin matrix increases further, the difference between the concentration profiles reduces, and at $F = 0.9$, the water concentration profiles of both materials are approximately equal.

Conditioning Relative Humidity of 85%

The water concentration profile behaviour of the phenolic resin matrix, within the two different materials, is similar to that observed at the two lower relative humidities. However, when the fractional water content of the phenolic resin matrix is 0.7, the trend is reversed. The concentration of water within the phenolic resin matrix of the composite material, is now greater, in the region closer to the material surface, than the concentration of water within the phenolic resin matrix of the pure resin material. Similarly, in the region closer to the material centre, the concentration of water within the phenolic resin matrix of the composite, is less than the concentration of water within the phenolic resin matrix of the pure resin material.

5.3.8.6. Effect of Low-fired Carbon-fibre on the T_g Profile of Phenolic Resin during Hygrothermal Conditioning

In Figure 126, Figure 127, and Figure 128 below, the glass transition temperature profiles of the two materials (pure phenolic resin, and resin/fibre composite), are predicted at the three different relative humidities, for a range of phenolic resin matrix fractional water contents.

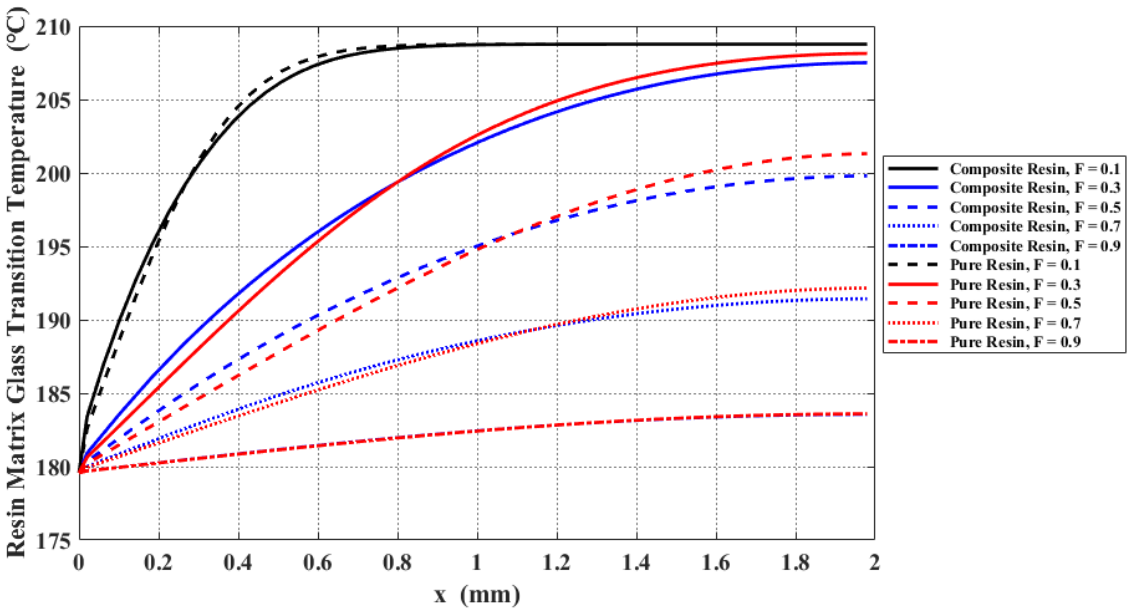

Figure 126: T_g profile of the phenolic resin matrix within the two different materials. One is composed entirely of phenolic resin ('Pure Resin'), the second is a composite of both resin and fibre ('Composite Resin') with a fibre volume fraction of 0.7. T_g profiles are shown for a range of phenolic resin matrix fractional water contents (F): 0.1, 0.3, 0.5, 0.7, and 0.9. Both materials were initially dry before being exposed to a conditioning environment at 45% relative humidity.

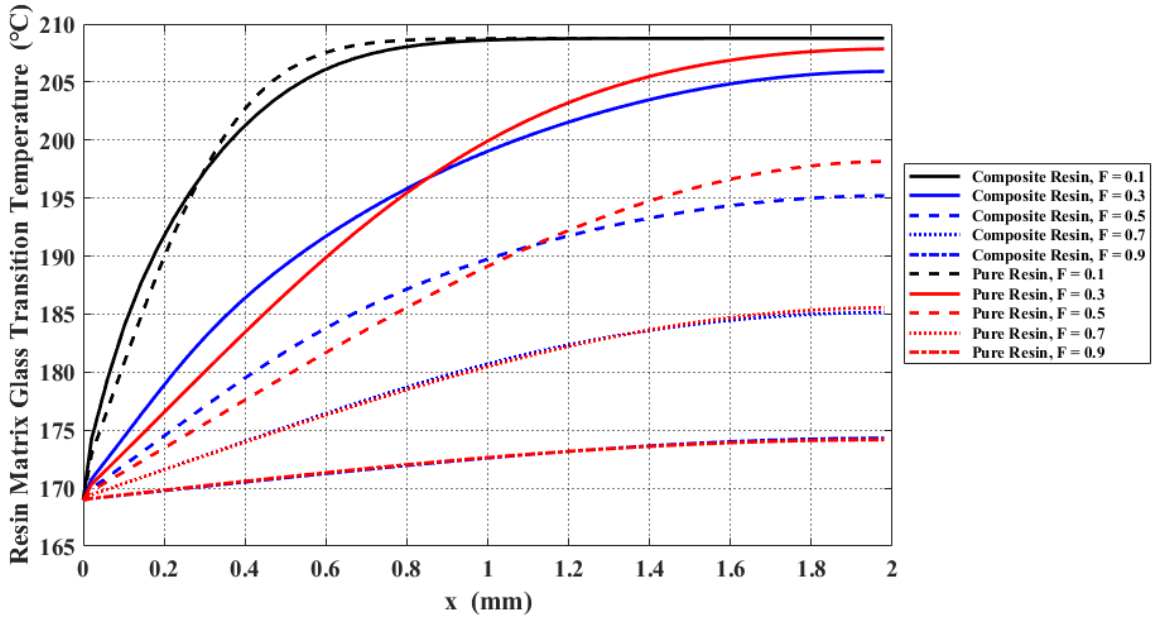

Figure 127: T_g profile of the phenolic resin matrix within the two different materials. One is composed entirely of phenolic resin ('Pure Resin'), the second is a composite of both resin and fibre ('Composite Resin') with a fibre volume fraction of 0.7. T_g profiles are shown for a range of phenolic resin matrix fractional water contents (F): 0.1, 0.3, 0.5, 0.7, and 0.9. Both materials were initially dry before being exposed to a conditioning environment at 65% relative humidity.

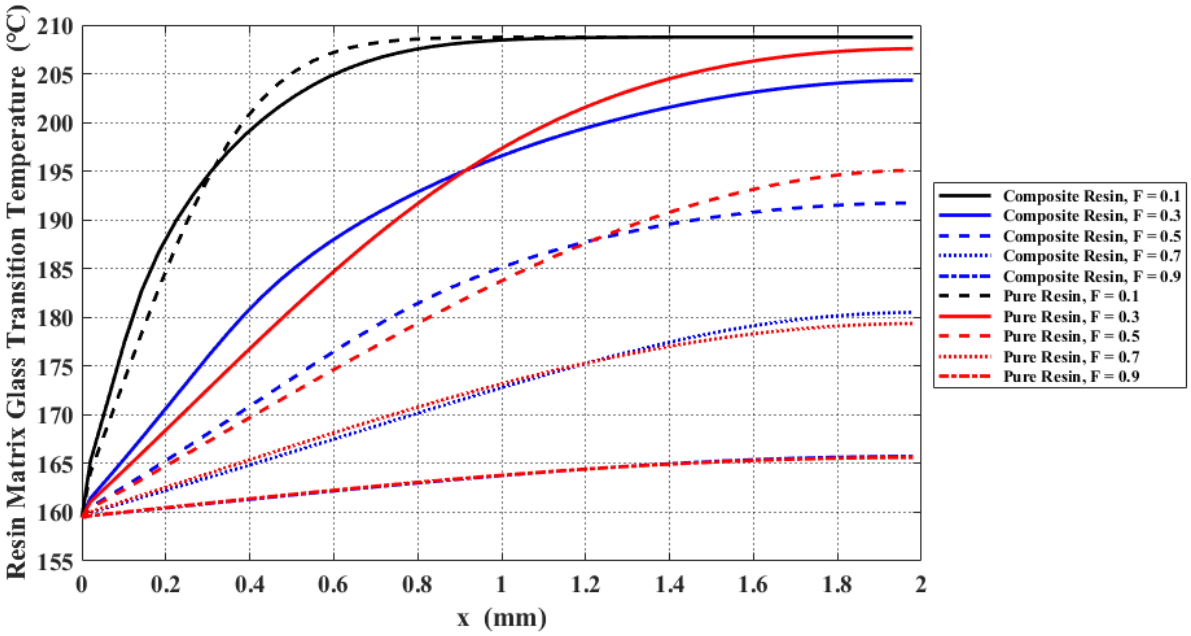

Figure 128: T_g profile of the phenolic resin matrix within the two different materials. One is composed entirely of phenolic resin ('Pure Resin'), the second is a composite of both resin and fibre ('Composite Resin') with a fibre volume fraction of 0.7. T_g profiles are shown for a range of phenolic resin matrix fractional water contents (F): 0.1, 0.3, 0.5, 0.7, and 0.9. Both materials were initially dry before being exposed to a conditioning environment at 85% relative humidity.

As has been discussed earlier in this work, the magnitude of the reduction in resin glass transition temperature that occurs as a result of moisture absorption, is proportional to the quantity of moisture that is absorbed (see section 1.4.2, page 18). Thus, as expected, the greater the difference in water concentration between the phenolic resin matrices of the two different materials, the greater the difference in the glass transition temperature. The largest difference observed is ~5℃ when the two materials, conditioned at 85% relative humidity, both have a phenolic resin matrix fractional water content of 0.3.

The overall conclusions drawn from this modelling work are as follows. For two different materials (one composed purely of phenolic resin, the second a composite composed of both resin and fibre) in which the fractional water contents of their phenolic resin matrices are identical, the one containing low-fired carbon-fibre (i.e. the composite) will have a lesser concentration of water in the region of the material that is closer to the atmosphere, and a greater concentration of water in the region that is closer to the material centre, before equilibrium is attained Thus, in general, the presence of low-fired carbon-fibre within a composite causes the distribution of water throughout the phenolic resin matrix of that material, during conditioning, to take a more uniform profile than that which would be observed if the material was composed entirely of phenolic resin, with no fibre being present ($v_f = 0$). This implies that the property gradients caused by the presence of absorbed water (Young's modulus, molar volume), will be smaller in the composite (resin and fibre) than in the pure phenolic resin material. It can be hypothesised that this may be beneficial with regards to certain material properties. For example, during conditioning the non-uniform profile of water throughout the phenolic resin matrix of the material, causes the resin closer to the material/atmosphere interface to swell more than resin deeper within the material. This difference in volume expansion will induce stress within the material. However, in the composite (resin and fibre), the water concentration gradient of the phenolic resin matrix throughout the material, is reduced. Thus, the difference in the swelling response of the phenolic resin is reduced, with an accompanying reduction in internal stress.

5.3.8.6.1. Calculating the Percentage Difference Between the Glass Transition Temperature Profile of the Composite with that of the Pure Resin Material

Previously, it was observed that increasing the relative humidity of the conditioning environment had the effect of increasing the magnitude of the difference in glass transition temperature between the two different materials (pure phenolic resin, and resin/fibre composite) (Figure 126, Figure 127, Figure 128). During conditioning, the average water concentration within the phenolic resin matrix of both materials, is greater at higher relative humidity. Thus, any difference in the concentration of water within the phenolic resin matrices of these materials,

will be amplified. As glass transition temperature reduction is directly proportional to water concentration, it follows that any difference in the glass transition temperature of the resin, between the two materials, will also be greater at higher relative humidity. In the work that follows, the degree to which the increase in the difference between the glass transition temperature of resin within the two different materials, can be attributed to the increased average water concentration of the phenolic resin matrix at higher relative humidity, is investigated. This was achieved by first determining the overall reduction in the glass transition temperature of the resin matrix that occurs when a material is conditioned to equilibrium at a specific relative humidity:

$$\Delta T_g(RH) = T_{g_{dry}} - T_{g_{eq}}(RH) \tag{287}$$

Where $\Delta T_g(RH)$ is the overall reduction in the glass transition temperature of the resin matrix when it is at equilibrium, at a relative humidity RH, $T_{g_{eq}}(RH)$ is the glass transition temperature of the resin matrix when it is at equilibrium, at a relative humidity RH, and $T_{g_{dry}}$ is the glass transition temperature of the dry resin matrix before conditioning has begun. The difference in the glass transition temperature of the resin matrix of the composite (resin and fibre), and that of the pure resin material (only resin), was then expressed as a percentage of the total change in glass transition temperature occurring at that conditioning relative humidity.

$$P = 100\left(\frac{T_{g_c} - T_{g_p}}{\Delta T_g(RH)}\right) \tag{288}$$

Where T_{g_c} and T_{g_p} are the glass transition temperatures of the resin matrix within the composite, and within the pure resin material, respectively.

In the analysis that follows, x_f is defined as:

$$x_f = \frac{x}{(d/2)} \tag{289}$$

Where x is the depth below the material surface, and d is the thickness of the material. Thus, $x_f = 1$ represents a position at the centre of the material, $x_f = 0.5$ represents a position halfway between the material surface and centre etc.

In Figure 129, Figure 130, and Figure 131 below, the result of plotting P against x_f is shown for the three different relative humidities investigated in this work: 45%, 65%, and 85%.

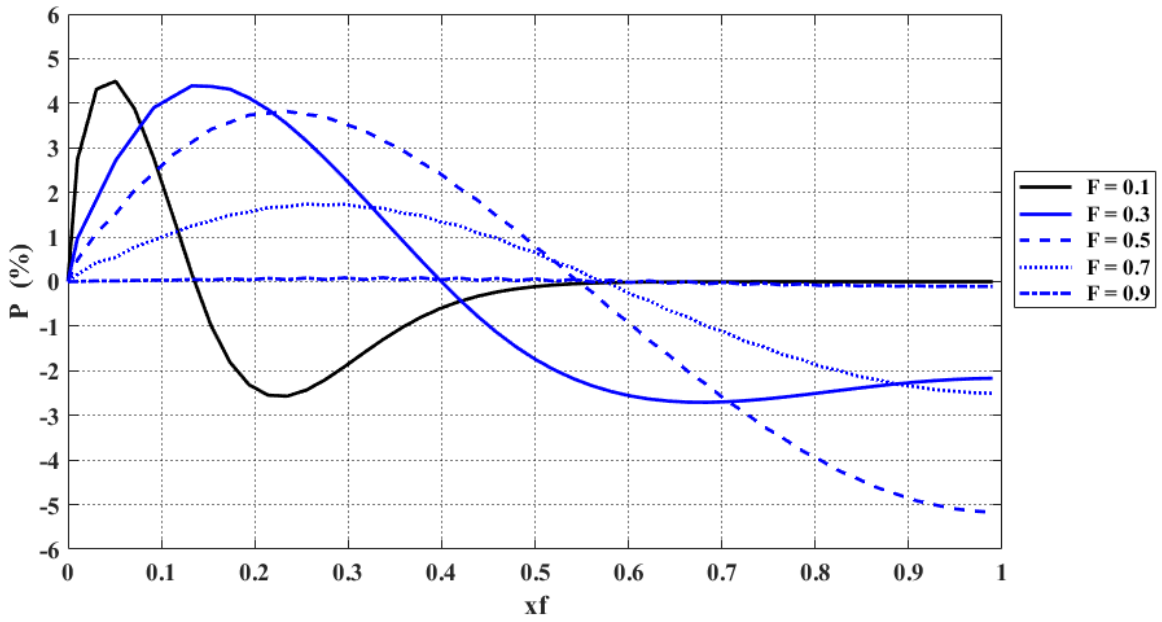

Figure 129: Difference between the glass transition temperature of a phenolic resin matrix within a composite, compared to that of a phenolic resin matrix within a pure resin material, as a function of the fractional water content of the phenolic resin matrix at 45% relative humidity.

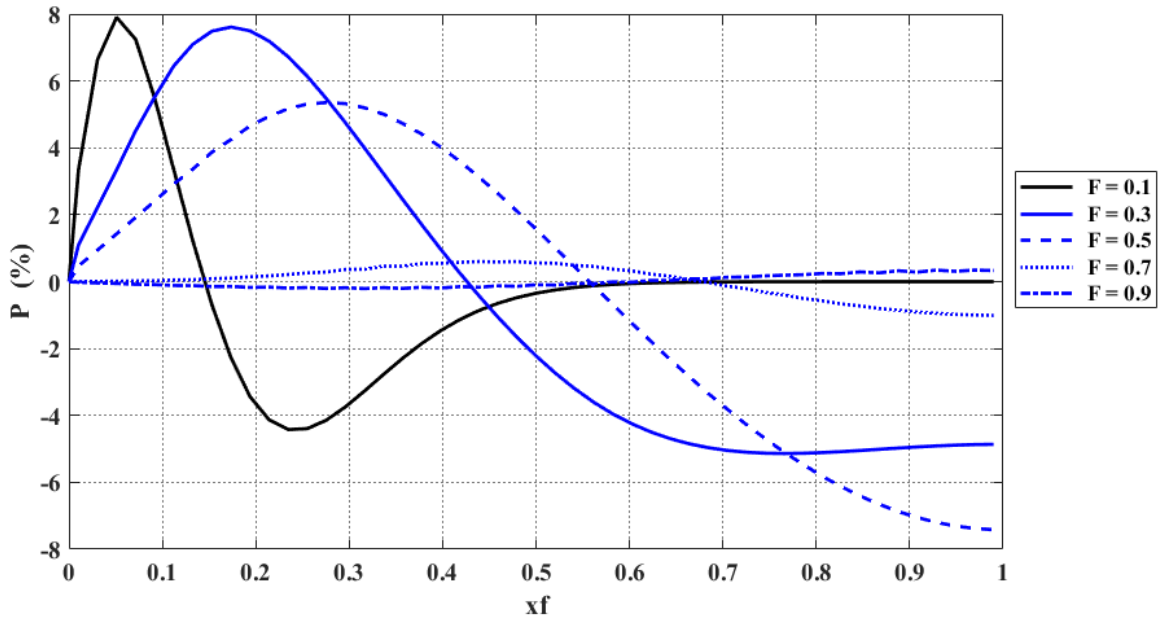

Figure 130: Difference between the glass transition temperature of a phenolic resin matrix within a composite, compared to that of a phenolic resin matrix within a pure resin material, as a function of the fractional water content of the phenolic resin matrix at 65% relative humidity.

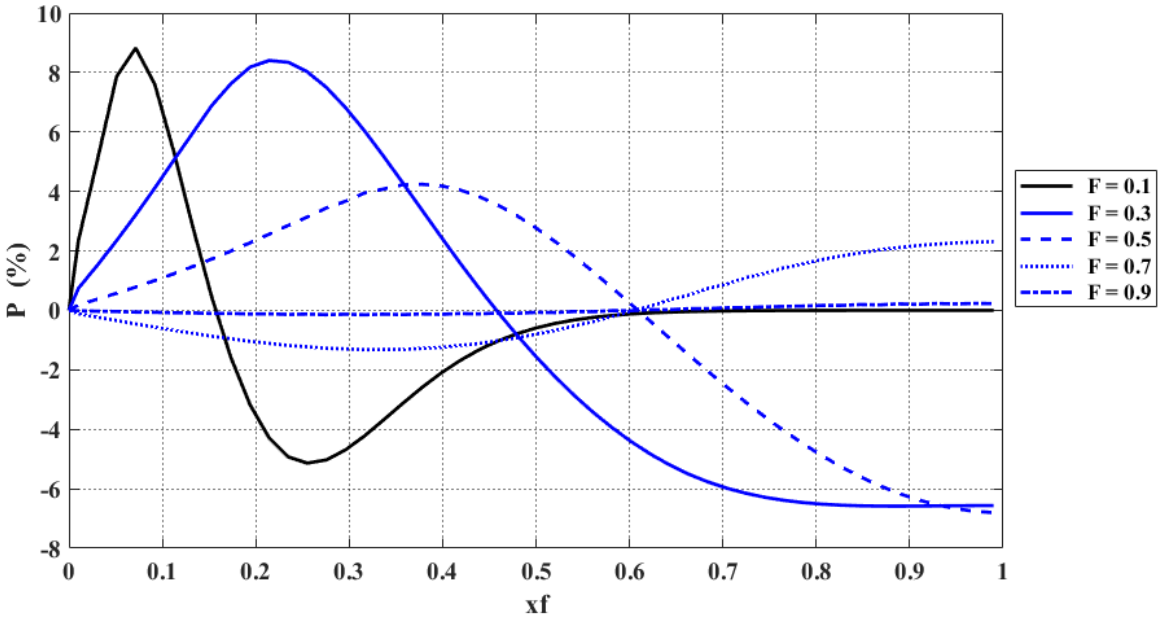

Figure 131: Difference between the glass transition temperature of a phenolic resin matrix within a composite, compared to that of a phenolic resin matrix within a pure resin material, as a function of the fractional water content of the phenolic resin matrix at 85% relative humidity.

These results indicate that for two materials, (one composed purely of phenolic resin, the second a composite composed of phenolic resin and fibre) with identical phenolic resin matrix fractional water contents, the increase in the difference in glass transition temperature with increasing relative humidity cannot be fully attributed to the greater equilibrium water content of

the resin matrix at higher relative humidity. This implies that the overall behaviour of the fibre at higher relative humidities, has a large effect on the difference in the glass transition temperature profiles of the two materials (pure resin and composite) that is observed during conditioning.

5.4. Chapter Conclusions

A simple model has been developed to describe the hygrothermal behaviour of low-fired carbon-fibre based on that which is observed in activated carbons. Although a comprehensive model for the water uptake of activated carbons has been proposed by Do et al [65], it is mathematically complex, with a large number of fitting parameters. The model developed in this work simplified the fibre uptake process by assuming that the low-fired carbon-fibre behaved as a simple sink/source for water molecules. This model was then fit to DVS data, provided by Stone [123], characterising the moisture uptake behaviour of a low-fired carbon-fibre under a range of relative humidity conditions. This allowed the equilibrium constant governing the uptake process, to be deduced. This analysis showed that the simple fibre model is capable of approximating the hygrothermal behaviour of the fibre. It was observed that the forward rate constant, describing the rate at which water becomes associated with the fibre, is constant below a certain threshold fibre water concentration, thereafter increasing rapidly with increasing fibre water concentration. This was attributed to the concentration of water at the fibre surface becoming sufficient to promote the formation of water clusters. Thus, further adsorption of water then occurs through the adsorption of water molecules to water molecules already adsorbed at the fibre surface, and the model suggests that this process occurs more rapidly than the initial adsorption of water molecules to fibre surface functional groups. This observation is in agreement with that of Do et al [65] who found that the rate constant, governing the adsorption of water molecules to other water molecules already adsorbed at the surface of activated carbon, is much greater than that governing the adsorption of water molecules to activated carbon's surface functional groups.

The low-fired carbon-fibre model was then modified to describe the hygrothermal behaviour of low-fired carbon-fibre phenolic resin composites. A range of different fibre volume fractions were investigated, from 0 to 0.7, and the equilibrium moisture content of the composite was predicted from 0%, to 100%, relative humidity. This analysis showed that at low relative humidity (<25%), the effect of fibre volume fraction has a negligible impact upon the equilibrium moisture content of the composite. This suggests that, in this relative humidity range, the concentration of water absorbed within the phenolic resin is similar to that associated with the fibre. In the relative humidity range 25-55%, the presence of low-fired carbon-fibre introduces a step in the equilibrium moisture content/relative humidity relationship. This can be attributed to

the absorption of water clusters into fibre pore volume, with the magnitude of this step increasing with increasing fibre volume fraction.

The fractional water content of a composite material (composed of both phenolic resin and fibre) with a fibre volume fraction of 0.7, as a function of time and relative humidity, was compared to that of a pure phenolic resin material (only phenolic resin). These results showed that the presence of low-fired carbon-fibre increases the time required for the material to attain equilibrium with its conditioning environment. The time increased with increasing relative humidity, up to a relative humidity of 45%. The quantity of water that is required for the composite to attain equilibrium is greater than that of the pure resin material, as the fibre must also be filled with water. As this water must be supplied by diffusion through the resin matrix, the net result is an increase in the time required for the composite material to reach equilibrium when compared to a pure resin material. At relative humidities of 65% and higher, the time taken to reach equilibrium begins to decrease, and is quickest at 85% relative humidity. It is still, however, slower than for the pure phenolic resin material. The decrease in the time taken to attain equilibrium at higher relative humidities, results from the increased flux of water molecules diffusing into the material under these conditions. At high fibre water concentrations, the forward rate constant also increases significantly which reduces the time required for the material to attain equilibrium.

The fractional water content of the phenolic resin matrix, as a function of conditioning time and relative humidity, was investigated to determine the effect of low-fired carbon-fibre on the hygrothermal behaviour of the resin matrix. The results of this modelling indicated that the time taken for the resin matrix to reach equilibrium, with increasing relative humidity, exhibited a similar trend to that observed for the bulk composite material (resin and fibre). However, at relative humidities of 65% and above, the fractional water content of the resin matrix appeared to reach a plateau, before increasing rapidly to a final plateau of higher fractional moisture content. This was attributed to water concentrations within the material becoming sufficient to promote water cluster formation, with the subsequent filling of fibre pore volume. This results in an initial, partial plateau, in resin matrix moisture content as water fills the fibre pore volume. When fibre pore volume becomes saturated, the resin matrix can then be filled, resulting in a rapid increase in its fractional water content with conditioning time.

The effect of low-fired carbon fibre on the water concentration profile of the phenolic resin matrix of a composite (resin and fibre), at various times in the conditioning process, was investigated. This analysis showed that, for a given resin matrix fractional water content, the presence of low-fired carbon-fibre has the effect of reducing the concentration gradients throughout the geometry of the resin matrix. It was shown that a similar effect on the resin matrix T_g profile also occurred. An implication of these results is that the presence of low-fired carbon-fibre may be beneficial by reducing the water concentration gradients within the resin matrix, and thus the corresponding moisture induced property gradients, during the conditioning process. For example, stress induced through the variation of the swelling response of the resin matrix, throughout its geometry, would be reduced. The potential beneficial effect of low-fired carbon-fibre on the hygrothermal stability of composites has not been reported previously in the literature. Only one other work on the effect of moisture content on the thermo-mechanical properties of a phenolic resin matrix, within a low-fired carbon-fibre composite, exists [89]. In this work, only the average moisture content of the composite, along with its corresponding average T_g, were considered at any given conditioning time. Thus, any effect of the fibre on the concentration profile, and thus property profile, of the resin matrix was not observable in the modelling they undertook.

6. Thesis Conclusions

In this work the hygrothermal behaviour of both epoxy and phenolic resins has been investigated, both experimentally, and through a combined diffusion/structure-property modelling approach.

The investigation into the hydrolysis of DGEBA-DDA resin, in chapter two, has shown how the impact of coupling, between various phenomena, can affect the interpretation of experimental results. In previous work on the hydrolysis of DGEBA-DDA, the chosen sample dimensions resulted in the time scale over which the material attained equilibrium, with its conditioning environment, to be similar to that over which observable hydrolysis occurred. As a result, the initial equilibrium moisture content and diffusion coefficient of DGEBA-DDA were not detectable by gravimetric analysis [5-7]. This lead to probable inaccuracies in the calculation of the diffusion coefficient and prevented the change in the solubility of water within the material, as polar OH groups are added to the polymer network during hydrolysis, from being observed. Previous work has suggested that, when immersed in liquid water at temperatures below 70℃, DGEBA-DDA absorbs water up to an equilibrium moisture content of 5%-6.75% w/w [6, 7, 43]. Absorption is accompanied by hydrolysis with a resulting reduction in the glass transition temperature of the resin. In this work, the diffusion and hydrolysis processes have been decoupled allowing the measurement of the initial diffusion coefficient and solubility, of the resin, before hydrolysis occurs. This has provided a new description of the behaviour of DGEBA-DDA resin under hygrothermal conditions. Initially, the uptake of moisture is more rapid than previously suggested [6, 7, 43], however the initial equilibrium moisture content of the material is only 2.55% w/w. Thus, the extent of polymer network plasticisation may initially be lower than previously suggested. However, as hydrolysis occurs, the solubility of water within the material increases and thus the equilibrium moisture content is increased, to a final value of ~5.86% w/w in fully hydrolysed DGEBA-DDA resin. This increase in material solubility is accompanied by a reduction in the diffusion coefficient. In conclusion, this work shows that, in investigating the hygrothermal behaviour of polymer materials, it is important to measure the absorption behaviour for a wide range of sample dimensions as this allows for the identification of other phenomena that may be affecting the experimental data.

In chapter three, Group Interaction Modelling [71] was applied to model the effect of chemical constituents on the thermo-mechanical properties of phenolic resins. This analysis showed that the formation of ether bridges had an effect on the overall engineering properties of

the resin, which has been suggested previously by Parameswaran et al [108]. Ether bridges are formed through the reaction of two methylol groups, and thus their quantity increases as the F/P ratio of the reactants is increased. Ether bridges can undergo molecular rearrangement to form methylene bridges and it has been proposed that this can only occur at elevated temperatures (T >160℃) [15]. Thus, this work highlights the importance of curing phenolic resins at temperatures sufficient for the removal of ether bridges if their effect, upon resin thermo-mechanical properties, is to be avoided. Group Interaction Modelling was also applied to predict the evolution of chemical species within phenolic resins, during cure, as a function of their F/P ratio. This work employed arbitrary values for the rate constants to demonstrate the application of GIM to modelling the cure of phenolic resins. However, a large amount of experimental data showing the evolution of chemical structures within phenolic resins, during cure, is available in the literature [18, 20, 23]. Thus, a focus of future work would be to use this experimental data as an input for GIM, allowing the evolution of the thermo-mechanical properties of real phenolic resin systems to be predicted.

Group Interaction Modelling [71] has been employed previously by Fu et al [78] to predict the effect of absorbed moisture on the T_g of spider silks. However, it has not been applied in predicting the swelling response of phenolic materials as a result of moisture absorption. In chapter four, GIM was applied to predict the swelling response of phenolic resins as a function of relative humidity, and the results of this analysis were shown to disagree with that behaviour expected experimentally. It was hypothesised that this resulted from combining the van der Waals volume of the water molecule with that of the mer unit, as water molecules do not covalently bond to the polymer network. GIM was modified to describe the volume of absorbed water molecules in terms of their apparent volume in the liquid phase. The predictions of this modified model agreed more closely with the expected behaviour, although the swelling of the material was slightly overestimated. This was attributed to the thermal energy of water molecules being overestimated by its inclusion in the model in both the degrees of freedom, and in the apparent volume of water molecules in the liquid phase; this being a function of temperature. The molar volume equation of GIM was then further modified to account for the free volume of polymer materials. This led to the unexpected prediction that, before free volume has been filled by water molecules, the effect of absorbed water is to increase the Young's modulus of some phenolic resins. A review of the literature found only limited evidence to support this [120], although if the free volume of the material is small, the model predicted that such an effect would only be observable at very low relative humidities (<40%). Conditioning experiments are seldom performed at low relative humidity and thus this may account for the absence of evidence of this effect in the present literature. At present, it is not possible to speculate on the possible importance of this model implication as there is not enough data available to verify its validity.

In chapter five, a model was developed to describe the hygrothermal behaviour of low-fired carbon-fibre. The fibre behaviour was reduced to that of a simple source/sink of water molecules and this model had some success in describing the uptake/time relationship of the fibre for a range of relative humidities. It was observed that, at early conditioning times, the model underestimated the fibre water content and at extended conditioning times, but before equilibrium, the moisture content was overestimated. This suggested that the hygrothermal behaviour of the fibre could only be approximated by a process governed by a single equilibrium constant. A diffusion model based on Fick's second law was then combined with the fibre model allowing the hygrothermal conditioning process, within a phenolic based low-fired carbon-fibre composite, to be modelled. The general results of this analysis show that the addition of low-fired carbon-fibre, to a pure phenolic resin material, increases the time required for the material to attain equilibrium. This was attributed to the time required for water to diffuse into, and fill, the fibre during the conditioning process. The effect of low-fired carbon-fibre upon the concentration profile of water molecules, within the resin matrix of a composite (resin and fibre), was also investigated. This showed that, compared to a pure phenolic resin material (only resin), the presence of low-fired carbon-fibre reduces the water concentration gradients throughout the phenolic resin matrix. This would have important implications for the long-term ageing behaviour of the composite, as a reduction in water concentration gradients will also reduce moisture induced property gradients within the resin matrix. Absorbed water is known to cause a swelling response in polymer materials [4, 50]. Differential swelling throughout the geometry of the resin matrix results in the development of internal stresses. As low-fired carbon-fibre reduces the concentration gradients within the resin matrix, the swelling gradients will also be reduced, with an accompanying reduction in internal stress. Thus, low-fired carbon-fibre may be beneficial in reducing swelling induced stresses in the resin matrices of composite materials during hygrothermal conditioning. Sullivan et al [89] modelled the moisture uptake of phenolic based low-fired carbon-fibre composites. However, they didn't consider the concentration of water in the resin matrix, and fibre, as two separate entities. As a result, the concentration profile of water within the matrix was not investigated with only the bulk composite material property changes, not dimension dependent, being explored. Thus, no such beneficial effect of low-fired carbon-fibre, upon the ageing resistance of phenolic matrices, has been previously reported in the literature for these types of composites.

Appendix A

Sample	t (hrs)	$\sqrt{t}$ $(\sqrt{hrs})$	H	w (℃)	T_g (℃)	$tan\delta_b$	H_a
ResinB-EdgePiece-Unconditioned	0	0	0.6607	13.66	182.65	0.0123	0.6729
Unconditioned-NonEdgePiece	0	0	0.6779	12.91	182.17	0.0124	0.6903
Unconditioned-NonEdgePiece-Sample2	0	0	0.6727	13.16	182.48	0.0055	0.6782
Unconditioned-NonEdgePiece-Sample3	0	0	0.6576	13.45	183.09	0.0072	0.6648

Table 62: Lorentzian fit obtained parameter values for unconditioned samples.

Sample	t (hrs)	$\sqrt{t}$ $(\sqrt{hrs})$	H	w (℃)	T_g (℃)	$tan\delta_b$	H_a
L2	145.07	12.04	0.6860	13.11	179.29	0.0132	0.6992
L3	145.07	12.04	0.6888	13.71	179.56	0.0097	0.6985
L4	145.07	12.04	0.6607	14.07	179.95	0.0109	0.6716
L5	313.23	17.70	0.6482	14.63	177.40	0.0332	0.6814
L6	313.23	17.70	0.6662	14.68	177.68	0.0109	0.6770
L7	313.23	17.70	0.6665	14.66	178.13	0.0124	0.6790
L8 (A)	483.45	21.99	0.6715	-	176.28	0.0138	0.6853
L9	483.45	21.99	0.6493	14.57	175.83	0.0153	0.6646
L10	483.45	21.99	0.6583	14.71	175.66	0.0151	0.6734
L11	649.95	25.49	0.6932	14.09	174.09	0.0108	0.7040
L12	649.95	25.49	0.6859	14.48	173.30	0.0092	0.6951
L13	649.95	25.49	0.6648	14.58	174.19	0.0102	0.6750

Table 63: Lorentzian fit obtained parameter values for samples conditioned at 35℃ and 100% relative humidity.

Sample	t (hrs)	$\sqrt{t}$ $(\sqrt{hrs})$	H	w (℃)	T_g (℃)	$tan\delta_b$	H_a
SBT3	145.64	12.07	0.6094	14.06	174.16	0.0380	0.6473
SBT4 (E)	338.39	18.40	-	-	169.83	-	-
SBT22	40.09	6.33	0.6343	13.98	178.58	0.0207	0.6551
SBT23	65.29	8.08	0.6482	13.49	178.00	0.0328	0.6810
SBT31	18.40	4.29	0.6430	13.08	180.19	0.0462	0.6892
SBT32	42.77	6.54	0.5902	15.34	178.50	0.0501	0.6403
SBT33	114.10	10.68	0.6402	14.14	175.07	0.0382	0.6784
SBT34	67.13	8.19	0.6976	13.06	176.13	0.0140	0.7115
SBT35	263.65	16.24	0.7382	13.57	170.32	0.0110	0.7491
SBT36	500.27	22.37	0.7794	13.14	165.24	0.0092	0.7886
SBT37	18.70	4.32	0.6290	14.11	179.58	0.0238	0.6529
SBT38	42.73	6.54	0.6714	14.09	177.72	0.0157	0.6871
SBT39	195.80	13.99	0.7161	13.49	172.00	0.0139	0.7300
SBT310	528.73	22.99	0.7967	13.57	163.98	0.0070	0.8037

Table 64: Lorentzian fit obtained parameter values for samples conditioned at 50℃ and 100% relative humidity.

Sample	t (hrs)	$\sqrt{t}$ $(\sqrt{hrs})$	H	w (℃)	T_g (℃)	$tan\delta_b$	H_a
H1	8.61	2.93	0.6667	13.82	178.70	0.0146	0.6813
H2	8.61	2.93	0.6350	13.77	179.41	0.0192	0.6542
H3	8.61	2.93	0.6567	14.05	178.66	0.0147	0.6714
H4	25.85	5.08	0.6758	13.98	175.72	0.0134	0.6892
H5	25.85	5.08	0.6868	13.64	175.89	0.0140	0.7008
H6	25.85	5.08	0.6762	14.19	175.72	0.0169	0.6930
H7	52.85	7.27	0.7003	13.58	172.59	0.0170	0.7173
H8	52.85	7.27	0.6825	14.06	172.61	0.0151	0.6976
H9	52.85	7.27	0.6949	13.98	171.73	0.0121	0.7070
H10	223.97	14.97	0.7913	13.31	161.89	0.0134	0.8046
H11	223.97	14.97	0.7737	12.83	162.70	0.0231	0.7968
H12	223.97	14.97	0.7709	14.15	163.02	0.0151	0.7860
H13	368.38	19.19	0.8424	13.93	159.40	0.0082	0.8505
H14	368.38	19.19	0.8402	14.20	158.82	0.0080	0.8482
H15	368.38	19.19	0.8312	14.27	158.38	0.0037	0.8349
H17	2960.20	54.41	1.1910	11.58	146.03	0.0000	1.1910
H18	2960.20	54.41	1.1859	12.23	146.42	0.0000	1.1859
H19	3147.90	56.11	1.1952	12.25	144.99	0.0000	1.1952
H20 (A)	3147.90	56.11	1.1987	-	144.93	0.0048	1.2036
H21	3147.90	56.11	1.1196	12.68	144.93	0.0000	1.1196
H22	3318.57	57.61	1.1988	12.26	144.76	0.0000	1.1988
H23	3318.57	57.61	1.1975	12.28	145.63	0.0078	1.2053
H24	3318.57	57.61	1.2567	12.29	144.93	0.0000	1.2567
H25	3910.07	62.53	1.2454	10.65	143.64	0.0000	1.2454
H26	5089.10	71.34	1.2926	11.89	142.89	0.0000	1.2926
HN1	993.50	31.52	1.0468	13.02	151.11	0.0006	1.0473
HN2	993.50	31.52	1.0348	12.89	151.00	0.0143	1.0491
HN3	993.50	31.52	1.0458	13.04	150.71	0.0051	1.0510
HN4	1503.43	38.77	1.1023	12.90	148.73	0.0000	1.1023
HN5	1503.43	38.77	1.0946	12.78	148.56	0.0034	1.0980
HN8	2003.60	44.76	1.0824	11.87	148.35	0.0506	1.1330
HN9	2003.60	44.76	1.1087	12.25	148.27	0.0000	1.1087
HC2-FullyAged-Film1	5279.29	72.66	1.1559	12.66	145.68	0.0053	1.1612
HC2-FullyAged-Film2-2 (A)	5279.29	72.66	1.1328	-	146.31	0.0037	1.1365
HC6-CoreSample-2	5183.30	72.00	1.1605	13.19	144.68	0.0000	1.1605

Table 65: Lorentzian fit obtained parameter values for samples conditioned at 60℃ and 100% relative humidity.

Appendix B

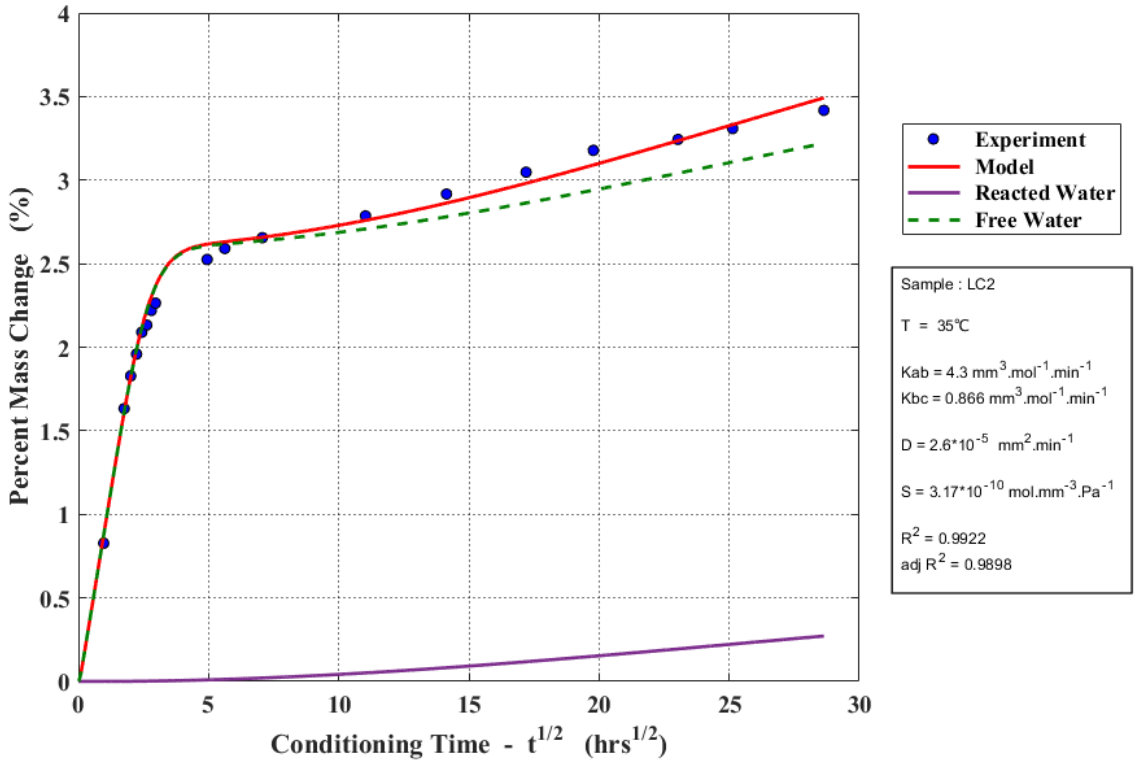

Figure 132: Result of model/data fitting process for sample LC2 conditioned at 35℃ and 100% relative humidity.

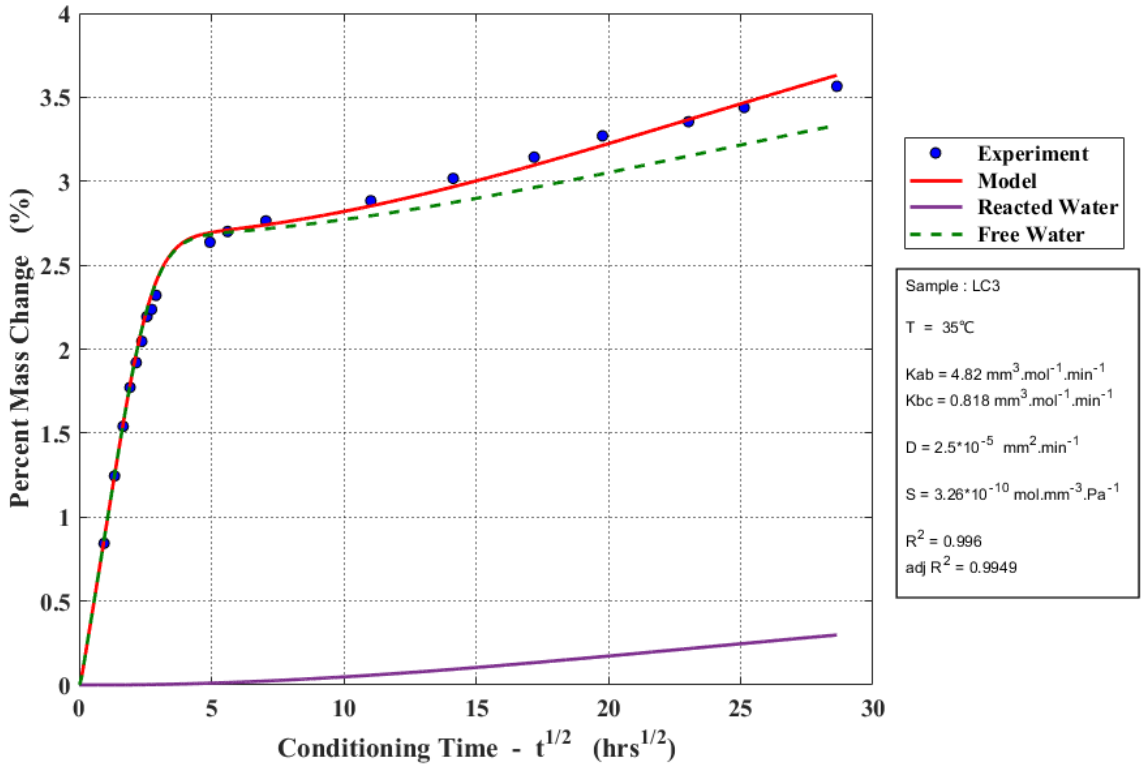

Figure 133: Result of model/data fitting process for sample LC3 conditioned at 35℃ and 100% relative humidity.

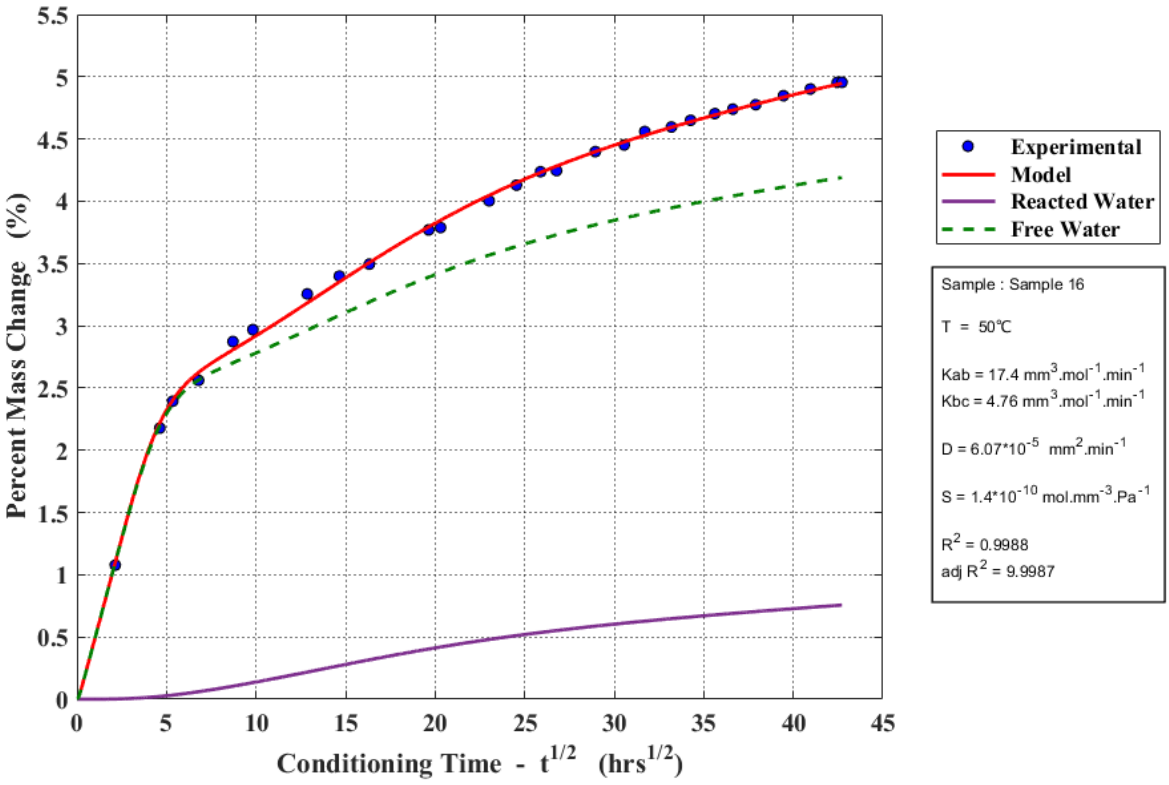

Figure 134: Result of model/data fitting process for Sample 16 conditioned at 50℃ and 100% relative humidity.

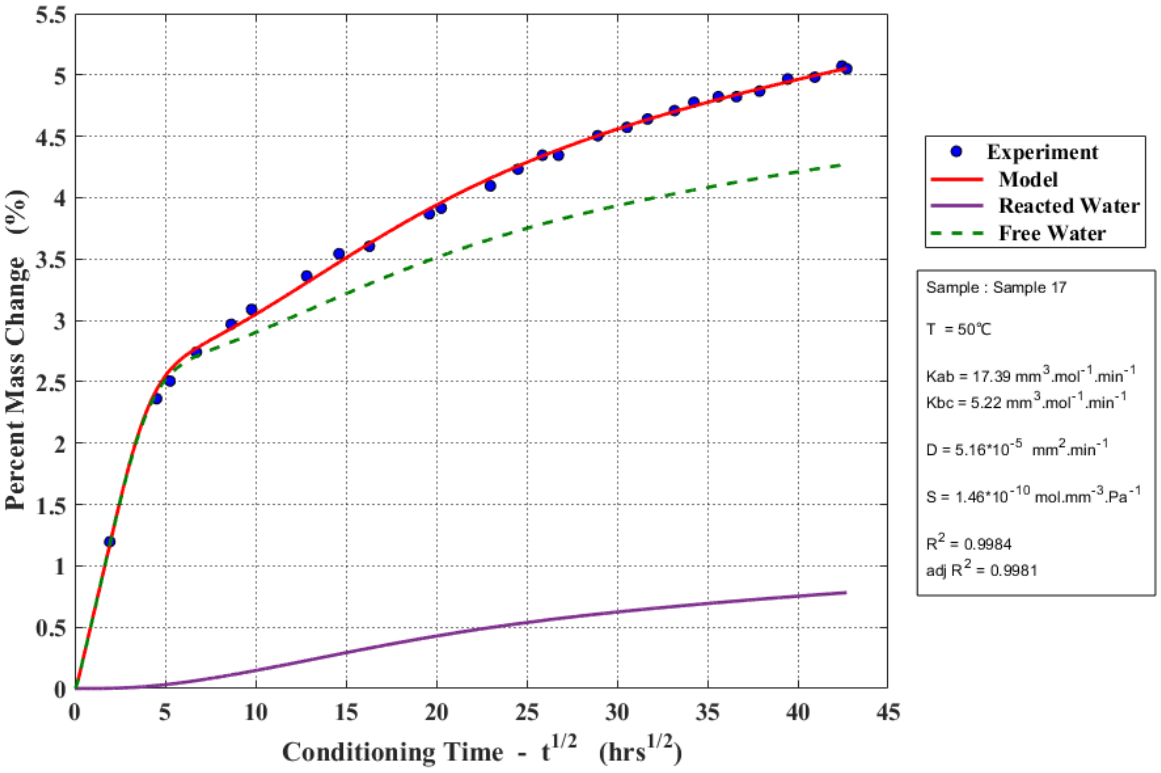

Figure 135: Result of model/data fitting process for Sample 17 conditioned at 50℃ and 100% relative humidity.

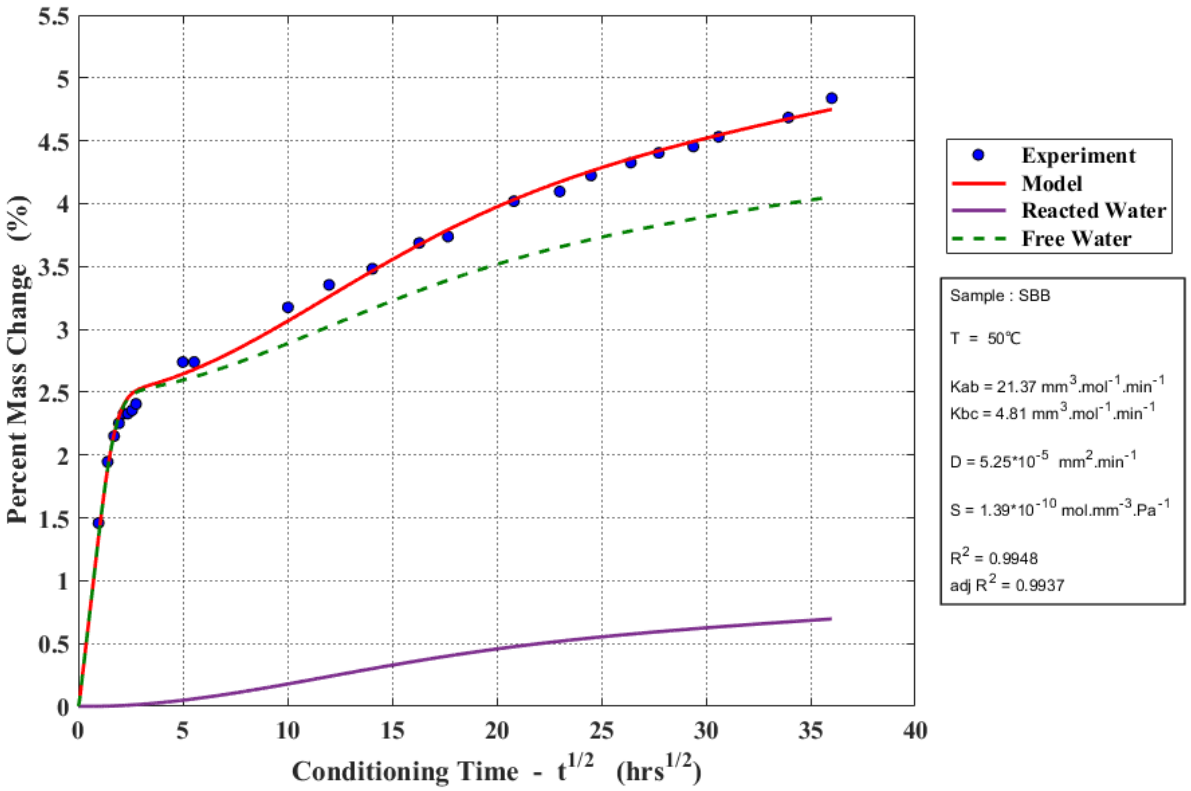

Figure 136: Result of model/data fitting process for sample SBB conditioned at 50℃ and 100% relative humidity.

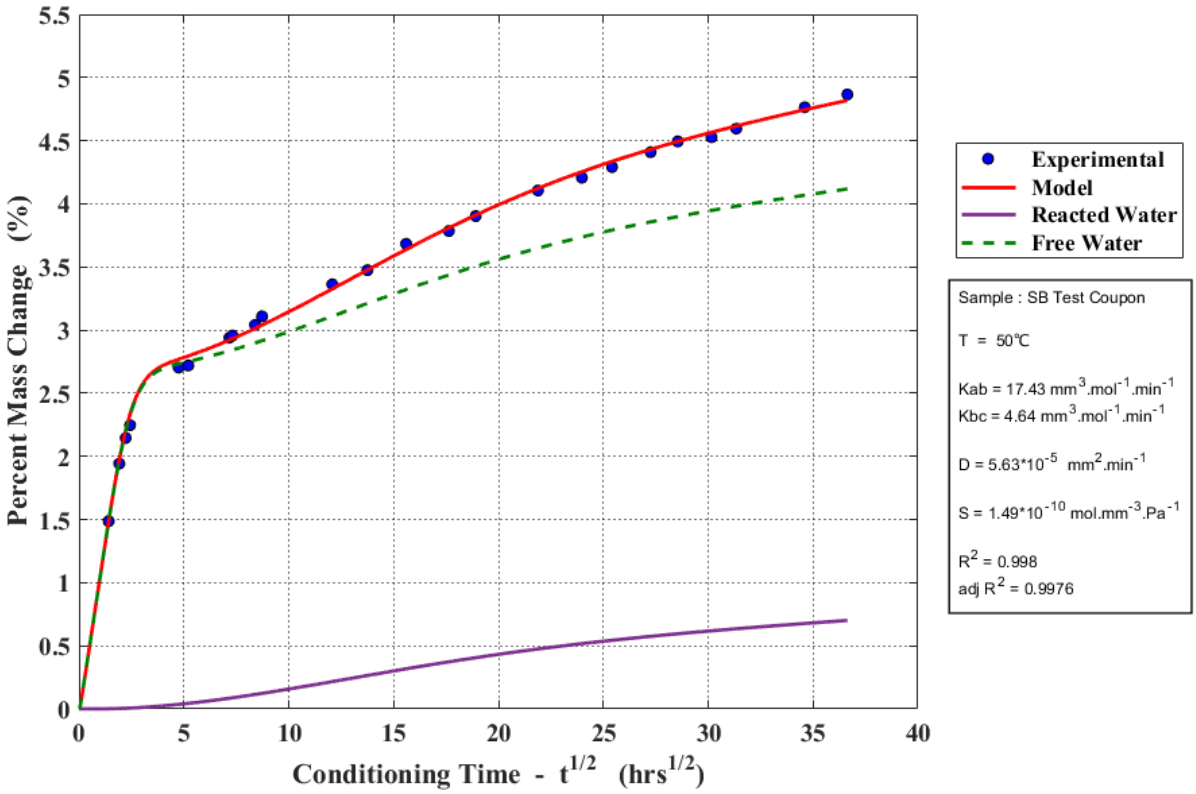

Figure 137: Result of model/data fitting process for sample SB-Test Coupon conditioned at 50℃ and 100% relative humidity.

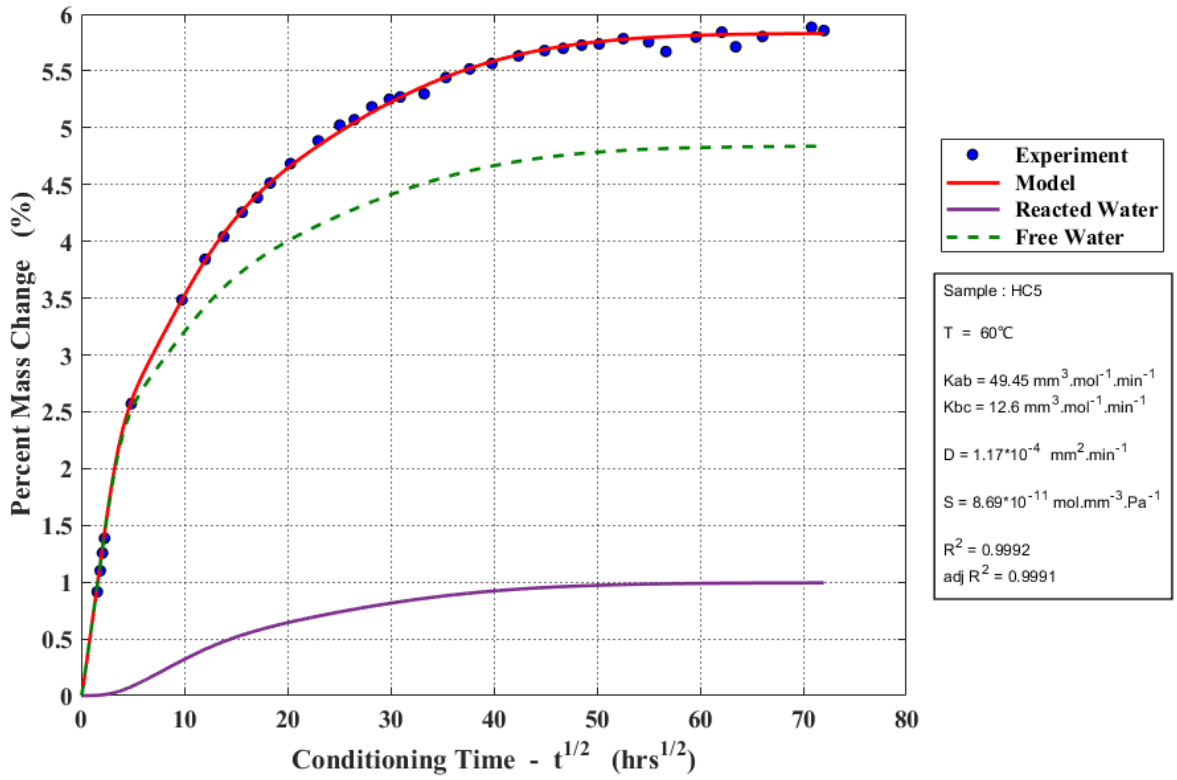

Figure 138: Result of model/data fitting process for sample HC5 conditioned at 60°C and 100% relative humidity.

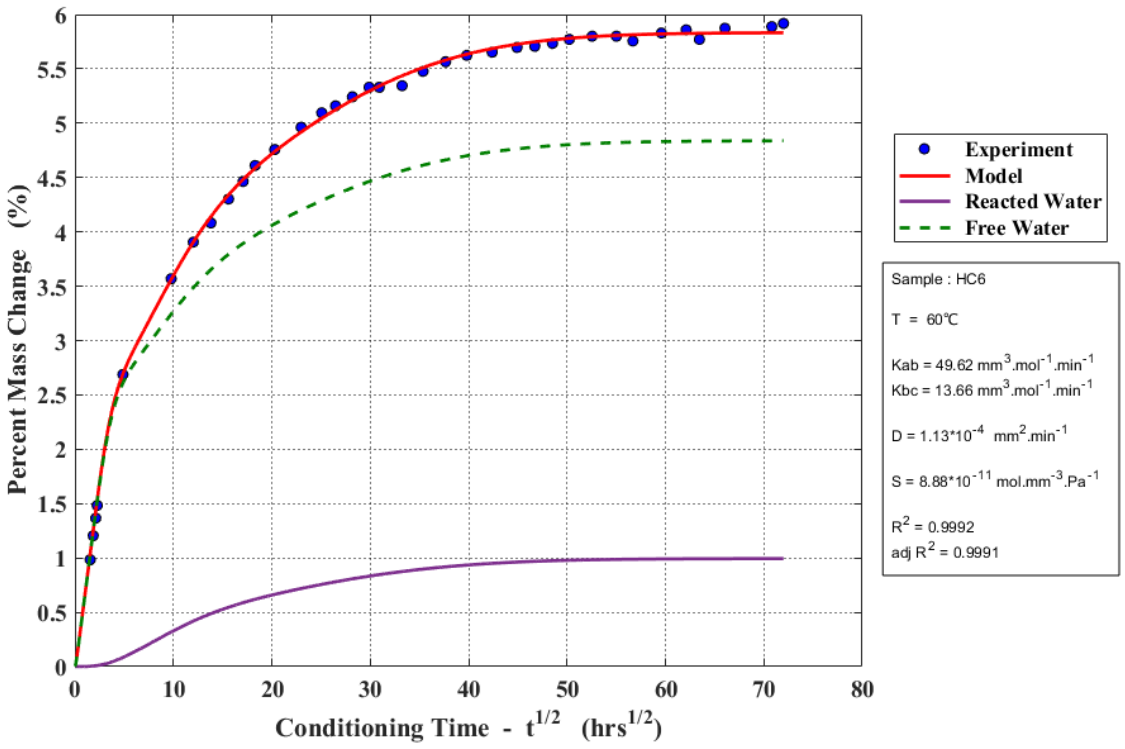

Figure 139: Result of model/data fitting process for sample HC6 conditioned at 60°C and 100% relative humidity.

Appendix C

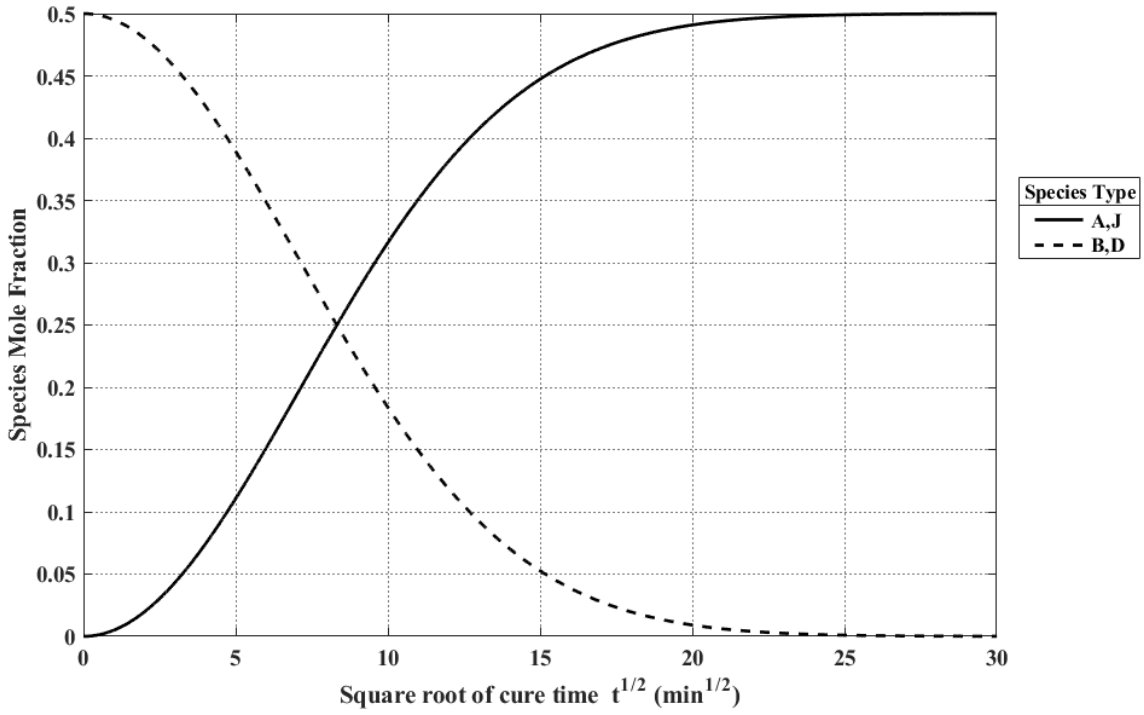

Figure 140: Species evolution as a function of cure time (F/P = 1.5).

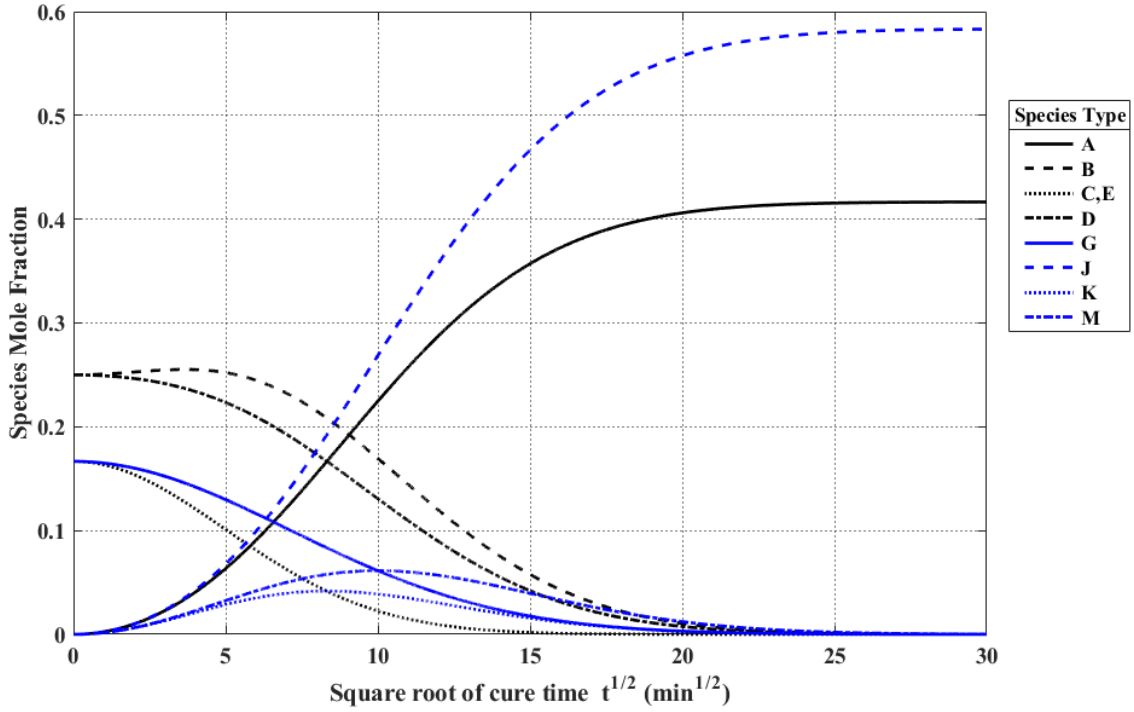

Figure 141: Species evolution as a function of cure time (F/P = 1.75).

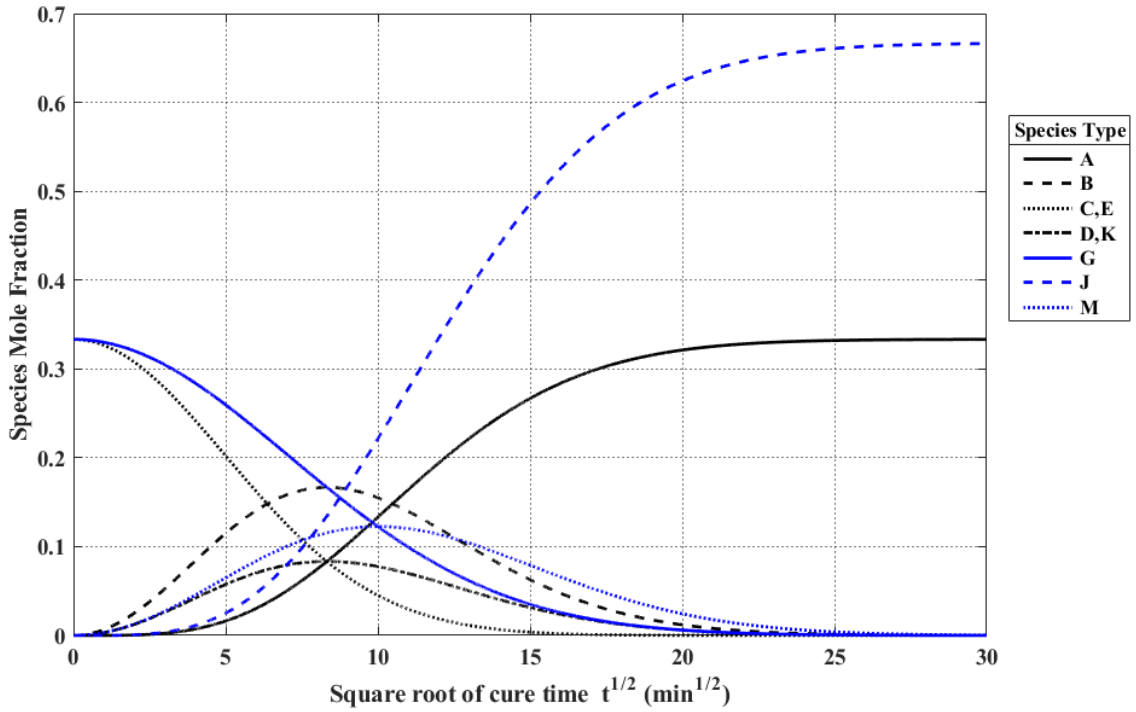

Figure 142: Species evolution as a function of cure time (F/P = 2).

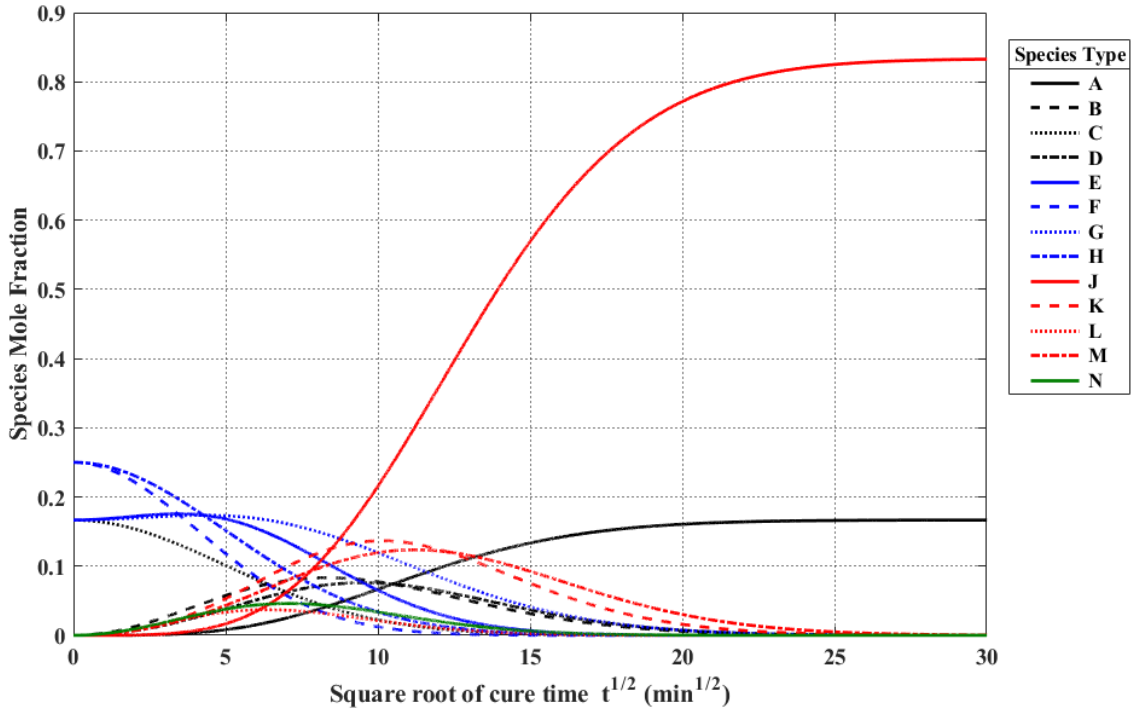

Figure 143: Species evolution as a function of cure time (F/P = 2.25).

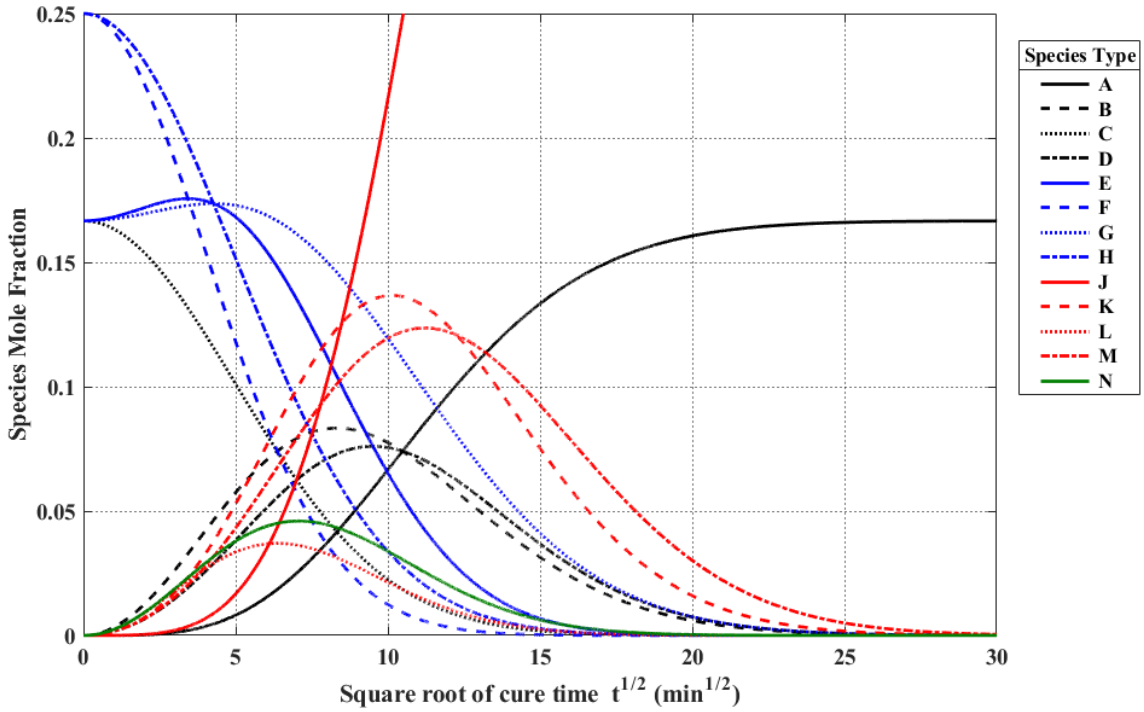

Figure 144: Species evolution as a function of cure time (F/P = 2.25). Figure has been scaled to allow the behaviour of species with low fractional proportions to be observed.

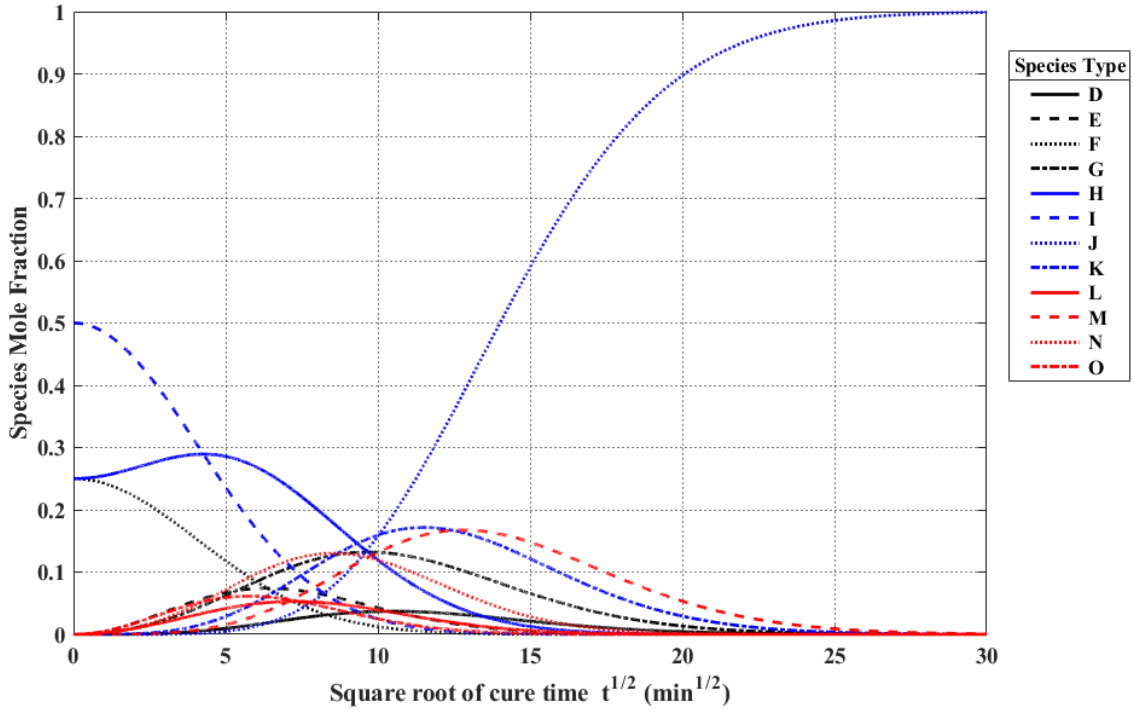

Figure 145: Species evolution as a function of cure time (F/P = 2.75).

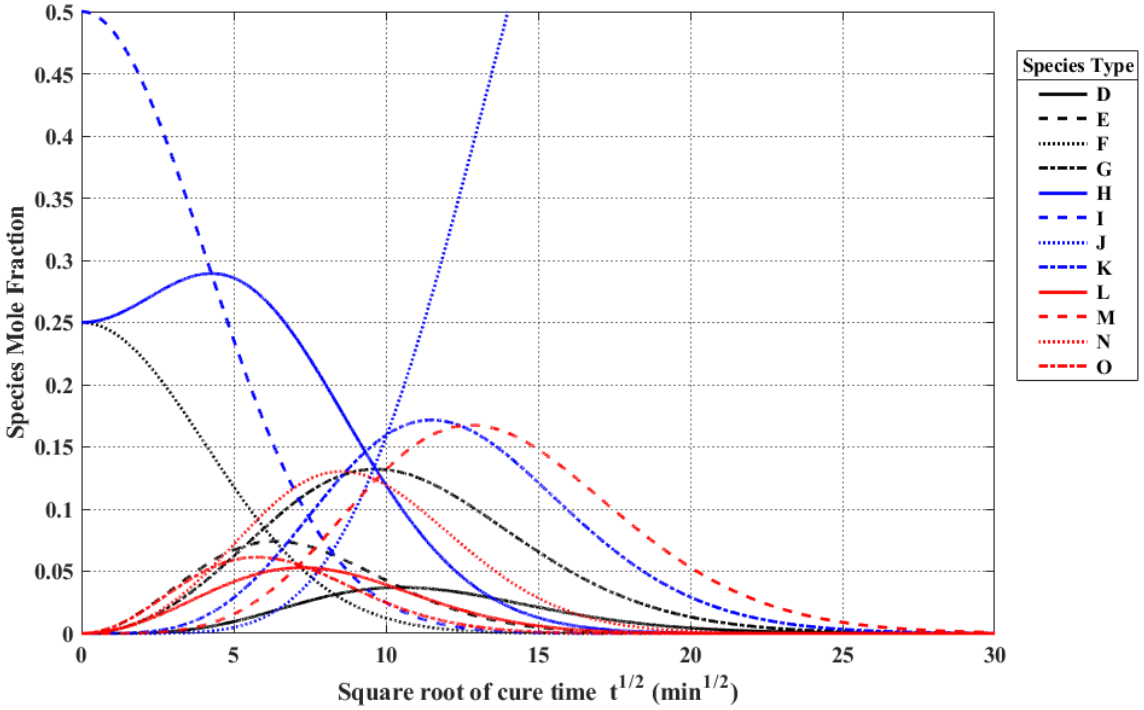

Figure 146: Species evolution as a function of cure time (F/P = 2.75). Figure has been scaled to allow the behaviour of species with low fractional proportions to be observed.

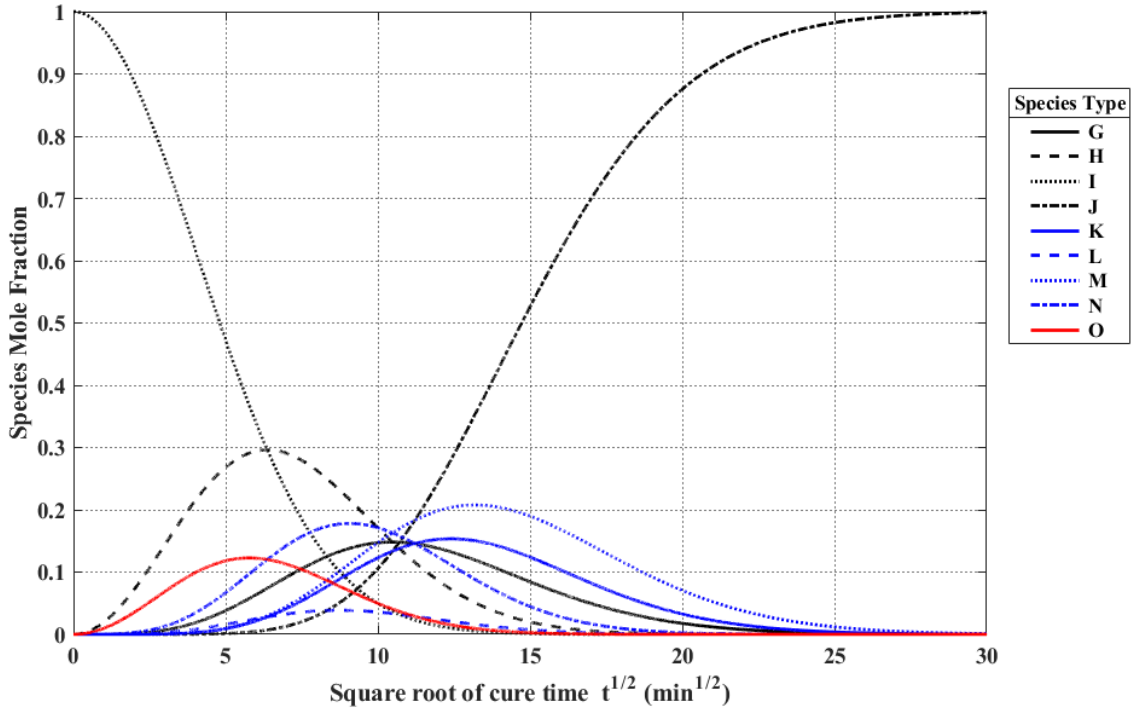

Figure 147: Species evolution as a function of cure time (F/P = 3).

Appendix D

```
%////////////////////////////////////////////////////////////////////////////%
%//////////////////  Diffusion-Hydrolysis  Model  ///////////////////////////%
%////////////////////////////////////////////////////////////////////////////%


conditioningPeriod = 1000000;    %(min)

maximumConcentrationChangePerStep = 0.00000001;     %(mol.mm^-3)

rowsMax = 50;



thickness = 1.2;                            %(mm)
width = 1000000;                            %(mm)
length = 1000000;                           %(mm)

deltax = thickness/(2*(rowsMax - 1));       %(mm)

materialVolume = thickness*width*length;    %(mm^3)
elementVolume = deltax*width*length;        %(mm^3)

pResin = 0.001225896;                       %(g.mm^-3)

cf = (1 + (thickness/width) + (thickness/length))^2;



binMolesA = zeros(rowsMax,1);
binMolesB = zeros(rowsMax,1);
binMolesC = zeros(rowsMax,1);

fA = zeros(rowsMax,1);
fB = zeros(rowsMax,1);
fC = zeros(rowsMax,1);

binS = zeros(rowsMax,1);
binD = zeros(rowsMax,1);
binC = zeros(rowsMax,1);

binCAbs = zeros(rowsMax,1);

binS3 = zeros(rowsMax,1);
binD3 = zeros(rowsMax,1);
binC3 = zeros(rowsMax,1);

binS1 = zeros(rowsMax,1);
binD1 = zeros(rowsMax,1);
binC1 = zeros(rowsMax,1);

xVector = zeros(rowsMax,1);

A1 = zeros(rowsMax,1);
A2 = zeros(rowsMax,1);
A3 = zeros(rowsMax,1);
A4 = zeros(rowsMax,1);
A5 = zeros(rowsMax,1);

fluxGradient = zeros(rowsMax,1);

solubilityFraction = zeros(rowsMax,1);

Ca = zeros(rowsMax,1);

delta = zeros(rowsMax,1);
deltaAbs = zeros(rowsMax,1);

deltaMolesA = zeros(rowsMax,1);
deltaMolesB = zeros(rowsMax,1);
deltaMolesC = zeros(rowsMax,1);

totalWaterMassPerElement = zeros(rowsMax,1);
```

```
time = zeros(1000000,1);
uptake = zeros(1000000,1);
uptakeAbsorbed = zeros(1000000,1);



T = 273 + 50;      %(K)
RH = 1;


v = 1 - (T/647.096);

a1 = -7.85951783;
a2 = 1.84408259;
a3 = -11.7866497;
a4 = 22.6807411;
a5 = -15.9618719;
a6 = 1.80122502;

pSat = 22.064*(10^6)*exp((647.096/T)*((a1*v) + (a2*(v^1.5)) + (a3*(v^3)) + (a4*(v^3.5))
+ (a5*(v^4)) + (a6*(v^7.5))));      %(Pa)


absorbedUptake = 0.994130049;     %(%)

molesFundamentalUnits = ((absorbedUptake*pResin)/3600)*elementVolume;       %(mol)


Ekab = 80720;               %(J.mol^-1)
Ekbc = 80270;               %(J.mol^-1)

Koab = 2.21*(10^14);        %(mm^3.mol^-1.min^-1)
Kobc = 4.81*(10^13);        %(mm^3.mol^-1.min^-1)


Kab = Koab*exp(-Ekab/(8.31*T));         %(mm^3.mol^-1.min^-1)
Kbc = Kobc*exp(-Ekbc/(8.31*T));         %(mm^3.mol^-1.min^-1)



binMolesA(1:rowsMax,1) = molesFundamentalUnits;     %(mol)
binMolesB(1:rowsMax,1) = 0;                         %(mol)
binMolesC(1:rowsMax,1) = 0;                         %(mol)


fA = binMolesA./molesFundamentalUnits;
fB = binMolesB./molesFundamentalUnits;
fC = binMolesC./molesFundamentalUnits;



SoA = 8.89*(10^-18);      %(mol.Pa.mm^-3)
SoC = 1.52*(10^-17);      %(mol.Pa.mm^-3)

EsA = -44540;             %(J.mol^-1)
EsC = -44740;             %(J.mol^-1)


SA = SoA*exp(-EsA/(8.31*T));                    %(mol.Pa^-1.mm^-3)
SC = SoC*exp(-EsC/(8.31*T));                    %(mol.Pa^-1.mm^-3)
SB = 0.5*(SA + SC);                             %(mol.Pa^-1.mm^-3)


DoA = 22511;               %(mm^2.min^-1)
DoC = 3847;                %(mm^2.min^-1)

EdA = 52970;               %(J.mol^-1)
EdC = 50130;               %(J.mol^-1)


DA = DoA*exp(-EdA/(8.31*T));                    %(mm^2.min^-1)
DC = DoC*exp(-EdC/(8.31*T));                    %(mm^2.min^-1)
DB = 0.5*(DA + DC);                             %(mm^2.min^-1)


binS(1:rowsMax,1) = (fA(1:rowsMax,1).*SA) + (fB(1:rowsMax,1).*SB) +
(fC(1:rowsMax,1).*SC);               %(mol.Pa^-1.mm^-3)
```

```
binD(1:rowsMax,1) = cf.*((fA(1:rowsMax,1).*DA) + (fB(1:rowsMax,1).*DB) +
(fC(1:rowsMax,1).*DC));          %(mm^2.min^-1)



binC(2:rowsMax,1) = 0;                          %(mol.mm^-3)
binC(1,1) = binS(1,1).*pSat.*RH;                %(mol.mm^-3)

binCAbs(1:rowsMax,1) = 0;       %(mol.mm^-3)



binS3(1:rowsMax-1,1) = binS(2:rowsMax,1);
binS3(rowsMax,1) = binS(rowsMax,1);

binS1(2:rowsMax,1) = binS(1:rowsMax-1,1);
binS1(1,1) = binS(1,1);


binD3(1:rowsMax-1,1) = binD(2:rowsMax,1);
binD3(rowsMax,1) = binD(rowsMax,1);

binD1(2:rowsMax,1) = binD(1:rowsMax-1,1);
binD1(1,1) = binD(1,1);


binC3(1:rowsMax-1,1) = binC(2:rowsMax,1);
binC3(rowsMax,1) = binC(rowsMax,1);

binC1(2:rowsMax,1) = binC(1:rowsMax-1,1);
binC1(1,1) = binC(1,1);



time(1,1) = 0;       %(min)
uptake(1,1) = 0;     %(%)



xVector(1,1) = 0;    %(mm)


counter1 = 2;

while counter1 <= rowsMax

    xVector(counter1,1) = (counter1 - 1.5)*deltax;     %(mm)

    counter1 = counter1 + 1;

end



t = 0;       %(min)

counter = 2;
counter3 = 1;



while t < conditioningPeriod

    A1(2:rowsMax,1) = (binS3(2:rowsMax,1) + binS1(2:rowsMax,1) -
    (2.*binS(2:rowsMax,1)))./(deltax*deltax);    % A1 = d^2S/dx^2
    A2(2:rowsMax,1) = (binS3(2:rowsMax,1) - binS1(2:rowsMax,1))./(2*deltax);
    % A2 = dS/dx
    A3(2:rowsMax,1) = (binC3(2:rowsMax,1) + binC1(2:rowsMax,1) -
    (2.*binC(2:rowsMax,1)))./(deltax*deltax);    % A3 = d^2C/dx^2
    A4(2:rowsMax,1) = (binC3(2:rowsMax,1) - binC1(2:rowsMax,1))./(2*deltax);
    % A4 = dC/dx
    A5(2:rowsMax,1) = (binD3(2:rowsMax,1) - binD1(2:rowsMax,1))./(2*deltax);
    % A5 = dD/dx

        fluxGradientWater(2:rowsMax,1) =
        ((binC(2:rowsMax,1).*A5(2:rowsMax,1).*A2(2:rowsMax,1))./binS(2:rowsMax,1)) +
```

```
    ((binD(2:rowsMax,1).*A4(2:rowsMax,1).*A2(2:rowsMax))./binS(2:rowsMax,1)) -
    ((binD(2:rowsMax,1).*binC(2:rowsMax,1).*((A2(2:rowsMax,1)).^2))./
    ((binS(2:rowsMax,1)).^2)) +
    ((binD(2:rowsMax,1).*binC(2:rowsMax,1).*A1(2:rowsMax,1))./(binS(2:rowsMax,1))) -
    (A4(2:rowsMax,1).*A5(2:rowsMax,1)) - (binD(2:rowsMax,1).*A3(2:rowsMax,1));



solubilityFraction = SA./binS;

Ca(1:rowsMax,1) = ((2.*Kab.*binMolesA(1:rowsMax,1)) +
(Kbc.*binMolesB(1:rowsMax,1))).*((solubilityFraction(1:rowsMax,1).*
binC(1:rowsMax,1))./elementVolume);     %(mol.mm^-3.min^-1)



delta = -fluxGradientWater(2:rowsMax,1) - Ca(2:rowsMax,1);       %(mol.mm^-3.min^-1)


deltaAbs = abs(delta);                    %(mol.mm^-3.min^-1)
deltaAbsMax = max(delta);                 %(mol.mm^-3.min^-1)

deltat = maximumConcentrationChangePerStep/deltaAbsMax;           %(min)



if deltat > 1

    deltat = 1;     %(min)

end



deltaMolesA(1:rowsMax,1) = (-2.*Kab.*solubilityFraction(1:rowsMax,1).*
binC(1:rowsMax,1).*binMolesA(1:rowsMax,1)).*deltat;          %(mol)
deltaMolesB(1:rowsMax,1) = ((2.*Kab.*solubilityFraction(1:rowsMax,1).*
binC(1:rowsMax,1).*binMolesA(1:rowsMax,1)) - (Kbc.*solubilityFraction(1:rowsMax,1).*
binC(1:rowsMax,1).*binMolesB(1:rowsMax,1))).*deltat;         %(mol)
deltaMolesC(1:rowsMax,1) = (Kbc.*solubilityFraction(1:rowsMax,1).*
binC(1:rowsMax,1).*binMolesB(1:rowsMax,1)).*deltat;          %(mol)



binMolesA(1:rowsMax,1) = binMolesA(1:rowsMax,1) + deltaMolesA(1:rowsMax,1); %(mol)
binMolesB(1:rowsMax,1) = binMolesB(1:rowsMax,1) + deltaMolesB(1:rowsMax,1); %(mol)
binMolesC(1:rowsMax,1) = binMolesC(1:rowsMax,1) + deltaMolesC(1:rowsMax,1); %(mol)



binCAbs(1:rowsMax,1) = binCAbs(1:rowsMax,1) + (Ca(1:rowsMax,1).*deltat);
%(mol.mm^-3)



binC(2:rowsMax,1) = binC(2:rowsMax,1) + (delta.*deltat);       %(mol.mm^-3)



t = t + deltat;    %(min)



materialDryMass = pResin*elementVolume*(rowsMax - 1);   %(g)

totalWaterMassPerElement(2:rowsMax,1) = (binC(2:rowsMax,1) +
binCAbs(2:rowsMax,1)).*elementVolume.*18;        %(g)
totalWaterMass = sum(totalWaterMassPerElement);  %(g)

percentageUptake = 100*(totalWaterMass/materialDryMass);           %(%)


absorbedWaterMassPerElement(2:rowsMax,1) = binCAbs(2:rowsMax,1).*elementVolume.*18;
%(g)
absorbedWaterMass = sum(absorbedWaterMassPerElement(2:rowsMax,1));     %(g)

percentageUptakeAbsorbed = 100*(absorbedWaterMass/materialDryMass);    %(%)
```

```
    time(counter,1) = t;                                            %(min)
    uptake(counter,1) = percentageUptake;                           %(%)
    uptakeAbsorbed(counter,1) = percentageUptakeAbsorbed;           %(%)



    counter = counter + 1;



    fA = binMolesA./molesFundamentalUnits;
    fB = binMolesB./molesFundamentalUnits;
    fC = binMolesC./molesFundamentalUnits;



    binS(1:rowsMax,1) = (fA(1:rowsMax,1).*SA) + (fB(1:rowsMax,1).*SB) +
   (fC(1:rowsMax,1).*SC);                %(mol.Pa^-1.mm^-3)

    binD(1:rowsMax,1) = cf.*((fA(1:rowsMax,1).*DA) + (fB(1:rowsMax,1).*DB) +
   (fC(1:rowsMax,1).*DC));          %(mm^2.min^-1)

    binC(1,1) = binS(1,1).*pSat.*RH;    %(mol.mm^-3)



    binS3(1:rowsMax-1,1) = binS(2:rowsMax,1);
    binS3(rowsMax,1) = binS(rowsMax,1);

    binS1(2:rowsMax,1) = binS(1:rowsMax-1,1);
    binS1(1,1) = binS(1,1);


    binD3(1:rowsMax-1,1) = binD(2:rowsMax,1);
    binD3(rowsMax,1) = binD(rowsMax,1);

    binD1(2:rowsMax,1) = binD(1:rowsMax-1,1);
    binD1(1,1) = binD(1,1);


    binC3(1:rowsMax-1,1) = binC(2:rowsMax,1);
    binC3(rowsMax,1) = binC(rowsMax,1);

    binC1(2:rowsMax,1) = binC(1:rowsMax-1,1);
    binC1(1,1) = binC(1,1);



end


%////////////////////////////////////////////////////////////////////////%
%//////////////////  End Conditioning Simulation  ////////////////////////%
%////////////////////////////////////////////////////////////////////////%
```

Bibliography

[1] A. Zafar, F. Bertocco, J. Schjødt-Thomsen, and J. C. Rauhe, "Investigation of the long term effects of moisture on carbon fibre and epoxy matrix composites", *Composites Science and Technology,* vol. 72, no. 6, pp. 656-666, 2012.

[2] O. Kläusler, S. Clauß, L. Lübke, J. Trachsel, and P. Niemz, "Influence of moisture on stress–strain behaviour of adhesives used for structural bonding of wood", *International Journal of Adhesion and Adhesives,* vol. 44, pp. 57-65, 2013.

[3] G. Xian and V. M. Karbhari, "DMTA based investigation of hygrothermal ageing of an epoxy system used in rehabilitation", *Journal of Applied Polymer Science,* vol. 104, no. 2, pp. 1084-1094, 2007.

[4] M. Adamson, "Thermal expansion and swelling of cured epoxy resin used in graphite/epoxy composite materials", *Journal of Materials Science,* vol. 15, no. 7, pp. 1736-1745, 1980.

[5] B. De'Nève and M. E. R. Shanahan, "Water absorption by an epoxy resin and its effect on the mechanical properties and infra-red spectra", *Polymer,* vol. 34, no. 24, pp. 5099-5105, 1993.

[6] D. Fata and W. Possart, "Aging behavior of a hot-cured epoxy system", *Journal of Applied Polymer Science,* vol. 99, no. 5, pp. 2726-2736, 2006.

[7] G. Z. Xiao and M. E. R. Shanahan, "Irreversible effects of hygrothermal aging on DGEBA/DDA epoxy resin", *Journal of Applied Polymer Science,* vol. 69, no. 2, pp. 363-369, 1998.

[8] J. El Yagoubi, G. Lubineau, F. Roger, and J. Verdu, "A fully coupled diffusion-reaction scheme for moisture sorption–desorption in an anhydride-cured epoxy resin", *Polymer,* vol. 53, no. 24, pp. 5582-5595, 2012.

[9] B. Ellis, "Chemistry and Technology of Epoxy resins", *1st ed. Springer Netherlands*, 1993, p. 332.

[10] A. J. Lesser and E. Crawford, "The role of network architecture on the glass transition temperature of epoxy resins", *Journal of Applied Polymer Science,* vol. 66, no. 2, pp. 387-395, 1997.

[11] L. Pilato, "Phenolic Resins: A Century of Progress", *1st ed. Springer-Verlag Berlin Heidelberg*, 2010, p. 545.

[12] D. Puglia, L. B. Manfredi, A. Vazquez, and J. M. Kenny, "Thermal degradation and fire resistance of epoxy–amine–phenolic blends", *Polymer Degradation and Stability,* vol. 73, no. 3, pp. 521-527, 2001.

[13] H. Chtourou, A. Atarsia, and B. Fisa, "Prediction of Thermal and Fire Resistance of Phenolic Resins by Dynamic TG Analysis", *Journal of Reinforced Plastics and Composites,* vol. 18, no. 4, pp. 339-345, 1999.

[14] A. R. Bahramian, M. Kokabi, M. H. N. Famili, and M. H. Beheshty, "Ablation and thermal degradation behaviour of a composite based on resol type phenolic resin: Process modeling and experimental", *Polymer,* vol. 47, no. 10, pp. 3661-3673, 2006.

[15] G. E. Maciel, I. S. Chuang, and L. Gollob, "Solid-state carbon-13 NMR study of resol-type phenol-formaldehyde resins", *Macromolecules,* vol. 17, no. 5, pp. 1081-1087, 1984.

[16] J. D. M. Jr, C. G. Silva, E. C. Ramires, and E. Frollini, "Thermoset matrix reinforced with sisal fibers: Effect of the cure cycle on the properties of the biobased composite", *Polymer Testing,* vol. 28, no. 8, pp. 793-800, 2009.

[17] F. Abrams and M. Ungarish, "Effect of pressure on phenolic cure", pp. 59-68: Publ by Technomic Publ Co Inc, Lancaster, PA, United States.

[18] J. H. Freeman and C. W. Lewis, "Alkaline-catalyzed Reaction of Formaldehyde and the Methylols of Phenol; A Kinetic Study", *Journal of the American Chemical Society,* vol. 76, no. 8, pp. 2080-2087, 1954.

[19] G. Astarloa Aierbe, J. M. Echeverría, C. C. Riccardi, and I. Mondragon, "Influence of the temperature on the formation of a phenolic resol resin catalyzed with amine", *Polymer,* vol. 43, no. 8, pp. 2239-2243, 2002.

[20] J. Monni, L. Alvila, and T. T. Pakkanen, "Structural and Physical Changes in Phenol−Formaldehyde Resol Resin, as a Function of the Degree of Condensation of the Resol Solution", *Industrial & Engineering Chemistry Research,* vol. 46, no. 21, pp. 6916-6924, 2007.

[21] L. B. Manfredi, O. de la Osa, N. G. Fernández, and A. Vázquez, "Structure-properties relationship for resols with different formaldehyde/phenol molar ratio", *Polymer,* vol. 40, no. 13, pp. 3867-3875, 1999.

[22] L. B. Manfredi, C. C. Riccardi, O. d. l. Osa, and A. a. Vázquez, "Modelling of resol resin polymerization with various formaldehyde/phenol molar ratios", *Polymer International,* vol. 50, no. 7, pp. 796-802, 2001.

[23] C. C. Riccardi, G. A. Aierbe, J. M. Echeverría, and I. Mondragon, "Modelling of phenolic resin polymerisation", *Polymer,* vol. 43, no. 5, pp. 1631-1639, 2002.

[24] S. G. Lee, J. I. Choi, W. Koh, S. S. Jang, J. Kim, and G. Kim, "Effect of Temperature on Water Molecules in a Model Epoxy Molding Compound: Molecular Dynamics Simulation Approach", *IEEE Transactions on Components, Packaging and Manufacturing Technology,* vol. 1, no. 10, pp. 1533-1542, 2011.

[25] C. L. Soles, F. T. Chang, B. A. Bolan, H. A. Hristov, D. W. Gidley, and A. F. Yee, "Contributions of the nanovoid structure to the moisture absorption properties of epoxy resins", *Journal of Polymer Science Part B: Polymer Physics,* vol. 36, no. 17, pp. 3035-3048, 1998.

[26] Y. Nishitani *et al.*, "Use of Hoy's solubility parameters to predict water sorption/solubility of experimental primers and adhesives", *European journal of oral sciences,* vol. 115, no. 1, pp. 81-86, 2007.

[27] C. Carfagna, A. Apicella, and L. Nicolais, "The effect of the prepolymer composition of amino-hardened epoxy resins on the water sorption behavior and plasticization", *Journal of Applied Polymer Science,* vol. 27, no. 1, pp. 105-112, 1982.

[28] C. Grave, I. McEwan, and R. A. Pethrick, "Influence of stoichiometric ratio on water absorption in epoxy resins", *Journal of Applied Polymer Science,* vol. 69, no. 12, pp. 2369-2376, 1998.

[29] E. H. Stokes, "Equilibrated moisture content of several carbon phenolic composites", *AIAA Journal,* vol. 30, no. 6, pp. 1597-1601, 1992.

[30] B. Xie, X. J. Fan, X. Q. Shi, and H. Ding, "Direct Concentration Approach of Moisture Diffusion and Whole-Field Vapor Pressure Modeling for Reflow Process—Part I: Theory and Numerical Implementation", *Journal of Electronic Packaging,* vol. 131, no. 3, pp. 031010-031010-7, 2009.

[31] J. Crank, "The Mathematics of Diffusion", *Oxford University Press*, 1975, p. 424.

[32] E. Dermitzaki, B. Wunderle, J. Bauer, H. Walter, and B. Michel, "Structure property correlation of epoxy resins under the influence of moisture and temperature; and comparison of diffusion coefficient with MD-simulations", in *2008 2nd Electronics System-Integration Technology Conference*, 2008, pp. 897-902.

[33] P. K. Aditya and P. K. Sinha, "Diffusion Coefficients of Polymeric Composites Subjected to Periodic Hygrothermal Exposure", *Journal of Reinforced Plastics and Composites,* vol. 11, no. 9, pp. 1035-1047, 1992.

[34] P. Musto, L. Mascia, G. Ragosta, G. Scarinzi, and P. Villano, "The transport of water in a tetrafunctional epoxy resin by near-infrared Fourier transform spectroscopy", *Polymer,* vol. 41, no. 2, pp. 565-574, 2000.

[35] C. Maggana and P. Pissis, "Water sorption and diffusion studies in an epoxy resin system", *Journal of Polymer Science Part B: Polymer Physics,* vol. 37, no. 11, pp. 1165-1182, 1999.

[36] I. Merdas, F. Thominette, A. Tcharkhtchi, and J. Verdu, "Factors governing water absorption by composite matrices", *Composites Science and Technology,* vol. 62, no. 4, pp. 487-492, 2002.

[37] C. Damian, M. Escoubes, and E. Espuche, "Gas and water transport properties of epoxy–amine networks: Influence of crosslink density", *Journal of Applied Polymer Science,* vol. 80, no. 11, pp. 2058-2066, 2001.

[38] H. G. Carter and K. G. Kibler, "Langmuir-type model for anomalous moisture diffusion in composite resins", *Journal of Composite Materials,* vol. 12, no. 2, pp. 118-131, 1978.

[39] G. Z. Xiao, M. Delamar, and M. E. R. Shanahan, "Irreversible interactions between water and DGEBA/DDA epoxy resin during hygrothermal aging", *Journal of Applied Polymer Science,* vol. 65, no. 3, pp. 449-458, 1998.

[40] M. D. Placette, X. Fan, J.-H. Zhao, and D. Edwards, "Dual stage modeling of moisture absorption and desorption in epoxy mold compounds", *Microelectronics Reliability,* vol. 52, no. 7, pp. 1401-1408, 2012.

[41] S. Popineau, C. Rondeau-Mouro, C. Sulpice-Gaillet, and M. E. R. Shanahan, "Free/bound water absorption in an epoxy adhesive", *Polymer,* vol. 46, no. 24, pp. 10733-10740, 2005.

[42] B. De Neve and M. E. R. Shanahan, "Physical and Chemical Effects in An Epoxy Resin Exposed to Water Vapour", *The Journal of Adhesion,* vol. 49, no. 3-4, pp. 165-176, 1995.

[43] G. Z. Xiao and M. E. R. Shanahan, "Swelling of DGEBA/DDA epoxy resin during hygrothermal ageing", *Polymer,* vol. 39, no. 14, pp. 3253-3260, 1998.

[44] G. Z. Xiao and M. E. R. Shanahan, "Water absorption and desorption in an epoxy resin with degradation", *Journal of Polymer Science Part B: Polymer Physics,* vol. 35, no. 16, pp. 2659-2670, 1998.

[45] C. Damian, E. Espuche, and M. Escoubes, "Influence of three ageing types (thermal oxidation, radiochemical and hydrolytic ageing) on the structure and gas transport properties of epoxy-amine networks", *Polymer Degradation and Stability,* vol. 72, no. 3, pp. 447-458, 2001.

[46] J. Konnerth, F. Stöckel, U. Müller, and W. Gindl, "Elastic properties of adhesive polymers. III. Adhesive polymer films under dry and wet conditions characterized by means of nanoindentation", *Journal of Applied Polymer Science,* vol. 118, no. 3, pp. 1331-1334, 2010.

[47] A. Apicella, L. Nicolais, G. Astarita, and E. Drioli, "Effect of thermal history on water sorption, elastic properties and the glass transition of epoxy resins", *Polymer,* vol. 20, no. 9, pp. 1143-1148, 1979.

[48] M. Akay, S. K. A. Mun, and A. Stanley, "Influence of moisture on the thermal and mechanical properties of autoclaved and oven-cured Kevlar-49/epoxy laminates", *Composites Science and Technology,* vol. 57, no. 5, pp. 565-571, 1997.

[49] J. Zhou and J. P. Lucas, "Hygrothermal effects of epoxy resin. Part II: variations of glass transition temperature", *Polymer,* vol. 40, no. 20, pp. 5513-5522, 1999.

[50] W. K. Loh, A. D. Crocombe, M. M. A. Wahab, and I. A. Ashcroft, "Modelling anomalous moisture uptake, swelling and thermal characteristics of a rubber toughened epoxy adhesive", *International Journal of Adhesion and Adhesives,* vol. 25, no. 1, pp. 1-12, 2005.

[51] K. P. Menard, "Dynamic Mechanical Analysis: A Practical Introduction", *2nd ed. CRC Press*, 2008.

[52] D. Bikiaris, J. Prinos, M. Botev, C. Betchev, and C. Panayiotou, "Blends of polymers with similar glass transition temperatures: A DMTA and DSC study", *Journal of Applied Polymer Science,* vol. 93, no. 2, pp. 726-735, 2004.

[53] D. Li and J. Brisson, "DMTA and FTIR Investigation of the Phase Behavior of Poly(methyl methacrylate)−Poly(4-vinylphenol) Blends", *Macromolecules,* vol. 29, no. 3, pp. 868-874, 1996.

[54] M. G. Prolongo, C. Arribas, C. Salom, and R. M. Masegosa, "Phase separation, cure kinetics, and morphology of epoxy/poly(vinyl acetate) blends", *Journal of Applied Polymer Science,* vol. 103, no. 3, pp. 1507-1516, 2006.

[55] M. Xie, Z. Zhang, Y. Gu, M. Li, and Y. Su, "A new method to characterize the cure state of epoxy prepreg by dynamic mechanical analysis", *Thermochimica Acta,* vol. 487, no. 1, pp. 8-17, 2009.

[56] M. R. Vanlandingham, R. F. Eduljee, and J. W. Gillespie, "Moisture diffusion in epoxy systems", *Journal of Applied Polymer Science,* vol. 71, no. 5, pp. 787-798, 1999.

[57] S. K. Karad, D. Attwood, and F. R. Jones, "Moisture absorption by cyanate ester modified epoxy resin matrices. Part V: effect of resin structure" *Composites Part A: Applied Science and Manufacturing,* vol. 36, no. 6, pp. 764-771, 2005.

[58] K. I. Ivanova, R. A. Pethrick, and S. Affrossman, "Hygrothermal aging of rubber-modified and mineral-filled dicyandiamide-cured DGEBA epoxy resin. II. Dynamic mechanical thermal analysis" *Journal of Applied Polymer Science,* vol. 82, no. 14, pp. 3477-3485, 2001.

[59] S. Alessi, G. Pitarresi, and G. Spadaro, "Effect of hydrothermal ageing on the thermal and delamination fracture behaviour of CFRP\ composites" *Composites Part B: Engineering,* vol. 67, no. 0, pp. 145-153, 2014.

[60] J. Zhou and J. P. Lucas, "Hygrothermal effects of epoxy resin. Part I: the nature of water in epoxy" *Polymer,* vol. 40, no. 20, pp. 5505-5512, 1999.

[61] A. Chateauminois, B. Chabert, J. P. Soulier, and L. Vincent, "Dynamic mechanical analysis of epoxy composites plasticized by water: Artifact and reality" *Polymer Composites,* vol. 16, no. 4, pp. 288-296, 2004.

[62] N. Yusof and A. F. Ismail, "Post spinning and pyrolysis processes of polyacrylonitrile (PAN)-based carbon fiber and activated carbon fiber: A review" *Journal of Analytical and Applied Pyrolysis,* vol. 93, pp. 1-13, 2012.

[63] E. H. Stokes, "Anomalous swelling behavior of FM 5055 carbon phenolic composite" *AIAA Journal,* vol. 31, no. 3, pp. 584-589, 1993.

[64] F. Stoeckli, T. Jakubov, and A. Lavanchy, "Water adsorption in active carbons described by the Dubinin-Astakhov equation" *Journal of the Chemical Society, Faraday Transactions,* vol. 90, no. 5, pp. 783-786, 1994.

[65] D. D. Do, S. Junpirom, and H. D. Do, "A new adsorption–desorption model for water adsorption in activated carbon" *Carbon,* vol. 47, no. 6, pp. 1466-1473, 2009.

[66] M. M. Dubinin, "Generalization of the theory of volume filling of micropores to nonhomogeneous microporous structures" *Carbon,* vol. 23, no. 4, pp. 373-380, 1985.

[67] F. Ellyin and C. Rohrbacher, "Effect of Aqueous Environment and Temperature on Glass-Fibre Epoxy Resin Composites" *Journal of Reinforced Plastics and Composites,* vol. 19, no. 17, pp. 1405-1427, 2000.

[68] J. Zhou and J. P. Lucas, "The effects of a water environment on anomalous absorption behavior in graphite/epoxy composites" *Composites Science and Technology,* vol. 53, no. 1, pp. 57-64, 1995.

[69] R. H. Newman, "Auto-accelerative water damage in an epoxy composite reinforced with plain-weave flax fabric" *Composites Part A: Applied Science and Manufacturing,* vol. 40, no. 10, pp. 1615-1620, 2009.

[70] J.-E. Lundgren and P. Gudmundson, "Moisture absorption in glass-fibre/epoxy laminates with transverse matrix cracks" *Composites Science and Technology,* vol. 59, no. 13, pp. 1983-1991, 1999.

[71] D. Porter, *Group Interaction Modelling of Polymer Properties*. CRC Press, 1995, p. 512.
[72] V. R. Gumen, F. R. Jones, and D. Attwood, "Prediction of the glass transition temperatures for epoxy resins and blends using group interaction modelling" *Polymer,* vol. 42, no. 13, pp. 5717-5725, 2001.
[73] H. Liu, A. Uhlherr, and M. K. Bannister, "Quantitative structure–property relationships for composites: prediction of glass transition temperatures for epoxy resins" *Polymer,* vol. 45, no. 6, pp. 2051-2060, 2004.
[74] J. P. Foreman, D. Porter, S. Behzadi, K. P. Travis, and F. R. Jones, "Thermodynamic and mechanical properties of amine-cured epoxy resins using group interaction modelling" *Journal of Materials Science,* vol. 41, no. 20, pp. 6631-6638, 2006.
[75] J. P. Foreman, D. Porter, S. Behzadi, P. T. Curtis, and F. R. Jones, "Predicting the thermomechanical properties of an epoxy resin blend as a function of temperature and strain rate" *Composites Part A: Applied Science and Manufacturing,* vol. 41, no. 9, pp. 1072-1076, 2010.
[76] J. Guan *et al.*, "Glass transitions in native silk fibres studied by dynamic mechanical thermal analysis" *Soft Matter,* vol. 12, no. 27, pp. 5926-5936, 2016.
[77] D. Porter, F. Vollrath, and Z. Shao, "Predicting the mechanical properties of spider silk as a model nanostructured polymer" *The European Physical Journal E,* vol. 16, no. 2, pp. 199-206, 2005.
[78] C. Fu, D. Porter, and Z. Shao, "Moisture Effects on Antheraea pernyi Silk's Mechanical Property" *Macromolecules,* vol. 42, no. 20, pp. 7877-7880, 2009.
[79] D. W. Van Krevelen and K. Te Nijenhuis, "Properties of Polymers", 4th ed. Elsevier, 2008.
[80] R. LeVeque, *Finite Difference Methods for Ordinary and Partial Differential Equations* (Other Titles in Applied Mathematics). Society for Industrial and Applied Mathematics, 2007, p. 342.
[81] T. J. R. Hughes, "The Finite Element Method: Linear Static and Dynamic Finite Element Analysis", *1st ed. Dover Publications*, 2000.
[82] ASTM D5229/D5229M-14 *Standard Test Method for Moisture Absorption Properties and Equilibrium Conditioning of Polymer Matrix Composite Materials.*
[83] S. Akbar and T. Zhang, "Moisture Diffusion in Carbon/Epoxy Composite and the Effect of Cyclic Hygrothermal Fluctuations: Characterization by Dynamic Mechanical Analysis (DMA) and Interlaminar Shear Strength (ILSS)" *The Journal of Adhesion,* vol. 84, no. 7, pp. 585-600, 2008.
[84] R. J. Morgan, J. E. O'Neal, and D. L. Fanter, "The effect of moisture on the physical and mechanical integrity of epoxies" *Journal of Materials Science,* vol. 15, no. 3, pp. 751-764, 1980.
[85] C. Soutis and D. Turkmen, "Moisture and Temperature Effects of the Compressive Failure of CFRP Unidirectional Laminates" *Journal of Composite Materials,* vol. 31, no. 8, pp. 832-849, 1997.
[86] C.-H. Shen and G. Springer, "Moisture Absorption and Desorption of Composite Materials" *Journal of Composite Materials,* vol. 10, no. 1, pp. 2-20, 1976.
[87] N. L. Post, F. Riebel, A. Zhou, T. Keller, S. W. Case, and J. J. Lesko, "Investigation of 3D Moisture Diffusion Coefficients and Damage in a Pultruded E-glass/Polyester Structural Composite" *Journal of Composite Materials,* vol. 43, no. 1, pp. 75-96, 2008.
[88] M. T. Aronhime, S. Neumann, and G. Marom, "The anisotropic diffusion of water in Kevlar-epoxy composites" *Journal of Materials Science,* vol. 22, no. 7, pp. 2435-2446, 1987.
[89] R. M. Sullivan, E. H. Stokes, and E. H. Baker, "Effect of Time at Temperature on the Ply-Normal Modulus of Carbon Phenolic" *AIAA Journal,* vol. 49, no. 11, pp. 2482-2490, 2011.
[90] Y. Joliff, W. Rekik, L. Belec, and J. F. Chailan, "Study of the moisture/stress effects on glass fibre/epoxy composite and the impact of the interphase area" *Composite Structures,* vol. 108, pp. 876-885, 2014.

[91] A. Mubashar, I. A. Ashcroft, G. W. Critchlow, and A. D. Crocombe, "Modelling Cyclic Moisture Uptake in an Epoxy Adhesive" *The Journal of Adhesion,* vol. 85, no. 10, pp. 711-735, 2009.

[92] D. Liu and S. Park, "A Note on the Normalized Approach to Simulating Moisture Diffusion in a Multimaterial System Under Transient Thermal Conditions Using ansys 14 and 14.5" *Journal of Electronic Packaging,* vol. 136, no. 3, pp. 034501-034501-3, 2014.

[93] C. Jang, S. Park, B. Han, and S. Yoon, "Advanced Thermal-Moisture Analogy Scheme for Anisothermal Moisture Diffusion Problem" *Journal of Electronic Packaging,* vol. 130, no. 1, pp. 011004-011004, 2008.

[94] R. Leger, A. Roy, and J. C. Grandidier, "Non-classical water diffusion in an industrial adhesive" *International Journal of Adhesion and Adhesives,* vol. 30, no. 8, pp. 744-753, 2010.

[95] ISO 483:2005 *Plastics - Small enclosures for conditioning and testing using aqueous solutions to maintain the humidity at a constant value*, 2005.

[96] M. Gundjian and C. Cole Kenneth, "Effect of copper on the curing and structure of a DICY-containing epoxy composite system" *Journal of Applied Polymer Science,* vol. 75, no. 12, pp. 1458-1473, 2000.

[97] A. Tcharkhtchi, P. Y. Bronnec, and J. Verdu, "Water absorption characteristics of diglycidylether of butane diol–3,5-diethyl-2,4-diaminotoluene networks" *Polymer,* vol. 41, no. 15, pp. 5777-5785, 2000.

[98] C. J. Gibbins, "A survey and comparison of relationships for the determination of the saturation vapour pressure over plane surfaces of pure water and of pure ice" *Annales Geophysicae,* Article vol. 8, no. 12, pp. 859-885, 1990.

[99] P. R. Lowe, "An Approximating Polynomial for the Computation of Saturation Vapor Pressure" *Journal of Applied Meteorology,* vol. 16, no. 1, pp. 100-103, 1977.

[100] W. Wagner and A. Pruß, "The IAPWS Formulation 1995 for the Thermodynamic Properties of Ordinary Water Substance for General and Scientific Use" *Journal of Physical and Chemical Reference Data,* vol. 31, no. 2, pp. 387-535, 2002.

[101] "DMA 8000 Manual" PerkinElmer.

[102] J. Yu Bai and Li, "Characterization of frequency-dependent glass transition temperature by Vogel–Fulcher relationship" *Journal of Physics D: Applied Physics,* vol. 41, no. 15, p. 152008, 2008.

[103] K. Li, K. Wang, M.-s. Zhan, and W. Xu, "The change of thermal–mechanical properties and chemical structure of ambient cured DGEBA/TEPA under accelerated thermo-oxidative aging" *Polymer Degradation and Stability,* vol. 98, no. 11, pp. 2340-2346, 2013.

[104] X. Ramis, A. Cadenato, J. M. Morancho, and J. M. Salla, "Curing of a thermosetting powder coating by means of DMTA, TMA and DSC" *Polymer,* vol. 44, no. 7, pp. 2067-2079, 2003.

[105] K. A. Connors, "Chemical Kinetics: Study of Reaction Rates in Solution", *John Wiley and Sons*, 1990.

[106] N. Melanitis, P. L. Tetlow, C. Galiotis, and S. B. Smith, "Compressional behaviour of carbon fibres" *Journal of Materials Science,* vol. 29, no. 3, pp. 786-799, 1994.

[107] C. Harwood, G. H. Wostenholm, B. Yates, and D. V. Badami, "Thermodynamic properties of phenol–formaldehyde resin" *Journal of Polymer Science: Polymer Physics Edition,* vol. 16, no. 5, pp. 759-766, 1978.

[108] P. S. Parameswaran and E. T. Thachil, "Influence of Ether Linkages on the Properties of Resol Phenolic Resin" *International Journal of Polymeric Materials and Polymeric Biomaterials,* vol. 56, no. 2, pp. 177-185, 2007.

[109] N. Gabilondo, L. Martin, A. Retegi, I. Mondragon, and A. Berglund Lars, "Property tailoring of phenol–formaldehyde matrices by control of reactant molar ratio and thermoplastic modification" *Polymer International,* vol. 60, no. 5, pp. 851-858, 2011.

[110] D. Porter and F. Vollrath, "The role of kinetics of water and amide bonding in protein stability" *Soft Matter,* vol. 4, no. 2, pp. 328-336, 2008.

[111] S. Alston and C. Arnold, "DMTA Spectrum of a Phenolic Resin", Unpublished work, Swansea University, 2017.
[112] S. Alston and C. Arnold, "Gravimetric Analysis of a Phenolic Resin in a Cyclic Conditioning Environment", Unpublished work, Swansea University, 2017.
[113] G. S. Kell, "Density, thermal expansivity, and compressibility of liquid water from 0.deg. to 150.deg.. Correlations and tables for atmospheric pressure and saturation reviewed and expressed on 1968 temperature scale" *Journal of Chemical & Engineering Data,* vol. 20, no. 1, pp. 97-105, 1975.
[114] S. Alston and C. Arnold, Unpublished work, Swansea University.
[115] L. W. Davies, R. J. Day, D. Bond, A. Nesbitt, J. Ellis, and E. Gardon, "Effect of cure cycle heat transfer rates on the physical and mechanical properties of an epoxy matrix composite" *Composites Science and Technology,* vol. 67, no. 9, pp. 1892-1899, 2007.
[116] A. Apicella, L. Nicolais, M. R. Nobile, and M. A. Castiglione-Morelli, "Effect of processing variables on the durability of epoxy resins for composite systems" *Composites Science and Technology,* vol. 24, no. 2, pp. 101-121, 1985.
[117] F. Franks, *Water: A Matrix of Life*, 2nd ed. Royal Society of Chemistry, 2000.
[118] M. P. Zanni-Deffarges and M. E. R. Shanahan, "Evaluation of adhesive shear modulus in a torsional joint: influence of ageing" *International Journal of Adhesion and Adhesives,* vol. 13, no. 1, pp. 41-45, 1993.
[119] Z. Yang, G. Xian, and H. Li, "Effects of alternating temperatures and humidity on the moisture absorption and mechanical properties of ramie fiber reinforced phenolic plates" *Polymer Composites,* vol. 36, no. 9, pp. 1590-1596, 2014.
[120] E. C. Botelho, M. L. Costa, L. C. Pardini, and M. C. Rezende, "Processing and hygrothermal effects on viscoelastic behavior of glass fiber/epoxy composites" *Journal of Materials Science,* vol. 40, no. 14, pp. 3615-3623, 2005.
[121] T. P. Ferguson and Q. Jianmin, "Elastic modulus variation due to moisture absorption and permanent changes upon redrying in an epoxy based underfill" *IEEE Transactions on Components and Packaging Technologies,* vol. 29, no. 1, pp. 105-111, 2006.
[122] W. N. Nkeuwa, B. Riedl, and V. Landry, "UV-cured clay/based nanocomposite topcoats for wood furniture. Part II: Dynamic viscoelastic behavior and effect of relative humidity on the mechanical properties" *Progress in Organic Coatings,* vol. 77, no. 1, pp. 12-23, 2014.
[123] C. Stone, "DVS of a Low-fired Carbon-fibre", Unpublished work, Defence Science and Technology Laboratory (DSTL), 2017.
[124] S. Alston and C. Arnold, "Composite Moisture Content as a Function of Relative Humidity", Unpublished work, Swansea University, 2018.
[125] K. A. Denham, "Measurement of Composite Fibre Volume Fraction", Unpublished work, Defence Science and Technology Laboratory (DSTL), 2016.